Evolution of Canadian Shield Groundwaters and Gases: Influence of Deep Permafrost

by

Randy L. Stotler

A thesis
presented to the University of Waterloo
in fulfillment of the
thesis requirement for the degree of
Doctor of Philosophy
in
Earth Sciences

Waterloo, Ontario, Canada, 2008

Author's Declaration

I hereby declare that I am the sole author of this thesis. This is a true copy of the thesis, including any required final revisions, as accepted by my examiners.

I understand that my thesis may be made electronically available to the public.

Abstract

Numerous glacial advances over the past 2 million years have covered the entire Canadian and Fennoscandian Shield outcrop. During glacial advance and retreat, permafrost is expected to form in front of the glacier. The question of how permafrost and freezing impact the formation and evolution of brines in natural systems may be vital to understanding the chemistry of groundwater in crystalline rocks. Investigations of groundwater conditions beneath thick permafrost can provide valuable information that can be applied to assessing safety of deep, underground nuclear waste repositories and understanding analogues to potential life-bearing zones on Mars. However, very little scientific investigation of cryogenic processes and hydrogeology deep within crystalline systems has been published. The purpose of this research is to evaluate the impacts of thick permafrost (>300m) formation on groundwater chemical and flow system evolution in the crystalline rock environment over geologic timescales.

A field investigation was conducted at the Lupin Mine in Nunavut, Canada, to characterize the physical and hydrogeochemical conditions within and beneath a thick permafrost layer. Taliks, or unfrozen channels within the permafrost, are found beneath large lakes in the field area, and provide potential hydraulic connections through the permafrost. Rock matrix waters are dilute and do not appear to affect groundwater salinity. Permafrost waters are Na-Cl and Na-Cl-SO_4 type, and have been contaminated with chloride and nitrate by mining activities. Sulfide oxidation in the permafrost may be naturally occurring or is enhanced by mining activities. Basal permafrost waters (550 to 570 mbgs) are variably affected by mining. The less contaminated basal waters have medium sulfate concentrations and are Ca-Na dominated. This is similar to deeper, uncontaminated subpermafrost waters, which are Ca-Na-Cl or Na-Ca-Cl type with a wide range of salinities (2.6 to 40 $g \cdot L^{-1}$). The lower salinity subpermafrost waters are attributed to dissociation of methane hydrate and drawdown of dilute talik waters by the hydraulic gradient created by mine dewatering. This investigation was unable to determine the influence of talik waters to the subpermafrost zone in undisturbed conditions. Pressures are also highly variable, and do not correlate with salinity. Fracture infillings are scarce and calcite $\delta^{18}O$ and $\delta^{13}C$ values have a large range. Microthermometry indicates a large range in salinities and homogenization temperatures as well, indicative of a boiling system. *In situ* freezing of fluids and methane hydrate formation may have concentrated the remaining fluids.

Field activities at the Lupin mine also provided an opportunity to study the nature of gases within crystalline rocks in a permafrost environment. Gases were generally methane-dominated (64 to 87), with methane $\delta^{13}C$ and $\delta^{2}H$ values varying between -56 and -42‰ VPDB and -349 to -181 ‰

VSMOW, respectively. The gases sampled within the Lupin mine have unique ranges of chemical and isotopic compositions compared with other Canadian and Fennoscandian Shield gases. The gases may be of thermogenic origin, mixed with some bacteriogenic gas. The generally low δ^2H-CH_4 ratios are somewhat problematic to this interpretation, but the geologic history of the site, a metaturbidite sequence, supports a thermogenic gas origin. The presence of gas hydrate in the rock surrounding Lupin was inferred, based on temperature measurements and hydrostatic pressures. Evidence also suggests fractures near the mine have been depressurized, likely due to mine de-watering, resulting in dissipation of methane hydrate near the mine. Modeling results indicate methane hydrates were stable throughout the Quaternary glacial-interglacial cycles, potentially limiting subglacial recharge.

The effects of deep permafrost formation and dissipation during the Pleistocene glacial/interglacial cycle to deep groundwaters in the Canadian Shield were also investigated by compiling data from thirty-nine sites at twenty-four locations across the Canadian Shield. Impacts due to glacial meltwater recharge and surficial cryogenic concentration of fluids, which had been previously considered by others, and *in situ* freeze-out effects due to ice and/or methane hydrate formation were considered. At some Canadian Shield sites, there are indications that fresh, brackish, and saline groundwaters have been affected by one of these processes, but the data were not sufficient to differentiate between mixed, intruded glacial meltwaters, or residual waters resulting from either permafrost or methane hydrate formation. Physical and geochemical data do not support the cryogenic formation of Canadian Shield brines from seawater in glacial marginal troughs.

The origin and evolution of Canadian and Fennoscandian Shield brines was explored with a survey of chlorine and bromine stable isotope ratios. The δ^{37}Cl and δ^{81}Br isotopic ratios varied between -0.78 ‰ and 1.52 ‰ (SMOC) and 0.01 ‰ and 1.52 ‰ (SMOB), respectively. Variability of chlorine and bromine isotope ratios decreases with increasing depth. Fennoscandian Shield groundwaters tend to be more enriched than Canadian Shield groundwaters for both ^{37}Cl and ^{81}Br. Other sources and processes which may affect δ^{37}Cl and δ^{81}Br composition are also explored. Primary processes such as magmatic and/or hydrothermal activity are thought to be responsible for the isotopic composition of the most concentrated fluids at each site. Positive correlations between δ^{81}Br, and δ^{37}Cl with δ^2H-CH_4 and δ^{13}C-CH_4 were noted. At this time the cause of the relationship is unclear, and may be a result of changing redox, pH, temperature, and/or pressure conditions during hydrothermal, metamorphic, or volcanogenic processes. The data suggest solute sources and fluid evolution at individual sites would be better constrained utilizing a multi-tracer investigation of δ^{37}Cl, δ^{81}Br, and ^{87}Sr/^{86}Sr ratios comparing fluids, rocks, and fracture filling minerals (including fluid inclusions).

Acknowledgements

A project of this magnitude and duration cannot be completed without the gracious assistance of many individuals and groups. In no particular order, I would like to express my gratitude to the all those that assisted.

This project could not have been completed without financial, logistical, technical, and personnel support from the Geological Survey of Finland (Kiitos!). I am grateful to Lasse Ahonen for field assistance and discussions concerning site geochemistry, Juha Kaija for maintaining the vast amounts of data collected Ilmo Kukkonen, Jussi Leveinen, and Marrku Paananen for helping to refine the Lupin site conceptual model with thermal and hydraulic modeling and geophysical interpretation, and Antero Lindberg for supervising the diamond drilling. Geophysical soundings were also conducted by geophysicists Jukka Lehtimäki, Heikki Forss, and Juha Majaniemi. Ossi Ikävalko from Kivikonsultit Oy provided the downhole video surveys. Even after Runar Blomqvist became director of the Survey office in Kokkala, he continued to offer support for the project and hospitality in Helsinki and Punkalaidun. Finally, I cannot thank Timo Rukeeniemi enough. His tireless work as project coordinator made everything possible. Through his hard work, Timo taught me about managing, organizing, and planning big projects in remote, inaccessible locations, spent countless hours reviewing reports and early versions of several of these chapters, and immensely helped me to understand hard rock systems. I appreciated the hospitality of Timo and his family in Kirkkonummi during the yearly Finnish progress meetings.

Participants in the yearly progress meetings in Finland provided research direction, feedback, and support. I particularly appreciated technical discussions with Paul Degnan, Kimmo Lehto, Ignasi Puigdomenech, and John Smellie. I am especially grateful to Kimmo for demonstrating how true Finns go ice fishing on that spring day at Lupin, and to John for proving that Shaun's Siberia stories were not embellished, but rather somewhat watered down. Support was also provided by Lena Moren, Margit Snellman, and Peter Vidstrand. It was especially helpful that most of this group also assisted in the field at Lupin at one time or another.

Monique Hobbs technically reviewed several chapters and reports, provided field assistance at Lupin, and provided additional support throughout the project. I cannot thank Monique enough for all the help she has provided me throughout my PhD.

The Indiana-Princeton-Tennessee-Astrobiology-Initiative (IPTAI) group provided additional funding, field expertise, and opened my eyes to research at the interface of scientific fields and for teaching me so much about enhancing public support for research. Tullis Onstont, Susan Pfiffner,

Lisa Pratt, and Barb Sherwood-Lollar provided encouragement, and reviewed and provided comments portions of an early draft of this thesis. Thanks also to Peter Suchecki from Redstart Studios for making me famous in all those NASA documentaries, and all the great discussions.

Access to Lupin was provided by Echo Bay Mines Ltd. and Kinross Gold Corp. Both companies provided hospitality and assistance to the project beyond expectation. Numerous employees including Doug Bencharski, Bill Danyluk, Hugh Ducasse, Phil Geusebroek, Wayne Grudzinski, Quinton Hamilton, Andy Hureau, Dave Hohnstein, Yves Levesque, Barry Lowe, Graham McNally, Richard McPherson, Richard McPherson, Bruce Penner, Mike Tansey, and many others contributed to the work at a practical level.

Access to High Lake was provided by Wolfden Resources Inc. and Zinifex Ltd. Assistance and hospitality from individuals at High Lake including Tom Collett, Ian Neill, Trish Toole, and Bruno Zerban helped with a very difficult part of the project.

It was also great to get to work with Barry Freifeld, Brian Holden, Bob Ingleton, Adam Johnson, and Dan McGown at High Lake. Paul Johnson also assisted by making some down-hole devices for Lupin. Bob and Paul, I really appreciated the opportunity to work with two of the best field minds around.

I cannot thank individuals from the Chlorine-Bromine-Strontium Lab enough, particularly Oya Albak, Humam El Mugammar, and Matt Vanderkooy. I am especially greatful to Orfan Shouakar-Stash and Bob Drimmie for helpful discussions.

I would also like to acknowledge two mentors who have helped me along the way. Ed Harvey, thanks for giving me a start, for all the help along the way, and for all the advice. I also appreciated the opportunity to help Will Robertson coordinate field school for all those years.

I also appreciate the support of Sue Fisher and Lorraine Albrecht. Thanks for keeping on top of everything and helping with all the details.

There are too many friends in the Earth Sciences Department to list everyone. You helped keep me sane, and I think we had a little bit of fun along the way as well. I would especially like to thank Ed Cey, J.P. Jones, Matt Lindsay, Mike Moncur and Jen Parks for the advice, friendship, and laughter.

In whole or in part, sections of this thesis were also reviewed by Ian D. Clark, Jean-Michel Lemeiux, W. Richard Peltier, and Lev Tarasov. I appreciate the time and effort put forth by all who assisted, and the thoughtful suggestions they provided. I also thank Lev for making adjustments to the

MUN/UT glacial systems model and providing me with the resulting simulations, and Jean-Michel for providing modeling results from his dissertation work. David Blowes, graciously provided access to the Lac de Gras dataset.

I am grateful to my PhD committee members, Tom Edwards, Dave Rudolph, and Ed Sudicky for their time, advice, guidance, and constructive comments throughout this project. I also appreciate the many constructive comments from my external examiners, Warren Wood and Bill Annable.

I would sincerely like to thank my supervisor Shaun Frape for his friendship, invaluable advice, conferences in exotic locals, the coolest field sites in the department, and of course, Ukrainian Christmas.

Financial contributions from other the funding partners National Aeronautics and Space Administration (NASA), USA, Ontario Power Generation (OPG) / Nuclear Waste Management Organization (NWMO), Canada, Posiva Oy, Finland, Svensk Kärnbränslehantering AB (SKB), Sweden, and UK Nirex Ltd, United Kingdom are also appreciated. Additional funding was provided by a Natural Sciences and Engineering Research Council (NSERC) grant to Shaun Frape. I also appreciated assistance from the Bob Farvolden Scholarship.

Finally, I would like to dedicate this thesis to my family. Mom and Dad, I appreciate all the support, love, and patience you have given me over the years. Andrea, I could not have done this without you. Thank you for your friendship and love, and for all your support.

Table of Contents

List of Figures ..... **xi**

List of Tables ..... **xvii**

Foreword ..... **xviii**

Chapter 1 Introduction **1**

1.1 Background 1

1.2 Objectives 4

Chapter 2 Hydrogeochemistry of Groundwaters In and Below the Base of Thick Permafrost at Lupin, Nunavut, Canada **8**

2.1 Executive Summary 8

2.2 Introduction 8

2.3 Site Description 10

2.3.1 Geology 12

2.3.2 Fracturing and Hydraulic Parameters 12

2.3.3 Permafrost 12

2.3.4 Taliks 13

2.4 Methods 13

2.5 Results and Discussion 18

2.5.1 Precipitation and Surface Waters 18

2.5.2 Taliks 22

2.5.3 Matrix Fluids 22

2.5.4 Permafrost Waters 24

2.5.5 Waters at the Base of the Permafrost 30

2.5.6 Subpermafrost Waters 31

2.5.7 Gases 35

2.5.8 Calcite Fluid Inclusions 35

2.5.9 Evolution of Waters at the Lupin Site 38

2.5.10 Comparison with "Cryogenic Freezing of Seawater" Hypothesis 40

2.6 Conclusions 41

Chapter 3 Thermogenic Methane Hydrate in a Crystalline Shield **43**

3.1 Executive Summary 43

3.2 Introduction 43

3.3 Methods 44

3.4 Results and Discussion 46

3.4.1 Origin and Evolution of the Gas 46
3.4.2 Physical Nature of Gas 55
3.5 Summary 60
Chapter 4 Interglacial-Glacial Cycling and the Geochemical Evolution of Canadian Shield Groundwaters 62
4.1 Executive Summary 62
4.2 Introduction 62
4.3 Freeze-out Experiments 68
4.4 Sites in Permafrost Regions 71
4.5 Sites Not Currently in Regions of Permafrost 78
4.5.1 Fresh, Brackish, and Saline Fluids 78
4.5.2 Canadian Shield Brines and Freezing 84
4.6 Are There Deep Freezing Affected Waters? 90
4.6.1 Mine De-watering 91
4.6.2 Deep Paleo-permafrost 92
4.6.3 Intruded Glacial Meltwater 93
4.6.4 Methane Hydrates 93
4.7 Summary 97
Chapter 5 An Isotopic Survey of $\delta^{81}Br$ and $\delta^{37}Cl$ of Dissolved Halides in the Canadian and Fennoscandian Shields 99
5.1 Executive Summary 99
5.2 Introduction 99
5.3 Methods 101
5.4 Results 103
5.5 Discussion 109
5.5.1 Formational Processes: High Temperatures 112
5.5.2 Internal & External Modifications: Intermediate to Low Temperatures 117
5.5.3 Other Relationships: Gases 124
5.6 Conceptual Model 131
5.7 Summary 134
Chapter 6 Conclusions and Future Study 136
6.1 Conclusions 136
6.2 Recommendations 139

Appendices

Appendix A. Overview of Permafrost and the Freezing Process 141

Appendix B. Lupin Datasets 158

Appendix C. Review of Methane Hydrate Isotopic Geochemistry 187

Appendix D. Canadian and Fennoscandian Shield $\delta^{37}Cl$ and $\delta^{81}Br$ Data 208

References 222

List of Figures

Figure 1-1. Salinity with depth in crystalline rocks..... 2
Figure 1-2. Conceptual model of surficial freezing of seawater hypothesis for the origin of Canadian and Fennoscandian Shield brines..... 3
Figure 1-3. Relationship between Na/Cl and Br/Cl ratios for experimental seawater evaporation and freezing..... 3
Figure 2-1. (A) Location of Lupin within Canada and zone of continuous permafrost (B) Surface geology of the study area..... 11
Figure 2-2. The Lupin mine 1130 m level plan and drillhole location map..... 15
Figure 2-3. Piper diagram of waters sampled in the Lupin area..... 19
Figure 2-4. Chemical trends with depth at Lupin (A) TDS (B) Cl, (C) SO_4 (D) NO_3 (E) ^3H. 20
Figure 2-5. Stable isotopic composition of Lupin Waters..... 20
Figure 2-6. Radioactive tracers ^{36}Cl and ^{14}C vs. TDS, and ^{36}Cl vs. Br/Cl*1000 for waters sampled at the Lupin mine..... 21
Figure 2-7. Reflection profiles from GPR surveys conducted at the Lupin mine, courtesy Geological Survey of Finland.
(A) Three GPR survey lines conducted at 400 MHz frequency
(B) 40 MHz survey line..... 23
Figure 2-8. (A) Na/Cl vs. Br/Cl trends for evaporating seawater, freezing seawater, and Shield fluid freezing experiments.
(B) Na/Cl vs. Br/Cl results for samples collected at the Lupin mine
(C) Ca/Na vs. Br/Cl for samples collected at the Lupin mine..... 25
Figure 2-9. $\delta^{37}Cl$ (A) vs. Br/Cl, (B) vs. Cl for samples collected at the Lupin mine. 26
Figure 2-10. Stable isotopes of nitrate in Lupin groundwaters..... 27
Figure 2-11. Stable isotopes of sulfur in Lupin groundwaters..... 29
Figure 2-12. Changes in pressure (A) and salinity (B) with time in boreholes from the subpermafrost zone of the Lupin Mine, Nunavut, Canada. 32
Figure 2-13. (A) Lupin calcites $\delta^{18}O$ and $\delta^{13}C$ vs. Canadian Shield calcites
(B) Isotopic thermometric plot for Lupin calcites. 37
Figure 2-14. Conceptual hydrogeologic model of the Lupin area..... 40

Figure 3-1. Lupin gas relationships, compared with other sites
(A) $\delta^{13}C$-CH_4 versus $C_1/(C_2+C_3)$ ratios
(B) $\delta^{13}C$ values of individual hydrocarbons versus carbon number.
(C) Comparison of $\delta^{2}H$ and $\delta^{13}C$ grouped with respect to permafrost conditions
(D). Relationship between $\delta^{13}C$ vs. $\delta^{2}H$ between C1, C2, C3..... 48
Figure 3-2. Results for gases sampled at the Lupin mine
(A) $\delta^{13}C$-C1 vs. $\delta^{13}C$-C2 and (B)$\delta^{13}C$-C2 vs. $\delta^{13}C$-C3..... 49
Figure 3-3. Relationship between $\delta^{13}C$-CH_4 and nitrogen gas content of Lupin gases. 49
Figure 3-4. Relationship between $\delta^{2}H$-CH_4 and $\delta^{2}H$-H_2O for Lupin gases..... 51
Figure 3-5. Relationship between the carbon isotopic ratios of methane and carbon dioxide for Lupin gas samples..... 53
Figure 3-6. Results of noble gas analyses from samples collected at the Lupin mine
(A) Correlation of He*10,000 and Ar versus methane.
(B) Xe and Kr versus Ne..... 55
Figure 3-7. Potential for gas hydrate formation at Lupin.
(A) Pressure-temperature fields for boreholes sampled at the 890 and 1130m levels.
(B). Results of borehole video survey for three boreholes, showing frequency of fractures and gas producing fractures. 56
Figure 3-8. Lupin borehole temperature variation..... 58
Figure 3-9. Results of glacial systems modeling of eight different climate scenarios. 59
Figure 3-10. Predicted subsurface hydraulic conditions over the last 120 ky at Lupin, Nunavut. 60
Figure 4-1. Map of Canadian Shield sample sites in relation to permafrost distribution. 64
Figure 4-2. Na/Cl vs. Br/Cl ratios from freezing experiments 69
Figure 4-3. Relationship between $\delta^{2}H$ and $\delta^{18}O$ during freezing of shield groundwaters..... 70
Figure 4-4. Relationship between $\delta^{18}O$ and Cl during freezing..... 71
Figure 4-5. Geochemical relationships of groundwaters sampled from Canadian Shield sites located in continuous permafrost regions.
(A) A comparison of Na/Cl and Br/Cl ratios
(B) Freezing and evaporation experiment results
(C) Isotopic relationships between $\delta^{2}H$ and $\delta^{18}O$.
(D) The relationship between Cl and $\delta^{18}O$, with three end-member mixing diagram. 73

Figure 4-6. Geochemical relationships of groundwaters sampled from Canadian Shield sites located in discontinuous permafrost regions.
(A) A comparison of Na/Cl and Br/Cl ratios
(B) Freezing and evaporation experiment results
(C) Isotopic relationships between δ^2H and $\delta^{18}O$.
(D) The relationship between Cl and $\delta^{18}O$, with three end-member mixing diagram 75
Figure 4-7. Geochemical relationships of groundwaters sampled from Canadian Shield sites located near sporadic and isolated permafrost regions.
(A) A comparison of Na/Cl and Br/Cl ratios
(B) Freezing and evaporation experiment results
(C) Isotopic relationships between δ^2H and $\delta^{18}O$.
(D) The relationship between Cl and $\delta^{18}O$, with three end-member mixing diagram 76
Figure 4-8. Relationship of $\delta^{18}O$ with depth in groundwaters
(A) for Canadian Shield sites located in or near permafrost areas
(B) and sites not currently located within permafrost areas..... 77
Figure 4-9. Ensemble mean permafrost depth difference between the Last Glacial Maximum (~20 ka) and present..... 79
Figure 4-10. Wisconsinan glacial extent and exposed, unglaciated land in North America and Greenland at the last glacial maximum..... 80
Figure 4-11. Relationship of Na/Cl and Br/Cl ratios for Canadian Shield groundwater samples from sites not located in or near permafrost.
(A) Displays results from all sites
(B) Displays only results from brackish and saline results from Eye Dashwa and Lac du Bonnet, and all results from Val d'Or and Kirkland Lake.
(C) Freezing and evaporation experiment results. 81
Figure 4-12. Relationship of δ^2H and $\delta^{18}O$ for Canadian Shield groundwater samples from sites not located in or near permafrost by salinity. (A) All sites, (B) South Bay Mine and East Bull Lake, (C) Lac du Bonnet and Elliot Lake.. 82
Figure 4-13. Relationship of Cl^- and $\delta^{18}O$ for Canadian Shield groundwater samples from sites not located in or near permafrost. (A) All sites, (B) South Bay Mine and East Bull Lake, (C) Lac du Bonnet, Elliot Lake, and Eye-Dashwa..... 83
Figure 4-14. Comparison of flow under glacial ice from Starinsky and Katz (*2003*) hypothesis with currently accepted conceptual model of subglacial pressures and flow 85

Figure 4-15. Geochemical trends of Canadian Shield brines.
(A) Relationship of Na/Cl and Br/Cl ratios for Canadian Shield brines
(B) Na/Cl vs. Br/Cl freezing and evaporation experiment results
(C) Relationship of δ^2H and $\delta^{18}O$ for Canadian Shield brines.
(D) Relationship of Cl^- and $\delta^{18}O$ for Canadian Shield brines. 87
Figure 4-16. Relationships between $\delta^{18}O$ and (A) $^{87}Sr/^{86}Sr$, (B) $\delta^{81}Br$, and (C) $\delta^{37}Cl$.. 89
Figure 4-17. Comparison of seawater freezing pathways.
(A) Gitterman pathway.
(B) Ringer-Nelson-Thompson pathway
(C) Relative salt precipitation during freezing to the eutectic temperature along each pathway..... 90
Figure 4-18. Mixing due to mine dewatering on a δ^2H vs. $\delta^{18}O$ plot. 92
Figure 4-19. Methane-hydrate and ice phase equlibria in fresh water.
(A) The Lupin geothermal gradient and modern hydrostatic pressures
(B) Hydrate stability field if a kilometer thick glacier, exerting 10000 kPa of pressure, is present with a "warm" glacial base and a conservative geothermal gradient. 94
Figure 4-20. (A) Different trends observed in Mackenzie Delta gas hydrate research well.
(B) Canadian Shield gas compositions compared with gas hydrates sampled in the Mackenzie Delta. 96
Figure 5-1. Groundwater sample locations in Canada and Finland for samples analyzed in this study..... 102
Figure 5-2. Frequency of (A) $\delta^{37}Cl$ and (B) $\delta^{81}Br$ from the Canadian and Fennoscandian Shields..... 104
Figure 5-3. Distribution of $\delta^{37}Cl$ and $\delta^{81}Br$ at individual sites. 105
Figure 5-4. $\delta^{81}Br$ vs. $\delta^{37}Cl$ for Canadian and Fennoscandian Shield groundwater samples analyzed in this study,..... 106
Figure 5-5. Ca/Na vs. (A) $\delta^{81}Br$ and (B) $\delta^{37}Cl$; Br/Cl vs. (C) $\delta^{81}Br$ and (D) $\delta^{37}Cl$ for Canadian and Fennoscandian shield groundwater samples analyzed in this study..... 107
Figure 5-6. $\delta^{37}Cl$ vs. (A) $\delta^{18}O$ and (B) δ^2H; $\delta^{81}Br$ vs. (C) $\delta^{18}O$ and (D) δ^2H for Canadian and Fennoscandian Shield groundwaters analyzed in this study. 108
Figure 5-7. Relationship of $\delta^{37}Cl$ (A) and $\delta^{81}Br$ (B) with depth in Canadian and Fennoscandian Shield groundwaters analyzed in this study. 109

Figure 5-8. Geology, major element water chemistry, Eh and pH, and stable chlorine isotope analyses of rock and water as functions of depth in drill hole Ju/Mi-116, eastern Finland. 111
Figure 5-9. $^{87}Sr/^{86}Sr$ vs. $\delta^{81}Br$ and $^{87}Sr/^{86}Sr$ vs. $\delta^{37}Cl$ for Canadian and Fennoscandian Shield groundwaters analyzed in this study. 118
Figure 5-10. Comparison of $^{87}Sr/^{86}Sr$ ratios and $\delta^{37}Cl$ values in the groundwater and in the host rock and $\delta^{81}Br$ values in the groundwater around Sudbury. 120
Figure 5-11. $\delta^{37}Cl$ vs. Residual Factor for Samples Taken from the Column (A) and Batch Freezing Experiments(B). 124
Figure 5-12. $\delta^{81}Br$ vs. $\delta^{2}H$-CH_4 (A), $\delta^{13}C$-CH_4 (C), and $\delta^{37}Cl$ vs. $\delta^{2}H$-CH_4 (B), $\delta^{13}C$-CH_4 (D) for Canadian and Fennoscandian Shield groundwater and gas samples. 125
Figure 5-13. $\delta^{81}Br$ vs. $\delta^{2}H$-C2 (A), $\delta^{13}C$-C2 (C), and $\delta^{37}Cl$ vs. $\delta^{2}H$-C2 (B), $\delta^{13}C$-C2 (D) for Canadian and Fennoscandian Shield groundwater and gas samples. 126
Figure 5-14. The relationship between Br^- and SO_4^{-2} for groundwaters sampled in crystalline rocks 127
Figure 5-15. Conceptual model of influences to halide isotope composition in the Canadian Shield, (A). Archean, (B) Proterozoic. 132
Figure 5-15 (cont.). (C). Shield during Plio-Pleistocene glaciation, (D). Conceptual model of current influences affecting halides isotopic ratios in the Shield. 133
Figure A-1. Comparison of seawater freezing pathways. (A) Gitterman pathway (B) Ringer-Nelson-Thompson pathway (C) Relative salt precipitation during freezing to the eutectic temperature along each pathway 142
Figure A-2. Isotopic fractionation of (A) $\delta^{2}H$ and $\delta^{18}O$ and (B) $\delta^{37}Cl$, during freezing of Palmottu fluids 146
Figure A-3. Typical geothermal profile through permafrost, with definitions 151
Figure C-1. Map of known and inferred hydrate occurrences, marine and permafrost. 189
Figure C-2. Conceptualization of methane hydrate formation environments: (A) passive margins, Blake Ridge as an example (B) accretionary margins, (C) continental permafrost. 192
Figure C-3. Blake Ridge Data, DSDP/ODP Legs 11, 76, 164, and 172.
(A) Site Locations with bathymetry and depth to sulfate-methane interface
(B) Legs 11, 76, and 164
(C) Leg 172 194

Figure C-4. Cascadia Margin
(A) Sites with methane hydrates
(B) sites with methane and hydrogen sulfide hydrates
(C) sites without hydrates. 195
Figure C-5. Accretionary margin sites with gas hydrates.
(A) Nankai Trough, ODP Leg 131, Site 808
(B) Middle America Trench, Leg 84 and Leg 170
(C) Peruvian Outer Continental Margin
(D) Chilean Triple Junction 197
Figure C-6. Carbon isotope-depth profiles at other passive margin sites. Gulf of Mexico sites
(A) with gas hydrates and (B) without gas hydrates.
(C) Sites with probable, but unconfirmed gas hydrate offshore New Jersey Leg
174A and (D) Vøring Plateau, Norway, Leg 104 198
Figure C-7. Other marine gas profiles at sites without gas hydrates. (A) Cariaco Trench |(B)
various oceanic sites from early DSDP
(C) Philippines 199
Figure C-8. Isotopic results of hydrate depressurization. 200
Figure C-9. Permafrost depth trends from the Mackenzie Delta, Mallik 2L-38 and Mallik 5L-38
boreholes 203
Figure D-1. δ^{81}Br vs. (A) TDS, (B) Br, (C) Na, (D) Cl, (E), Ca, (F), SO4, (G) Mg, and (H) K
for Canadian and Fennoscandian Shield groundwaters. 211
Figure D-2. Br vs. δ^{37}Cl and vs. δ^{81}Br for Canadian and Fennoscandian Shield groundwaters 212
Figure D-3. Cl vs. δ^{37}Cl and vs. δ^{81}Br for Canadian and Fennoscandian Shield groundwaters. 213
Figure D-4. Na vs. δ^{37}Cl and vs. δ^{81}Br for Canadian and Fennoscandian Shield groundwaters 214
Figure D-5. Ca vs. δ^{37}Cl and vs. δ^{81}Br for Canadian and Fennoscandian Shield groundwaters 215
Figure D-6. Mg vs. δ^{37}Cl and vs. δ^{81}Br for Canadian and Fennoscandian Shield groundwaters 216
Figure D-7. K vs. δ^{37}Cl and vs. δ^{81}Br for Canadian and Fennoscandian Shield groundwaters 217
Figure D-8. Ca/Na vs. Br/Cl for Canadian and Fennoscandian Shield groundwaters 218
Figure D-9. δ^{2}H vs. δ^{37}Cl and vs. δ^{81}Br for Canadian and Fennoscandian Shield groundwaters 219
Figure D-10. δ^{18}O vs. δ^{37}Cl and vs. δ^{81}Br for Canadian and Fennoscandian Shield groundwaters ... 220
Figure D-11. δ^{18}O vs. δ^{2}H for Canadian and Fennoscandian Shield groundwaters 221

List of Tables

Table 4-1. Host rock types and ages, water chemistry, and groundwater geochemical data sources for studies from the Canadian Shield. 65
Table 5-1. Statistical evaluation of $\delta^{37}Cl$ and $\delta^{81}Br$ distributions in Canadian and Fennoscandian Shield samples 103
Table 5-2. Summary of processes and known effects to $\delta^{37}Cl$ ratios, predicted behavior of $\delta^{81}Br$ ratios, and behavior of Cl^- vs. Br^-. 135
Table A-1. Summary of mineral precipitation from seawater through the different freezing pathways. 143
Table A-2. Relationship of temperature and water content in permafrost terminology. 149
Table A-3. Chemical comparison of talik waters. Data sources are listed in text. 155
Table B-1. Borehole completion information 158
Table B-2. Final redox (Eh) and dissolved oxygen values measured in flow-through cell. 158
Table B-3. Major ion geochemistry of Lupin Mine water samples. 159
Table B-4. Isotopic geochemistry of water samples from the Lupin Mine. 161
Table B-5. Description of crush and leach matrix fluids and drill salt samples. 164
Table B-6. Chemistry of crush and leach matrix fluids and drill salt. Alkalinity was analyzed to complete charge balance calculations. 165
Table B-7. Fluid inclusion microthermometry data. 166
Table B-8. Calcite isotope data. 174
Table B-9. $\delta^{34}S$ of sulfide minerals associated with calcite filled fractures from the Lupin mine. 176
Table B-10. Summary of molecular gas compositions sampled at Lupin. 177
Table B-11. Summary of gas isotopic compositions sampled at Lupin. 178
Table B-12. Complete Lupin gas composition data. 179
Table B-13. Complete Lupin gas isotopic data. 180
Table B-14. Gas volume per liter of water. 181
Table B-15. Temperature, Pressure, and Salinity Measurements. 182
Table B-16. Lupin static borehole pressure data with time (in bars) 186
Table C-1. Site characteristics of the passive margin marine hydrate occurrences discussed in this paper. 206
Table C-2. Site characteristics of the accretionary margin marine hydrate occurrences discussed in this paper. 207
Table D-1. Canadian and Fennoscandian Shield $\delta^{37}Cl$ and $\delta^{81}Br$ data from this study. 208

Foreword

This thesis was written in paper format, with the intention that each chapter (excepting the introduction and overall conclusion) will be publishable as an individual journal article, keeping the overall thesis objectives in mind. Therefore, some repetition within individual chapters was unavoidable. An introduction to the research objectives and justification is provided in Chapter 1. Chapter 2 is a discussion and overview of the major findings from the field study at the Lupin permafrost research site. Geochemical and physical data are utilized in developing a conceptual model of the hydrogeochemical conditions existing at Lupin today. Expectations for how permafrost would affect conditions at a site undisturbed by mining are also discussed. Chapter 3 describes the origin, evolution, and quantification of terrestrial methane hydrates at the Lupin crystalline rock permafrost site. The potential for gas hydrate formation and dissipation associated with past climate change is also explored. Chapter 4 compares the Lupin geochemical data with data collected over the last 25 years at other Canadian and Fennoscandian Shield study sites, investigating the influence of the glacial/interglacial cycle at these sites. Chapter 5 is an overview of the stable isotopic compositions of bromide and chloride in the Canadian and Fennoscandian Shields. Relationships of bromine and chlorine isotopic compositions with carbon and hydrogen isotopic composition of methane gas and strontium isotopic composition of the waters are also be explored. Potential processes are discussed which should be explored in future research. Finally, Chapter 6 summarizes the conclusions of this work and provides recommendations for future research.

The several appendices provide additional background and reviews of some of the processes discussed, to allow a more detailed overview of certain processes than allowed by the paper format chosen for this thesis, as well as a compilation of the data compiled for this thesis. Appendix A provides background information regarding permafrost and the freeze-out process. Definitions relevant to permafrost, a review of previous deep permafrost and crystalline rock permafrost investigations, and the compiled talik geochemical dataset may also be found in this section. Appendix B is a compilation of all data collected at the Lupin site as part of the overall GTK-OPG-SKB-POSIVA PERMAFROST project. Appendix C is a review of the geochemistry of methane hydrates. The Canadian and Fennoscandian Shield $\delta^{37}Cl$ and $\delta^{81}Br$ database and several extra diagrams relevant to chlorine and bromine isotope geochemistry are included in Appendix D. Finally, a compilation of freeze-out experiment methods and data from experiments conducted by other researchers is available in Appendix E.

Chapter 1

Introduction

1.1 Background

Fluid salinity increases with depth in crystalline Shields, with salinities reaching 340 $g \cdot L^{-1}$ in some localities (Figure 1-1, *Frape et al. 2004*). The formation and evolution of Canadian and Fennoscandian Precambrian Shield brines have been attributed to several different processes, broadly grouped as allocthonous or autochthonous (*Frape et al. 2004*). Allocthonous brines are derived from saline fluids which have moved into the crystalline rock. Their formation is related to concentrated seawater through processes such as (1) evaporative concentration and emplacement of fluid and/or migration and emplacement of seawater or sedimentary formation fluids (e.g.. *Nurmi and Kukonen 1986, Nurmi et al. 1988, Purdy 1989, Gascoyne et al. 1989, Bottomley et al. 1994, 1999, Bottomley and Clark 2004*), (2) dissolution of sedimentary evaporite deposits (*Michelot et al. 1983, Michelot and Fontes 1987*), and/or (3) freezing of seawater or seawater derivatives (e.g. *Herut et al. 1990, Bein and Arad 1992, Starinsky and Katz 2003*). Autochthonous Shield brines form through water-rock interaction as a result of: (1) dissolution of mineral phases (e.g. *Fuge 1979*) and interactions with Cl^- bearing minerals such as amphibole or biotite (e.g. *Ito and Anderson 1983, Kamineni 1986, Vanko 1986, Kamineni 1987, Morrison 1991, Enami et al. 1992, Zhu and Sverjensky 1992*), (2) mineral alteration (e.g. *Frape et al. 1984, Kelly et al. 1986, Sherwood Lollar et al. 1993b*), and/or (3) leakage of fluid inclusions (e.g. *Nordstrom and Olsson 1987, Nordstrom et al. 1989a,b, Sie and Frape 2002*). It has been suggested hydrothermal systems may drive both allocthonous and/or autochthonous brine formation. Further background information on Shield groundwaters is available in Chapter 4 and also several reviews which discuss the processes contributing solutes to groundwater composition in crystalline rocks, as well as the origin and evolution of brines in crystalline rocks (*Bucher and Stober 2000, Frape et al. 2004*).

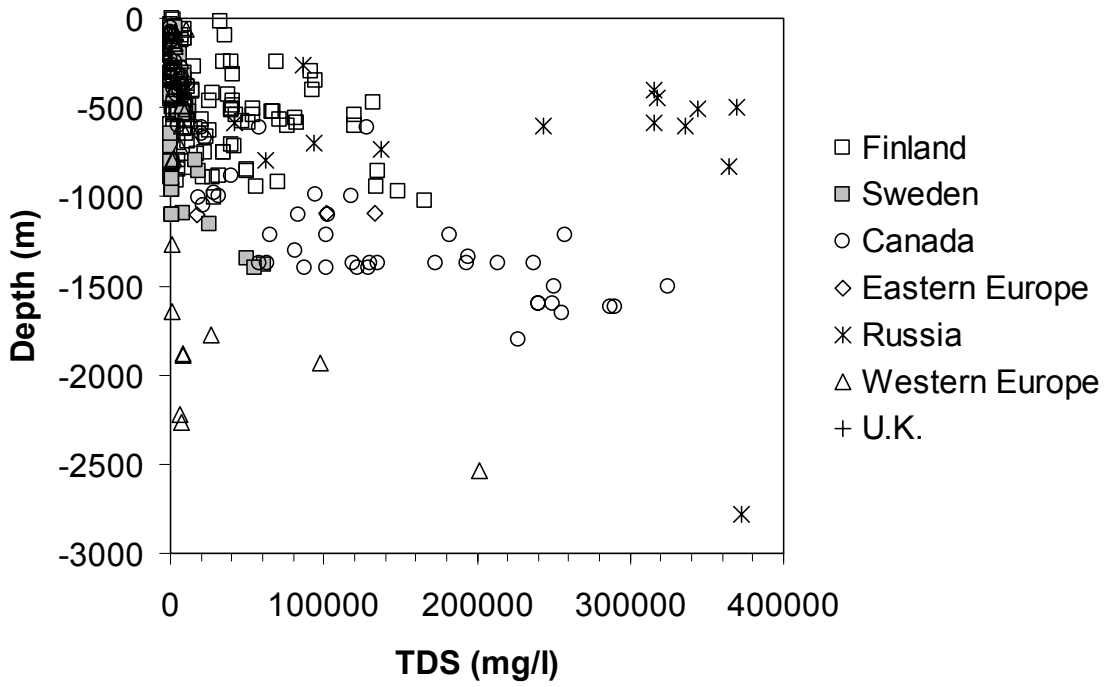

Figure 1-1. Salinity with depth in crystalline rocks (From Frape et al. 2004).

Recently, solute concentration due to fluid freezing has been investigated as a possible evolutionary pathway for Canadian and Fennoscandian Shield brines (*Herut et al. 1990, Bein and Arad 1992, Bottomley et al. 1999, Starinsky and Katz 2003*). Experimental and field investigations have hypothesized that freezing of seawaters along glacial margins during glacial periods will create Ca-Na-Cl brines, which then recharged the Canadian and Fennoscandian Shields (Figure 1-2, *Herut et al. 1990, Starinsky and Katz 2003*). Geochemically, this hypothesis was supported primarily with a comparison of Na/Cl and Br/Cl solute ratios of different fluids. Seawater was experimentally frozen and compared with solute ratios from seawater evaporation (Figure 1-3 *Herut et al. 1990*). Although data gathered during freezing of seawater only plotted in a small area, the data was interpolated (Figure 1-3). Throughout this thesis, this hypothesis will be referred to as the "surficial freezing of seawater hypothesis."

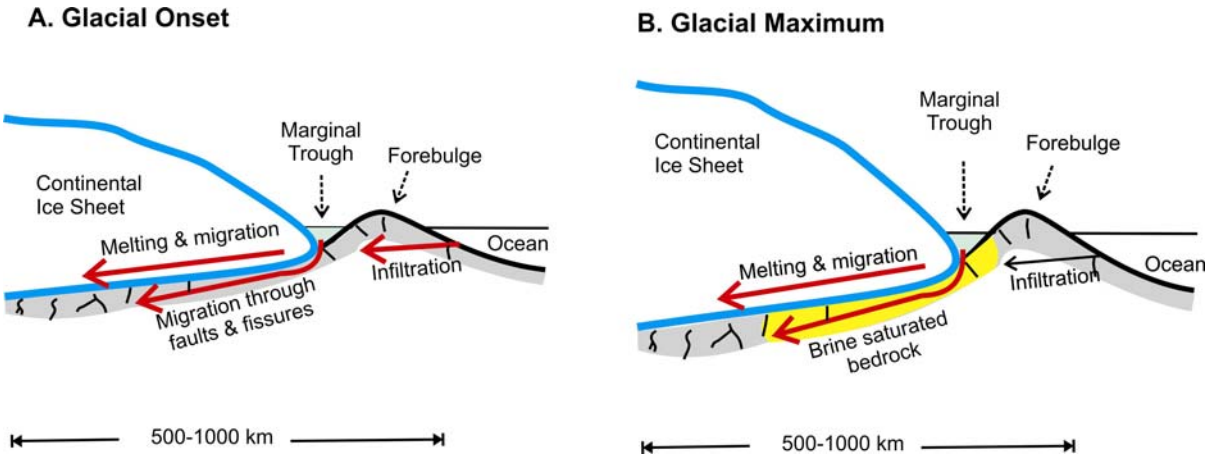

Figure 1-2. Conceptual model of surficial freezing of seawater hypothesis for the origin of Canadian and Fennoscandian Shield brines (From Starinsky and Katz 2003).

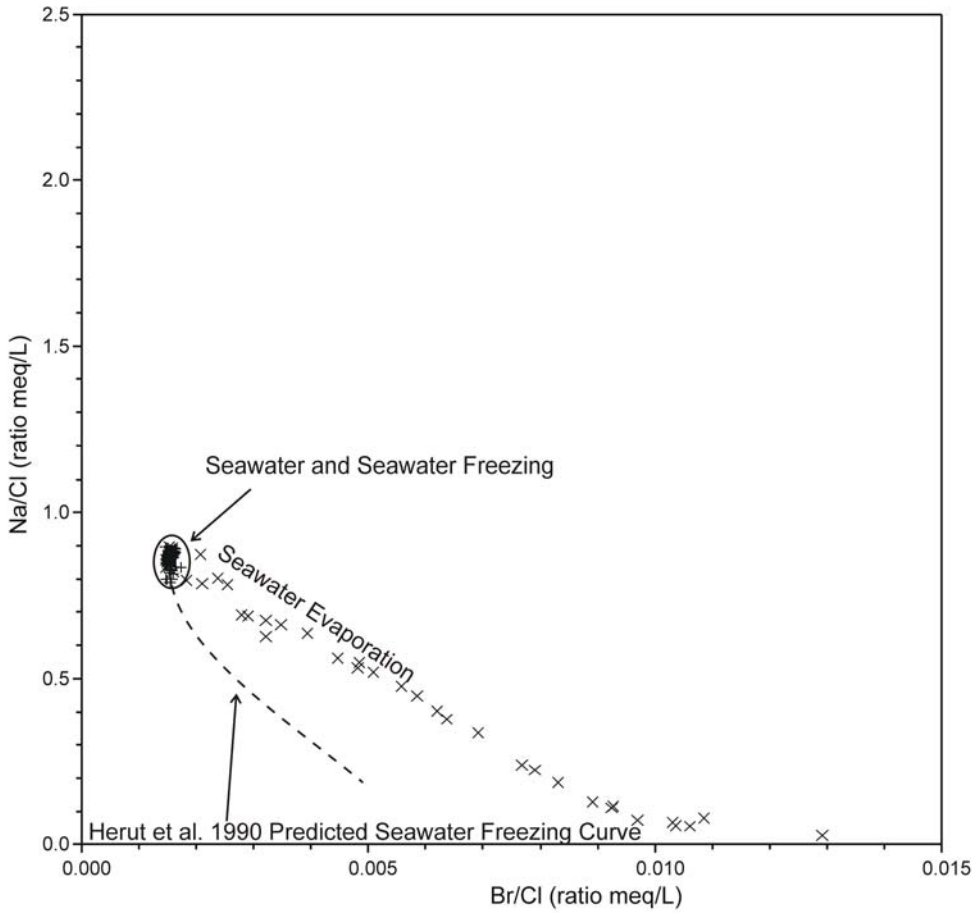

Figure 1-3. Relationship between Na/Cl and Br/Cl ratios for experimental seawater evaporation (McCaffrey et al. 1984) and freezing (Herut et al. 1990). Extrapolated seawater freezing curve (Herut et al. 1990) is also shown.

The entire outcrop area of the Canadian and Fennoscandian Shields was subject to numerous glacial events over the last 2 million years. During the glacial-interglacial cycle, permafrost formation is expected at the margin of advancing and receeding glaciers. In soils, freeze-thaw cycles have suggested *in situ* freeze-out can occur, concentrating solutes in the remain fluids (*Konrad and McCamon 1990*). Therefore, the question of how freezing and permafrost impacts the formation and evolution of brines in natural systems may also be vital to understanding the chemistry of groundwater in crystalline rocks. Some aspects of geochemical concern related to permafrost have been extensively studied in shallow systems and in sedimentary environments (e.g. *Dallimore et al. 1999, Alexeev and Alexeeva 2002, 2003, Dallimore and Collett 2005, Shouakar-Stash et al. 2007*). However, due to the complexity and difficulty of studying groundwater flow systems beneath thick permafrost, very few scientific studies have been conducted regarding cryogenic processes and hydrogeology in crystalline systems. Column experiments have shown that while solutes do concentrate in residual fluid beneath a progressively frozen column, temperatures below the hydrohalite eutectic point (-21°C) with very low volumes of residual fluid would be required to account for the high salinities typical of Shield fluids (*Zhang and Frape 2002*). Additionally, freezing cannot account for the large deuterium excess found in many Shield groundwaters (e.g. *Frape et al. 1987, Zhang and Frape 2002*). Additional background information on permafrost processes and definitions can be found in Appendix A.

1.2 Objectives

The purpose of this research is to evaluate the impacts of cryogenic concentration of fluids to groundwater and flow system evolution in the crystalline rock environment over geologic timescales. This thesis will specifically In addition to the surficial freezing of seawater hypothesis previously described, will also examine the effects of thick permafrost (>300m) formation on groundwater in the crystalline rock environment.. This scientific research will contribute to several areas of societal interest including:

- Provide assistance to the development of the Safety Case and Performance Assessment for long-term (100,000-1,000,000 years) isolation of nuclear fuel wastes in Deep Geologic Repositories (DGR) excavated at a depth between 500 and 1000 m in the plutonic crystalline rock of the Canadian and Fennoscandian Shields. Over the life span of a DGR, permafrost is expected to reoccur in northern Europe and central North America at latitudes expected to host a repository (e.g. *Vieno and Ikonen*

2005). Thus constraining permafrost scenarios relevant to the evolution of crystalline groundwater flow systems will enhance the scientific basis for safety and performance assessment. This investigation will contribute to better understanding of modern permafrost systems and how those systems have evolved, which is vital to developing the permafrost scenarios for performance and safety assessment.

- The search for life on Mars and other planetary bodies. The current strategy for Mars exploration is "follow the water" (*National Research Council 2008*). Water on the Martian surface is expected to be locked in or beneath permafrost (e.g. *Clifford 1993*). Thus permafrost conditions on Earth may be similar to the environment in which Martian H_2O based microbes could be found. The understanding of the chemical fluid environments in which microbes live is fundamental to the understanding of the microbes. The results of this work have been utilized by members of the Indiana-Princeton-Tennessee Astrobiology Initiative (e.g. *Bakermans et al. 2008*), providing important details of the living environment of microbes sampled beneath the permafrost.

- Increased understanding of potential climate change impacts. Consistent with climate change predictions (*Holland and Bitz 2003, ACIA 2004, Serreze and Francis 2006*), over recent decades the arctic permafrost regions of North America and Asia have experienced the greatest annual average temperature increases (*Overpeck et al. 1997, Serreze and Francis 2006, Hansen et al. 2006*). This study provides a baseline for future evaluation of the evolution of groundwater chemical and flow systems as climate change occurs in the Arctic and attempts to predict potential impacts of climate change.

- The potential for greenhouse gas contributions from crystalline permafrost. Melting gas hydrates may have added significant amounts of greenhouse gases as a result of past climate change (*Nisbet 1990, 1992, Beerling et al. 2002, Holbrook et al. 2002, Kirschvink and Raub 2003, Buffett and Archer 2004, Retallack and Krull 2006*). The conditions of natural gases in crystalline rocks under permafrost conditions have not been previously studied. Investigation of gas hydrates and understanding how permafrost melting might affect gas hydrate stability are important to current climate change discussions. By analyzing relative gas concentration, isotopic composition, and quantity, this study will investigate the occurrence, origin, and evolution of gases beneath permafrost in crystalline environments, and will provide a first step towards

understanding the relative influence of crystalline rock methane hydrate to influence global climate.

- Mine safety, planning, and environmental assessment. Changing climate has renewed interest in the Northwest Passage and northern ports. With the development of northern ports, many mineral prospects in the Arctic may become economic. However, a changing climate will also impact on permafrost stability, which then can impact on mine safety. Therefore, understanding groundwater conditions and subsurface gases in crystalline rocks may be more important in permafrost areas. Further, relatively little is known of the long-term environmental impacts of mining in this type of environment. This research is an important step in understanding groundwater conditions beneath permafrost.
- Potential for flow through permafrost. While permafrost typically reduces permeability, the presence of unfrozen areas (taliks) beneath lakes provides potential pathways for groundwater flow. The connection through taliks between surface water and groundwater beneath the permafrost in crystalline environments is not well documented. Understanding the nature of groundwater flow through taliks is vital for several reasons
    - The proper environmental assessment of the construction of mine tailings and other waste lagoons for these new mines must take potential groundwater-surface water connections into account
    - A number of the mineral deposits are located under lakes, thus the connection of surface waters and the presence or absence of frozen ground will have a significant impact on the amount of mine dewatering that may be required. Through a review of the permitting process, it is evident a number of assumptions are currently made about surface water-groundwater interactions through taliks with little actual data behind modeling studies (e.g. *Golder Associates 2004, SRK Consulting 2005, Gartner Lee Limited 2006a, 2006b*).
    - An understanding of GW-SW connections may be vital to understanding why certain microbes are found beneath the permafrost layer.
    - Talik surface-water-groundwater connections will also play an important role in safety and performance assessment.

This research investigates possible connections between taliks and subpermafrost groundwater by examining deep groundwaters in a mine near the end of its life cycle, near a large lake with a through-talik (Lake Contwoyto). This work will also attempt to understand whether taliks should be a concern to deep excavations.

Chapter 2

Hydrogeochemistry of Groundwaters In and Below the Base of Thick Permafrost at Lupin, Nunavut, Canada

2.1 Executive Summary

This chapter furthers scientific understanding of permafrost and its role in influencing deep flow system evolution, fluid movement, and chemical evolution of waters in crystalline rocks by characterizing hydrogeologic and geochemical conditions at a Canadian Shield site located in an area with 400-600 m of permafrost. Taliks, or unfrozen channels through the permafrost, were investigated beneath lakes by the Geological Survey of Finland utilizing ground penetrating radar. Temperature and hydraulic pressure measurements were collected as part of the hydrogeologic characterization. Water and gas samples were collected throughout the subsurface for geochemical characterization. Salinities at the base and beneath the permafrost are particularly important, as the effects of freezing may affect water chemistry and concentrate solutes. Fracture filling calcite samples are utilized to investigate paleo-fluid movement. A conceptual model of the site is developed to provide a baseline for investigations at other locations. Results are then compared with a hypothesis for the origin of Canadian Shield brines. Finally, implications for deep geologic disposal of radioactive waste are presented. This investigation of hydrogeochemical conditions provides important baseline information for long-term environmental impacts of mine operations in permafrost and expectations for extraterrestrial subpermafrost geochemical conditions.

2.2 Introduction

Although little is known about groundwater conditions beneath thick permafrost (>500m) in crystalline rock, investigations of these systems can benefit several diverse research interests. Understanding permafrost environments on earth is fundamental to topics as diverse as safe nuclear waste disposal and the search for life on Mars. In the Finnish and Swedish concepts for long-term isolation of nuclear fuel waste, Deep Geologic Repositories will be constructed at depths of 500 to 1000 m within crystalline rock of the Fennoscandian Shield (e.g. *SKB 1992*, *TVO 1992*, *Posiva 2000*, *SKB 2004*). In Canada, both the crystalline rocks of the Canadian Shield and sedimentary rock units

are being considered (*NWMO 2005*). The large temporal scale (>1 million yrs) over which a safety case must demonstrate repository performance requires consideration of glacial and interglacial conditions which will alter the thermal, hydraulic and mechanical boundary conditions. These changes could potentially affect engineered barrier systems, radionuclide mobility and groundwater flow system stability (e.g. *Vieno & Ikonen 2005*). On the other hand, water, the key to known life, is likely trapped in or beneath permafrost on Mars (e.g. *Clifford 1993*), and recent investigations have probed the possible cold origins of life (*Bada et al. 1994, Levy et al. 2000, Miyakawa et al. 2002a, 2002b, Priscu and Christner 2004, Bada 2004, Price 2006*). Characterizing the geochemical environment on Earth is an important step in understanding the potential for life on Mars. Research programs studying waters in crystalline rocks in the Canadian and Fennoscandian Shields have concluded that waters with total dissolved solids (TDS) ranging between 2 and 340 g l^{-1} are derived from water-rock interactions (*Fritz and Frape 1982, Frape et al. 1984*, *Frape and Fritz 1987*, *Gascoyne et al. 1987, Lahermo and Lampen 1987, Nordstrom and Olsson 1987, McNutt 1987, Kamineni 1987, Nurmi et al. 1988, McNutt et al. 1990, Ruskeeniemi et al. 1996, Bucher and Stober 2000*), with intrusion of sedimentary brines at Shield margins (*Gascoyne et al. 1989*).

The possibility for brine formation in Canadian and Fennoscandian Shields through surficial freezing of marine and/or sedimentary waters with subsequent deep penetration during glacial times has also been discussed (*Herut et al 1990, Bein and Arad 1992, Bottomley et al. 1999, Starinsky and Katz 2003*). This cryogenic brine formation hypothesis implies that Canadian and Fennoscandian Shield brines have formed since the Pleistocene as part of a "highly dynamic flow" system (*Starinsky and Katz 2003*).

The Canadian and Fennoscandian Shields were subject to the glacial-interglaical cycle over the last 2 million years, with several glacial advances covering the entire outcrop area of both Shields, including the most recent Wisconsinan glaciation. During the glacial-interglacial cycle, permafrost formation is expected at the margin of advancing and receeding glaciers. In soils, freeze-thaw cycles have suggested *in situ* freeze-out can occur, concentrating solutes in the remain fluids (*Konrad and McCamon 1990*), and that the cold temperatures in permafrost create a strong thermodynamic sink that may allow advection of water (and solutes) against the concentration gradient (e.g. *Cary and Maryland 1972, Gray and Granger 1986, Qiu et al. 1988, Perfect et al. 1991*). Concentrations in the freezing front may become sufficiently high as to "leap" over solute pockets, resulting in alternating bands of high and low concentration fluids in frozen soils (*Romanov and Levchenko 1989*) although this may not be a significant macroscale phenomenon (*Kay and Groenvelt 1983*). A review of *in situ* freeze-thaw processes is provided by Marion (*1995*) and Yershov (*1998*). *In situ* freezing may

account for increased concentrations of carbonate, sulfate, sodium, magnesium, and calcium in groundwaters found in the Siberian Platform under thick permafrost (*Alexeev and Alexeeva 2002, 2003*). Other processes, including evaporation and halite dissolution have also influenced brine formation in Siberian Platform groundwaters (*Shouakar-Stash et al. 2007*). Therefore, the question of how freezing and permafrost impacts the formation and evolution of brines in natural systems may also be vital to understanding the chemistry of groundwater in crystalline rocks. This study specifically addresses the impact of these processes on groundwater chemistry within the Canadian Shield at a location currently under cryogenic conditions.

The purpose of this study was to further the scientific understanding of permafrost and its role in influencing deep flow system evolution, fluid movement, and chemical evolution of waters in crystalline rocks. This was accomplished by conducting a surface and subsurface hydrogeologic and geochemical characterization at a permafrost site that had been an active mine for over twenty years. The salinity and chemistry of waters at and below the base of the permafrost are of particular interest for this investigation. Exploration and mine development in northern parts of Canada has increased dramatically in recent years, and very few investigations into long-term environmental effects have been conducted. Evaluation of mining impacts in permafrost environments was also possible from this dataset. Other field activities at the Lupin site are described in several reports published by the Geological Survey of Finland (*Ruskeeniemi et al. 2002, 2004*).

2.3 Site Description

The Lupin Gold Mine (65º45’29”N, 111º13’10”W) in Nunavut, Canada (Figure 2-1), was active from 1982 to 2005. All mining activities are located underground, with workings extending to 1450 m below ground surface. The Lupin area is approximately 450 m above sea level, and is relatively flat with a height variation in the range of 30-40 m. Current isostatic rebound in nearby regions is on the order of 6 mm·yr (Stella et al. 2007).

(A)

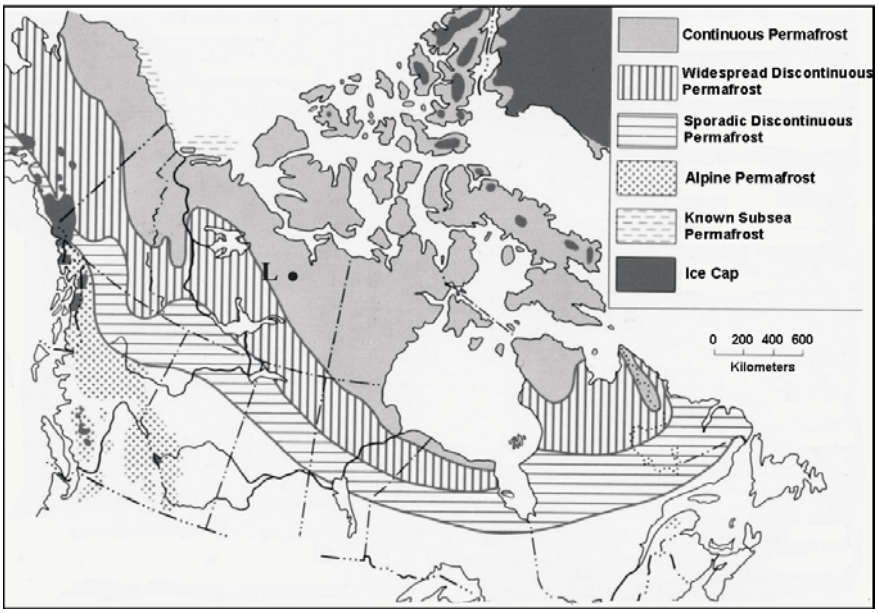

(B)

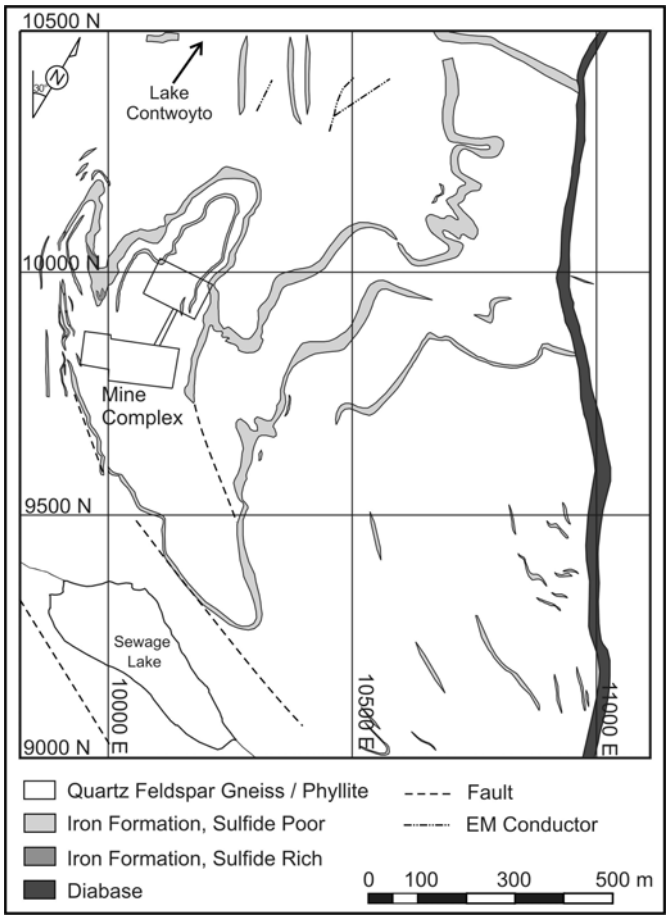

Figure 2-1. (A) Location of Lupin (L) within Canada and zone of continuous permafrost (after *Natural Resources Canada 1995*), (B) Surface geology of the study area (after *King et al. 1989*).

2.3.1 Geology

The Lupin mine is a Banded-Iron-Formation gold deposit located in an Archean metaturbidite sequence that has been subjected to regional and contact metamorphism, resulting in a number of low to high grade metasedimentary rock types. Three major deformation phases have been identified, creating a complex fold structure (*Bullis et al. 1994*). Amphibolite facies metamorphism from multiple intrusions and metamorphic events altered turbidite mudstones and greywackes to the crystalline rock types meta-greywacke/quartzite, phyllite and quartz-feldspar-gneiss (*King et al. 1988, Ford and Duke 1993, Bullis et al. 1994, Geusebroek and Duke 2004*). Peak metamorphism occurred between 2.680 and 2.585 Ga, however faulting caused contact metamorphism as late as 1.84-1.81Ga (*Geusebroek and Duke 2004*). Metamorphism imparted a high angle foliation (80-85°) or planar structural element to the lithological units at the site (Figure 2-1B). Up to six plutonic events also occurred in the area (*King et al. 1989*). A more detailed overview of the metamorphic and structural history of Lupin is provided by Geusebroek and Duke (*2004*).

2.3.2 Fracturing and Hydraulic Parameters

Jointing is common and includes two vertical joints sets that are nearly perpendicular to each other, and one sub-horizontal set with the following dip direction/dip angles: 110/80°, 005/75°, 195/13°, respectively. Most fractures appeared tight, open fractures with irregular distribution were observed by video survey in all boreholes surveyed. Typically, apertures were 1-2 mm wide; 5 mm was the largest fracture observed. A majority of open fractures appeared to be parallel to foliation. Major identified fault zones in the area (Figure 2-1) vary in size, but are less than 10m wide. Three fracture zones were identified in the subsurface (*Ruskeeniemi et al. 2002*). Fracture zone V1 was located approximately 495-510 m east of the mine, and intersected by boreholes at 890 and 1130m levels, and is believed to have an orientation of 090/85° (dip direction/dip angle). Fracture zone V2, known as the "ramp fault" intersects the mine spiral ramp, and is generally 1-2m wide, with intense cross-cutting fracturing. The fault was readily observed between the 250 m and 610 m levels. Below this, level the ramp trends away from the N-S fault. Finally, a thin (< 0.5 m) subvertical fault was observed between 890m and 1105 m levels, with an orientation of 014/72-86° (dip direction/dip angle). Transmissivities were estimated between 2.2×10^{-6} m^2·and 1.1×10^{-6} m^2 s (Frape et al. 2004).

2.3.3 Permafrost

The site is well within the zone of continuous permafrost (Figure 2-1). Permafrost depth (as defined by the 0 °C isotherm) in the Lupin Mine area currently extends between 400 and 600 meters below ground surface (mbgs). Variance in permafrost depth is due to differences in porosity and heat

conductivity of the main rock types as well as surficial features such as vegetation, snow cover or soil types (e.g. *Kukkonen and Šafanda 2001*). Temperature measurements within the mine shaft indicate a permafrost depth of 541 mbgs. Extrapolation of the observed thermal gradient (16 mK/m) indicates that the lowest rock temperature below the seasonally affected zone is around -8 ºC, somewhere between 50 and 80 mbgs. These observations are important when considering the potential for precipitation of various mineral phases during freezing (or 'freezing out') and will be discussed later in the thesis (*Chapter 4*).

The age or onset of permafrost formation at Lupin has not yet been determined. The warmest climate scenario results from an ensemble glacial systems modeling approach presented by Tarasov and Peltier (*2007*) indicates an 80% probability that permafrost completely melted at the site following the last glacial maximum, although relict permafrost cannot be completely ruled out. Permafrost at Lupin therefore likely started to form following the rapid retreat of the ice sheet at the start of the last interglacial period, which began approximately 8000 to 6000 years ago (*Smith et al. 2001*).

2.3.4 Taliks

Taliks are unfrozen channels which may provide routes for discharging or recharging groundwaters through thick, continuous permafrost. They are typically found beneath large watercourses where mean annual bottom temperatures remain above the freezing point (e.g., the watercourse does not freeze down to the bottom). Taliks such as these formed by water above 0°C are termed "hydrothermal taliks" (*van Everdingen 1976*). According to Mackay (*1992*) and Burn (*2002*), conditions favorable for the existence of a talik typically occur when water depth is greater than 2/3 of the maximum ice thickness.

Of the many lakes in the Lupin area, Lake Contwoyto is of particular interest. It is 1.3 km from the Lupin mine, 100 km long, and ranges between 2 and 5 km wide near the mine. The bathymetry of the lake is uncertain, but except for areas near the shoreline, depths are much greather than two-thirds of the maximum ice thickness. Its linear geometry suggests a fault-valley type origin with deep fractured roots. Therefore, a potentially unfrozen hydraulic conduit may exist beneath Lake Contwoyto.

2.4 Methods

Waters sampled at Lupin are grouped into the following categories: precipitation, surface waters, waters in the permafrost zone, waters at the base of the permafrost, subpermafrost waters, and rock

matrix fluids. Several precipitation samples were collected in October 2000 and June 2002, but additional data was available from earlier studies (*Gibson 1996, Gibson et al. 1999*). Surface water samples were collected from lakes and flowing streams in June 2002. Permafrost waters were sampled from drips along a north-south trending, 1-2m wide fault zone bisected by the main mine access ramp (known as the "ramp fault") between 250 and 540 mbgs. The ramp fault zone showed evidence of cross-fracturing. Research boreholes *550-112*, and *570-105* (boreholes are identified as *collar depth mbgs-borehole number*) were drilled specifically to sample waters at the base of the permafrost. Borehole *550-112* was a short, 15m borehole, drilled upwards to intersect the ramp fault at 12m. Borehole *570-105* was drilled 515m at +2° (up angle), but avoided the ramp fault. Both boreholes ended within the permafrost and had very low flows. Consequently, most samples from these boreholes were collected over periods ranging between one day and several weeks. An additional research borehole, *570-106* was drilled 387 m at -25° (down angle), but due to difficulty obtaining water samples, only the rock core was utilized for matrix fluid analysis.

Ten predominately horizontal and sub-horizontal exploration boreholes, drilled underground in a direction to the east of the mine and below the permafrost (most with a minimum length of 450 m), were selected for study of subpermafrost waters and gases on the 890, 1130, and 1300 m levels of the mine (Figure 2-2). Exceptions to this are boreholes *1130-273* (drilled 225 m northwards), *1130-64* (drilled 30 m upwards), and *1130-175* (drilled 920 m vertically down). Most boreholes were drilled across the steeply dipping foliation and away from the mine workings. Additional drip samples were collected from a 3m bolt-hole on the 1130 m level. Nine boreholes were sealed on the 1130 m level, providing investigation of hydraulic conditions over a planar area of 500 x 500 m^2. The horizontal subpermafrost boreholes were sealed with 3m Margot® packers, allowing pressure to build up within the boreholes. All boreholes drilled in this section produce water and gas. Borehole *890-188* was also sealed for study, and is located above and in a comparable vertical position to borehole *1130-197*. Several fractured zones with vertical to subvertical orientation (perhaps parallel to foliation) were identified through geological mapping, examination of rock core, borehole logging, as well as borehole camera logging. Details of individual borehole construction, including length, azimuth, diameter, dates drilled and sealed, are provided in Appendix B.

Matrix fluids were extracted from drilled core by crush and leach from the *550-112*, *570-105*, and *570-106* research boreholes and the *890-188* exploration borehole. Techniques and rationale for examining matrix pore fluids by crushing and leaching of core are detailed by Waber and Frape (*2002*), Smellie et al. (*2003*) and Frape et al. (*2004*). Briefly summarized, rock core was quickly rinsed in deionized water, then crushed (<63 μm), weighed, and added to double-deionized nano-pure

water in a solid to liquid ratio of 1 g to 1 mL. The mixture was put on a shaker for 24 hours. The solution was then extracted from the rock particles by vacuum sieve. For the calculation of mass-solute-per-kg-of-rock, it was assumed that all available chloride was released into the fluid phase during the 24 hour reaction period, which had proven sufficient due to repeated crush and leaching of samples in previous studies (*Smellie et al. 2003*).

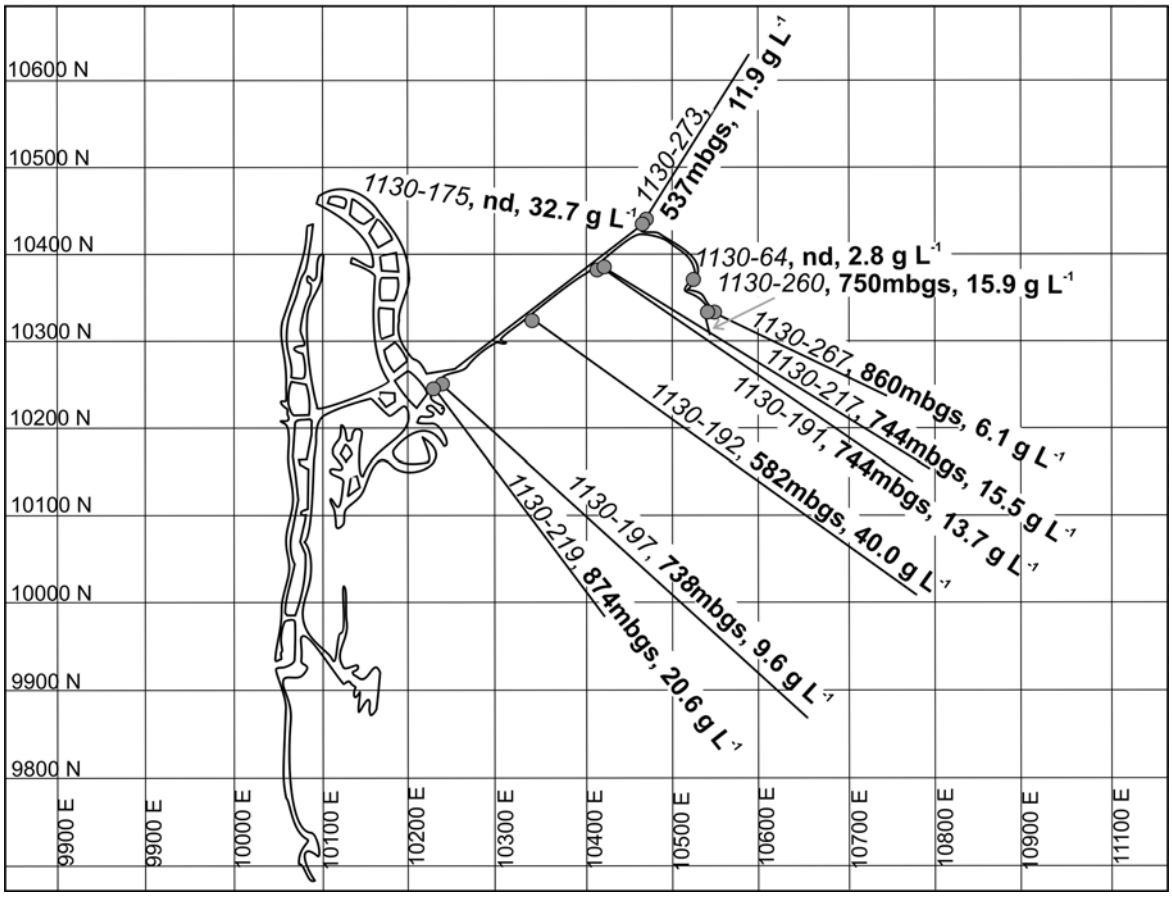

Figure 2-2. The Lupin mine 1130 m level plan and drillhole location map. Boreholes are labeled with *Borehole number*, the highest measured Hydrostatic Pressure (depth of the equivalent fresh water table), and highest measured total dissolved solids (grams per liter). Borehole *1130-175* is drilled downwards 920m and *1130-64* is drilled upwards 30m.

Precipitation, surface water, groundwater, and crush and leach samples were analyzed for major and trace elements. Multiple samples were collected from each sampling point over the six year study period in connection with other sampling activities (gases, microbes, dating) to observe any changes in groundwater chemical conditions, and to achieve as complete a characterization of the groundwater system as possible at any given sampling opportunity. Gas samples were collected using an inverted bottle headspace displacement method. Glass bottles (500 mL or 1 L) were filled with

borehole fluid by placing nylon tubing from the borehole packer to the bottom of the bottle. The sample bottle was allowed to overflow into a container. Once the water level in the container topped the sampling bottle, the bottle was carefully inverted, keeping the bottle opening below the water surface. Gas then displaced the fluid in the sampling bottle, until only ~20 mL of borehole fluid remained. The bottles were sealed underwater. During transport and storage, bottles were kept upside down until analyzed.

Redox and oxygen concentrations were measured from six boreholes using a flow-through cell (*Ruskeeniemi et al. 2004*). A platinum electrode with a combined Ag/AgCl reference was used for redox measurements. The outflow rate from the borehole was between 1-1.5 $L \cdot min^{-1}$. The monitoring time varied from 20 to 55 hours. Therefore, about 1 – 5 m^3 of water was removed during the monitoring cycle, and thus in principal the water volume in the holes changed at least 1 – 5 times. The pH and electrical conductivity values were recorded after the oxygen and redox values had stabilized (Table B-2). Dissolved oxygen concentrations were below the detection limit (0.0 mg/L). Eh-values, ranging from -10 mV to 25 mV, were still slowly decreasing at the end of the measurement period. The field-measured pH-values are rather uniform (pH 8.2 – pH 8.6) for waters from all boreholes monitored. The pH values measured in laboratory are uniformly about two units lower than these *in situ* results, indicating atmospheric CO_2 diffusion into the sample occurred during transportation, and that pCO_2 levels in the groundwater were low or below atmospheric.

Field-filtered (0.45 μm) water samples were taken for the determination of physico-chemical parameters and ionic analysis in the Geolaboratory of the Geological Survey of Finland (GTK). A filtered and acidified (0.5 ml concentrated suprapure HNO_3 /100 ml water) sample was taken for metal and trace element analyses. Electrical conductivity and pH were measured in the field and in the laboratory. Total alkalinity (as mmol $HCO_3 \cdot L^{-1}$) was determined in the laboratory using an automatic titrator. No adjustments were made for atmospheric CO_2 diffusion during transport. The main anions, F^-, Cl^-, NO_3^-, and SO_4^{2-}, were analyzed using ion chromatographic (IC) technique. All cations and other elements were analyzed by ICP-AES or ICP-MS technique. The detection limits for Ca, Na, K, Mg, Li, and Sr of the ICP-MS/ICP-AES method are 100, 200, 10, 100, 0.1, and 0.1 μg/L, respectively. Charge balance errors in the samples reported are below 10%.

Tritium, δ^2H, $\delta^{18}O$, $\delta^{37}Cl$, $\delta^{15}N$, $\delta^{34}S$, and $\delta^{13}C$ were analyzed at the University of Waterloo Environmental Isotope Laboratory (UW EIL). Tritium values were determined by the electrolytic enrichment method of Taylor (*1977*), and counted in a LKB Wallac 1220 Quantalus liquid scintillation counter, with a detection limit of 0.8 T.U. Deuterium determinations were made following the Mn reduction preparation method of Shouakar-Stash et al. (*2000*) and the Cr reduction

method of Morrison et al. (*2001*) and analyzed on an Isoprime IRMS coupled with a Eurolecton elemental analyzer. Oxygen isotope analysis was performed on a Micromass 903 triple collector mass spectrometer using the preparation procedures of Epstein and Mayeda (*1953*) with Moser's (*1977*) modification. Analytical reproducibility of $\pm\delta^{18}O$ and $\pm\delta^{2}H$ are 0.2 and 2.0 ‰ respectively. Dissolved chloride was converted to CH_3Cl which was then analyzed for $\delta^{37}Cl$ on a dual inlet Isoprime IRMS following the method of Eggenkamp (*1994*), with an accuracy of ±0.15‰. Nitrates were separated from other anions using an ion-exchange resin column packed with Bio-Rad AG 1-X8 and combusted in EA-Isochrom-Carlo Erba continuous flow elemental analyzer-IRMS with a precision of ±0.3‰. Samples analyzed for NO_3-^{18}O were combusted with excess graphite to generate CO_2 which was then analyzed using a Dual Inlet Prism II MS, with an accuracy of ±0.5‰. $\delta^{34}S$ analyses were prepared following the method of Yanaglsawa and Sakai (*1983*) and analyzed on a Robo-CN Europa Tracemass IRMS with an accuracy of ±0.3‰. Sulfate $\delta^{18}O$ was prepared by combustion of $BaSO_4$ which was analyzed on an HEKATECH high temp-EA-IsoPrime IRMS, with an accuracy of ± 0.3‰, following the method of Shakur (*1982*). Chlorine-36 was analyzed by accelerator mass spectrometry at ETH in Zurich, Switzerland.

The Indiana University Stable Isotope Facility and the UW-EIL analyzed $\delta^{13}C$ using Micromass Isoprime and Finnigan MAT Deltas for $\delta^{2}H$ isotopes of gases. Accuracy and reproducibility of $\delta^{13}C$ and $\delta^{2}H$ are typically ±0.3‰ VPDB and ±5‰ VSMOW, respectively. Gas compositions were analyzed at the UW Organic Geochemistry Laboratory; N_2 and CO_2 on a Fisher/Hamilton Gas Partitioner, Model 29 gas chromatograph, and alkane-hydrocarbons on a Varian 3800 gas chromatograph equipped with a flame ionization detector and capillary injection port. Detection limits for CO_2, N_2, C_1, C_2, C_3, nC_4 and iC_4 are 0.5 ppm, 30 ppm, 0.3 µg/L, 0.2 µg/L, 0.2 µg/L, 0.8 µg/L, and 1.6 µg/L, respectively.

Samples for ^{14}C analysis were collected in 2 L glass containers. The containers were filled with water by holding tubing leading from the borehole at the bottom of the container, allowing the water to displace the air in a non-turbulent manner. The containers were allowed to over flow into a plastic bag for at least 6 L (3 container volumes) and then sealed underwater to eliminate the possibility of air contamination. Carbon-14 was analyzed by accelerator mass spectrometry at Rafter Radiocarbon Laboratory in New Zealand. Stable carbon isotope samples ($^{13}C/^{12}C$) were prepared at the University of Waterloo EIL. The ^{14}C content is corrected for the $\delta^{13}C$ value and reported according to the conventions of Stuiver & Polach (*1977*).

Observations of the talik boundary beneath Lake Contwoyto were obtained by conducting a ground penetrating radar (GPR) survey. The survey was conducted by the Geological Survey of

Finland in May, 2004, the time of year when ice cover is at its maximum thickness and the mean diurnal temperatures are still well below zero. Two frequencies were used: a 400 MHz frequency to investigate the depth of ice on the lake surface and a 40 MHz frequency for investigation of the properties of lake bottom sediments and to determine the location of the interface between frozen and unfrozen ground. The snow/ice and ice/water boundaries could not be observed using the 40 MHz survey, but the properties of the lake bottom sediments were studied to depths of 30 to 35 m. The total length of all survey lines was 28.9 km.

2.5 Results and Discussion

The groundwaters found in the fracture systems intersected by drilling activity have potentially mixed with or been influenced by several fluid and solute end members. Mining activity (such as dewatering) has introduced fresh surface waters into the mine, and drilling within the permafrost necessitated the use of a drilling brine solution made from fresh lake water and imported NaCl salt (with low SO_4^-). According to mine personnel, at least one large spill of drilling brine solutions occurred within the upper part of the mine during operations. Blasting introduced large quantities of nitrogen to the subsurface. Long term water/rock interactions may result in matrix pore fluids influencing groundwater compositions. Pleistocene glaciations and isostasy have changed ground surface elevation and pressure conditions. Determining which, if any, of these components affect the resident groundwaters in the subsurface is important to understanding the geochemical evolution of the waters at the site. A summary of analytical results are provided in Appendix B (Table B-3).

2.5.1 Precipitation and Surface Waters

Precipitation and surface waters in the Lupin area contain very low concentrations of most ions. These waters are dilute; with mean concentrations of sodium, 0.32 and 4.64 mg l^{-1}, and calcium, 0.29 and 4.2 mg l^{-1}, for precipitation and surface waters respectively. Precipitation samples are Na-dominated, but buffering by local surficial water/rock interaction results in Ca-dominated surface water samples (Figure 2-3). Total dissolved solids (TDS) (2.6-22.5 mg·L^{-1}), chloride (0.2-3.5 mg·L^{-1}), sulfate (0.1-10.6 mg·L^{-1}), and nitrate (0.2-0.9 mg·L^{-1}) concentrations in the precipitation and surface waters are also low (Figure 2-4).

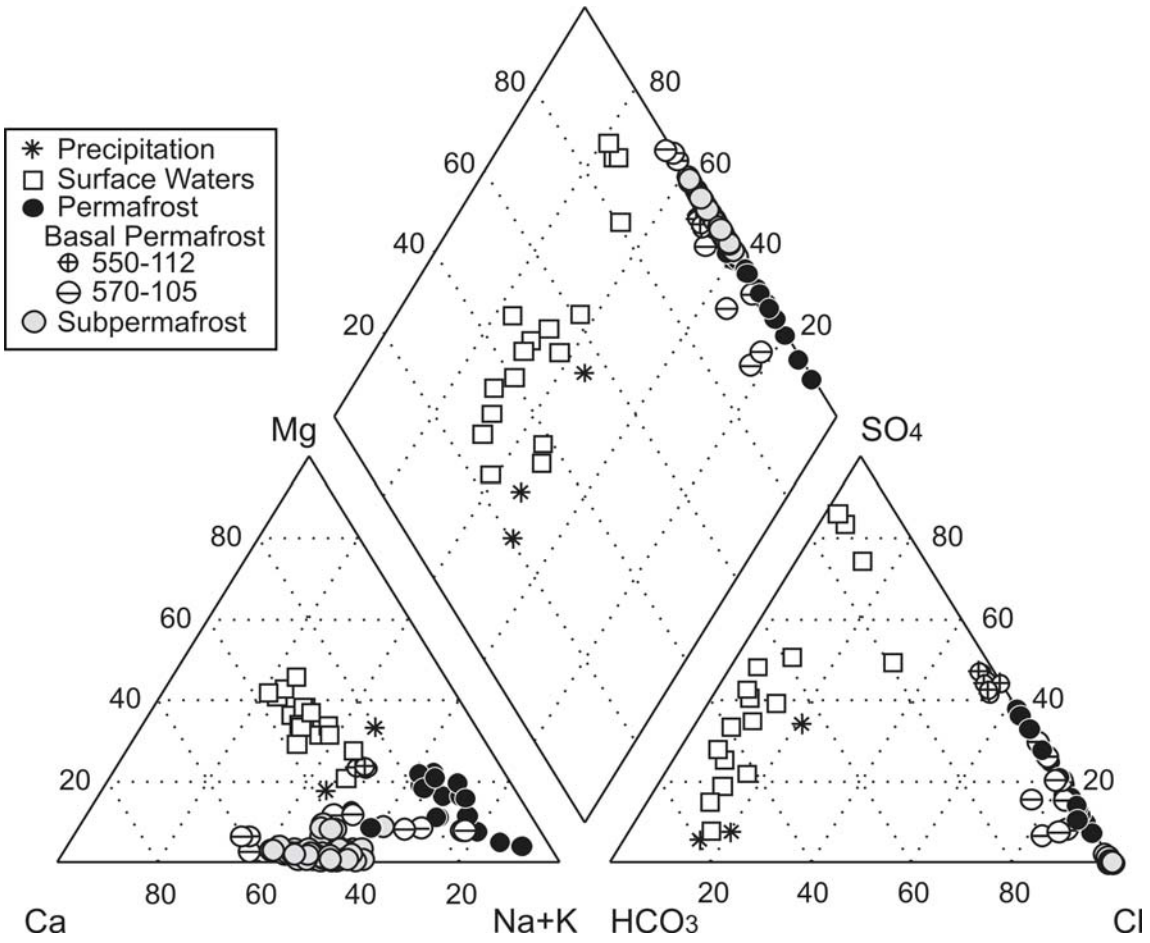

Figure 2-3. Piper diagram of waters sampled in the Lupin area.

Stable isotopic composition (δ^2H, $\delta^{18}O$) of waters sampled are shown in Figure 2-5. Precipitation δ^2H varies between -119 and -279 ‰ VSMOW, and $\delta^{18}O$ varies between -15.7 and -37.6 ‰ VSMOW (not shown on graph, *Gibson 1996*). Precipitation $\delta^{18}O$-δ^2H values vary seasonally along the local meteoric waterline. A Local Meteoric Waterline (LMWL) for the Lupin area was estimated ($\delta^2H=7.32\cdot\delta^{18}O-4.46$, $R^2 = 0.98$) from precipitation data collected by Gibson (*1996*). Reported stable isotopic values of surface waters are similar to other studies in this area of the Canadian Arctic (*Rossi 1999, Gibson 1996, 2002, Gibson et al. 1999, Gibson and Edwards 2002*), and plot along the observed Local Evaporation Line (LEL) ($\delta^2H=5.37\cdot\delta^{18}O-52.4$) for surface waters in the Lupin area (*Gibson et al. 1999, 2008*).

Tritium values (Figure 2-4E) ranged between 6 and 13 TU in precipitation samples and 14 and 21 TU in surface water samples. These values are similar to the tritium distributions reported over a limited geographical area in the region (*Rossi 1999*).

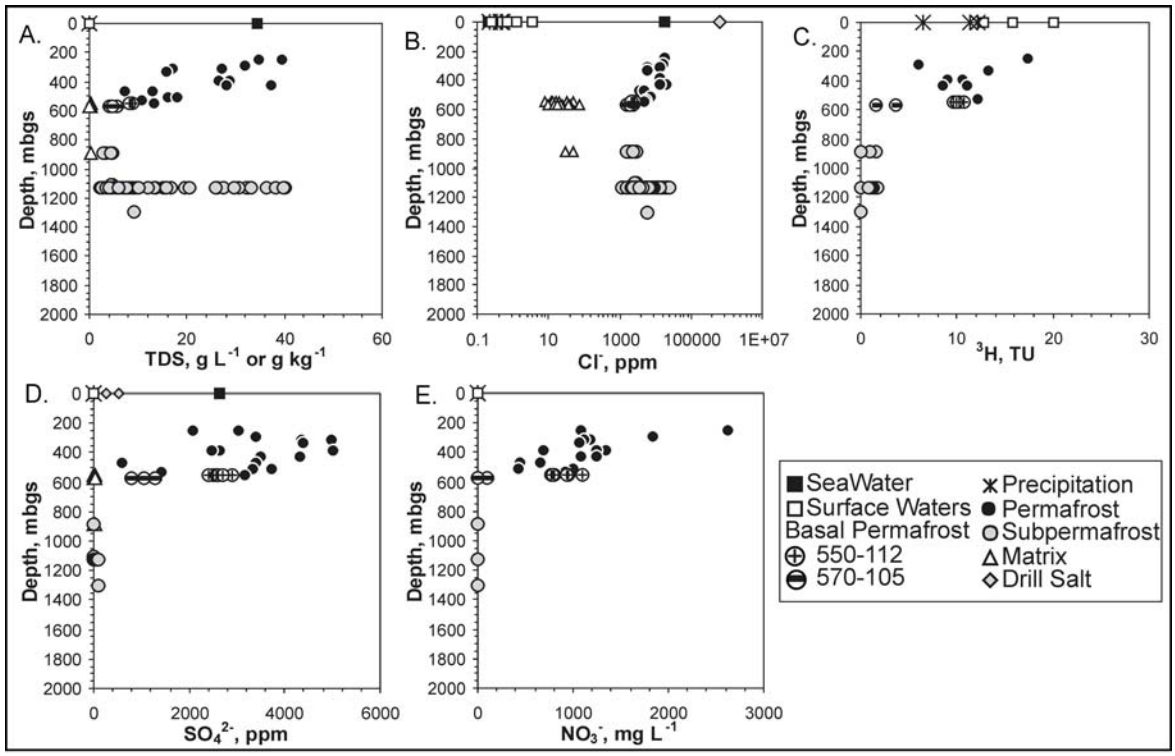

Figure 2-4. Chemical trends with depth at Lupin (A) TDS (B) Cl, (C) SO_4 (D) NO_3 (E) ^3H.

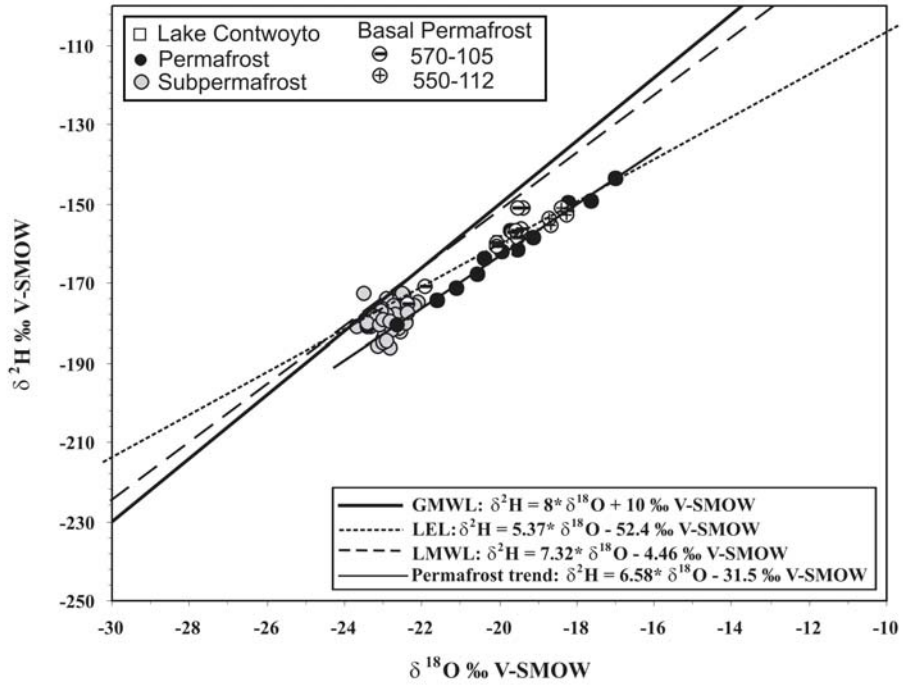

Figure 2-5. Stable isotopic composition of Lupin Waters. LEL from Gibson et al. (*1999*), LMWL from Gibson (*1996*), GMWL after Craig (*1961*). Surface water samples are slightly hidden behind 570-105 and permafrost samples.

The ^{36}Cl value for Lake Contwoyto is anomalously high (1073.8 x 10^{-15} $^{36}C{\cdot}Cl^{-1}$) for an uncontaminated environment, and was unexpected (Figure 2-6). However, similar values have been found in surface waters with low chlorine concentrations in the Antarctic dry valleys (*Carlson et al. 1990*). Lake Contwoyto has very low chloride content (3.5 $mg{\cdot}l^{-1}$); therefore any amount of ^{36}Cl will have a large influence on the $^{36}Cl{\cdot}Cl^{-1}$ value. Thus, the high ^{36}Cl value is likely attributable to a proportionally large atmospheric chlorine contribution, low weathering rates, and higher cosmic flux due to lowered atmospheric ozone (*Carlson et al. 1990, Lyons et al. 1998*).

(A)

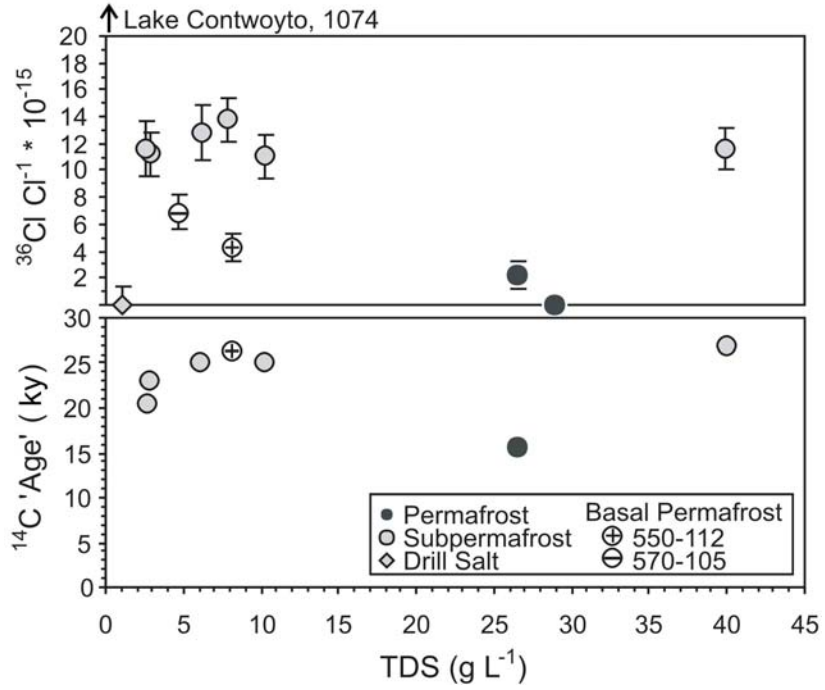

(B)

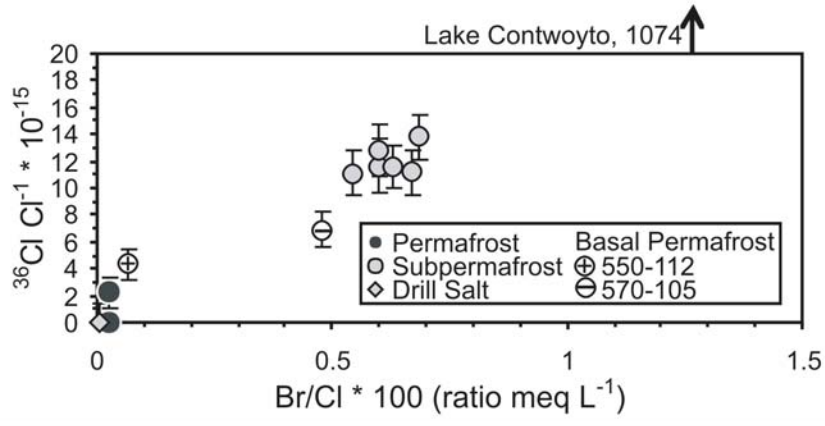

Figure 2-6. Radioactive tracers (A) ^{36}Cl and ^{14}C vs. TDS, (B) ^{36}Cl vs. Br/Cl*1000 for waters sampled at the Lupin mine. Radiocarbon error is less than the size of the data point.

2.5.2 Taliks

Example results from the GPR survey are provided in Figure 2-7. The GPR surveys conducted at a frequency of 400 MHz (Figure 2-7A) over Lake Contwoyto revealed that completely frozen lake water extends for several tens of meters from the shoreline, beyond which water exists beneath the ice. Free water below the ice layer, when the ice thickness is at its maximum indicates the mean annual temperatures at the lake bottom are above 0°C. The 400 MHz results indicate a talik could be located 30 – 60 m from the shoreline, which is comparable to the distances of 50-100 m predicted by Mackay (*1992*) and Burn (*2002*), assuming that the geometry of the lake bottom is constant. With the lower 40 MHz frequency surveys (Figure 2-7B), areas of frozen and unfrozen ground (talik) were distinguished. The results indicate the interface between permafrost and the talik is almost vertical at least to survey penetration depths (30-35 m). The survey results indicate that smaller lakes in the study area, with an area of at least 500 m x 250 m and a depth of at least 1.5 – 2.5 m, have free water below the ice cover. Open taliks could therefore be expected beneath lakes of this size.

The GPR results have important hydrogeologic implications. Although deep permafrost may effectively seal many of the potential flow routes in the crystalline bedrock, there are likely hydrothermal through-taliks in the area of the Lupin Mine that could provide potential pathways for waters through the permafrost.

2.5.3 Matrix Fluids

Crush and leach experiments on rock core (matrix fluids) from several boreholes yield a very low salinity NaCl solution (Table B-6 in Appendix B). The matrix fluids are NaCl-type waters with the exception of one $CaCl_2$-type water, which was the only sample analyzed from a sulfide-bearing amphibolite rock (sample *570-106*, 385 m). This sample had the largest Ca/Na ratio (6.1) of any fluid sampled at the Lupin site.

The subpermafrost fracture waters at the Lupin mine are typically more saline (2.2-40.0 g·l-1) than the matrix waters (0.09-0.38 g·kg-1). The lack of matrix salts would mean that for most parameters, the rock pore fluid would most likely be unable to substantially overprint the geochemical signature of saline fluids found in faults. Low matrix salinities at Lupin are similar to those found at High Lake, another Canadian Shield site located in permafrost about 90 km north of Lupin (*Stotler et al. 2008*). However it is not possible with this limited dataset to determine whether the low matrix salinity is related to site specific (local), or interglacial/glacial processes (e.g. freeze out, cold temperature gradients affecting solute transport, or dilute glacial water flushing). It is also possible

the rock salinity is concentrated in fracture minerals, which are discussed later in this chapter. In general, fracture infillings are scarce, potentially limiting influence to fluids.

(A)

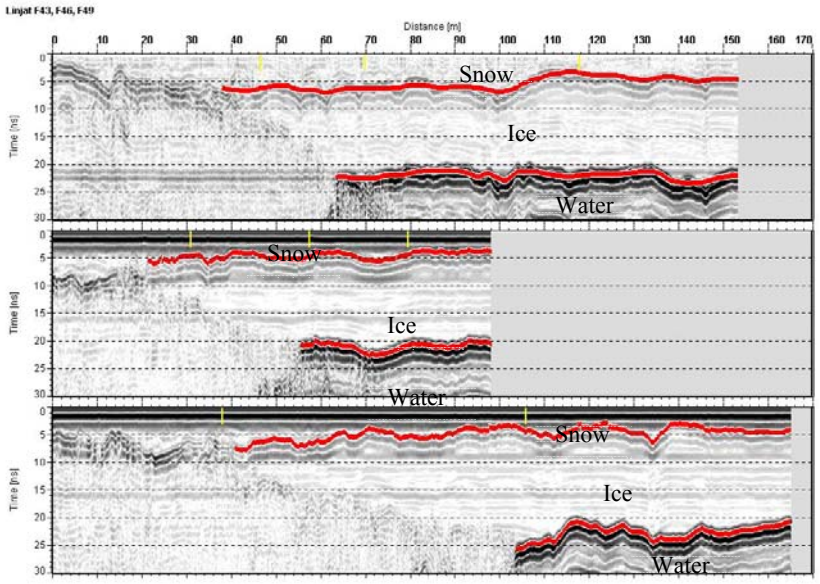

(B)

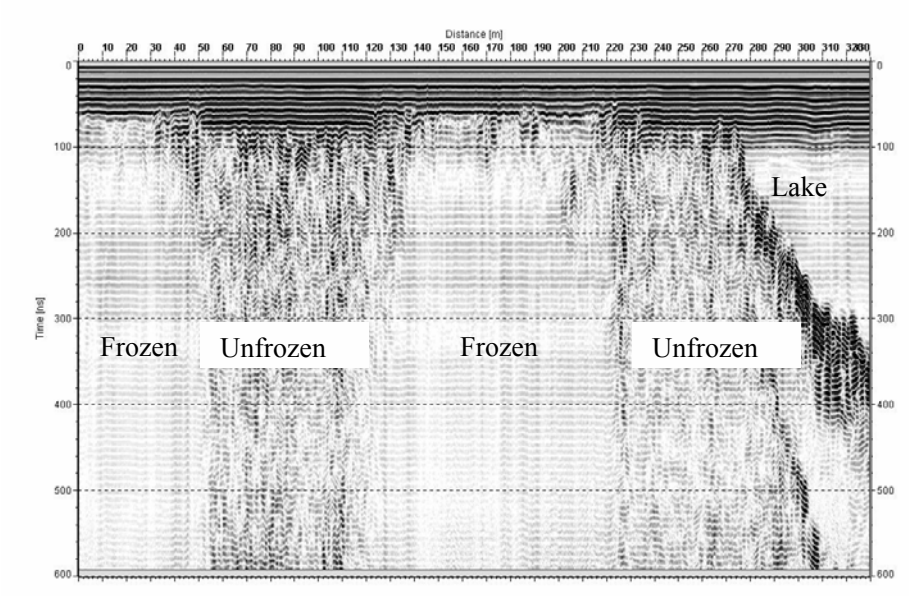

Figure 2-7. Reflection profiles from GPR surveys conducted at the Lupin mine, courtesy Geological Survey of Finland. (A) Three GPR survey lines (F43, F46 and F49) conducted at 400 MHz frequency and their interpretation. Upper thick line: snow/ice boundary; lower thick line: ice/water boundary. Maximum survey depth is 5m. (B) Survey line F116, 40 MHz. The line runs from the mainland to the lake. In the middle of the line, a shoal is encountered. The areas of frozen and unfrozen ground are clearly visible. Maximum survey depth is 35m.

2.5.4 Permafrost Waters

The dissolved load in permafrost fluids at the site (12.9 - 39.6 g l^{-1}) is higher than expected based on freezing experiments (*Zhang and Frape 2002*), and previous studies of Mackenzie Valley sedimentary hydrate research boreholes drilled through a similar permafrost thickness (*Matsumoto et al. 2005*). In order of frequency of occurrence, permafrost waters are Na-Cl, Na-Cl-SO_4, or Na-Mg-Cl-SO_4 (Figure 2-3). Permafrost fluids have similar chloride concentrations to those of deeper subpermafrost groundwaters.

Geochemical data (ionic ratios, ^{3}H, and ^{36}Cl) indicate that the chloride sampled in permafrost waters associated with the ramp fault is contaminated by the NaCl drilling brine. Unlike the Na-Ca fluids found deeper in the site, permafrost fluids are Na-dominated (Figure 2-3). The relationships between Na and Ca, Br and Cl, and Na/Ca and Br/Cl ratios indicate permafrost fluids trend towards the introduced drilling salt end member, compared with matrix and subpermafrost waters. The Br versus Cl plot and the Ca/Na vs. Br/Cl ratio plot (Figure 2-8) also suggest the drilling salt used at the site resulted in the large salt load observed in the permafrost waters. High ^{3}H concentrations (6.0 to 17.3 TU) also reflect the influence of water pumped down for mining activity (drilling brine, washing, etc.) (Figure 2-4E).

Permafrost ^{36}Cl values are much lower than measured in deeper subpermafrost waters (Figure 2-6), but have a signature similar to the drilling salt ($<0.0014 \times 10^{-15}$ $^{36}Cl \cdot Cl^{-1}$). Because most salt is mined from salt domes with negligible U and Th, $^{36}Cl \cdot Cl^{-1}$ ratios less than 1×10^{-15} are typical for imported drilling salt (*Bentley et al. 1986, Fabryka-Martin et al. 1987, Phillips 2000*). This further indicates a majority of chloride sampled in the permafrost was introduced by mining activities.

Conversely, stable isotopic $\delta^{37}Cl$ values in the permafrost waters are similar to the matrix fluid, rather than the salt currently stored at the mine site (Figure 2-9). It is possible that Cl in the drilling fluids was fractionated by the freezing process. As saline water freezes, ^{37}Cl is preferentially incorporated into the ice, resulting in up to a 1‰ fractionation (*Zhang and Frape 2002*). However, the fractionation is typically only observed in chloride incorporated in the ice, because chloride concentrations in the fluid reservoir are large enough that the chloride mass ratio is generally unaffected. Therefore, freezing provides a rather unsatisfying explanation for the observed variation in $\delta^{37}Cl$ in the permafrost. It was not possible to ascertain if the same salt source was utilized for mixing the drilling brine throughout the twenty years of mine operations prior to the research team's arrival. A change in salt source could also explain the observed variation of $\delta^{37}Cl$ ratios in permafrost fluids.

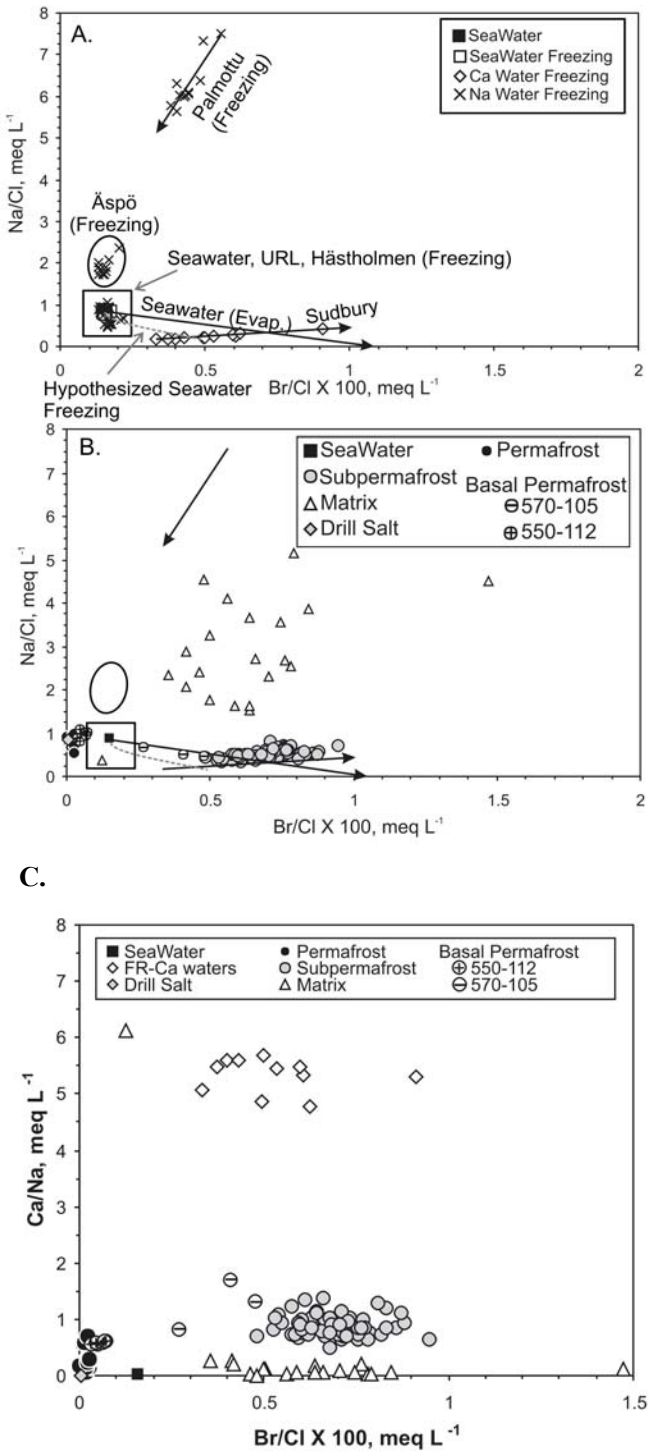

Figure 2-8. Na/Cl vs. Br/Cl. (A) Trends for evaporating seawater (McCaffrey et al. 1987), Sudbury Ca-Cl water freezing experiment (*Frape et al., unpubl.*), Palmottu Na-Cl water freezing experiment (*Zhang and Frape 2002*), Äspö Na-Cl-HCO_3 water freezing experiment (*Zhang and Frape 2002*), are shown. Data inside the box include Sea Water, sea water freezing experiment results and hypothesized freezing trend (Herut et al. 1990), URL Na-Cl water freezing experiment results (*Zhang and Frape 2002*), and Hästholmen freezing experiment results (*Zhang and Frape 2002*). (B) Results from Lupin (C) Ca/Na vs. Br/Cl for samples collected at Lupin.

(A)

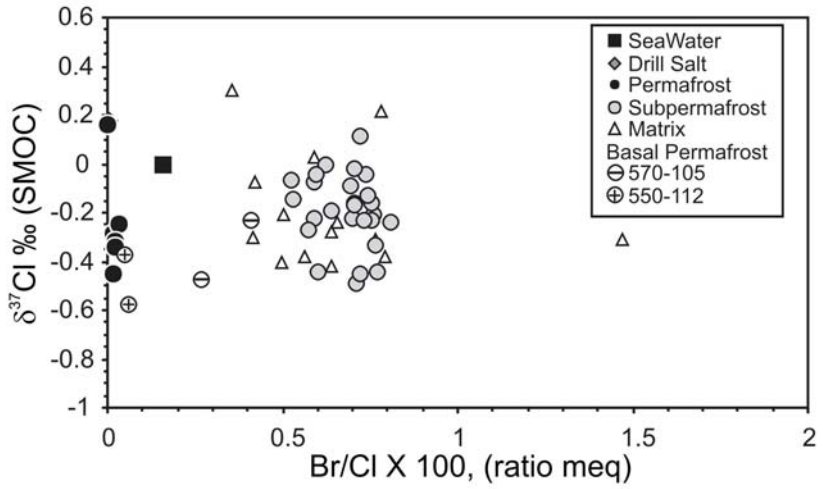

(B)

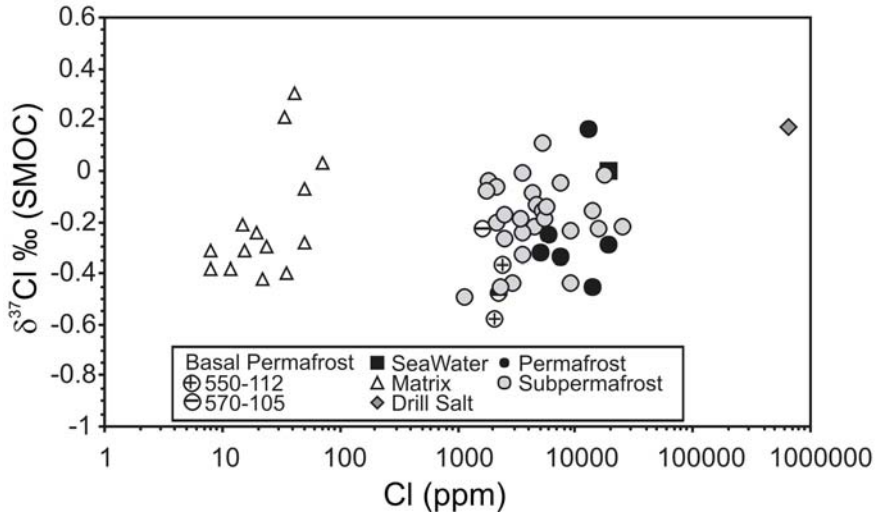

Figure 2-9. δ^{37}Cl (A) vs. Br/Cl, (B) vs. Cl for samples collected at the Lupin mine.

High nitrate concentrations (423 to 2630 mg l^{-1}) were sampled in permafrost zone waters (Figure 2-4D). Out of nearly fifty Canadian and Fennoscandian Shield sites previously studied (e.g. *Frape and Fritz 1981, 1987, Frape et al. 1984*, *2004, MacDonald 1986, Jones 1987, Sherwood-Lollar 1990, Gascoyne et al. 1987, Ruskeeniemi et al. 1996, Blomqvist 1999, Blomqvist et al. 2000*), samples from only three mines (Macassa Mine in Kirkland Lake, ON; Sigma Mine in Val d'Or, PQ; and Con Mine in Yellowknife, NWT) have recorded nitrate concentrations greater than 100 mg·l^{-1}. Macassa was the only other site with nitrate concentrations exceeding 1000 mg·l^{-1} (3070 mg·l^{-1}) (*Frape and Fritz 1981, MacDonald 1986, Jones 1987*). High nitrate concentrations in the Lupin mine

are intriguing, because studies at the Whiteshell Underground Research Laboratory site (URL) in Manitoba showed only small increases in NO_3^- concentrations in fractures adjacent to blast sites. Nitrate concentrations then returned to pre-blast concentrations, within two hours of the blast, in fractures with higher flow rates at the URL (*Gascoyne and Thomas 1997*).

The δ^{15}N-NO_3 (+2.62 to +11.73 ‰ AIR) and δ^{18}O-NO_3 (-0.78 to +27.62 ‰ VSMOW) isotopic compositions are similar to ammonium-nitrate fertilizer isotopic compositions (Figure 2-10) and mine water sampled in other mines (*Mislowack et al. 2008*). This suggests the increased nitrate concentrations are related to blasting compounds and residuals. The isotopic composition of ammonium-nitrate used by the mine for blasting was not analyzed (safety and security regulations prohibit its removal from site), but fertilizer and blasting ammonium-nitrate should have similar isotopic compositions. Denitrification is not likely occurring within the permafrost, as shown by a plot of δ^{15}N vs. ln [NO_3^-] concentration (Figure 2-10).

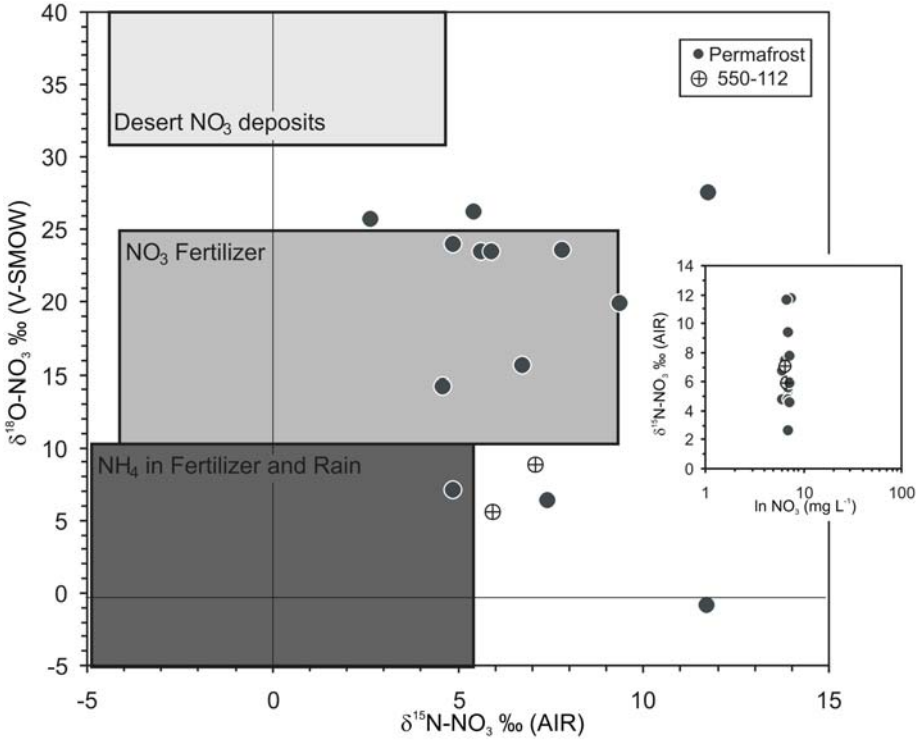

Figure 2-10. Stable isotopes of nitrate in Lupin groundwaters. Boxes showing typical desert and fertilizer values after Kendall and Aravena (*2000*). Inset box is a semi-log plot of δ^{15}N vs. ln NO_3^-.

Microbial studies in subpermafrost boreholes at Lupin have isolated several denitrifying bacteria, however the bacteria are not obligate denitrifiers, and there is no direct evidence for denitrification in the subpermafrost waters (*Bakermans et al. 2008*). No information is available

regarding the presence or activity of these microbes in the permafrost. δ^{15}N-NO_3 ratios remained very similar in three repeat sampling events over four years, although δ^{18}O-NO_3 ratios changed up to ~20‰ in some samples. These data and high nitrate concentrations suggest that denitrification is not an active or significant process in the permafrost. Subpermafrost nitrate concentrations were too low for isotopic analysis, and it is unclear whether the low concentrations in the subpermafrost are due to denitrification or some other process.

The wide range of stable isotope ratios and the slight deviation away from the global meteoric waterline (GMWL) and LMWL observed in permafrost water samples reflect the mixing of introduced surface waters from drilling with natural permafrost waters. Stable isotopic values of permafrost waters plot linearly along and slightly below the LEL, with a slope of 6.58 and a 7 ‰ VSMOW range in δ^{18}O (Figure 2-5). In laboratory experiments, freezing impacted waters were found to plot linearly with slopes between 4.32 and 7.44 (*Souchez and Jouzel 1984, Zhang and Frape 2002*). The sampled permafrost waters plot along a slope similar to a freezing line, but originating near the LEL. This is attributed to mixing between natural frozen waters and the drill waters that have also been affected by the freezing process. Large amounts of ice and hoarfrost were observed to occur in many of the mined openings in the permafrost zone, indicating freezing is an on-going process. Although considerable evaporation likely occurs in open areas of the mine as a result of the strong ventilation, the relationship of δ^{2}H and δ^{18}O does not indicate evaporation is a significant process in the sampled permafrost waters.

Three possibilities were investigated to determine the source of the increased dissolved sulfate concentrations (578-5000 $mg \cdot L^{-1}$) observed in permafrost fluids compared with subpermafrost fluids (1-41 $mg \cdot L^{-1}$): (1) importation of sulfate with the drilling brine (2) dissolution of sodium sulfate precipitated due to permafrost formation, or (3) oxidation of iron formation sulfide minerals. Sulfate concentrations and SO_4/Cl ratios in the drill salt are much lower than observed in permafrost fluids, and are therefore not considered to be the sulfate source in the permafrost fluids. In the permafrost of the Siberian Platform, crystallization of hexahydrite ($MgSO_4 \cdot 6H_2O$, eutectic -4.8 °C) and mirabilite ($Na_2SO_4 \cdot 10H_2O$, eutectic -3.5 to -8.2 °C) was considered as a sulfate source (*Alexeev and Alexeeva 2003*). At Lupin, the minimum temperature (-6.8 °C at 87 mbgs) is low enough for the precipitation of both hexahydrite and mirabilite. Although Mg concentrations are much higher in permafrost (239-1150 $mg \cdot L^{-1}$) than subpermafrost fluids (6-366 $mg \cdot L^{-1}$), permafrost sodium concentrations are clearly related to drill brine inputs (Figure 2-8B). If the permafrost SO_4^{2-} were related to dissolution of hexahydrite and mirabilite, a component of sodium would be distinct from the drilling brine. Precipitation of mirabilite is expected to have the same effect on hydrogen and oxygen isotope

fractionation as ice formation (*Stewart 1974*). Therefore, the relationship between δ^2H and $\delta^{18}O$ is not able to further constrain the potential for mirabilite precipitation.

Isotopic evidence suggests oxidation of sulfide minerals in the iron formation and in other lithologies resulted in the increased permafrost SO_4^{2-} concentrations. Isotopic values for the sulfide mineral end members are reported in Table B-9 (in Appendix B). One sample from the 440 m level has a value of -33.2 ‰ CDT. The sample is mostly chalcopyrite but contains considerable impurities. The other samples are more typical of sulfides in this type of geological environment (e.g. *Rye and Rye 1974*) with $\delta^{34}S$ values between -2.5 and 12.5 ‰ CDT.

In most environments, a sulfide to sulfate transition is accompanied by a $\delta^{34}S$ depletion of 2.0 to 5.5 ‰ if biological processes are involved (*Toran and Harris 1989*). Therefore, the oxidation of sulfides is considered to be a conservative process with only a very minor depletion of the sulfide isotopic value. Examination of Figure 2-11 shows that the $\delta^{34}S\text{-}SO_4$ values measured within the permafrost ($\delta^{34}S\text{-}SO_4$: -1.8 to +2.9 ‰ CDT) reflect the abiogenic oxidation of pyrite ($\delta^{34}S_{pyrite}$ = -2.5 ‰ CDT) in the permafrost groundwaters. However, both sulfide oxidizers and reducers have been isolated in Lupin groundwaters (*Bakermans et al. 2008*), and the sulfur isotopic value of the chalcopyrite sample (-33.2 ‰ CDT) indicates microbial sulfate reduction may have occurred in the past. In a process similar to acid mine drainage, *in situ* oxidation of permafrost sulfate has resulted in acidification of permafrost waters (pH range 3.2 to 7.6).

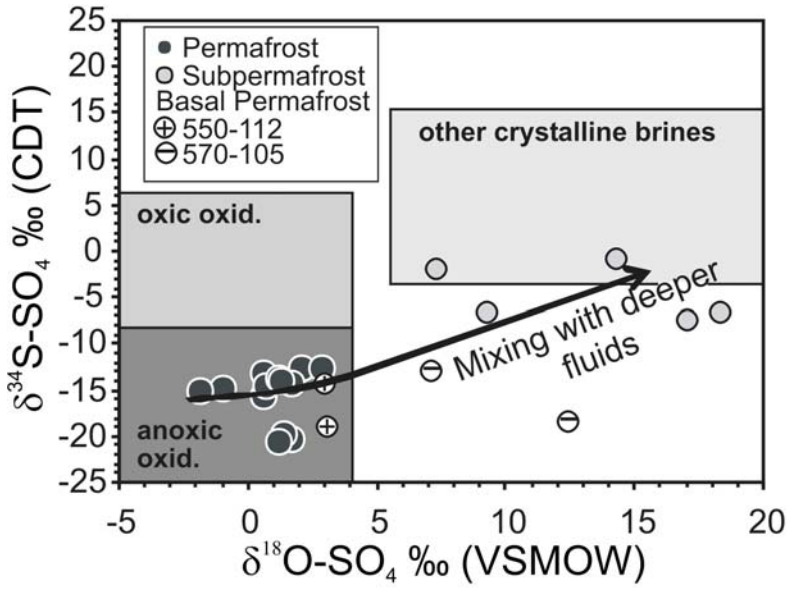

Figure 2-11. Stable isotopes of sulfur in Lupin groundwaters. Crystalline brine sulfate values are from Fritz et al. (*1994*). Justification of the oxic and anoxic boxes provided in the text.

Analysis of $\delta^{18}O$ was conducted to try to determine if sulfide oxidation was a naturally occurring process, or induced by mining activities. The two most probable sources of oxygen in sulfate in permafrost fluids are oxygen bound to water molecules and gaseous or dissolved oxygen in groundwater ($\delta^{18}O\text{-}SO_{4\text{-Atmospheric}}$ = +23.7 ‰ VSMOW, *Kroopnick and Craig 1972*). Abiogenic fractionation of $\delta^{18}O$ from atmospheric or dissolved oxygen into sulfate is -10 ‰ (VSMOW), but fractionation associated with SO_4 derived from the H_2O molecule is only -3 ‰ (*Krouse and Mayer 2000*).

The $\delta^{18}O\text{-}SO_4$ values in the permafrost fluids (-12 to -16 ‰ VSMOW) indicate the most important source of oxygen for SO_4^{2-} is from H_2O molecules, although a very small component of the oxygen could be from atmospheric or dissolved oxygen. Combined with the slightly acidic conditions and saturated water conditions, a very low fractionation is favored (+2 to +4 ‰) (*Toran and Harris 1989*). With a water $\delta^{18}O$ value of -17 to -20 ‰, the sulfate in the permafrost zone should have values identical to those seen at the site. Figure 2-11 shows the sulfate in water within this zone is a result of local sulfide oxidation under anoxic conditions. While oxidation is likely enhanced by the mining activity, it is probably also naturally occurring. However, it was not possible to determine to what degree oxidation increased due to mining activities.

The isotopic fractionation accompanying mirabilite and hexahydrite precipitation are unknown; however, at most, there is a 2.4 ‰ fractionation of $\delta^{34}S$ when gypsum precipitates during seawater evaporation (*Raab and Spiro 1991*). It is likely there is a similar isotopic fractionation during mirabilite and hexahydrite precipitation. Considering the deeper subpermafrost waters as an end-member, it is not likely precipitation of mirabilite and hexahydrite could account for the large isotopic sulfur fractionation (~20‰) between permafrost and subpermafrost waters, although precipitation of oxidized sulfides within the permafrost cannot be ruled out. Lower SO_4^{2-} values in the subpermafrost are related to microbial sulfate reduction (*Bakermans et al. 2008*).

The chemistry of permafrost waters indicates both mining and freezing related impacts. Major ion chemistry, particularly Cl^-, Na^+, and NO_3^- are introduced through mining activities. Freezing has affected the δ^2H, $\delta^{18}O$, and $\delta^{37}Cl$ signatures of the introduced drilling brine. High SO_4^{2-} concentrations may or may not be enhanced due to mining activities; regardless they are a result of oxidation of naturally occurring sulfide in the rocks.

2.5.5 Waters at the Base of the Permafrost

Contamination was a concern in waters sampled from the two drilled research boreholes (*550-112*, *570-105*) at the base of the permafrost. Water samples from both of the boreholes initially had ^3H and

stable isotopic (δ^2H, $\delta^{18}O$) values equivalent to the surface waters used as drill fluids. Packer tests conducted shortly after the borehole was drilled show water chemistry is significantly more dilute further from the mine and closer to the permafrost. However, as the drill fluid slowly drained from *570-105*, the ^3H levels dropped and Na-rich waters were replaced by the older, non-tritiated, Ca-rich resident groundwaters in the rock mass (Figure 2-3, Figure 2-8B), with a steady increase in Br^- and Cl^- concentrations. While the *550-112* borehole has high concentrations of both sulfate (2400-2910 $mg \cdot L^{-1}$) and nitrate (768-1100 $mg \cdot L^{-1}$), the final samples from *570-105* had very low to no nitrate (<20 mg L^{-1}) and intermediate sulfate concentrations (1050 mg l^{-1}) (Figure 2-4). Decreases in nitrate with time were observed in both boreholes as the influence of uncontaminated water in the boreholes increases. Basal permafrost waters sampled from *550-112* are Na-Ca-Mg-Cl-SO_4 type, and from *570-105* are typically Na-Ca-Cl-SO_4 or Ca-Na-Cl-SO_4 type (Figure 2-3). The sulfate in these waters has a similar origin to that of the permafrost waters.

Ionic ratios (Figure 2-8), $\delta^{18}O$, δ^2H (Figure 2-5), and ^{36}Cl compositions (Figure 2-6) suggest the waters sampled from *550-112* are heavily influenced by the drilling brine contamination similar to permafrost fluids, while *570-105* waters likely represent predominately "natural" waters, more similar to matrix and subpermafrost fluids. With each sampling, every geochemical parameter sampled in *570-105* waters became more like the subpermafrost fluids. The data from these basal permafrost boreholes suggests that the final few samples in borehole *570-105* are dominantly uncontaminated basal permafrost water (Table B-3).

2.5.6 Subpermafrost Waters

2.5.6.1 Pressure and TDS Measurements

Large differences in hydraulic pressures were observed in the eight closely spaced boreholes on the 1130 m level and in borehole *890-188* that were sealed. This indicates that the boreholes are either not interconnected, or are only poorly connected. Based on the calculated groundwater table derived from hydraulic pressure measurements, the boreholes can be divided into three groups (Figure 2-2, Figure 2-12A): high (*890-188*, *1130-192* and *-273*), medium (*1130-191*, *-197*, *-217* and *-260*) and low (*1130-219* and *-267*). Mine dewatering has resulted in measured hydraulic pressures much lower than hydrostatic pressures (See *Chapter 3*).

The water salinity varied up to 10 $g \cdot l^{-1}$ in any one sealed borehole on the 1130 level during the study. Over the 5 years of the study, only waters from *890-188* and *1130-64* showed a constant TDS; while *1130-192* and *1130-175* both exhibited an increasing trend in TDS, and the remaining

boreholes sampled displayed no consistent TDS pattern. The fluids are also divided into 3 groups of differing salinities; a high salinity water (~38 $g \cdot l^{-1}$), a medium salinity water (between 8 and 20 $g \cdot l^{-1}$), and a low salinity water (< 5 $g \cdot l^{-1}$) (Figure 2-12B).

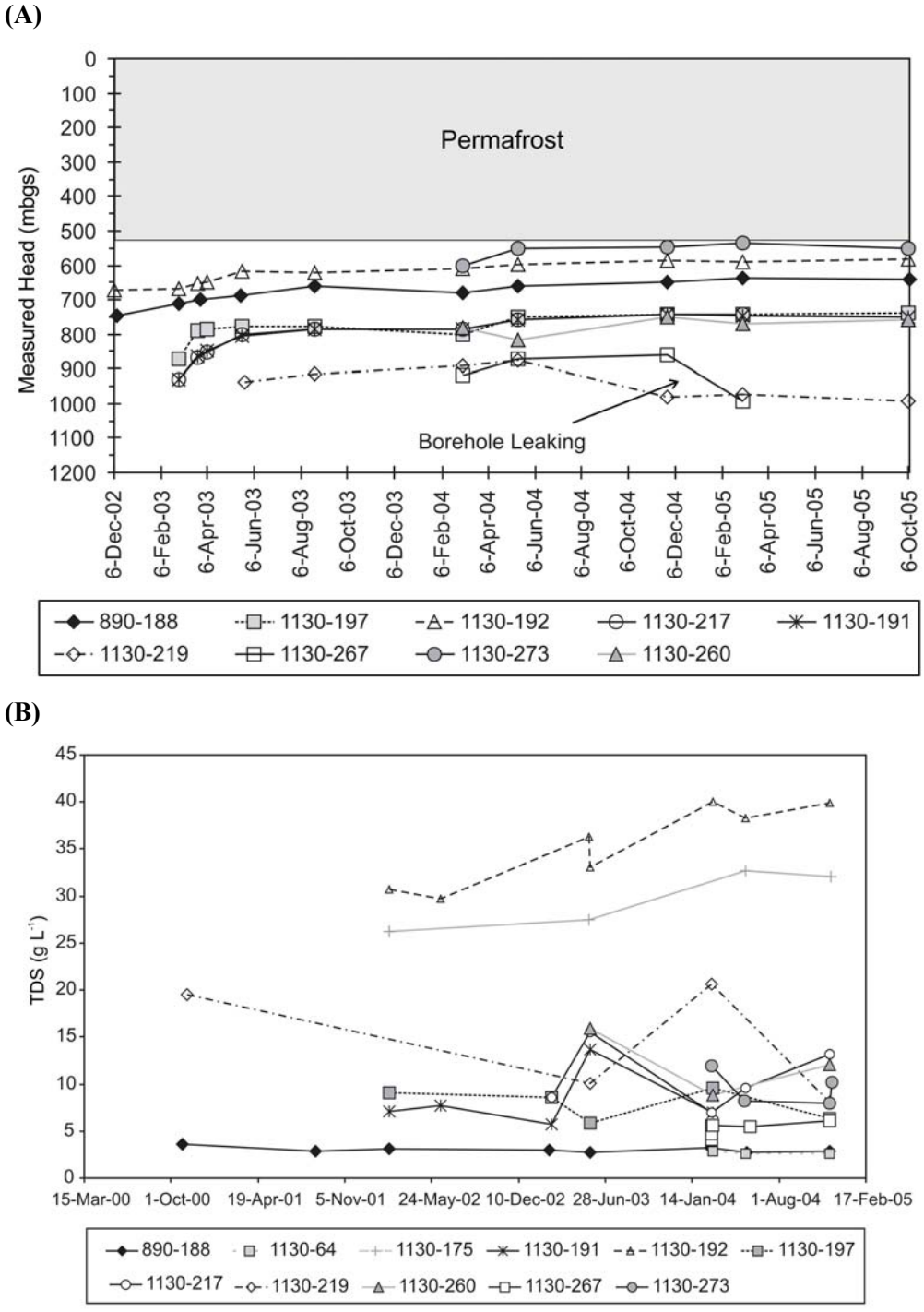

Figure 2-12. Changes in pressure (A) and salinity (B) with time in boreholes from the subpermafrost zone of the Lupin Mine, Nunavut, Canada.

There is no or little correlation between TDS and pressure (Figure 2-12). As an example, the two boreholes with the highest pressures, *1130-273* and *1130-192*, are among the lowest (8-12 $g \cdot l^{-1}$) and the highest (38 $g \cdot l^{-1}$) TDS measured at the site, respectively, while waters from the remaining boreholes displayed no consistent pattern in TDS. As individual boreholes were opened and hydraulic pressures decreased, TDS and temperatures also decreased. This may be attributable to the presence and dissociation of gas hydrates, which have been inferred to occur in the area (*Chapter 3*). As gas hydrates dissociate, an endothermic reaction occurs, lowering temperatures. At the same time, TDS decreases as fresh waters in the crystalline hydrate structure are released.

The TDS and pressure data suggest the boreholes are intersecting and connecting different fracture networks of very different salinities and densities. The variations in pressure and TDS suggest two to three once-independent fracture systems were connected by the boreholes. It is hypothesized that higher TDS water is pushed up from depth. As boreholes are sealed, this water tends to replace the less dense water in the boreholes and some fracture networks, resulting in a transient state. In most boreholes, these waters mix to varying degrees relative to fracture network transmissivities. When mine work extended below the permafrost, some dewatering was conducted by the mine, essentially depressurizing the area immediately surrounding the mine. Relatively dilute water flows down from the permafrost and/or talik in fractures closer to the mine. The drawdown caused by pumping in the mine (*Chapter 3*) encourages the downward flow in these fractures.

2.5.6.2 Major Ions and Stable Isotopes

Subpermafrost fracture waters are either Na-Ca-Cl or Ca-Na-Cl type (Figure 2-3). The Na/Cl and Br/Cl ratios of deep subpermafrost waters plot near the evaporitic concentration pathway (e.g. *McCaffrey et al. 1996*), but along a different slope (Figure 2-8A). Subpermafrost waters are generally more enriched in calcium than the matrix and contaminated permafrost fluids (Figure 2-8B). It is possible the matrix fluids of sulfide-bearing amphibolites, which had a high Ca/Na ratio in the one sample analyzed, increase the calcium content of the waters relative to the phyllite rock mass, which had significantly lower Ca/Na ratios. Br/Cl ratios and $\delta^{37}Cl$ in subpermafrost waters are indistinguishable from the matrix waters (Figure 2-9).

Although the subpermafrost samples do not follow the hypothesized seawater freezing pathway presented by *Herut et al.* (*1990*) (Figure 2-8A), modification of subpermafrost waters *in situ* by freezing cannot be completely ruled out. Several different Canadian and Fennoscandian Shield type brines were experimentally frozen, including a Sudbury CaCl-type fluid (*Zhang and Frape 2002*). The deep Lupin waters follow a similar slope to the frozen CaCl Sudbury water (Figure 2-8A).

Stable isotopes of subpermafrost waters sampled at the Lupin mine generally plot in one area near and below the intersection of the LEL with the global meteoric waterline (GMWL) (Figure 2-5). The deepest sample (1300-105) is in the center of the grouping. Unlike many other saline Canadian/Fennoscandian groundwaters (e.g. *Frape et al. 2004*), none of the deep Lupin groundwaters plots above the GMWL.

2.5.6.3 Age Tracers

Four age tracers (^{3}H, ^{14}C, ^{36}Cl) were analyzed in the deep waters and indicate waters of at least three different ages are mixing. The occasional presence of ^{3}H suggests there is some connection with modern surface waters. Radiogenic carbon isotopic (Figure 2-6A) evidence from four boreholes indicate a recharge event around 25,000 ybp. The high He concentrations suggest a component of water with between 50 and 500 million years of radiogenic accumulation (*Bakermans et al. 2008*). Nucleogenic ^{36}Cl production in crystalline rocks is typically less than 50 x 10^{-15} $^{36}Cl{\cdot}Cl^{-1}$, and generally between 10 x 10^{-15} and 30 x 10^{-15} $^{36}Cl{\cdot}Cl^{-1}$ (*Bentley et al. 1986, Phillips 2000, Cecil 2000*). Although subsurface nucleogenic ^{36}Cl production was not determined at Lupin, ^{36}Cl values in subpermafrost waters are within the range expected for equilibration with subpermafrost nucleogenic production. Thus, the Cl^{-} in the subpermafrost system is likely older than the 0.5 to 1 million year limit of the ^{36}Cl dating method (*Phillips 2000*).

Occasionally, samples from approximately half of the subpermafrost boreholes monitored contained minor amounts of tritium (<2 T.U.) during the 7 year sampling period, with the exceptions of *1130-176*, *-192*, *-195*, *-260*, *-273* and *1300-105* (Figure 2-4E). Although minor tritium values were occasionally observed in some boreholes, tritium concentrations were typically below detection. The long length of time subpermafrost boreholes were purged prior to sealing would suggest negligible drill fluid impacts.

Four waters sampled with a wide range of salinity (3 to 40 g l^{-1}) from the horizontal boreholes at the 1130 m level produced radiocarbon dates between 22 and 25 ky, roughly the same time as glaciers were forming over the site. The salinity was not a factor in the dateable carbon. Calcite mineralization ($CaCO_3$) was sparse, and the thin calcite veins were not observed to be producing water. Low bicarbonate values may indicate a lack of carbonate/water interaction, and calculated saturation indices of calcite were typically near saturation in deep waters. Recent models have suggested most groundwater recharge during glacial periods would occur as glaciers form, rather than from glacial meltwater during retreat (*Lemieux 2006, Lemieux et al. 2008*). Direct impacts of glaciation on Lupin groundwater chemistry are unclear at this time, but radiogenic carbon (^{14}C)

suggests a recharge event of some kind may have occurred at ~25 ky. This data supports the conclusions of Lemieux et al. (*2008*).

2.5.7 Gases

Evidence concerning the origin and occurrence of methane and other hydrocarbon gases at Lupin are discussed extensively in Chapter 3 of this thesis, but aspects and implications are previewed in this chapter to allow complete development of the Lupin hydrogeochemical conceptual model. Methane hydrates are inferred to occur in the Lupin area based on temperature/pressure conditions, TDS and thermal variations during borehole depressurization, and gas saturation. Important hydrogeologic and geochemical implications of methane hydrate formation include the potential for sealing of porosity, fracture space, and permeability (e.g. *Kleinberg et al. 2003*), elevated ion concentrations, and relative depletion of ^{2}H and ^{18}O in associated groundwaters (e.g. *Trofimuk et al. 1974, Hesse and Harrison 1981, Hesse et al. 1985, Ussler and Paull 1995, Ussler and Paull 2001, Hesse 2003*), similar to the ice formation process (e.g. *Burt and Williams 1976*). Water chemistry can be affected by the ion-exclusion process well below the base of the permafrost, to the base of hydrate formation, because methane hydrates are stable well beneath the base of the permafrost (e.g. *Sloan 1998*). However, directly beneath hydrothermal through-taliks, thermal conditions are likely outside the range of hydrate stability.

Due to the low permeability of crystalline rocks, methane in these environments may be trapped in gas pockets well beneath the base of the permafrost (i.e. permafrost is not the primary gas trapping mechanism). Depending on the gas concentration and distribution within the rock mass, several ion exclusion zones may form within crystalline permafrost. Because gas was only found at certain depths well below the permafrost at Lupin (between 890-1130 m), up to three ion exclusion zones may form, including the base of ice-bonded permafrost, and deeper zones above and below individual methane hydrate formation zones.

Melting of gas hydrates can subsequently cause a dilution in groundwaters (e.g. *Hesse and Harrison 1981, Hesse et al. 2000, Hesse 2003, Haeckel et al. 2004*). In the Lupin area, mine induced depressurization is believed to have resulted in melting of methane hydrates, contributing the dilution observed in some sampled subpermafrost waters.

2.5.8 Calcite Fluid Inclusions

In general, fracture infillings are scarce. Most fracture surfaces are polished and may contain some chlorite and/or graphite. Thin calcite fillings are observed in a few fractures. Some fracture calcites

were massive (over 5 cm in width), while other calcites occurred as large vugs and what appeared to be accreted geochemical veins and vugs. In some shear zones, complex calcite-sulfide assemblages were observed. The euhedral nature of the calcite and pyrite in these assemblages suggests the crystals formed from hydrothermal solutions. Textural features within these fractures indicate several reactivation episodes. Many of the most prominent infillings occur in sub-horizontal fractures. Very few calcite veins or vugs appeared to be water-bearing.

Isotopic composition ($\delta^{13}C$, $\delta^{18}O$) and fluid inclusion microthermometry analyses were performed on a number of hand specimens and drill core fracture calcite samples collected from throughout the Lupin mine. The measured calcite isotopic compositions have the largest range of any Canadian Shield site studied (Figure 2-13A) and are also beyond the range of calcites found at Fennoscandian sites (*Frape et al. 1992, Blyth 1992, 2004, Blyth et al. 2000, 2004*). One especially large subhorizontal calcite vein, found at the 540 level along the access ramp had a particularly wide range of values ($\delta^{13}C$ -2.08 ‰ to +30.09 ‰ and $\delta^{18}O$ -14.49 ‰ to -6.29 ‰). The Lupin calcite samples are among the most enriched ^{13}C (+30‰ PDB) sampled in the Canadian or Fennoscandian shields, although Ylivieska, Outokumpu, Stripa, and Gidea are also relatively enriched (+20‰ PDB) (*Frape et al. 1992, Blyth 1993, Blyth et al. 2000, Blyth et al. 2004, Blyth 2004*).

The carbon isotopic compositions of the methane from Lupin (-56 to -40 ‰ PDB, *Chapter 3*) and some of the calcites ($\delta^{13}C$ +14 to +30 ‰ PDB) indicates that a group of the calcites may be syn-depositional to a portion of methane formed through the CO_2 reduction pathway. CO_2-CH_4 has a fractionation between -25 to -68 ‰ at temperatures between 60 and 300°C (*Rosenfeld and Silverman 1959, Bottinga 1969*), the range found in microthermometry. CO_2 reduction may be a biotic or abiotic process within the Middle America Trench (*Claypool et al. 1985*), a modern, analogous depositional environment to that at Lupin. CO_2 reduction is not believed to be a major or a modern process in the boreholes sampled (*Chapter 3*).

Several different fluid inclusion assemblages (FIA) were observed in the calcites from the Lupin site. Homogenization temperatures (T_h) indicate all calcites formed at temperatures greater than 73 °C. One FIA consisted of only liquid phase inclusions. A second FIA consisted of liquid and gas phase inclusions. The liquid was a high salinity (>26 %), Ca/Mg fluid, with homogenization temperatures between 73 °C and 147 °C. The next FIA observed was three phase NaCl inclusions with salinity between 31 and 36 % and homogenization temperatures between 250 °C and 271 °C. Another FIA consisted of a low salinity (<3 %) fluid, with homogenization temperatures between 132 °C and 148 °C. Finally, there was a FIA consisting of what are believed to be CH_4 inclusions. Often, multiple sets of these FIA were found in the same fluid inclusion chip, in what seemed to be the same

crystal. This indicates a boiling system at the time of crystallization. High salinity Ca/Mg fluid inclusions also provide an additional but small source of high salinity and calcium for the subpermafrost waters.

(A)

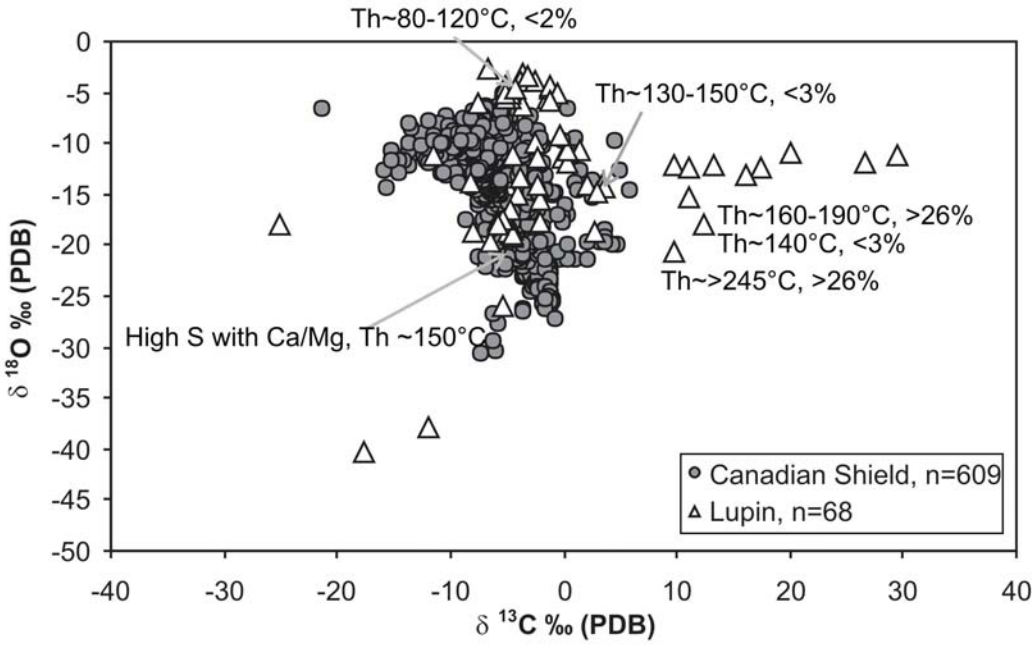

(B)

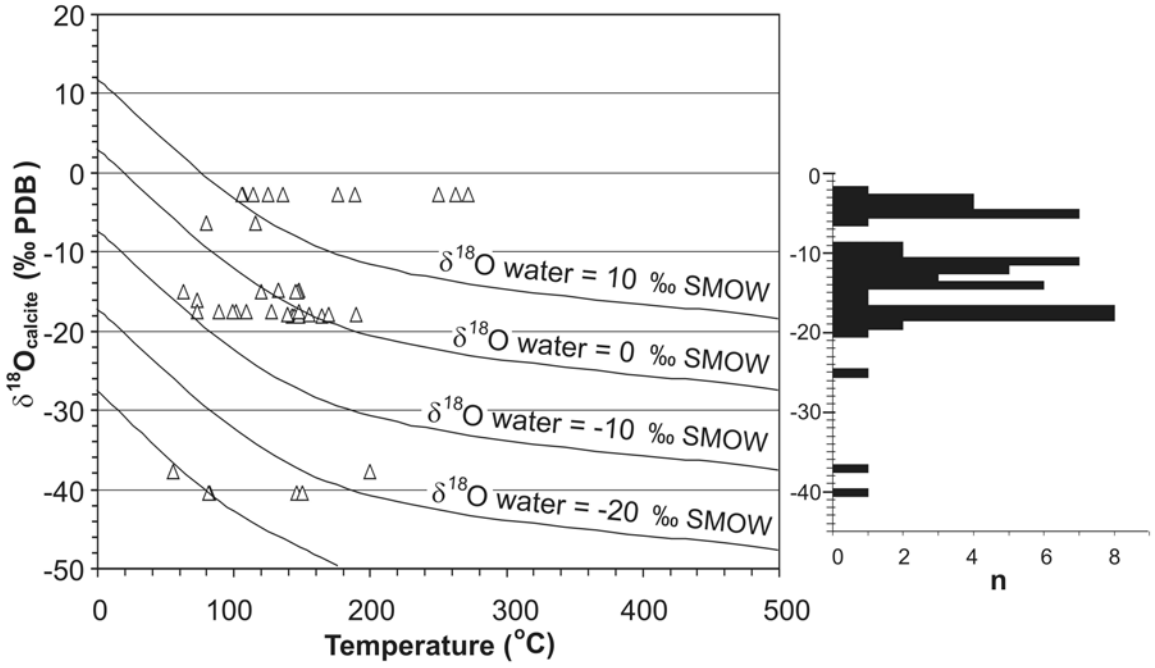

Figure 2-13. Lupin calcites with microthermometry data (A) vs. Canadian Shield calcites (*Jones 1987, Frape et al. 1992, Blyth 1993*) and (B) Isotopic thermometric plot for Lupin calcites.

Oxygen isotopic compositions and T_h of the calcite emplacement waters were interpreted following the methods of Blyth et al. (*2000, 2004*) to determine the isotopic composition of the fluid from which the calcites formed. Some of the most saline waters with the highest homogenization temperatures were likely emplaced by a heavy water, $\delta^{18}O > +10‰$ SMOW (Figure 2-13B). Another set appears to have been carried by a slightly lighter water, $0‰ \text{ SMOW} > \delta^{18}O > -10‰$ SMOW. Finally, a group appeared to crystallize from an extremely light water, $-20‰ \text{ SMOW} > \delta^{18}O > -30‰$ SMOW. Although this water is isotopically light, homogenization temperatures indicates this is still a higher temperature hydrothermal fluid. Further comparison of the microthermometric data with isotopic data (Figure 2-13) shows no apparent trends or patterns.

The system was very chaotic at formation as evidenced by indications of boiling and the random and diverse nature of ^{13}C-^{18}O values between and within calcite crystals. Many inclusions contain some gas phase (methane or carbon dioxide), while others appear to have very low salinity. If the calcite inclusions reflect the host rock, the low salinities from crush and leach studies are consistent with the low salt contents observed in some fracture fillings, although this conclusion is only tentative based on the heterogeneous salinities observed in the fluid inclusions.

^{13}C and ^{18}O isotopic analyses and geothermometry calculations of calcite formation conditions appeared to suggest that some calcites were formed by a depleted cold climate fluid. Although subglacially precipitated calcite has been reported in the literature (*Hanshaw and Hallett 1978*), fluid inclusion geothermometry indicates that the Lupin minerals calculated to have the most extreme isotopic signature were in fact precipitated from hydrothermal waters at temperatures greater than 80°C and salinities often greater than 20 weight percent. The hydrothermal, possible metamorphic nature of the calcites suggests they are greater than one billion years in age, possibly as old as peak (2.5-2.7 Ga) or retrograde metamorphism (1.84-1.81 Ga) (*Geusebroek and Duke 2004*). However, determining the relative ages of the fracture fillings was beyond the scope of this study.

2.5.9 Evolution of Waters at the Lupin Site

The origin and evolution of the deep waters at the Lupin is not completely understood. Because the sampled dissolved load is much greater in the fracture waters than the matrix waters, the rock matrix is not likely able to substantially overprint fracture water chemistry. However, some calcite fluid inclusions have sufficient salinity to account for the observed TDS in the most saline deep waters. Basal permafrost waters have similar salinities as the most dilute deep subpermafrost waters. Elevated sulfate in the basal subpermafrost waters is a result of natural and mining- enhanced oxidation of sulfides in the rock. Introduction of mine-brine, mine-induced drawdown and gas hydrate melting

complicates direct investigation into the impact of in situ freezing effects, but there is a possibility that in situ freezing of formation waters has affected the groundwater chemistry. The formation of methane hydrate should cause similar ionic fractionations as ice formation. Thus, while ice formation within the permafrost is not necessarily the cause of the observed ionic trends in the subpermafrost, the methane hydrate formation process is a type of freezing with similar geochemical impacts to residual fluids. Although ^{14}C-ages indicate a recent recharge event within the last 20,000 years, dissolved ^{36}Cl in equilibrium with subsurface nucleogenic ^{36}Cl production indicates the dissolved chloride component has been in the system longer than the range of the method (> 1 million years). High He concentrations provide further evidence the waters have equilibrated between 50 and 500 million years (*Bakermans et al. 2008*). These varied ages indicate mixing of fluids is occurring.

Under the right conditions of fracture/foliation interconnection, intersection with taliks, and a hydraulic gradient (e.g. established due to mine dewatering activities), a hydraulic pathway could be present for the recharge of fresh waters to depth. Given that many of the horizontal boreholes sampled intercept numerous geological structural elements while cutting almost perpendicular across the foliation, it is possible that the small amounts of dilute water observed in some of the deep saline water zones were transported to depth under these conditions. The brackish waters observed at the 890 and 1130 m levels thus may represent subsurface transport of fluids from the talik existing below Lake Contwoyto, but is more likely related to destabilization of methane hydrates in the area of the mine.

The complete conceptual model for the Lupin area is presented in Figure 14. A thin active layer only affects the upper ~1-8 m. Shallow lakes freeze completely and have no talik, while other larger, deeper lakes (300 m wide) contain open taliks. Even larger lakes (>500 m wide), including Lake Contwoyto, have hydrothermal through-taliks. Permafrost fluids are mixtures of drilling salt, blasting remnants, and natural fluids. Although mine dewatering may provide a downward gradient for dilute talik water, there is no evidence of the contaminated permafrost fluids at depth. Therefore, the primary dilute water source at the 890 and 1130 m levels is likely provided by gas hydrate melting, related to anthropogenic mine depressurization. In the final component of the conceptual model, methane hydrates would not exist beneath hydrothermal through-taliks, due to the warmer subsurface temperature conditions.

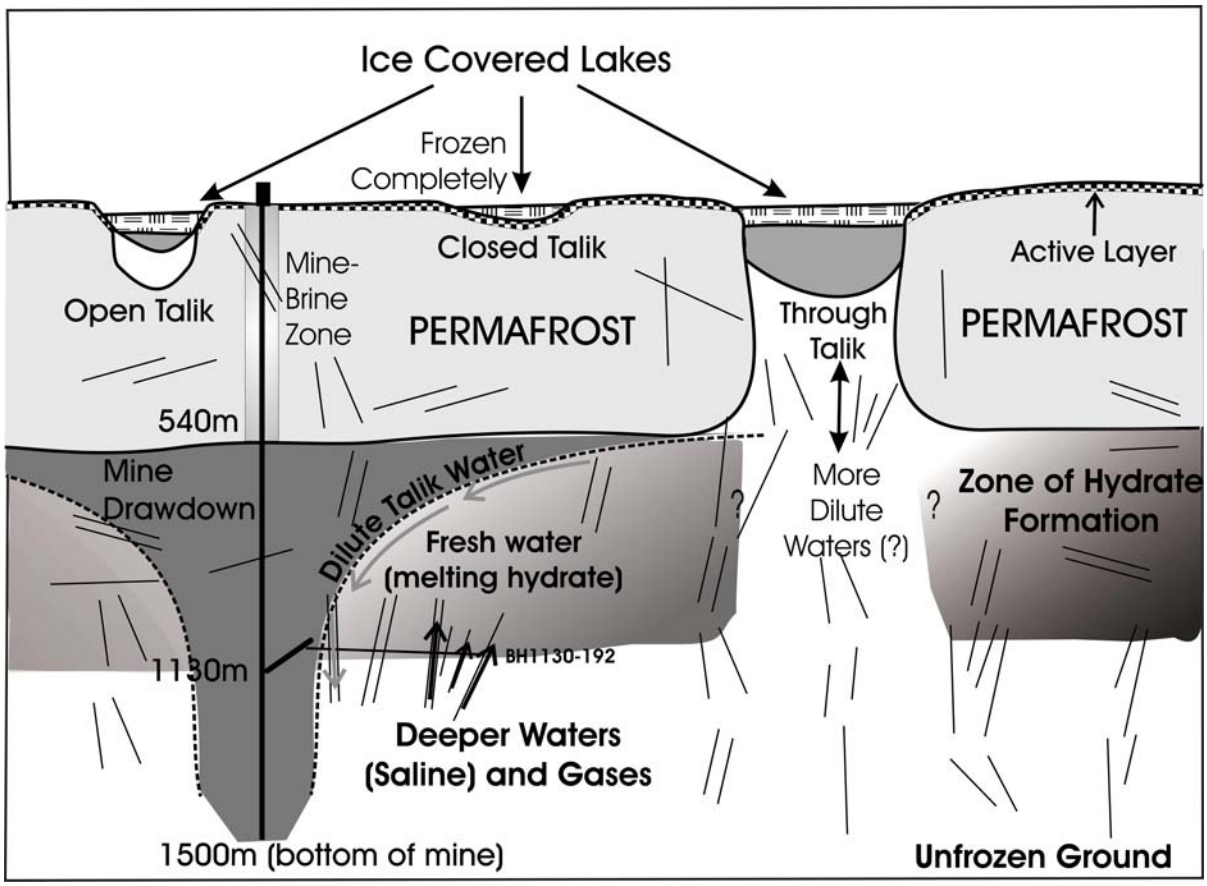

Figure 2-14. Conceptual hydrogeologic model of the Lupin area.

2.5.10 Comparison with "Cryogenic Freezing of Seawater" Hypothesis

The cryogenic formation of crystalline brines from seawater hypothesis (*Starinsky and Katz 2003*) does not account for several important observations from this permafrost study. First, as shown in Figure 2-8, the relationship between Na/Cl and Br/Cl ratios for subpermafrost Lupin groundwaters is significantly different from seawater evaporation (*McCaffrey et al. 1996*), hypothesized seawater freezing (*Herut et al. 1990*), and the hypothesized freshwater dilution trend (*Starinsky and Katz 2003*). The extrapolated seawater freezing trend presented by *Herut et al.* (*1990*) forms the basis of the cryogenic formation of brines from seawater presented by *Starinsky and Katz* (*2003*). Additional information provided by age tracers (He, ^{36}Cl) also suggests brine formation at Lupin occurred well before the last glacial maximum, contrary to the proposal by *Starinsky and Katz* (*2003*). While ^{14}C ages do indicate a recharge event during the last glacial advance, there is no apparent correlation of ^{14}C age with the salinity. If the saline waters at Lupin formed through freezing on the surface in a glacially-created lagoon, there should be a clear correlation between salinity and ^{14}C age, since the most saline fluids would have formed within the range of the ^{14}C methodology (~50 ka). However,

the predicted presence of methane hydrates throughout the glacial cycle (Chapter 3) would significantly reduce the permeability and porosity of the rock. Additional modeling is needed to evaluate thermal regimes and the effect of pre-existing taliks. Finally, Lupin waters do not have the chemical signature predicted by the seawater freezing hypothesis. Therefore, the combined data strongly suggest that surficial seawater freezing has not affected deep subsurface waters at Lupin.

2.6 Conclusions

Geochemical data from the Lupin site clearly show the contaminated permafrost water is distinct from the subpermafrost water, however the degree to which freezing modified the chemistry at the site is difficult to quantify. The observed deep groundwater chemistry at Lupin does not appear to have evolved due to surficial freezing of seawater. Large variations of the isotopes of chlorine, hydrogen, and oxygen is apparent in the permafrost. For hydrogen and oxygen isotopes, this is attributed to freezing of the introduced drill brine. At the extreme, the freezing/methane hydrate formation process has only resulted in the formation of moderately saline water at Lupin.

Although various geochemical parameters suggest the waters associated with the "ramp fault" sampled in the permafrost have been heavily affected by mining activities, natural geochemical components are observed as well. Much of the dissolved load analyzed in the permafrost waters is from the use of drilling brine for work in the permafrost areas by mine personnel. Nitrate accumulation is a result of blasting activities, and its persistence is due to oxic to suboxic conditions. However some constituents (e.g. SO_4^{2-}) within the permafrost may be a result of natural processes, although it is unclear to what extent its formation was influenced by mining operations.

For hydrogeologic modeling, permafrost in areas with numerous large lakes should be treated as a leaky confining layer, rather than a completely impermeable barrier. Although ice and methane hydrate formation in deep permafrost may seal many potential flow routes in the crystalline bedrock, through-taliks can form conduits through frozen ground. The presence of through-taliks beneath Lake Contwoyto and several smaller lakes in the area is suspected. It is unclear from the investigation what impacts taliks would have on waters at depth at an undisturbed location. Many large lakes in the Canadian and Fennoscandian shields, including Lake Contwoyto, appear to be associated with fracture zones. Thus taliks may provide the hydraulic pathways required for recharge through permafrost.

There are several implications of this research for deep geologic radioactive waste disposal. Even considering the contamination, brines were not found at Lupin at repository depth. Thus, *in situ* freeze-out during permafrost/methane hydrate formation is not considered able to create such strongly

concentrated fluids. Deep (~1 km) recharge of glacial meltwater was not ruled out, although artificially induced hydraulic gradients from mining appear to cause mixing of different age fluids at the sample depths. Challenges are also presented by the possible formation and destabilization of methane hydrates. Dilute fluids created by melting hydrates could negatively impact engineered barriers. An upper limit to potential fluid salinities during methane hydrate formation should be investigated. A repository placed in an area currently in permafrost conditions with methane hydrates would need to constrain what changes to the physical and geochemical environment could occur if hydrate dissociation occurs due to heat generated from the repository. Heat generated by the repository may also create a hydrothermal talik to form through the permafrost, thus understanding how talik formation affects deep groundwater flow system evolution in permafrost environments is critical for safe radioactive waste disposal in northern countires.

Different rock chemistries and subsurface thermal conditions will influence the final water chemistry beneath permafrost on Mars. Regardless, this investigation is an important step towards constraining subpermafrost fluid chemistries in tectonically inactive crystalline rocks on Earth and Mars.

Chapter 3

Thermogenic Methane Hydrate in a Crystalline Shield

3.1 Executive Summary

Although significant proportions of the Canadian arctic is underlain by crystalline rocks, the occurrence, phase, and origin of alkanes in crystalline rocks under thick permafrost conditions (>500m) have not been explored. Relatively little attention has been given to the stability of permafrost hydrates during past periods of climate change. For the first time, gas data from a crystalline shield environment currently under permafrost conditions is presented. Evidence indicates the formation of natural gases by thermogenic processes mixed with some bacteriogenic gas, unique compared with other gases previously described in the Canadian Shield, although the data are somewhat contradictory.. It is suggested these gases have been stabilized as methane-hydrates throughout Quaternary glacial cycles, despite severe climate changes. Significant formation of gas hydrates could limit subglacial recharge. This study is a first step towards understanding the nature of methane-hydrates in crystalline rocks.

3.2 Introduction

Methane is formed through three natural processes: (1) thermogenically, through thermal decomposition of organic matter; (2) bacteriogenically, from methanogenic microbes; and (3) abiogenically, from CO_2 reduction to CH_4 through non-biological reactions (*Sackett et al. 1970, Des Marais et al. 1981, James 1983, Sherwood Lollar et al. 1993a, 1993b, 2002, Berndt et al. 1996, McCollom and Seewald 2001, 2003*). While methane in marine and sedimentary basins are of thermogenic or bacteriogenic origin (e.g. *Sackett et al. 1970, Des Marais 1981, James 1983*), gases of primarily abiogenic origin have been documented in the Canadian and Fennoscandian crystalline Shields from volcanogenic greenstone belts, granitic batholiths, and meteor impact sites (*Voytov 1991, Sherwood Lollar et al. 1993a,b, 2002, 2006*). During metamorphism of certain rock units, methane may be abiogenically produced through Fischer-Tropsch-type synthesis (*Szatmari 1989*, *Sherwood Lollar et al. 1993b, Salvi and Williams-Jones 1997, Taran et al. 2007*), decarboxylation of organic acids (*McCollom and Seewald 2003*), and serpentinization reactions (e.g. *Berndt et al. 1996*),

although recent investigations suggest hydrocarbon formation during serpentinization may be limited (*McCollom and Seewald 2001*).

Gas hydrates form in certain low temperature and medium pressure conditions when water and gas mixtures crystallize into ice-like solids, storing >160 times more gas per unit volume than free gas (*Sloan 1998*). Large thermogenic alkane (with bacteriogenic components) and methane-hydrate reservoirs have been found in permafrost-affected sedimentary rocks, including those of the Arctic Archipelago and Mackenzie Delta in Canada (*Dallimore and Collett 1995, Dallimore et al. 1999, Majorowicz and Osadetz 2001, Dallimore and Collett 2005*), the North Slope Basin in Alaska (*Collett et al. 1990*), and Siberia (*Yakushev and Chuvilin 2000*). Because studies of methane-hydrates have focused on oil- and gas-producing regions (concentrated in existing marine and sedimentary basins), currently no information is available regarding the nature of gas associated with crystalline Shields in permafrost environments.

Field activities at the Lupin Au mine (65º45'29"N, 111º13'10"W) in Nunavut, Canada (Figure 2-1), provided an opportunity to study the nature of gases within crystalline rocks in a permafrost environment. Understanding the properties of gas in a Shield environment under permafrost conditions is important for assessing the safe long-term storage of radioactive materials in Canada, Finland, and Sweden. Additionally, it is hypothesized that water on Mars should be found in permafrost and in an environment similar to a geologically inactive Shield. Characterizing the nature of gas in an analogous environment on Earth can help to constrain the expected geochemical environment on Mars.

The metamorphosed Lupin banded-iron-formation gold deposit is part of an Archean metaturbidite sequence. Today, Lupin is well within the continuous permafrost zone. Permafrost depth, defined by the 0°C isotherm, varies from 400 to 600 m in the area. Mineshaft temperature measurements indicate permafrost depth (541 m) was unchanged during the 23 years that the mine operated.

3.3 Methods

Water and gas samples were collected between 250 and 1130 meters below ground surface (mbgs) from fractures, dripping exploration boreholes, and packer-sealed research boreholes. Natural gas was identified between 890 and 1130 mbgs. Gas samples were collected from one fracture fed pool, nine sub-horizontal and three sub-vertical research boreholes. The boreholes had been drilled across steeply dipping foliation and away from mine workings for lengths from 60 to 500 m. They were sealed with 3 m Margot® packers, allowing pressure to build up within the boreholes. One borehole

was sampled on the 890 mbgs level, and eleven on the 1130 mbgs level. The eleven boreholes on the 1130 mbgs level allow investigation of hydraulic conditions over a planar area of 500 x 500 m^2, with the total distance between collars about 300 m. Samples were analyzed for gas chemistry, $\delta^{13}C$ and δ^2H composition of the gases, dissolved ions, and $\delta^{18}O$ and δ^2H composition of the water. Noble gas samples were collected using two different methods: copper tubes and a gas diffusion sampler (*Greene 2005*). Fractures and fracture zones were mapped in each borehole under unpressurized conditions using a borehole camera. Gas was readily observed effervescing from several fracture openings in each borehole.

The Indiana University Stable Isotope Facility and the University of Waterloo (UW) Environmental Isotope Laboratory analyzed $\delta^{13}C$, and δ^2H isotopes using a Micromass Isoprime GC-C-IRMS for carbon isotopes and Finnigan MAT Delta GC-PYR-IRMS for hydrogen isotopes. Accuracy and reproducibility of $\delta^{13}C$ and δ^2H are typically ±0.3‰ VPDB and ±5‰ VSMOW, respectively. Gas compositions were analyzed at the UW Organic Geochemistry Laboratory; N_2 and CO_2 on a Fisher/Hamilton Gas Partitioner, Model 29 gas chromatograph, and alkane-hydrocarbons on a Varian 3800 gas chromatograph equipped with a flame ionization detector and capillary injection port. Detection limits for CO_2, N_2, C_1, C_2, C_3, nC_4 and iC_4 are 0.5 ppm, 30 ppm, 0.3 µg/L, 0.2 µg/L, 0.2 µg/L, 0.8 µg/L, and 1.6 µg/L, respectively. Noble gas concentrations were measured at the University of Ottawa (*Greene 2005*) using an isotope dilution method (*Youngman 1989*).

The climate/subsurface modeling results are from a large ensemble calibration of the Memorial University/University of Toronto (MUN/UofT) Glacial Systems Model (GSM) for the last glacial cycle. The model includes a 3-D thermo-mechanically coupled ice-sheet model, permafrost resolving bed thermal model, diagnostic surface drainage, visco-elastic bedrock response, and positive degree day surface mass-balance module (*Tarasov and Peltier 2007*). Climate forcing is derived from an ensemble of General Circulation Model results for the last glacial maximum that defines a glacial climate state. The climate forcing is interpolated between this glacial state and present day observational climatology via a glaciological inversion of the last 120 kyr regional climate over Greenland. The climate forcing is subject to 20 ensemble parameters (governing regional climate changes and the definition of the glacial climate state) calibrated against a large set of relative sea-level observations, geodetic observations, strandline elevations (proxy for pro-glacial lake levels), and an inferred deglacial ice margin chronology. Eleven other parameters governing ice calving, fast flow controls, and ice marginal mass-balance are also calibrated. The eight model runs presented are a hand-picked set of high-scoring runs that roughly bound possible climate ranges. Model results prior to the last glacial maximum are poorly constrained due to limited data. Detail of the calibration can be

found in Tarasov and Peltier (*2005*). The pressure-melting point of gas-hydrates was determined by utilizing a best fit of previously compiled data (*Sloan 1998*). For temperatures above 0°C this relationship is defined by: T(P)=9.0416·ln(P/2492.6)*;* and for temperatures below 0°C: T(P)=30.338·ln(3.917·10-4·P), where T = temperature [°C] and P = pressure [kPa]. Hydraulic conditions were modeled for one of the GSM scenarios, accounting for density-dependent flow, hydromechanical loading, subglacial infiltration, isostasy, and permafrost development utilizing the HydroGeoSphere model (*Therrien et al. 2007*), and applied to the Wisconsinan glaciation over the Canadian landscape. Further discussion of the rationale for the use of this model may be found in Lemieux et al. (*2008 a,b,c*) and Lemieux (*2006*).

3.4 Results and Discussion

A summary of the Lupin gas molecular and isotopic compositions may be found in Appendix B (Table B-10 and Table B-11). Gases were generally methane-dominated (64-87 %), with nitrogen as the next largest component (10-37 %), with smaller amounts of ethane, carbon dioxide, and propane. Very small amounts of butane and iso-butane were detected in most samples. Methane and carbon dioxide carbon isotopic compositions varied between -56 and -42 ‰ VPDB and -55 and -15 ‰ VPDB, respectively. A smaller range was detected for ethane (-37 to -27 ‰ VPDB) and propane (-34 to -27 ‰ VPDB). Similarly, methane hydrogen isotopes showed a larger range (-349 to -181 ‰ VSMOW) than either ethane (-330 to -228 ‰ VSMOW) or propane (-196 to -172 ‰ VSMOW).

3.4.1 Origin and Evolution of the Gas

Trends in relative abundance and isotopic composition are widely used to identify thermogenic gas reservoirs (e.g. *Sackett et al. 1970, Des Marais 1981, James 1983, Prinzhofer and Huc 1995*) and to differentiate thermogenic from abiogenic hydrocarbon gases (e.g. *Sherwood-Lollar et al. 2002, Taran et al. 2007*). As gas is thermogenically formed, higher hydrocarbons are thermally cracked, resulting in a low (<100) methane (C_1) to ethane plus propane (C_2+C_3) ratio. Lighter isotopes are preferentially removed from longer chain hydrocarbons during thermal cracking, resulting in lower $\delta^{13}C$ values for C_1 than for higher hydrocarbons such as C_2 or C_3. Contrasting with that, during bacteriogenic methane formation, a -70‰ fractionation occurs between the carbon source (typically CO_2 or acetate) and the resulting methane. Very few higher hydrocarbons are formed by bacteria, resulting in a high $C_1/(C_2+C_3)$ ratio (>1000). Empirical data suggest abiogenic gases generally evolve with a low $C_1/(C_2+C_3)$ ratio (<100), similar to thermogenic gases, but with progressively lower $\delta^{13}C$ values as hydrocarbon chains lengthen (i.e., from C_1 towards C_3), opposite from that of thermogenic gases (e.g.

Des Marais et al. 1981, Taran et al. 2007). Abiogenic gas formation and subsequent fractionation is still the subject of investigation and debate (*Taran et al. 2007*).

Compared to other gases previously sampled from the Canadian and Fennoscandian Shield, the Lupin gases appear to have a unique origin. Similar to gases of thermogenic and abiogenic origins, Lupin gases have low $C_1/(C_2+C_3)$ values (Figure 3-1A). On the other hand, the enrichment trend of $\delta^{13}C$ from C_1 to C_3 alkanes (Figure 3-1B) is typical of gases of a thermogenic origin. The wide range of $\delta^{13}C$-C_1 values and the relationship between the $C_1/(C_2+C_3)$ and $\delta^{13}C$-C_1 values (Figure 3-1A) indicate that some mixing with bacteriogenic gases has occurred. Because methanogenic bacteria were not isolated in parallel investigations (*Bakermans et al. 2008*), $\delta^{13}C$ of C_1, C_2, and C_3 were compared (Figure 3-2). The relationships between $\delta^{13}C$-C_1 values with $\delta^{13}C$-C_2 and $\delta^{13}C$-C_3 values provide additional evidence that C_1 gases have mixed with bacteriogenic gas. When thermogenic gases mix with bacteriogenic gases, $\delta^{13}C$-C_1 values decrease, but because very little ethane or propane is produced bacteriogenically, $\delta^{13}C$-C_2 and $\delta^{13}C$-C_3 values are relatively unchanged (*Berner and Faber 1988, Whiticar 1994, 1996*). The inverse correlation between nitrogen gas composition and methane carbon isotope composition (Figure 3-3) indicates the bacteriogenic component has higher nitrogen content. It is unclear why nitrogen would increase with bacteriogenic methane. Generally, nitrogen is an important component of deeply buried humic and other over-mature source rocks (*Whiticar 1994*). The inverse relationship observed in Lupin gases between $\delta^{13}C$-C_1 and N_2 content is unique compared with other natural gases from North America and Europe (*Whiticar 1994*).

Interestingly, the Lupin $\delta^{2}H$-C_1 ratios are lower than typically associated with thermogenic gases. The relationships between methane $\delta^{13}C$ and $\delta^{2}H$ ratios suggest a bacteriogenic origin from an acetate precursor (Group 1, Figure 3-1C). This comparison also reveals a similarity with some other abiogenic Canadian Shield gases currently located within or near permafrost. However a more comprehensive analysis considers the fractionation relationship between $\delta^{13}C$ and $\delta^{2}H$ for C_1, C_2, and C_3. The result of this analysis is consistent with gas of a thermogenic origin (Figure 3-1D), as both $\delta^{13}C$ and $\delta^{2}H$ become isotopically heavier from C_1 to C_2 to C_3 (e.g. *Sherwood-Lollar et al. 1994, Prinzhofer and Huc 1995*), and does not follow previously recognized abiogenic gas trends (e.g. *Sherwood-Lollar et al. 2002, Taran et al. 2007*). Therefore, despite the significantly more depleted $\delta^{2}H$ values, the gas isotopic fractionation pattern is more consistent with thermogenic gas than abiogenic gas trends.

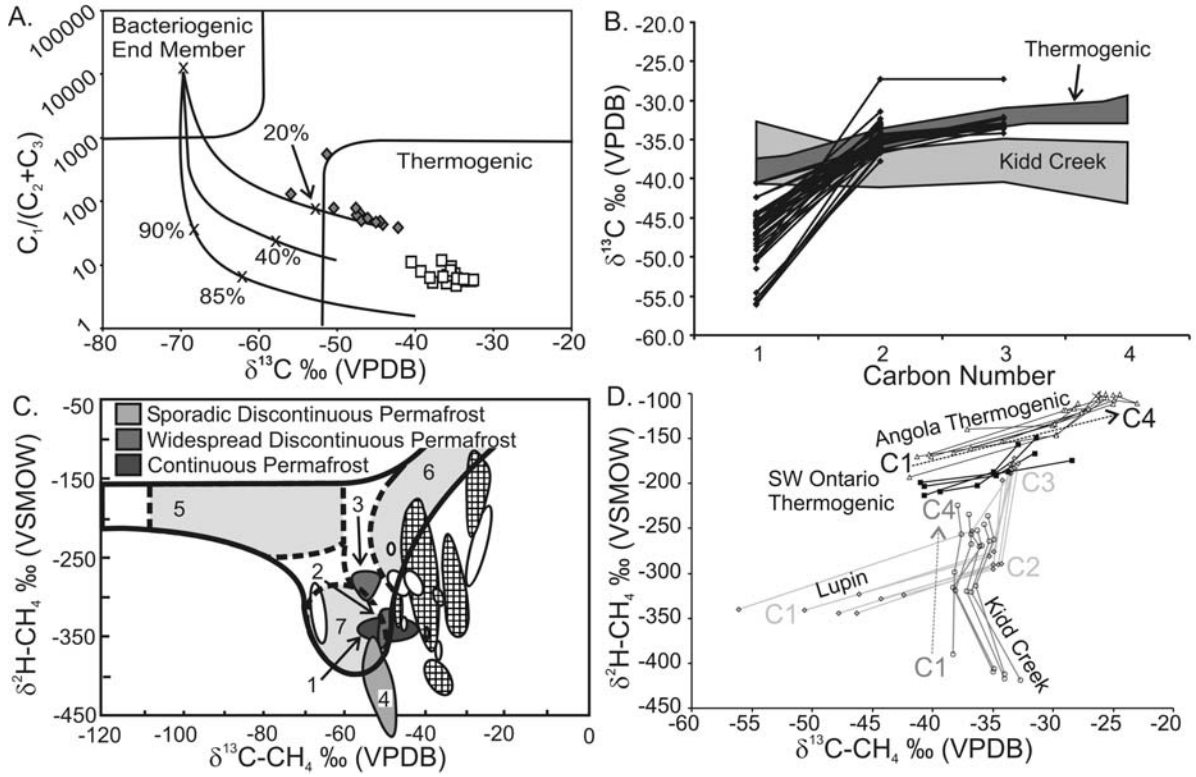

Figure 3-1. Lupin gas relationships, compared with other sites, including Canadian and Fennoscandian Shield gases (*Sherwood Lollar et al. 1993a,b*) southwest Ontario natural gas fields (*Sherwood Lollar et al. 1994*), Angola gas fields (*Prinzhofer and Huc 1995*), and Kidd Creek (*Sherwood Lollar et al. 2002*). (A) $\delta^{13}C$-CH_4 versus $C_1/(C_2+C_3)$ ratios for Lupin (filled diamonds) and Kidd Creek (open squares) gases. Various end-member mixing lines are provided, with relative locations for different percentages of each gas shown on each line for reference (B) $\delta^{13}C$ values of individual hydrocarbons versus carbon number. Black lines indicate individual samples from Lupin (C) Comparison of δ^2H and $\delta^{13}C$ from all Canadian (cross-hatched regions) and Fennoscandian (unshaded regions) Shield sites grouped with respect to permafrost conditions: discontinuous (2-Yellowknife), sporadic or isolated (3-Thompson, 4-Matagami/Norita) and continuous (1-Lupin) permafrost. Lightly shaded fields represent typical areas for bacterial carbonate reduction (5), thermogenic associated gases (6), and bacterial methyl-type fermentation (7). (D). Relationship between $\delta^{13}C$ vs. δ^2H between C1, C2, C3.

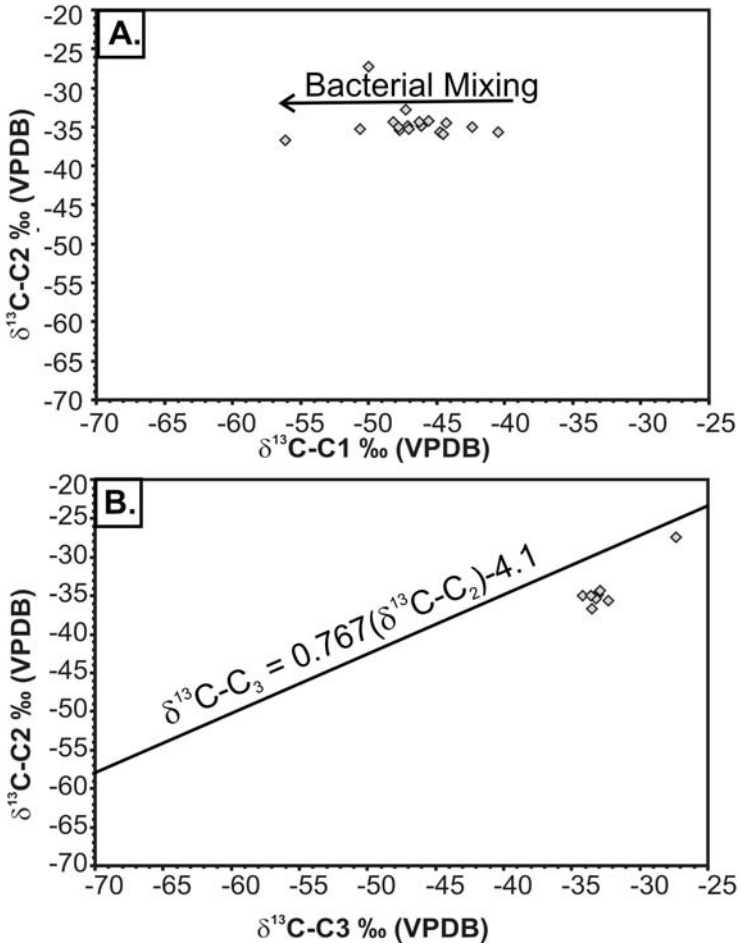

Figure 3-2. (A) δ^{13}C-C1 vs. δ^{13}C-C2 and (B)δ^{13}C-C2 vs. δ^{13}C-C3 for gases sampled at the Lupin mine. The relationship in B ($\delta^{13}C\text{-}C_3 = 0.767*\delta^{13}C\text{-}C_2 - 4.1$) is a thermogenic gas trend from Jenden (*1985*).

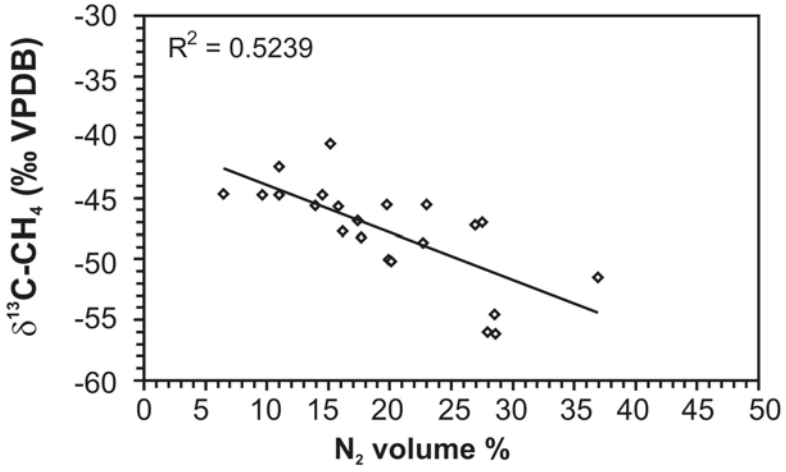

Figure 3-3. Relationship between $\delta^{13}C\text{-}CH_4$ and nitrogen gas content of Lupin gases.

However, if the major Lupin gas component does have a thermogenic origin, the depleted gas δ^2H values require special consideration. Hydrogen isotopic fractionation during primary production is controlled by δ^2H-H_2O or -H_2 values and/or metabolic processes (*Whiticar 1996, 1999*). On the other hand, during thermogenic methane formation, hydrogen molecules are believed to come from the decarboxylated organic material (e.g. *Schoell 1980, Whiticar 1996*). From field data, primary fields have been determined where δ^2H values have a range between -275 ‰ and -100 ‰ (VSMOW) for thermogenic gases, and for bacteriogenic methane, between -250‰ and -170 ‰ (VSMOW) for the carbonate reduction pathway, and between -531 ‰ and -250 ‰ (VSMOW) for the methyl-type fermentation pathway (*Whiticar 1999*). However, methane δ^2H ratios may change dramatically depending on hydrogen concentration; in one experiment increasing H_2 concentrations resulted in 150 ‰ decrease in δ^2H-CH_4 beyond the lower concentrations (*Burke 1993*). Further, during bacteriogenic methanogenesis, a specific proportion of hydrogen atoms are incorporated into methane from water molecules (*Whiticar 1999*). A range of empirical relationships comparing δ^2H -H_2O and -CH_4 have been published (e.g. *Schoell 1980, Jenden and Kaplan 1986, Whiticar et al. 1986, Waldron et al. 1999, Whiticar 1999*). Generally, this relationship has a slope of 1 during carbonate reduction and 0.25 during methyl-type fermentation, and intermediate slopes likely attributable to a combination of the pathways (*Whiticar 1999*). Additional evidence of carbon-bound hydrogen exchange over short (*de Graaf et al. 1996, Waldron et al. 1999*) and geologic timescales (*Sessions et al. 2004*) has been presented. Therefore, several possible scenarios are explored to explain the observed δ^2H-C_1 ratios:

- A bacteriogenic component produced by methyl-type fermentation. Although this possibility is consistent with the most depleted methane δ^2H and $\delta^{13}C$ ratios, δ^2H ratios do not vary significantly. Thus, δ^2H ratios for both the bacteriogenic and thermogenic gases must be the same or very similar. This flat trend between δ^2H and $\delta^{13}C$ may also be attributed to fermentation of ^{13}C-depleted acetate (e.g. *Burke 1993, Whiticar 1999*). Ethane and propane may be minor products of this process, resulting in a small carbon isotopic fractionation from precursor organic matter (e.g. *Oremland et al. 1988, Hinrichs et al. 2006*).

  However other aspects of the Lupin data are not characteristic of methyl-type fermentation. For instance, Lupin $\delta^{13}C$ -C_2 and -C_3 co-vary (Figure 3-2B) as expected during organic matter maturation for thermogenic gases (*James 1983, Jenden 1985, Martini et al. 2003*). The relationship between H_2O and CH_4 for δ^2H values in Lupin gas (Figure 3-4) is indicative of methanogenesis from the carbonate reduction pathway, given a hydrogen fractionation of -180 ± 20 ‰ VSMOW (*Whiticar et al.*

1986). In addition to data presented previously in this chapter, methyl-type fermentation does not seem a plausible explanation for the depleted δ^2H ratios.

- A bacteriogenic component produced by carbonate reduction. As discussed, the δ^2H-CH_4 and -H_2O values are within the range predicted by Whiticar et al. (*1986*), if the relationship is extended to the depleted δ^2H-H_2O ratios of Lupin groundwaters. Previous correlations between δ^2H-CH_4 and -H_2O have not considered δ^2H-H_2O values as depleted as found in Lupin groundwaters (e.g. *Whiticar et al. 1986, Whiticar 1999, Martini et al. 2003*). Thus if methane gas at Lupin formed from waters with depleted δ^2H-H_2O values similar to modern-day values, gas formed from a carbonate reduction pathway could have δ^2H-CH_4 values significantly more depleted than previously considered. Depending on the age of the gas, the δ^2H in modern waters may be in dis-equilibrium with the methane.

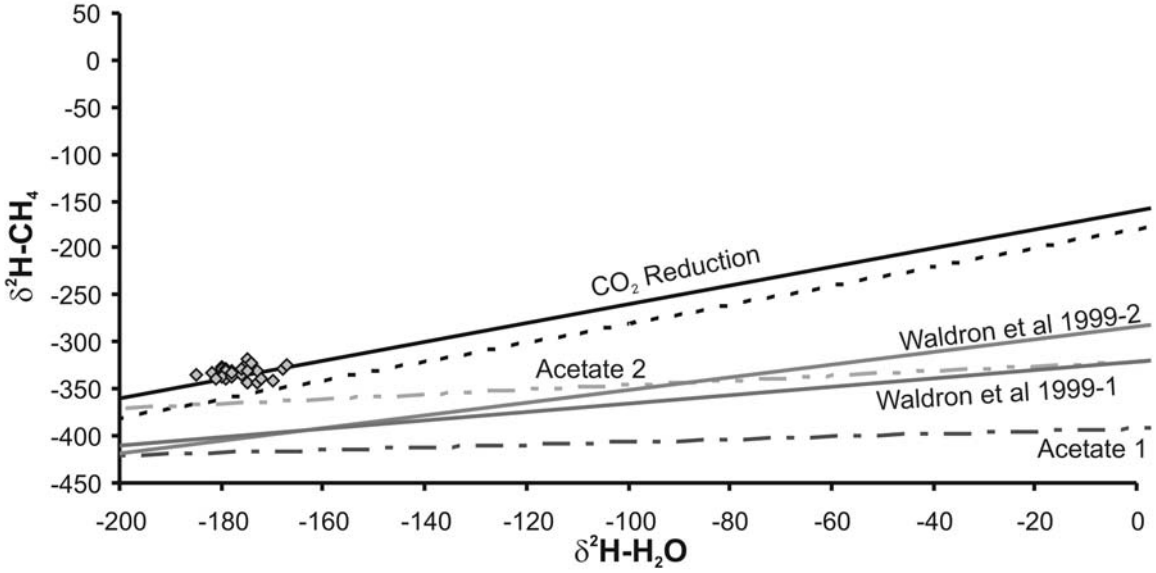

Figure 3-4. Relationship between δ^2H-CH_4 and δ^2H-H_2O for Lupin gases. CO_2 reduction line from Schoell (*1980*) Acetate fermentation 1 line from (*Jenden and Kaplan 1986*) Acetate fermentation 2 line from (*Whiticar et al. 1986*). The other two lines reflect shallow biogenic gas trends (*Waldron et al. 1999*).

A carbonate reduction methanogenic pathway may be supported by calcite isotopic and fluid inclusion microthermometry data (presented in detail in Chapter 2). Methane was observed in numerous calcite thick sections. Based fluid inclusion evidence, several "warm" (>100°C) calcites had very depleted $\delta^{18}O$ values (-20 to -30

‰, Figure 2-13 in Chapter 2), which could indicate substantially more depleted δ^2H-H_2O values than normally associated with gas formation. Further, some abnormally enriched δ^{13}C-calcite ratios (+30‰) indicate an enriched source δ^{13}C-CO_2. Bacteriogenic methane produced by carbonate reduction from such an enriched δ^{13}C-CO_2 could have δ^{13}C values as high as -50‰ (*Whiticar 1999*). Similar δ^{13}C-CO_2 and δ^{13}C-CH_4 values are found in the Middle America Trench, an analogous modern environment (*Claypool et al. 1985*). However, ethane and propane are not produced through this process, and δ^2H-CH_4 values should be different for both the biogenic and thermogenic components.

- Thermogenic gas formed from isotopically light source organic matter or water. Like biogenic gases, most thermogenic methanes are found in waters with δ^2H-H_2O values < -80 ‰ VSMOW (*Schoell 1980, Barker and Pollack 1984, Martini et al. 2003*). Unlike biogenic gases, thermogenic gases primarily derive hydrogen isotopic compositions from thermal cracking of larger organic chains rather than water (*Schoell 1980*). However, unlike carbon isotopes, methane hydrogen isotopic data do not show a dependence on maturity (*Whiticar 1996*). Source organic matters display a δ^2H range between -175 and -75‰ VSMOW due to differences in plant types and the δ^2H-H_2O during plant growth (e.g. *Shiegl and Vogel 1970, Yapp and Epstein 1977, Stahl 1979, Redding et al. 1980, Whiticar 1996*). Although the data presented here are from Archean metasedimentary units, previously described thermogenic gases are predominately from Proterozoic marine sediments. Thus unless organic matter δ^2H was significantly different during the Archean when initial deposition of Lupin sediments occurred (of which there is no evidence), there is not sufficient evidence to support thermogenic formation of isotopically light hydrogen.

- Hydrogen isotope exchange during methane oxidation in the presence of oxidized iron. Lupin gas δ^{13}C-CO_2 and δ^{13}C-CH_4 values generally plot between the methane oxidation and methyl fermentation fields (Figure 3-5) as defined by Whiticar (*1986*). During methane oxidation, δ^{13}C-CO_2 and δ^{13}C-CH_4 values decrease and increases, respectively. Loss of CH_4 also decreases the $C_1/(C_2+C_3)$ ratio. Thus, the trend in Figure 3-1A could be related to bacteriogenic gas mixing with thermogenic gas or methane oxidation. If kinetic isotope effects control δ^2H during methane oxidation, δ^2H-CH_4 will also become higher (e.g. *Kiyosu and Imaizumi 1996, Whiticar 1999*). However, laboratory experiments indicated hydrogen isotopes are not affected by

kinetic isotope effects during methane oxidation in the presence of Fe_2O_3, but are subject to exchange with H_2O (*Kiyosu and Imaizumi 1996*). There is abundant iron in Lupin rocks, and oxidized iron was observed in fractures higher in the mine, within the permafrost. However, oxidation rates in the Fe_2O_3 system were low below 500°C (*Kiyosu and Imaizumi 1996*). Therefore, if the observed δ^2H-CH_4 values are attributable to methane oxidation with an iron-oxide catalyst, the implied oxidation would have occurred over either a long geologic time period or at a time when temperatures were significantly higher than present.

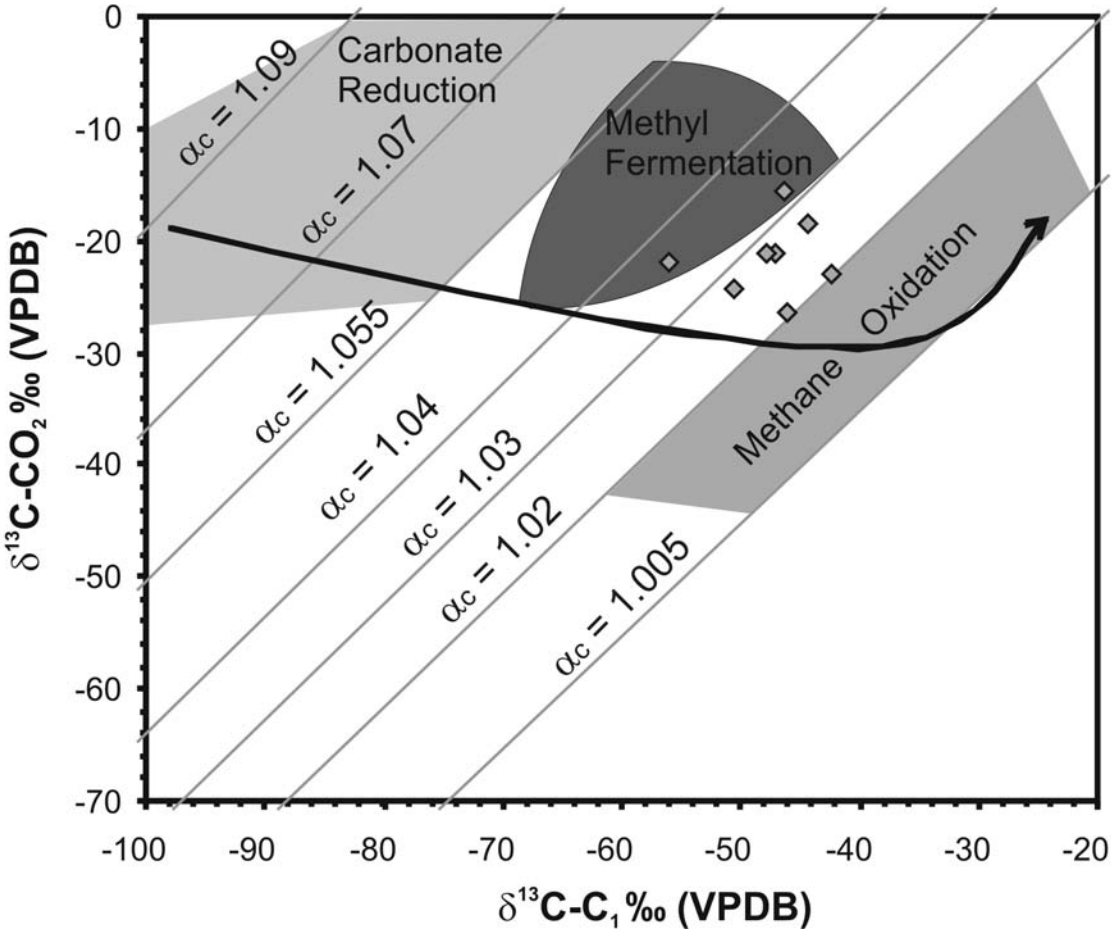

Figure 3-5. Relationship between the carbon isotopic ratios of methane and carbon dioxide for Lupin gas samples, compared with the oxidation trend and resulting oxidized methane field and established fields for bacteriogenic methane from carbonate reduction and methyl fermentation pathways (after *Whiticar et al. 1986*).

- Hydrogen isotope exchange over geologic time. Recent experiments indicate hydrogen isotope exchange may occur over geologic time (>350 Ma, *Sessions et al.*

2004). If the origins of the Lupin gas were metamorphic events, sufficient time would have elapsed for hydrogen isotope exchange to occur. However, given a methane to water fractionation factor ($\alpha_{O/W}$) of 0.692 (*Sessions et al. 2004*) and the current Lupin groundwater δ^2H ratio, methane δ^2H ratios would be much more enriched than actually observed (~ -250‰). Therefore, hydrogen isotope exchange over geologic time likely cannot account for the depleted δ^2H ratios.

This demonstrates that although the gas composition, carbon isotopic composition, and relative fractionation of carbon and hydrogen isotopes between the different gas species indicate gas of a thermogenic origin, the methane hydrogen isotopic data remain problematic. However, thermogenic gas generation at Lupin is reasonable given the geologic history of the area. About 2.8 Ga, the central Slave structural province was part of a marine accretionary margin and subject to proto-plate tectonic forces (*Kusky 1989*). At Lupin, amphibolite facies metamorphism (low-pressure, high-temperature) from multiple intrusions and metamorphic events (peaking 2.68-2.585 Ga) altered turbidite mudstones and greywackes to the crystalline rock types meta-greywacke/quartzite, phyllite and quartz-feldspar-gneiss (*King et al. 1988, Geusebroek and Duke 2004*). Proterozoic faulting (1.84-1.81 Ga), resulting in contact metamorphism, is the last dated metamorphic event in the area (*Geusebroek and Duke 2004*). The thermogenic gas component was likely derived from the regional metamorphic alteration of marine sediments (turbidites) into metaturbidites and amphibolitic gneisses. Organic carbon contents at Lupin range between 0.02 and 0.99 wt%, averaging 0.27 wt% (*L. Pratt, University of Indiana, personal communication*). Thus adequate carbon was available for thermogenic alteration. The original gases were generated and trapped in the meta-sediments during metamorphism. Graphitic carbon ($\delta^{13}C$: -22.62 and -27.1‰ VPDB) on fractures and bedding surfaces is a common occurrence in Lupin rock samples and is an inferred remnant of previously migrating hydrocarbon fluids. Bituminous rocks and oil-rich fluid inclusions have been found at other sites in the Canadian Shield, suggesting thermogenic gases may also be found at other Archean and Paleoproterozoic locations (*Petersilie and Sörensen 1970, Goodarzi et al. 1992, Mossman et al. 1993, Melezhik et al. 1999, Dutkiewicz et al. 2003*).

Various data suggest methane origins at the Lupin mine are not recent. The ^{14}C-DIC (dissolved inorganic carbon) from groundwater associated with the gas samples give ages of 20.5-26.8 ka (3.50±0.07 to 7.67±0.09 pMC), while analyses of ^{14}C-CH_4 (<0.3 to 0.7±0.1 pMC) suggests methane formed from an older carbon pool than datable by the radiocarbon methodology (50 ky). The ^{14}C data, combined with relatively low $\delta^{13}C$-CO_2 values (-15.7 to -26.4‰ VPDB), indicate the bacteriogenic methane component is not part of a modern process. Methane also correlates with He

and Ar concentrations (Figure 3-6A), which are significantly over-pressured, consistent with a geogenic source for these gases (e.g. *Ballentine et al. 2002, Kipfer et al. 2002*). Combined with the inferred metamorphic-thermogenic gas origin, this would suggest that gas has been present at this site for possibly billions of years.

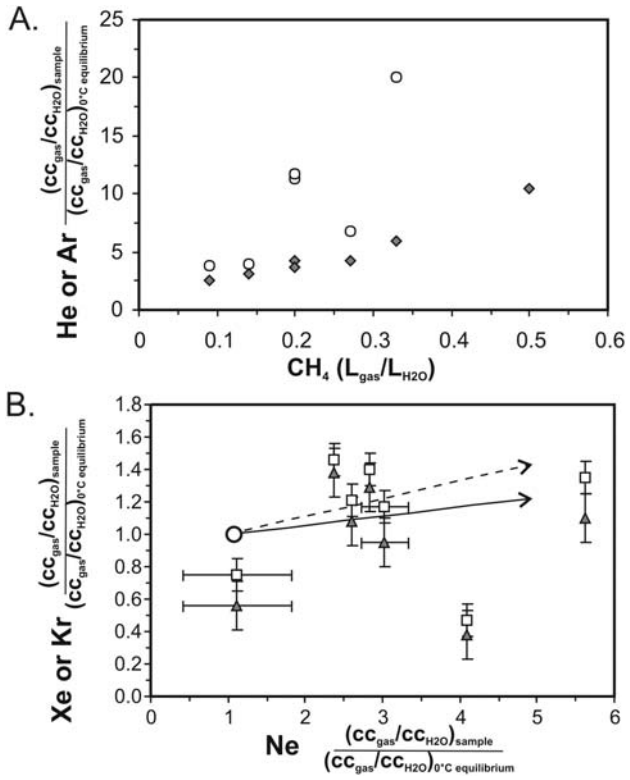

Figure 3-6. Results of noble gas analyses from samples collected at the Lupin mine, with all noble gas concentrations displayed as sample concentration normalized to fresh water concentrations at 0ºC. (A) Correlation of He*10,000 (open circles) and Ar (filled diamonds) versus methane. (B) Xe (open squares) and Kr (filled triangles) versus Ne, with the expected increased excess air trends with respect to Xe (dashed line) and Kr (solid line). Unlike Ar and He, the noble gases Ne, Kr, and Xe are largely unaffected by subsurface sources and in-situ production, with concentrations established from atmospheric concentrations and gas solubility during recharge (*Kipfer et al. 2002*). Displacement of samples below the excess air line is believed to be indicative of depressurization within the rock mass. Modified from Greene (*2005*).

3.4.2 Physical Nature of Gas

With the presence of methane gas at depth in a permafrost region, the potential for gas-hydrate formation was investigated. Temperatures (8-13 °C) and hydrostatic pressures (8,725-11,078 kPa) at the sampling depths are within the gas-hydrate stability field (Figure 3-7A). The physical setting in the area of the mine is therefore conducive to gas-hydrate formation. To determine the presence of gas hydrate, estimates of gas quantity are also required. However, it was not possible to quantify the

amount of gas in individual fractures. While average estimates of gas quantities were collected from each borehole (Appendix B-Table B-14), it was clear from video logging that gas was only produced from some fractures (Figure 3-7B). If only some fractures produce fluid, and only some fractures produce gas or gas and fluid, the concentration of gas produced by each borehole would be less than the amount in gas containing fractures. Certain boreholes (*1130-217, 1130-260*) were observed to produce significantly more gas than fluid prior to being sealed. Anomalous white chunks were also observed during borehole video logging, possibly indicative of methane hydrate; however it was not possible to collect samples for identification.

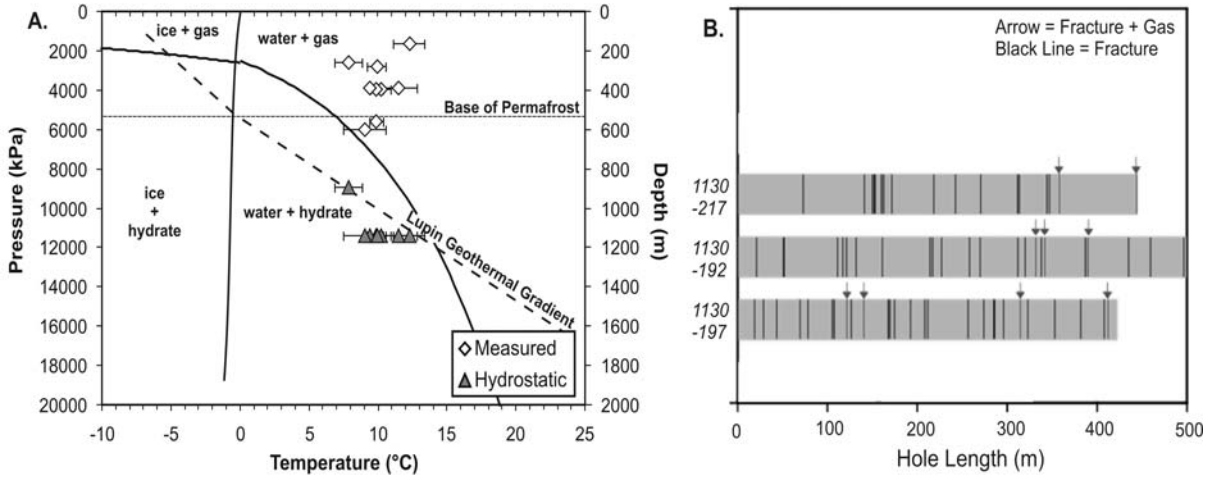

Figure 3-7. Potential for gas hydrate formation at Lupin. (A) Pressure-temperature fields for boreholes sampled at the 890 and 1130 m levels. Under hydrostatic conditions, gas hydrates are stable. Mine-induced depressurization has resulted in dissociation of gas hydrates. Maximum and minimum temperatures are represented by the error bars. (B). Results of borehole video survey for three boreholes, showing frequency of fractures and gas producing fractures. Measured gas concentrations are likely much lower than individual fracture concentrations.

During mining, the immediate area of the Lupin mine was drained (depressurized) to a depth of approximately 1500 mbgs. *In-situ* pressures measured along the 400 m-long tunnel at borehole collars have a significant range (1,550-5,930 kPa). At these pressures and the observed temperatures, gas hydrates would not be stable (Figure 3-7A). However, these *in situ* pressures are representative of only the most transmissive fractures in each borehole.

Pressures in gas-producing fractures are suspected to be greater than the measured *in-situ* pressure, a conclusion supported by noble gas data (*Greene 2005*). Low concentrations of Ne, Kr, and Xe relative to air-equilibrated water (Figure 3-6B) suggest a post-equilibrium process has affect gas

partial pressures. Gas equilibria in fluids are described by Henry's Law; temperature, pressure, and salinity all affect gas solubility (e.g. *Mazor 1972, Kipfer et al. 2002*). Generally, decreasing pressure or temperature, or increasing salinity, will result in decreasing gas solubilities, although the relative impact to individual noble gases varies (e.g. *Kipfer et al. 2002*). Compared with Ne, both Kr and Xe are significantly more sensitive to changes in temperature (e.g. *Mazor 1972*). However, concentrations of Ne, Kr, and Xe are all lower than expected (Figure 3-6B) and no relationship with salinity was observed (*Greene 2005*). Therefore, significant depressurization of the rock and water in fractures encountered by the boreholes would result in the observed noble gas separation (*Greene 2005*).

Short of visibly observing methane hydrate, identification of methane hydrate is often difficult without geophysical evidence. The presence or absence of hydrate is debated, even in areas where significant quantities of methane are extracted (e.g. *Collett and Ginsburg 1998*). After over thirty years of research, direct gas quantification of methane in marine hydrates has only recently been completed at two sites (*Dickens et al. 1997, Milkov et al. 2003*). At Lupin it was not possible to physically measure gas quantities within individual fractures, therefore the presence of gas hydrates can only be inferred from supporting physical and geochemical measurements.

Mine-induced depressurization would also cause dissipation of methane hydrates in fractures located near the mine or intersected by the drilled boreholes. When the pressures decrease within boreholes as they are drilled or opened for sampling, methane hydrate dissociation are expected to cause a decrease in temperature and a decrease in salinity (*Sloan 1998*). Substantial differences in measured salinity (2.2 g l^{-1} and 40 g l^{-1}) and temperatures (7.5-13.4 °C) were observed in eleven parallel boreholes sampled along a 400 m-long tunnel. Water temperatures varied over five years of study by more than 2.2 °C in five of the boreholes with a maximum variation of 3.5 °C (Figure 3-8, Table B-15).

The conclusion that gas hydrates are present at Lupin is supported by other geochemical data, including pressure, temperature, and salinity measurements, which have previously been utilized to determine the presence of gas hydrates (e.g. *Hesse and Harrison 1981, Wright et al. 1999, Tréhu et al. 2003*). Over the period of study, fluid temperatures generally decreased after drilling until the boreholes were sealed (Figure 3-8, Table B-15 in Appendix B). Fluid temperatures increased once boreholes were sealed, unless the boreholes were allowed to depressurize (Figure 3-8). Temperatures decreased during the study in the one borehole that was incompletely sealed (1130-267, Figure 3-8). During one experiment, several boreholes were allowed to completely depressurize over two days. Temperature decreased by up to 2 °C, while electrical conductivity decreased by up to 300 mS/m. All

of the trends described are consistent with the presence of methane hydrates, suggesting methane hydrates are present in the rock distally from the mine. Although mixing within boreholes may also explain these trends, the systematic nature of these trends within all of the boreholes is strong evidence to indicate the presence of methane hydrate.

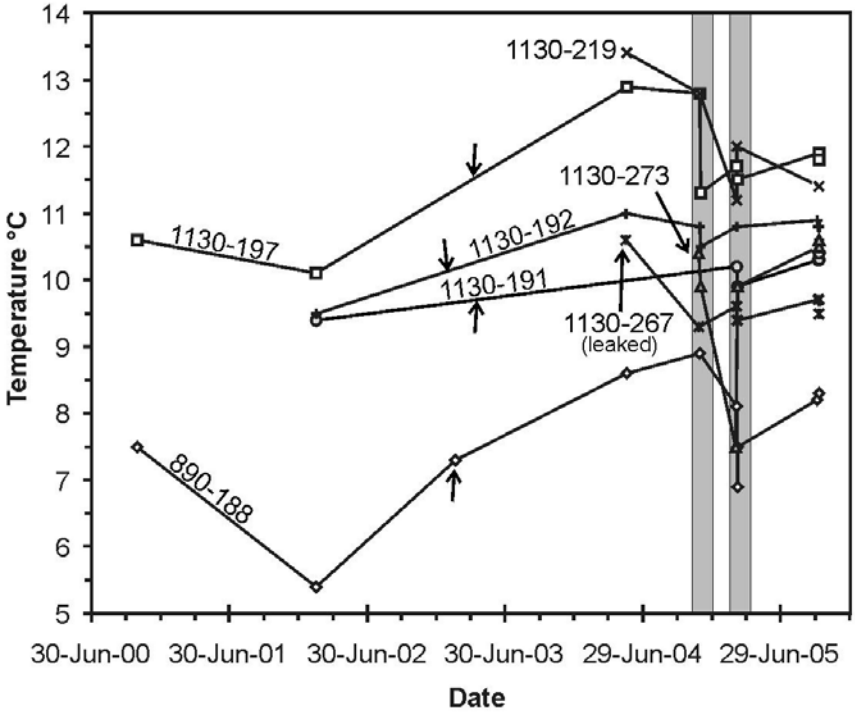

Figure 3-8. Lupin borehole temperature variation. Arrows indicate date boreholes were sealed. 1130-219 was sealed in May 2003, and 1130-273 was sealed in Feb. 2004. 1130-263 was sealed, but leaky. All boreholes except 267 and 273 were drilled in the 1990s. Grey shaded areas indicate periods when temperature measurements were taken before and after borehole depressurization. The final set of temperature measurements were taken at static conditions.

Evidence suggests marine methane hydrate releases occurred during Quaternary interstadials (*Kennett et al. 2000*), so hydrate stability at Lupin over the last 120 ky was evaluated. The effect of the glacial cycle to hydrate stability was examined with a combination of GSM and hydraulic modeling. Eight estimates of hydrate stability using subsurface temperature and pressure calculations were derived from a glacial systems model with different reconstructions constraining the possible climate ranges (*Tarasov and Peltier 2007*) (Figure 3-9). Up to four glacial advances and retreats are predicted to have affected the site over the last 120 ky (Figure 3-9h). Although permafrost stability fields are often reduced during glaciation by warm subglacial temperatures (e.g. *Tarasov and Peltier 2007*), the GSM results indicate the gas hydrate stability field actually increases. This is corroborated by hydraulic modeling, which suggests the effects of glacial pressures to subsurface hydrostatic

pressures are greatest when permafrost melts completely (Figure 3-10, *Lemieux et al. 2008*). All model simulations suggest gas hydrates have remained stable at the sampling depths, even in scenarios where permafrost melted completely.

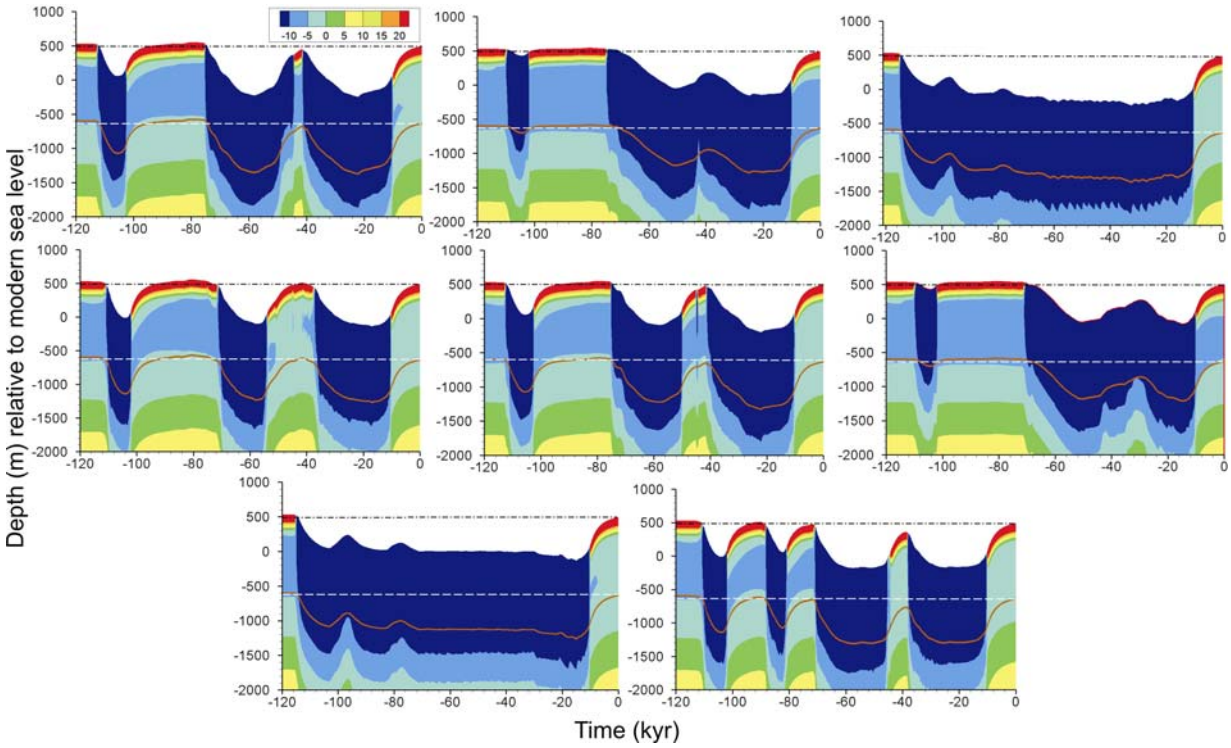

Figure 3-9. Results of glacial systems modeling of eight different climate scenarios. Contours show temperature with respect to methane hydrate pressure melting point over the last 120 ky at Lupin. Temperatures below zero (light green and blues) indicate hydrate stability. Elevation is shown with respect to modern sea level at 0 m. The changing land surface elevation due to isostatic loading and unloading of glacial ice is depicted. The black dash-dot line represents the modern land surface elevation. The 1130 m sampling depth is shown with respect to the modern land surface (dashed white line) and with respect to the isostatic land surface (solid red line). Isostacy results in a true sampling depth between these two lines. Methane hydrates were stable at the sampling depths throughout the Pleistocene for all modeled scenarios.

In areas currently affected by permafrost, gas hydrate stability throughout glacial cycles has important implications to subsurface hydraulic conditions. Similar to ice (e.g. *Burt and Williams 1976*), methane hydrates reduce porosity and permeability (e.g. *Kleinberg et al. 2003*). Thus even if permafrost melted sub-glacially, deep subsurface porosity and permeability would not necessarily increase substantially, depending on methane hydrate distribution. This would substantially limit the potential for deep sub-glacial recharge in areas with significant methane hydrate accumulations, even

in warm subglacial conditions. Because a core area of methane hydrate remains stable throughout the glacial cycles, methane release to the atmosphere would not likely occur.

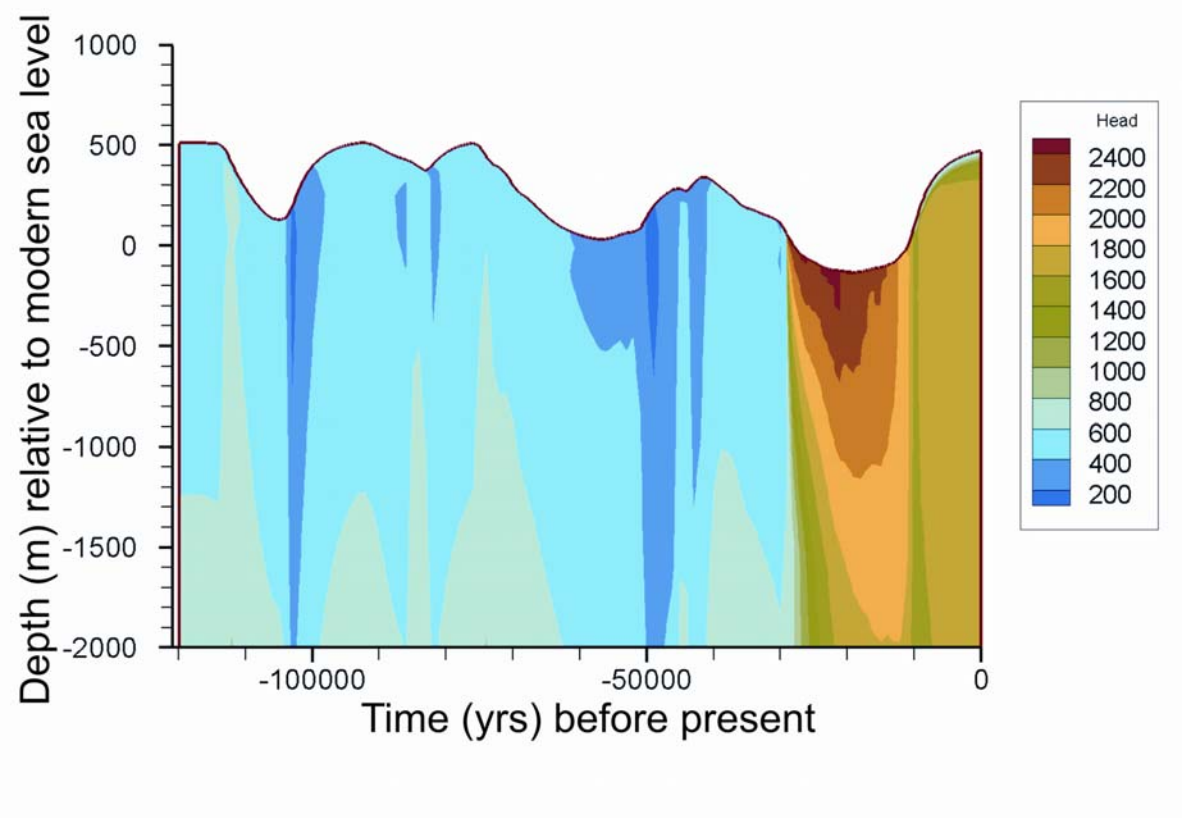

Figure 3-10. Predicted subsurface hydraulic conditions over the last 120 ky at Lupin, Nunavut. Glacial loading is indicated by a depressed land surface. In this modeled scenario, permafrost melted completely only during the last glacial advance, between ~30,000 and ~10,000 years ago. This results in drastically increased subsurface pressures.

3.5 Summary

The gases sampled at Lupin are unique compared with other crystalline shield gases. It is suggested the unique geochemical trends are evidence of thermogenic gas mixed with microbial gas, although methanogens were not found in parallel investigations. The site has considerable metasedimentary and higher-grade metamorphic rocks that were originally organic-rich mud rock. Gas genesis is tied to the metamorphic events, and suggests gas has been present between 1.81-2.68 Ga. It is possible thermogenic gas remnants may also occur at other Shield locations with a similar geologic setting. Radiocarbon and δ^{13}C-DIC support a conclusion the gases are not recently formed. The depleted δ^{2}H values are problematic to a thermogenic gas origin, but are not readily explained by other processes.

It is suggested the gases are present as gas hydrates in the absence of the mine. Hydrostatic pressures and temperatures are within hydrate stability fields. However, gas concentrations are lower than typical for gas hydrate formation, likely because the concentrations obtained were averages for entire boreholes. Borehole video surveys indicated gas was present only in certain fractures, where concentrations would be higher than the borehole average. Noble gas data and pressure measurements support a conclusion that de-watering of the mine depressurized the area near the mine, resulting in gas hydrate dissociation.

Although subsurface conditions have changed significantly over the last 120 ka, there is no evidence of large-scale methane releases at the Lupin site. Rather, during glacial advances, gas hydrate stability fields have actually increased in size without ever completely disappearing. Thus, gas trapped at Lupin during glacial cycles has not recently been an active part of the global carbon cycle.

The presence of gas hydrates over significant periods of time may significantly affect long-term stability scenarios for subsurface nuclear waste disposal in northern countries. If sufficient gas is present, gas hydrates may reduce subsurface permeability and porosity, similar to ice formation. This can then limit flow and hydraulic pathways, which could constrain the potential for subglacial recharge.

Chapter 4

Interglacial-Glacial Cycling and the Geochemical Evolution of Canadian Shield Groundwaters

4.1 Executive Summary

The results from the site characterization at Lupin and experimental column freezing experiments are compared with the geochemical data collected in the Canadian Shield over the past 25 years to investigate the relative influence of glaciers and permafrost on the evolution of Shield groundwaters. Several different geochemical indicators of fluids impacted by a freezing procees (either glacial or permafrost-related) were utilized: a comparison of Na/Cl and Br/Cl ratios, $\delta^{18}O$ and $\delta^{2}H$ values, and $\delta^{18}O$ values and Cl^- concentration. During freezing, fluids with different dominant cations follow distinctly different straight-line trends when Na/Cl and Br/Cl ratios are compared. Significantly, none of the freezing trends follow the trend hypothesized by *Herut et al.* (1990) for the evolution of seawater chemistry during freezing. Freezing experiments show a similar end-member would form during intrusion of glacial meltwater and *in situ* permafrost formation when $\delta^{18}O$ values and Cl^- are compared. The geochemical influence of a freezing process on fresh, brackish, and some saline fluids was identified at some, but not all Canadian Shield sites, regardless of site location with respect to permafrost. Significantly, physical and geochemical data do not support the formation of brines through any freezing process in the Canadian Shield, as hypothesized by *Starinsky and Katz* (2003). Rather on all diagnostic freezing plots, brines are an end-member, indicating a different evolutionary pathway. Significant depletions in ^{18}O with respect to modern precipitation, an indication of either glacial meltwater or a freezing process, were identified at depths of up to 1 km at some sites. The potential of this fluid to reach such depths could be attributable to artificial gradients and mixing, glacial recharge, permafrost or paleo-permafrost formation, methane hydrate or paleo-methane hydrate formation. With the current data-set, it was not possible to distinguish between the different scenarios.

4.2 Introduction

In the Canadian, Finnish, and Swedish concepts for long-term isolation of nuclear fuel waste, Deep Geologic Repositories may be constructed at depths of 500 to 1000 m within crystalline rock of the

Canadian and Fennoscandian Shields (e.g. *SKB 1992*, *TVO 1992*, *Posiva 2000*, *SKB 2004, NWMO 2005*). The large temporal scale (>1 million yrs) over which a safety case must demonstrate repository performance requires consideration of glacial and interglacial conditions which will alter the thermal, hydraulic and mechanical boundary conditions, potentially affecting engineered barrier systems, radionuclide mobility and groundwater flow system stability (*Vieno & Ikonen 2005*).

Very few investigations of groundwaters beneath deep permafrost (>300m) have been conducted. Most studies have been conducted in the sedimentary units of the Siberian Platform (e.g. *Pinnekar 1973*, *Alexeev and Alexeeva 2002*, *2003*, *Shouakar-Stash et al. 2007*). A series of gas hydrate research boreholes were also drilled in the sedimentary sequences of the Mackenzie Delta (*Dallimore et al. 1999, Dallimore and Collet 2005*). During freeze-thaw cycles in soils, solutes are concentrated in residual fluids, a process termed "freeze-out" in this chapter (*Mackay and Lavkulich 1974, Konrad and McCamon 1990*). *In situ* freezing may account for increased concentrations of carbonate, sulfate, sodium, magnesium, and calcium in groundwaters found in the Siberian Platform under thick permafrost, although other processes, including evaporation and halite dissolution, may have also influenced these groundwaters (*Alexeev and Alexeeva 2002, 2003, Shouakar-Stash et al. 2007*). Cold temperatures in permafrost create a strong thermodynamic sink that may allow advection of water (and solutes) against the concentration gradient, further complicating the freeze-out process (*Cary and Maryland 1972, Gray and Granger 1986, Qiu et al. 1988, Perfect et al. 1991*).

Numerous investigations have considered the origin and evolution of deep groundwaters in the Canadian Shield (Table 4-1, Figure 4-1). Some of the investigations discuss the potential effects of Pleistocene glaciations on deep groundwaters (*Herut et al. 1990, Douglas et al. 2000, Clark et al. 2000, Starinsky and Katz 2003*). However, only theoretical investigations have considered the impact of permafrost on deep groundwaters (*Lemieux 2006, Lemieux et al. 2008*). Groundwaters in the Canadian Shield with total dissolved solids (TDS) ranging between 2 and 340 $g \cdot l^{-1}$ are derived from water-rock interactions and mixing with meteoric waters (*Fritz and Frape 1982, Frape et al. 1984, Frape and Fritz 1987, Gascoyne et al. 1987, McNutt 1987, Kamineni 1987, McNutt et al. 1990*). Intrusion of sedimentary basin brines at the Shield margins has been noted (*Gascoyne et al. 1989*).

The purpose of this study was to investigate the effects of deep permafrost formation and dissipation during the Pleistocene glacial/interglacial cycle on deep groundwaters in the Canadian Shield. This comprehensive investigation of the Canadian Shield groundwater geochemical dataset will help constrain the role of the glacial/interglacial cycle and permafrost formation in influencing deep flow system evolution, fluid movement, and chemical evolution of groundwaters in Shield environments. Data from thirty-nine sites at twenty-four locations across the Canadian Shield were

compiled for this analysis (Table 4-1, Figure 4-1). Twelve sites are located within or near permafrost: Lac de Gras, High Lake, Lupin, and Meadowbank are currently located in continuous permafrost, Con, Giant, Thompson, Lynn Lake, Selbaie, Matagami, Norita, and Copper Rand are located in discontinuous, sporadic, or isolated permafrost. The other sites are not currently located within or near areas under the influence of permafrost. To investigate the potential effects of deep permafrost formation, experimental freezing data are examined, followed by data from sites currently located in permafrost regions. Fresh, brackish, and saline fluids from sites not currently located in permafrost regions will then be considered, followed by a detailed examination of highly saline and brine fluid data. Finally, the discussion will examine certain geochemical trends to determine the potential impact of freezing related process.

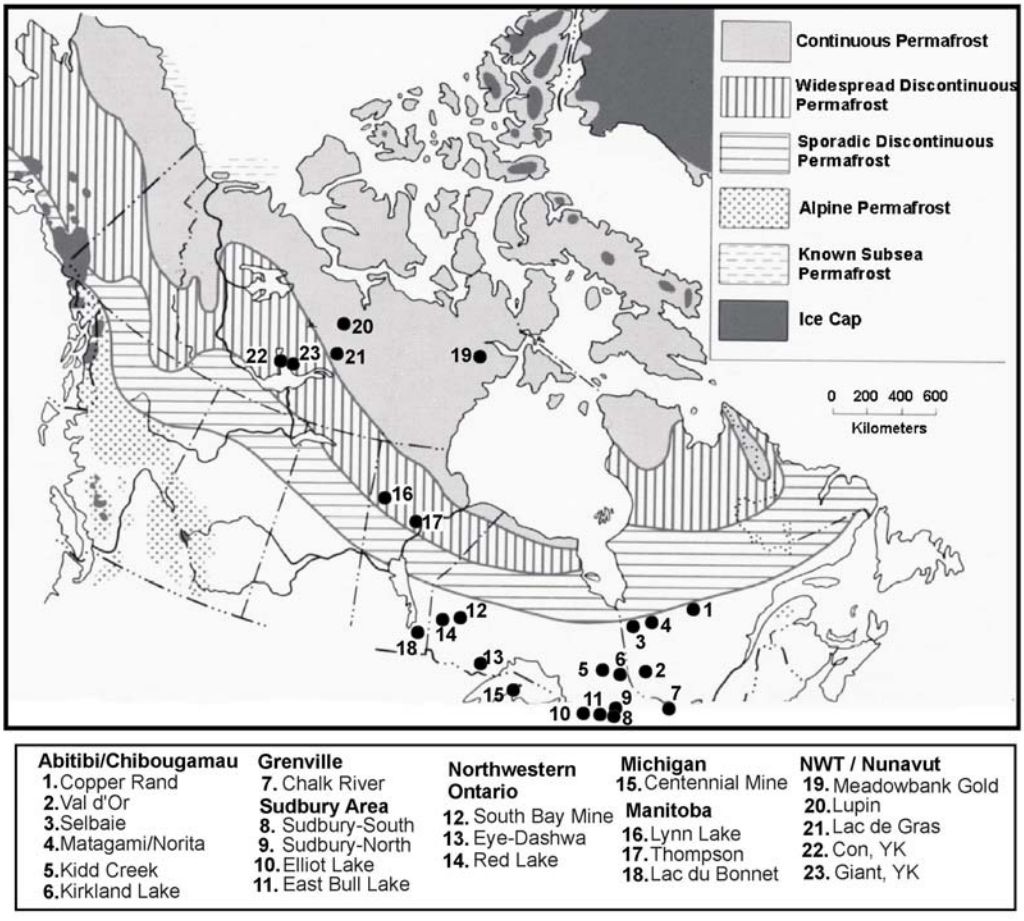

Figure 4-1. Map of Canadian Shield sample sites in relation to permafrost distribution. Permafrost map modified from Natural Resources Canada (*1995*).

Table 4-1. Host rock types and ages, water chemistry, and groundwater geochemical data sources for studies from the Canadian Shield.

Site	Permafrost?, depth (mbgs)	Rock types	Structural Province / Greenstone Belt	Sample Depth (m)	Water Types	TDS ($g \cdot l^{-1}$)	References***
NUNAVUT							
Lupin	Continuous, ~540	Metasediments, banded iron formation, quartzite, phyllite, amphibolite, Au	Slave	< 1300	Ca-Na-Cl, Na-Ca-Cl	8-40	Ruskeeneimi et al. 2002, 2004, Frape et al. 2004b, Stotler et al. 2007, Bakermans et al. 2008, This thesis
High Lake	Continuous	VMS, Metasediments, Cu, Zn	Slave/High Lake GB	45, 430	Ca-Mg-SO_4, Ca-Cl**		Gartner Lee 2005, 2006 a,b, Pfiffner et al. 2008, Stotler et al. 2008
Meadowbank	Continuous	Au		111-169	Na-SO_4, Ca-Mg-SO_4, Ca-Mg-Na-HCO_3-Cl, Ca-Mg-Cl	0.15-0.79	Golder 2004,
NWT							
Diavik	Continuous	Granite, Kimberlite	Slave	44-404	Na-Mg-Ca-HCO_3, Na-Mg-Ca-HCO_3-Cl, Na-Mg-Cl, Na-Mg-Ca-Cl	0.13-0.56	Blowes and Logsdon 1998
Yellowknife (Con Mine)	Extensive Discontinuous	Metabasalts in granodiorite, Au	Yellowknife GB / Slave Province	< 1600	Ca-Na-HCO_3, Na-Ca-Cl (d)	0.7-314	Frape and Fritz 1981, Fritz and Frape 1982, Frape et al. 1984, McNutt et al. 1984, MacDonald 1986, Frape and Fritz 1987, Kaufmann et al. 1987, Fritz et al. 1987, Sherwood-Lollar et al. 1988, Sherwood-Lollar et al. 1993a, Fritz et al. 1994, Bryant 1995, Douglas 1997, Bottomley et al. 1999, Douglas et al. 2000, Clark et al. 2000, Bottomley et al. 2002, Battye 2002, Frape et al. 2004, Bottomley and Clark 2004, Shouakar-Stash et al. 2005, Greene 2005, This Thesis,
Yellowknife (Giant Mine)	Extensive Discontinuous	Au	Slave	30-610	Ca-SO_4-Cl-HCO3, Ca-Mg-SO_4-HCO_3, Ca-Mg-SO_4, Ca-Na-SO_4, Ca-Mg-Na-SO_4-HCO_3, Ca-Mg-Na-SO_4, Ca-Na-SO_4-HCO_3, Ca-Na-SO4-HCO_3, Ca-Na-SO4-Cl, Na-Ca-SO_4-Cl-	0.7-80	Frape and Fritz 1981, Frape et al. 1984, MacDonald 1986, Frape and Fritz 1987, Sherwood-Lollar et al. 1988, 1993a, Fritz et al. 1994, This Thesis,

Site	Permafrost?, depth (mbgs)	Rock types	Structural Province / Greenstone Belt	Sample Depth (m)	Water Types	TDS ($g \cdot l^{-1}$)	References***
					HCO_3, Ca-Na-Cl		
MANITOBA							
Thompson	Sporadic Discontinuous	Quartzites, granite gneiss, schist, peridotite, Ni	Thompson Nickel GB	100-1500	Na-HCO_3, Na-SO_4-HCO3-Cl, Na-HCO3-Cl, Mg-HCO_3, Ca-SO_4, Ca-Na-Cl, Ca-Cl (d)	0.5-325	Frape and Fritz 1981, Fritz and Frape 1982, Frape et al. 1984, McNutt et al. 1984, Frape and Fritz. 1987, Kaufmann et al. 1987, Sherwood-Lollar et al. 1988, 1993a, Fritz et al. 1994, Bottomley et al. 1994, Bryant 1995, Frape et al. 2004, Bottomley and Clark 2004, This Thesis,
Lynn Lake (SGM Fox Mine)	Sporadic Discontinuous			61-792	Ca-HCO_3, Ca-Mg-SO_4, Mg-SO_4, Ca-SO_4, Ca-Cl	1.2-21.5	Frape and Fritz 1981, Fritz et al. 1994, This thesis
Lac du Bonnet (Whiteshell-URL)	None at present	Granitic gneiss	Superior	2.1-1098	Na-Ca-Cl-SO_4	0.22-33	Gascoyne et al. 1987, Purdy 1989, Frape et al. 2004, Gascoyne unpubl. data
MICHIGAN							
Keweenaw (Centennial Mine)	None at present	Basalts, tholeitic, conglomerates		2100-2800	Ca-Cl	326-406	Kelly et al. 1986
ONTARIO							
Red Lake (Campbell, Dickenson)	None at present	Mafic volcanics, ultramafics, metavolcanics, metasediments, granitic plutons	Birch-Uchi Lake GB	640, 660, ??	Mg-Ca-Na-SO_4-Cl*, Ca-Na-Cl	0.8*, 190	MacDonald 1986, Bottomley et al. 1994, Fritz et al. 1987, Sherwood Lollar et al. 1988, 1993b,
Atikokan (Eye-Dashwa)	None at present	Granodiorite-Granitic pluton	Superior	4-1050	Ca-Cl, Ca-SO_4, Ca-Cl-SO_4, Ca-HCO_3, Ca-Na-HCO_3, Na-HCO_3, Mg-HCO_3, Ca-Mg-HCO_3, Ca-Na-Mg-HCO_3, Ca-Na-Cl, Ca-Na-SO_4-HCO_3-Cl, Ca-Na-HCO_3-Cl	0.03-40	Dicken et al. 1984, Gascoyne et al. 1987, Franklyn thesis, Franklyn et al. 1991, This Thesis, Gascoyne unpubl. data,
Elliot Lake (Panel, Stanleigh, Dennison)	None at present	Huronian metasediments (conglomerate, quartzite, argillite), U		381-960	Na-Ca-Cl, Ca-Cl, Ca-Na-SO_4*, Ca-Na-Cl	2.1-50	MacDonald 1986, Fritz et al. 1987, Sherwood Lollar et al. 1988, 1993b, Bottomley et al. 1994, This Thesis
East Bull Lake (EBL)	None at present	Gabbro and anorthosite		0-836	Ca-HCO_3 (s) mixing to Na-Cl (d)	0.08-4.3	Kamineni 1987, McNutt et al. 1987, Gascoyne et al. 1987, Bottomley et al. 1990, Bottomley et al. 1994, Frape et al. 2004,
Sudbury – North (Creighton, Fraser,	None at present	Mafic intrusive (Norite)	Superior	152-1600	Ca-Na-SO_4-HCO_3, Ca-Na-SO_4-Cl-HCO_3, Na-Cl-	0.11-254	Frape and Fritz 1982, Fritz and Frape 1982, Frape et al. 1984, McNutt et al. 1984,

Site	Permafrost?, depth (mbgs)	Rock types	Structural Province / Greenstone Belt	Sample Depth (m)	Water Types	TDS ($g \cdot l^{-1}$)	References***
Garson, Lockerby, North, Onaping, Strathcona, Victor, Dowling Wells)					HCO_3, Mg-Ca-SO_4, Na-Cl, Ca-Na-Cl, Ca-Cl		Frape and Fritz 1987, Kaufmann et al. 1987, Sherwood-Lollar et al. 1988, Sherwood-Lollar et al. 1993b, Bottomley et al. 1994, Fritz et al. 1994, Bryant 1995, Frape et al. 2004, Bottomley and Clark 2004, Shouakar-Stash et al. 2005, This thesis
Sudbury – South (Copper Cliff South, Copper Cliff North)	None at present	Mafic intrusive (Norite)	Superior	121-1219	Ca-Cl, Ca-Mg-SO_4, Ca-Na-Cl-SO4	0.26-257	Frape and Fritz 1982, Frape et al. 1984, McNutt et al. 1984, Frape and Fritz 1987, Sherwood-Lollar et al. 1988, 1993b, Bottomley et al. 1994, Doig 1994, Fritz et al. 1994, Montgomery 1994, Bryant 1995, Sherwood-Lollar et al. 2006, This thesis
South Bay (Selco)	None at present	Felsic volcanics	Superior	15-595	Ca-Na-HCO_3, -Cl, Ca-HCO_3, Ca-HCO3-SO_4, Ca-SO_4 (0-320m) Ca-Na-SO_4, Ca-Na-Cl (595m)	0.05-7.9	Frape and Fritz 1981, Fritz and Frape 1982, MacDonald 1986, Fritz et al. 1994
Kirkland Lake (Macassa, Lakeshore)	None at present	Conglomerate, greywacke, tuff, syenite	Superior / Abitibi GB	61-1966	Ca-Mg-Na-SO_4, Ca-Mg-HCO_3, Ca-Mg-HCO_3-SO_4, Ca-Mg-Na-HCO_3, Ca-Mg-Na-HCO_3-SO_4 Nitrate	0.5-14.8	MacDonald 1986, Bottomley et al. 1994
Timmins (Kidd Creek)	None at present	Mafic and felsic metavolcanics, diorite	Superior / Abitibi GB	610*, 1402-1616	Na-Ca-Cl*, Ca-Cl	1.4*, 88-129	Bottomley et al. 1994, Doig 1994, Montgomery 1994, Bryant 1995, Westgate 1998, Sherwood Lollar et al. 2002
Chalk River	None at present	Metasedimentary gneiss, qtz. Monzonite, gneiss	Grenville	341-576	Na-Cl, Na-HCO_3	0.2-0.7	Gascoyne et al. 1987
QUEBEC							
Chibougamau (Copper Rand Mine)	Isolated	Meta-anorthosite, Cu-Au	Superior / Chibougamau-Abitibi GB	640, 869	Ca-Na-Cl, Ca-Cl	326-406	Guha and Kanwar 1987
Matagami / Norita	Isolated	Mafic volcanic and ultramafics	Superior / Abitibi GB	?-670?	Shallow: Ca-Na-Mg-HCO_3, Ca-Mg-SO_4, Ca-SO_4 Deep: Ca-Cl, Ca-Na-Cl	0.5-240	Frape and Fritz 1987, Jones 1987, Sherwood-Lollar et al. 1988, 1993a,b, Fritz et al. 1994, Frape et al. 2004, This thesis

Site	Permafrost?, depth (mbgs)	Rock types	Structural Province / Greenstone Belt	Sample Depth (m)	Water Types	TDS ($g \cdot l^{-1}$)	References***
Selbaie	Isolated	Felsic-intermediate volcanics, metasediments overly, Zn-Cu-Ag	Superior / Abitibi GB	60-240	Ca-Mg-HCO_3, Mg-Ca-HCO_3	0.4	MacDonald 1986, Fritz et al. 1994
Val d'Or (Sigma, Lamaque)	None at present	Mafic - Felsic volcanics,	Superior / Abitibi GB	73, 116, 1737	Ca-HCO_3-SO_4 (s), Ca-Cl (d)	0.4-66	MacDonald 1986, Fritz et al. 1987, Sherwood-Lollar et al. 1988, Sherwood-Lollar et al. 1993a, Fritz et al. 1994, This thesis

*Bottomley et al. 1994 significantly lower TDS than previous studies, ** Samples contaminated by drilling salt, *** $\delta^{37}Cl$ values reported in Kaufmann et al. 1987 have been shown to be incorrect by Bryant 1995.

4.3 Freeze-out Experiments

It has been suggested a comparison of the Na/Cl and Br/Cl ratios can differentiate between fluids affected by the freeze-out and evaporation processes (*Herut et al. 1990*, see Chapter 2). To further investigate this process, freeze-out experiments were conducted on seawater (*Herut et al. 1990*) and crystalline shield fluids of differing compositions (*Zhang and Frape 2002*). These experiments show that as freezing progressed (and residual fluid concentration increased), the Na/Cl ratio varied inconsistently with increasing residual fluid concentration for both Na- and Ca- dominated fluids (Figure 4-2). However, there was very little change in the Na/Cl ratio during the freezing process for several Na- dominated fluids, including seawater (Figure 4-2). Br/Cl ratios did not change in the Na-dominated fluids, and generally increased with increasing residual fluid concentration in Ca-dominated fluids, although this was not always the case (Figure 4-2). Anionic dominance (Cl vs. SO_4) did not affect Na/Cl or Br/Cl ratios significantly during freezing (Figure 4-2). When the resulting trends are plotted on a Na/Cl vs. Br/Cl graph (Figure 4-2), Na-dominated fluids have a near-vertical slope, Ca-dominated fluids have a slightly positive slope, and fluids with no Na-Ca dominance are expected to plot along a slope between pure Na- and Ca- dominant fluids, regardless of the initial anionic composition. The different slopes for the fluids with different cation dominance are a result of the precipitation of calcite ($CaCO_3$), ikaite ($CaCO_3 \cdot 6H_2O$), and gypsum ($CaSO_4 \cdot 2H_2O$) during freezing and the relative influence on solute ratios (*Zhang and Frape 2002*). None of the freezing experiments, including the seawater freezing experiment, follow the hypothesized and extrapolated "seawater freezing line" which was previously published (Figure 4-2, *Herut et al. 1990, Starinsky and Katz 2003*). For comparison, as seawater evaporation proceeds, the Na/Cl ratio decreases steadily while Br/Cl increases (Figure 4-2, *McCaffrey et al. 1987*).

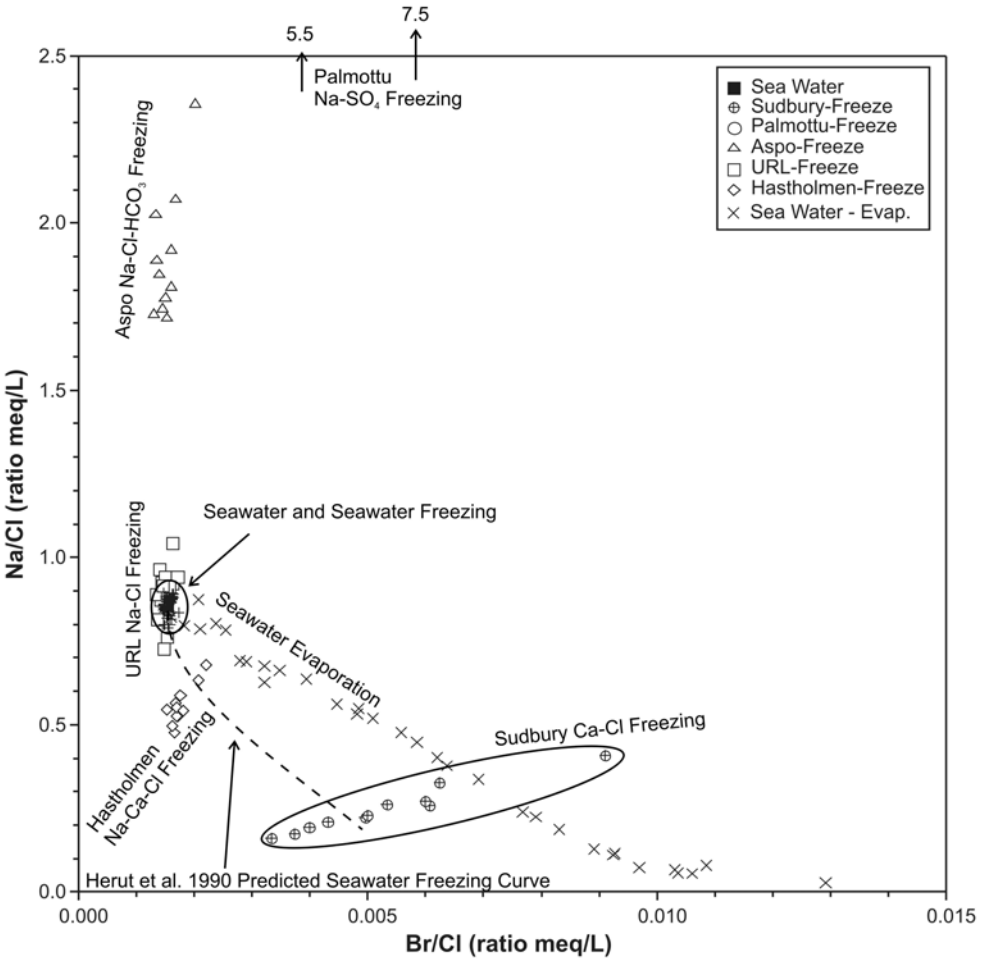

Figure 4-2. Na/Cl vs. Br/Cl ratios from freezing experiments. The seawater evaporation trend (*McCaffrey et al. 1987*) and predicted seawater freezing curve (*Herut et al. 1990*) are included for reference. Seawater freezing data plot in a small area (*Herut et al. 1990*). Shield groundwater freezing data from Zhang and Frape (*2002*).

Fluid freezing has a definable impact on the stable isotopic (δ^2H, $\delta^{18}O$) composition of the water and ice (e.g. *Mackay and Lavkulich 1974, Souchez and Jouzel 1984, Zhang and Frape 2002*). Regardless of ionic composition, fluids freeze such that the relationship between δ^2H and $\delta^{18}O$ ratios falls along lines with slopes between 4.32 and 7.44 (Figure 4-2, *Souchez and Jouzel 1984, Zhang and Frape 2002*). Fluid freezing therefore results in a slope that is distinct from the slope (8.0) for the global meteoric waterline (GMWL) (*Craig 1961*). The first ice that forms will have substantially higher δ^2H and $\delta^{18}O$ signatures than the original fluid, but will progressively become lighter as freezing progresses, until the final ice and residual fluid both have much lower δ^2H and $\delta^{18}O$ than the original fluid. Therefore, the stable isotopic compositions of fluids are a potentially powerful tool for determining whether a fluid has been affected by freezing. Stable isotopic compositions of fluids were not measured by Herut et al. (*1990*).

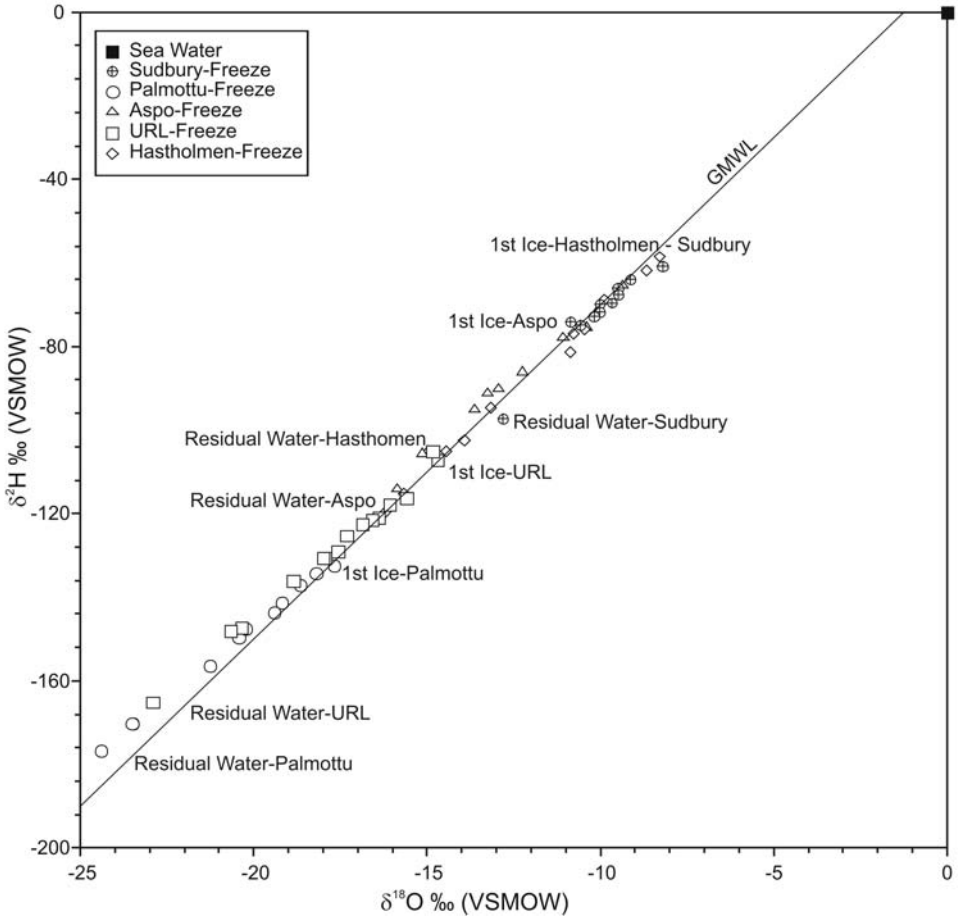

Figure 4-3. Relationship between δ^2H and $\delta^{18}O$ during freezing of shield groundwaters. The first ice is heavier than the initial fluids, with residual fluids significantly lighter. The slopes are slightly less than the GMWL. Shield ground-water freezing data from Zhang and Frape (*2002*).

Utilizing a comparison of $\delta^{18}O$ and chloride, Douglas et al. (*2000*) and Clark et al. (*2000*) proposed a three end-member mixing scenario which could account for the observed chemistry at the Con Mine within the zone of discontinuous permafrost. The three end-members were attributed to: (1) fresh, modern meteoric recharge, (2) glacial recharge, with a saline component leached from bedrock after glacial meltwater emplacement, and (3) geologically old Shield brine (Figure 4-4). The results of freezing experiments (Figure 4-4) suggest an *in situ* freeze-out process related to permafrost formation would result in a fluid end-member with a similar composition as the glacial meltwater component after dissolving residual salts described by Douglas et al. (*2000*) and Clark et al. (*2000*). During freeze-out, a nearly straight-line relationship exists between $\delta^{18}O$ and chloride for each of the fluids when plotted on a semi-log plot, with $\delta^{18}O$ ratios decreasing as chloride concentrations increase (Figure 4-4).

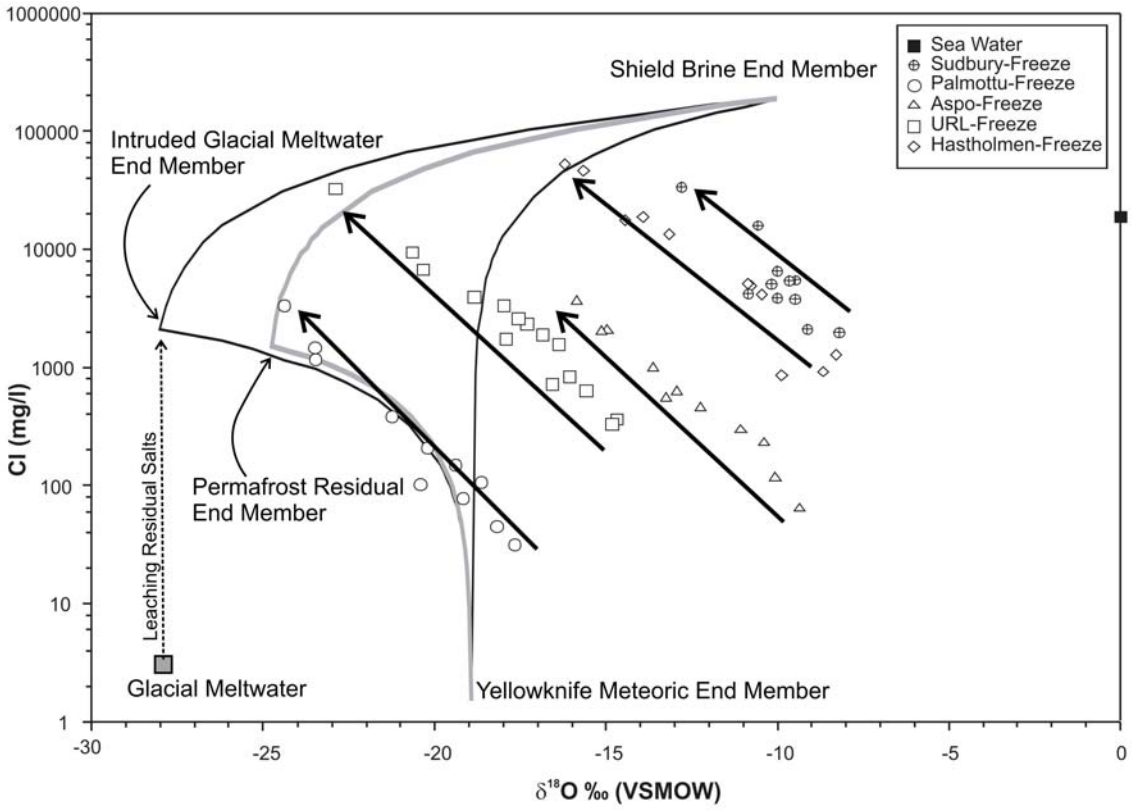

Figure 4-4. Relationship between $\delta^{18}O$ and Cl during freezing. Arrows indicate progression during freezing. Shield groundwater freezing data from Zhang and Frape (*2002*). The three end-member mixing diagram modified from Douglas et al. (*2000*) and Clark et al. (*2000*), shows the similarity between permafrost and intruded glacial meltwater end-members.

In the rest of this chapter, the experimental evidence will be compared with field data collected across the Canadian Shield. In the next two sections, fluids with salinities less than 50 $g \cdot L^{-1}$ will be considered. The more concentrated fluids will be examined separately.

4.4 Sites in Permafrost Regions

Of the twelve sites located within or near areas of permafrost (Figure 4-1), Lupin and Lac de Gras are the only sites currently located within continuous permafrost with extensive data available (subpermafrost samples are only available from Lupin); Con and Giant are within the zone of extensive discontinuous permafrost; Thompson and Lynn Lake are located in sporadic discontinuous permafrost; and Copper Rand (Chibougamau), Matagami, Norita, and Selbaie are in or very near the zone of isolated permafrost.

At Lupin, water samples collected were brackish to saline (8 - 40 g L^{-1}). The relationship of Na/Cl and Br/Cl ratios from subpermafrost waters is similar to what would be expected for freezing of Na-Ca fluids, between the Ca- and Na- dominated freezing trends (Figure 4-5A). Permafrost waters were contaminated by drilling brine, which was reflected in Na/Cl and Br/Cl ratios (Figure 4-5A). Permafrost, basal permafrost, and subpermafrost waters generally fall along either the global or local meteoric waterlines, but the relationships between δ^2H and $\delta^{18}O$ indicate permafrost water samples have been affected by freezing, with subpermafrost waters a depleted end-member (Figure 4-5C).

The Lac de Gras samples were collected within a hydrothermal talik. Taliks, unfrozen channels or conduits through the permafrost, can form due to thermal, chemical, or pressure conditions (*van Everdingen 1976*). A hydrothermal talik indicates the unfrozen conduit was formed by fluid at any temperature above the freezing-point depression of water (*van Everdingen 1976*). Typically, hydrothermal taliks are found beneath large water courses with mean annual bottom temperatures that remain above freezing. Because taliks remain unfrozen, they can provide hydraulic pathways through an otherwise impermeable permafrost barrier. Pressure data are currently unavailable from within hydrothermal taliks, therefore the potential for flow through this permafrost feature is not well understood. The Lac de Gras geochemical results were reported by Blowes and Logsdon (*1997*) (Table A-3 in Appendix A).

Comparing the relationship between Na/Cl and Br/Cl ratios (Figure 4-5A), the most dilute Lac de Gras talik waters have significant scatter, but the more concentrated waters (~0.30-0.56 g·L^{-1}), which have no dominant cation, follow a trend similar to freezing of Ca-dominated fluids, while more dilute fluids follow Na-dominated fluid freezing trends (Figure 4-5B). The relationships between the stable isotope composition (δ^2H, $\delta^{18}O$) of Lac de Gras talik water samples are consistent with freezing (Figure 4-5C). Comparing the relationships between Cl^- and $\delta^{18}O$ (Figure 4-5D), Lac de Gras talik waters follow the straight-line trend identified in the freeze-out experiments (Figure 4-4), further evidence these fluids were affected by a freezing process.

Very little hydrogeochemical data is available from other taliks in the Canadian Shield. Recently, limited talik samples have been collected within the Canadian Shield at two other sites: High Lake (*Gartner Lee 2004, 2005a,b*), and Meadowbank (*Golder 2004*). These talik waters are dilute (< 1 g L^{-1}), and are chemically and isotopically distinct from modern surface waters (*Gartner Lee 2004, 2005a,b, Golder 2004*). Unfortunately, no permafrost or subpermafrost water samples are available from these sites for further chemical comparison, so the interactions between hydrothermal talik fluids and permafrost, and talik fluids and sub-permafrost waters, remain poorly understood.

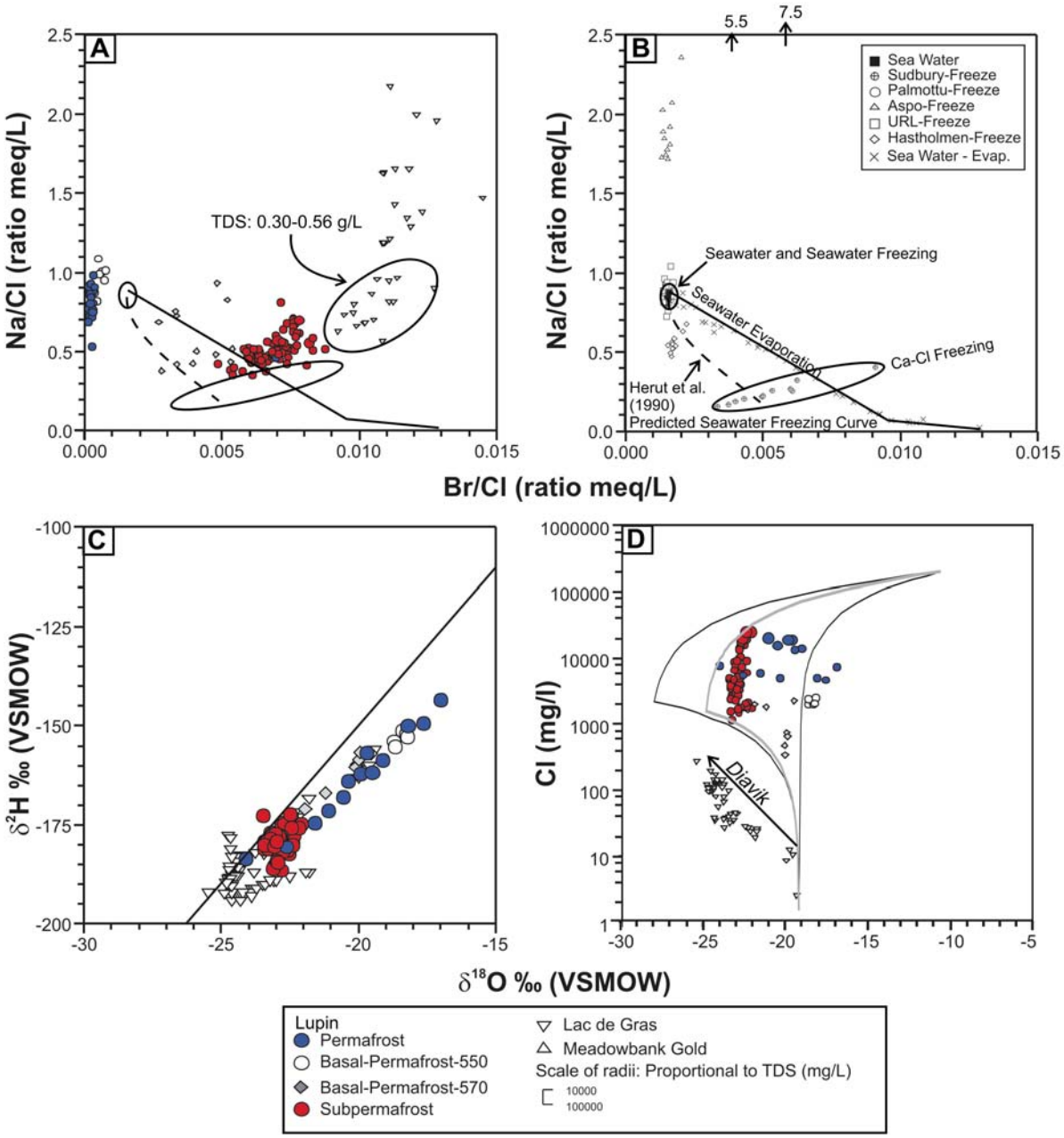

Figure 4-5. Geochemical relationships of groundwaters sampled from Canadian Shield sites located in continuous permafrost regions. (A) A comparison of Na/Cl and Br/Cl ratios (B) Freezing and evaporation experiment results for reference (references cited in Figure 4-2) (C) Isotopic relationships between δ^2H and $\delta^{18}O$. (D) The relationship between Cl and $\delta^{18}O$, with three end-member mixing diagram from Figure 4-4 for reference. Symbols scaled relative to TDS, brines are the largest symbol, brackish and fresh waters are the smallest, and saline fluids are in-between. Data are from references listed in Table 4-1.

Geochemical evidence for freezing is also found at sites located in regions of discontinuous permafrost (Con, Giant). The relationships between Na/Cl and Br/Cl ratios in fresh, brackish, and

some saline samples from Con and Giant (Figure 4-6A) are similar to the freezing experiment trends for Na- or Na-Ca- dominant fluids (Figure 4-6B). The stable isotope composition ($\delta^{18}O$, $\delta^{2}H$) of these same waters are significantly depleted relative to modern precipitation, but plot near the GMWL (Figure 4-6C). Chloride and $\delta^{18}O$ (Figure 4-6D) do not follow the exact straight-line trend exhibited in freezing experiments or Lac de Gras waters, due to three-end member mixing with deeper brines (*Douglas et al. 2000, Clark et al. 2000*). The brines sampled at these sites show evidence of mixing with the freezing-impacted fluids; the most concentrated samples are also the most enriched in ^{18}O (Figure 4-6D). Only a minor number of brine samples from Con fall along the GMWL (Figure 4-6C). These samples have tritium and are less concentrated than other brines from these sites, indicating mixing with modern waters was most likely a result of mining operations (*Frape et al. 1984*). This is supported by increasing tritium in many of the less concentrated brines closer to the meteoric waterline intersection.

Sites located in regions of sporadic permafrost (Thompson, Lynn Lake) are similar to sites located in regions of discontinuous permafrost. The relationships between Na/Cl and Br/Cl ratios in fresh, brackish, and some saline samples from Thompson (Figure 4-7A) are similar to the freezing experiment trends for Na- or Na-Ca- dominant fluids (Figure 4-7B). However, Thompson brines do not show similarities with this trend (Figure 4-7A). Generally Thompson fresh, brackish, and saline fluids plot near mean precipitation for the Thompson area and along the GMWL, but the brines are enriched in ^{2}H relative to the GMWL (Figure 4-7C). The relatively few fresh, brackish, and saline samples are scattered when the relationships between Cl and $\delta^{18}O$ are compared, and it is not possible to determine if the samples follow a three end-member mixing pattern (Figure 4-7D).

None of the geochemical trends identified in the freezing experiments were observed in samples from Matagami/Norita (Figure 4-7), located near the zone of isolated permafrost, indicating waters were not significantly impacted by the freezing process. Despite this, borehole water temperatures of 5-10°C were noted at 2 km depth, less than expected considering the geothermal gradient and modern mean atmospheric temperatures (*Jones 1987*). The sample population was not large enough at the Selbaie or Copper Rand mines to determine potential impacts of the glacial-interglacial cycle.

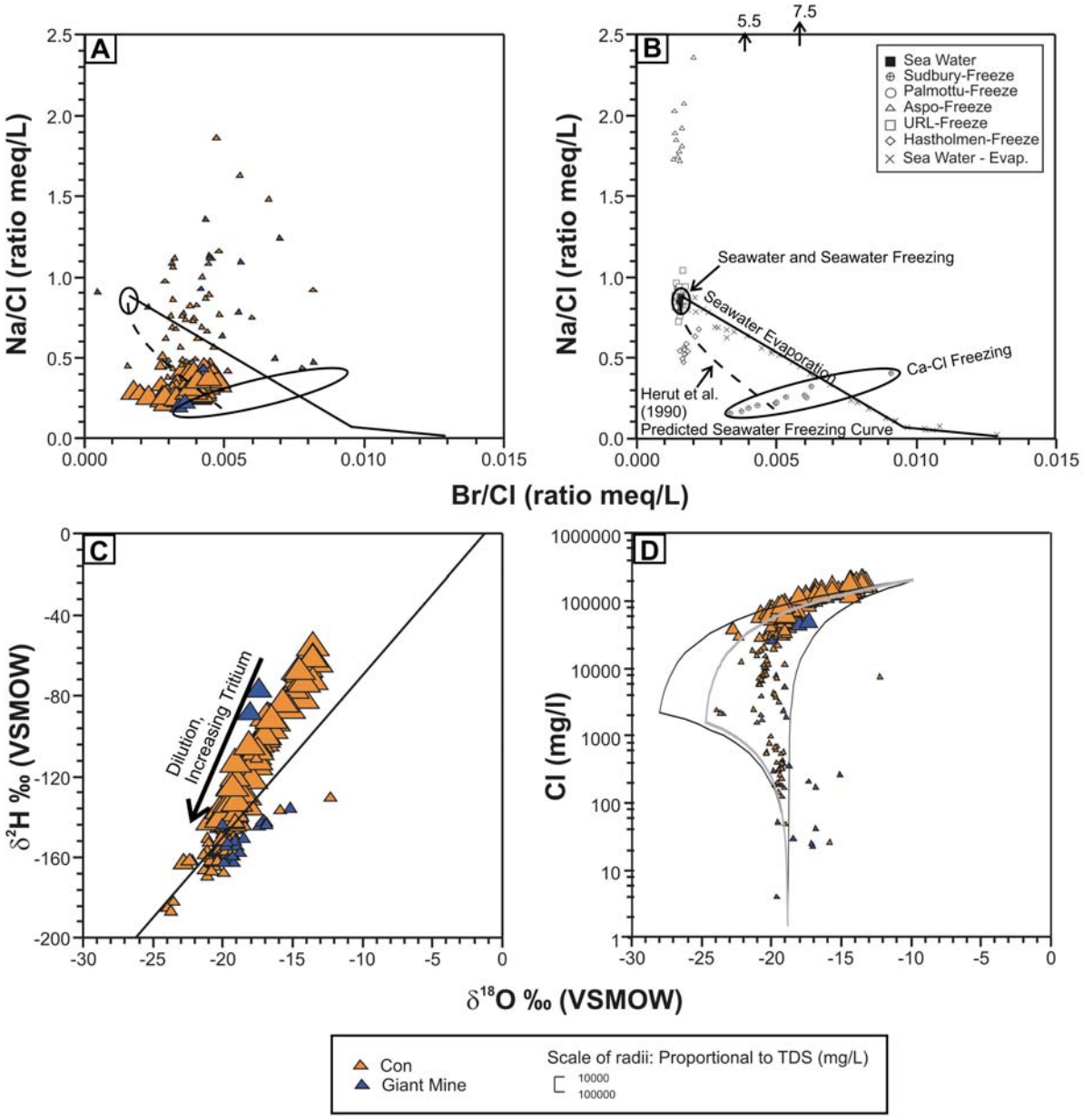

Figure 4-6. Geochemical relationships of groundwaters sampled from Canadian Shield sites located in discontinuous permafrost regions. (A) A comparison of Na/Cl and Br/Cl ratios (B) Freezing and evaporation experiment results for reference (references cited in Figure 4-2) (C) Isotopic relationships between δ^2H and $\delta^{18}O$. (D) The relationship between Cl and $\delta^{18}O$, with three end-member mixing diagram from Figure 4-4 for reference. Symbols scaled relative to TDS, brines are the largest symbol, brackish and fresh waters are the smallest, and saline fluids are in-between. Data are from references listed in Table 4-1.

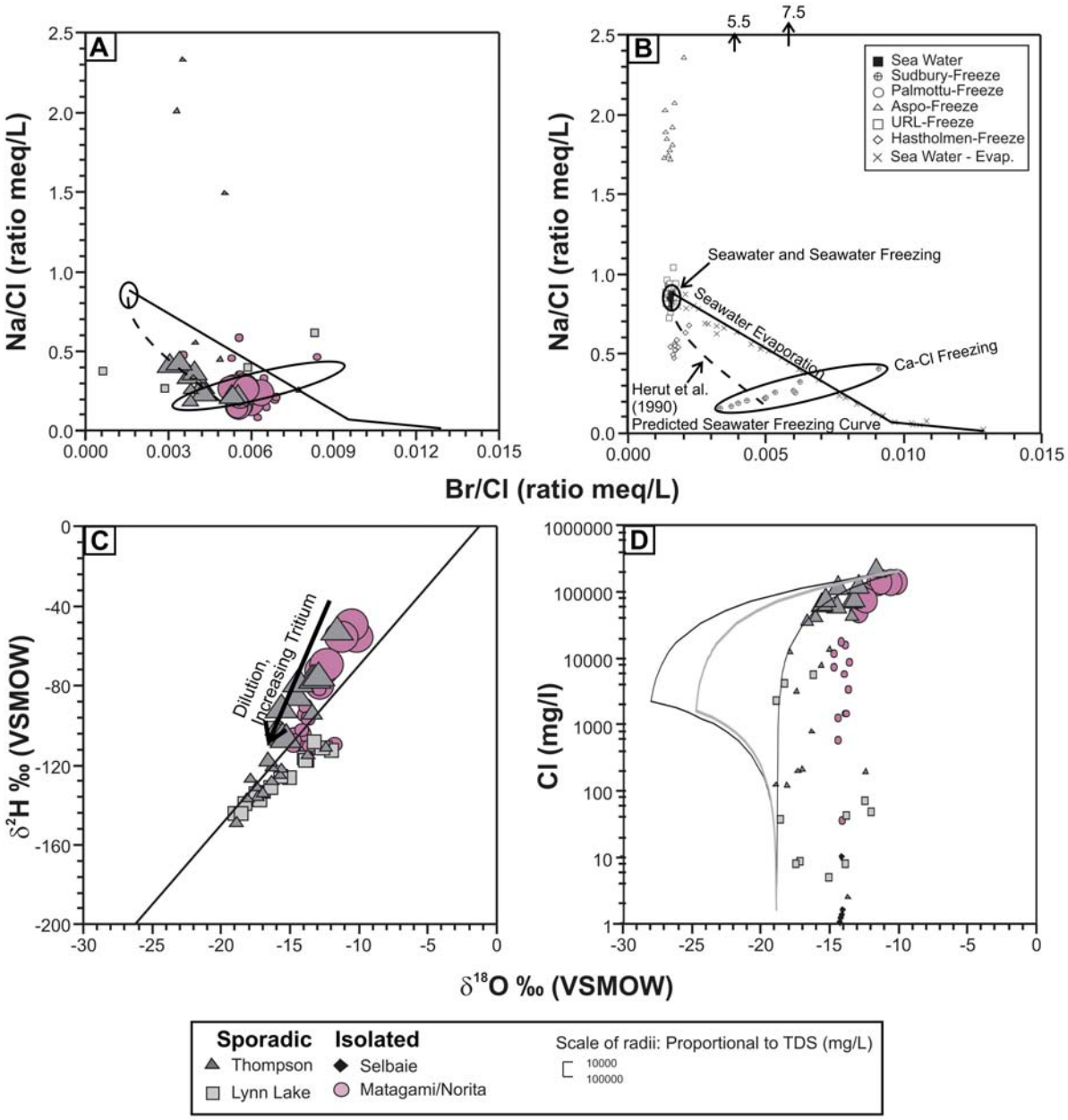

Figure 4-7. Geochemical relationships of groundwaters sampled from Canadian Shield sites located near sporadic and isolated permafrost regions. (A) A comparison of Na/Cl and Br/Cl ratios (B) Freezing and evaporation experiment results for reference (references cited in Figure 4-2) (C) Isotopic relationships between δ^2H and $\delta^{18}O$. (D) The relationship between Cl and $\delta^{18}O$, with three end-member mixing diagram from Figure 4-4 for reference. Symbols scaled relative to TDS, brines are the largest symbol, brackish and fresh waters are the smallest, and saline fluids are in-between. Data are from references listed in Table 4-1.

Overall, from the surface, $\delta^{18}O$ becomes depleted to a minimum between 700 and 1100 mbgs, then begins to become more enriched again with depth (Figure 4-8A). This pattern is most

pronounced at the Con, Giant, and Thompson Mines. However, the data are too sparse at most sites to better observe this relationship. On the other hand, Cl^- concentrations increase with depth (*Frape et al. 2004*).

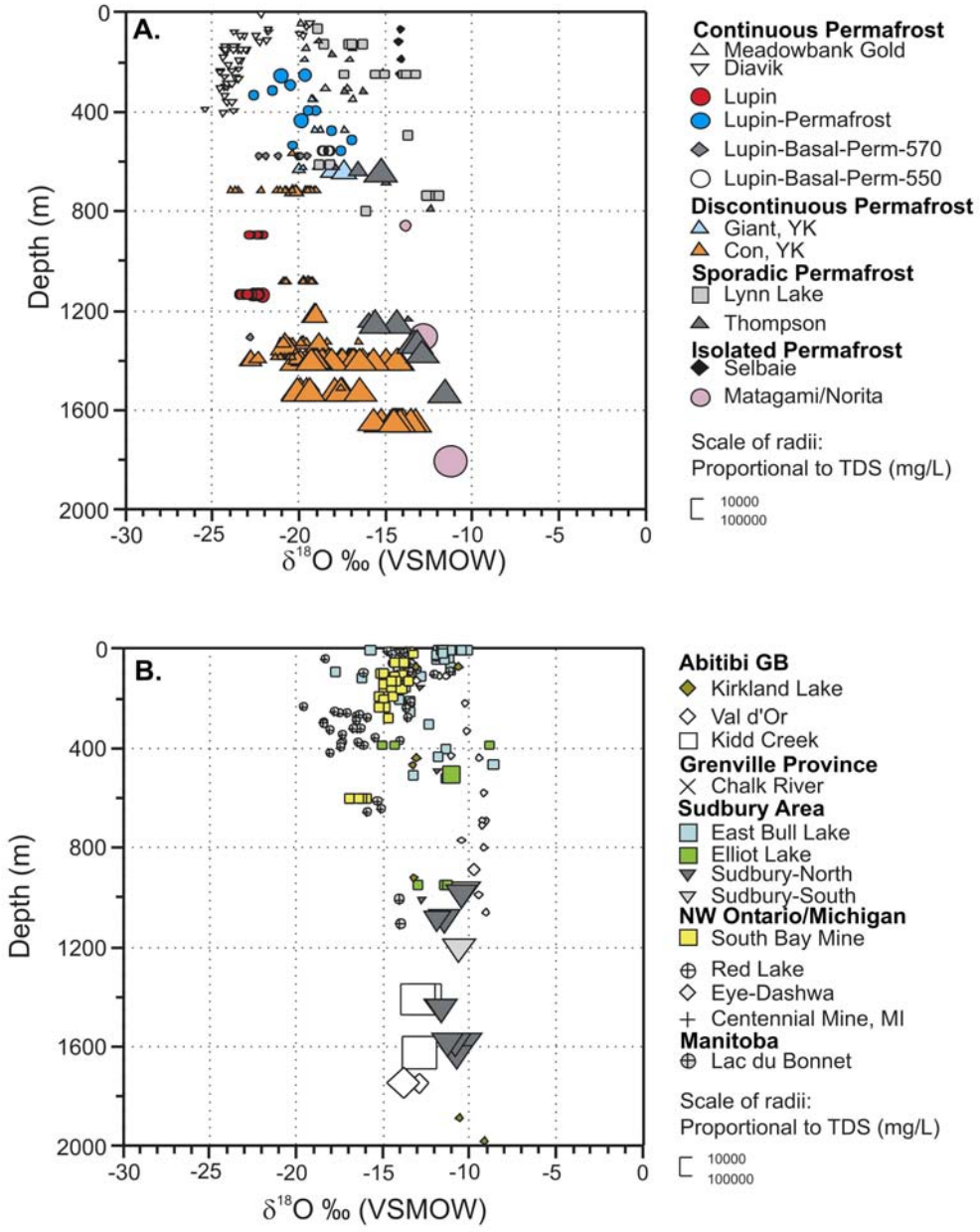

Figure 4-8. Relationship of $\delta^{18}O$ with depth in groundwaters for Canadian Shield sites located in or near permafrost areas (A) and sites not currently located within permafrost areas (B). Symbols are scaled relative to TDS, with brines the maximum size, brackish and fresh waters the smallest size, and saline waters in-between. Data are from various sources cited in Table 4-1.

The freezing experiments and groundwater investigations in areas of permafrost described provide guidelines for determining whether a fluid at a site has been impacted by freezing. On a plot comparing Na/Cl and Br/Cl ratios, freezing of Na-dominated fluids result in a vertical trend and freezing of Ca-dominated fluids result in a supra-horizontal trend, contrary to the evaporation and hypothesized seawater freezing trends, which are sub horizontal (Figure 4-2). Freezing of fluids also results in an initial enrichment of δ^2H and $\delta^{18}O$ in ice (Figure 4-3). As freezing progresses, ^2H and ^{18}O continue to enrich in the ice until both ice and residual fluid are significantly depleted relative to the initial fluid (Figure 4-3). This fluid-ice mixture evolves along a line with a slope slightly less than the GMWL (Figure 4-3). During freezing, solutes concentrate in residual fluids, resulting in a straight-line relationship between chloride and $\delta^{18}O$ on a semi-log plot (Figure 4-4). Mixing, as at the Con Mine, result in a curved line on the same plot, (Figure 4-7C). In groundwaters at permafrost sites, $\delta^{18}O$ values with depth follow a curve that has a minima significantly less than modern precipitation between two relative maxima at shallow and deeper parts of the sites (Figure 4-8A). At sites with enough data, $\delta^{18}O$ minima is reached between 700 and 1100 mbgs (Figure 4-8A). This may indicate the depth to which waters affected by a freezing process or processes related to the glacial-interglacial cycle (surficial freezing, *in situ* freezing, or glacial intrusion) have affected groundwaters.

4.5 Sites Not Currently in Regions of Permafrost

4.5.1 Fresh, Brackish, and Saline Fluids

Effects of the glacial/interglacial cycle on Canadian Shield sites not currently located in or near permafrost are investigated because a shallow southern Canadian Shield permafrost regime has been proposed by glacial climate models (Figure 4-9, *Tarasov and Peltier 2007*) in advance of and following the continental glaciations that covered the entire Canadian Shield at times during the Pliocene and Pleistocene (Figure 4-10, *Dyke and Prest 1987, Dyke et al. 2002*). Geochemical trends similar to those identified in the freezing experiments are evident in some fresh, brackish, and saline fluids at some individual sites, but are not ubiquitous.

When Na/Cl and Br/Cl ratios are compared with increasing salinity, data from most sites are scattered and only a couple of sites follow trends similar to the freezing experiments (Figure 4-11A). For instance, fluids from Val d'Or, Quebec show a slightly shallower trend than was observed for freezing of Ca-dominated fluids (Figure 4-11B). In brackish and saline fluids from Lac du Bonnet and Eye-Dashwa, Na/Cl ratios decrease, but Br/Cl ratios increase slightly in Lac du Bonnet samples, and decrease slightly in Eye-Dashwa samples (Figure 4-11B). This is similar to freezing experiment trends for Na-dominated and Na-Ca fluids, respectively (Figure 4-11C). However, there was more

scatter for both Lac du Bonnet and Eye-Dashwa samples, which was not observed in freezing experiments or fluids from permafrost sites with "freezing" trends. In Kirkland Lake samples, Na/Cl increases with increasing salinity, but Br/Cl does not change (Figure 4-11B), similar to freezing of Na-dominated fluids (Figure 4-11C).

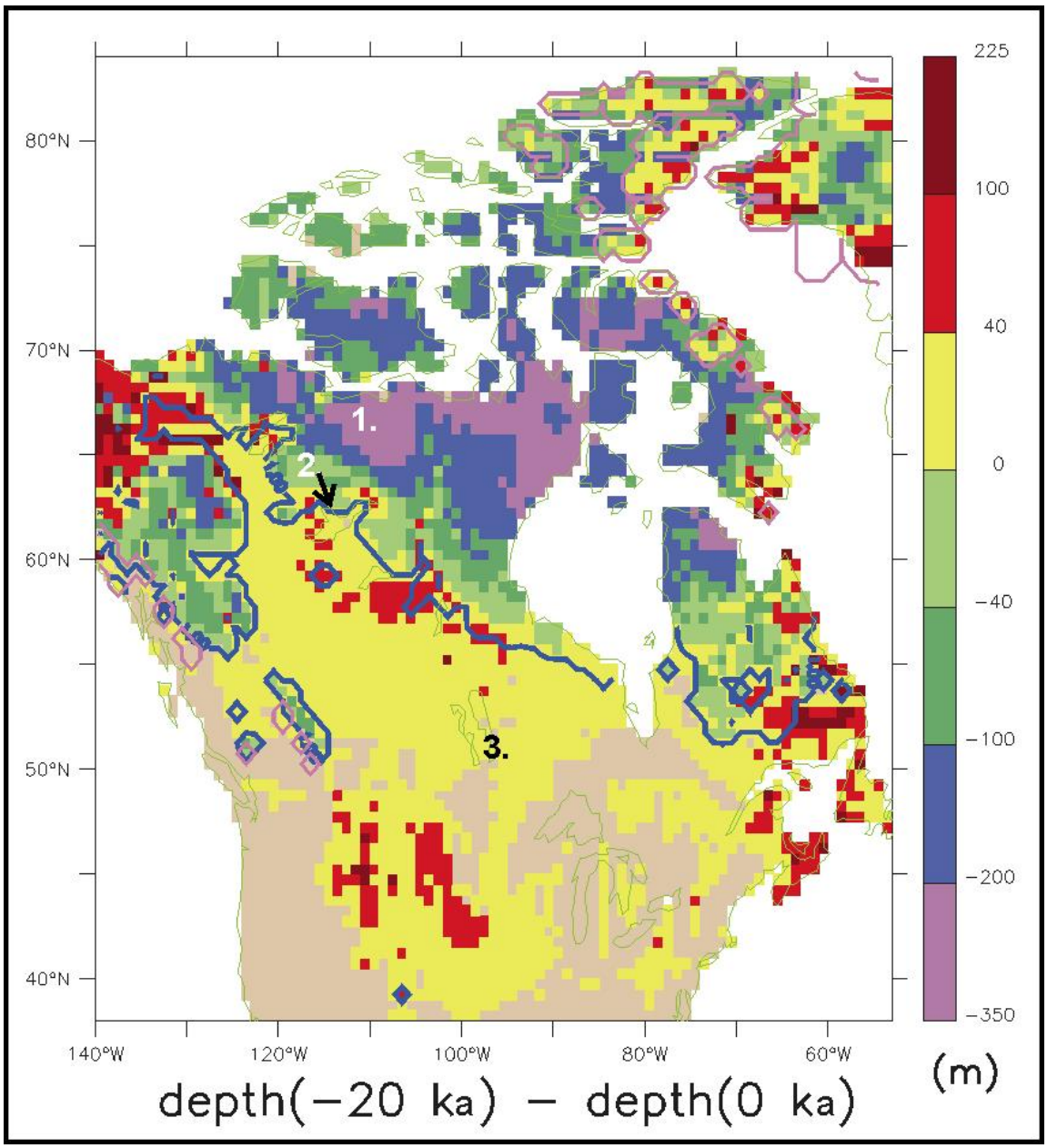

Figure 4-9. Ensemble mean permafrost depth difference between the Last Glacial Maximum (~20 ka) and present. Dark blue contour represents modern continuous permafrost extent. Dots next to numbers represent locations of: 1-Lupin, 2-Con, 3-URL. From Tarasov and Peltier (*2007*).

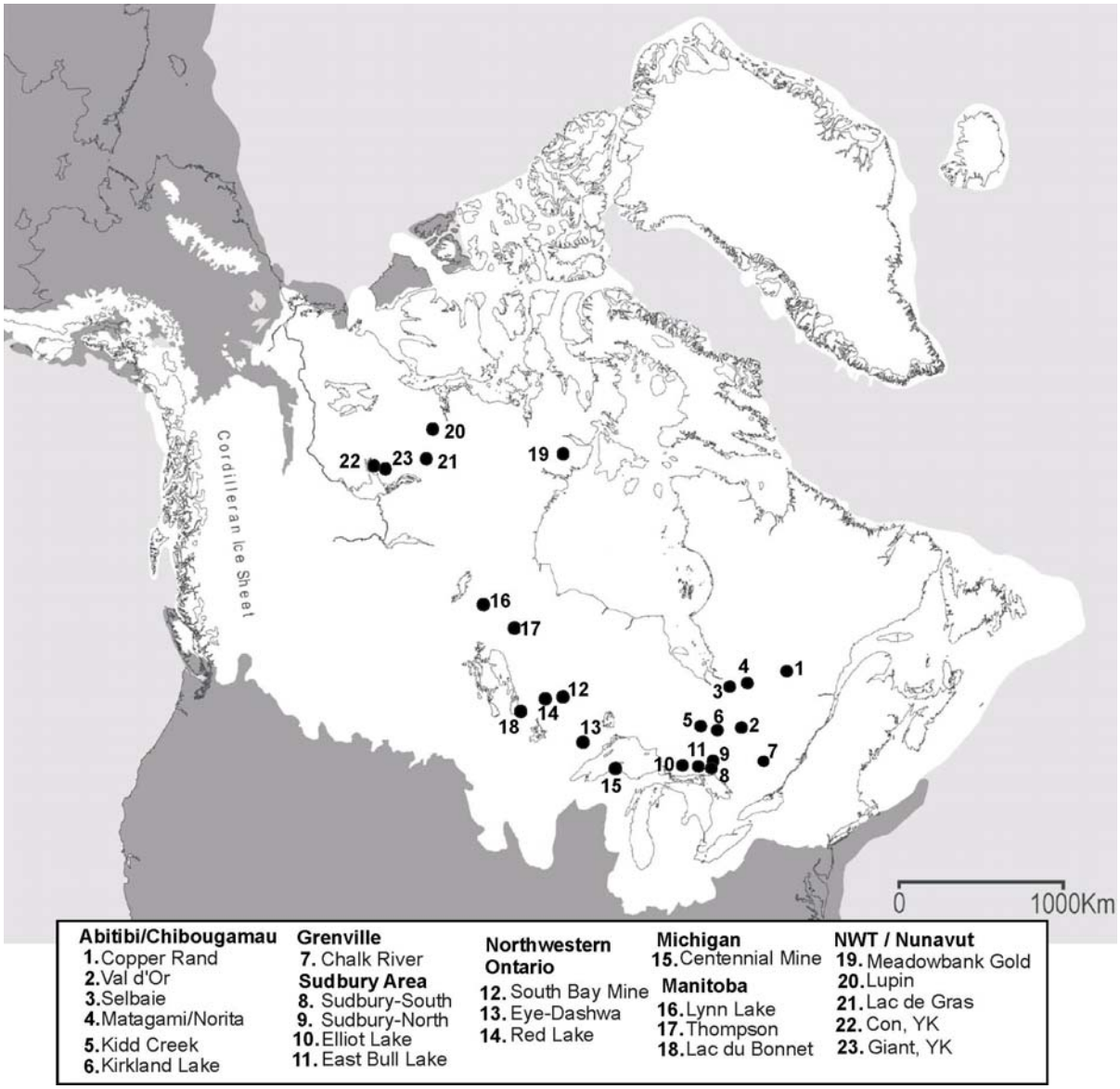

Figure 4-10. Wisconsinan glacial extent (white) and exposed, unglaciated land (dark grey) in North America and Greenland at the last glacial maximum. Modern land and water features are designated with lines for reference. From Dyke et al. (*2002*).

Fresh, brackish, and saline Canadian Shield groundwaters generally plot along the GMWL (with brines plotting above) (Figure 4-12A). At most sites not currently located in or near permafrost, δ^2H and $\delta^{18}O$ values are equal to or higher than modern precipitation. δ^2H and $\delta^{18}O$ values are lower than modern precipitation only at Lac du Bonnet, South Bay Mine, Elliot Lake, and East Bull Lake (Figure 4-12 B and C). The relationships between Cl and $\delta^{18}O$ also indicate samples from Lac du Bonnet, South Bay Mine, Elliot Lake, and possibly East Bull Lake and Eye-Dashwa waters were affected by the freezing process, as $\delta^{18}O$ values decrease with increasing salinity in fresh, brackish,

and some lower salinity fluids (Figure 4-13). However, there is significant scatter in the East Bull Lake and Eye-Dashwa trends, indicating mixing with other fluids also occurs.

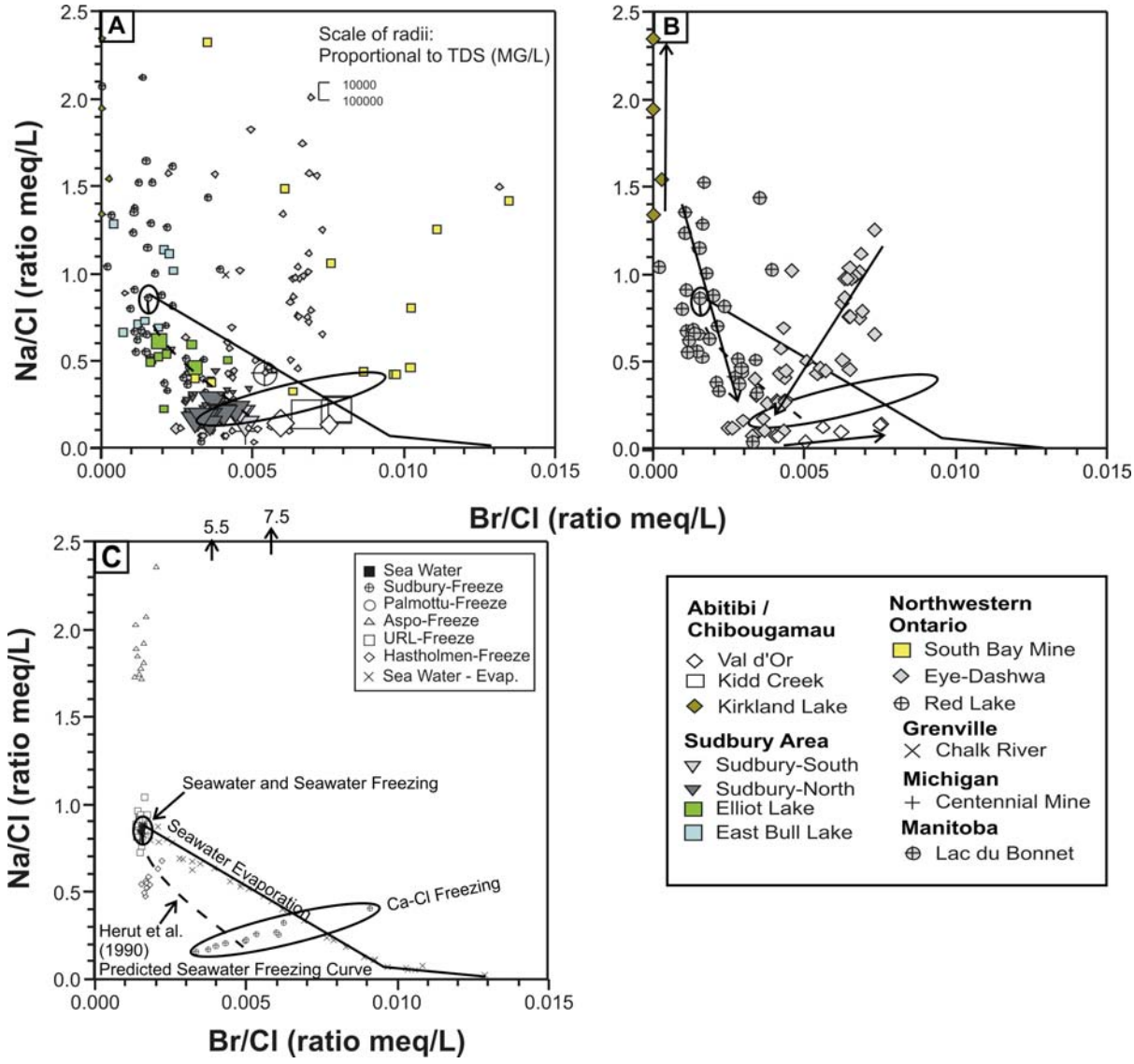

Figure 4-11. Relationship of Na/Cl and Br/Cl ratios for Canadian Shield groundwater samples from sites not located in or near permafrost. (A) Displays results from all sites, with data symbols scaled relative to TDS. Brines are the largest symbol, brackish and fresh waters are the smallest, and saline fluids are in-between. (B) Displays only results from brackish and saline results from Eye Dashwa and Lac du Bonnet, and all results from Val d'Or and Kirkland Lake. (C) Freezing and evaporation experiment results for reference (references cited in Figure 4-2). All data are from references listed in Table 4-1.

Therefore, there are some fresh, brackish, and saline waters at several sites not currently located in or near permafrost with geochemical characteristics indicative of glacial/interglacial impacts to groundwaters. At East Bull Lake and Eye-Dashwa, the lowest $\delta^{18}O$ values are found in

relatively shallow, fresh waters (Figure 4-8B). The observed relationship between Cl and $\delta^{18}O$ at these two sites (Figure 4-13) could indicate an intruded glacial meltwater which acquired less salinity from the rock and had intruded to shallower depths than at other sites, such as the Con mine (Figure 4-8A, *Clark et al. 2000, Douglas et al. 2000*). On the other hand, the similarity with freezing experiments and field data from Lac de Gras suggest the geochemical trend at these sites could also be the result of an *in situ* permafrost freeze-out process. The shallow, depleted $\delta^{18}O$ values in fresh waters would then be consistent with a more shallow permafrost depth in these southern sites than in the Con mine area, as indicated by glacial climate modeling (Figure 4-9, *Tarasov and Peltier 2007)*.

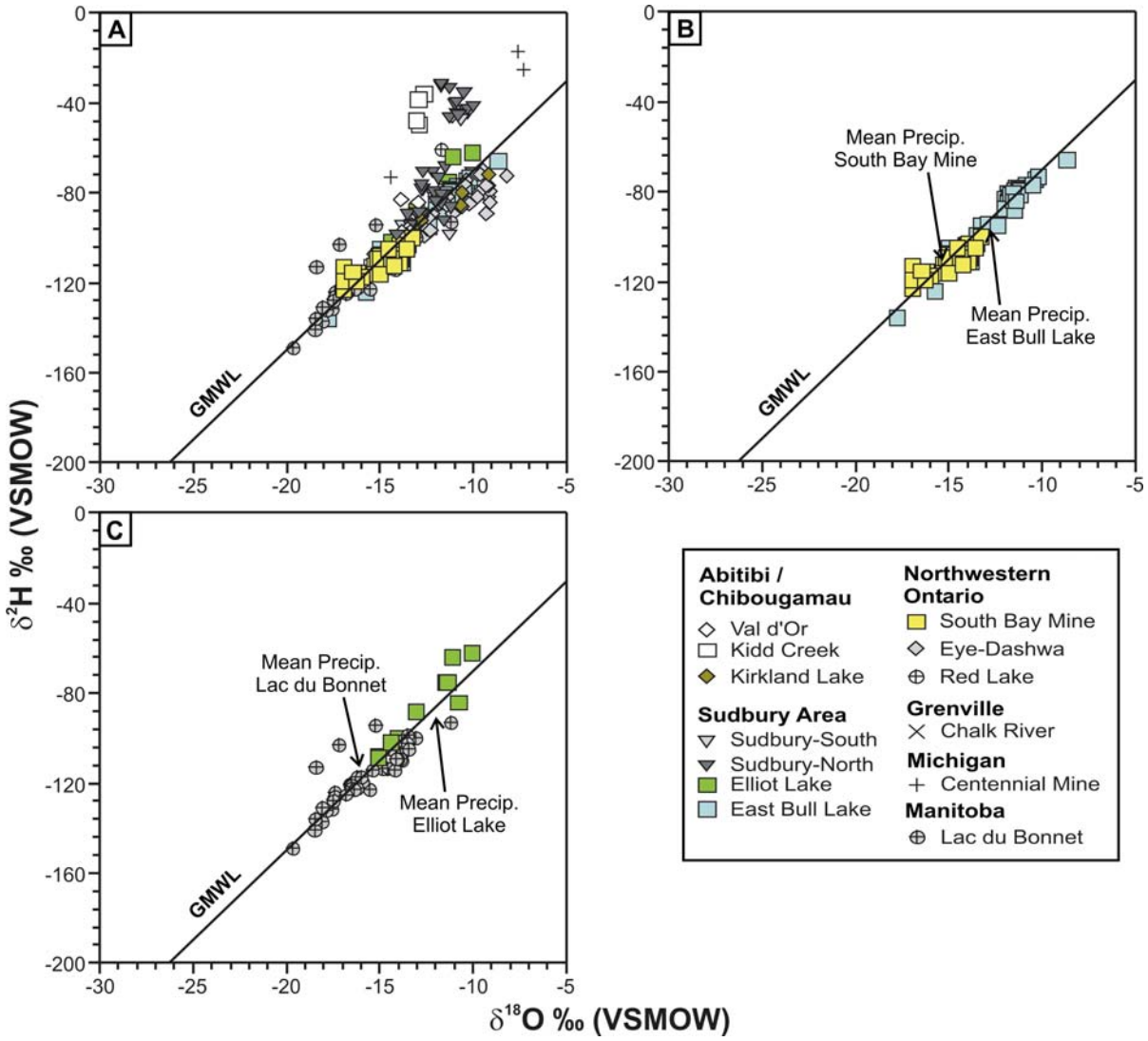

Figure 4-12. Relationship of $\delta^{2}H$ and $\delta^{18}O$ for Canadian Shield groundwater samples from sites not located in or near permafrost by salinity. (A) All sites, (B) South Bay Mine and East Bull Lake, (C) Lac du Bonnet and Elliot Lake. Data are from various sources listed in Table 4-1.

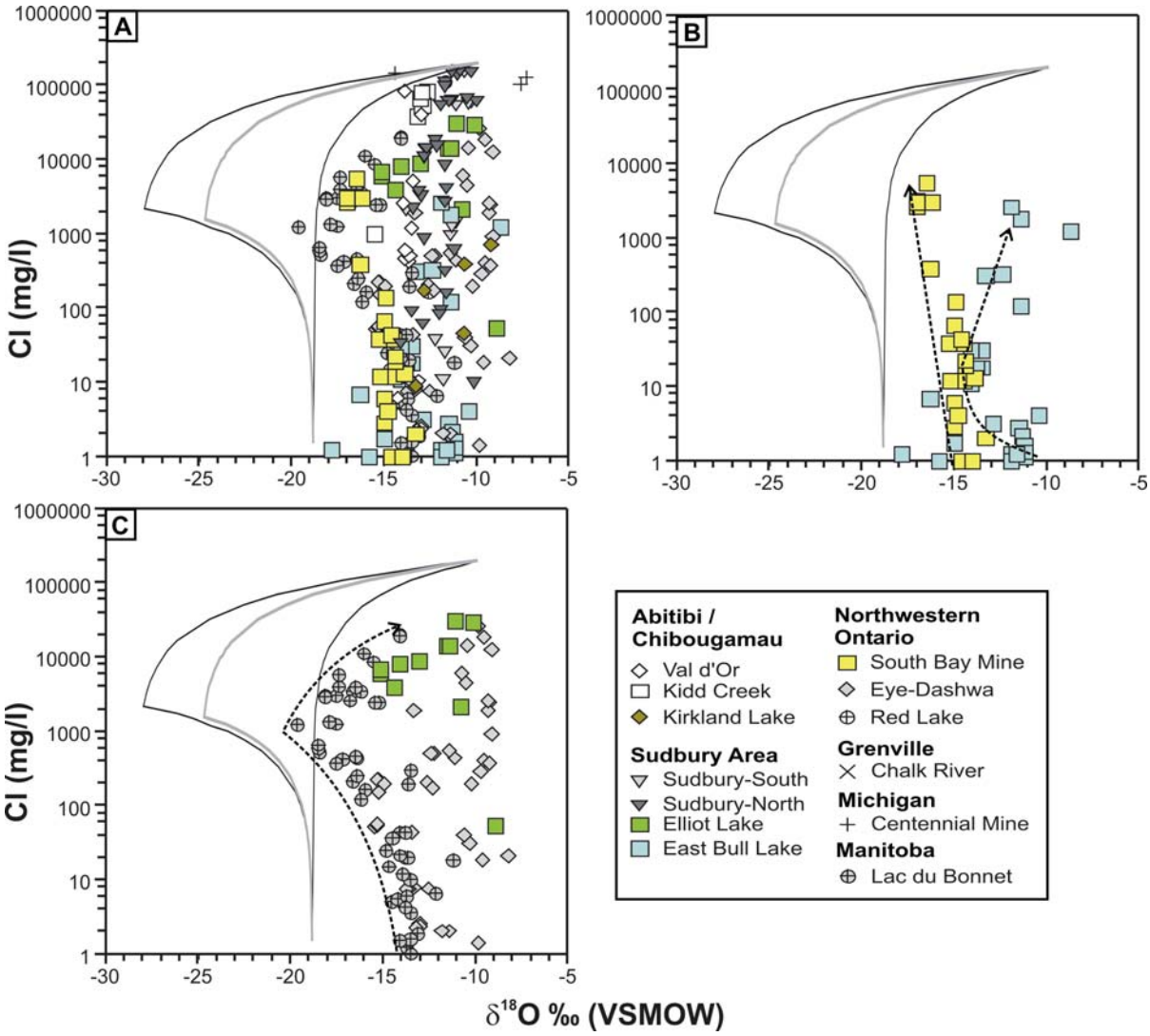

Figure 4-13. Relationship of Cl^- and $\delta^{18}O$ for Canadian Shield groundwater samples from sites not located in or near permafrost. (A) All sites, (B) South Bay Mine and East Bull Lake, (C) Lac du Bonnet, Elliot Lake, and Eye-Dashwa. Three end-member mixing plot shown for reference. Data are from various sources listed in Table 4-1.

Geochemical trends consistent with the freeze-out experiments were observed at several sites. However, only groundwaters from Lac du Bonnet follow every trend observed in the freeze-out experiments. Fluids at other sites such as Val d'Or had Na/Cl versus Br/Cl ratio patterns similar to freeze-out experiments, but $\delta^{18}O$ values were not similar. Elliot Lake, East Bull Lake, and South Bay groundwaters have $\delta^{18}O$ signatures similar to those that would be expected for waters influenced by a freezing process, but Na/Cl versus Br/Cl ratio patterns were much more scattered and generally did not follow freezing experiment trends. Finally, although some characteristics of freezing are observed in Eye-Dashwa fluids, the data is highly scattered.

4.5.2 Canadian Shield Brines and Freezing

Formation of the Canadian Shield brine component during Plio-Pliestocene glaciations due to surficial freezing of seawater along sub-arctic continental margins around ice-sheets and post-genetic emplacement has been hypothesized (*Starinsky and Katz 2003*). Alternative evidence was also presented that suggests at least some Canadian Shield brines are too old to support that hypothesis, and therefore are derived from evaporation of paleo-seawater (*Bottomley et al. 2002, Bottomley et al. 2003*). Additional physical and geochemical evidence, described below, also provide strong arguments against a surficial seawater freezing origin for Canadian Shield brines. Evidence provided from subglacial flow, permeability, distribution of saline glacial margin lakes, Na/Cl and Br/Cl ratios, stable isotope ratios, thermodynamic equilibrium models, all suggesting cryogenic freezing of seawater along continental margins is not the source of Canadian Shield brines, are explored

Physical evidence does not support flow towards the center of the continent. The surficial cryogenic brines hypothesis suggests brines formed in cryogenic troughs along subarctic continental margins around ice sheets, with density induced brine migration into the Canadian Shield away from the ocean (Figure 4-14 A & B*, Starinsky and Katz 2003*). However, this postulation ignores several other important physical processes. First, since the hypothesis suggests salinity is forming on the continental margins, a continental scale reversal of groundwater flow is required, significantly reversing the hydraulic gradient. Although flow reversal during glacial periods has been identified, this is due to the ice mass changing subsurface pressure fields, resulting in the groundwater flow outward from the ice sheets (*Grasby et al. 2000, Person et al. 2007, Lemieux et al. 2008*). Therefore, a groundwater divide could be expected beneath continental ice sheets, with groundwater flow still progressing towards the ocean. Recent investigations of continental scale flow and recharge, incorporating density-dependent flow, hydromechanical loading, subglacial infiltration, isostasy, and permafrost development suggest groundwater recharge typically occurs during glacial advance, with discharge occurring during glacial retreat, a result of reduced pressures as the weight of the ice mass is removed (*Lemieux et al. 2008*). This is illustrated in Figure 4-14 C & D, with groundwater flowing away from the center of the ice mass, with major recharge under the glacier only occurring during glacial onset. There is no evidence to suggest a hydraulic gradient would be created for infiltration of oceanic water through the forebulge.

The low permeability of the Canadian Shield is also ignored by the hypothesis. For instance at Copper Rand, the most concentrated fluids, with isotopic and geochemical characteristics similar to other Canadian Shield brines are located in vugs, which are not part of an active flow system (*Guha and Kanwar 1987*). Using a simple, “back of the envelope” groundwater flow calculation, given an

average hydraulic conductivity for intact rock of 10^{-12} m·s^{-1} (*Freeze and Cherry 1979*) and a large hydraulic gradient of 1.0 in the area surrounding the vug, water could be expected to travel only 31.5 meters in 100,000 years. This calculation indicates that there is barely enough time during a glacial cycle for fluid to travel to the vug from a nearby fracture, and clearly not from the edge of the continent, 1100 km away (Figure 4-10) during the last glacial maximum, even if highly permeable fractures were assumed to be present. Permeability within the Canadian Shield is too low for transport of brines formed on the continental margins to be feasible over the time scale proposed by Starinsky and Katz (*2003*). Only small penetrations of sedimentary formation waters have been observed at sites located along the Canadian Shield margins (*Gascoyne et al. 1987, Gascoyne et al. 1989, Frape et al. 2004*).

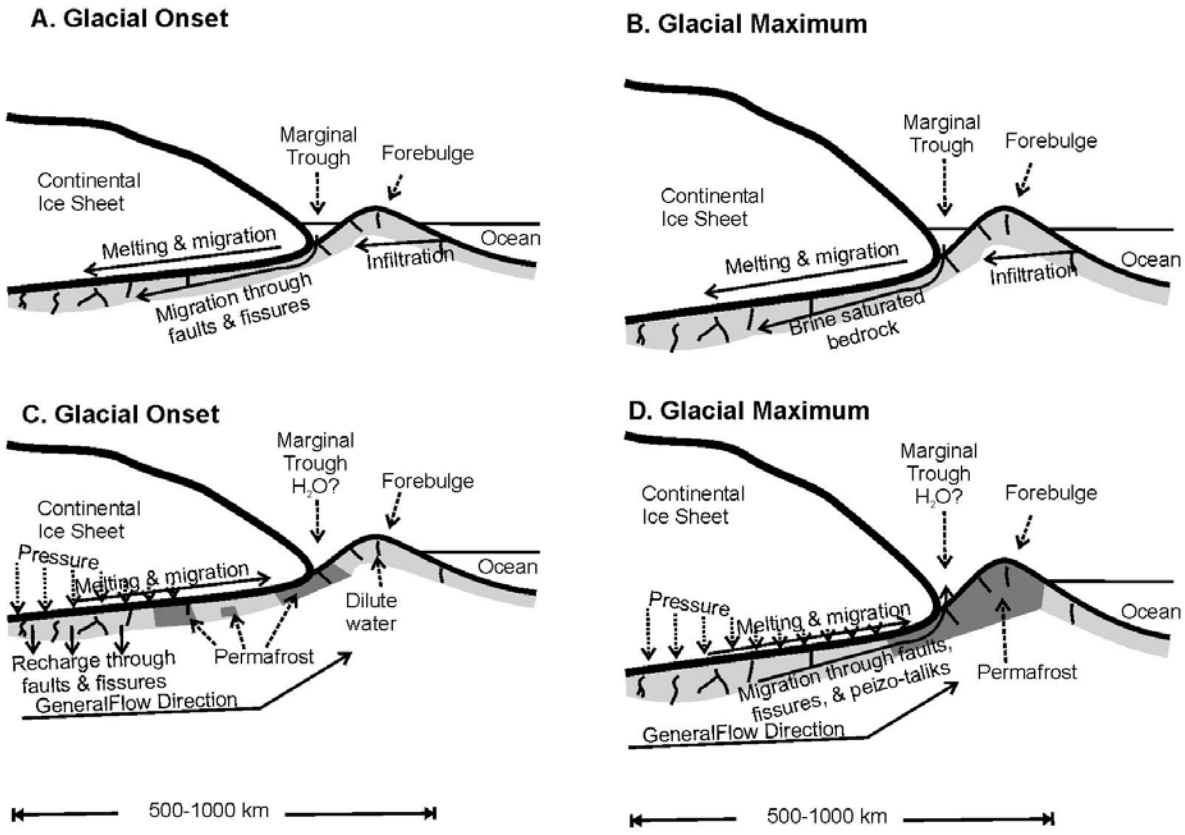

Figure 4-14. Comparison of flow under glacial ice from Starinsky and Katz (*2003*) hypothesis (A,B) with the currently accepted conceptual model of subglacial pressures and flow (*Person et al. 2007*, *Lemieux et al. 2008*) (C,D).

Today, saline lakes at glacial margins are the exception, although, there are instances of saline lakes near glacial margins today in the McMurdo dry valleys Antarctica and Greenland (*Anderson et al. 2001, Willemse et al. 2004, Lyons et al. 2005*). Individual saline lake chemistries in

the McMurdo dry valleys and Greenland are dominated by marine aerosols, glacial and chemical weathering, ancient marine waters, evaporation, and solute removal via mineral precipitation during cryogenic concentration (*Anderson et al. 2001, Lyons et al. 2005*). However a significant majority of lakes in Greenland, the Arctic, Antarctic, including along glacial fringes are composed of fresh water (*Douglas and Smol 1994, Rühland and Smol 1998, Anderson et al. 2001, Hamilton et al. 2001, Lim et al. 2001, Michelutti et al. 2002, Lim and Douglas 2003, Lim et al. 2005, Keatley et al. 2007, Kumke et al. 2007*). Indeed, it is not uncommon to find freshwaters in disequilibrium with modern ocean waters within continental shelf regions that were beneath former proglacial lakes during the last glacial maximum (*Pearson et al. 2006*). This is the area where the Starinsky and Katz (*2003*) hypothesis suggests concentrated brines should be found.

The relationships between Na/Cl and Br/Cl ratios do not support a seawater freezing origin for the brines. Shield brines have unique Na/Cl and Br/Cl ratios (Figure 4-15A) compared with experimental evaporation of seawater (*McCaffery et al. 1987*), or freezing of modern-day shield fluids (*Zhang and Frape 2002*) or seawater (*Herut et al. 1990*), and indicates the brines were not formed through these processes (Figure 4-15B). Although some Canadian Shield brines do fall near the hypothesized seawater freezing trend (Figure 4-15A, *Herut et al. 1990*), the Herut et al. (*1990*) trend is extrapolated significantly, and is not supported by experimental evidence (e.g. *Herut et al. 1990, Zhang and Frape 2002*).

The stable isotopes of water (δ^2H, $\delta^{18}O$) are also useful for determining the relative influence of glacial-interglacial cycling, freezing, and/or evaporative processes to groundwaters in the Canadian Shield. Unlike many other groundwaters, brines sampled in the Canadian Shield plot above the GMWL for δ^2H and $\delta^{18}O$ (Figure 4-15C), a result of water-rock interaction (*Fritz and Frape 1982, Frape et al. 1984, Pearson 1987*). This indicates Canadian Shield brines do not have a stable isotopic signature suggestive of either the evaporative or freezing processes, indicating the majority of brines and saline fluids were not formed or significantly affected by either freezing or evaporation (*Fritz and Frape 1982, Frape et al. 1984, Pearson 1987, Frape et al. 2004*). Thus, the most concentrated fluids sampled in the Canadian Shield could not have formed by *in situ* freezing of fluids (e.g. permafrost or methane-hydrate formation), surficial freezing of seawater, or evaporation of seawater. Rather, evidence indicates these fluids have evolved through water-rock interaction, particularly hydration of silicates (*Fritz and Frape 1982, Frape et al. 1984, Pearson 1987, Ziegler and Longstaffe 2000, Longstaffe 2000, Bucher and Stober 2000*).

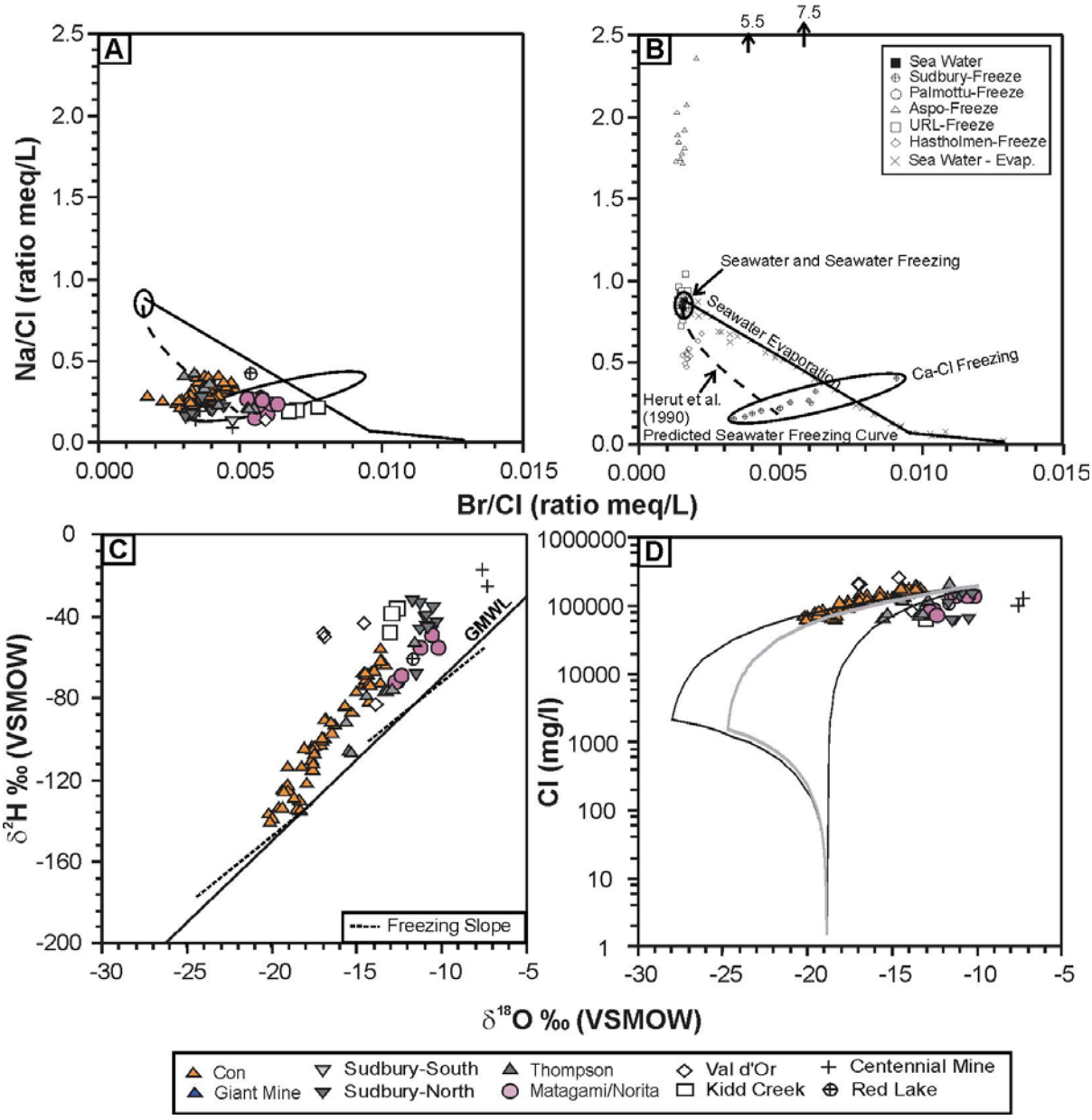

Figure 4-15. Geochemical trends of Canadian Shield brines. (A) Relationship of Na/Cl and Br/Cl ratios for Canadian Shield brines (B) Na/Cl vs. Br/Cl freezing and evaporation experiment results for reference (references cited in Figure 4-2). (C) Relationship of δ^2H and $\delta^{18}O$ for Canadian Shield brines. (D) Relationship of Cl^- and $\delta^{18}O$ for Canadian Shield brines. Three end-member mixing plot shown for reference. All data are from references listed in Table 4-1.

An examination of seawater during freezing using thermodynamic equilibrium models also suggests that the brines have not been affected by *in situ* freezing. Two different seawater freezing models (Figure 4-17, *Nelson and Thompson 1954, Marion et al. 1999*) suggest mirabilite ($Na_2SO_4 \cdot 10H_2O$) precipitation occurs between -6.3 and -8.2 °C, and hydrohalite ($NaCl \cdot 2H_2O$), is the

first chloride mineral to precipitate during freezing (-22.9°C). Antarcticite ($CaCl_2 \cdot 6H_2O$) precipitates at the eutectic of one freezing pathway (-53.8°C), but $MgCl_2 \cdot 12H_2O$ forms at the eutectic point of another pathway (-36.2°C). Significantly, only mirabilite is stable within or near the lowest temperatures (-7 to -8 °C, *Natural Resources Canada 1995*) currently found beneath the seasonally affected layer of permafrost on the Canadian Shield. Even as far north as 76°N, in the Arctic Archipelago, the subsurface thermal minima (-15°C) are typically found within the upper 100 mbgs (*Natural Resources Canada 1995*). Thus, temperatures have not become cold enough and have not persisted to depths great enough to freeze or affect brines within the Canadian Shield. From the evidence provided in this section, it is concluded the most concentrated Canadian Shield fluids were not significantly affected by evaporation, surficial freezing, permafrost formation or any other freezing process.

In the surficial cryogenic concentration of seawater hypothesis, Starinsky and Katz (*2003*) suggest that the brine Sr has a different origin than Ca. In their model Ca is derived from concentration of seawater through freezing and Sr is derived from water-rock interaction (*Starinsky and Katz 2003*). However, the co-evolution between Sr and Ca in Canadian Shield groundwaters is well-established (*McNutt et al. 1984, 1990, McNutt 1987*). If seawater were to cryogenically concentrate to form Ca-rich brines as hypothesized (*Starinsky and Katz 2003*), Sr would also concentrate in the residual fluid. Therefore, if the Sr sampled in Canadian Shield groundwaters were derived from seawater freezing, as suggested for Ca, the $^{87}Sr/^{86}Sr$ ratios (0.707-0.755) of Canadian Shield brines should be the same as Pleistocene seawater (~0.709, *Capo and DePaolo 1990*). Brines from one site (Matagami/Norita) have a $^{87}Sr/^{86}Sr$ composition similar to Pleistocene seawater, however these samples are from Rb-poor, ultramafic rocks, and the $\delta^{18}O$ signatures of these brines are not indicative of significant freezing (Figure 4-16A). Brines from the remainder of the sites do not have $^{87}Sr/^{86}Sr$ ratios similar to Pleistocene seawater, and therefore do not support a conclusion that Canadian Shield brines formed during surficial cryogenic concentration of seawater.

The surficial cryogenic freezing hypothesis is also not supported by $\delta^{37}Cl$ and $\delta^{81}Br$ values. Several researchers argue against $\delta^{37}Cl$ variation in seawater over the Phanerozoic (*Eastoe et al. 2001, Stewart and Spivack 2004, Eastoe et al. 2007, Sharp et al. 2007*). During freezing, ^{37}Cl enriches in ice, but because the amount of chloride incorporated into ice is so small, the effect on the fluid reservoir is negligible when compared to brine concentrations (15-30 $mg \cdot l^{-1}$ vs. 100's $g \cdot l^{-1}$, *Zhang and Frape 2002*). Fractionation processes for stable bromine isotopes are not well-documented, but may be expected to behave similarly to stable chlorine isotopes. Currently, it is accepted that oceanic $\delta^{37}Cl$ ratios do not vary from 0‰ standard mean ocean chloride (SMOC), except for small, semi-isolated

basins such as the Black Sea which have terrestrial Cl^- inputs, (*Kaufmann 1984, Kaufmann et al. 1984, Eggenkamp et al. 1995, Godon et al. 2004b, Eastoe et al. 2007*). Again, the bromine system is less well studied. The value of modern ocean bromide is 0‰ (SMOB). Thus if the salt source for brines in the Canadian Shield were derived directly from surficial freezing of seawater, both the $\delta^{37}Cl$ and $\delta^{81}Br$ values would be expected to equal the seawater value (0 ‰), as the amount of halide incorporated into ice is expected to be too small to change the isotopic ratios of the residual fluid. Even in samples with the most depleted $\delta^{18}O$ values, the $\delta^{37}Cl$ and $\delta^{81}Br$ values (Figure 4-16 B,C) are also not consistent with a seawater salt origin of Pleistocene age.

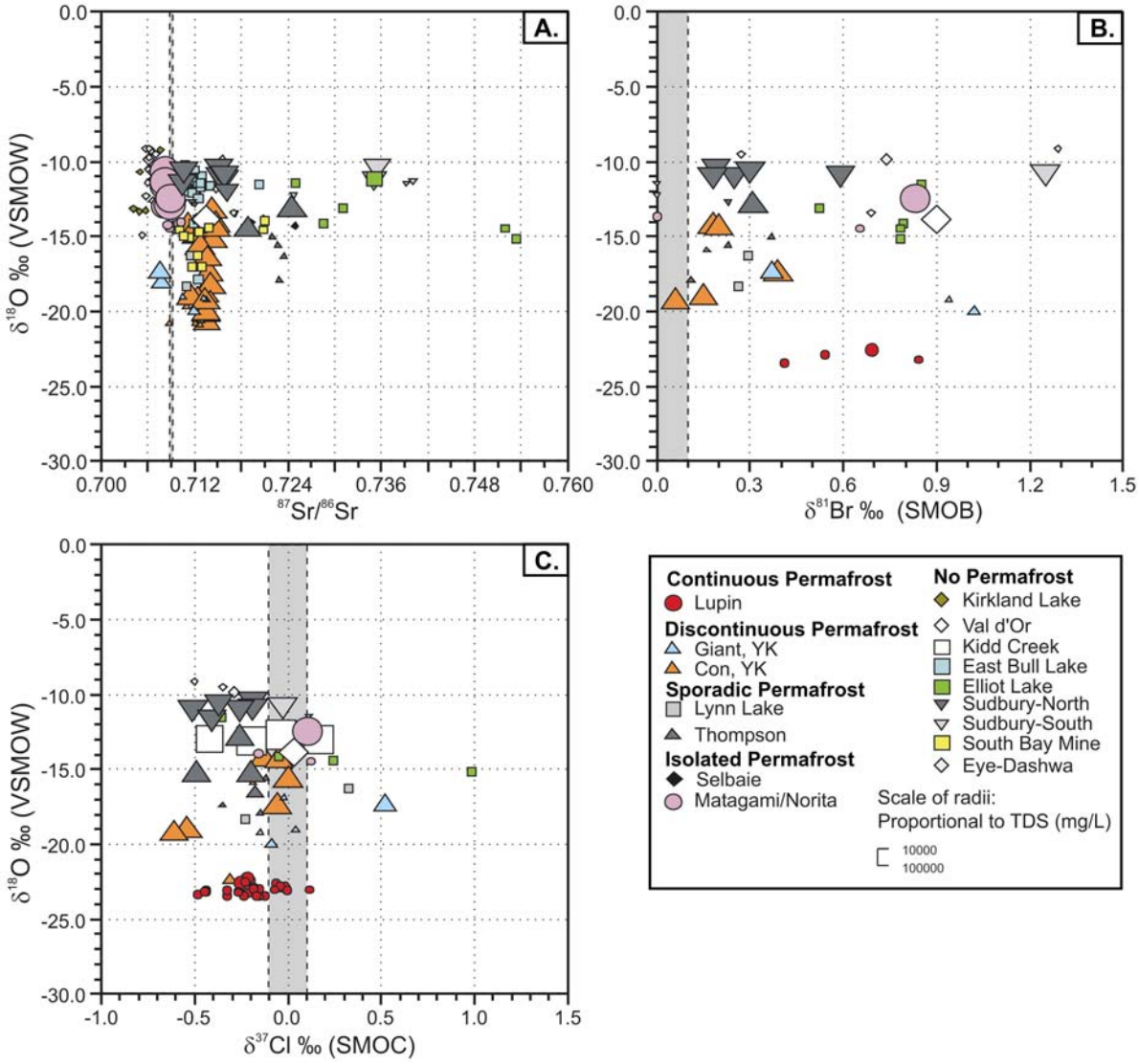

Figure 4-16. Relationships between $\delta^{18}O$ and (A) $^{87}Sr/^{86}Sr$, (B) $\delta^{81}Br$, and (C) $\delta^{37}Cl$. The grey shaded areas indicate seawater values, considering method detection limit.

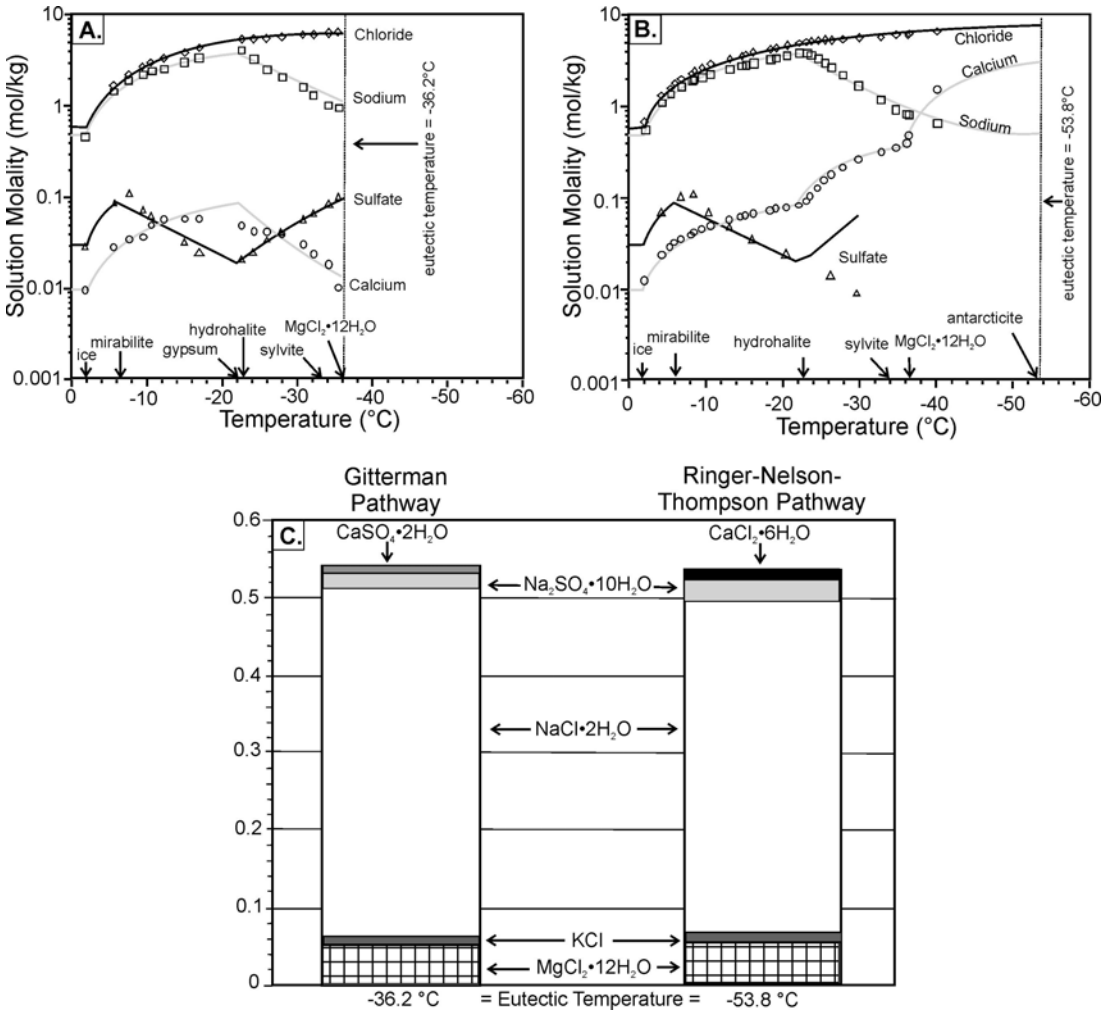

Figure 4-17. Comparison of seawater freezing pathways. (A) Gitterman pathway, after Marion and Farren (*1999*). (B) Ringer-Nelson-Thompson pathway, after Marion and Farren (*1999*). (C) Relative salt precipitation during freezing to the eutectic temperature along each pathway after Marion et al. (*1999*).

4.6 Are There Deep Freezing Affected Waters?

As discussed above, the depleted δ^2H and $\delta^{18}O$ values observed in fresh, brackish, and saline groundwaters from several Canadian Shield sites may be an indicator of either glacial meltwater recharge or *in situ* freeze-out. At many Canadian Shield sites, there is a decreasing trend of $\delta^{18}O$ with depth, until a local minima is reached, at which point $\delta^{18}O$ starts to increase again, resulting in a bow shaped curve (Figure 4-8). $\delta^{18}O$ values lower than that of modern precipitation are found at depths of up to 700-1100 m (Figure 4-8). If this trend is related to the glacial/interglacial cycle, this correlation indicates the geochemical effects of the glacial/interglacial cycle are found at considerable depths

within the Canadian Shield. Interestingly, depleted $\delta^{18}O$ values are found at the greatest depths at sites currently in permafrost areas, but are only between 200 m and 600 m in other areas (Figure 4-8B).

The maximum observed modern-day permafrost depth in the Canadian Arctic is only 700 m, in the Arctic Islands (*Natural Resources Canada 1995*). Permafrost is absent near Elliot Lake, the URL, and South Bay Mine. Additional insight is needed to determine if glacial or interglacial processes are responsible for the geochemical trends observed to depths of 1100 m within the Canadian Shield. Five possible explanations for these trends are:

1. Hydraulic gradients created by mine-dewatering has drawn permafrost-influenced or glacial meltwaters to depth,
2. Paleo-permafrost extended to depths greater than observed at present,
3. Natural groundwater flow/transport processes allowed waters influenced by permafrost formation to recharge to depth,
4. Samples are indicative of deep glacial meltwater intrusion,
5. Isotopic modification and solute concentration after water removal due to methane hydrate formation at depth.

Each of these possible scenarios will be discussed below.

4.6.1 Mine De-watering

Disturbances due to mine de-watering may have created sufficient downward gradients to draw shallower fluids to greater depths. Mixing in fractures, fracture zones, and faults due to the artificially induced gradient could then occur. Samples taken from long exploration boreholes could be mixed, as individual fracture zones were generally not sealed and therefore became cross-connected. Dewatering and cross-connected boreholes likely caused some of the observed geochemical variations at the Con and Lupin mines, where traces of tritium and evidence of mixing in $\delta^{18}O$-$\delta^{2}H$ signatures (Figure 4-18) were observed in some groundwater samples (*Frape et al. 1984, McNutt et al. 1990, Douglas et al. 2000, Chapter 3, Chapter 2*). Although anthropogenic gradients may have induced mixing between shallow and deep fluids at some sites, evidence of deep periglacial-glacial effects were also found at sites where surface-drilled boreholes (up to 1100 mbgs) were sampled from sealed sections, including Eye-Dashwa. This process therefore cannot explain the deep geochemical evidence of the freezing process at all locations.

In crystalline rocks, groundwater transport is dominated by fracture flow and diffusion within the rock mass. Currently, the limited studies of pressures beneath and within permafrost in crystalline areas are unable to determine a meaningful hydraulic gradient (*Gartner Lee 2005, 2006a,b*, *Stotler et al. 2008*). Salinities increase with increasing depth; therefore downward diffusion of freezing-affected waters is also not considered significant; rather concentration gradients would favor upward transport of solutes towards the more dilute waters within the permafrost. Thermal gradients would also favor upward solute transport from deeper, warmer fluid towards the colder permafrost.

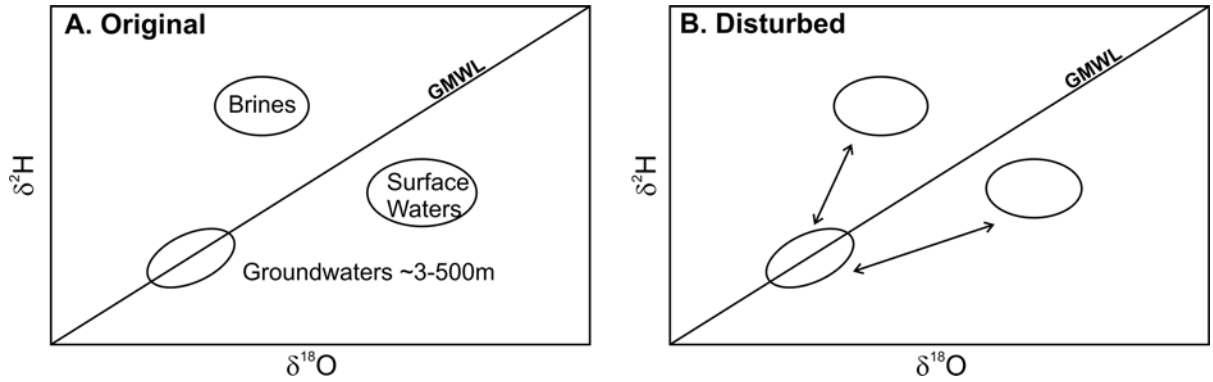

Figure 4-18. Mixing due to mine dewatering on a δ^2H vs. $\delta^{18}O$ plot.

4.6.2 Deep Paleo-permafrost

Although the maximum recorded depth of permafrost in Canada is 700 m, permafrost reaches depths of over 1580 m in Siberia (*Alexeev and Alexeeva 2002, 2003*). Siberia remained glacier-free during Plio-Pleistocene glaciations, thus allowing permafrost to persist. Although, it is possible that permafrost was deeper in North America in the past, glacial climate models of North America indicate maximum permafrost depths over the last 120 ky were similar to present day values. Rather, repeated continental glaciations likely acted to repeatedly melt some, if not all, of the permafrost (*Tarasov and Peltier 2007*, Chapter 3). However, as the glaciers advanced from the northern latitudes, permafrost also advanced in front of the ice sheet. During the last glacial maximum, the ice sheets advanced well beyond the Canadian Shield (Figure 4-10, *Dyke and Prest 1987, Dyke et al. 2002*). Thus, although permafrost was likely shallower in the past, it also affected a much larger area than at present (Figure 4-9). Along the southern extent of the Canadian Shield, where permafrost is currently absent, paleo-permafrost depths probably did not exceed 40-60 m at the Last Glacial Maximum

(Figure 4-9, *Tarasov and Peltier 2007*). Therefore, paleo-permafrost is not believed to have reached the depths required to directly affect the $\delta^{18}O$ trend.

4.6.3 Intruded Glacial Meltwater

The entire study area was covered by continental glaciations at the last glacial maximum (LGM), and then deglaciated within ~4000 years of each other (*Tarasov and Peltier 2004*). Surficial loading of glacial ice can dramatically change subsurface pressure regimes (*Grasby et al. 2000, Lemieux 2006, Person et al. 2007, Lemieux et al. 2008*). Previous assumptions have held that glacial meltwater would recharge groundwaters during de-glaciation (*Clark et al. 2000, Douglas et al. 2000*). However, recent studies have suggested glacially-induced recharge is more prevalent during glacier formation and advance, with discharge occurring during retreat (*Lemieux 2006, Lemieux et al. 2008*). Permafrost is typically considered to have extremely low permeability, and is generally considered "impermeable" (e.g. *Burt and Williams 1976*). Therefore, recharge of glacial waters is dependent upon melting of pre-existing permafrost to open recharge pathways, or it is restricted to pre-existing taliks. Deep recharge of any glacially-derived fluids would require an outlet for fluid already in the system. A glacial meltwater recharge scenario is complicated by the density of the recharging fluid and existing fluids, as dilute glacial fluids would have to displace the more dense brine fluids. However glacial recharge has been documented in some highly permeable sedimentary aquifer systems (*Siegel and Mandle 1984*, *Person et al. 2007*). A glacial meltwater recharge for the periglacial/glacial freeze-out component is not ruled out entirely.

4.6.4 Methane Hydrates

Methane hydrates have been found beneath sedimentary permafrost and beneath the ocean, and have been inferred within crystalline permafrost environments (*Chapter 3*). If methane and water are present in sufficient quantities, temperatures are low enough, and pressure is high enough, methane hydrates are stable (Figure 4-19A). Because of the transient nature of subsurface thermal and pressure fields in North America during the glacial-interglacial cycles, and the presence of methane within the Canadian Shield (*Sherwood-Lollar et al. 1988, 1993a,b, 2002, 2006, Doig 1994, Montgomery 1994, Westgate 1998*, Chapter 3), it is probable methane hydrate would have formed and dissipated at some locations on the Canadian Shield. In permafrost regions, gas hydrates may be stable between 200 and 2000 m, depending on the geothermal gradient (*Ershov and Yakushev 1992*). Even in areas of deep permafrost, methane hydrates are stable well below the base of permafrost (Figure 4-19).

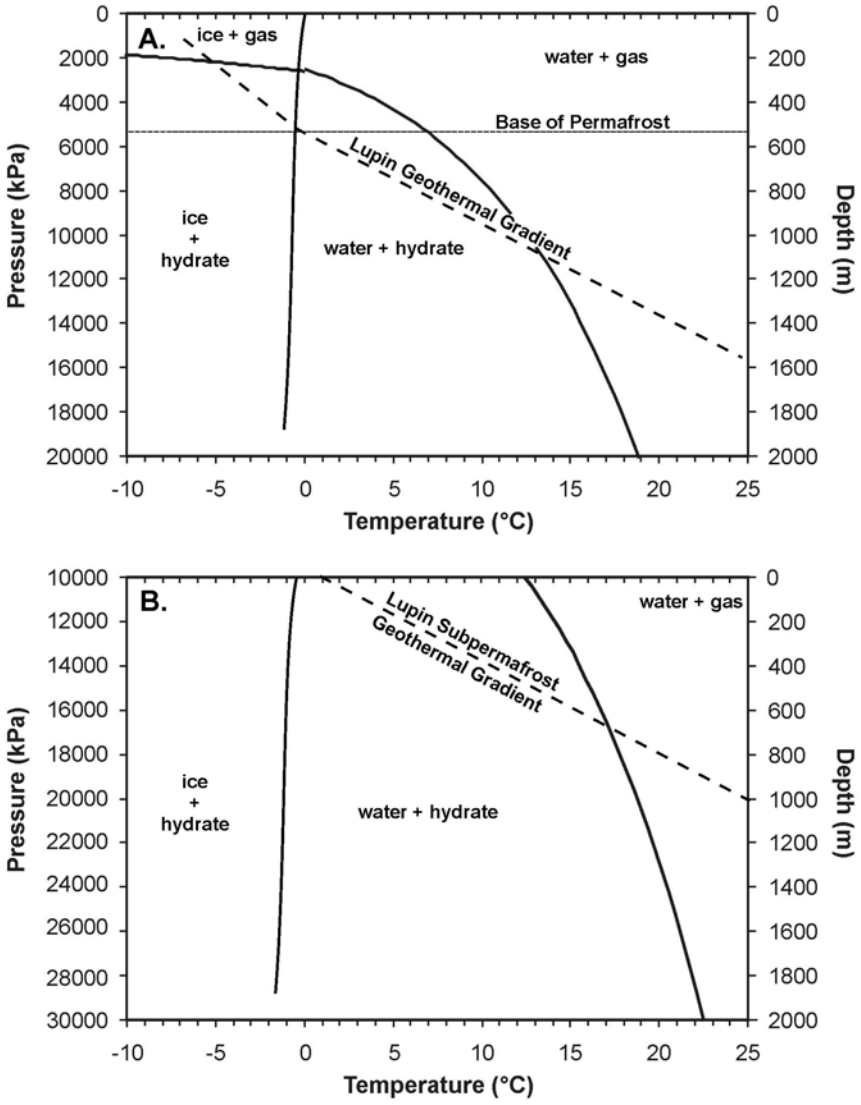

Figure 4-19. Methane-hydrate and ice phase equlibria in fresh water. (A) The Lupin geothermal gradient and modern hydrostatic pressures are provided as an example. (B) Hydrate stability field if a kilometer thick glacier, exerting 10000 kPa of pressure, is present with a "warm" glacial base and a conservative geothermal gradient. Hydrate stability fields based on fresh water, calculated from empirical measurements discussed by Sloan (*1998*).

Methane hydrate formation has the same geochemical effects on water and fluids as ice formation. Methane hydrate formation concentrates solutes in residual fluids and fractionates the stable isotopes of water (*Trofimuk et al. 1974, Hesse and Harrison 1981, Hesse et al. 1985, Ussler and Paull 1995, Ussler and Paull 2001, Hesse 2003*), similar to the formation of ice (e.g. Section 4.3). Therefore, the geochemical trends associated with fluid freezing (Section 4.3) could also indicate methane hydrate formation. However, geochemical trends associated with freezing could be found well below the base of permafrost, because gas hydrates are stable at greater depths than ice

(Figure 4-19). Methane is present at many of the Canadian Shield sites studied, and it is possible the deep geochemical evidence of the freezing process is related to paleo-hydrate formation. This could confirm terrestrial methane hydrate formation during cooler climates (e.g. *Nisbet 1990, Weitemeyer and Buffett 2006*), although further physical modeling needs to be conducted to determine time-scales and methane-hydrate stability depths in the more southerly sites.

The transient state of hydrate stability fields could be a crucial component to understanding glacial-interglacial cycling effects on groundwater recharge. In unglaciated conditions, permafrost needs to be at least 200 m thick for hydrates to form. As shown by the hydrate stability field (Figure 4-19A), methane hydrates are stable at higher temperatures if pressures are also higher. Subsurface pressures increase during glaciation, even if sub-glacial temperatures are high enough to melt permafrost, methane hydrates most likely would remain stable and might not dissipate, according to the hydrate stability fields (Figure 4-19). Hydrates would actually become stable at much shallower depths (Figure 4-19B), thus hydrates may form in the subsurface during glacial periods in the southern Canadian Shield, at sites such as the URL if methane gas is a substantial component of the subsurface geochemical system. The overall concept is supported by modeling at the Lupin site (*Chapter 3*).

Methane hydrate can act to further reduce permeability (*Kleinberg et al. 2003*), similar to the formation of ice (*Burt and Williams 1976*). Although it is unclear to what extent hydrates may be able to form in the low permeability rock matrix of crystalline shield rock, methane hydrates have been observed in fractures (*Kvenvolden et al. 1984*). If gas hydrates had formed prior to or during glacial advance, it is suggested the ability for glacial meltwater to recharge deep into the subsurface would be diminished. This would be contingent upon widespread methane hydrate formation within the shield.

Dissipation of methane hydrate typically results in fluid dilution and could slightly enrich $\delta^{18}O$ values (*Hesse and Harrison 1981, Hesse et al. 1985, Ussler and Paull 1995, 2001, Hesse 2003*). From the literature, it is unclear if there are any other geochemical markers of methane hydrates after formation and subsequent dissipation; although some carbonates (e.g. calcite) may form coincident with methane hydrate dissociation and subsequent oxidation (*Hein et al. 2006*).

Formation of Structure I methane hydrates, the most common hydrate structure observed in nature (e.g. *Sloan 1998*), can affect gas composition in nearby sediments (*Milkov et al. 2004*). This relationship is observed in two methane hydrate research boreholes drilled in the sedimentary units of the Mackenzie Delta (Figure 4-20A, *Lorenson et al. 1999, 2005*). Mixing between thermogenic and bacteriogenic gases within the wells result in significant gas shifts in composition [methane/(ethane + propane), or C1/(C2+C3)] and carbon isotopic signature ($\delta^{13}C\text{-}CH_4$) shifts. On the other hand, free

gas found in the zone where gas hydrates occur are characterized by significant shifts in gas composition (C1/(C2+C3)) accompanied by only minor changes in carbon isotopic signature (δ^{13}C-CH_4) (Figure 4-20A).

(A)

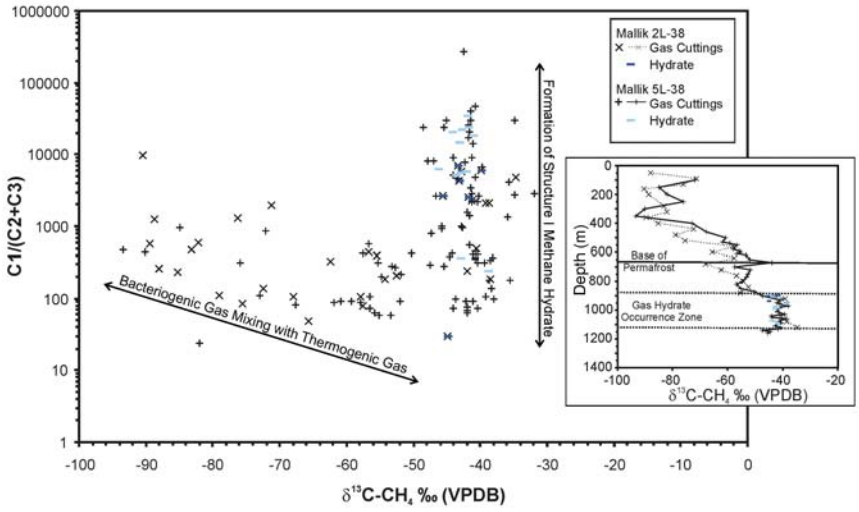

(B)

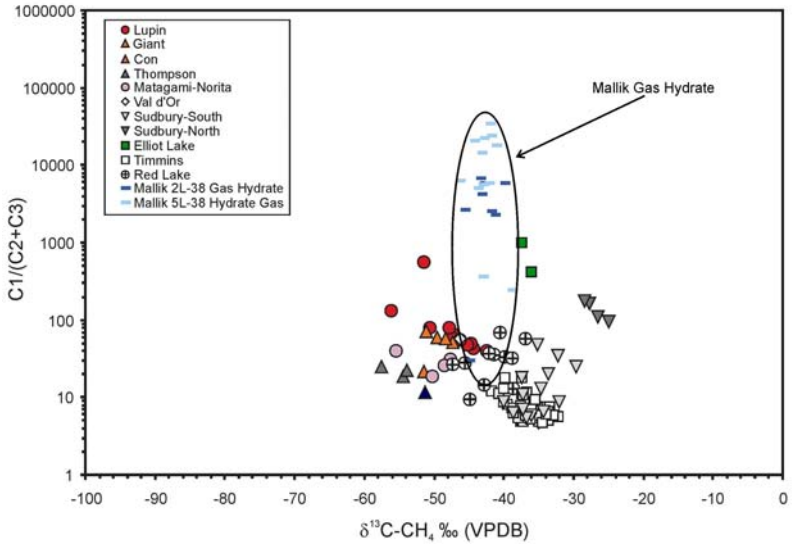

Figure 4-20. (A) Different trends observed in Mackenzie Delta gas hydrate research well. Inset shows carbon-methane isotopic relationship for gas cuttings and methane hydrate samples with depth. (B) Canadian Shield gas compositions compared with gas hydrates sampled in the Mackenzie Delta. With data from Sherwood-Lollar et al. 1988, 1993a,b, 2002, 2006, Doig 1994, Montgomery 1994, Westgate 1998, Lorenson et al. 1999, 2005, and Chapter 3 of this thesis.

A review of the relationship between gas composition (C1/(C2+C3)) and δ^{13}C-CH_4 for Canadian Shield gas data (Figure 4-20B) indicates an enrichment of methane relative to high

hydrocarbons at some sites, with only a small change in $\delta^{13}C\text{-}CH_4$ (i.e. Con, Lupin, Red Lake, Sudbury-South, Elliot Lake). However it is not clear how long changes to gas composition would be observed after hydrate dissipation, and may be dependent on gas transport, mixing and whether or not the system is "open". Thus it is not possible at this time to determine from the gas compositions if methane hydrates formed and dissipated during the glacial cycles within the Canadian Shield.

Investigation of unglaciated sedimentary basins with methane deposits in North America, where permafrost formed to depths of 100-200 m during the Pleistocene, may constrain the potential for methane hydrate formation to substantially affect deep groundwater geochemistry. However, the geochemical impact may be enhanced in crystalline rock compared with sedimentary rock, due to the smaller fluid reservoir in crystalline rock.

4.7 Summary

The glacial-interglacial cycle can impact deep subsurface geochemical conditions. In this chapter, the available geochemical data from across the Canadian Shield was examined to determine residual geochemical effects due to the glacial-interglacial cycle. Effects of glacial melt-water recharge and surficial freeze-out, which had been previously considered by others, and *in situ* freeze-out effects due to ice and/or methane hydrate formation were considered. The data are not sufficient to differentiate between mixed, intruded glacial meltwaters, or residual waters resulting from either permafrost or methane hydrate formation. At some Canadian Shield sites, there are indications that fresh, brackish, and saline groundwaters have been affected by one of these processes. The geochemical indications are found to depths of 1300 m at disturbed sites currently located in permafrost regions. Canadian Shield brines did not evolve as a result of evaporation, permafrost formation or the freeze-out process, as clearly shown by δ^2H, $\delta^{18}O$ and Na/Cl, Br/Cl relationships. However, it is important to note that not all sites exhibited the geochemical characteristics associated with the freezing process.

Physical and geochemical data do not support the cryogenic formation of Canadian Shield brines in glacial marginal troughs as outlined by Starinsky and Katz (*2003*). Groundwater flow, subglacial pressures, and rock permeability suggest that it would not be possible to move a hypothetical brine from a marginal trough on the continental margin to the center of North America during the recent glacial cycles. Cryogenic formation of the brines is also not supported by the present-day observation that although some saline lakes are present, they are not common in Polar Regions or near the margin of continental-scale ice sheets (Antarctica, Greenland). Geochemical evidence, including ionic ratios, and δ^2H, $\delta^{18}O$, $^{87}Sr/^{86}Sr$, $\delta^{37}Cl$ and $\delta^{81}Br$ data all suggest recent

surficial cryogenic freezing of seawater was not the origin of the brines in the Canadian Shield. Geochemical freezing models demonstrate that an *in-situ* freeze-out origin for the brines is also not possible, as subsurface temperatures in present day areas of permafrost are not low enough to create such concentrated solutions. Modern subsurface temperatures in permafrost areas are also not low enough for the freeze out process to have influenced any pre-existing concentrated Shield brines.

Methane is present at many of the study sites. It is suggested the observed dilute fluids, Na/Cl-Br/Cl, δ^2H-δ^{18}O, and Cl-δ^{18}O relationships observed at depths greater than paleo-permafrost may be related to formation and dissipation of paleo-methane hydrate at these locations. Evidence for geochemical modification of gas geochemistry was inconclusive. Methane hydrates could form during glacial advances due to increased pressures. This would act to reduce subsurface permeability, thereby reducing the potential for sub-glacial recharge. At this time, there is not enough evidence to support either methane hydrate formation or sub-glacial recharge as the main process influencing the observed geochemical trends.

This research indicates further consideration of deep fluids across the Canadian Shield is necessary for safe radioactive waste disposal. Although Shield brines were not formed through a freezing process, more dilute fluids (~<50 g·L^{-1}) have been affected. The possibility for deep glacial meltwater intrusion into the Canadian Shield versus an *in situ* freeze-out mechanism (permafrost or methane hydrate formation) needs to be better constrained by collecting geochemical data from relatively undisturbed locations and analyzing recharge age and geochemical indications of freezing. Pressure and salinity measurements from within hydrothermal taliks will provide an understanding of flow direction within taliks, and the relative importance of taliks to deep flow system evolution beneath the permafrost. Hydraulic modeling should incorporate talik formation, density, temperature effects, and the potential for methane hydrate formation. A better understanding of the subsurface thermal history at individual sites, talik-permafrost interaction, and glacial recharge-discharge will further constrain processes involved in the evolution of fresh to moderately saline waters in the Canadian Shield.

Chapter 5

An Isotopic Survey of $\delta^{81}Br$ and $\delta^{37}Cl$ of Dissolved Halides in the Canadian and Fennoscandian Shields

5.1 Executive Summary

Chlorine and bromine are two major anionic components of most brines, and typically behave conservatively in groundwater systems. The origin and evolution of brines in Canadian and Fennoscandian Shields are further explored through a survey of chlorine and bromine stable isotopes. Although chlorine isotopes have been utilized in past investigations and are relatively well understood, very few investigations have analyzed for bromine isotopes. Weak correlations between chlorine and bromine isotopes indicate there is a process or several processes that affect each isotopic system differently. Halogens are followed through the cycle from the oceanic reservoir, to the mantle and formation of rocks, to metamorphism of surface rocks, into shield fluids, and freezing of fluids to identify the proceeses which might cause significant isotopic fractionation. Comparisons with other isotopic systems, such as $^{87}Sr/^{86}Sr$, indicate water-rock interactions at some sites likely influence halogen isotopic composition ($\delta^{37}Cl$, $\delta^{81}Br$). Possible causes of a relationship between the fluid halide isotopic composition ($\delta^{37}Cl$, $\delta^{81}Br$) and methane gas isotopic composition ($\delta^{2}H$, $\delta^{13}C$) are discussed. At this time, knowing the bromine isotopic composition does not significantly add to the current understanding of Shield fluid evolution. However, as fractionation processes are defined and established, and isotopic values are obtained for various end-members such as rocks and fluid-inclusions, the chlorine and bromine isotopic tools will provide valuable information with regards to the evolution of brines in Shield envirinoments.

5.2 Introduction

Deep groundwaters in the Canadian and Fennoscandian Shields often have salinities exceeding 200 $g \cdot l^{-1}$ (e.g. *Fritz and Frape 1982, Frape and Fritz 1987, Lahermo and Lampen 1987, Nurmi et al. 1988, Frape et al. 2004*). The formation and evolution of these brines have been attributed to several different processes, broadly grouped as allochthonous or autochthonous (*Frape et al. 2004*). Allochthonous Shield brines are derived from saline fluids which have moved into the crystalline

rock environment, and are related to some form of concentrated seawater such as (1) evaporative concentration and emplacement of fluid, (2) migration and emplacement of sedimentary formation fluids, (3) dissolution of sedimentary evaporite deposits, and (4) freezing of seawater or seawater derivatives. Autochthonous brines form through water-rock interaction and include processes such as (1) dissolution of mineral phases, (2) mineral alteration, (3) leakage of fluid inclusions, and (4) magmatic fluid intrusions. It has been suggested hydrothermal systems may drive both allocthonous and/or autochthonous brine formation. The reader is referred to several reviews which discuss these processes as well as the origin and evolution of brines in crystalline rocks (*Bucher and Stober 2000, Frape et al. 2004*).

Halogens are usually considered conservative tracers in groundwater systems, providing a reliable indicator of fluid sources and interactions. In particular, chloride and bromide concentrations are used to identify processes that have impacted saline fluids and groundwaters (e.g. *Valyashko 1956, Ritenhouse 1967, Lundström and Olin 1986, Edmunds 1996*). Natural chlorine and bromine sources to groundwaters are marine (i.e. seawater, evaporites), crustal, or mantle (*Schilling et al. 1978*). Volcanic gases and hydrothermal fluids leave behind both fluid inclusions and minerals into which halogens have partitioned (e.g. *Yoshida et al. 1971, Kozłowski and Karwowski 1974, Unni and Schilling 1978, Roedder 1984*). Organic matter contains significant quantities of bromide, and provides bromide to waters in reservoirs high in organic matter, such as coal seams (*Edmunds 1996*). Precipitation and sea-spray provide halide inputs to groundwaters, particularly in coastal and semi-arid areas.

Chlorine stable isotopes ($^{37}Cl/^{35}Cl$) have been measured in conjunction with Br/Cl ratios to better constrain fluid and solute sources and processes. Several studies have investigated the natural distribution of $\delta^{37}Cl$ in waters, including Antarctic lakes (*Lyons et al. 1999*), sedimentary formation waters (e.g. *Eastoe and Guilbert 1992, Kaufmann et al. 1993, Eggenkamp 1994, Eastoe et al. 2001, Woulé Ebongué et al. 2005, Zhang et al. 2007, Shouakar-Stash et al. 2007, Shouakar-Stash 2008*), hot springs (*Kaufmann 1984, Kaufmann et al. 1984, Kaufmann 1989, Eggenkamp 1994, Zhang et al. 2004*), sedimentary formation waters and impacts of diagenesis (*Hesse et al. 2000, Deyhle et al. 2003, Kopf et al. 2003, Hess et al. 2006, Bonifacie et al. 2007b, Frape et al. 2007*), fluid inclusions (*Eastoe et al. 1989, Eastoe and Guilbert 1992, Banks et al. 2000, Chiaradia et al. 2006*) and crystalline brines (*Bryant 1995, Frape et al. 1995, 1998, 2004, 2007, Sie and Frape 2002,*). Chlorine isotopic composition may change due to mixing of fluid from different reservoirs, fluid rock interaction, and phase separation (e.g., *Magenheim 1995, Bonifacie et al. 2005, Liebscher et al. 2006b*). The effect of

fluid phase separation on chlorine isotopes is believed to be insignificant, but additional investigation is needed to determine pressure and temperature effects (*Liebscher et al. 2006b*).

Previous studies of crystalline Shield brines found $\delta^{37}Cl$ compositions to vary between -1.0 and +2.0‰ SMOC (*Frape et al. 1998, 2004*). $\delta^{37}Cl$ values are likely derived from local bedrock (e.g. *Sie and Frape 2002*), with mafic-hosted waters generally more enriched in ^{37}Cl than felsic-hosted waters (*Frape et al. 2004*).

The analysis of bromine stable isotopes ($^{81}Br/^{79}Br$) is now practical due to new analytical techniques (*Eggenkamp and Coleman 2000, Shouakar-Stash et al. 2005b*). To date, only the natural distribution of $\delta^{81}Br$ has been reported for sedimentary formation waters (*Eggenkamp and Coleman 2000, Shouakar Stash et al. 2005b, 2007, Frape et al. 2007, Shouakar-Stash 2008*), and fractionation processes are poorly documented. However, due to the chemical similarities between chlorine and bromine, $\delta^{81}Br$ should generally behave in a similar manner to $\delta^{37}Cl$. Bromine isotopes (^{81}Br, ^{79}Br) have greater masses and the percentage of heavy to light isotopes is approximately equal (49:51), therefore theoretically any fractionation may be less than for stable chlorine isotopes.

As pointed out earlier, bromide and chloride ions are believed to behave in a conservative fashion in most natural processes. Therefore, combining analyses of $\delta^{37}Cl$ and $\delta^{81}Br$ should provide more detailed information on processes affecting salinity in shield environments. The purpose of this study was to characterize $\delta^{81}Br$ and extend the database for $\delta^{37}Cl$ in Canadian and Fennoscandian Shield groundwaters, as well as assess the usefulness of $\delta^{37}Cl$ and $\delta^{81}Br$ isotopes as tools for evaluating evolutionary processes in crystalline environments.

Canadian and Fennoscandian Shield fluids have been affected by multiple evolutionary processes. Geochemical anomalies were observed between the Lupin field site, located in permafrost, and other Canadian Shield sites, such as depleted $\delta^{2}H\text{-}CH_4$ (*Chapter 3*) and high nitrate concentrations (*Chapter 2*). During freezing, solutes, including Cl^- and Br^-, are concentrated in the fluids. One aim of this survey of $\delta^{37}Cl$ and $\delta^{81}Br$ in Canadian and Fennoscandian Shield groundwaters is to provide an evaluation of processes that have the potential to fractionate the halide stable isotopic compositions, including freezing during permafrost formation.

5.3 Methods

Seventy samples from crystalline shield environments were selected for $\delta^{37}Cl$, and $\delta^{81}Br$ analyses. These included new samples collected at the Lupin field site and archived samples collected by previous researchers. Twenty of these samples were also analyzed for $^{87}Sr/^{86}Sr$ ratios to expand a previously published dataset and allow a comparison with an isotopic parameter used as an indicator

of water-rock interaction in crystalline environments (*Frape et al. 1984, McNutt et al. 1984, McNutt 1987, McNutt et al. 1987, Smalley et al. 1988, McNutt et al. 1990, Franklyn 1987, Franklyn et al. 1991, Negrel et al. 2003, Frape et al. 2004, Negrel et al. 2005*). Figure 5-1 displays sample locations in the Canadian and Fennoscandian Shields. Major ionic chemistry (Ca, Na, Mg, K, SO_4, Cl, HCO_3, Br) was available and previously published for each of the archived samples. The samples targeted for analyses were selected with the following criteria in mind: (1) to represent as many previously sampled Shield sites as possible, (2) to cover a range of $\delta^{37}Cl$ values (where previously analyzed), (3) to examine extreme Br/Cl or Ca/Na ratios, (4) to represent a range of salinities, and (5) to analyze samples where hydrocarbon and other gas data was available. Stable chlorine and bromine isotopic ratios were analyzed at the University of Waterloo Environmental Isotope Laboratory, following the procedures described by Eggenkamp (*1994*) and Shouakar Stash et al. (*2005a*) for chlorine isotopes and Shouakar Stash et al. (*2005b*) for bromine isotopes. Isotopic ratios of $^{37}Cl/^{35}Cl$ and $^{81}Br/^{79}Br$ were analyzed by Isotope Ratio Mass Spectrometry (IRMS), and are reported in permil (‰) deviation from an isotopic standard reference material using the conventional δ notation, where $\delta = ((R_{sample}/R_{standard})-1)*1000$. The reference materials for chlorine isotope analyses are Standard Mean Ocean Chloride (SMOC) and Standard Mean Ocean Bromide (SMOB) for bromine isotope analyses. Analytical precision is ±0.1‰ for both $\delta^{37}Cl$ and $\delta^{81}Br$. Strontium isotopic ratios were determined using Thermal Ionization Mass Spectrometry (TIMS) with an analytical precision of $2\sigma = 0.00004$, following procedures described by McNutt et al. (*1990*). Analyses were corrected to the standard NIST-987 (NIST-987 = 0.710249).

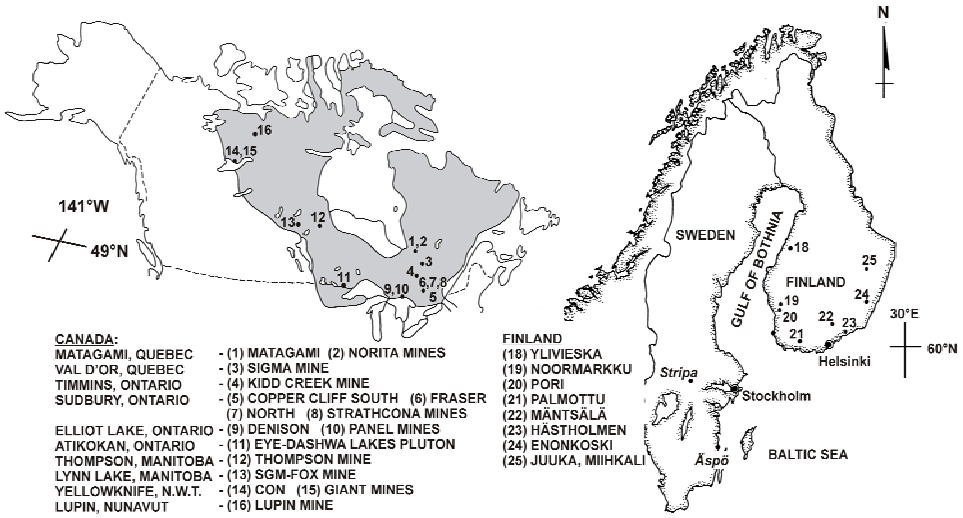

Figure 5-1. Groundwater sample locations in Canada and Finland (not at same scale) for samples analyzed in this study.

5.4 Results

The $\delta^{37}Cl$ and $\delta^{81}Br$ isotopic ratios of samples analyzed in this study varied between -0.78 ‰ and 1.52 ‰ (SMOC) and 0.01 ‰ and 2.04 ‰ (SMOB), respectively (Table D-1 in Appendix D). Isotopic compositions sampled from the Fennoscandian Shield ($\delta^{37}Cl$: -0.54 ‰ to 1.52 ‰, SMOC; $\delta^{81}Br$: 0.26 ‰ to 2.04 ‰, SMOB) are more positive and have a greater range than those sampled from the Canadian Shield ($\delta^{37}Cl$: -0.78 ‰ to 0.98 ‰, SMOC; $\delta^{81}Br$: 0.01 ‰ to 1.29 ‰, SMOB). The $\delta^{37}Cl$ ratios for samples analyzed in this study have a smaller range than previously analyzed samples. Figure 5-2, Figure 5-3, and Table 5-1 display the complete $\delta^{37}Cl$ and $\delta^{81}Br$ dataset for groundwater samples collected in the Canadian and Fennoscandian Shields. The $\delta^{37}Cl$ and $\delta^{81}Br$ values exhibit a skewed distribution (Figure 5-2, Table 5-1).

Table 5-1. Statistical evaluation of $\delta^{37}Cl$ and $\delta^{81}Br$ distributions in Canadian and Fennoscandian Shield samples $\delta^{37}Cl$ data are from Bryant (*1995*), Sie (*1999*), Pitkanen et al. (*1999*), Sie and Frape (*2002*), Frape et al. (*2004*), Palmen and Hella (*2003*), S.K. Frape unpublished data, and this study.

	All Samples		Canada		Finland		Sweden
	$\delta^{37}Cl$	$\delta^{81}Br$	$\delta^{37}Cl$	$\delta^{81}Br$	$\delta^{37}Cl$	$\delta^{81}Br$	$\delta^{37}Cl$
n	327	62	63	44	172	18	92
Max (‰)	2.07	2.04	0.98	1.29	2.07	2.04	0.72
Min (‰)	-1.32	0.01	-0.78	0.01	-0.62	0.26	-1.32
Mean (‰)	0.11	0.77	-0.16	0.49	0.32	1.44	-0.10
Median (‰)	0.12	0.68	-0.19	0.37	0.31	1.70	-0.10
Mode (‰)	-0.19	0.23	-0.19	0.23	0.12	1.70	-0.23
Std. Dev. (‰)	0.46	0.59	0.28	0.34	0.42	0.52	0.46
Variance	0.22	0.34	0.08	0.11	0.18	0.27	0.21
Skew	0.42	0.74	1.03	0.73	1.03	-1.02	-0.35
Kurtosis	1.99	-0.71	3.61	-0.43	3.58	-0.06	-0.17

Considering all of the data, $\delta^{37}Cl$ has a weak, but statistically insignificant (R^2 = 0.36), positive correlation with $\delta^{81}Br$ isotopic ratios for all sites (Figure 5-4). Deeper fluids generally have lower $\delta^{37}Cl$ and $\delta^{81}Br$ values (Figure 5-4A), but there is little correlation with TDS (Figure 5-4B). Two trends are apparent when $\delta^{81}Br$ is compared with Ca/Na ratio. On Figure 5-5A, a plot of the Ca/Na ratio versus $\delta^{81}Br$, a minor trend of increasing Ca and enriched $\delta^{81}Br$ appears to exist in fluids with higher concentrations. Many of the less concentrated fluids form a more or less horizontal line across the diagram around a Ca/Na ratio of 1.0, regardless of isotopic value. As Ca/Na ratios increase, the variability of $\delta^{37}Cl$ compositions decreases (Figure 5-5B). On Figure 5-5C, a plot of Br/Cl versus $\delta^{81}Br$, no trends are apparent in the dataset; although the range of Br/Cl values appears to narrow as the isotopic value becomes more enriched. A similar trend may be found when Br/Cl ratios are compared with $\delta^{37}Cl$ composition, however the data are more scattered (Figure 5-5D). Variability of

fluid $\delta^{37}Cl$ composition decreases as stable isotopic compositions ($\delta^{2}H$, $\delta^{18}O$) of the fluids sampled become more depleted (Figure 5-6A,B). There is a slight positive trend when stable isotopic compositions ($\delta^{2}H$, $\delta^{18}O$) are compared with $\delta^{81}Br$ (Figure 5-6C,D).

(A)

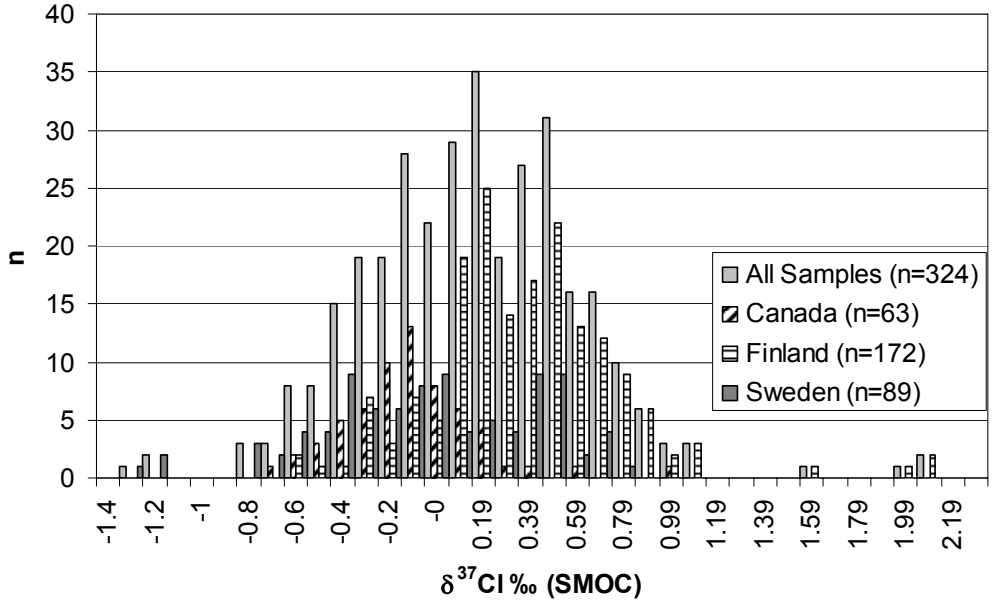

(B)

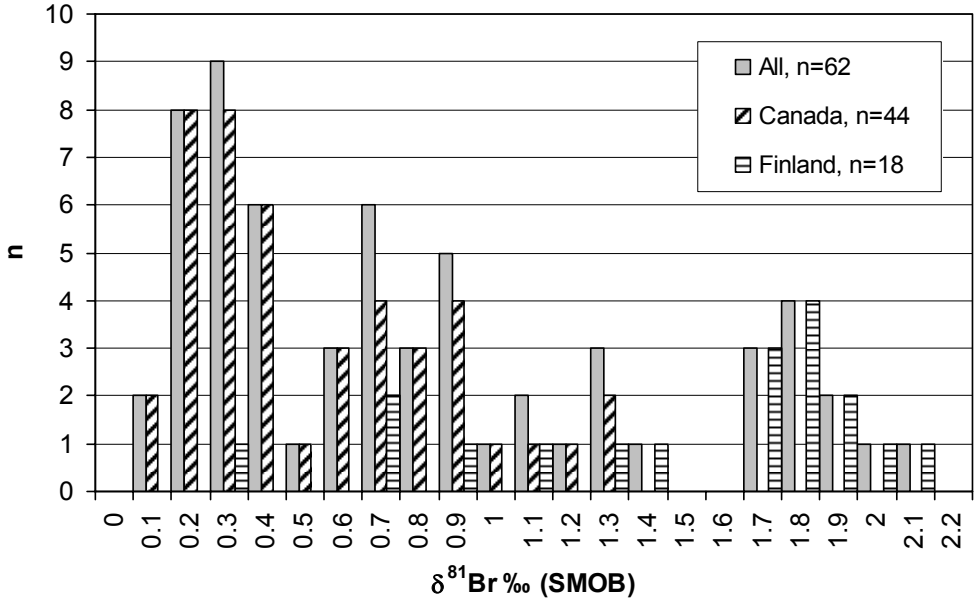

Figure 5-2. Frequency of (A) $\delta^{37}Cl$ and (B) $\delta^{81}Br$ from the Canadian and Fennoscandian Shields. All data analyzed in this and previous investigations are displayed. $\delta^{37}Cl$ data are from Bryant (*1995*), Sie (*1999*), Pitkanen et al. (*1999*), Sie and Frape (*2002*), Frape et al. (*2004*), Palmen and Hella (*2003*), S.K. Frape unpublished data, and this study.

(A)

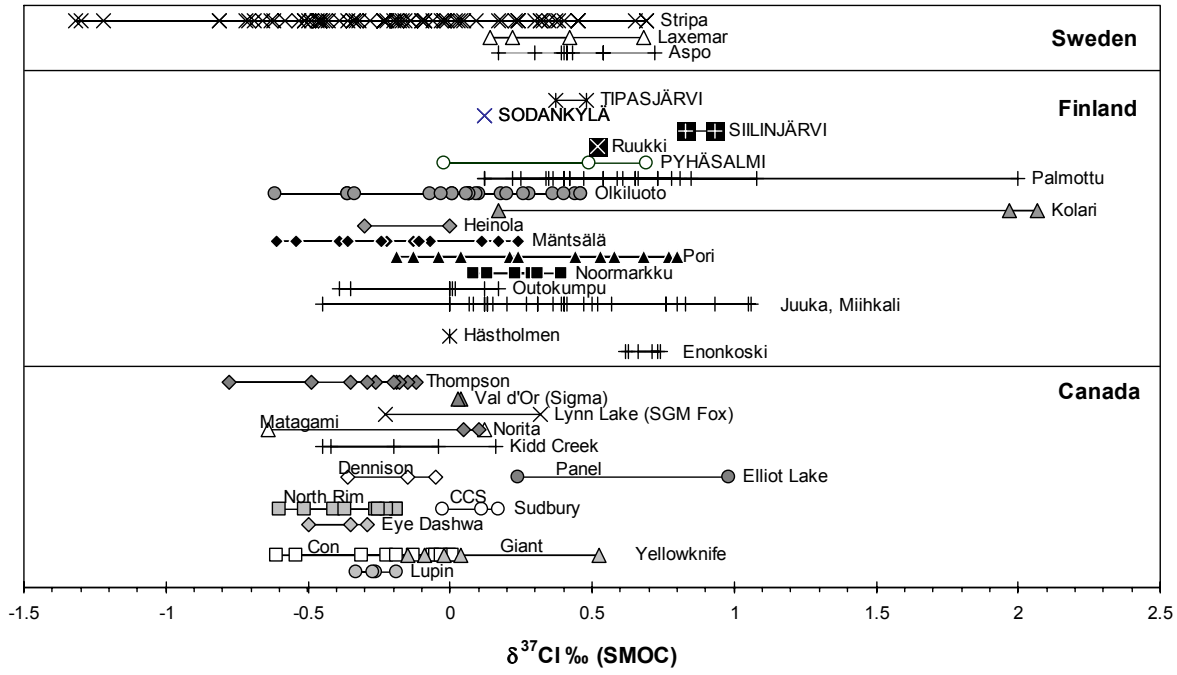

(B)

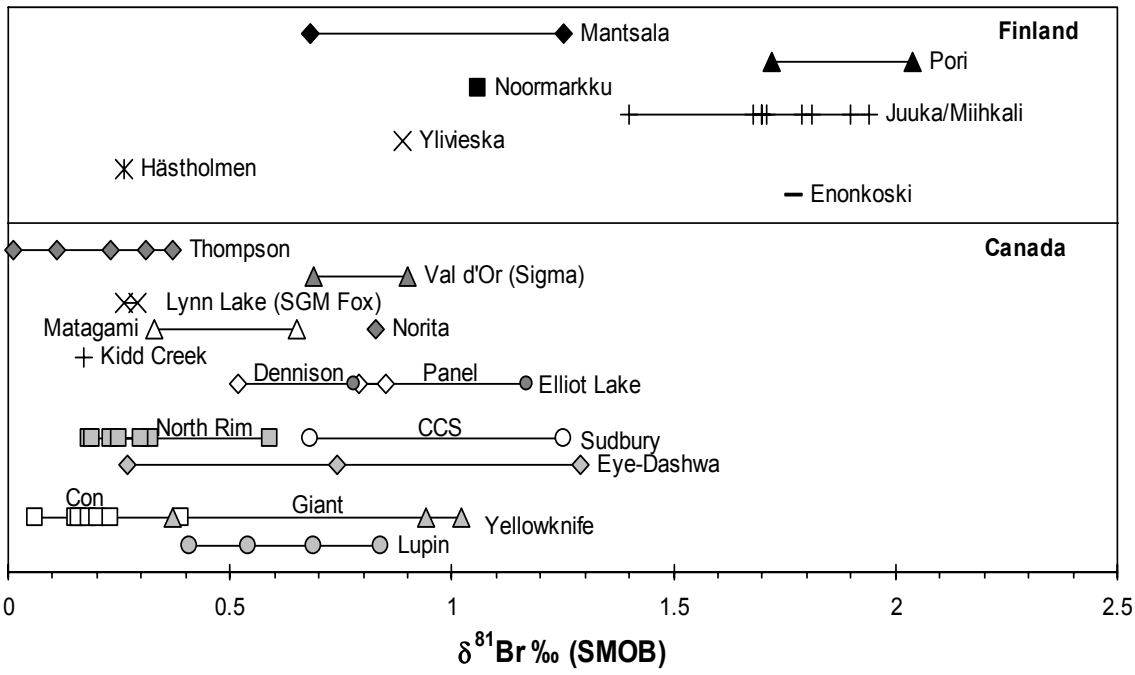

Figure 5-3. Distribution of $\delta^{37}Cl$ and $\delta^{81}Br$ at individual sites. All data analyzed in this and previous investigations are displayed. $\delta^{37}Cl$ data are from Bryant (*1995*), Sie (*1999*), Pitkanen et al. (*1999*), Sie and Frape (*2002*), Frape et al. (*2004*), Palmen and Hella (*2003*), S.K. Frape unpublished data, and this study.

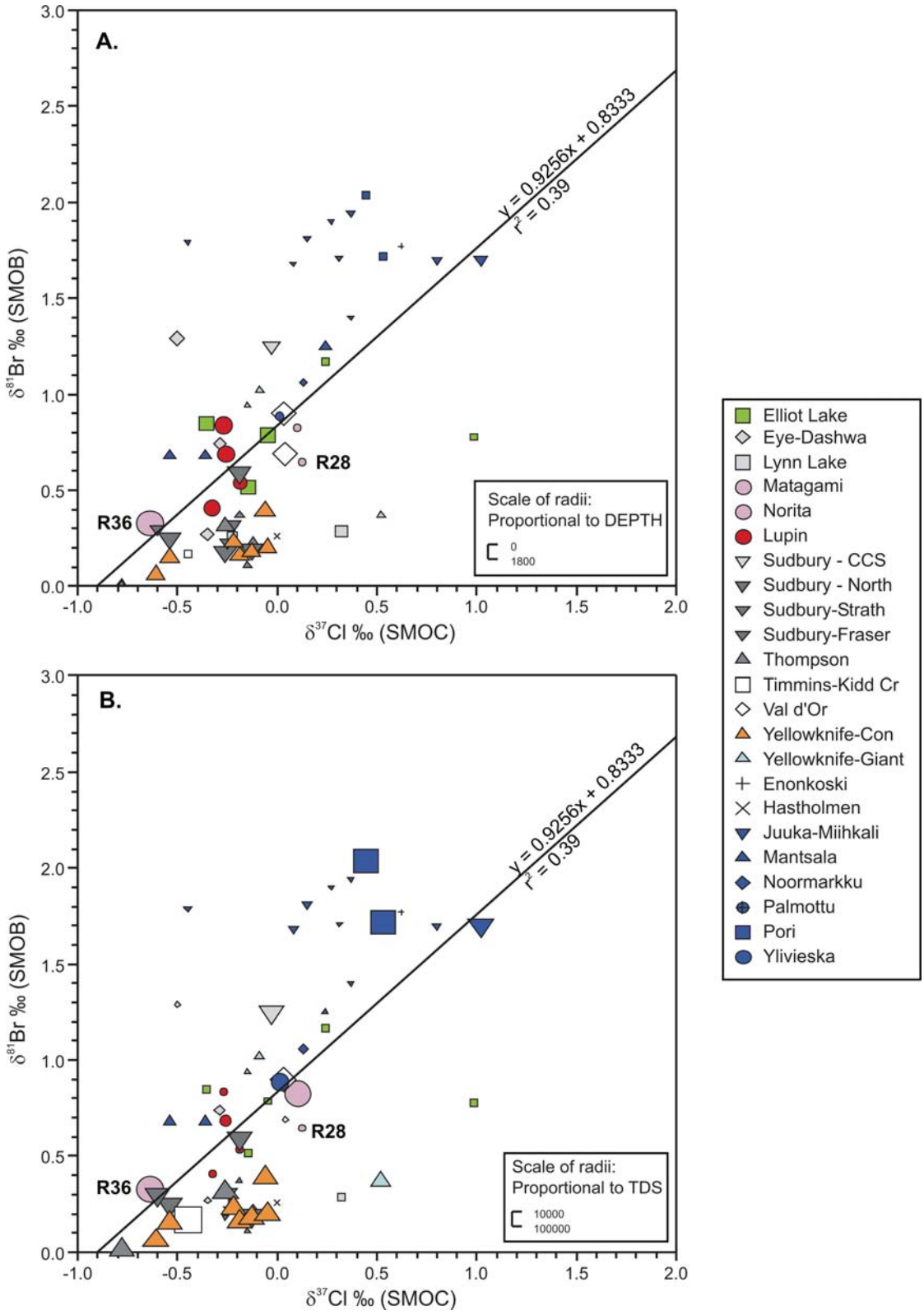

Figure 5-4. δ^{81}Br vs. δ^{37}Cl for Canadian and Fennoscandian Shield groundwater samples analyzed in this study, (A) with symbols scaled with respect to sample depth (deeper samples are larger) and (B) TDS (brines are the largest symbol size, fresh and brackish the smallest).

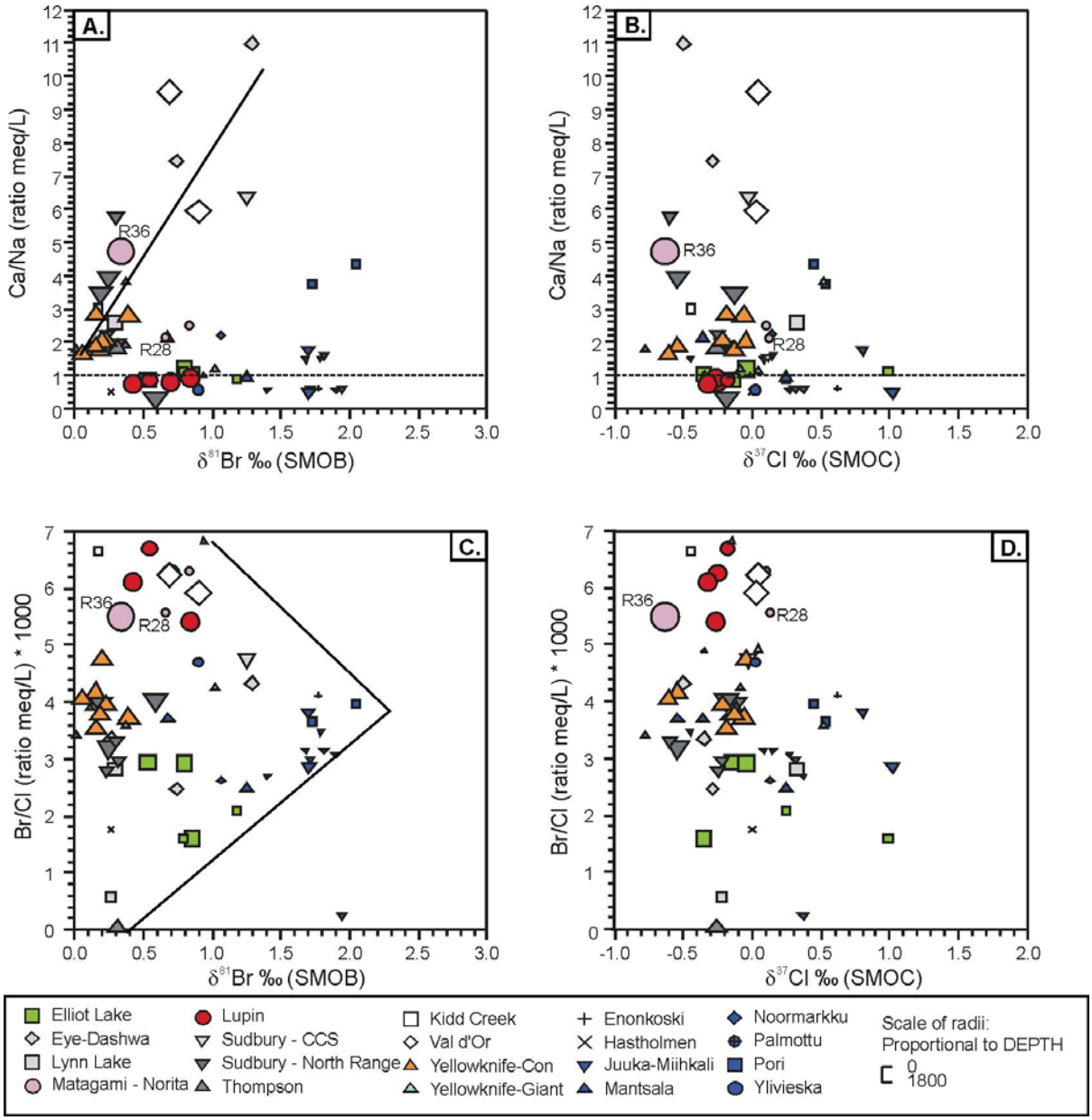

Figure 5-5. Ca/Na vs. (A) δ^{81}Br and (B) δ^{37}Cl; Br/Cl vs. (C) δ^{81}Br and (D) δ^{37}Cl for Canadian and Fennoscandian shield groundwater samples analyzed in this study. Symbols are scaled relative to depth (larger symbols reflect deeper samples).

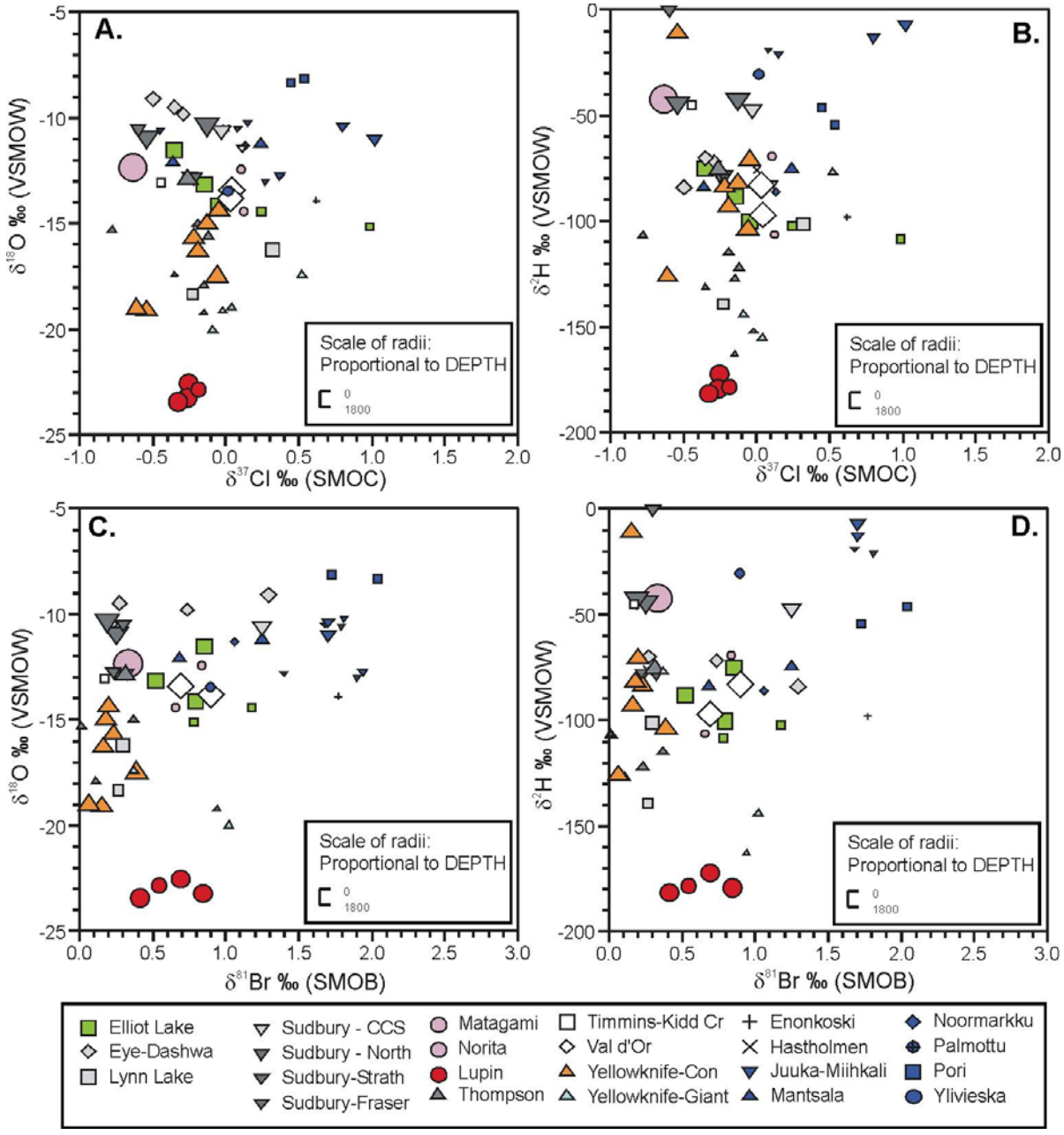

Figure 5-6. $\delta^{37}Cl$ vs. (A) $\delta^{18}O$ and (B) $\delta^{2}H$; $\delta^{81}Br$ vs. (C) $\delta^{18}O$ and (D) $\delta^{2}H$ for Canadian and Fennoscandian Shield groundwaters analyzed in this study. Symbols are scaled relative to depth (larger symbols reflect deeper samples).

Variability in $\delta^{37}Cl$ and $\delta^{81}Br$ ratios in crystalline groundwater samples decreases with increasing depth, with a trend towards depletion of the heavy isotopes (Figure 5-7). Since the major chloride and bromide fluid reservoirs are found at depth, depletion or loss of light isotopes (^{35}Cl and ^{79}Br) should occur in shallow compared with deep groundwaters. In the shallower groundwater system, loss of light isotopes may result from a number of processes, including diffusion, acidification and volatilization, or oxidation, all of which preferentially remove light isotopes. These processes will be discussed in more detail later in this chapter.

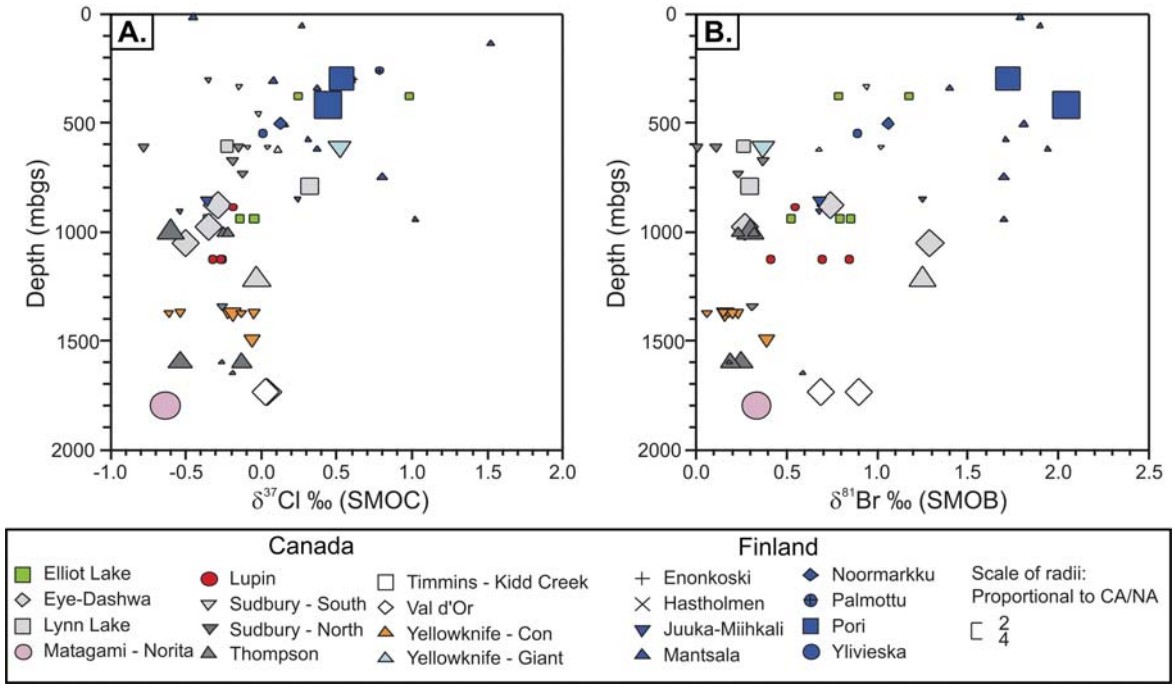

Figure 5-7. Relationship of $\delta^{37}Cl$ (A) and $\delta^{81}Br$ (B) with depth in Canadian and Fennoscandian Shield groundwaters analyzed in this study. Symbols are scaled with respect to Ca/Na ratios, such that calcium-type waters are large symbols, sodium-type waters are small symbols, and sodium-calcium or calcium-sodium type waters are medium sized symbols.

5.5 Discussion

The results indicate both $\delta^{37}Cl$ and $\delta^{81}Br$ in crystalline shield groundwaters have a similar range of approximately 2 ‰. This is consistent with studies in sedimentary basins, where the range for $\delta^{81}Br$ was found to be similar to that of $\delta^{37}Cl$ (*Shouakar-Stash et al. 2007, Shouakar-Stash 2008*). The $\delta^{81}Br$ ratios in Shield fluids are heavier than modern seawater, while $\delta^{37}Cl$ values vary withn ± 1 ‰ from

ocean chloride. The heavy bromide isotopic values may be indicative of a significant fractionation process or solute source. Fennoscandian Shield groundwaters tend to be heavier than Canadian Shield groundwaters for both $\delta^{37}Cl$ and $\delta^{81}Br$ (Figure 5-2).

Previous investigations of stable chlorine isotopes noted a large range of variable and dominantly non-marine $\delta^{37}Cl$ ratios in Fennoscandian waters compared with the Canadian Shield, and suggested the most concentrated Fennoscandian Shield fluids have similar $\delta^{37}Cl$ signatures to those of the rock matrix fluids. Less concentrated fluids varied from the rock $\delta^{37}Cl$ signature, some of which were were identified as intruded Baltic Seawater (*Bryant 1995, Frape et al. 1995, 1998, Sie and Frape 2002*). Generally, the rocks had positive $\delta^{37}Cl$ ratios and dilute waters were more negative (*Frape et al. 1995, Frape et al. 1998, Sie and Frape 2002*). This resulted in two patterns in Fennoscandian Shield waters: a trend towards increasing Cl^- concentration associated with ^{37}Cl enrichment, and a number of samples with a wide range of $\delta^{37}Cl$ values and little or no change in the Cl^- concentration (*Frape et al. 1995*). Primary processes such as magmatic/hydrothermal activity were believed to be responsible for the $\delta^{37}Cl$ ratios in the most concentrated fluids at each site (*Frape et al. 1995*).

A relationship between ultra-mafic and mafic rocks and higher $\delta^{37}Cl$ values was previously observed in the Fennoscandian Shield (*Bryant 1995, Frape et al. 1995, 1998*). As an example, the $\delta^{37}Cl$ signatures were sampled at the Miihkali site in Finland, located in a Proterozoic metaturbidite sequence of mica gneiss; often referred to as actinolite-albite rock, which is part of an ophiolite complex overthrusted onto continental crust (*Lahermo et al. 1989, Halonen et al. 1990*) The $\delta^{37}Cl$ values sampled from deep fluids associated with serpentinite units at the Juuka-Miihkali site are amongst the most enriched sampled in a Shield environment (+1.1 to + 1.3 ‰ SMOC, *Frape et al. 1998, Frape et al. 2004*), and are similar to other rock and mineral $\delta^{37}Cl$ values from boreholes at the same site not shown on Figure 5-8 (+1.3 to +1.5 ‰ SMOC, *Frape et al. 1998*). Shallow groundwater samples are less saline and $\delta^{37}Cl$ values deviate from rock values, indicating mixing and intruded waters (*Frape et al. 2004,* Figure 5-8). Deeper fluids have similar chlorine isotopic values as the altered-ultramafics, and fluid chemistry abrubtly changes, suggesting long-term equilibrium has occurred (Figure 5-8, *Frape et al. 2004*).

Fluid $\delta^{37}Cl$ values from boreholes sampling ultramafic and mafic units in the Canadian Shield exhibit a different relationship compared with the Fennoscandian Shield. For example at the Matagami Mine, borehole R36 samples mafic units, while borehole R28 was drilled through felsic units. The $\delta^{37}Cl$ value in R36 (-0.64 ‰ SMOC) is amongst the lowest sampled from the Canadian Shield, compared with R28 (+0.12 ‰ SMOC) which is amongst the highest (Figure 5-4). Lower $\delta^{37}Cl$

values were also observed at the Thompson Mine (-0.70 to -0.12 ‰ SMOC), another mafic Canadian Shield site (Figure 5-4).

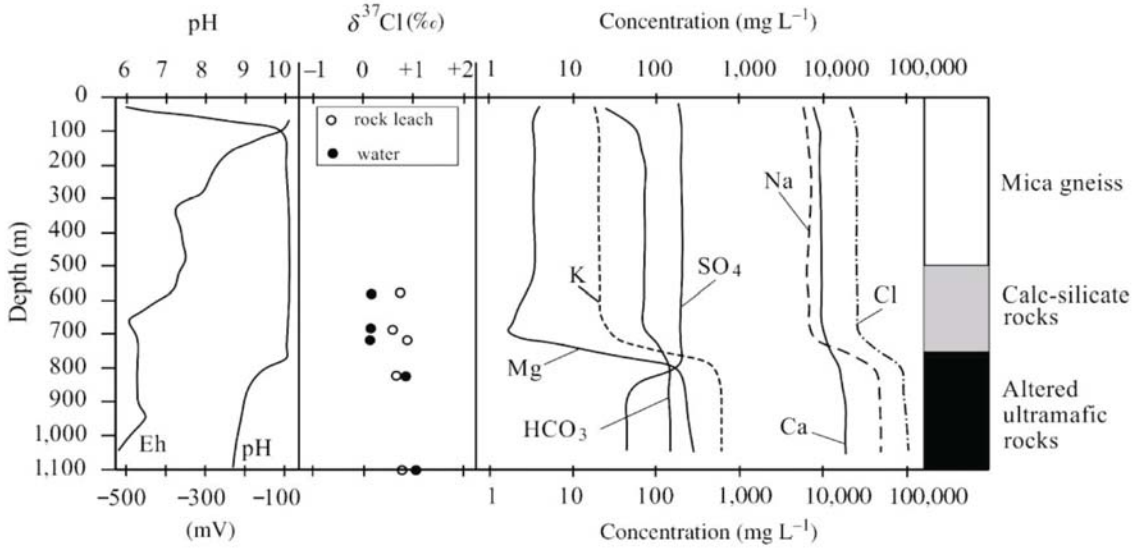

Figure 5-8. Geology, major element water chemistry, Eh and pH, and stable chlorine isotope analyses of rock and water as functions of depth in drill hole Ju/Mi-116, eastern Finland. From Frape et al. (*2004*).

A similar trend is also observed for δ^{81}Br values. In the Canadian Shield, the mafic Thompson Mine and the Matagami Mine R36 samples are all less than +0.4 ‰ SMOB (Figure 5-4), amongst the lowest sampled in either Shield, but the felsic Matagami Mine R28 sample had a δ^{81}Br value of +0.7 ‰ SMOB. Also similar to the δ^{37}Cl trend, the Juuka-Miihkali δ^{81}Br values are consistently amongst the highest values in the study, between +1.4 and +1.9 ‰ SMOB.

Unlike Matagami, δ^{81}Br from the Juuka/Miihkali site is relatively invariant between different water samples, despite significant change in δ^{37}Cl, resulting in a near- horizontal trend on a plot comparing the two isotopes (Figure 5-4). Halide dissolution could conceivably cause this fractionation pattern (*Shouakar Stash 2008*). Peridotite alteration products are serpentinites and salt (*Fyfe 1987*), and the relationship between δ^{37}Cl and δ^{81}Br in fluids sampled in the Juuka/Miihkali serpentinites may represent the salt phase created during serpentinite formation.

It is likely the halides in the rock units have also influenced the isotopic ratios at Matagami, even though the relationship is opposite to that of mafic units in the Fennoscandian Shield. Unlike the Miihkali region, mafic units in the Matagami area are of submarine volcanic-exhalative origin, with subsequent hydrothermal alteration of rhyolitic units (*Roberts 1975, MacGeehan 1978, MacGeehan and MacLean 1980, MacGeehan et al. 1981, Piché et al. 1993*). Halide isotope signatures found in

rocks associated with submarine volcanic-exhalative origins and subsequent hydrothermal alteration should be different from halides in serpentinites affected by fluid-dehydration-mineral hydration reactions, ion filtration, and salt dissolution because of the different processes involved. Fumarolic minerals formed from gases typically have very negative $\delta^{37}Cl$ values (-5 ‰ SMOC) due to repeated sublimation and condensation, although $\delta^{37}Cl$ values directly associated with base metals are typically enriched (+6 ‰ SMOC) (*Eggenkamp and Schuiling 1995*). During open-system serpentinization, serpentinites become enriched due to incorporation of ^{37}Cl into the rock and loss of ^{35}Cl back into the ocean (*Barnes and Sharp 2006*). However, a study of the alteration product, reactant, and unaltered rock should better illuminate how hydrothermal fluids affected halides in the system. A thorough investigation of both $\delta^{37}Cl$ and $\delta^{81}Br$ in rocks, minerals, fluid inclusions, and fluids at individual sites should therefore provide important details to the origin and evolution of halides in both fluids and rocks.

Halide sources and processes affecting halides should have a role in defining the observed isotopic values in groundwaters. This discussion will examine the halide cycle, focusing on the sources and the processes that change halide concentrations in fluids to determine which processes may be important to isotopic fractionation in the crystalline Shield environment. Investigations of $\delta^{81}Br$ to date have focused on characterizing the natural distribution (*Eggenkamp and Coleman 2000, Shouakar Stash et al. 2005b, 2007, Frape et al. 2007, Shouakar-Stash 2008*). To guide future studies, the following discussion provides an overview of stable chlorine isotope fractionation processes which are relevant to Shield waters, and hypothesize the relative effects of these processes to $\delta^{81}Br$ ratios to focus future research.

5.5.1 Formational Processes: High Temperatures

The Canadian and Fennoscandian Shields have evolved as a result of volcanism, magmatic processes, and numerous metamorphic events (e.g. *Häkli 1971, Roberts 1975, Härme 1978, Paktunç 1984, Maas et al. 1986, Robert and Brown 1986a,b, Piché 1993, Ruskeeniemi et al. 1996, Hanley et al. 2005, 2006*). Mantle chlorine is attributed to primordial chlorine and assimilated altered crust (*Unni and Schilling 1978, Michael and Schilling 1989*). Mantle halides return to the earth's surface via magmatic fluids, resulting in partitioning between fluids, melts, and gaseous phases. Halogens are generally incompatible elements in melts, and display a large spectrum of distribution coefficients between fluids and melts (*Villemant and Boudon 1999*). The slightly larger size of the Br^- ion (1.68 to1.96 Å – *Shannon 1976, Elliott et al. 1981*) means the smaller Cl^- ion (between 1.62 and 1.81 Å – *Fumi and Tosi 1964, Tosi and Fumi 1964, Shannon 1976*) is favored for partitioning into the solid phase, resulting in a fractionation of the Br/Cl ratio (e.g. *Schilling et al. 1980, Johnson et al. 2000*).

The $\delta^{37}Cl$ of the mantle is currently postulated to have a value between 0.0 and +7.2 ‰ SMOC (*Magenheim et al. 1995, Philippot et al. 1998, Banks et al. 2000, Stewart and Spivack 2004, Sharp et al. 2007*), and there are no estimates of the $\delta^{81}Br$ signature of the mantle, but by analogy to $\delta^{37}Cl$, an enriched signature is very likely.

5.5.1.1 Magmatic

Temperature, pressure, Cl/H_2O ratios, and melt composition (including solubilities of Cl, H_2O, SO_2, and CO_2) all affect halide solubility during melt solidification (*Webster 2004*). The halides have similar chemical properties and therefore, processes could be expected to affect Br and Cl solubility in a similar fashion. Phase changes are dependent on solubility conditions; therefore these factors may also contribute to halogen stable isotope fractionation (variations in $^{37}Cl/^{35}Cl$ and $^{81}Br/^{79}Br$).

In the subsurface, as mantle-derived fluids rise, boiling occurs at pressures less than ~150 MPa, resulting in separation of Cl-rich fluids into two immiscible phases. One is a low density, Cl-poor vapor, which may easily migrate to the surface, and the other is a hypersaline, high-density, liquid enriched in chloride-complexed metals capable of generating hydrothermal ore deposits at depth (*Hedenquist and Lowenstren 1994*). The large density contrast between the vapor and hypersaline liquid commonly results in the phases separating within the magma chamber or its adjacent hydrothermal system (*Henley and McNabb 1978*). The aqueous vapor, often containing CO_2, SO_2, H_2S and/or HCl, tends to ascend on formation, either discharging to the surface as volcanic fumaroles or becoming absorbed at depth, resulting in an acidic water capable of leaching the host rock (*Henley and McNabb 1978, Hedenquist and Lowenstern 1994*).

Partial degassing during magma assent can result in chemical fractionation (or a change in Br/Cl ratio), since the larger Br^- anion degasses more readily than Cl^-, especially in acidic environments (*Schilling et al. 1980, Berndt and Seyfried 1997, Bureau et al. 2000, Liebscher et al. 2006a*). Temperature-dependent isotope fractionation is expected during phase transformations between aqueous, gaseous, and solid phases, with the lighter chlorine isotope (^{35}Cl) preferentially enriched in the vapor phase (*Bonifacie et al. 2005*). This process should result in fluids with a wide range in $\delta^{37}Cl$ values from very negative to +1.0‰ (*Bonifacie et al. 2005*). Light isotope enrichment in the vapor or gas phase and heavy-isotope enrichment in the solid phase is commonly observed in other isotope systems, as the molecules containing the heavy isotope are more stable and have higher dissociation energies than those containing the light isotope (e.g. during equilibrium exchange, ^{18}O in ice, ^{16}O in vapor), a result of stronger bond strength of heavier isotopes (*Clark and Fritz 1997*).

Therefore, based on the behavior of other elements including chlorine, light bromine isotopes (^{79}Br) are also postulated to be enriched in the vapor phase during boiling and phase transformations.

5.5.1.2 Rocks

There are only limited studies of $\delta^{37}Cl$ in igneous and metamorphic rocks, thus much is yet to be learned about these reservoirs and their internal geochemical interactions (*Stewart and Spivack 2004*). Chloride is known to substitute for OH^- in non-sedimentary minerals including sodalite and scapolite (*Pan and Dong 2003*) and hydrated silicates, particularly amphiboles, biotite, and apatite (*Ito and Anderson 1983, Kamineni 1986, Vanko 1986, Morrison 1991, Enami et al. 1992, Zhu and Sverjensky 1992*). Chloride substitution for OH^- can occur over a wide range of pressure, temperature, and fluid compositions in geothermal, igneous, and metamorphic environments (*Ito and Anderson 1983, Kamineni 1986, Vanko 1986, Morrison 1991, Enami et al. 1992*).

Bromide has also been found to substitute into apatite, sodalite, and scapolite group minerals (*Elliot et al. 1981, Pan and Dong 2003*). Unlike halides and apatite-group minerals which have a preference for Cl^- over Br^- (*Siemann and Schramm 2002, Pan and Dong 2003*), Br and Cl are equally incorporated into scapolite-group minerals and sodalite (*Pan and Dong 2003*). Crystallization of a Cl^- bearing phase, such as apatite or Cl-bearing mica, would remove Cl relative to Br, due to their incompatible nature (*Johnson et al. 2000*). Cl-OH partitioning is pH-dependent (*Johnson et al. 2000*), with chloride preferentially substituting within the apatite structure in alkaline environments. Discussion of $\delta^{37}Cl$ ratios in amphiboles is found in Section 5.5.1.4. Ion size is an important factor in halide substitution in amphiboles and biotite. Because ionic radii increase from OH^- to Cl^- to Br^-, the size of the OH^- cavity is integral to halide substitution (*Enami et al. 1992, Oberti et al. 1993*). The smaller size allows the Cl^- ion to substitute more readily than the Br^- ion, increasing the Br/Cl ratio of the remaining fluid (*Martin 1999*). Isotopic fractionation could be expected, depending on the completeness of the reaction. Typically, heavier isotopes are thermodynamically preferred in the solid phase.

5.5.1.3 Volcanic

Halogen contents have been measured in some volcanic gases (*Sugiura et al. 1963, Jordan 2003, Bobrowski et al. 2003*, *Gerlach 2004, Lee et al. 2005, Aiuppa et al. 2005*), however both volcanic gases, and the phase and form of halogens, are difficult to measure under *in situ* conditions (*Symonds et al. 1990*). The Br/Cl ratios in volcanic gases vary significantly (*Sugiura et al. 1963*, references in *Jordan 2003*, *Gerlach 2004*). A wide variety of brominated and chlorinated compounds are found in

volcanic gases, including HBr, HCl, chlorofluorocarbons, methyl halides, halogenated aromatics, and halogen oxides (*Jordan 2003, Bobrowski et al. 2003*, *Gerlach 2004*, *Lee et al. 2005*). Many of these compounds may be key ingredients in the relationship between co-existing hydrocarbon gases and bromine and chlorine stable isotopic signatures in fluids as discussed at the end of this chapter. It is likely most of these compounds form during high-temperature mixing in the atmosphere or near-vent environments (*Jordan 2003, Gerlach 2004*), but it is possible they may also form in the subsurface for short periods during high-temperature reactions with CH_4 and other carbon compounds as crustal organic matter undergoes thermal cracking during magma upwelling, reacting with halogens (*Jordan 2003*). Therefore, volcanoes emit reactive bromine and chlorine compounds, with a range of oxidation numbers, as opposed to the (-1) oxidation number for bromide and chloride.

The variation in redox states and pH implied by the formation of the compounds discussed above can be expected to cause significant isotopic fractionation of Cl and Br. Higher oxidation states of chlorine are predicted to be enriched in ^{37}Cl (*Schauble et al. 2003*). As well, fractionation is increased depending on the cations that bond with Cl; for instance +2 cations will have greater ability to cause fractionation than +1 cations, and silicates should be 2-3 ‰ enriched compared to co-existing brines (*Schauble et al. 2003*). Gas phase HCl should also be enriched with ^{37}Cl compared to dissolved Cl^- (*Richet et al. 1977, Volpe 1998, Schauble et al. 2003*), but the fractionation should be small at high temperatures (<0.3‰ at T>200°C) (*Richet et al. 1977*). The overall effect to the larger volcanic halogen reservoir should be minimal, because the reactions described above predominately occur in the near-vent/atmospheric environment and account for only trace amounts of the total reservoir of Br and Cl (*Jordan 2003, Gerlach 2004*). However, the result may be observed in volcanic gases. Volcanic gas condensate $\delta^{37}Cl$ values range between -1.2 ‰ to 5.69 ‰ (*Eggenkamp 1994, Godon et al. 2004a*), and values for fumarolic minerals range between -0.46 ‰ to -4.88 ‰ (*Eggenkamp and Schuiling 1995*). Two different processes may act to influence the isotopic signatures near volcanic vents: (1) lighter isotopes are transported in gases with incorporation of heavier isotopes into rocks and/or (2) acidification of gases results in transport of heavy isotopes (^{37}Cl, ^{81}Br). The effects of changing pH and redox conditions to $\delta^{81}Br$ values are currently unquantified. However, bromine oxidizes more readily than chlorine (e.g. *Ericksen 1981*), particularly in acidic conditions (*Eggenkamp and Coleman 1999, Shouakar Stash et al. 2005b*) and therefore the potential for fractionation is greater (*Eggenkamp and Coleman 1999*).

5.5.1.4 Metamorphic

The processes described in the previous sections likely have had a significant impact upon the original $\delta^{37}Cl$ and $\delta^{81}Br$ values of rocks in the Canadian and Fennoscandian Shields. However,

subsequent metamorphism at most sites likely altered the rock isotopic ratios further and thus would be more likely to influence $\delta^{37}Cl$ and $\delta^{81}Br$ values in Canadian and Fennoscandian Shield groundwaters. The changing influences to $\delta^{37}Cl$ and $\delta^{81}Br$ values over time in the Shields will be further discussed in a conceptual model developed at the end of this chapter.

Chlorinity decreases in marine pore waters as a result of clay mineral dehydration reactions, alteration of biogenic silica, and ash alteration (*Deyhle et al. 2003*). High bromine concentrations and low Cl/Br ratios in peridotites and other ophiolites altered by serpentinization are likely caused by the clay-like properties of the serpentinites (*Rehtijärvi 1984, Appel 1997*, *Orberger et al. 1990*). The serpentinites act as a semi-permeable membrane to retain Br^- from brines created during peridotite alteration in the presence of seawater, resulting in serpentinites with high Br contents (*Appel 1997*). Chloride can be hosted in two sites in serpentinites, a structurally bound site and a water-soluble site (*Sharp and Barnes 2004*). Depleted $\delta^{37}Cl$ values (-1 to -8 ‰ SMOC) in some marine pore fluids may be the result of the alteration process (*Ransom et al. 1995*, *Deyhle et al. 2003, Godon et al. 2004a, Hesse et al. 2006*). Chlorine isotope fractionation due to ion filtration can be affected by P-T conditions, tectonic stress, chemistry and mineralogy of sediments involved and their physical hydraulic properties such as porosity, permeability, hydraulic conductivity (*Godon et al. 2004a*).

Fluid dehydration-mineral hydration reactions lead to progressively more saline fluids, increasing chloride content in amphiboles, biotites, and other granulite-facies mineralogy, and salt deposition in granulites (*Markl and Bucher 1998, Nijland et al. 1993, Kullerud 1996*). Prograde metamorphic devolatilization/dehydration and mineral precipitation/transformation reactions cause Cl isotope fractionation, with ^{35}Cl released to fluid, enriching the solid in ^{37}Cl (*Ransom et al. 1995, Spivack et al. 2002, Godon et al. 2004a*). The effect on $\delta^{81}Br$ would likely be similar, with ^{79}Br enrichment in the fluid and ^{81}B enrichment in the solid. On the other hand, it has also been suggested that chlorine isotopic compositions in granulite facies may be unrelated to either mantle degassing or metamorphism (*Markl et al. 1997*).

High temperature hydrothermal alteration of amphiboles favors the formation of Cl^--rich hornblende, but depending on water/rock ratios, Cl^--poor actinolite or Cl^-rich amphiboles can form during lower temperature alteration (*Vanko 1986*). The observed enrichment in ^{37}Cl relative to seawater in amphiboles is interpreted as the result of fractionation during incorporation of Cl^- from the fluid phase (*Magenheim et al. 1995*). Temperature and pressure also affect the $\delta^{37}Cl$ values of hydrothermal amphiboles. Lower $\delta^{37}Cl$ values are found in amphiboles that formed at higher temperature/pressures (*Magenheim et al. 1995*). If Br^- were present in the amphiboles instead of Cl^-,

Br should fractionate isotopically in a similar manner. It is unclear how $\delta^{37}Cl$ and $\delta^{81}Br$ values would be affected if both Br and Cl were present.

The processes associated with metamorphism have been shown to affect $\delta^{37}Cl$ values, and as well can reasonably be assumed to fractionate Br. With the given data, the effect on modern Shield fluids is difficult to discern. There are no correlations between halide isotopes with $\delta^{2}H$ or d-excess (d-excess = $\delta^{2}H - 8*\delta^{18}O$) in groundwaters (Figure 5-6). Excess deuterium relative to the GMWL is an indicators of moderate to low temperature silicate alteration in Canadian and Fennoscandian Shield fluids (*Frape et al. 1984, Pearson 1987*). Further, because fluid mixing is likely at individual sites (Chapter 4), detailed analyses of the $\delta^{37}Cl$ and $\delta^{81}Br$ signatures in rocks and fluid inclusions are likely required to constrain long-term effects of metamorphic processes to Shield groundwaters.

5.5.2 Internal & External Modifications: Intermediate to Low Temperatures

5.5.2.1 Water-Rock Interaction

Bonifacie et al. (*2007b*) demonstrated that during metamorphism, if there is a high water-chloride to rock-chloride ratio, the influence of $\delta^{37}Cl$ from the original rock will be small, but $\delta^{37}Cl$ from the water may significantly influence the rock $\delta^{37}Cl$. If there is a low water-chloride to rock-chloride ratio, the reverse would be true. Two studies by Bonifacie et al. (*2005, 2007b*) show low temperature interactions impart more negative $\delta^{37}Cl$ values on fluids; consequently, secondary minerals formed from these fluids have a more negative signature than those formed from seawaters (*Sharp and Barnes 2004, Bonifacie et al. 2007a*). A similar relationship has been observed for oxygen isotopes (*Taylor 1977b*). Given the observed results in oxygen and chlorine isotopic systems, a similar scenario is hypothesized for bromine isotopes. If there is a high water-bromide to rock-bromide ratio during metamorphism, fluid $\delta^{81}Br$ values should also significantly influence rock $\delta^{81}Br$.

Water-rock interactions in the Canadian and Fennoscandian Shields have been previously investigated utilizing $^{87}Sr/^{86}Sr$ ratios (*Frape et al. 1984, 2004, McNutt et al. 1984, 1987, 1990, McNutt 1987, Smalley et al. 1988, Franklyn 1987, Franklyn et al. 1991, Negrel et al. 2003, 2005*). In crystalline shield groundwaters, strontium is a proxy for calcium, and correlates positively with Br (*McNutt et al. 1984, 1990*). The $^{87}Sr/^{86}Sr$ ratio in waters is typically equilibrated with one or more minerals (mineral phase of whole rock or fracture-filling) at a given locality. Therefore brines typically have a uniform $^{87}Sr/^{86}Sr$ ratio, and are sensitive indicators of mixing (*McNutt 1987, McNutt et al. 1990*). It is expected that closely comparing the $\delta^{37}Cl$ and $\delta^{81}Br$ values with $^{87}Sr/^{86}Sr$ at individual sites may provide additional information concerning the formation and evolution of brines

in crystalline shield groundwaters (Figure 5-9). More detailed discussion of strontium isotopes at each of the sites discussed below is available in other publications (*McNutt et al. 1984, 1990, McNutt 1987, Franklyn et al. 1991*).

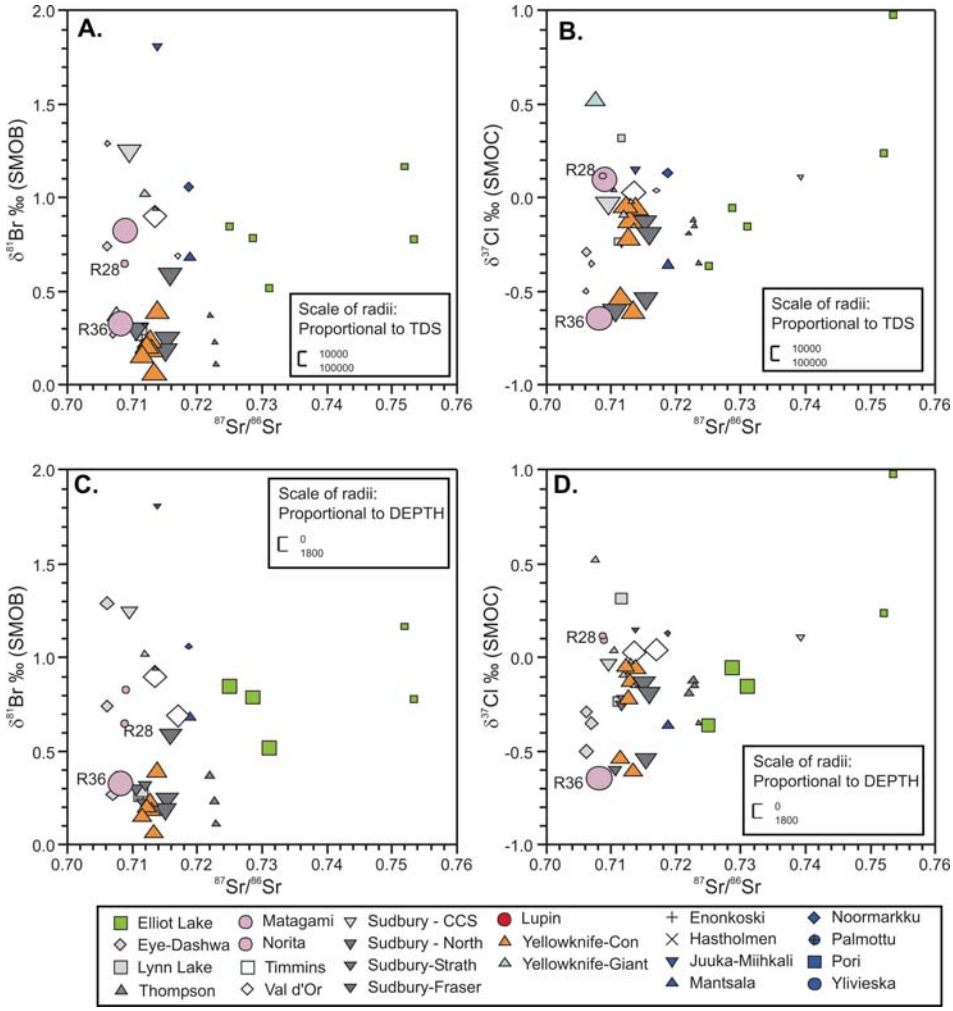

Figure 5-9. $^{87}Sr/^{86}Sr$ vs. $\delta^{81}Br$ (A and C), and $^{87}Sr/^{86}Sr$ vs. $\delta^{37}Cl$ (B and D) for Canadian and Fennoscandian Shield groundwaters analyzed in this study. Symbols are scaled relative to TDS (A and B), with the largest symbols representing brines, and relative to depth (C and D) with the largest symbols representing the deepest samples.

At Matagami/Norita, fluid $^{87}Sr/^{86}Sr$ ratios are similar to fracture-filling calcites (*McNutt et al. 1990*). As discussed, the $\delta^{81}Br$ and $\delta^{37}Cl$ values at these sites are higher in felsic than mafic units. The $^{87}Sr/^{86}Sr$ ratio is slightly higher in the felsic sample (0.7086) than the mafic sample (0.7081). This may indicate lithologic control, with some influence from calcite fluid inclusions to salinity of the

fluids at these sites. Chloride and bromide isotopic analyses of rocks and fluid inclusions are necessary to further define such a relationship.

At Eye-Dashwa, fluid $^{87}Sr/^{86}Sr$ ratios reflect dissolution of plagioclase (*Franklyn et al. 1991*). However, the plagioclase structure does not contain either Br^- or Cl^-, thus $^{87}Sr/^{86}Sr$ should not evolve like $\delta^{37}Cl$ or $\delta^{81}Br$ at this site. Higher $\delta^{81}Br$ values are associated with the plagioclase "fingerprint" $^{87}Sr/^{86}Sr$ ratios at Eye-Dashwa, but there are no trends when TDS, Sr, Br, or $\delta^{37}Cl$ are considered. The 1 ‰ range for $\delta^{81}Br$ values in water samples is associated with a smaller range in $\delta^{37}Cl$ (0.2 ‰) and in $^{87}Sr/^{86}Sr$ (0.7061-0.7070). As expected, the data therefore indicate Br and Cl evolve separately from Sr at this site.

Sudbury waters are divided into three groups based on geography and $^{87}Sr/^{86}Sr$ ratios: (1) Copper-Cliff Offset (South Sudbury), (2) North Range, east of a fault, and (3) North Range, west of, and within, a fault. The $^{87}Sr/^{86}Sr$ ratio for each of these groups is unique from the other, and is attributed to differences in norite composition at each location (Figure 5-10, *McNutt et al. 1984*). The $\delta^{37}Cl$ values obtained from minerals sampled from the North and South Ranges vary between -1.25 and 1.61 ‰ SMOC depending on mineral type and sample location (Figure 5-10, *Hanley et al. 2006*). Although a few groundwater samples from the North Range, both east and west of the fault, have $\delta^{37}Cl$ ratios consistent with North Range biotite, most are more enriched. This may indicate the groundwaters have contributions of norite-associated scapolite, which have more enriched $\delta^{37}Cl$ values (Figure 5-10, *Hanley et al. 2006*). With one exception, the $\delta^{37}Cl$ and $\delta^{81}Br$ values from both North Range groups are similar; the North-West of Fault group sample with the highest TDS also has the highest $\delta^{81}Br$ value of either group, with a slightly higher $^{87}Sr/^{86}Sr$ ratio. The overall similarity of $\delta^{37}Cl$ values in North Range groundwaters is striking, considering the multiple halogen-rich fluids that have been identified (*Hanley and Mungall 2003, Hanley et al. 2005, Hanley et al. 2006*). The brine sample from Copper Cliff South has the second highest $\delta^{81}Br$ value analyzed from the Canadian Shield, and the lowest $^{87}Sr/^{86}Sr$ ratio in the Sudbury area (0.014 less than other samples from the South group). The saline sample from the Copper Cliff Offset has a similar $^{87}Sr/^{86}Sr$ ratio as other samples from the group (*McNutt et al. 1984*), and a higher $\delta^{37}Cl$ value than the brine sample.

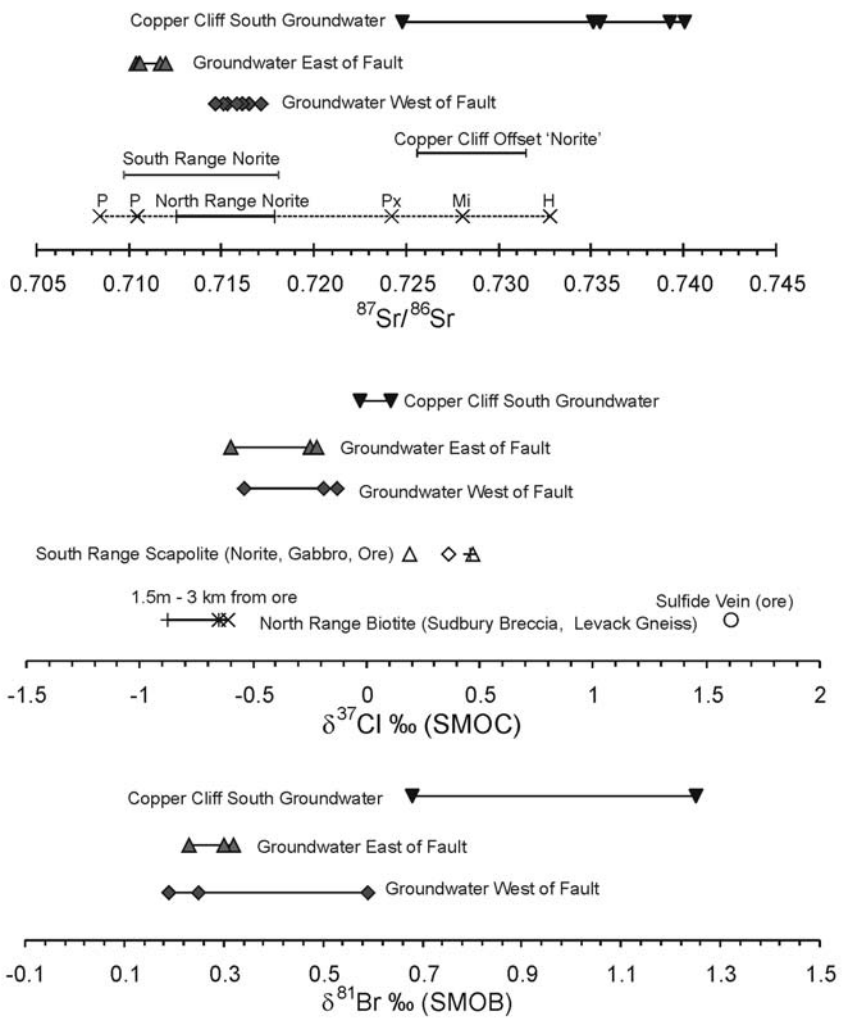

Figure 5-10. Comparison of $^{87}Sr/^{86}Sr$ ratios and $\delta^{37}Cl$ values in the groundwater and in the host rock and $\delta^{81}Br$ values in the groundwater around Sudbury. The $^{87}Sr/^{86}Sr$ plot is updated from McNutt et al. (*1984*), with rock and mineral data from Gibbins and McNutt (*1975*) and Hurst and Farhat (*1977*) (P = plagioclase, Px = pyroxene, Mi = micrographic intergrowth, H = hornblende), and fluid $^{87}Sr/^{86}Sr$ values from McNutt et al. (*1984*) and this study. Rock $\delta^{37}Cl$ values are from Hanley et al. (*2007*).

At other sites, rock influence on $^{87}Sr/^{86}Sr$ ratios is less identifiable, and fluid mixing may dominate (*McNutt et al. 1984, 1990, McNutt 1987*). For instance, in Thompson samples, $\delta^{81}Br$ values increase with decreasing $^{87}Sr/^{86}Sr$ ratios, but $\delta^{37}Cl$ values are statistically the same. The relationship between $\delta^{81}Br$ values and $^{87}Sr/^{86}Sr$ ratios does not correlate with TDS, Br, or Sr concentrations. Yellowknife samples (Con and Giant), exhibit a significant change in $\delta^{37}Cl$ values with very little change in $^{87}Sr/^{86}Sr$ ratios. However at the Con mine, $\delta^{81}Br$ values and $^{87}Sr/^{86}Sr$ ratios plot in a group,

compared with samples from the Giant mine which show significant difference in both $\delta^{81}Br$ values and $^{87}Sr/^{86}Sr$ ratios. At all sites, there is greater variance in $^{87}Sr/^{86}Sr$ ratios in more dilute, shallower waters, attributed to mixing (*McNutt et al. 1990*). In Elliot Lake waters, there are distinctly different $^{87}Sr/^{86}Sr$ ratios (0.7095 to 0.7309 vs. 0.7519 to 0.7533) and $\delta^{37}Cl$ values (-0.36 to -0.05 ‰ SMOC vs. 0.24 to 0.98 ‰ SMOC) for each of the two mines investigated (Dennison, Panel), however the $\delta^{81}Br$ range (0.52 to 0.82 ‰ SMOB vs. 0.78 to 1.17 ‰ SMOB) is too large to differentiate between the sites. The large variations between the different isotopic tracers at these sites are indicative of different solute sources.

Correlations between stable halide isotopes and strontium isotopes may be useful at sites where strontium-rich rocks, such as plagioclase, are present. In heterogeneous systems like crystalline Shields, different rocks may control different parts of the chemistry. A multiple isotope approach, similar to the analysis for $\delta^{37}Cl$ and $^{87}Sr/^{86}Sr$ at Sudbury (Figure 5-10), can help distinguish the rocks contributing to the salinity, providing valuable information about the fluid chemical evolution.

5.5.2.2 Marine Chlorine and Bromine

Although the mass of the crust is far greater than the oceans, concentrations of Cl^- and Br^- in seawater are significantly greater than in the continental crust (*Schilling et al. 1978*). Chloride and bromide concentrations in modern seawater are 19,000 and 65 $mg \cdot L^{-1}$, respectively (e.g. *Herrmann et al. 1973*), although seawater Br/Cl ratios may have changed significantly through time due to changes in the mid-ocean ridge hydrothermal brine flux (*Hardie 1996, Channer et al. 1997, Siemann 2003*), seawater evaporation rates (*Holland et al. 1996*), and/or deposition of marine organic sediments (*Channer et al. 1997*). One estimate suggests Archean seawater Br/Cl ratios were as high as 2.5×10^{-3} (ratio mmol/L) (*Channer et al. 1997*), compared with the present value of 1.3×10^{-3} (ratio mmol/L). It is generally accepted that there are no significant $\delta^{37}Cl$ variations in modern seawater ($\delta^{37}Cl$ = 0‰ SMOC, *Kaufmann 1984, Kaufmann et al. 1984, Eggenkamp et al. 1995, Godon et al. 2004b, Eastoe et al. 2007*), although several exceptions have been described, including ocean water above the Central Indian Ridge, where $\delta^{37}Cl$ varied within the water column between -0.53 and +0.94‰ SMOC (*Xiao et al. 2002, Shirodkar et al. 2003*), and in smaller, slightly isolated basins, such as the Black Sea (+0.4‰ SMOC, *Eastoe et al. 2007*), and the Baltic Sea (-0.21‰ SMOC, *Bryant 1995*). Several researchers argue against $\delta^{37}Cl$ variation in seawater over the Phanerozoic (*Eastoe et al. 2001, 2007, Stewart and Spivack 2004, Sharp et al. 2007*). Considering a mantle isotopic value of -1‰, it is estimated 10 Ga would be required to make a detectable change in the oceanic $\delta^{37}Cl$ signature (*Eastoe et al. 2007*). However, recent investigations of basin brines have implied that ocean $\delta^{37}Cl$ values vary with time (*Shouakar-Stash 2008*).

During NaCl and KClsalt precipitation, heavy isotope (^{37}Cl) enrichment in the solid and light isotope (^{35}Cl) enrichment in the fluid phase occurs, with fractionation factors varying depending on the particular salt mineral precipitating (*Eggenkamp et al. 1995*). The opposite effect occurs during hydration, as the heavy isotope is preferentially incorporated in the aqueous phase (*Musashi et al. 2007*). Bromine bearing salts form only at late stages of evaporation (*McCaffrey et al. 1987*), although bromide partitions into chloride precipitates throughout evaporation (*Valyashko 1956, Rittenhouse 1967*, *Hermann et al. 1973*, *Hermann 1980*, *McCaffrey et al. 1987, Siemann and Schramm 2000, 2002, Siemann 2003*). Bromide partitioning into chloride precipitates is not hypothesized to have a significant impact on fluid $\delta^{81}Br$ values, because only a small amount of bromide partitions into the chloride minerals (e.g. *Valyashko 1956*). Therefore during most of the evaporation process, $\delta^{81}Br$ fractionation may be insignificant. Likewise, it is postulated that bromine will not fractionate isotopically through salt dissolution.

In Canadian and Fennoscandian Shield groundwaters, fluids resulting from marine intrusions with very little external inputs can be expected to have $\delta^{37}Cl$ and $\delta^{81}Br$ ratios within ± 0.1‰ (the analytical precision) of seawater. This relationship was not observed in any of the shield fluids analyzed. The Hästholmen sample was previously interpreted as impacted by Litorina seawater (*Nordstrom 1986*). The $\delta^{37}Cl$ value is indicative of a marine origin (0.00‰ SMOC), but the $\delta^{81}Br$ sample is not (0.26‰ SMOB). However in small, semi-isolated marine basins like the Baltic and Black Seas, the modern $\delta^{37}Cl$ values vary (0.0±0.2‰ SMOC, *Bryant 1995, Eastoe et al. 2007*), likely due to non-marine inputs (*Eastoe et al. 2007*). Therefore, considering the Hästholmen sample as representative of the Litorina Sea, the $\delta^{81}Br$ value may either indicate non-marine inputs into a semi-isolated Litorina Sea, or post-emplacement enrichment of ^{81}Br. Due to the lack of $\delta^{81}Br$ analyses in modern semi-isolated seas, fluids with $\delta^{37}Cl$ values of 0.0 ± 0.1‰ SMOC and $\delta^{81}Br$ ratios of 0.00 to 0.26 ± 0.1‰ SMOB, are then considered as potentially of marine origin. However, from this study, only the most concentrated sample analyzed from the Con mine (237 g L^{-1}) falls in that range of values (sample 4500-6C, Table D-1). This concentrated sample is an end-member resulting from water-rock interaction (e.g. *Frape et al. 1984, Frape and Fritz 1987*), and therefore the chlorine is most likely non-marine in origin.

Fluids formed in sedimentary basins can migrate into crystalline shield environments (*Gascoyne et al. 1987, Gascoyne et al. 1989*). Fractionation observed in sedimentary basin fluids (0 ± 2 ‰ SMOC) is attributed to halite dissolution and/or precipitation (*Ransom et al. 1995*). However a significant range of $\delta^{37}Cl$ and $\delta^{81}Br$ values have been observed in sedimentary formation waters

(*Shouakar-Stash 2008*), and large isotopic variations in halite (0.0 ± 0.9‰ SMOC) are partially attributed to the addition of non-marine chloride (*Eastoe et al. 2001*).

5.5.2.3 Diffusion and Halide Escape

During diffusion, the diffusing Cl^- ions are depleted in ^{37}Cl relative to the initial, high-Cl^- fluids, as $\delta^{37}Cl$ values decrease away from the source (*Desaulniers et al. 1986, Phillips and Bentley 1987, Eggenkamp et al 1994, Eggenkamp et al. 1997, Eastoe et al. 2001*). In diffusion-dominated environments, similar behavior has also been observed in other isotopic systems, particularly in non-reactive systems, including $^2H/^1H$-H_2O, $^3H/^3He$, ^4He, $^{18}O/^{16}O$-H_2O, ^{36}Cl (*Desaulniers et al. 1981, Andrews 1985, Phillips and Bentley 1987, Solomon and Sudicky 1991, Fabryka-Martin et al. 1991*). Therefore, ^{81}Br is hypothesized to be depleted in diffusing fluids relative to the initial source fluids.

The increased variability and enriched $\delta^{37}Cl$ and $\delta^{81}Br$ values at shallower depths in the Canadian Shield could be attributed to diffusion (Figure 5-7). Rocks exposed at surface today in the Canadian and Fennoscandian Shields were once buried under kilometers of rock. In crystalline Shields, permeabilities decrease with depth (*Stober and Bucher 2000*). As the surface erodes over geologic time, new rock is exposed and permeabilities gradually increase in rock that was once deeply buried. Fluid inclusions also become more susceptible to rupture as pressures decrease and stresses are released. As the system opens, the 'escape' of matrix/rock halides becomes more likely. If the system is still dominantly diffusive, then over geologic time lighter isotopes (^{35}Cl, ^{79}Br) diffuse out of the shallow system, leaving an enriched isotopic reservoir. Light isotope removal may be enhanced by several processes including stronger concentration gradients due to more dilute meteoric fluids in shallow systems, volatilization due to reduced pressures as erosion occurs, and more acidic shallow flow systems that favor selective mobilization and removal of Br over Cl.

5.5.2.4 Fluid Freezing

Five different Canadian Shield fluids were carefully frozen to determine the effects of freezing on $\delta^{37}Cl$ (*Zhang and Frape 2002, Frape et al. unpubl. data*). These experiments demonstrated that in some, but not all fluids, ^{37}Cl enriches in the ice phase. However, the effect on the fluid reservoir is negligible, because the amount of chloride incorporated into the ice is very limited (~15 mg l^{-1}, *Zhang and Frape 2002*). Similar experiments to determine the effects of freezing on $\delta^{81}Br$ should have similar results. Except in situations where fluids are extremely limited, permafrost formation is not expected to significantly alter stable chlorine and bromine isotopic compositions, and may thus not be sensitive indicators for evaluating permafrost evolutionary pathways.

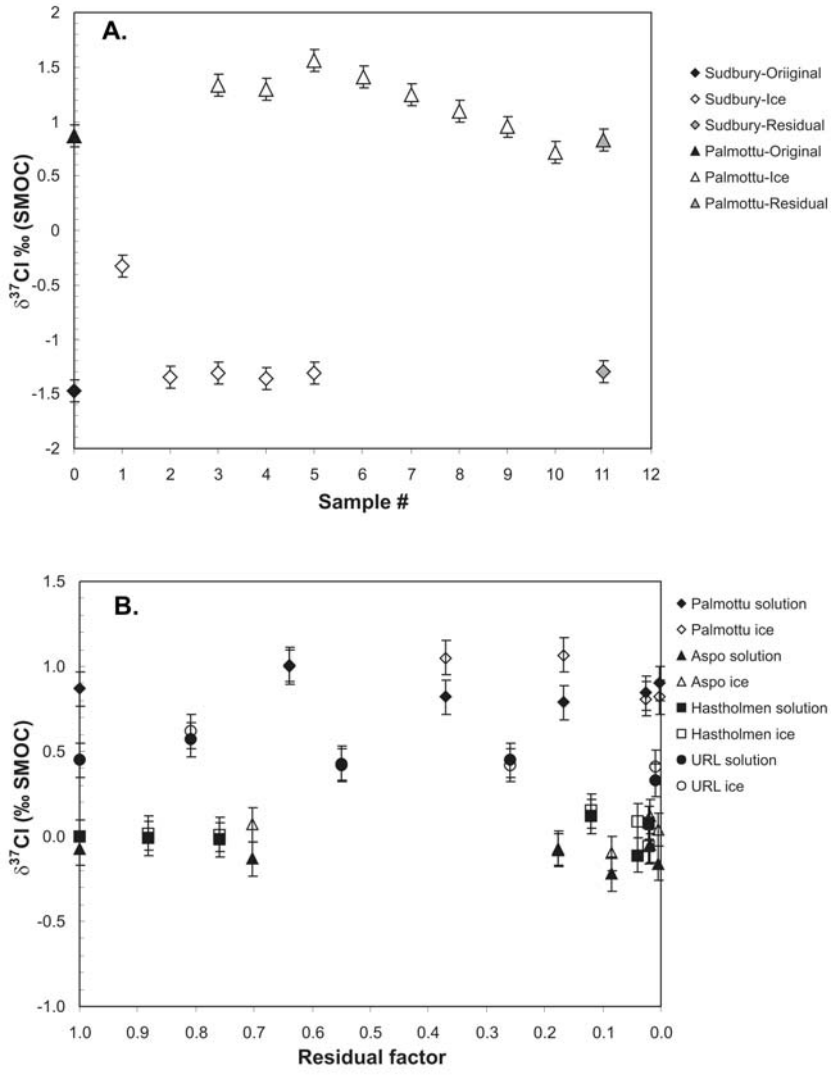

Figure 5-11. $\delta^{37}Cl$ vs. Residual Factor for Samples Taken from the Column (A) and Batch Experiments(B). Error bars represent analytical uncertainty. Modified from Zhang and Frape (*2002*), with data from Zhang and Frape (*2002*), Frape et al. (*unpublished*).

5.5.3 Other Relationships: Gases

There appears to be an increasing trend when $\delta^{37}Cl$ and $\delta^{81}Br$ are compared with the isotopic ratios of methane ($\delta^{2}H\text{-}CH_4$ and $\delta^{13}C\text{-}CH_4$) associated with the fluids (Figure 5-12). A much weaker correlation also exists between $\delta^{37}Cl$ and $\delta^{81}Br$ and the isotopic ratios of ethane ($\delta^{2}H$-C2 and $\delta^{13}C$-C2), for which there are fewer data available (Figure 5-13). In all instances, the trends with $\delta^{37}Cl$ are less apparent. The relationships with $\delta^{2}H\text{-}CH_4$ are particularly interesting, given the possibility of hydrogen-isotope exchange over long time-scales (*Waldron et al. 1999, Sessions et al. 2004*). Samples from three sites (Matagami, Sudbury North Range, and Pori) do not follow the trend, indicating locations where either

there is no link between the dissolved halide and the evolved gas components, or there is an additional, unknown process or processes occurring. Generally, an inverse relationship also exists between Br^- and SO_4^{2-} concentrations in Shield groundwaters (Figure 5-14). Previous studies in crystalline groundwaters indicated geochemical processes, rather than primary origin, control isotopic composition of sulfate (*Fritz et al. 1994*).

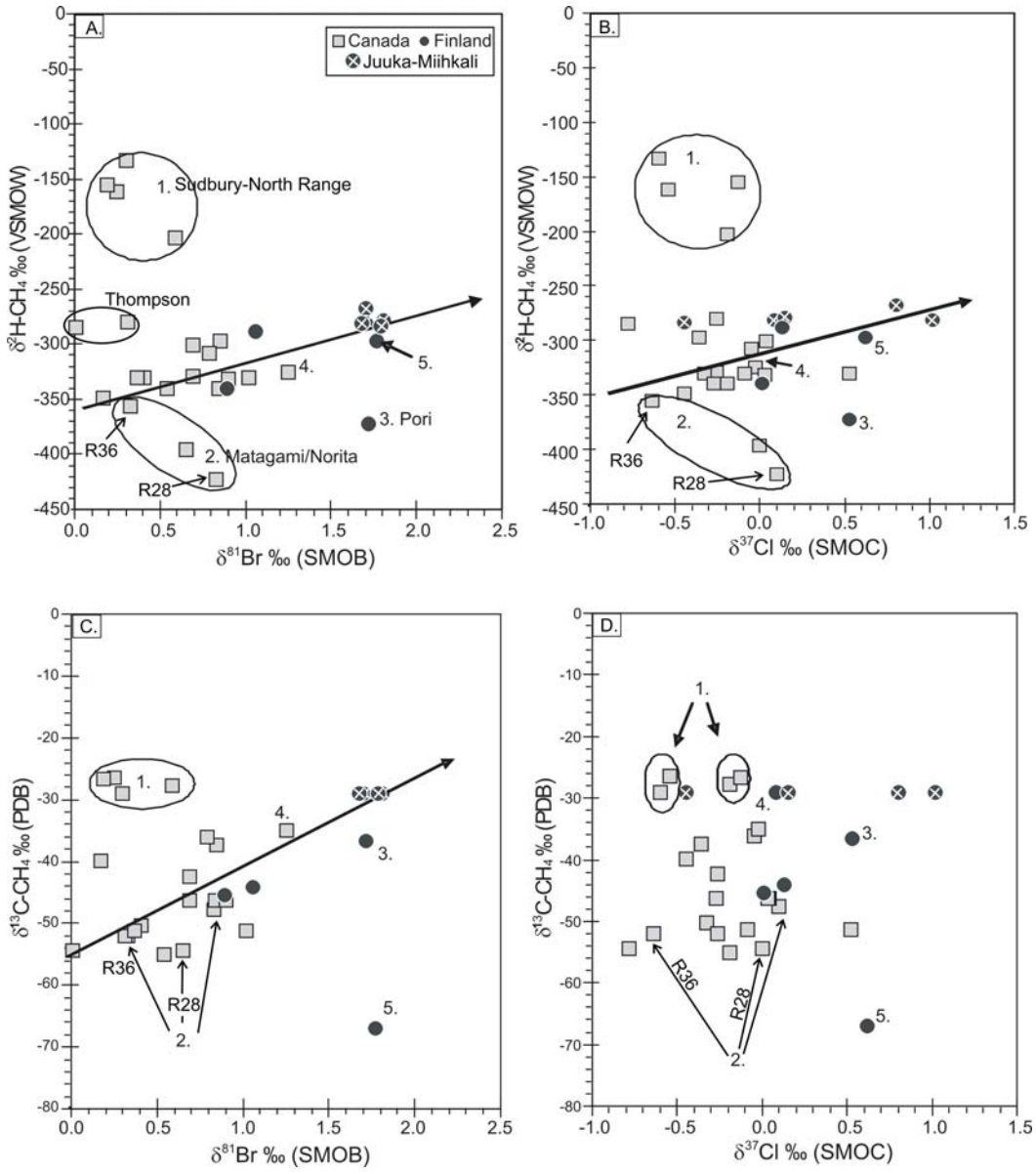

Figure 5-12. $\delta^{81}Br$ vs. $\delta^{2}H\text{-}CH_4$ (A), $\delta^{13}C\text{-}CH_4$ (C), and $\delta^{37}Cl$ vs. $\delta^{2}H\text{-}CH_4$ (B), $\delta^{13}C\text{-}CH_4$ (D) for Canadian and Fennoscandian Shield groundwater and gas samples. Sample Groups: (1) North Rim, Sudbury, (2) Matagami (boreholes R28 and R36 are discussed in the text) and Norita, (3) Pori, (4) Copper Cliff South, Sudbury, and (5) Enonkoski.

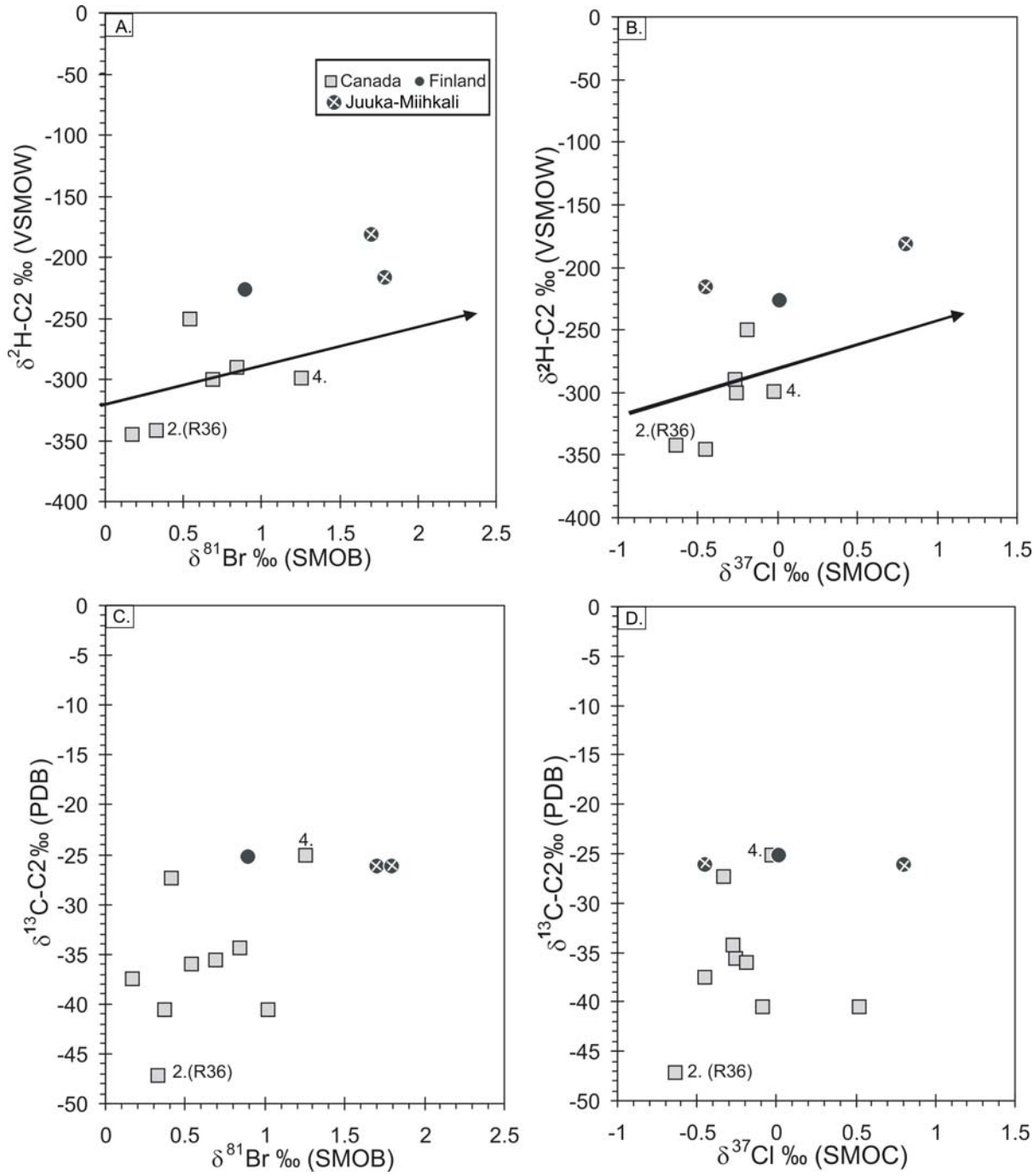

Figure 5-13. δ^{81}Br vs. δ^2H-C2 (A), δ^{13}C-C2 (C), and δ^{37}Cl vs. δ^2H-C2 (B), δ^{13}C-C2 (D) for Canadian and Fennoscandian Shield groundwater and gas samples. Sample Groups: (2) Matagami (borehole R36 is discussed in the text) and Norita, and (4) Copper Cliff South, Sudbury.

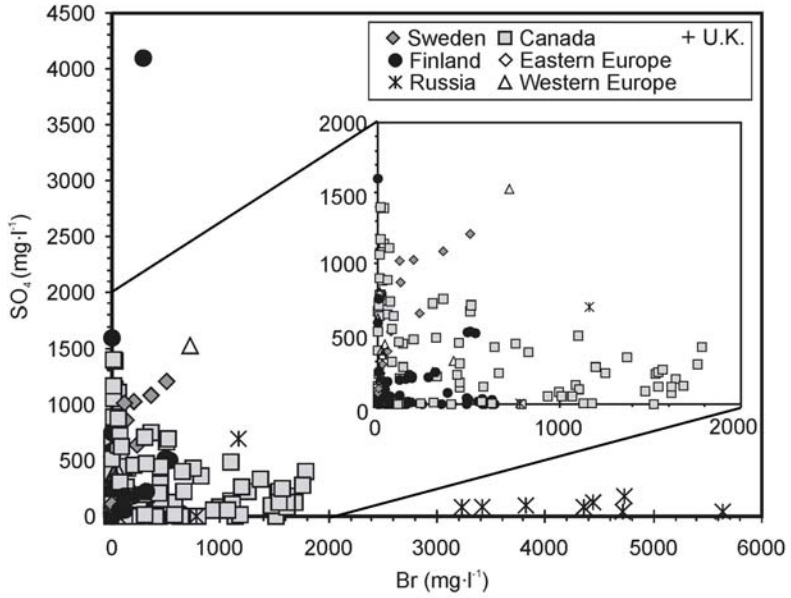

Figure 5-14. The relationship between Br^- and SO_4^{-2} for groundwaters sampled in crystalline rocks. Data from Frape et al. (*2004*).

The relationships described above may indicate that different chemical systems have co-evolved in shield groundwaters. Several SO_4^{2-} minerals, including gypsum, precipitate as salinity increases in Ca-dominated fluids similar to most shield fluids. The relationship between SO_4^{2-} and Br^- concentrations in shield groundwaters may also indicate several processes which could control bromide in shield groundwaters including diffusion, dissolution of early stage (SO_4^{2-}) vs. late stage (Br^-) evaporites, organic matter evolution, pH and redox, and changing in temperature and pressure conditions.

5.5.3.1.1 Diffusion

Isotope partitioning due to diffusion can be important for Cl and Br stable isotopes (Figure 5-7, Section 5.5.2.3), as there are relatively few chemical or biological reactions to mask the effects (*Desaulniers et al. 1986*). However, diffusion is not a very significant fractionation process for hydrocarbon gases (*Fuex 1980*). Biological and chemical effects cause significantly larger fractionation to gas isotopic compositions compared with diffusion (e.g. *Whiticar et al. 1986, Zhang and Krooss 2001*), thus the trend is not likely related to isotopic-diffusion for gases (Figure 5-12).

5.5.3.1.2 Evaporite Dissolution

Likewise, evaporite dissolution could not account for the relationships with CH_4 and C_2H_6 (Figure 5-12, Figure 5-13). Evaporite dissolution will primarily affect only $\delta^{37}Cl$ signatures, unless there is

significantly more Br^- in the evaporite than the initial fluid (*Shouakar-Stash 2008*). Likewise, methane and ethane would only be affected if large inclusions were found in the evaporite. However, even if methane and ethane were included in the evaporite, dissolution itself would not be the process responsible for the δ^2H and $\delta^{13}C$ signatures of the gases. Rather, a process related the gas genesis is much more likely to affect the δ^2H and $\delta^{13}C$ signatures of the gases. Therefore, the remaining possibilities will be explored in more detail.

5.5.3.1.3 Organic Matter Evolution

Bromide may be associated to one process associated with organic matter evolution, acetate fermentation. Therefore, the gas-halide trend (Figure 5-12, Figure 5-13) may be related to organic matter evolution. Bromine has been linked to dehydrogenation of acetate through the reaction (*Mallard et al. 1993*):

$$CH_3COOH + Br \rightarrow CH_3COO^- + HBr$$

As a part of acetate fermentation, it is possible the complete reaction may extend to:

$$CH_3COOH + Br \rightarrow CH_4 + CO_2 + HBr.$$

However, most Shield gases are of abiogenic origin, and the organic matter content in Shield rocks is typically low, (*Sherwood-Lollar et al. 1993a, 1993b*), and Cl^- concentrations and $\delta^{37}Cl$ values are not affected by organic matter evolution (*Eggenkamp et al. 1995, Lüders et al. 2002*). This further suggests organic matter evolution is not the process affecting the isotopic relationships (Figure 5-12, Figure 5-13).

5.5.3.1.4 Redox/pH

Changes in redox and pH are two mechanisms which may cause the isotopic compositions of halides and hydrocarbon gases to co-vary (Figure 5-12, Figure 5-13). Methane formation is redox-dependent, but Cl^- and Br^- are expected to be the dominant species for each respective element in most deep subsurface environments. As described earlier, pH affects partitioning of Br and Cl during rock formation and metamorphism, resulting in isotopic fractionations of Cl and likely Br. Acidic conditions during low- to mid- temperature metamorphism and hydrothermal/volcanic fluid flow often result in formation of HCl and HBr, encouraging the volatilization of halogens (*Hedenquist and Lowenstern 1994*). On the other hand, if buffering capacity exists within the host rock during magmatic-vapor/meteoric water interactions, acidic gases in magmatic vapor will exchange H^+ for cations in the host rock (*Hedenquist and Lowenstern 1994*). Changing redox conditions cause

fractionation in some isotopic systems, often with the help of bacteria (*Coleman et al. 1981, Whiticar et al. 1986, Krouse and Mayer 2000*). Methane oxidation can be initiated or catalyzed by halogens, following the equations (*Lary and Toumi 1997*):

$$Br^- + CH_4 \rightarrow CH_3^- + HBr,$$
$$Cl^- + CH_4 \rightarrow CH_3^- + HCl.$$

This hydrogen abstraction process is a function of temperature, pressure, and halide concentration. Therefore, the observed relationships between gas isotopes (δ^2H, $\delta^{13}C$) and halide isotopes ($\delta^{37}Cl$, $\delta^{81}Br$) in Shield environments (Figure 5-12) may be related to coupled changes in pH and redox.

5.5.3.1.5 Temperature and Pressure – Metamorphism

In subsurface Shield environments, metamorphism causes temperature and pressure changes. Thus it is possible the relationships between gas and halide isotopes (Figure 5-12, Figure 5-13) reflect the metamorphic processes and/or fluids which formed or influenced rocks at each site. Isotopic fractionations for many systems have been shown to be temperature and/or pressure dependent including hydrogen, carbon, and chlorine isotopic systems (e.g. *Friedman and O'Neil 1977, Richet et al. 1977*).

The different chemical components in the observed relationships (Figure 5-12) can be linked during serpentinization. The effects of serpentinization on halide concentrations and isotopic compositions were discussed earlier. Methane and other alkenes may also form abiogenically during serpentinization and silicate hydration reactions (*Szatmari 1989*, *Voytov 1991, Sherwood Lollar et al. 1993b, 2002, McCollom and Seewald 2001, 2003, Salvi and Williams-Jones 1997*). Although the serpentinization process has not occurred at all Shield locations, low-temperature silicate hydration accounts for enrichment of ^2H-H_2O in brines relative to the global meteoric waterline (*Fritz and Frape 1982, Pearson 1987*). Abiogenic CO_2 reduction during serpentinization follows the general reaction (e.g. *Lancet and Anders 1970*):

$$8H^+ + CO_2 \rightarrow CH_4 + 2H_2O$$

Carbon as CO_2 may also be involved with halides in a reduction reaction:

$$8HBr + CO_2 \rightarrow CH_4 + 2H_2O + 8Br^-$$

or, it is possible bromine may be reduced as well:

$$8HBr + CO_2 \rightarrow CH_4 + 2H_2O + 4Br_2$$

The different chemical components in the observed relationships (Figure 5-12) may also be linked at other metamorphic grades. For instance, in granulite facies, fluid inclusions are typically

CO_2-dominated, with N_2 and CH_4 (*Andersen et al. 1993, Van Reenen et al. 1994*), and hydrosilicates are Cl-enriched (See Section 5.5.1.2). As igneous rocks are heated significantly, sublimation of Cl^-, Br^-, F^-, I^-, NH_4^+, Na^+, and K^+ occurs, until Br^- and Cl^- are redeposited with NH_4^+ as temperatures drop below 200ºC (*Yoshida et al. 1965*). Investigations in some metamorphosed terrains indicate nitrogen may fractionate up to 10‰ between different grade metamorphic rocks, with higher $\delta^{15}N$ values correlating with higher grade rocks (*Mingram and Bräuer 2001*). This demonstrates that each of the chemical components (Cl^-, Br^-, CH_4, N_2) is linked during metamorphic processes. The original unmetamorphosed rocks at the sites could be expected to have significantly different $\delta^{37}Cl$ and $\delta^{81}Br$ ratios from metamorphosed rocks and different δ^2H-CH_4, $\delta^{13}C$-CH_4, and $\delta^{15}N$-N_2 values. Therefore, although the trends most likely reflect the temperatures and/or pressures which resulted in metamorphosing the rocks in equilibrium with the waters, additional studies to determine rock isotopic signatures and the temperature-pressure-isotope fractionation relationship are needed.

5.5.3.1.6 Outliers

The Sudbury North Range samples are significantly enriched in both ^2H-CH_4 and ^{13}C-CH_4 from the trends with $\delta^{37}Cl$ and $\delta^{81}Br$ (Figure 5-12, Figure 5-13). Unlike other metamorphic Shield sites (including Copper Cliff South), the Sudbury North Range was of magmatic origin, due to a large bolide impact (*Dietz 1964*, *Therriault et al. 2002, Mungall et al. 2004*). Fluid inclusion evidence suggests methane co-existed with a brine phase at much higher temperatures in the North Range (*Hanley et al. 2005*) than at most other Shield locations (*Sherwood-Lollar 1990, Sherwood-Lollar et al. 1993b*). Higher temperatures of formation would typically result in less overall fractionation, and values closer to the source. On Figure 5-12A, the Sudbury North Range outlier may occur because of the unique origin and high temperatures of fluids at this site. Alternatively this may indicate a unique origin for the gases or a de-coupling of Cl^- and Br^- from the gases.

Two Matagami/Norita samples are slightly enriched in ^1H-CH_4 relative to the overall ^2H-CH_4 vs. $\delta^{37}Cl$ and $\delta^{81}Br$ trends (Figure 5-12). The Matagami sample that is enriched in ^1H-CH_4 is located in a hydrothermally altered felsic rock unit, but no core description was available for the Norita sample. Since the samples are considerably closer to the trends between $\delta^{37}Cl/\delta^{81}Br$ and $\delta^{13}C$ (Figure 5-12), the deviation from the trend may therefore indicate hydrogen isotope exchange during hydrothermal alteration affected the gases at this site (*Waldron et al. 1999, Sessions et al. 2004*).

Water and gas from the Juuka/Miihkali site do not plot along the methane gas vs. $\delta^{37}Cl$ trends (Figure 5-12). As discussed previously, halite dissolution is one possible process affecting the $\delta^{37}Cl$ ratios at this site. The deepest, most saline samples do plot along the trend. The fluids sampled higher

in the boreholes at this site are believed to have intruded, and are not in equilibrium with the rock matrix (*Frape et al. 2004*).

Enonkoski gases are predominately bacteriogenic (*Sherwood-Lollar et al. 1993a*). The Enonkoski sample follows the $\delta^{2}H$ vs. $\delta^{37}Cl$ or $\delta^{81}Br$ trends (Figure 5-12), but the bacteriogenic gas has affected the $\delta^{13}C$ ratios, resulting in a discrepancy on the $\delta^{13}C$ vs. $\delta^{37}Cl$ or $\delta^{81}Br$ plots (Figure 5-12). Other samples which are slightly below the overall trend between $\delta^{81}Br$ and $\delta^{13}C\text{-}CH_4$ may also indicate mixing with bacteriogenic gas.

5.6 Conceptual Model

The conceptual model for halide isotope evolution in groundwaters or fluids found in the Canadian Shield is presented in Figure 5-15. The original Shield halide isotopic signatures were derived from primary processes (Figure 5-15A). Beneath the seafloor, diffusion and dehydration reactions during subduction result in light isotope ($^{35}C.$, ^{79}Br) enrichment in fluids beneath the seafloor. Light isotopes are transported from the mantle into the atmosphere and ocean by boiling and degassing, with heavier isotopes transported by acidic volcanic gases. Heavy isotopes are incorporated into minerals and rocks. Isotopic exchange occurs during early secondary processes, including metamorphism of the Shield resulting in further influence on the isotopic signatures.

Over time, the surface of the Shield eroded, with increased fracturing and depressurization of the rock mass resulting in increased fluid inclusion cracking, degassing, out-diffusion, and oxidation (Figure 5-15B). Combined, these processes result in the escape of ^{79}Br and ^{35}Cl from the Shield subsurface. These processes continue today, resulting in deeper fluids that are more enriched in ^{81}Br and ^{37}Cl with less variability when compared with shallower fluids. Sedimentation occurs beneath Paleozoic oceans, primarily along Shield margins. Over time, fluids from these sediments intrude the Shield, but are confined to the margins.

During Plio-Pleistocene glaciations, dilute glacial meltwaters intrude, but are primarily restricted to shallow depths (Figure 5-15C). These dilute waters increase the concentration gradient, increasing halide diffusion out of the rock mass. Permafrost formation at the front of the glacier also results in shallow dilute water formation. Today, permafrost is still present in some parts of the Shield, but processes connected to erosion and the shallow intrusion of meteoric waters remains the primary active influences to subsurface halide isotopic composition (Figure 5-15D).

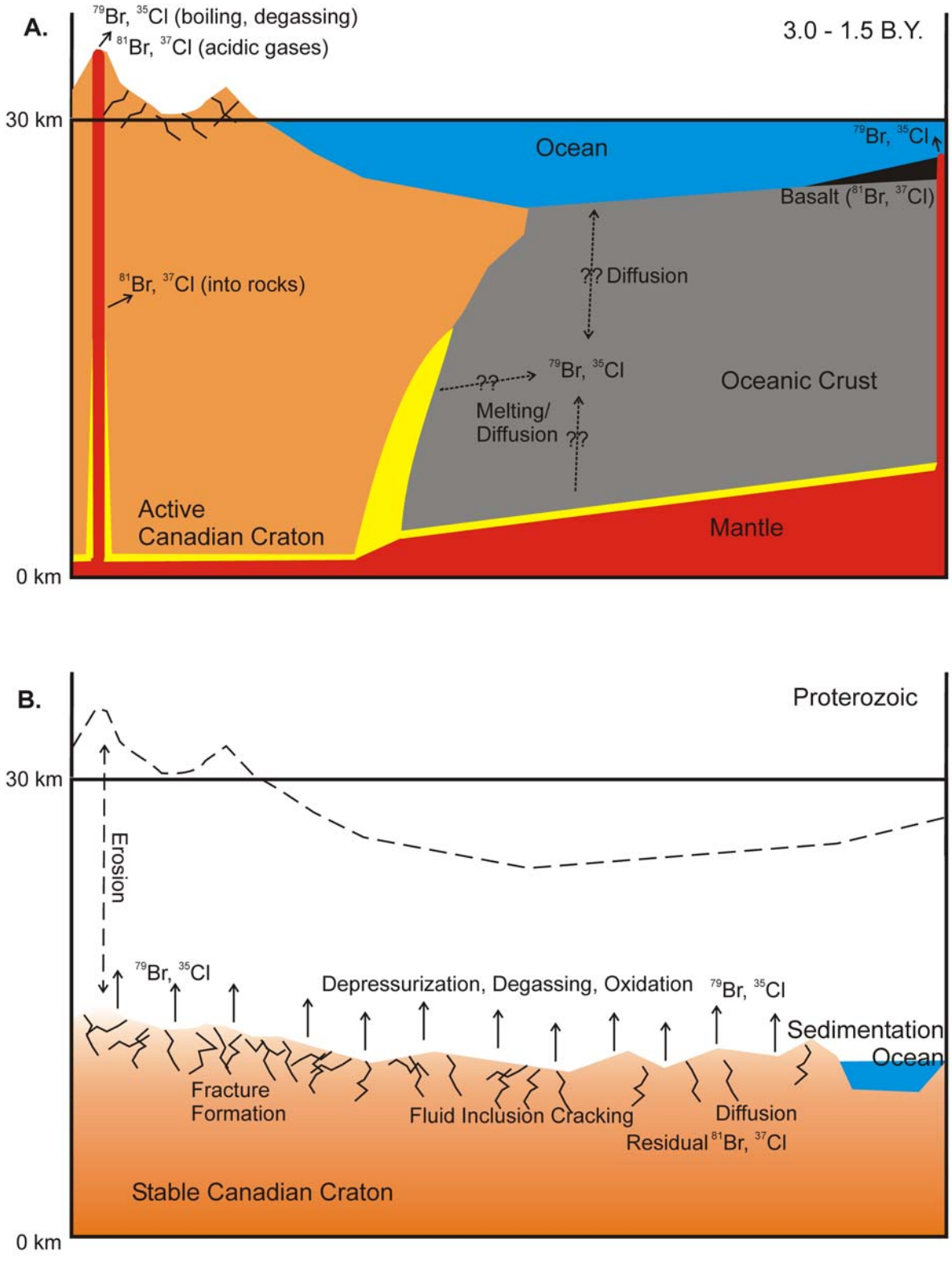

Figure 5-15. Conceptual model of influences to halide isotope composition in the Canadian Shield, (A). Archean, (B) Proterozoic.

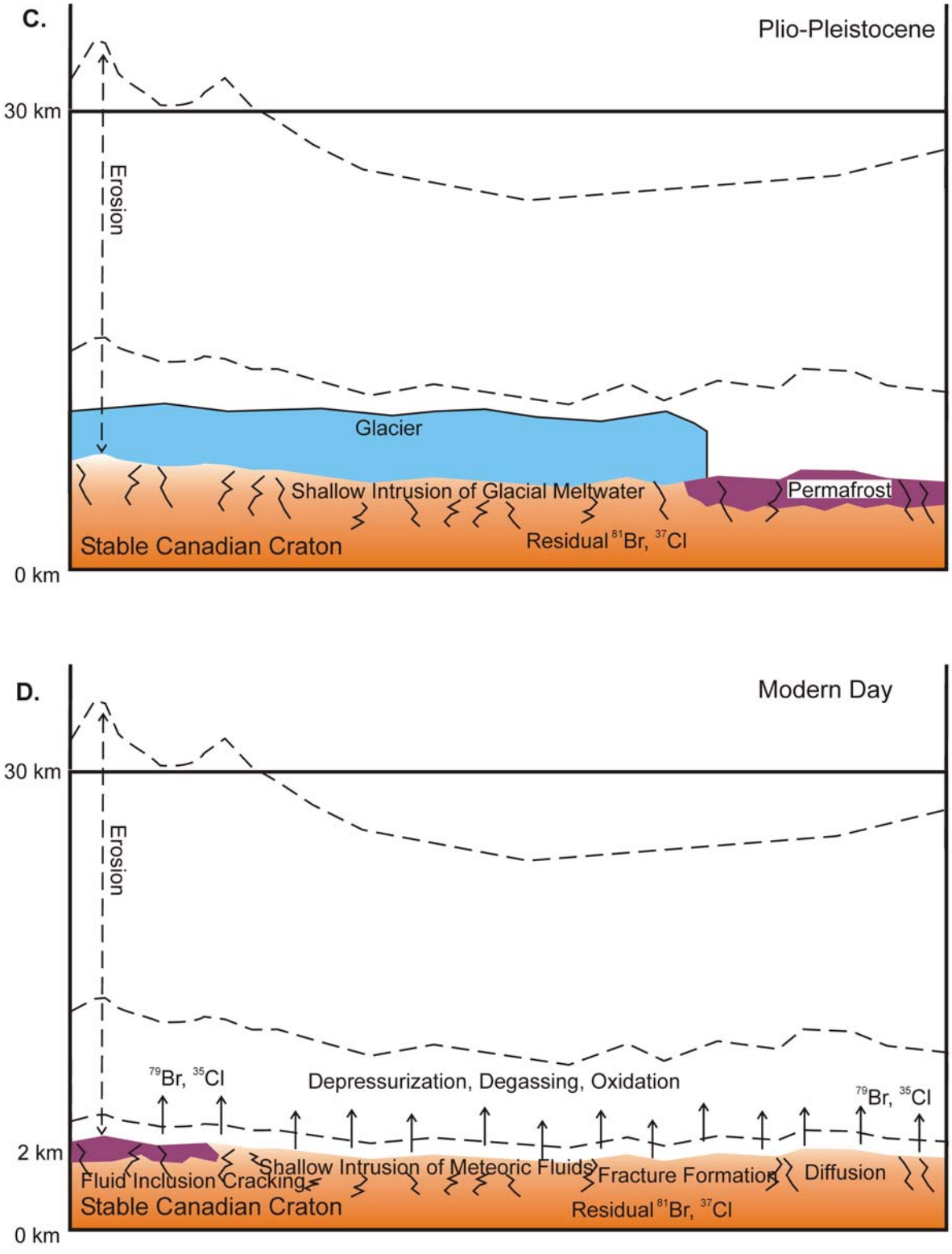

Figure 5-15 (cont.). (C). Shield during Plio-Pleistocene glaciation, (D). Conceptual model of current influences affecting halides isotopic ratios in the Shield.

5.7 Summary

The $\delta^{37}Cl$ and $\delta^{81}Br$ signatures for Fennoscandian Shield groundwaters are more positive and have a greater range than Canadian Shield groundwaters. No significant trends were observed when $\delta^{81}Br$ was compared with other chemical constituents. In Canadian Shield fluids, $\delta^{81}Br$ values changed significantly in brackish and saline Na-Ca and Ca-Na waters within individual sites, but typically varied between +0.0 and +0.3 ‰ SMOB for calcium dominated brines. The higher $\delta^{81}Br$ value was associated with higher Ca/Na ratios. Slightly increasing trends were observed between $\delta^{81}Br$ and $\delta^{37}Cl$, and $\delta^{81}Br$ and the stable isotopes of water ($\delta^{2}H$, $\delta^{18}O$). Halide stable isotopic ratios did not indicate a recent marine origin for fluids.

Chloride and bromide ions are typically considered conservative tracers, but chemical fractionation can occur during subsurface halide cycling. Under modern conditions in Shield groundwaters, Br/Cl ratios can be expected to change significantly, primarily during water-rock interactions. These processes can include metamorphic and low temperature reactions such as: hydration of silicates, interactions with or dissolution of minerals that contain Cl in the structure (e.g. scapolite and hydrated silicates like amphibole, biotite), and dissolution of or interactions with minerals containing saline fluid inclusions. Mixing with fluids having different Br/Cl ratios can also change the fluid Br/Cl ratio. Other processes discussed in this chapter, such as partitioning, had a greater influence on the rock Br/Cl ratios, which in turn affected fluid Br/Cl. These processes have been shown by others to affect $\delta^{37}Cl$ vlaues. $\delta^{81}Br$ is expected to generally behave similar to $\delta^{37}Cl$ during partitioning and other subsurface processes, although the intensity of fractionation may be different. $\delta^{37}Cl$ does not appear to be useful in differentiating fluids that have been affected by the freezing process, but evaluation of $\delta^{81}Br$ data is not yet complete. A summary of the processes known to fractionate to Cl isotopically and expected to fractionate Br isotopically is provided in Table 5-2.

Currently, the overall utility of the fluid $\delta^{81}Br$ values obtained in this study is limited, because very little is known about non-fluid end-members and fractionation processes. Groundwater $\delta^{37}Cl$ values at several Shield locations indicate leaching from the rocks. Mixing or intrusion of an external fluid has likely occurred in instances where fluid $\delta^{37}Cl$ values vary from rock values. It is reasonable to expect a similar relationship between $\delta^{81}Br$ in rocks and fluids as $\delta^{37}Cl$. When such relationships are investigated in the future, fluid $\delta^{81}Br$ values should be useful for determining brine evolutionary pathways in Shield environments. Similar to other ions in Canadian and Fennoscandian Shield rocks, the heterogeneity of crystalline shields likely precludes a single source of, or process controlling the evolution of, bromide to groundwaters.

Positive correlations between $\delta^{81}Br$, and $\delta^{37}Cl$ with $\delta^{2}H\text{-}CH_4$ and $\delta^{13}C\text{-}CH_4$ were noted and compared with previously observed negative correlations between $\delta^{15}N\text{-}N_2$ and $\delta^{2}H\text{-}CH_4$. Changing redox, pH, temperature, and/or pressure conditions during hydrothermal, metamorphic, and volcanogenic processes may have influenced the observed trends. The increased scatter in $\delta^{37}Cl$ values against $\delta^{13}C\text{-}CH_4$ may be related to additional Cl^- inputs. Alternatively, the increased correlation between $\delta^{37}Cl$ and $\delta^{81}Br$ with $\delta^{2}H\text{-}CH_4$ may be an indication of long-term hydrogen exchange and equilibrium.

The data suggest solute sources and fluid evolution at individual sites would be better constrained utilizing a multi-tracer investigation of $\delta^{37}Cl$, $\delta^{81}Br$, and $^{87}Sr/^{86}Sr$ ratios comparing fluids, rocks, and fracture filling minerals (including the fluid inclusions). This approach should be investigated to further refine the use of chlorine and bromine isotopes to document solute sources and fluid evolution in crystalline shield groundwaters.

Table 5-2. Summary of processes and known effects to $\delta^{37}Cl$ ratios, predicted behavior of $\delta^{81}Br$ ratios, and behavior of Cl^- vs. Br^-.

Process	$\delta^{37}Cl$ fractionation	Predicted $\delta^{81}Br$ fractionation	Behavior of Cl^- vs. Br^-
Ion Filtration	^{35}Cl repelled, resulting fluid on inflow side of membrane Cl^- and ^{35}Cl enriched	^{79}Br repelled, resulting fluid on inflow side of membrane Br^- and ^{79}Br enriched	
Diffusion	^{35}Cl diffuses, diffusing fluid is enriched in ^{35}Cl relative to initial Cl^- mass	^{79}Br diffuses, diffusing fluid is enriched in ^{79}Cl relative to initial Br^- mass	
Halite precipitation	^{37}Cl enrichment in solid phase	No fractionation or change	Primarily Cl^- affected
Halite dissolution	No fractionation; change in fluid $\delta^{37}Cl$ only if halite has different isotopic ratio	No observed fractionation or change due to small amount incorporated	Primarily Cl^- affected
Other salt/mineral precipitation	^{37}Cl enrichment in solid phase if Cl^- incorporated into mineral / salt structure	^{81}Br enrichment in solid phase if Br^- incorporated into mineral / salt structure	Cl^- favored for mineral precipitation over Br^- due to ion size; Br^- salts precipitate only at late stages of evaporation
Boiling/Degassing	^{35}Cl enriches vapor phase; fractionation greater at lower temperatures	^{79}Br enriches vapor phase; fractionation greater at lower temperatures	Br^- degasses more readily than Cl^-
Acidification	Acids enriched with ^{37}Cl compared with dissolved Cl^-	Acids enriched with ^{81}Br compared with dissolved Br^-	Br^- more readily aerosolizes when acidified than Cl^-
Oxidation	Higher oxidation states enriched with ^{37}Cl	Higher oxidation states enriched with ^{81}Br	Br^- oxidizes more readily than Cl^-, particularly in acid conditions
Fluid dehydration-Mineral hydration	^{35}Cl released to fluid, ^{37}Cl enriched in solid	^{79}Br enriched in fluid, ^{81}Br enriched in solid	Depends on Cl^- and Br^- concentrations
Metamorphism: water-halide to rock-halide ratio	High water-Cl^- to rock-Cl^- ratio, fluid $\delta^{37}Cl$ will affect rock values and vise-versa for low water-Cl^- to rock-Cl^- ratio	High water-Br^- to rock-Br^- ratio, fluid $\delta^{81}Br$ will affect rock values and vise-versa for low water-Br^- to rock-Br^- ratio	Depends on Cl^- and Br^- concentrations
Fluid Freezing	Generally no change observed; ^{37}Cl may enrich into ice (inclusions or structure)	Experiments on-going	Depends on solution chemistry

Chapter 6

Conclusions and Future Study

6.1 Conclusions

The hydrogeochemical effects of permafrost on Canadian Shield groundwaters were examined through characterization of sites currently located within permafrost, analyzing new components of archived samples, and re-evaluating previously collected data. This thesis provides the first detailed hydrogeochemical characterization of deep subpermafrost fluids in a crystalline environment.

The characterization of permafrost effects on hydrogeology and geochemistry at the Lupin field site required first understanding the effects of mine operations. Permafrost waters were contaminated by the use of brine for drilling and other operations in subzero conditions. High nitrate concentrations in permafrost waters were a result of blasting. Elevated permafrost fluid sulfate concentrations from oxidation of rock sulfides may or may not be a result of mining activities. Although the chemistry of permafrost fluids was overwhelmed by the drill brine, it seems possible the permafrost fluids were dilute and oxic. Deep sub-permafrost water chemistry was less affected by mining operations, but mine dewatering resulted in depressurization of the rock mass near the mine. Measured pressures were significantly below expected hydrostatic pressure in the deep boreholes.

Some geochemical trends are evident despite the contamination. In the permafrost, hydrogen and oxygen isotopes exhibit fractionation typical for freezing-impacted waters. The narrow isotopic range of subpermafrost waters is indicative of the end result for this process. Fluid salinity varied extensively within and between boreholes in the subpermafrost. Borehole salinities indicate mixing of brackish and saline fluids is occurring. Fluids had either Na-Ca-Cl or Ca-Na-Cl composition. Some relatively uncontaminated samples were collected at the base of the permafrost. These fluids were fresh to brackish, and generally more similar in composition to subpermafrost fluids than the contaminated fluids found in the permafrost. Relatively higher SO_4^{2-} concentrations were observed in these basal permafrost fluids, but NO_3^- concentrations were generally low.

Age tracers indicate mixtures of at least three different age fluids were sampled in the subpermafrost. Small and inconsistent amounts of tritium were attributed to drill fluids. A second component recharged prior to the last glacial maximum, while the saline portion of the fluids was beyond the dating methodologies employed. The younger components were likely drawn to depth by

the artificial gradient created by mine dewatering. The latter component precludes a surficial freeze-concentrated origin of the salinity at the site.

In undisturbed conditions, methane hydrate is likely present in the rock surrounding the Lupin mine to depths of 1100 m, or 600 m below the base of permafrost, although hydrates were not directly observed. Mine dewatering and exploration boreholes depressurized the area near the mine, destabilizing the methane hydrate. This process results in decreasing temperatures and salinities in sampled fluids, and can also affect the fluid stable isotopic composition. Conversely, methane hydrate formation can concentrate solutes and fractionate stable isotopes similar to ion-exclusion during fluid freezing. The relative importance of methane hydrate formation as a concentration process may be increased in crystalline rock relative to sedimentary and marine units, due to the low water to rock ratio. Modeling indicates methane hydrate was stable in the subsurface around the Lupin mine throughout Quaternary glaciations and climate change. Methane hydrates can reduce porosity and permeability. Therefore, depending on hydrate distribution, the potential for deep sub-glacial recharge could be limited.

The isotopic and molecular compositions of gases at Lupin are unique compared with other Shield gases, although this does not appear to be related to glacial or periglacial processes. The gas genesis is tied to metamorphism of marine turbidites 1.8 – 2.8 Ga, and appears to have a thermogenic origin. However, the δ^{2}H-CH_4 is significantly lower than other known thermogenic gases, and if the gases are thermogenic, the cause of the light H is not clear.

Taliks through the permafrost exist beneath lakes of significant size. Although permafrost is often described as impermeable, taliks represent potential hydraulic flow paths. The talik under Lake Contwoyto at Lupin was not sampled directly, but taliks beneath other lakes across the arctic have been sampled. Sampled talik fluids are dilute waters, with δ^{18}O-Cl compositions that evolve similar to fluids concentrated during freezing, and show no evidence of mixing with deeper saline fluids. Thermal conditions beneath lakes with taliks preclude methane hydrate formation. Taliks should be carefully considered when modeling long-term hydrologic flow in permafrost regions.

A review of Canadian Shield groundwaters revealed some deep (400 to 1300 m) fluids potentially affected by the freezing process. However, evidence of freezing was not observed at all sites, and no evidence was found to suggest that Shield brines were formed from ion-exclusion during freezing. Several possible processes related to freezing and the glacial-interglacial cycle were identified and considered which have the ability to affect solute concentration and isotopic composition at depth. The processes include deep glacial meltwater intrusion, an *in situ* freeze-out mechanism such as permafrost or methane hydrate formation, and artificial mine-dewatering

gradients. The data are not sufficient to differentiate between the processes at all sites. This is significant, as similar geochemical signatures were previously considered to have only a glacial meltwater origin. The possibility for an *in situ* freeze out process, such as permafrost and/or methane hydrate formation to affect geochemical signatures deep within the Canadian Shield, is a new concept. Additional investigation is required to better constrain the relative influence of each process to the evolution of Canadian Shield groundwaters.

Surficial freezing of seawater in glacial marginal troughs with subsequent transport of brines into the Canadian Shield was discounted. A review of groundwater flow, subglacial pressures, and rock permeability preclude the possibility for transport of a hypothetical brine from a marginal trough on the continental margins to the center of North America during the recent glacial cycles. Geochemical evidence, including ionic ratios, and $\delta^{2}H$, $\delta^{18}O$, $^{87}Sr/^{86}Sr$, $\delta^{37}Cl$ and $\delta^{81}Br$ data also do not support a recent freeze-concentrated seawater salinity source.

There are several implications of this research for deep geologic radioactive waste disposal. Even considering the contamination, permafrost formation at Lupin did not create brines at repository depth (500-1000mbgs). Deep (~1 km) recharge of glacial meltwater was not ruled out, although artificially induced hydraulic gradients from mining appear to cause mixing of different age fluids at the sample depths. The possibility for deep glacial meltwater intrusion into the Canadian Shield versus an *in situ* freeze-out mechanism (permafrost or methane hydrate formation) needs to be better constrained by collecting geochemical data from relatively undisturbed locations and analyzing recharge age and geochemical indications of freezing. Challenges are also presented by the possible formation and destabilization of methane hydrates. Dilute fluids created by melting hydrates could negatively impact engineered barriers. An upper limit to potential fluid salinities during methane hydrate formation should be investigated. A repository placed in an area currently with methane hydrates would need to constrain the changes to the physical and geochemical environment possible if hydrate dissociation occurs due to heat generated from the repository. Heat generated by the repository may also create a hydrothermal talik through the permafrost; thus understanding how talik formation affects deep groundwater flow system evolution in permafrost environments is critical. Pressure and salinity measurements from within hydrothermal taliks will provide an understanding of flow direction within taliks, and the relative importance of taliks to deep flow system evolution beneath the permafrost. Hydraulic modeling should incorporate talik formation, density, temperature effects, and the potential for methane hydrate formation. A better understanding of the subsurface thermal history at individual sites, talik-permafrost interaction, and glacial recharge-discharge will

further constrain processes involved in the evolution of fresh to moderately saline waters in the Canadian Shield.

In the Canadian Shield, the glacial-interglacial cycle did not result in brine formation. This is significant for the search for life on Mars, as life is currently believed to begin in a brine solution (*Bada 2004*). The results of this investigation indicate that subsurface life on Mars might not have evolved as a direct result of *in situ* freeze-out. However, on Mars, different rock chemistries and cooler subsurface thermal conditions will influence the final water chemistry beneath permafrost, and may result in more concentrated fluids. Regardless, this investigation is an important step towards constraining subpermafrost fluid chemistries in tectonically inactive crystalline rocks on Earth and Mars.

The origin and evolution of Canadian and Fennoscandian Shield groundwaters were further investigated through a survey of fluid $\delta^{37}Cl$ and $\delta^{81}Br$. Generally, Fennoscandian Shield fluids have higher $\delta^{37}Cl$ and $\delta^{81}Br$ values and cover a larger range than Canadian Shield fluids. Although Br and Cl are generally conservative tracers in fluids, several processes were identified that are known to fractionate Cl and Br concentrations and Cl isotopes. These processes should be further explored to determine their potential for fractionation of Br isotopes. These processes include both metamorphic and low-temperature reactions such as diffusion, silicate hydration, dissolution of or interactions with minerals containing saline fluid inclusions, exchange with hydrothermal or metamorphic fluids. Diffusion and escape of halides may result in enriched halide isotope signatures at shallower depths. Positive correlations between $\delta^{81}Br$, and $\delta^{37}Cl$ with $\delta^{2}H\text{-}CH_4$ and $\delta^{13}C\text{-}CH_4$ may be related to changes in pressure, temperature, redox, and/or pH during hydrothermal, metamorphic, or volcanogenic processes. Multi-tracer investigations including $\delta^{37}Cl$, $\delta^{81}Br$, and $^{87}Sr/^{86}Sr$ ratios should constrain solute sources and fluid evolution at individual sites. The halide stable isotopic ratios did not indicate a recent marine origin for most fluids.

6.2 Recommendations

The results of this thesis have provided new information about deep permafrost-groundwater interaction. However, several important questions either remain unanswered or were developed by this research. The research at Lupin was the first investigation to specifically study effects of deep permafrost to groundwaters. Additional less contaminated sites in permafrost regions should be investigated to corroborate the Lupin site scientific findings. Two specific targets of investigation should include:

1. Taliks. The potential for flow through taliks needs to be better documented, and additional geochemical samples are needed to confirm that talik fluids are dilute. Flow through taliks should be investigated by collecting pressure information and analyzing the age of talik fluids. Modeling exercises should include

    a. The fate of taliks and their role for aquifer recharge during glacial periods.

    b. Understanding how melting permafrost affects flow through taliks.

2. Methane Hydrates. Beyond this investigation, methane hydrates have not been investigated in crystalline rock environments. Methane hydrate behavior in fractures, vugs, and low porosity materials is not currently well documented. Experimental and field investigations should be considered to examine geochemical and hydrogeological changes that occur. The distribution of methane hydrates in the Canadian Shield should also be investigated.

Previously investigated Canadian Shield sites should also be re-sampled. Most of the early studies specifically targeted the most saline fluids. Complete depth and salinity profiles were not often collected. These overlooked fluids may provide key components to understanding the influence of the glacial-interglacial cycle on the evolution of Canadian Shield groundwaters.

A survey of age tracers and geochemistry within Canadian Shield groundwaters would also be highly beneficial to better constrain the origin of depleted ^{18}O observed at several locations in the Canadian Shield. Young ^{14}C ages would indicate significant glacial recharge; other tracers would provide constraints for fluid mixing scenarios. Ideally, this survey would be conducted in relatively undisturbed conditions to minimize the potential for anthropogenically induced groundwater mixing.

This initial investigation of $\delta^{81}Br$ values in crystalline shield environments indicates that more detailed investigation of bromine isotopes in rocks, fracture filling minerals, and fluid inclusions should constrain the solute sources and fluid evolution in individual crystalline shield sites. Further investigation of Br isotopic fractionation should be conducted, focusing on the processes identified with potential to fractionate bromine isotopic ratios. In particular, detailed investigation of pH-, redox-, temperature-, and pressure- fractionation relationships should be considered.

Appendix A.

Overview of Permafrost and the Freezing Process

A.1 Freezing Studies

Ice and methane hydrate formation excludes solutes from the solid phase, concentrating solutes in the remaining liquid phase (*Ringer 1906a, 1906b, Gitterman 1937, Lewis and Thompson 1950, Nelson and Thompson 1954, Thompson and Nelson 1954, Thompson and Nelson 1956, Trofimuk et al. 1974, Richardson 1976, Hesse and Harrison 1981, Hesse et al. 1985, Herut et al. 1990, Spencer et al. 1990, Marion and Grant 1994, Ussler and Paull 1995, Mironenko et al. 1997, Marion et al 1999, Marion and Farren 1999, Ussler and Paull 2001, Hesse 2003, Zhang and Frape 2002*), a process termed cryogenic metamorphism in the Russian literature (*Tolstikhin and Tolstikhin 1974*). This review of the cryogenic brine concentration and salt deposition process begins with experiments conducted with seawater, continued by experiments and studies on soils and fluids of different chemical compositions, and finally investigations of methane hydrate.

A.1.1 Seawater Freezing

Relatively few experiments have investigated brine and precipitate composition during sea-water freezing. Two freezing pathways have been proposed, termed the "Ringer-Nelson-Thompson" pathway (*Ringer 1906a, 1906b, Lewis and Thompson 1950, Nelson and Thompson 1954, Thompson and Nelson 1954, Thompson and Nelson 1956*) and the "Gitterman" pathway (*Gitterman 1937*). The "Ringer-Nelson-Thompson" pathway is supported by other experiments (*Richardson 1976, Herut et al 1990*) and theoretical work (*Spencer et al. 1990, Marion and Grant 1994, Mironenko et al. 1997*). Additional theoretical and experimental evidence also suggest the "Gitterman" pathway is thermodynamically stable (*Marion et al 1999, Marion and Farren 1999*).

The most notable difference between the two pathways concerns the precipitation of calcium sulfate minerals (Table A-1, Figure A-1). Calcium sulfate minerals do not precipitate in the "Ringer-Nelson-Thompson" pathway until antarcticite forms at -54°C, however gypsum precipitates in the "Gitterman" pathway at -22.9°C. Experiments and modeling by Marion et al. (*1999*) suggest gypsum will not actually precipitate until -22°C, with the speed at which freezing occurs the primary factor determining which pathway is followed. If freezing occurs quickly, the "Ringer-Nelson-Thompson"

pathway is favored. This is because gypsum precipitation is only favored if the freezing solution is saturated in sulfate, which can only occur if mirabilite has sufficient time to dissolve during hydrohalite precipitation. Additional experiment design factors also contribute to determining which pathway is favored (*Marion et al. 1999*, *Marion and Farren 1999*).

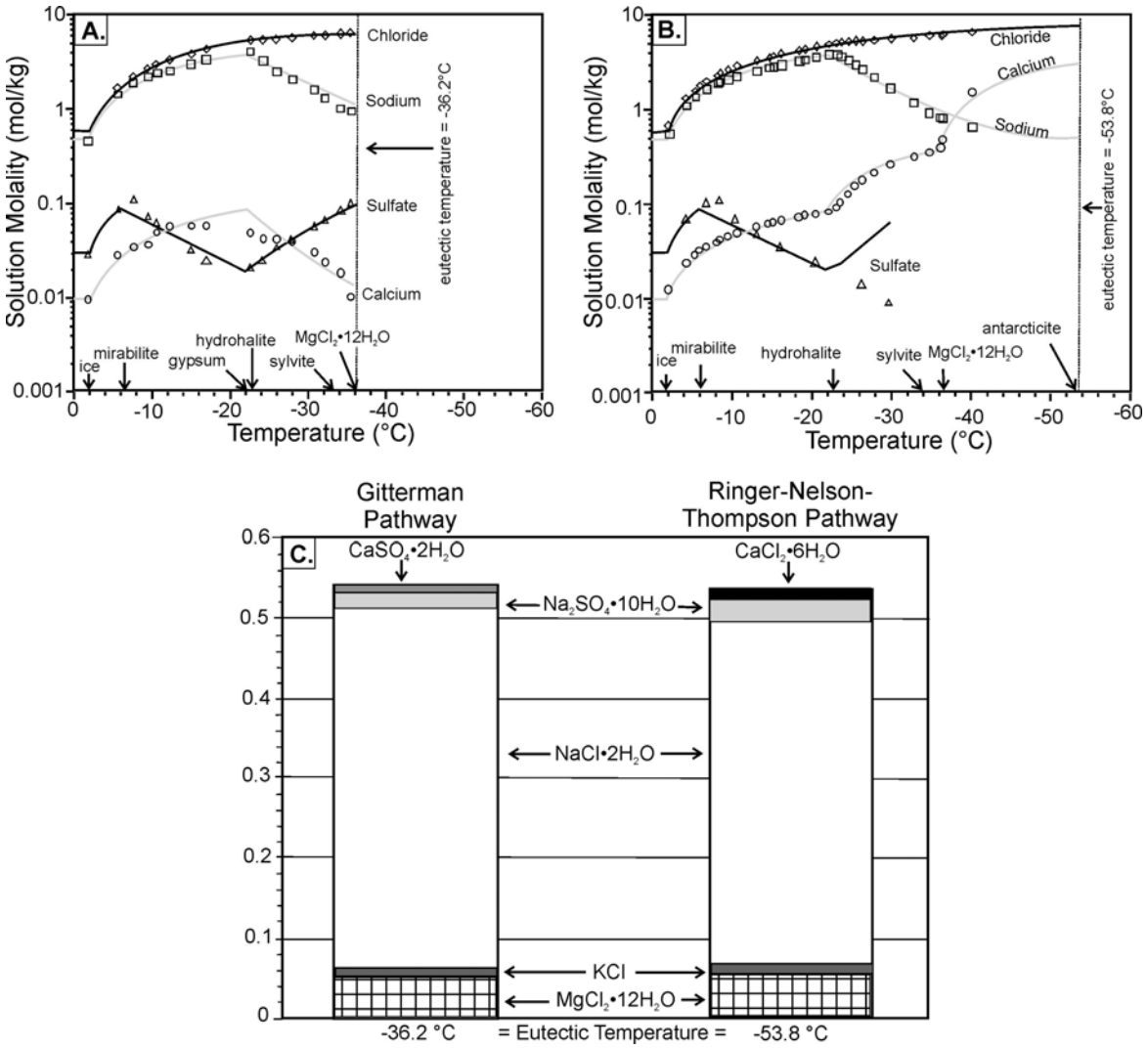

Figure A-1. Comparison of seawater freezing pathways. (A) Gitterman pathway, after Marion and Farren (*1999*). (B) Ringer-Nelson-Thompson pathway, after Marion and Farren (*1999*). (C) Relative salt precipitation during freezing to the eutectic temperature along each pathway after Marion et al. (*1999*).

Seawater freezing naturally occurs during sea ice formation and in the polar ice shelves, as atmospheric temperatures in Polar Regions can reach the eutectic of both freezing pathways. Mirabilite and brine formation during freezing within the McMurdo Ice Shelf results in brines

concentrated to 200 g L^{-1} (*Cragin et al. 1986*). Mirabilite salt beds over a meter thick have been found on top of the Ross Ice Shelf, a result of basal ice shelf brine freezing after being injected onto the surface of the ice shelf (*Brady and Batts 1981*).

Bromide data is available from only one set of seawater freezing experiments (*Herut et al. 1990*); most other studies have focused on chloride and/or sulfate. Data provided by Herut et al. (*1990*) shows that bromide/chloride ratios did not change during freezing to temperatures of -14°C; however predictions were made suggesting Na/Cl and Br/Cl ratios would change significantly as hydrohalite precipitates. This data is further discussed in Chapter 4.

Table A-1. Summary of mineral precipitation from seawater through the different freezing pathways.

Mineral Precipitated	Chemical Formula	Temperature °C		
		Ringer-Nelson-Thompson	Gitterman	Marion et al. 1999
Ice	H_2O	-1.9	-1.9	-1.9
Mirabilite	$Na_2SO_4 \cdot 10H_2O$	-8.2	-7.3	≥-7.3[1]
Gypsum	$CaSO_4$	DNP[2]	-15	-22.2[3]
Hydrohalite	$NaCl \cdot 2H_2O$	-22.9	-22.9	-22.9
Sylvite	KCl	-36	-36	-36
$MgCl_2 \cdot 12H_2O$	$MgCl_2 \cdot 12H_2O$	-36	-36[4]	-36.2
Antarcticite	$CaCl_2 \cdot 6H_2O$	-54	DNP	-54[3]

1.Cited values for mirabilite precipitation range between -8.2°C and -6.3°C (Marion and Farren 1999)
2.DNP = Does not precipitate
3.Discrepancies in gypsum and antarcticite precipitation temperatures exist in literature, probably related to experimental protocols, indicating precipitation of these species is reaction time dependent (Marion and Farren 1999)

The stable isotopes of hydrogen ($^2H/^1H$) and oxygen ($^{18}O/^{16}O$) fractionate during ice and methane hydrate formation. For hydrogen isotopes the fractionation factor for water and ice is between 1.0178 and 1.0206 (*Craig and Hom 1968, O'Neill 1968, Suzuoki and Kimura 1973*), and for oxygen isotopes the water to ice fractionation factor is between 1.0027 and 1.0035 (*Craig and Hom 1968, O'Neill 1968, Suzuoki and Kimura 1973*). Experimental results suggest that regardless of ionic composition, this fractionation results in fluids with a relationship between δ^2H and $\delta^{18}O$ that falls

along lines with slopes between 4.32 and 7.44 (e.g. *Souchez and Jouzel 1984, Zhang and Frape 2002*), less than the slope (8.00) of the Global Meteoric Waterline (*Craig 1961*).

A.1.2 Freezing of other fluids

Freezing of fluids with different chemistries and in other environments has also been studied. Investigations into solute concentration during freeze-thaw cycles in soils are useful, as annual cycling in a small column could be an analogue to deep permafrost formation and dissipation over geologic timescales. This section also reviews investigations into the evolution of the Antarctic saline lakes, which might loosely be considered modern analogues to the large glacial seawater lakes or lagoons proposed by Starinsky and Katz (*2003*). A series of experiments are also discussed, in which a range of Canadian and Fennoscandian Shield brines are frozen. Finally, freezing experiments conducted on a dilute Ca-HCO_3 solution are reviewed.

Freeze-thaw cycle research in soils suggests *in situ* freeze-out concentrate solutes (e.g. *Konrad and McCamon 1990*), and the cold temperatures in permafrost create a strong thermodynamic sink that may promote advection of water (and solutes) against the concentration gradient (e.g. *Cary and Maryland 1972, Gray and Granger 1986, Qiu et al. 1988, Perfect et al. 1991*). Concentrations in the freezing front may become sufficiently high that the freezing front "leaps" over solute pockets, resulting in alternating bands of high and low concentrations in frozen soils (*Romanov and Levchenko 1989*) although this may not be a significant macroscale phenomenon (*Kay and Groenvelt 1983*). Solutes and gases were also found to segregate during freezing of dilute Ca-HCO_3 solutions (*Killawee et al. 1998*). A more thorough discussion of *in situ* freeze-thaw processes in soils is provided by Marion (*1995*).

The origin and evolution of saline lakes in Antarctica's dry valleys have been studied extensively (e.g. *Burton 1981, Carlson et al. 1990, Marion 1997 Lyons and Welch 1997, Lyons et al. 1999, Stark et al. 2003, Lyons et al. 2005*). Unlike brine formation within and under sea-ice, which are dominated by the freezing process, Antarctic lakes are also subject to evaporation. Individual lake chemistries are dominated by marine aerosols, glacial and chemical weathering, ancient marine waters, and solute removal via mineral precipitation during cryogenic concentration (Lyons et al. 2005).

A series of experiments froze saline Canadian and Fennoscandian Shield groundwaters of different compositions from Palmottu, Finland (Na-SO_4), Aspö, Sweden (Na-HCO_3-Cl), Hästholmen, Finland (Na-Cl), Underground Research Laboratory (URL), Canada (Na-Cl) (*Zhang and Frape*

2002), and Sudbury, Canada (Ca-Cl) (unpublished data). Based on modern permafrost measurements (discussed further in Section A.2.2) fluids were only cooled to between -1°C and -7°C, temperatures found in modern permafrost terrain. Generally, as freezing progressed, the resulting concentrated solution became included into the ice as large fluid inclusions. For individual solutes, the results varied dependent on initial fluid chemistry. Barite formation during freezing of Aspo groundwater was suspected. There was no preferential solute incorporation or precipitation observed as Palmottu fluid was frozen. Ca and HCO_3 in Hastholmen fluids appeared to be solubility controlled. Gypsum and calcium carbonate precipitation likely occurred, evidenced by decreasing SO_4 concentrations. Gypsum precipitation was also suspected during freezing of URL fluids. Although gypsum, barite, and carbonated precipitated in these experiments, a suitable supply of CO_2 is required. However, this may not always occur in closed system. Uranium was the only minor ion which appears to have been significantly affected by freezing. Comparison of experimental data with FREZCHEM model (*Marion and Grant 1994, Mironenko et al. 1997*) simulations suggested the predicted results agreed reasonably well at low concentration factors (10-30), but simulations were unable to match experimental results at higher concentration factors.

Isotopic behavior during freezing was also investigated by Zhang and Frape (*2002*). During freezing, the first ice is heaviest, generally 1-2‰ for $\delta^{18}O$ and 5-15 ‰ for $\delta^{2}H$ with the last ice 4-5‰ and 20-30‰ lighter, respectively. As expected, heavier isotopes are incorporated into ice structure due to stronger bonding; lighter isotopes remain in solution (e.g. *Criss 1999*). As discussed previously (Section A.1.1), the relationship between $\delta^{2}H$ and $\delta^{18}O$ for both ice and fluids plot along lines with slopes between 6.86 and 7.44. For chlorine stable isotopes ($\delta^{37}Cl$), as chloride is incorporated into fluid inclusions in the ice, the observed fractionations were small and generally greater when there was not much Cl- in solution. Variation between ice and fluid increased as freezing progressed. Reflective of the mass in each respective pool, $\delta^{37}Cl$ in the fluid generally remained constant, but a gradual depletion in ice was observed from beginning to the end of experiment. An example of these processes is provided in Figure A-2. Additional aspects of these freezing experiments are discussed in Chapter 4.

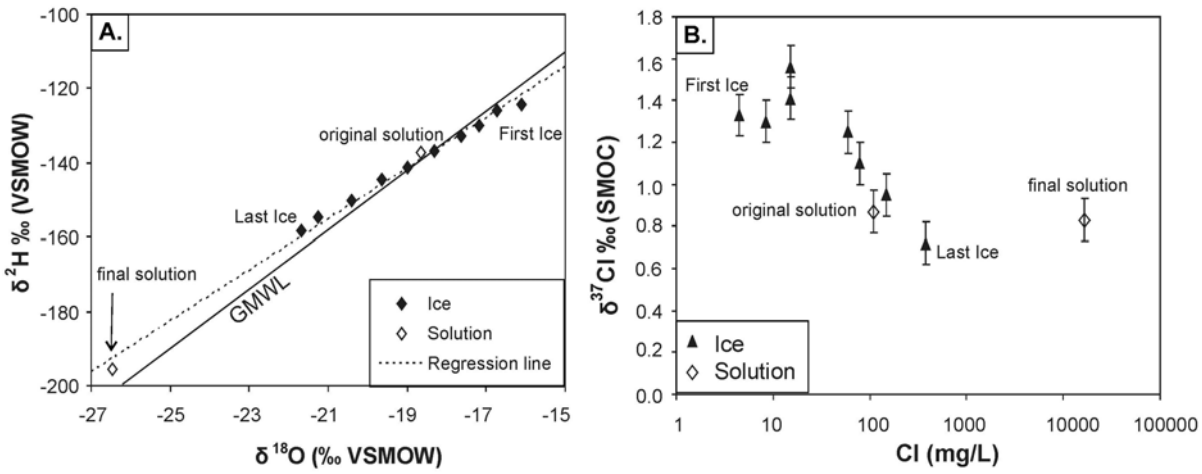

Figure A-2. Isotopic fractionation of (A) δ^2H and $\delta^{18}O$ and (B) $\delta^{37}Cl$, during freezing of Palmottu fluids, after Zhang and Frape (*2002*).

A.1.3 Methane Hydrates

Gas hydrates, or *clathrates*, form when mixtures of water and gases crystallize into ice-like solids in certain low temperature and high pressure conditions. In situ gas hydrates are found in marine or permafrost environments. Formation temperature, pore pressure, gas chemistry, and pore water salinity all control gas hydrate stability, while the availability of gas and water and the presence of reservoir rocks and seals affect gas hydrate formation (*Collett 1994*). Gas hydrate decomposition in unfrozen rocks can initiate permafrost formation because of the heat loss (*Ershov and Yakushev 1992*) Further background on gas hydrates is available in Chapter 3, Chapter 4, and Appendix C.

The impact of gas hydrate formation and dissociation on pore water salinity and isotopic composition has been well established (*Trofimuk et al. 1974, Hesse and Harrison 1981, Hesse et al. 1985, Ussler and Paull 1995, Ussler and Paull 2001, Hesse 2003*). Salt is normally excluded from the gas hydrate structure as it is from ice, thus increasing the salinity of pore waters during gas hydrate formation. Thus if gas hydrates form from the surface downwards, deeper pore waters should have a higher salinity than shallow pore fluids. The salt exclusion effect may be masked by transport processes (e.g. diffusion or advection) or in the marine environment, by burial compaction (*Hesse 2003*). On the other hand, melting of gas hydrates dilutes pore fluids, even if salt exclusion occurred during hydrate formation (e.g. *Hesse and Harrison 1981*). Published interstitial water chemistry datasets typically do not report *Br* and *Na* (or if one parameter is reported, the other is not), thus the effect of methane hydrate formation on Cl/Br, Na/Cl, or Na/Ca ratios is unknown.

Solid-fluid isotope fractionation results in isotopically heavy δ^2H and $\delta^{18}O$ in the hydrate lattice and isotopically light δ^2H and $\delta^{18}O$ in the remaining fluids (*Trofimuk et al. 1974, Davidson et al. 1983*). The fractionation factor (α) for oxygen and hydrogen isotopes between water and hydrate are 1.0024-1.0040 (*Kvenvolden and Kastner 1990, Matsumoto and Borowski 2000, Maekawa and Imai 2000, Tomaru et al. 2006*) and 1.016 and 1.022 (*Maekawa and Imai 2000, Tomaru et al. 2006*), respectively. These values are similar to the fractionation factors for water to ice (Section A.1.1). Fractionation of $\delta^{37}Cl$ during methane hydrate formation does not occur, although transport (e.g. diffusion, advection) related fractionation was reported in and beneath methane hydrate occurrences (*Hesse et al. 2000, 2006, Kopf et al. 2003, Deyhle et al. 2003*).

A.1.4 Preferential Solute Loss from Melting Ice and Snow

Preferential ion release from snow and ice may be analogous to subsurface melting of permafrost. Experimental evidence also suggests solutes are preferentially lost during ice and snow melt. Generally, sulfate and nitrate were preferentially released from snow and ice with respect to chloride, while magnesium and potassium were more readily released than sodium, with no information available with respect to calcium (*Brimblecombe et al. 1987*). This suggests if partial melting occurs, sodium and chloride would remain in snow and ice.

A.1.5 Weathering and Freezing

Mechanical and chemical weathering in permafrost environments is largely driven by ice formation and melting. Because ice has a greater volume than water, expansion in the rock matrix can mechanically weather rocks, creating fresh surfaces and increasing surface areas (*Tyutyunov 1964*). When permafrost ice melts, the dilute melt water could act in a similar fashion to dilute glacial melt waters, where comparable or higher chemical weathering rates occur than in temperate streams (*Nezat et al. 2001, Gooseff et al. 2002*). This weathering would likely occur over much longer time scales in permafrost than glacial melt water streams, because flow is substantially less in permafrost. At the other extreme, saline fluids and salts created during solute exclusion can also weather certain types of rocks and minerals (e.g. *Cooke and Smalley 1968*).

A.2 Permafrost Studies

Permafrost is an important part of the glacial-interglacial cycle. *Periglacial* is defined as a broad range of non-glacial cold conditions regardless of glacial proximity, suggesting areas where

permafrost processes dominate (*Washburn 1979*). Permafrost extends in front of and beneath glaciers during glacial advance and retreat. As a result, permafrost has affected a greater percentage of the earth's surface than glaciers, particularly during the Plio-Pleistocene glaciations. Permafrost covers nearly 20% of the continental land surface today, and nearly 50% of the Canadian land surface, but is estimated to have covered an additional 25% more during the last glacial maximum (*Vakimäe et al. 1995*, *French 1996*). Distribution of permafrost is influenced by climate and climate history, topography, geology and subsurface lithology, and vegetation (*Rossi 1999*). Permafrost occurs at high latitudes and altitudes, but conditions in these regimes are quite different (*Gascoyne 2000*). This review will focus on high-latitude permafrost, which occurs in Antarctica, Greenland, Canada, Alaska, Russia, and China.

A majority of the permafrost literature is concerned with surficial processes (geomorphology, hydrology, and agriculture) and engineering (e.g. foundation construction and pipeline design) affected by the active layer (*Vidstrand 2003*). New research focusing on permafrost degradation due to climate change is also available (*Smith and Riseborough 1983, Jorgenson et al. 2006*). However, information on the deep subpermafrost, relevant to this thesis, has primarily been obtained only from deep-drilling in sediments for oil and gas, with relatively little reported from fractured rock.

This section of the review will define various terms unique to permafrost literature and discuss previous investigations of the subpermafrost environment and the effects of freezing. The focus will be on freezing and other processes which affect groundwater chemistry in the permafrost and subpermafrost. Although permafrost in crystalline environments is a key focus of this dissertation, studies of subpermafrost sediments and sedimentary environments are more prevalent, and therefore will be included in this review of permafrost and deep groundwaters.

A.2.1 Definitions

Permafrost is defined as ground remaining below 0°C for at least two consecutive years (*National Research Council of Canada 1988*). This definition has nothing to do with water content, even though 'frozen ground' implies the presence of ice. Thus *cryotic* has also been accepted to describe ground with temperatures below 0°C (*van Everdingen 1976*). Although groundwater in permafrost environments may occur above (*suprapermafrost*), within (*intrapermafrost*), and below (*subpermafrost*) the permafrost layer, most hydrologic research focuses on the *active layer*, or the upper few meters of permafrost which seasonally thaws and freezes. A summary of temperature-moisture content terminology is provided in Table A-2.

Table A-2. Relationship of temperature and water content in permafrost terminology, (after van Everdingen 1976).

<table>
<tr><th>H_2O Content →
Temp↓</th><th colspan="2">No H_2O (except chemically bound and adsorbed)</th><th colspan="2">Some H_2O (less than porosity)</th><th colspan="2">Pore spaces filled with H_2O</th><th colspan="2">Containing “excess” H_2O</th><th colspan="2">Zone descriptions</th></tr>
<tr><th></th><th colspan="2"></th><th colspan="2"></th><th colspan="2"></th><th colspan="2"></th><th>Phase</th><th>Temp</th></tr>
<tr><td>T>0°C</td><td colspan="2">Dry, noncryotic</td><td colspan="2">Moist or unsaturated, noncryotic</td><td colspan="2">Wet or saturated, noncryotic</td><td colspan="2"></td><td>Nonfrozen</td><td>Noncrotic</td></tr>
<tr><td>T<0°C</td><td rowspan="2">Dry, cryotic</td><td rowspan="2">Dry Permafrost</td><td>Moist or unsaturated, cryotic</td><td>Moist Permafrost</td><td>Wet or saturated, cryotic</td><td>Wet permafrost</td><td colspan="2"></td><td rowspan="2">Partially Frozen</td><td rowspan="3">Cryotic</td></tr>
<tr><td rowspan="2">T<0°C</td><td>Ice-poor, partially frozen</td><td rowspan="2">Ice-poor permafrost</td><td>Partially frozen</td><td rowspan="2">Permafrost</td><td>Ice-rich, partially frozen</td><td rowspan="2">Ice-rich permafrost</td></tr>
<tr><td>Ice-poor, frozen</td><td>Frozen</td><td>Ice-rich, frozen</td><td>Frozen</td></tr>
</table>

Areas of unfrozen ground within permafrost are defined as *taliks*. A *cryopeg* is a special type of talik, and refers to ground that is below 0°C, but unfrozen due to saline waters in an intrapermafrost or subpermafrost lens (*van Everdingen 1976*). Taliks formed by water above 0°C are *hydrothermal taliks* and those formed by saline subzero temperatures are *hydrochemical taliks*. *Pressure taliks*, *thermal taliks*, *chemical taliks*, and *piezochemical taliks*, have also been defined (*van Everdingen 1976*). Taliks are often found beneath rivers and lakes that do not freeze to the bottom. If the talik is open through the permafrost, it is known as an *open talik* or *through talik*, but if it does not open through the permafrost, it is termed a *closed talik*. *Continuous permafrost* regions are characterized by the presence of permafrost everywhere expect for localized taliks beneath lakes and rivers. *Discontinuous permafrost* regions have larger areas of unfrozen ground separating the permafrost. *Sporadic permafrost* occurs on the warm fringe of the discontinuous permafrost zone where isolated ‘islands’ of frozen ground are present.

A.2.2 Permafrost Thermal Regimes

A thermal profile from an area with thick permafrost is shown in Figure A-3. Temperatures vary seasonally in the upper 15m of permafrost in crystalline areas, from -25°C to +10C°, with the largest range of values in the upper 5m (*Ruskeeniemi et al. 2002, Cumberland Resources 2005*, *BGC*

Engineering 2005, Gartner Lee 2005, 2006a,b). As seasonal effects become negligible, temperatures steadily decrease to depths between 60 to 150m below surface (*Zhang and Frape 2002, Freifeld et al. 2008*), or about 10-15% of total permafrost depth. Below seasonally affected ground, the minimum recorded temperatures in the subsurface are between -7 and -8°C (*Natural Resources Canada 1995, Ruskeeniemi et al. 2002, Henninges et al. 2005, BGC Engineering 2005, Gartner Lee 2005, 2006a,b, Freifeld et al. 2008*). Some Russian researchers have hypothesized Siberian subsurface temperatures within the upper 80 to 150m below surface may have been as low as -18°C and -21°C in the past (*Balobaev 1991*), however Siberia remained free of glacial ice throughout the Pleistocene (*Gerasimov and Markov 1941*). It has also been noted in the Russian literature that "degradation of the frozen zone from below is capable of leading to an abrupt lowering of the piezometric levels" (*Tolstikhin and Masimov 1955* in *Ginsburg and Neizvestnov 1973*).

A.2.3 Deep Permafrost Studies

A.2.3.1 Sedimentary Permafrost

As mentioned previously, investigation of deep subpermafrost fluids has been concentrated in oil and gas producing sedimentary sequences, such as the Mackenzie Delta in N.W.T., Canada and in Siberia. Published investigations of the North Slope oil and gas region of Alaska focus on the oil and gas composition, with very little information regarding fluid chemistry. Significantly more information has been collected by Russian scientists; however the available translations of early investigations are generally synopsis of work and lack the data from which the conclusions were made. Early investigations in sedimentary units in North America suggested permafrost influence on chemistry of the 25 and 300 g L^{-1} NaCl type fluids was minor (*Williams and van Everdingen 1973*).

A general description of water flow through permafrost in sedimentary rock in Siberia was presented by Tolstikhin and Tolstikhin (*1974*), and is summarized here. Subpermafrost piezometric pressures in sedimentary units are more stable than for other aquifers. Typically, only a small lag is observed between surface water level fluctuations and piezometric levels in the "upper horizons of sedimentary water," even for relatively thick permafrost (250 – 400 m), indicating taliks provide a hydraulic link through the permafrost. A "piston-effect" during frozen zone development can create piezometric levels which are commonly found in large artesian basins. The lower subpermafrost regime is less well documented, but pressures and piezometric levels are typically higher than observed closer to the base of the permafrost. Cryopegs, or unfrozen saline pockets within the permafrost, are common in sedimentary permafrost areas of Russia. The cryopegs typically have low

Ca-CO_3 and $MgSO_4$ contents. Cryopeg formation may be related to significant fluctuations in the base of permafrost.

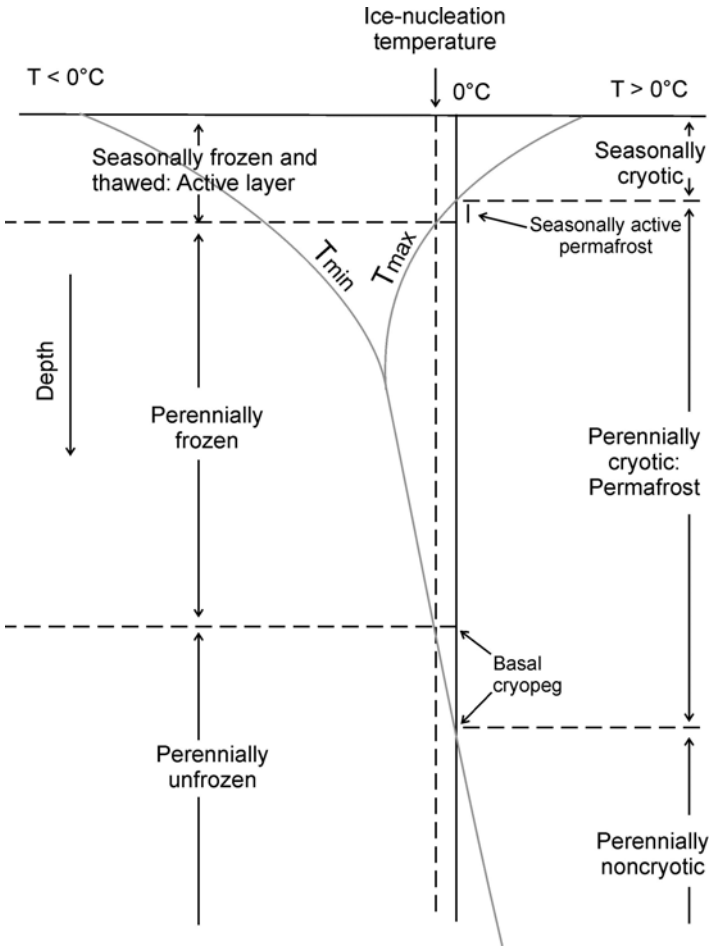

Figure A-3. Typical geothermal profile through permafrost, with definitions, after van Everdingen (*1990*). Temperatures vary seasonally in the upper portion of the permafrost.

Subpermafrost fluids in the Siberian Platform are affected by several geochemical processes. *In situ* freezing may account for increased concentrations of carbonate, sulfate, sodium, magnesium, and calcium in groundwaters found in the Siberian Platform under thick permafrost (*Alexeev and Alexeeva 2002, 2003*). Other processes, including evaporation and halite dissolution have also influenced brine formation in Siberian Platform groundwaters (*Shouakar-Stash et al. 2007*). Pinneker (*1973*) proposed that CaCl brines in the Siberian platform migrated downwards due to freezing but were not necessarily created by the freezing process.

In the Mallik area of the Mackenzie Delta, pore water chemical data are available through the permafrost and methane hydrate stability zone. However, gas hydrates were the focus of the

investigation, and very little attention was given to pore fluids in the permafrost or basal permafrost areas. The Mallik 2L-38 and 5L-38 boreholes were drilled to 1150 m below ground surface (bgs), and 1188 m bgs, respectively, well below the base of permafrost (~600 m bgs), and near the base of the hydrate stability zone (~1100 m bgs) (*Dallimore et al. 1999, Dallimore and Collett 2005*). In gas hydrate bearing samples, the magnesium/salinity ratio increases (for unknown reasons), and salinity decreases. Over time, it is expected that excess salt from non-gas hydrate bearing sections would diffuses from the high concentrations to low concentration sections (*Cranston 1999*). In the gas hydrate core section, Cl^- values varied widely between 0.7 $g \cdot kg^{-1}$ and 26.6 $g \cdot kg^{-1}$, related to pore water freshening from gas hydrate decomposition during sampling and solute exclusion during gas hydrate formation (*Clark et al. 1999*). Salinity also varied substantially (between 1 $g \cdot kg^{-1}$ and 38 $g \cdot kg^{-1}$) over small intervals (9 m and 24 m) in twenty samples analyzed in the permafrost section, and did not correlate with depth (*Clark et al. 1999*). Similar geochemical results were found in the nearby Mallik 5L-48 borehole (*Matsumoto et al. 2005, Ethier et al. 2005*). The original salinity in pore waters is attributed to the nearby Beaufort Sea, and mixing with fluids affected by the salt exclusion process during methane hydrate formation (*Clark et al. 1999, Matsumoto et al. 2005*). δ^2H and $\delta^{18}O$ values in the permafrost section ranged between -153 ‰ and -198 ‰ -18.9‰ and -24.4‰, respectively, generally decreasing with depth. Values in the deeper gas hydrate section were much higher, ranging between -74 ‰ and -118 ‰ and -8.4 ‰ and -14.8 ‰ for δ^2H and $\delta^{18}O$, respectively, with values generally increasing in zones where gas hydrate was found (*Clark et al. 1999*). There was a stepwise increase of δ^2H and $\delta^{18}O$ values with depth through the gas hydrate zone of the Mallik 5L-38 borehole, possibly related to changes in the pressure-temperature conditions (and the resulting impact on gas hydrate solubility) since the last glacial epoch (*Tomaru et al. 2005*). The overall increase is from -146 ‰ to -79 ‰ and -18 ‰ to -8.5 ‰, respectively.

A.2.3.2 Crystalline Permafrost

As mentioned previously, there have been relatively few crystalline permafrost studies outside of alpine regions in Russia, China, and Canada. The most recent of the limited references available are associated with the mine permitting process in Canada, where numerous ore deposits are currently being actively explored.

A general description of water flow through permafrost in fractured rock in Siberia was presented by Tolstikhin and Tolstikhin (*1974*), and is summarized here. Typical fractured rock aquifers, fluids are concentrated in fractures, particularly in fracture zones and larger tectonic faults. Recharge to subpermafrost aquifers is controlled by taliks in the permafrost, thus major water-courses in permafrost areas may be extremely important. In areas of discontinuous permafrost, recharge is

more common. In continuous permafrost zones, subpermafrost water is only recharged through open taliks, and is therefore "linked with the intrapermafrost water in open taliks." Piezometric head in subpermafrost waters are generally described as tied to surface boundary conditions, such as precipitation and surface water levels. Subpermafrost fluid chemistry may be influenced by suprapermafrost, intrapermafrost, or deeper "tectonic" fluids. If the primary water source is intrapermafrost fluid, subpermafrost waters should show the effects of "cryogenic metamorphism" or *in-situ* "freeze-out," due to limited water supply and the length of time for waters to migrate through taliks. This causes subpermafrost fluids to have higher TDS and sodium ion content compared to surface and suprapermafrost fluids.

Freeze-out effects on the basaltic arctic islands of Franz-Josef Land are generally described by Ginsburg and Neizvestnov (*1973*). Sodium sulfate was observed in soils, as was mirabilite. Subpermafrost water densities increased with depth; from "several tens of meters to the first hundreds of meters" TDS increased from 40- g L-1 to 160-190 g L^{-1}, however beneath the brines, lower TDS fluids were observed.

Isolated permafrost was reported to depths ranging from 30 to 100m in granitic bedrock in Huloa River basin, northeastern China. Investigations into subpermafrost chemistry revealed generally dilute Ca-Mg-HCO_3 fluids which likely were recharged in surrounding uplands through the widespread taliks (*Wang 1990*).

Yellowknife, Canada is within the discontinuous permafrost zone. Groundwater chemistry in two Yellowknife mines, Con and Giant, have been extensively studied (citations), however the only direct investigation of permafrost effects at these sites is found in Chapter 4 of this thesis. At Giant, permafrost is found in bedrock above the 70m level, mostly below a surface valley with a clay and gravel insulating layer (*Espley 1969*), with similar conditions within the Con mine. Some researchers have investigated the possibility that groundwater compositions are related to freezing of seawater on the surface during glacial periods, with subsequent deep emplacement (*Bottomley et al 1999, Starinsky and Katz 2003*). More recent research discounts the possibility that surficial sea water freezing occurred at the Con mine (e.g. *Douglas et al. 2000, Clark et al. 2000, Bottomley et al. 2002, Bottomley et al. 2005*).

Several other Canadian Shield study sites are currently located within sporadic discontinuous permafrost or isolated permafrost, including Lynn Lake, Thompson, Selbaie, Matagami, and Norita. The only investigation of the geochemical impact of permafrost at these sites is the subject of Chapter 4 of this thesis.

Geochemical data are also available from project descriptions, baseline environmental condition reports, and environmental assessments from three arctic ore deposits: High Lake Project, Meadowbank Gold Project, and Diavik Mine. Pressure transducers at High Lake have determined subpermafrost piezometric head in two wells to within ±50m, rock permeabilities within the permafrost were investigated, and dilute talik water was collected from 60m beneath High Lake (*Gartner Lee 2005, 2006a,b*). A thermal profile and hydraulic conductivity data has also been collected (*Friefeld et al. 2008, Stotler et al. 2008*). At the Meadowbank Gold Project, permafrost is approximately 550 m deep. Talik water samples were collected to depths of 175m, and hydraulic conductivities were determined to similar depths, geochemical conditions within the Lac de Gras talik at the Diavik mine were characterized to a depth of 405m below lake surface (*Blowes and Logsdon 1998*). TDS values, >600 mg L^{-1}, increased with depth. Talik geochemical data are extensively discussed in Chapter 4 and provided in Table A-3.

Table A-3. Chemical comparison of talik waters. Data sources are listed in text.

Sample	Depth mbgs	pH	Temp °C	Ca	Na	Mg	K	Cl	Br	SO_4	HCO_3	TDS	δ^2H ‰ VSMOW	$\delta^{18}O$ ‰ VSMOW	^3H T.U.
								mg/l							
High Lake															
BH06-T1 (GW-9-L40)	44.5	7.4		14	3	4.5	< 2.0	4.9	< 0.050	34	53				
Meadowbank Gold															
MW03-01	150	7.4		66	20	23	5.7	626		16	37	793			
MW03-02	143	7.7		63	6.3	32	5.4	5.4		260	125	500			
MW03-03	111	8.6		26	17	17	3.3	50		27	114	254			
MW03-04	169	7.7		15	53	3.8	5.4	13		64		154			
Diavik-Lac de Gras															
Port A	77	9.4	1.7	26	33	12	5.9	26	0.7	6.7	151	205	-187	-21.8	9.1
Port A	77	9.2	1.3	26	34	13	5.9	24	0.6	6.4	162	203			9.4
Port A	77	7.9	9.3	26	35	13	6.0	23		6.0	177	200			
Port A	77	7.8	3.1	25	35	18	3.0	28		0.5	205	214	-182	-23.8	<6
Port B	137	7.1	3.3	26	36	19	4.1	39	1.0	0.1	227	240	-191	-23.7	<0.8
Port B	137	7.6	3.4	29	39	21	4.6	37	0.9	0.2	227	245	-187	-23.8	<0.8
Port B	137	8.0	7.4	25	36	19	4.4	34	0.9	<0.1	219	230			
Port B	137	7.6	4.4	26	38	20	4.5	36		0	219	236	-184	-24.3	<6
Port C	150.5	9.3	4.2	31	31	17	7.0	40	1.0	3.7	194	240	-190	-23.5	<0.8
Port C	150.5	8.4	3.7	29	35	18	7.6	45	1.1	3.4	206	242	-189	-23.1	<0.8
Port C	150.5	8.4	3.7	32	34	18	7.6	45	1.1	3.5	211	247	-189	-23.0	<0.8
Port C	150.5	8.4	3.7	30	34	18	7.6	45	1.1	3.4	208	244	-190	-23.4	<0.8
Port C	150.5	8.4	3.7	29	35	18	7.6	45	1.1	3.5	208	244	-190	-23.4	<0.8
Port C	150.5	8.4	2.5	33	35	19	8.0	37	1.2	3.0	211	242			
Port C	150.5	8.8	4.5	35	37	21	7.6	56		6.2	195	267	-183	-24.1	<6
Port D	150	7.8	1.2	23	32	20	5.0	36	1.0	0.5	197	216			<0.8
Port D	150	7.8	2.9	24	33	21	5.3	38	1.0	0.1	196	221			<0.8
Port D	150	8.1	5	22	31	19	5.0	37	1.0	0.3	194	213			
Port D	150	7.7		23	32	20	5.0	38		0.3	188	213	-186	-24.4	<0.8
Port E	117.5	7.5	2	23	31	19	4.9	37		0.3	196	214			<0.8
Port E	117.5	7.5	1.5	27	35	18	4.0	28	0.8	0.2	213	221			<0.8
Port E	117.5	7.7	2.7	25	37	19	4.2	28	1.4	0.4	218	223			
Port E	117.5	9.1	2.6	24	34	12	5.8	22		6.1	153	196			
Port E	117.5	9.1	2.3	24	34	13	5.4	28		5.9	162	200	-172	-22.3	<6
Port F	94	8.2	0.5	34	39	18	6.3	37	0.9	2.5	233	255			1.9
Port F	94	8.2	0.5	35	39	18	6.5	37		2.4	236	255			
Port F	94	8.2	0.5	34	39	18	6.2	37		2.4	234	252			
Port F	94	8.2	0.5	35	38	18	6.3	36		2.4	232	252			
Port F	94	8.2	0.5	36	38	18	6.3	36		2.3	232	252			
Port F	94	8.2	2.7	30	39	18	4.8	35	0.9	2.3	226	242	-189	-23.2	3.1
Port F	94	8.9	5	26	38	17	4.6	31		2.1	221	229			
Port F	94	8.9	5	27	38	18	4.6	31		2.1	217	228			
Port F	94	8.0	0.4	26	37	17	4.2	32		1.7	205	222	-182	-23.4	<6
Port G	66	8.6	0.9	22	28	14	3.2	24		1.3	163	176	-168	-21.8	9.4
Port H	147	9.8	0.6	18	39	12	16	66	1.9	46	16	226		-23.8	<0.8
Port H	147	9.5	0.7	14	39	13	16	63	1.5	36	36	217	-191		
Port H	147	10.2	3	12	42	14	16	68	1.7	28	44	223			
Port H	147	10.2	3	12	41	14	16	66		27	44	220			
Port H	147	10.2	3	12	42	14	16	66		27	61	220			
Port H	147	10.2	3	13	42	14	16	68		27	54	222			
Port H	147	10.2	3	13	42	15	17	68		27	57	223			
Port H	147	9.8	1.5	11	44	17	16	81		21	55	236	-183	-24.3	<6
Seep1	66			22	31	15	3.3	31		0.8	187	198			
Seep1	66			26	33	17	3.6	31		1.0	168	208			
Seep1	66			20	29	14	3.2	25		1.3	161	176			
Seep2	75			15	25	12	3.3	9.8		0.7	162	150			
Seep2	75			16	26	12	3.7	9.1		0.8	160	151			<0.8
Seep2	75			16	24	11	3.3	8.5		0.9	160	147			
Seep2	75			14	23	10	3.1	7.0		1.2	139	132			
Seep3	82.5			21	32	14	2.8	21	1.0	0.7	206	197			
Seep3	82.5			26	34	16	3.1	19		0.6	204	201			
Seep3	82.5			20	31	14	2.8	17		1.1	179	178			
Seep4	94			22	34	17	3.7	28		0.8	204	209	-188	-22.5	4.6
Seep4	94			26	34	18	3.8	29		0.9	201	214			

Sample	Depth mbgs	pH	Temp °C	Ca	Na	Mg	K	Cl	Br	SO_4	HCO_3	TDS	δ^2H	$\delta^{18}O$	^3H
				mg/l									‰ VSMOW		T.U.
Seep4	94			20	32	15	3.5	23		1.3	183	188			
Seep5	110			22	31	17	4.4	19		0.5	194	192	-187	-21.9	4.9
Seep5	110			16	27	14	4.4	20		0.8	155	162			
Seep5	110			18	28	14	4.6	20		0.8	157	167			
Seep6	117			15	25	13	4.6	16		0.5	155	155			
Seep6	117			15	25	13	4.6	16		0.5	154	155			
Seep6	117			16	25	13	4.7	16		0.4	151	154			
Seep6	117			19	30	15	4.8	23		0.5	171	181			
Seep6	117			19	30	16	4.2	18		0.8	188	184			
Seep7	137			20	34	18	6.5	34		0.1	185	206			
Seep7	137			20	34	18	6.3	34		<0.1	187	207			
Seep8	140.8			23	35	19	6.1	39		0.2	197	223			
Seep8	140.8			24	37	20	6.3	43		0.3	195	230			
Seep8	140.8			24	37	20	6.0	43		1.1	191	228			
Seep9	145			41	45	28	5.3	122		4.1	211	352			
Seep9	145			42	48	30	5.8	102		4.3	211	338			
Seep9	145			41	47	29	5.5	95		7.7	211	332			
Seep10	160.5	8.2	4.3		33	17	8.4			1.9		213			
Seep10	160.5	8.2	4.3		33	17	8.2			1.9		215			
Seep10	160.5	8.2	4.3		33	16	8.2			1.9		212			
Seep10	160.5	8.2	4.3		33	17	8.2			2		215			
Seep10	160.5	7.4	4.4		34	16	8.5			1.7		215			
Seep11	150.5	8.2	3.7		35	13	9.7			6.5		230			
Seep11	150.5	7.5	4.5		39	17	10			4.5		250			<0.8
Seep11	150.5	8.8	3.2		40	20	10			3.7		260			
Seep12	148.5	7.6	3		34	20	5.7			4.5		235			<0.8
Seep12	148.5	8.0	2.9		31	20	5.0			4.4		238			
Seep12	148.5	7.5	3.7		32	20	5.2			0.6		212			
Seep13	150	7.3	0		32	20	4.7			0.4		232			
Seep13	150	7.9	2.4		32	21	4.9			0.4		228			
A154 Seep	NA	9.6	5.4		40	17	27			2.4		222			
A418 Seep	147	8.7	2.8		35	14	12			0.4		172			
A418 Seep	147	9.2	0.4		34	13	12			0.2		173			
A418 Seep	147	9.3	2.7		33	13	11			0.3		164			
Pipe A154-25	206.6	9.1	3.2		50	23	39			1.5		289			1.6
Pipe A154-25	226.7	9.3	3.5		59	24	35			1.7		342	-190	-23.5	1.7
Pipe A154-25	264.6	8.1	3.3		50	30	14			0.7		346			<0.8
Pipe A154-26	193.9	10.7	3.2		75	1.4	61			1.4		296	-190	-23.5	<0.8
Pipe A154-26	192.7	9.9	3.1		75	1.5	62			2.7		299	-190	-23.4	1.3
Pipe A154-26	262.4	8.6	3.7		48	34	21			2.7		323	-191	-23.7	<0.8
Pipe A154-27	179.6	8.1	3.1		49	30	11			18		362	-193	-24.4	
Pipe A154-27	234.4	8.1	4		52	31	17			16		379	-192	-24.6	<0.8
Pipe A154-27	239.3	9.3	5.6		74	40	26			2.5		482	-194	-24.6	<0.8
Pipe A154-28	257.1	8.2	9.8	40	54	31	17	122	2.8	19	200	384	-192	-24.3	<0.8
Pipe A154-28	295.7	8.2	3	37	56	31	21	130	2.9	16	196	389	-192	-24.3	<0.8
Pipe A154-28	361.8	8.2	3.4	42	53	33	13	130	2.7	21	193	388	-192	-24.2	<0.8
Pipe A154-28	404.5	8.6	3.4	31	59	30	25	143		11	173	385	-192	-24.4	
Pipe A154-29	136.6	7.8	2.4	37	45	25	5.0	81	1.9	<0.1	211	300	-187	-23.8	<0.8
Pipe A154-29	212.4	6.8	3.4	43	50	33	6.0	135	3.3	0.8	207	372	-192	-24.1	
Pipe A154-29	266.1	8.3	5	37	44	25	11	100	2.3	5.9	195	320	-190	-23.5	1.5
Pipe A154-29	302	9.3	3.3	26	66	22	26	136	3	1.1	158	372	-192	-24.2	<0.8

Sample	Depth mbgs	pH	Temp °C	Ca	Na	Mg	K	Cl	Br	SO_4	HCO_3	TDS	δ^2H	$\delta^{18}O$	^3H
				mg/l									‰ VSMOW		T.U.
Pipe A154-29	358.9	8.9	3	27	59	24	27	113	2.5	3.4	188	354	-191	-23.9	2.3
Pipe A154-29	394.2	9.0	3.4	33	58	27	24	122	2.6	2.8	183	366	-191	-23.8	
Pipe A154-30	303.9	7.9	1.5	59	60	43	7.2	199		4.6	190	467	-192	-24.6	
Pipe A154-30	387.3	8.5	4.4	65	67	53	13	274		3.8	165	559	-192	-25.5	<6
Pipe A418-16	232.3			38	71	23	9.5	113	2.9	6.2	204	364	-192	-23.9	<0.8
Pipe A418-16	286.3			46	76	21	8.7	144	3.6	0.2	190	392	-192	-24.2	
Pipe A418-16	286.3			43	77	22	8.8	146	3.7	0.1	188	392	-193	-23.9	<0.8
Pipe A418-16	334.7	8.0	2.6	42	81	24	21	177	4.2	0.7	178	435	-194	-24.3	<0.8
PT97-1	21/Jan/97	8.9	3.2	49	56	30	12	125		38	182	401	-191	-24.8	<0.8
PT97-1	21/Jan/97	8.5	3.2										-192	-24.9	<0.8
PT97-1	21/Jan/97	8.6	3.2	47	54	30	11	122		24	189	382	-190	-24.8	<0.8
PT97-1	21/Jan/97	8.4											189	-24.7	<0.8
PT97-1	22/Jan/97	8.2	3.4	47	51	29	10				191		-189	-24.8	<0.8
PT97-1	22/Jan/97	8.2	3.5										-189	-24.7	<0.8
PT97-1	22/Jan/97	8.2	3.4	46	52	30	11	110		15	196	363	-188	-24.7	<0.8
PT97-1	22/Jan/97	8.4	4	44	49	29	10	110		13	194	352	-190	-24.6	<0.8
PT97-1	22/Jan/97	8.4	3.4	43	52	29	11	106		17	195	356	-189	-24.8	<0.8
PT97-1	23/Jan/97	8.4	3.6										-188	-24.7	<0.8
PT97-1	23/Jan/97	8.3	3.5	41	49	28	10	97		11	194	333	-188	-24.6	<0.8
PT97-1	23/Jan/97	8.4	3	42	49	28	10	98		12	196	336	-188	-24.5	<0.8
PT97-1	24/Jan/97	8.5	4.2	44	50	29	10	107		10	194	348	-181	-24.7	<0.8
PT97-1	24/Jan/97	8.6	3.5	45	50	29	10	112		9.5	193	352	-186	-24.7	1.1
PT97-1	24/Jan/97	8.6	3.6										-186	-24.4	<0.8
PT97-1	24/Jan/97	8.5	3.6										-183	-24.3	<0.8
PT97-1	25/Jan/97	7.5	4	44	48	28	9.9	108		8.4	195	345	-186	-24.7	<0.8
PT97-1	25/Jan/97	8.1	3.3										-184	-24.4	<0.8
PT97-1	25Jan/97	7.7	3.3	44	49	29	9.9	109		8.0	194	346	-183	-24.6	<0.8
PT97-1	25/Jan97	8.3	3.3										-188	-24.5	<0.8
PT97-1	26/Jan/97	8.6	3.3	39	48	28	9.6	93		6.6	196	322			
PT97-1	26/Jan/97	8.4	3.2										-186	-24.4	<0.8
PT97-1	26/Jan/97	8.7	3.3	40	48	28	9.8	97		10	195	331			
PT97-1	26/Jan/97	8.9	3.3										-188	-24.4	<0.8
PT97-1	27/Jan/97			39	47	28	9.5	97		6.2	193	324	-178	-24.6	<0.8
PT97-1	27/Jan/97			37	47	27	9.5	100		5.9	195	324			
PT97-1	28/Jan/97	8.2	3.3	38	46	27	9.2	96		5.5	195	320	-178	-24.8	<0.8

Appendix B.

Lupin Datasets

Table B-1. Borehole completion information.

Borehole	[1]Collar elevation (m)	Northing	Easting	Azimuth (°)	Angle (°)	Length (m)	Completion Date	Date Sealed
550-112					+15	23.8	May-2004	-
570-105	1433.57	10130.88	10125.86	087	+2	515	Nov-2002	-
570-106	1432.57	10130.88	10125.86	070	-25	387	Nov-2002	-
890-188	~1123.0	10193.5	10209	130	?	522.71	Jun-1990	5-Dec-2002
1130-64								-
1130-175	877.76	10433.64	10463.40	309.51	-80.68[2]	920.00	Jul-1993	-
1130-176	876.73	10433.63	10462.61	289.71	-73.38[3]	713.00	Sep-1993	-
1130-181	877.39	10407.96	10433.54	119.18	+0.95	995.05	Dec-1993	26-Feb-2003
1130-191	876.74	10391.90	10414.51	125.16	-0.49	440.78	Dec-1993	24-Feb-2003
1130-192	875.35	10329.94	10336.49	125.86	+0.63	549.00	Dec-1993	3-Dec-2002 / 22-Feb-2003
1130-195	872.26	10257.20	10230.79	121.51	+1.16	579.09	Jan-1994	-
1130-197	872.25	10257.04	10230.43	132.40	+0.40	573.91	Feb-1994	25-Feb-2003 / 29-Feb-2004
1130-217	874.4	10392	10414.8	122	0	450	Sep-1994	24-Feb-2003
1130-219	872	10256.4	10224.2	144	0	336.0	Sep-1994	24-May-2003
1130-260								Mar-2004
1130-267	880.72	10338.79	10540.34	114	0	270	Jun-2003	02-Mar-2004
1130-273	877+	10439	10467	32	0	225	Jul-2003	28-Feb-2004

[1]Zero point elevation in the mine coordinate system is 2000m below ground surface
[2]Acid Tube Data at 900m:-58°
[3]Acid Tube Data at 700m: -44°

Table B-2. Final redox (Eh) and dissolved oxygen values measured in flow-through cell.

Depth-Borehole No.	Date	Eh (mV)	O_2 (mg L^{-1})	pH	EC (mS/cm)
890-188	21-Feb-2003	24	0.0	8.34	545
1130-192	22-Feb-2003	-18	0.0	8.22	4430
1130-217	24-Feb-2003	-16	0.0	8.60	1370
1130-197	25-Feb-2003	11	0.0	8.48	1410
1130-181	27-Feb-2003	-10	0.0	8.43	1230

Table B-3. Major ion geochemistry of Lupin Mine water samples.

Sample type	Date	Depth m	Ca mg/l	Mg mg/l	Na mg/l	K mg/l	Sr mg/l	Cl mg/l	SO_4 mg/l	HCO_3 mg/l	Br mg/l	NO_3 mg/l	TDS g/l
Precipitation													
Rain	22/06/02	0	0.4	0.1	0.3	0.23	0.0031	0.5	1.1	2	0.1	0.88	0.0057
Snow	23/06/02	0	0.1	0.1	0.2	0.11	0.0003	0.2	0.1	1	0.1	0.20	0.0026
Snow	27/10/00	0	0.4	0.1	0.4	0.31	0.0019	0.5	0.2	4	0.0	0.20	0.0064
Surface Water													
Lake Contwoyto	22/06/02	0	2.4	1.1	2.1	0.65	0.0156	3.5	7.5	4	0.1	0.86	0.0225
Permafrost													
Drips	26/10/00	250	1130	381	11600	326	13	20200	3040	217	9.4	2630	39.6
Drips	19/05/04	250	618	271	11300	157	6.6	19000	2090	167	7.0	1080	34.8
Drips	07/10/05	250	804	366	9750	171	7.5	15900	2970	406	13.1	1190	31.6
Drips	28/10/00	290	1250	452	8820	224	11	15800	3400	93	5.9	1830	31.9
Drips	26/10/00	310	899	765	6240	183	9.4	13200	4350	1	4.8	1180	27.3
Drips	25/05/04	310	692	666	3520	95	6.6	5960	4970	1	4.4	1110	17.2
Drips, cable hole	26/10/00	330	754	587	2980	174	7.8	5670	4400	50	4.0	1070	15.8
Drips	26/10/00	390	924	1050	6820	233	17	13700	5000	1	8.0	689	28.8
Drips, wza[1], bolt	25/05/04	390	1760	640	7470	187	27	14300	2630	157	5.9	1350	28.6
Drips, wza[1], bolt	27/11/04	390	1580	579	6600	161	24	13500	2470	162	8.3	1250	26.5
Drips, wza[1], bolt	07/10/05	390	1300	589	6040	177	20	15500	2650	197	13.2	1020	27.5
Drips	26/10/00	430	1280	1150	9730	337	23	19300	4320	91	8.2	1080	37.4
Drips	14/06/02	430	1180	650	7890	317	14	13200	3490	71	<0.1	1250	28.2
Drips, wza[1]	08/10/05	450	1590	623	6570	164	23	12300	2650	13	12.3	1460	25.4
Drips	25/05/04	470	703	452	2740	70	6.9	5010	3400	3	2.5	450	12.9
Drips	26/10/00	510	664	585	3320	131	7.9	7120	3740	30	3.9	423	16.1
Drips	25/05/04	510	870	581	4470	128	9.8	7390	3320	13	3.5	1000	17.9
Drips	26/10/00	530	1080	239	1790	77	8.2	5140	1430	155	2.8	916	10.9
Drips	25/05/03	550	762	477	3040	105	8	4750	3170	10	3.0	813	13.2
Basal Permafrost													
BH 112	25/05/03	550	742	392	1550	72	9.0	2410	2500	281	2.7	958	8.9
BH 112	12/06/03	550	756	371	1380	85	8.0	2100	2400	244	3.4	1100	8.5
BH 112	25/05/03	550	763	398	1570	61	8.9	2220	2410	15	2.4	934	8.4
BH 112	27/02/04	550	672	359	1370	56	7.9	2410	2580	262	1.8	810	8.6
BH 112	25/05/04	550	700	366	1350	49	8.4	2060	2600	175	2.9	768	8.2
BH 112	27/11/04	550	696	360	1340	61	8.0	2510	2910	202	2.5	794	8.9
BH 112	30/11/04	550	704	346	1290	60	8.1	2090	2690	217	3.2	793	8.2
BH 112	05/10/05	550	548	18	773	4	7.7	2130	25	220	2.0	630	4.3
BH 105*	31/10/02	570	70	16	206	48	0.8	341	87	13	3.7	6	0.8
BH 105*	02/11/02	570	103	19	256	49	1.6	478	134	91	5.6	5	1.2
BH 105, 0-45 m^2	19/11/02	570	661	18	453	13	12	1845	638	1	11.6		3.9
BH 105,.45-160 m^2	19/11/02	570	161	33	251	44	0.3	750	98	76	9.1	12	1.4
BH 105, 160-515 m^2	19/11/02	570	69	21	350	68	0.8	743	81	166	5.6	7	1.5
BH 105, 160-515 m^2	19/11/02	570	60	19	321	56	24	655	80	92	4.9	5	1.3
BH 105[2]	20/05/03	570	799	55	542	9	18	1663	799	1	15.3	<2	4.0
BH 105, 0-150 m	12/06/03	570	805	53	497	19	14	1800	630	49	16.0	<2	3.9
BH 105, 0-515 m	02/03/04	570	778	65	535	6	16	1960	942	<1.2	14.8	16	4.4
BH 105, 0-515 m	25/05/04	570	712	132	1010	15	15	2270	1300	1	13.8	93	5.7
BH 105, 0-515 m	27/11/04	570	732	86	630	11	14	2020	1050	<1.2	21.7	<20	4.6
BH 105, 0-515 m	05/10/05	570	757	69	495	5	15	1640	1050	1	18.1	<20	4.0
Subpermafrost													
BH 188	28/10/00	890	588	43	735	6	15	2160	7.8	15	37.0	2	3.6
BH 188	30/08/01	890	284	51	636	4	7.3	1770	1.0	29	27.1	<2	2.8
BH 188	14/02/02	890	485	44	613	5	11	1860	11	10	32.0	<2	3.1
BH 188, pressurized	20/02/03	890	444	55	561	4	10	1850	7.0	15	30.8	<0.2	3.0
BH 188, pressurized	24/05/03	890	429	54	619	4	11	1540	7.6	8	27.0	<0.2	2.7
BH 188, pressurized	26/02/04	890	385	47	532	3	8.5	2110	9.1	18	25.0	<1	3.2
BH 188, pressurized	18/05/04	890	394	47	552	2	9.2	1620	9.2	15	26.1	<1	2.7
BH 188, pressurized	26/11/04	890	407	56	526	2	9.3	1780	9.4	16	26.9	<2	2.8
BH 188, pressurized	08/10/05	890	428	57	539	3	9.7	1670	12	18	30.4	<1	2.8
BH 64	23/05/03	1130	343	20	610	1	7.1	1160	34	12	18.6	<2	2.2
BH 64	01/03/04	1130	389	20	575	2	6.8	1750	35	10	23.2	<1	2.8
BH 64	17/05/04	1130	352	19	580	2	6.4	1580	35	10	23.6	<1	2.6
BH 64	26/11/04	1130	361	20	533	1	6.5	1590	28	11	21.5	<2	2.6
BH 64	06/10/05	1130											
BH 175, flowing	15/02/02	1130	4220	93	5260	45	122	16200	3.1	5	268	<4	26.2
BH 175, flowing	22/05/03	1130	4090	133	7170	39	162	15600	1.2	10	266	<2	27.5
BH 175, flowing	16/05/04	1130	4430	148	7270	33	158	20100	<5	7	323	<10	32.7
BH 175, flowing	28/11/04	1130	4500	143	7120	46	167	19700	1.2	8	362		32.1
BH 175, flowing	06/10/05	1130	4670	157	6910	52	156	19100	<0.1	11	384	<1	31.3

Sample type	Date	Depth m	Ca mg/l	Mg mg/l	Na mg/l	K mg/l	Sr mg/l	Cl mg/l	SO_4 mg/l	HCO_3 mg/l	Br mg/l	NO_3 mg/l	TDS g/l
BH 191	16/02/02	1130	1430	39	1370	9	30	4110	29	7	77.0	<2	7.1
BH 191	14/06/02	1130	1350	36	1530	10	28	4590	24	10	72.2	<0.2	7.7
BH 191, pressurized	24/02/03	1130	1080	50	962	6	21	3570	30	13	65.0	<0.2	5.8
BH 191, pressurized	23/05/03	1130	2500	28	3340	12	70	7540	20	9	125	<2	13.7
BH 191, pressurized	01/03/04	1130	1140	28	1290	5	28	4340	30	13	61.6	<2	7.0
BH 191, pressurized	08/10/05	1130	742	34	940	3	17	3150	29	18	56.2	<1	5.0
BH 192	15/02/02	1130	4800	40	6000	33	137	19400	13	6	290	<4	30.7
BH 192	14/06/02	1130	4570	38	6550	38	147	18000	11	7	286	<0.2	29.7
BH 192, pressurized	22/05/03	1130	6130	69	9060	35	199	20400	7.4	9	350	<2	36.3
BH 192, pressurized	24/05/03	1130	4830	61	8620	31	187	19000	8.6	9	334	<0.2	33.1
BH 192, pressurized	01/03/04	1130	5120	44	8570	21	192	25600	18	9	342	<20	40.0
BH 192, pressurized	15/05/04	1130	5510	72	8630	28	174	23300	9.0	8	368	<10	38.3
BH 192, pressurized	26/11/04	1130	5860	70	8140	33	184	25200	7.0	8	357	<2	39.9
BH 192, pressurized	08/10/05	1130	5900	81	9040	41	183	24000	8.4	79	436	<20	39.6
BH 197	15/02/02	1130	1730	52	1800	13	43	5340	8.0	6	105	<2	9.1
BH 197, pressurized	25/02/03	1130	1450	47	1710	11	36	5310	8.8	10	86.0	<0.2	8.6
BH 197, pressurized	23/05/03	1130	916	39	1450	7	27	3390	10	10	57.8	<0.2	5.9
BH 197, pressurized	01/03/04	1130	1490	45	1720	7	37	6150	9.9	11	83.7	<4	9.6
BH 197, pressurized	26/11/04	1130	869	40	1240	6	23	4080	12	12	60.2	<2	6.4
BH 197, pressurized	09/10/05	1130	905	41	1240	7	23	3590	16	13	76.3	<2	5.9
BH 217, pressurized	24/02/03	1130	1540	47	1530	9	34	5200	27	12	82.9	<0.2	8.5
BH 217, pressurized	23/05/03	1130	2660	30	3620	17	76	8930	20	9	152	<2	15.5
BH 217, pressurized	28/02/04	1130	1120	29	1360	5	28	4350	29	12	58.1	<2	7.0
BH 217, pressurized	15/05/04	1130	1720	19	2040	8	34	5610	23	9	91.9	<4	9.6
BH 217, pressurized	25/11/04	1130	1950	19	2040	10	47	8910	22	9	108	<2	13.2
BH 217, pressurized	08/10/05	1130	1230	27	1400	7	30	4360	28	91	84.5	<1	7.2
BH 219	08/11/00	1130	3670	121	3050	21	54	12300	17	17	183	<6	19.5
BH 219, pressurized	25/05/03	1130	1830	80	2080	10	50	5940	10	9	103	<0.2	10.1
BH 219, pressurized	28/02/04	1130	3600	121	3070	13	89	13400	4.8	9	184	<6	20.6
BH 219, pressurized	26/11/04	1130	1380	60	1400	6	31	5090	14	10	73.7	<2	8.1
BH 219, pressurized	09/10/05	1130	1370	65	1450	7	33	4750	15	12	101	<4	7.8
BH 260	23/05/03	1130	2770	33	3690	17	78	9150	19	8	159	<0.2	15.9
BH 260	02/03/04	1130	1540	42	1570	6	39	5410	29	12	78.1	<2	8.8
BH 260	25/11/04	1130	2050	50	1920	8	48	7810	23	9	101	<2	12.1
BH 260, pressurized	06/10/05	1130	1460	30	1790	10	37	5010	27	15	112	<2	8.5
BH 267, 3-24 m	28/02/04	1130	553	26	853	4	13	2520	34	16	32.7	<2	4.1
BH 267, 45-66 m	29/02/04	1130	616	28	935	4	15	2980	34	15	40.3	<2	4.7
BH 267, 150-269m	29/02/04	1130	744	15	1170	4	20	3550	35	15	46.7	<2	5.6
BH 267, 187-269 m	01/03/04	1130	747	15	1160	4	20	3500	34	15	49.0	<2	5.6
BH 267, pressurized	26/05/04	1130	790	17	1200	2	18	3280	41	14	52.9	<2	5.4
BH 267, pressurized	25/11/04	1130	809	18	1140	5	20	3970	31	14	53.7	<2	6.1
BH 267, leaking	08/10/05	1130	766	23	1080	3	18	2780	30	19	60.4	<2	4.8
BH 273, pressurized	29/02/04	1130	1780	39	2250	10	46	7580	6.9	8	102	<4	11.9
BH 273, pressurized	14/05/04	1130	1250	34	1690	7	25	5050	3.4	8	71.8	<2	8.2
BH 273, pressurized	25/11/04	1130	1230	40	1560	8	27	4920	3.7	9	75.9	<2	7.9
BH 273, pressurized	30/11/04	1130	1460	44	1760	8	32	6700	3.4	9	82.4	<2	10.2
BH 273, pressurized	08/10/05	1130	1320	44	1730	10	30	5110	3.5	13	96.5	<4	8.3
Drips, Bolthole	26/02/03	1130	612	20	781	5	9.6	2470	25	10	39.2	<0.2	3.9
Drips, Bolthole	02/03/04	1130	472	17	768	3	7.9	2790	26	11	30.3	<2	4.1
Drips, Bolthole	28/11/04	1130	481	16	728	3	8.5	2220	27	11	33.9	<2	3.6
Drips, Bolthole	06/10/05	1130	548	18	773	4	9.2	2130	25	15	41.8	<2	3.6
BH 105	01/03/04	1300	1460	18	1640	6	37	5800	24	9	69.5	<2	9.1

[1]WZA = West Zone Access. All other permafrost drip samples collected along mine ramp.
[2]Sample corrected for uranine tracer (drill fluid contamination)

Table B-4. Isotopic geochemistry of water samples from the Lupin Mine.

Sample type	Date	Depth m	$\delta^{18}O$ ‰	$\delta^{2}H$ ‰	^{3}H TU	$\delta^{37}Cl$ ‰	$\delta^{34}S_{SO4}$ ‰	$\delta^{18}O_{SO4}$ ‰	$\delta^{15}N_{NO3}$ ‰	$\delta^{18}O_{NO3}$ ‰	$\frac{^{36}Cl}{Cl*10^{-15}}$	±	$\delta^{13}C$-DIC ‰	^{14}C pmc	±	^{14}C 'Age' yrs	±
Precipitation																	
Rain	22/06/02	0	-20.3	-156	12.1												
Snow	23/06/02	0	-29.2	-226	11.3												
Snow	27/10/00	0	-25.7	-195	6.5												
Surface Water																	
Lake Contwoyto	22/06/02	0	-20.0	-160	12.8						1073.8	22.5					
Permafrost																	
Drips	26/10/00	250	-21.1	-171	17.3												
Drips	19/05/04	250	-19.7	-157		-0.29	0.6	-13.1	5.4	26.2							
Drips	07/10/05	250	-20.7	-170	12.9	0.14	1.7	-20.2	5.9	23.5							
Drips	28/10/00	290	-20.6	-168	6.0		2.1	-12.8	11.7	27.6							
Drips	26/10/00	310					-1.0	-14.7	2.6	25.7							
Drips	25/05/04	310	-21.6	-175		-0.25	0.6	-15.6	5.6	23.5							
Drips, cable hole	26/10/00	330	-22.6	-180	13.2												
Drips	26/10/00	390					-1.8	-15.0	7.4	6.4	0.0	0.4					
Drips, wza[1], bolt	25/05/04	390	-19.1	-159	10.5	-0.45	0.7	-14.4	7.8	23.6							
Drips, wza[1], bolt	27/11/04	390	-19.5	-162	9.0						2.2	1.1	-9.8	14.02	0.10	15729	60
Drips, wza[1], bolt	07/10/05	390	-19.4	-161	10.0	-0.03	1.4	-19.9	9.4	20.0							
Drips	26/10/00	430	-19.9	-162	8.5												
Drips	14/06/02	430			11.0	0.16											
Drips, wza[1]	08/10/05	450	-19.3	-159	10.0	-0.06	1.2	-20.7	4.6	14.2							
Drips	25/05/04	470	-18.2	-150		-0.32	1.7	-14.2	6.7	15.7							
Drips	26/10/00	510					1.2	-13.8	4.8	24.1							
Drips	25/05/04	510	-17.0	-144		-0.34	1.3	-14.0	4.8	7.1							
Drips	26/10/00	530	-20.4	-164	12.2		2.9	-12.6	11.7	-0.8							
Drips	25/05/03	550	-17.6	-149	10.4												
Basal Permafrost																	
BH 112	25/05/03	550	-18.7	-155	9.6	-0.37											
BH 112	12/06/03	550	-18.3	-152	10.8												
BH 112	25/05/03	550															
BH 112	27/02/04	550															
BH 112	25/05/04	550	-18.7	-154	10.2	-0.58	2.9	-14.3	5.9	5.5							
BH 112	27/11/04	550	-18.2	-153	10.7												
BH 112	30/11/04	550	-18.4	-151	10.0						4.3	1.1	-11.0	3.86	0.07	26080	140
BH 112	05/10/05	550	-18.5	-154	8.3	-0.08	3.1	-19.0	7.1	8.8							
BH 105*	31/10/02	570	-20.1	-160	13.7												
BH 105*	02/11/02	570	-20.1	-161	13.0												
BH 105, 0-45 m^2	19/11/02	570	-21.2	-167	8.0												
BH 105,.45-160 m^2	19/11/02	570															
BH 105, 160-515 m^2	19/11/02	570	-20.0	-159	16.1												
BH 105, 160-515 m^2	19/11/02	570	-19.9	-157	11.7												
BH 105[2]	20/05/03	570	-22.4	-175	1.5	-0.23											
BH 105, 0-150 m	12/06/03	570															
BH 105, 0-515 m	02/03/04	570															
BH 105, 0-515 m	25/05/04	570	-19.6	-157	3.7	-0.48	7.1	-13.0									
BH 105, 0-515 m	27/11/04	570	-21.9	-171	1.5						6.9	1.3	-14.0				
BH 105, 0-515 m	05/10/05	570	-21.8	-173	1.7	-0.01	12.4	-18.5									
Subpermafrost																	
BH 188	28/10/00	890	-22.4	-178	<0.8	-0.20											
BH 188	30/08/01	890	-22.1	-175	1.6												
BH 188	14/02/02	890	-22.4	-180	<0.8												
BH 188,	20/02/03	890	-22.8	-176	0.9	-0.04											

Sample type	Date	Depth m	$\delta^{18}O$ ‰	$\delta^{2}H$ ‰	^{3}H TU	$\delta^{37}Cl$ ‰	$\delta^{34}S_{SO4}$ ‰	$\delta^{18}O_{SO4}$ ‰	$\delta^{15}N_{NO3}$ ‰	$\delta^{18}O_{NO3}$ ‰	$\frac{^{36}Cl}{Cl*10^{-15}}$	±	$\delta^{13}C$-DIC ‰	^{14}C pmc	±	^{14}C 'Age' yrs	±
pressurized																	
BH 188, pressurized	24/05/03	890	-22.9	-179	<0.8												
BH 188, pressurized	26/02/04	890	-22.5	-182	<0.8	-0.07											
BH 188, pressurized	18/05/04	890															
BH 188, pressurized	26/11/04	890	-22.8	-178	<0.8						11.2	1.7	-5.2	5.58	0.07	23130	100
BH 188, pressurized	08/10/05	890	-22.7	-179	<0.8	0.05											
BH 64	23/05/03	1130	-23.3	-181	0.9	-0.49											
BH 64	01/03/04	1130	-23.0	-184	1.2	-0.08											
BH 64	17/05/04	1130															
BH 64	26/11/04	1130	-23.4	-181	<0.8						11.6	2.0					
BH 64	06/10/05	1130	-23.3	-182	<0.8	-0.21	17.0	-7.4					-22.8	7.67	0.09	20570	95
BH 175, flowing	15/02/02	1130	-22.6	-177	1.1												
BH 175, flowing	22/05/03	1130	-22.8	-174	<0.8	-0.23											
BH 175, flowing	16/05/04	1130															
BH 175, flowing	28/11/04	1130	-22.5	-173	<0.8												
BH 175, flowing	06/10/05	1130															
BH 191	16/02/02	1130	-23.2	-179	<0.8												
BH 191	14/06/02	1130	-23.2	-179	<0.8	-0.22											
BH 191, pressurized	24/02/03	1130	-23.4	-180	1.5	-0.24											
BH 191, pressurized	23/05/03	1130	-23.0	-179	<0.8												
BH 191, pressurized	01/03/04	1130	-23.0	-182	1.2												
BH 191, pressurized	08/10/05	1130															
BH 192	15/02/02	1130	-22.6	-181	<0.8												
BH 192	14/06/02	1130	-22.8	-175	<0.8	-0.02											
BH 192, pressurized	22/05/03	1130	-22.7	-175	<0.8												
BH 192, pressurized	24/05/03	1130															
BH 192, pressurized	01/03/04	1130	-22.2	-176	<0.8	-0.22	7.4	-2.0									
BH 192, pressurized	15/05/04	1130															
BH 192, pressurized	26/11/04	1130	-22.5	-172	<0.8						11.6	1.5					
BH 192, pressurized	08/10/05	1130	-22.6	-173	<0.8	-0.16							10.5	3.50	0.07	26870	150
BH 197	15/02/02	1130	-22.8	-186	<0.8												
BH 197, pressurized	25/02/03	1130	-23.0	-178	<0.8	0.11											
BH 197, pressurized	23/05/03	1130	-22.9	-179	0.9												
BH 197, pressurized	01/03/04	1130	-22.4	-180	<0.8												
BH 197, pressurized	26/11/04	1130	-22.8	-178	1.0												
BH 197, pressurized	09/10/05	1130	-22.7	-179	<0.8	-0.06							-1.7	4.41	0.08	25030	150
BH 217, pressurized	24/02/03	1130	-23.5	-179	<0.8	-0.16											
BH 217, pressurized	23/05/03	1130	-23.2	-180	<0.8												
BH 217, pressurized	28/02/04	1130	-22.9	-182	1.4												
BH 217, pressurized	15/05/04	1130															
BH 217, pressurized	25/11/04	1130	-23.1	-179	<0.8												

Sample type	Date	Depth m	$\delta^{18}O$ ‰	$\delta^{2}H$ ‰	^{3}H TU	$\delta^{37}Cl$ ‰	$\delta^{34}S_{SO4}$ ‰	$\delta^{18}O_{SO4}$ ‰	$\delta^{15}N_{NO3}$ ‰	$\delta^{18}O_{NO3}$ ‰	$\frac{^{36}Cl}{Cl*10^{-15}}$	±	$\delta^{13}C$-DIC ‰	^{14}C pmc	±	^{14}C 'Age' yrs	±
BH 217, pressurized	08/10/05	1130															
BH 219	08/11/00	1130															
BH 219, pressurized	25/05/03	1130	-23.0	-179	<0.8												
BH 219, pressurized	28/02/04	1130	-22.9	-179	<0.8												
BH 219, pressurized	26/11/04	1130	-22.9	-178	1.4												
BH 219, pressurized	09/10/05	1130															
BH 260	23/05/03	1130	-23.0	-177	<0.8	-0.44											
BH 260	02/03/04	1130	-23.0	-183	<0.8	-0.19											
BH 260	25/11/04	1130	-23.1	-179	<0.8												
BH 260, pressurized	06/10/05	1130															
BH 267, 3-24 m	28/02/04	1130	-23.1	-185	1.7	-0.27											
BH 267, 45-66 m	29/02/04	1130	-23.1	-186	1.3	-0.44											
BH 267, 150-269m	29/02/04	1130															
BH 267, 187-269 m	01/03/04	1130	-23.0	-185	1.1	-0.01											
BH 267, pressurized	26/05/04	1130															
BH 267, pressurized	25/11/04	1130	-23.4	-180	0.9						12.8	2.0					
BH 267, leaking	08/10/05	1130	-23.2	-183	1.9	-0.08	18.3	-6.6									
BH 273, pressurized	29/02/04	1130	-22.8	-182	<0.8	-0.04	9.2	-6.6									
BH 273, pressurized	14/05/04	1130															
BH 273, pressurized	25/11/04	1130	-23.2	-178	<0.8						13.8	1.6					
BH 273, pressurized	30/11/04	1130	-23.2	-179	<0.8						11.1	1.6					
BH 273, pressurized	08/10/05	1130	-23.0	-180	1.3	-0.11							9.6	4.40	0.70	25040	130
Drips, Bolthole	26/02/03	1130	-23.4	-180	<0.8	-0.17											
Drips, Bolthole	02/03/04	1130	-22.9	-184	0.8												
Drips, Bolthole	28/11/04	1130															
Drips, Bolthole	06/10/05	1130															
BH 105	01/03/04	1300	-22.8	-180	<0.8	-0.14	14.3	-0.8									

Table B-5. Description of crush and leach matrix fluids and drill salt samples.

Borehole, distance(m)	Geology
Drill Salt	Halite (imported to site)
550-112, 6.6	Phyllite
550-112, 9.5	Phyllite - before fracture (10.5m-12m)
550-112, 12	Phyllite - after fracture (10.5-12m)
550-112, 14	Phyllite
550-112, 16	Phyllite
550-112, 18	Phyllite
550-112, 19.1	Phyllite
550-112, 20.2	Phyllite
550-112, 21.1	Phyllite
570-105, 32.1	Phyllite/Greywacke (fine grained, mica bearing, and homogeneous)
570-105, 123.6	Phyllite, coarser, dark minerals (mica, amphibole) clearly visible
570-105, 155.4	Muscovite Granite (fine grained, grey)
570-105, 353.9	Phyllite, fine grained corderite bearing
570-105, 416.9	Quartz-Feldspar Gneiss, locally contains garnet and amphibole
570-105, 511.69	Quartz-Feldspar Gneiss
570-106, 99.1	Phyllite (Garnet-Amphibole, sulfides)
570-106, 128.2	Mica-Gneiss, corderite porphyroblasts (medium grained)
570-106, 179.6	Muscovite Granite
570-106, 385.7	Amphibole, sulfide-bearing, heterogeneous
890-188, 42.8	Mudstone/greywacke
890-188, 93.1	Muscovite Granite

Table B-6. Chemistry of crush and leach matrix fluids and drill salt. Alkalinity was analyzed to complete charge balance calculations.

Borehole, distance (m)	B	Li	Mn	Sr	Fe	Na	K	Ca	Mg	Br	Cl	SO_4	HCO_3[(2)]	$\delta^{37}Cl$
	mg·kg^{-1}													‰ SMOC
Drill Salt	<4	0.02	2.69	2.74	<1	358000	917	110	5.6	45	639000	263	-	0.17
550-112, 6.6	0.10	0.065	0.052	0.024	5.2	56	32	1.5	2.3	0.6	34	17	116	0.21
550-112, 9.5	0.03	0.009	0.008	0.012	0.72	32	36	0.8	1.4	0.2	12	8.7	116	-0.38
550-112, 12	0.03	0.066	0.005	0.068	< 0.03	50	67	7.5	6.3	0.7	51	36	159	-0.28
550-112, 14	0.02	0.051	0.000	0.016	< 0.03	35	43	1.9	1.1	0.3	20	5.9	140	-0.24
550-112, 16	0.03	0.028	0.001	0.018	< 0.03	24	52	2.5	1.0	0.3	8.1	4.0	159	-0.31
550-112, 18	0.03	0.083	0.119	0.012	11	27	56	0.6	4.9	0.1	8.1	8.7	140	-0.38
550-112, 19.1	0.04	0.099	0.049	0.016	3.6	31	47	1.6	1.6	0.2	12	6.6	140	NES[(1)]
550-112, 20.2	0.02	0.068	0.004	0.023	< 0.03	27	31	5.1	2.3	0.3	16	26	104	-0.31
550-112, 21.1	0.04	0.062	0.053	0.014	6.4	30	72	1.4	2.4	0.2	13	6.9	177	NES[1]
570-105, 32.1	0.06	0.111	0.002	0.030	< 0.03	45	66	9.9	1.0	0.2	24	38	151	-0.30
570-105, 123.6	0.10	0.091	0.002	0.038	< 0.03	62	60	4.3	1.8	0.7	41	30	153	NES[1]
570-105, 155.4	0.06	0.022	0.004	0.103	< 0.03	62	32	15	0.8	0.3	41	34	132	0.30
570-105, 353.9	0.15	0.009	0.001	0.041	0.09	32	44	3.4	1.5	0.2	15	14	116	-0.21
570-105, 416.9	0.05	0.005	0.001	0.037	< 0.03	40	36	4.0	1.5	0.4	35	1.9	146	-0.40
570-105, 511.69	0.07	0.011	0.005	0.018	0.44	53	56	2.1	1.0	0.3	22	30	134	-0.42
570-106, 99.1	0.03	0.001	0.000	0.004	< 0.03	15	19	0.5	0.9	0.1	9.5	2.1	45	NES[1]
570-106, 128.2	0.04	0.023	0.002	0.006	< 0.03	43	71	0.4	0.5	0.2	15	14	148	NES[1]
570-106, 179.6	0.05	0.004	0.004	0.023	< 0.03	75	54	3.6	0.6	0.9	72	30	137	0.03
570-106, 385.7	0.02	0.023	0.002	0.131	< 0.03	4.3	5.7	23	3.8	0.0	17	18	54	NES[1]
890-188, 42.8	0.03	0.030	0.000	0.014	< 0.03	32	90	1.6	0.6	0.4	31	15	145	NES[1]
890-188, 93.1	0.05	0.012	0.006	0.045	< 0.03	68	28	12	2.8	0.5	51	25	143	-0.07

[(1)]NES = not enough sample

[(2)]Alkalinity was analyzed on the matrix fluids for charge balance calculations

Table B-7. Fluid inclusion microthermometry data.

Sample ID	Stable Isotope		Chip No	Description	Fluid Inclusion	Microthermometric Measurement (°C)				Comments
	$\delta^{13}C$	$\delta^{18}O$				T_{freeze}	T_{fm}	T_m	T_h	
LuF47	-1.8	-18.1	3	mostly two-phase	(1) FIA, two phase, regular, 1-5 um					Cool down to -148.2 °C, no changes were observed
				regular shape	(2) A two-phase FI, 8 um, triangular, V/L = 15%					Cool down to -115.3 °C, no changes were observed
				2-5 um, V/L ≈ 20%	(3) A two-phase FI, 3 um, with a moving bubble	-73.5		<-37.9		T_m was determined based on the first move of the bubble
				uneven distribution some		-73.9		-40.3		" "
				crystals full of FIs some are free of FIs		-74.0		-40.9		" "
									164.7	
					(4) A two-phase FI, 4 um					Cool down to -133.5 °C, no changes were observed
					(5) Two two-phase Fis, 4-5 um, V/L = 20%					Cool down to -112.9 °C, no changes were observed
					(6) A two-phase FI, 2 um, with a moving bubble					Cool down to -102.3 °C, no changes were observed
										Cool down to -129.5 °C, no changes were observed
										Cool down to -112 °C, no changes were observed
					(7) A two-phase FI, 8 um, V/L = 10%	-85.0	-65.0	-39.2		Breaking and melting of ice were observed
						-84.5	-65.7	-40.2		" "
						-85.6	-65.0	-40.0		Eutectic temperature should be a little lower than T_{fm}
									142.6	Using cycling technique, so the last measurement
									144.1	represents the T_h
									146.5	
									147.3	
										Conclusion: very low T_{fm} and T_m imply a Ca/Mg system
LuF44	-1.1	-6.3	1	mostly liquid-phase	(1) A two-phase FI, highly irregular, 15x8 um, V/L = 15%					Cool down to -164 °C, no changes were observed
				irregular shape	(2) A two-phase FI, highly irregular,					Cool down to -130.6 °C, no changes were

Sample ID	Stable Isotope		Chip No	Description	Fluid Inclusion	Microthermometric Measurement (°C)				Comments
	$\delta^{13}C$	$\delta^{18}O$				T_{freeze}	T_{fm}	T_m	T_h	
					8x4 um, V/L =50%					observed
				some two-phase FIs	(3) A two-phase FI, 5x3 um, V/L = 15%					Cool down to -106.8 °C, no changes were observed
				small, <5 um	(4) A two-phase FI, 2-3 um, V/L = 30%					Cool down to -131.4 °C, no changes were observed
				V/L = 15-25%	(5) A two-phase FI, 3-4 um, V/L = 20%					Cool down to -114.8 °C, no changes were observed
					(6) A two-phase FI, 3-4 um, triangular, V/L=25%					Cool down to -122.7 °C, no changes were observed
										Conclusion: no FIs suitable for microthermometric meas.
LuF51	10.0	-21.1	2	mostly small, liquid-phase	(1) A two-phase FI, 3 um, but clear					Cool down to -123 °C, no changes were observed
				some very irregular FIs	(2) A two-phase FI, regular, 4-5 um, V/L =25%					Cool down to -143.1 °C, no changes were observed
				(high relief?)						Heat up to 125 °C, bubble still present
			1	two-phase FI rare	(1) A two-phase FI, regular, 4-5 um, V/L =20%					Cool down to -118.9 °C, no changes were observed
				three-phase FI, cubic crystal	(2) A two-phase FI, regular, 10 um, V/L =15%					Cool down to -158 °C, no changes were observed
				usually >7 um, V/L <10%	(3) A two-phase FI, regular, 8um, V/L < 5%				>245.3	Cool down to -158 °C, no changes were observed
					(4) A three-phase FI, 8 um, with a 1 um crystal				190.5	Halite dissolved at 190.5 °C
					(5) A two-phase FI, 6x3 um, V/L=10%				117.7	
					(6) A three-phase FI, 7 um, with a 2 um crystal				195.7	Bubble disappeared before reaching 150 °C
									194.2	Bubble disappeared before reaching 160 °C
										Conclusion: Salinity of 31.64% was determined based on T_{NaCl} = 195 °C
LuF14	-17.6	-40.4	2	Lots of dark FIs (CH_4?)	(1) A two-phase FI, 3 um, regular, V/L =40%					Cool down to -185 °C, no changes were observed
				Liquid-phase FIs	(2) A two-phase FI, V/L <5%, with a					Bubble expanded during cooling

Sample ID	Stable Isotope		Chip No	Description	Fluid Inclusion	Microthermometric Measurement (°C)				Comments
	$\delta^{13}C$	$\delta^{18}O$				T_{freeze}	T_{fm}	T_m	T_h	
					moving bubble					
				Two types of two-phase FIs (1) V/L<5%, similar to 3-P FIs (2) V/L>60%, CH_4 dominant? three-phase FIs, low V/L with a cubic crystal	(3) A two-phase FI, 15x4 um, V/L <5%	-60.0		<-10		Bubble started moving around -30 °C when heated
						-61.7		-15.9		T_m was determined based on the first move of the bubble
						-61.4			81.3	
									82.5	
									81.2	
					(4) A two-phase FI, 6x3 um, V/L <5%, a moving bubble	-48.0		-8.9		Bubble stopped moving at -48 °C, and Hydrohalite (?) disappeared at -8.9 °C
					(5) A three-phase FI, with a halite crystal				146.0	T_h here is indicated by dissolution of halite crystal
					(6) A three-phase FI, with a halite crystal				150.0	T_h here is indicated by dissolution of halite crystal **Conclusion**: Salinity 29.5% was calculated based on T_h
LuF52	-11.9	-37.8	4	large quantity of small, liquid-phase, irregular FIs some two-phase FIs	(1) A two-phase FI, 5 um, V/L = 20%	-7.2		6.2		This is likely a H_2O-dominant inclusion with CH_4 T_{freeze} is likely the formation of clathrate, indicated by deformation of bubble; T_m is indicated by normalization of bubble Cool down to -104.4 °C, no changes were observed **Conclusion**: further work will be needed to understand different types of FIs in this sample.
						-6.9		6.4		
									55.3	
									55.5	
					(2) A two-phase FI, 5 um, V/L = 20%					
					(3) A two-phase FI, 4 um, V/L = 25%				199.8	
LuF42	18.1	-12.9		small (<1 um), liquid-phase FIs						**Conclusion**: not suitable for microthermometric meas.
LuF43	20.8	-11.5		small (<1 um), liquid-phase FIs						**Conclusion**: not suitable for microthermometric meas.

Sample ID	Stable Isotope		Chip No	Description	Fluid Inclusion	Microthermometric Measurement (°C)				Comments
	$\delta^{13}C$	$\delta^{18}O$				T_{freeze}	T_{fm}	T_m	T_h	
LuF45	10.1	-12.6		very clean, few FIs						**Conclusion**: not suitable for microthermometric meas.
LuF37	12.4	-17.9	3	Lots of dark FIs (CH_4?)	(1) A three-phase FI, 15x8 um, halite = 2.5 um				189.7	T_h here is indicated by dissolution of halite crystal
				Two-phase FIs, V/L = 5-15%	(2) A three-phase FI, same FIA as (1)				155.4	T_h here is indicated by dissolution of halite crystal
				Three-phase FIs	(3) A three-phase FI, same FIA as (1)				169.1	T_h here is indicated by dissolution of halite crystal
				with a cubic crystal	(4) A two-phase FI, 6x2 um, V/L = 15%			-2.2		Melting of ice was observed
						-45.1		-1.9		Melting of ice was observed
						-44.9		-2.2		Melting of ice was observed
						-44.3	-22.4			The FI brightened at -22.4 °C
									139.0	
									139.2	
					(5) Dark FI, 12x4, CH_4-dominant but two-phase (?)					Cool down to -146.49 °C, no changes were observed
			1	Dark FIs dominant, various sizes	(1) A two-phase FI, 12 um, V/L =15-20%	-83.0		-27.9		T_m - bubble moved and returned to normal size
				Two-phase FIs, regular shape		-82.8	-48.1	-28.7		T_{fm} - big crystals of ice shown
						-82.9	-51.3	-28.5		T_{fm} - disintegration of ice
					(2) A two-phase FI, 5 um, V/L = 15%	-85.0		-36.5		T_m - bubble moved and returned to normal size
										Conclusion: different types of FI in this sample high salinity three-phase FIs: 29.5 - 31% NaCl low salinity two-phase FIs: 3% NaCl
LuF29	3.0	-14.7	3	mostly liquid-phase FIs various V/L ratios	(1) A two-phase FI, 12 um, V/L =15%	-36.0				
						-36.8				
						-38.5	-21.1	0.8		T_m - appearance of bubble
									148.0	
					(2) A two-phase FI, 5x2.5 um, V/L = 15%			-2.4		T_m - appearance of bubble
						-33.5	-21.4			
						-33.6	-20.9	-1.9		
						-33.8	-21.2			
									132.7	

Sample ID	Stable Isotope		Chip No	Description	Fluid Inclusion	Microthermometric Measurement (°C)				Comments
	$\delta^{13}C$	$\delta^{18}O$				T_{freeze}	T_{fm}	T_m	T_h	
									132.9	
										Conclusion: FIs with salinity of less than 3%
LuF20	-3.6	-6.3	3	mostly one-phase (liquid) FIs	(1) A two-phase FI, irregular, 40 um, V/L = 40%	-37.2	-21.5	-0.4		T_m - appearance of bubble
				large, irregular some are two-phase FIs			-21.5	-0.2		T_m - appearance of bubble
									79.9	
					(2) A two-phase FI, 10 um, V/L = 8%					Cool down to -101.7 °C, no changes were observed
					(3) A two-phase FI, irregular, 30 um, V/L = 20%	-20.8				T_{freeze} - disappearance of bubble
						-16.9		-0.8		T_m - appearance of bubble
						-13.7		-1.1		T_m - appearance of bubble
						-12.9		-1.1		T_m - appearance of bubble
									47.2 (?)	Bubble became a black dot since 47.2 °C (up to 96.5 °C)
					(4) A two-phase FI, regular, 20x10 um, V/L = 8% different appearance from the other FIs measured			-0.6		Bubble expanded during cooling; T_m - bubble moved
									115.9	
									116.1	
					(5) A two-phase FI, regular, 50 um, V/L = 8%	-37.4		0.4		T_m - appearance of bubble
						-37.4		0.4		T_m - appearance of bubble
									79.3	
LuF46	0.5	-12.6		irregular, liquid-phase FIs various sizes						**Conclusion**: not suitable for microthermometric meas.
LuF40	0.0	-11.9		some small liquid-phase FIs						**Conclusion**: not suitable for microthermometric meas.
LuF15	-3.8	-13.4		small liquid-phase FIs some maybe two-phase (<3 um)						**Conclusion**: not suitable for microthermometric meas.
LuF41	-2.1	-16.1		both one- and two-	(1) A two-phase FI, 12 um, V/L=5%					Bubble deformed gradually during cooling (-102.6 °C)
				phase FIs various V/L ratios,	(2) A two-phase FI, 20 um, V/L=25%					No change was observed during cooling (-102.6

Sample ID	Stable Isotope		Chip No	Description	Fluid Inclusion	Microthermometric Measurement (°C)				Comments
	$\delta^{13}C$	$\delta^{18}O$				T_{freeze}	T_{fm}	T_m	T_h	
				mostly <5%						°C) and warming up (32.3 °C)
					(3) A two-phase FI, 5 um, V/L=5%					Bubble expanded during cooling to -118 °C
					(4) A two-phase FI, 10x4 um, V/L=10%	-16.5		-7.5		Bubble deformed (oval shape) at -16.5 °C due to the formation of clathrate (?)
						-16.7				
						-16.9		-8.2		Bubble returned to the normal shape
									72.9	
									72.9	
					(5) A highly-irregular one-phase FI, 15 um					Cool: -35.1 °C, bubble form; warm: -1.2 °C, bubble disapp.
										Cool: -33.4 °C, bubble form; warm: -1.1 °C, bubble disapp.
					(6) A one-phase FI, 15x7 um	-24.8				Cool: -3.9 °C, bubble form; warm: 30 °C, bubble disapp.
						-25.2				Cool: -3.6 °C, bubble form; warm: 30.5 °C, bubble disapp.
						-26.1				Cool: -2.9 °C, bubble form; warm: 32.1 °C, bubble disapp. **Conclusions:** Formation of clathrate?
LuF50	3.7	-14.9	4	lots of liquid-phase FIs (<1 um)	(1) A two-phase FI, 5 um, V/L=15%, with a moving bubble					Cool down to -111.7 °C, no changes were observed
				two-phase FI are present	(2) A two-phase FI, 4 um, V/L=15%					Cool down to -121.3 °C, no changes were observed
					(3) A two-phase FI, 6 um, V/L<10%					Cool down to -114.2 °C, bubble expanded during cooling
					(4) A two-phase FI, 8 um, V/L =10%					Cool down to -113.6 °C, no change was observed
					(5) A two-phase FI, 6 um, V/L=10%		-65.3			
							-66.4	-26.4		Melting of last bit of ice and appearance of bubble occurred simultaneously at -26.4 °C
						-81.4				
							-67.1	-26.6		

Sample ID	Stable Isotope		Chip No	Description	Fluid Inclusion	Microthermometric Measurement (°C)				Comments
	$\delta^{13}C$	$\delta^{18}O$				T_{freeze}	T_{fm}	T_m	T_h	
									119.8	
					(6) A two-phase FI, 7x2 um, with a moving bubble				147.2	
			3	CH_4 FIs was big as 15 um a few two-phase FIs closely associated with CH4 FIs	(1) A highly-irregular two-phase FI, 7 um	>-74		-21.0		Bubble disappeared at -74 °C, melting of ice was observed
								-20.3		Melting of ice was observed
								-20.4		Last bit of ice melt and bubble appeared at the same time
									63.0	
						-65.7	-44.0			
					(2) A two-phase FI, 4 um, V/L=15%, with a moving bubble	-67.7				Jerking of bubble was observed
								-31.4		Melting of last bit of ice was observed
								-31.3		Melting of last bit of ice was observed
									145.0	
										Conclusions: High salinity fluids containing Ca/Mg
#2A	13.2	-12.2		Liquid-phase FIs only						**Conclusion**: not suitable for microthermometric meas.
#2C	-6.6	-2.7	2	Lots of small, liquid-phase FIs	(1) A two-phase FI, 6 um, V/L=25%					Cool down to -115.4 °C, no changes were observed
				Two-phase FI, irregular, various	(2) A two phase FI, 7 um, V/L=25%					Cool down to -143.6 °C, no changes were observed
					(3) A two-phase FI, 10 um, V/L=5%				135.5	Bubble expanded gradually during cooling (-101.7 °C)
				V/L rations, mostly 15-20%	(4) A two-phase FI, 8x3 um, V/L=10%					Bubble expanded gradually during cooling (-105 °C)
				Three-phase FIs, small bubble	(5) A two-phase FI, 15x5 um, V/L=15%					Bubble expanded gradually during cooling (-107.1 °C)
				(V/L=5%), a cubic crystal	(6) A two-phase FI near FI (3)				106.6	
				CH_4 FIs	(7) A two-phase FI near FI (3)				114.5	
					(8) A two-phase FI near FI (3)				105.5	
					(9) A three-phase FI (10 um) with a bubble (1.5				249.7	Bubble disappeared at 138.6 °C

Sample ID	Stable Isotope		Chip No	Description	Fluid Inclusion	Microthermometric Measurement (°C)				Comments
	$\delta^{13}C$	$\delta^{18}O$				T_{freeze}	T_{fm}	T_m	T_h	
					um) and a cubic crystal (2 um)					
					(10) A three-phase FI (10 um) with a bubble (1 um) and a cubic crystal (1.5 um), near FI (9)				188.6	
					(11) A two-phase FI near FI (9)				124.9	
					(12) A three-phase FI (15 um) with a bubble (1.5 um) and a cubic crystal (3 um), near FI (9)				262.2	
					(13) A two-phase FIs near FI (12)				271.6	
					(14) A three-phase FIs				<170	Bubble disappeared at 134.4 °C
					(15) A two phase FI with a big cubic crystal				176.5	
										Conclusion: Salinity between 31 and 36% was determined based on the T_{NaCl} = 188 - 262 °C
#5C	0.3	-10.8		Liquid-phase FIs only						**Conclusion**: not suitable for microthermometry.
#6-1	-3.8	-3.9		Liquid-phase FIs only						**Conclusion**: not suitable for microthermometry
890AB	-1.2	-5.8		Liquid-phase FIs only						**Conclusion**: not suitable for microthermometry
1130-2	-5.9	-17.4		Lots of small, liquid-phase FIs	(1) A two-phase FI, 12x4 um, V/L=8%		-69.3			Bubble expanded during cooling (-124 °C)
									147.7	
				Two-phase FI, irregular-regular	(2) A two phase FI, 12x12 um, V/L=10%		-64.1	-42.6		Bubble expanded during cooling (-111.6 °C)
				V/L mostly 5-20%	(3) A two phase FI, 8x6 um, V/L=10%		-61.5	-43.2		
							-64.3	-43.1		
							-64.5			
					(4) A two phase FI, 8x6 um, V/L=10%		-72.4	-46.3		Bubble expanded during cooling (-100.3 °C)
					(5) A two phase FI, 15 um, V/L<10%		-79.2	-48.8		Bubble expanded during cooling (-92.6 °C)
							-79.0	-47.6		Bubble expanded during cooling (-

Sample ID	Stable Isotope		Chip No	Description	Fluid Inclusion	Microthermometric Measurement (°C)				Comments
	$\delta^{13}C$	$\delta^{18}O$				T_{freeze}	T_{fm}	T_m	T_h	
										97.3 °C)
									73.4	
					(6) A two-phase FIs near FI (5), 3-6 um				89.1	
					(7) A two-phase FIs near FI (5), 3-6 um				101.9	
					(8) A two-phase FIs near FI (5), 3-6 um				127.7	
					(9) A two-phase FIs near FI (5), 3-6 um				99.3	
					(10) A small two-phase FI near FI (1)				109.4	
										Conclusion: high salinity Ca/Mg fluid

Table B-8. Calcite isotope data.

Sample Description	Calcite Type	Isotope ID	Thin Section ID	$\delta^{13}C$ ‰ (VPDB)	$\delta^{18}O$ ‰ (VPDB)
570-105 116.30-116.33 Lupin	massive	LU A		-2.6	-9.8
310-FAR Lupin	powdery	LU B	LUF 49	-7.7	-6.1
310-FAR Lupin	powdery	LU C	LUF 49	-7.5	-6.1
570-105 116.0-116.10	massive	LU D	LUF 40	-0.1	-11.4
570-105 231.40-231.45	powdery	LU E	LUF 50	3.5	-14.0
570-105 231.40-231.45		LU F	LUF 50	3.4	-14.5
huge calcite vein clear rhomb. Middle (1)	crystalline	LU G	LUF 43	20.1	-11.0
huge calcite vein cloudy right side (2)	crystalline	LU H	LUF 41	-2.2	-15.7
huge calcite vein clear right side (3)	crystalline	LU I	LUF 42	17.5	-12.4
huge calcite vein bottom 1mm	powdery	LU J		-4.4	-11.3
huge calcite vein top surface (5)	crystalline	LU K	LUF 46	0.4	-12.0
huge calcite vein top surface fine coating (6)	crystalline?	LU L		2.0	-14.0
huge calcite vein, 1 rhomb crystal right side part a clear		LU M		29.5	-11.3
huge calcite vein, 1 rhomb crystal right side part b clear		LU N		26.7	-11.8
Lupin 490 Level, borehole 195, 123.0		LU O	LUF 51	9.7	-20.7
huge calcite vein , crystal from vug cloudy		LU P	LUF 44	-1.5	-5.6
huge calcite vein , crystal from vug cloudy		LU Q	LUF 44	-1.3	-5.5
huge calcite vein, rhomb crystal from vug, clear		LU R	LUF 45	9.9	-12.1
huge calcite vein, rhomb crystal from vug, clear		LU S	LUF 45	9.8	-12.0
550-112 calcite, 6.23	massive	LU T		-8.0	-18.6
1130 NED Lupin	powdery	LU U	LUF 52	-11.9	-37.8
Lupin 570-106, 336.15 - 336.27	massive	LU V	LUF 47	-2.0	-17.6
exploration drift	powdery?	LU W		-25.1	-17.9
570-106, 27.62-27.83, Lupin clear	powdery	LU X		-6.5	-19.7
570-106, 27.62-27.83 Lupin cloudy	powdery	LU Y		-4.0	-15.1
570-106 277.40-277.65		LU Z		11.2	-15.2
190 B 15 Dip up ramp		LU 1		-11.6	-11.3
190 B 15 Dip up ramp		LU 2		-11.6	-11.3

Sample Description	Calcite Type	Isotope ID	Thin Section ID	$\delta^{13}C$ ‰ (VPDB)	$\delta^{18}O$ ‰ (VPDB)
Safety Bay L 330 25 Down Ramp		LU 3		-5.8	-17.6
490m level borehole 195 164.35		LU 4		1.7	-16.9
1300 m west zone south drift N dipping		LU 5		2.8	-18.8
1300 m west zone south drift N dipping		LU 6		3.3	-18.8
570-105 320.69-320.80		LU 7		-8.2	-13.7
570-106 233.50-233.64		LU 9		0.5	-16.5
890-188 493.26-493.48		LU 11	LuF 1	1.2	-18.3
570-105 283.17-283.39		LU 12	LuF 12	-5.7	-20.3
570-105 416.90-417.08		LU 14	LuF 13	-3.2	-14.5
890-188 61.75-62.11		LU 13	LuF 14	-17.6	-40.4
170-135 60.75		LU 18	LuF 15	-3.8	-13.4
490-195 291.1 (2 diff. calcites?)		LU 17	LuF 21	-4.1	-13.2
490-195 291.1 (2 diff. calcites?)		LU17b		-5.9	-17.7
570-106 304.22-304.42 (2 diff. calcites?)		LU 16	LuF 30	3.5	-14.1
570-106 304.22-304.42 (2 diff. calcites?)		LU 16b		-5.4	-25.9
490-195 83.35		LU 20	LuF 36	-5.3	-13.8
570-106 226.60-226.75		LU 15	LuF 37	12.4	-17.9
		#1A	#1A	-4.6	-18.9
		#1B	#1B	-4.6	-19.1
		#1C	#1C	-4.5	-18.9
		#1D	#1D	-4.5	-18.5
		#1E	#1E	-4.4	-18.4
		#2A	#2A	13.2	-12.2
		#2B	#2B	-3.6	-3.2
		#2C	#2C	-6.6	-2.7
		#3	#3	-4.9	-18.7
		#4	#4	-4.5	-18.9
		#5A	#5A	-2.3	-11.5
		#5B	#5B	1.4	-10.7
		#5C	#5C	0.3	-10.8
		#5D	#5D	-0.3	-9.3
		#6-1A	#6-1A	-3.8	-3.9
		#6-1B	#6-1B	-4.8	-5.6
		#6-2A	#6-2A	-5.1	-5.7
		#6-2B	#6-2B	-2.6	-3.8
		#6-2C	#6-2C	-3.2	-3.3
		#6-2D	#6-2D	-4.7	-5.1
		#6-3A	#6-3A	-5.1	-4.5
		#6-3B	#6-3B	-5.2	-5.1
		#6-3C	#6-3C	-4.4	-4.7
		#6-3D	#6-3D	-1.3	-4.6
		#6-3E	#6-3E	-1.1	-4.4
		#7	#7	-2.4	-14.1
		#8	#8	-0.5	-5.1
		890A	890A	-1.2	-5.8
		890B	890B	16.2	-13.1
		890C	890C	11.0	-12.4
		1130-1	1130-1	-4.6	-16.5
		1130-1-G	1130-1-G		
		1130-2	1130-2	-5.9	-17.4
		1130-5	1130-5	-5.8	-17.4
		1130-3	1130-3	-5.3	-17.6
		1130-4	1130-4	-5.9	-17.9

Table B-9. $\delta^{34}S$ of sulfide minerals associated with calcite filled fractures from the Lupin mine.

Sample Depth	Mineral	$\delta^{34}S$ (‰CDT)
300m	Pyrite, some chalcopyrite	-2.5
440m	Chalcopyrite	-33.2
475m	Pyrite	12.5
490m	Pyrite, some chalcopyrite	2.1

Table B-10. Summary of molecular gas compositions sampled at Lupin. Noble gas data from Greene (*2005*).

Sample ID	Ne	He·10,000	Ar	Kr	Xe	N_2	CO_2	C_1	C_2	C_3	i-C_4	n-C_4	$\frac{C_1}{(C_2+C_3)}$
		$\frac{[(cc_{gas}/cc_{H2O})_{sample}]}{[(cc_{gas}/cc_{H2O})0°C_{equilibrium}]}$				Vol. %*							
890-188	2.4	3.8	2.5	1.4	1.5	28.5	0.47	74.4	0.55	0.014	ND	0.0002	132
1130-64	NA	NA	NA	NA	NA	36.9	0.14	64.4	0.11	0.004	0.000	0.0001	565
1130-160	NA	NA	NA	NA	NA	NA	NA	69.6	2.40	0.169	NA	NA	55
1130-175	NA	NA	NA	NA	NA	9.63	1.67	86.7	1.89	0.094	0.007	0.007	44
1130-176	NA	NA	NA	NA	NA	11.0	1.42	84.7	1.60	0.089	0.008	0.007	50
1130-NED-Pool	NA	NA	NA	NA	NA	26.9	0.98	72.6	1.09	0.002	0.003	0.003	66
1130-191	5.6	20.0	5.9	1.1	1.4	15.8	1.38	81.1	1.49	0.080	0.004	0.004	52
1130-192	4.1	5.9	10.5	0.4	0.5	11.0	1.92	86.7	2.05	0.124	0.006	0.006	40
1130-197[1]	2.8	11.3	4.2	1.3	1.4	22.7	0.88	77.4	0.93	0.033	0.001	0.001	80
1130-217	3.0	6.7	4.3	0.9	1.2	15.1	1.43	81.5	1.61	0.083	0.004	0.004	48
1130-219	1.1	4.0	3.1	0.6	0.8	16.2	1.17	82.2	1.27	0.046	0.001	0.001	62
1130-267	NA	NA	NA	NA	NA	27.5	0.79	69.5	0.93	0.037	0.002	0.002	80
1130-273	NA	NA	NA	NA	NA	13.9	1.32	81.8	1.42	0.068	0.004	0.005	55

Table B-11. Summary of gas isotopic compositions sampled at Lupin.

Sample ID	δ^2H ‰ (VSMOW)			$\delta^{13}C$ ‰ (VPDB)			
	C_1	C_2	C_3	C_1	C_2	C_3	CO_2
890-188	-340	-253	-189	-56.1	-36.7	-33.5	-21.9
1130-64	-181	-330	ND	-50.3	-27.3	-27.3	-55.3
1130-160	-323	-276	-172	-46.1	-34.9	-33.2	-26.4
1130-175	-328	-290	-179	-44.3	-34.5	-33.3	-18.6
1130-176	-344	-243	ND	-44.7	-35.7	-32.3	ND
1130-NED-Pool	-329	-312	ND	-47.3	-32.8	ND	ND
1130-191	-319	-305	ND	-47.1	-34.9	-33.1	-21.1
1130-192	-324	-295	-196	-42.4	-35.0	-34.2	-23.0
1130-197[1]	-341	-281	-183	-50.6	-35.3	-33.2	-24.3
1130-217	-337	-308	ND	-45.2	-36.6	ND	ND
1130-219	-349	-228	ND	-47.7	-35.5	ND	ND
1130-267	-344	-290	-179	-47.8	-35.0	-33.6	-21.1
1130-273	-344	-289	-178	-46.3	-34.3	-32.9	-15.7

Table B-12. Complete Lupin gas composition data.

Sample	Date	N_2	O_2	CO_2	CH_4	C2	C3	i-C4	n-C4
						Vol %			
890-188	19-Feb-03[1]	28.62	1.34	0.50	68.6	0.51	0.002	ND	ND
890-188	21-Feb-03[2]	27.94	1.22	0.47	69.8	0.51	0.002	ND	0.0002
890-188	24-May-03	28.54	1.12	0.47	74.4	0.55	0.014	ND	0.0002
1130-64	07-Oct-05	36.96	2.06	0.14	64.4	0.11	0.004	0.0003	0.0001
1130-160	01-Oct-05[3]				69.6	2.40	0.169		
1130-175	22-May-03	9.63	0.89	1.67	86.7	1.89	0.094	0.007	0.007
1130-176	22-May-03	11.00	0.93	1.42	84.7	1.60	0.089	0.008	0.007
NED-Ground	26-Feb-03	26.92	2.05	0.98	72.6	1.09	0.002	0.0028	0.003
1130-191	25-Feb-03[4]	23.00	1.41	0.98	73.4	1.04	0.002	0.0025	0.003
1130-191	25-Feb-03[4]	19.76	1.56	1.15	73.4	1.18	0.002	0.002	0.003
1130-191	23-May-03	15.82	1.01	1.38	81.1	1.49	0.080	0.004	0.004
1130-192	21-Feb-03[1]	14.48	1.66	1.64	19.5	0.48	0.002	ND	0.001
1130-192	22-Feb-03[2]	64.97	15.89	0.50	81.0	1.69	0.002	0.0001	0.004
1130-192	22-May-03	11.00	1.13	1.92	86.7	2.05	0.124	0.006	0.006
1130-197	24-Feb-03[1]	19.93	1.53	1.07	75.2	0.97	0.002	0.007	0.001
1130-197	25-Feb-03[2]	20.11	1.65	1.07	72.6	0.92	0.002	ND	0.001
1130-197	23-May-03	22.69	1.01	0.88	77.4	0.93	0.033	0.001	0.001
1130-217	24-Feb-03	17.38	1.42	1.23	76.6	1.29	0.002	0.0003	0.002
1130-217	23-May-03	15.13	1.03	1.43	81.5	1.61	0.083	0.004	0.004
1130-219	25-May-03	16.16	1.01	1.17	82.2	1.27	0.046	0.001	0.001
1130-267	16-May-04	27.5	1.24	0.79	69.5	0.83	0.037	0.0018	0.002
1130-273	15-May-04	13.92	1.13	1.32	81.8	1.42	0.068	0.0042	0.005
1130-273	07-Oct-05	17.66	1.04	1.03	78.9	1.02	0.004	0.0003	0.0001

[1]Sample taken shortly after borehole opened
[2]Sample taken after redox measurements had stabilized; borehole was flowing continuously from prior sample
[3]Sample analyzed at University of Indiana
[4]Two samples taken; initial sample taken immediately after borehole was sealed and was predominately gas, second sample taken after borehole stabilized and was fluid and gas

Table B-13. Complete Lupin gas isotopic data.

Sample	Date	δ^2H (‰ SMOW)			$\delta^{13}C$ (‰ PDB)				$\delta^{15}N$
		CH_4	C2	C3	CH_4	C2	C3	CO_2	(‰ AIR)
890-188	19-Feb-03[1]	-336	-249	ND	-56.1	-33.0			
890-188	21-Feb-03[2]	-336	-290	ND	-56.0	-35.1			
890-188	24-May-03	-340	-310	ND	-54.6	-37.8	ND		-0.34
890-188	18-May-04	-335	BLOQ	ND	-55.4	-36.6	BLOQ		
890-188	01-Oct-05	-340	-253	-189	-56.1	-36.7	-33.5	-21.9	
1130-64	07-Oct-05	-339	BLOQ		-51.5				
1130-64	01-Oct-05	-330			-50.3	-27.3	-27.3	-55.3	
1130-160	01-Oct-05	-323	-276	-172	-46.1	-34.9	-33.2	-26.4	
1130-175	22-May-03	-326	-300	ND	-44.7	-35.2	-32.1		-0.09
1130-175	28-Nov-04	-330	-312	ND	-44.6	-35.1	BLOQ		
1130-175	01-Oct-05	-328	-290	-179	-44.3	-34.5	-33.3	-18.6	
1130-176	22-May-03	-329	-287	ND	-44.7	-35.7	-32.3		-0.23
NED-Ground	26-Feb-03	-329	-312	ND	-47.3	-32.8			
1130-191	25-Feb-03[3]	-334	-306	ND	-45.6	-33.4			
1130-191	25-Feb-03[3]	-327	-314	ND	-45.5	-31.4			
1130-191	23-May-03	-329	-314	ND	-45.7	-35.3	ND		
1130-191	01-Mar-04	-332	-312	ND	-46.0	-36.5	BLOQ		
1130-191	01-Oct-05	-319	-305		-47.1	-34.9	-33.1	-21.1	
1130-192	21-Feb-03[1]	-326	-283	ND	-44.7	-33.5			
1130-192	22-Feb-03[2]	-322	-307	ND	-44.7	-33.6			
1130-192	22-May-03	-323	-316	ND	-42.4	-35.5	-33.0		0.95
1130-192	15-May-04	-328	-306	ND	-44.6	-35.5	BLOQ		
1130-192	01-Oct-05	-324	-295	-196	-42.4	-35.0	-34.2	-23.0	
1130-197	24-Feb-03[1]	-329	304	ND	-50.0	-32.3			
1130-197	25-Feb-03[2]	-330	-306	ND	-50.2	-33.9			
1130-197	23-May-03	-333	-314	ND	-48.7	-36.1	ND		0.11
1130-197	01-Mar-04	-338	-302	ND	-49.0	-36.6	BLOQ		
1130-197	01-Oct-05	-341	-281	-183	-50.6	-35.3	-33.2	-24.3	
1130-217	24-Feb-03	-328	-303	ND	-46.8	-33.1			
1130-217	23-May-03	-328	-317	ND	-40.5	-35.7	ND		0.08
1130-217	15-May-04	-337	-308	ND	-45.2	-36.6	BLOQ		
1130-219	25-May-03	-330	-313	ND	-47.7	-35.5	ND		-0.34
1130-219	28-Feb-04	-331	-306	ND	-44.5	-35.9	BLOQ		
1130-267	16-May-04	-335	-307	ND	-47.0	-35.3	BLOQ		
1130-267	01-Oct-05	-344	-290	-179	-47.8	-35.0	-33.6	-21.1	
1130-273	15-May-04	-336	BLOQ	ND	-45.6	-34.2	BLOQ		
1130-273	07-Oct-05	-333	-319		-48.2	-34.4			
1130-273	01-Oct-05	-344	-289	-178	-46.3	-34.3	-32.9	-15.7	

(1)Sample taken shortly after borehole opened

(2)Sample taken after redox measurements had stabilized; borehole was flowing continuously from prior sample

(3)Sample analyzed at University of Indiana

(4)Two samples taken; initial sample taken immediately after borehole was sealed and was predominately gas, second sample taken after borehole stabilized and was fluid and gas

Table B-14. Gas volume per liter of water.

Depth-Borehole No.	Gas Vol. (L)	Flow (L/min)	Collection time (min)	Water Vol. (L)	Gas Vol. (L)/ 1 L water	pH	Pressure during sampling (kPa)
890-188	0.4	0.62	7.3	4.53	0.09		
1130-191	0.7	0.47	4.5	2.13	0.33	8.18	3240
1130-192	0.4	0.27	3.0	0.80	0.50	8.40	4960
1130-197	0.7	0.54	6.5	3.51	0.20	8.36	3720
1130-217	1	0.91	4.1	3.73	0.27	8.13	3240
1130-219	0.4	0.45	6.1	2.78	0.14	8.28	1930

Table B-15. Temperature, Pressure, and Salinity Measurements.

Sample ID	Date Borehole Sealed	Measurement Date	Pressure KPa	Temperature °C	TDS $g \cdot l^{-1}$
890-188	05-Dec-2002	28-Oct-2000	-	7.5	3.6
		30-Aug-2001	-	NA	2.8
		14-Feb-2002	-	5.4	3.1
		19-Feb-2003		7.3	3.0
		24-May-2003	2040	NA	2.7
		26-Feb-2004	2110	NA	3.2
		18-May-2004	2310	8.6	2.7
		26-Nov-2004		8.9	2.8
		5-Mar-2005		8.1	
		7-Mar-2005		6.9	
		8-Mar-2005		7.5	
		5-Oct-2005		8.2	
		8-Oct-2005		8.3	
		10-Oct-2005		8.3	
1130-64	Not Sealed	23-May-2003	-	NA	2.2
		1-May-2004	-	NA	2.8
		16-May-2004	-	10.0	2.6
		26-Nov-2004	-	9.4	2.6
		4-Mar-2005	-	9.3	
		7-Mar-2005	-	9.9	
		6-Oct-2005	-	9.7	
		7-Oct-2005	-	9.4	
1130-175	Not Sealed	15-Feb-2002	-	NA	26.2
		22-May-2003	-	NA	27.5
		16-May-2004	-	NA	32.7
		26-Nov-2004	-	9.4	-
		28-Nov-2004	-	9.7	32.1
		30-Nov-2004	-	9.7	-
		6-Mar-2005	-	9.6	
		8-Mar-2005	-	9.7	
		6-Oct-2005	-	9.6	

Sample ID	Date Borehole Sealed	Measurement Date	Pressure KPa	Temperature °C	TDS $g \cdot l^{-1}$
1130-176	Not Sealed	22-May-2003	-	NA	25.9
		28-Nov-2004	-	10.4	15.7
1130-191	24-Feb-2003	15-Feb-2002	-	9.4	7.1
		14-Jun-2002	-	NA	7.7
		24-Feb-2003	2000	NA	5.8
		23-May-2003	3290	NA	13.7
		1-Mar-2004	3410	NA	7.0
		14-May-2004	3700	NA	NA
		4-Mar-2005		10.2	
		7-Mar-2005		9.9	
		6-Oct-2005		10.3	
		8-Oct-2005		10.3	
		10-Oct-2005		10.4	
1130-192[1]	03-Dec-2002	15-Feb-2002	-	9.5	30.7
	22-Feb2003	14-Jun-2002	-	NA	29.7
		22-May-2003		NA	36.3
		24-May-2003		NA	33.1
		1-Mar-2004		NA	40
		16-May-2004		11.0	38.3
		26-Nov-2004		10.8	39.9
		30-Nov-2004		10.5	
		4-Mar-2005		10.8	
		5-Oct-2005		10.9	
		6-Oct-2005		10.8	
		7-Oct-2005		10.8	
		8-Oct-2005		10.8	
		10-Oct-2005		10.6	
1130-195	Not Sealed	28-Oct-2000	-	NA	15.3
		26-Nov-2004	-	10.1	16.8
		5-Mar-2005	-	10.0	
		6-Mar-2005	-	9.9	
		19-Oct-2005	-	9.9	
1130-197[2]	25-Feb-2003	28-Oct-2000	-	10.6	
	29-Feb-2004	15-Feb-2002		10.1	9.1

Sample ID	Date Borehole Sealed	Measurement Date	Pressure KPa	Temperature °C	TDS $g \cdot l^{-1}$
		25-Feb-2003	2600	NA	8.6
		23-May-2003	3530	NA	5.9
		1-Mar-2004	3280	NA	9.6
		17-May-2004	3790	12.9	
		26-Nov-2004		12.8	6.4
		30-Nov-2004		11.3	
		5-Mar-2005		11.7	
		7-Mar-2005		11.5	
		9-Oct-2005		11.9	
		10-Oct-2005		11.8	
1130-198	Not Sealed	25-Nov-2004	-	9.4	4.4
		8-Mar-2005	-	9.4	
		8-Oct-2005	-	9.4	
1130-201	Not Sealed	17-Feb-2002	-	NA	4.3
		27-Feb-2003	-	NA	5.2
		28-Nov-2004	-	9.6	4.3
		3-Mar-2005	-	9.6	
		6-Mar-2005	-	9.7	
		6-Oct-2005	-	9.6	
		8-Oct-2005	-	9.8	
1130-217	24-Feb-2003	24-Feb-2003	2000	NA	8.5
		23-May-2003	3270	NA	15.5
		28-Feb-2004	3370	NA	7
		15-May-2004	3700	NA	9.6
		25-Nov-2004		NA	13.2
		8-Mar-2005		9.4	
		8-Oct-2005		10.2	
		10-Oct-2005		10.4	
1130-219	24-May-2003	8-Nov-2000		NA	19.5
		25-May-2003		NA	10.1
		28-Feb-2004		NA	20.6
		17-May-2004		13.4	
		26-Nov-2004		12.8	8.1
		5-Mar-2005		11.2	

Sample ID	Date Borehole Sealed	Measurement Date	Pressure KPa	Temperature °C	TDS $g \cdot l^{-1}$
		6-Mar-2005		12	
		9-Oct-2005		11.4	
1130-260	02-Mar-2004	23-May-2003	-	NA	15.9
		2-Feb-2004	3420	NA	8.8
		25-Nov-2004		9.4	12.1
		6-Oct-2005		9.5	
1130-267	02-Mar-2004	28-Feb-2004	2120	NA	4.1
		16-May-2004	2590	10.6	5.4
		25-Nov-2004		9.3	6.1
		5-Mar-2005		9.6	
		6-Mar-2005		9.4	
		8-Mar-2005		9.4	
		6-Oct-2005		9.7	
		8-Oct-2005		9.7	
		10-Oct-2005		9.5	
1130-273	28-Feb-2004	29-Feb-2004	5280	NA	11.9
		14-May-2004	5770	NA	8.2
		25-Nov-2004		10.4	7.9
		30-Nov-2004		9.9	10.2
		3-Mar-2005		7.5	
		7-Mar-2005		9.9	
		8-Oct-2005		10.5	
		10-Oct-2005		10.6	
1130-bolt drip	Not Sealed	26-Feb-2003	-	NA	3.9
		2-Mar-2004	-	NA	4.1
		16-May-2004	-	11.2	
		28-Nov-2004	-	NA	3.6
		3-Mar-2005	-	9.8	
		6-Mar-2005	-	9.2	
		6-Oct-2005	-	9.4	

Table B-16. Lupin static borehole pressure data with time (in bars).

Depth	890	1130							
Borehole	188	192	197	191	217	219	260	267	273
6-9 Dec-02	14.5	45.8							
27-Feb-03	18	46.0	26	20	20				
25-28 Mar-03	19.2	47.9	41.1	26.2	26.2				
5-Apr-03		48.3	34..5	28.3	27.6				
20-25 May-03	20.4	51.1	35.3	32.4	32.7	19.3			
24-Aug-03	22.8	51.0	35.2	34.5	34.8	21.7			
3-Mar-04	21.1	51.9	32.8	34.6	34.6	23.9	35.0	21.2	52.8
14-May-04	23.1	53.1	37.9	37.0	37.0	25.6	31.5	25.9	57.7
25-Nov-04	24.3	54.4	38.8	38.6	38.6	14.9	38.0	27.0	58.1
3-Mar-05	25.3	53.8	38.6	38.3	38.6	15.5	36.0	13.8*	59.3
5-6 Oct-05	25.0	55.0	39	38.0		14.0	37.0	*leaking	58.0

Appendix C.

Review of Methane Hydrate Isotopic Geochemistry

C.1 Introduction

Gas hydrates, or clathrates, form when mixtures of water and gases crystallize into ice-like solids in certain low temperature and high pressure conditions. Structure I methane hydrate is the most common gas hydrate (*Kvenvolden 1988, Kvenvolden 1995*), but small amounts of heavier hydrocarbons, carbon dioxide, and hydrogen sulfide are sometimes incorporated into different crystals (*Sloan 1998*). Gas hydrates are able to store >180 times more gas per unit volume than free gas (*Sloan 1998*), thus natural deposits are potentially both an economic resource (*Makogon et al. 1971, Makogon 1981, Collett 1992, Collett 1993*) and a factor in climate change (e.g. *Nisbet 1990, Nisbet 1992, Beerling et al. 2002, Holbrook et al. 2002, Kirschvink and Raub 2003, Buffett and Archer 2004, Retallack and Krull 2006*). In situ gas hydrates are found in marine or permafrost environments, and have been observed as (1) occupying pores of coarse-grained rocks, (2) disseminated nodules within fine-grained rocks, (3) as a solid, filling fractures; or (4) as a massive unit of solid gas hydrate with minor amounts of sediment (*Sloan 1998*). Formation temperature, pore pressure, gas chemistry, and pore water salinity all control gas hydrate stability, while the availability of gas and water and the presence of reservoir rocks and seals affect gas hydrate formation (*Collett 1994*). Gas hydrates themselves can act as a hydrocarbon trap (*Collett 1994*).

A sufficient supply of both water and gas is required for gas hydrate formation; therefore an understanding of origins of the gas phase is integral to understanding gas hydrate systems (*Collett 1994*). Origins of methane and light natural hydrocarbons, including zones of hydrate formation, are typically determined through their chemical and isotopic compositions (*Bernard et al. 1976, Schoell 1980, Whiticar 1999*). Three distinct natural processes are known to form methane and light hydrocarbons: thermogenic (thermal decomposition of organic matter), bacteriogenic (metabolic activities of methanogenic microbes), and abiogenic (reduction of CO_2 through non-biological reactions).

The origin of methane (and methane in hydrates) found in sedimentary and marine settings are typically thermogenic or bacteriogenic gas (e.g. *Bernard et al. 1976, Schoell 1980, Schoell 1983a, Martini et al. 1998, Whiticar 1999*). Thermogenic gases typically have a $\delta^{13}C\text{-}CH_4$ content more

enriched than -50‰ PDB and a C1/(C2+C3) {methane/(ethane+propane)} ratio less than 100 (*Bernard et al. 1976*). In thermogenic gases, ^{13}C is progressively enriched from C1 to C4 alkanes (methane, ethane, propane, and butane), due to kinetic isotopic fractionation during cracking of heavier carbon compounds. Bacteriogenic gases however, are characterized by a $\delta^{13}C$-CH_4 content more depleted than -55‰ and a C1/(C2+C3+C4) ratio greater than 1000 (*Bernard et al. 1976*), as bacteria typically only produce methane and small amounts of ethane. Intermediate values are typically associated with mixing and/or oxidation. Additional information, such as $\delta^{13}C$-CO_2 and $\delta^{13}C$-DIC (often measured as total carbon dioxide, ΣCO_2) can provide constraints to the origin and evolution of a natural gas. The interpretation of natural gas origins is complicated if the gases are affected by post genetic processes such as mixing or methane oxidation. During methane oxidation, the lighter isotopes are preferentially oxidized, leaving the remaining gas enriched in ^{13}C compared with the original gas (e.g. *Coleman et al. 1981*).

Controversial views on the origin of gas hydrate systems are a result of the lack of extensive and comprehensive direct measurements of the molecular and isotopic properties of hydrate-bound gases, largely because of the difficulty of studying gas hydrates (*Milkov et al. 2005*). Occurrences of gas hydrate have been determined through changes in stable isotopic composition and/or dilution of pore waters (*e.g. Hesse and Harrison 1981*), presence of bottom simulating reflectors (BSR) and other seismic reflections (*e.g. Hyndman et al. 1992, Bangs et al. 1993*), downhole geophysics (e.g. *Holbrook et al. 1996, Collett and Lee 2005, Collett et al. 2005*), thermal imaging of newly retrieved core (*Tréhu et al. 2003*) ramen spectroscopy (*Hester et al. 2007*) and direct observation (*e.g. Kvenvolden et al. 1984, Kvenvolden and McDonald 1985*). Recent studies have suggested changes in molecular gas chemistry (*Milkov et al. 2004*) or shallow sulfate-methane interfaces (SMI) (*Borowski et al. 1999*) might also be useful for finding and defining gas hydrate accumulations.

Previous reviews of methane hydrates have focused on geological occurrence (*Kvenvolden 1998*, *Kvenvolden and Lorenson 2001*), kinetics and physical properties (*Sloan 1998*), geophysical recognition of hydrate occurrence (*Chand and Minshull 2003*), and chemical and isotopic compositions of the hydrates themselves (*Kvenvolden 1995, Borowski 2004, Milkov 2005a*. However, there has been no comprehensive review of how the parameters which are used to define natural gas origin (chemical and isotopic composition) vary with depth from the sea floor (or land surface in the case of permafrost) through the base of the hydrate stability field; and there have been no comparisons of the isotopic composition of methane with depth between marine and permafrost methane hydrate.

A review of available chemical and isotopic depth dependent data from locations with gas hydrates will be useful in determining the potential impact of gas hydrates to these parameters, increase the overall understanding the process of methane hydrate formation, and better define gas transport through hydrate accumulations. This will be constructive in identifying post-genetic processes which affect methane and other light hydrocarbons in areas of hydrate accumulation. While this review focuses on $\delta^{13}C$ data; molecular gas and $\delta^{2}H$ compositions will also be noted, which are also useful in the delineation of gas origin and evolutionary pathways. Figure C- shows the location of all known gas hydrate occurrences and highlights those which have methane isotopic data reviewed in this paper.

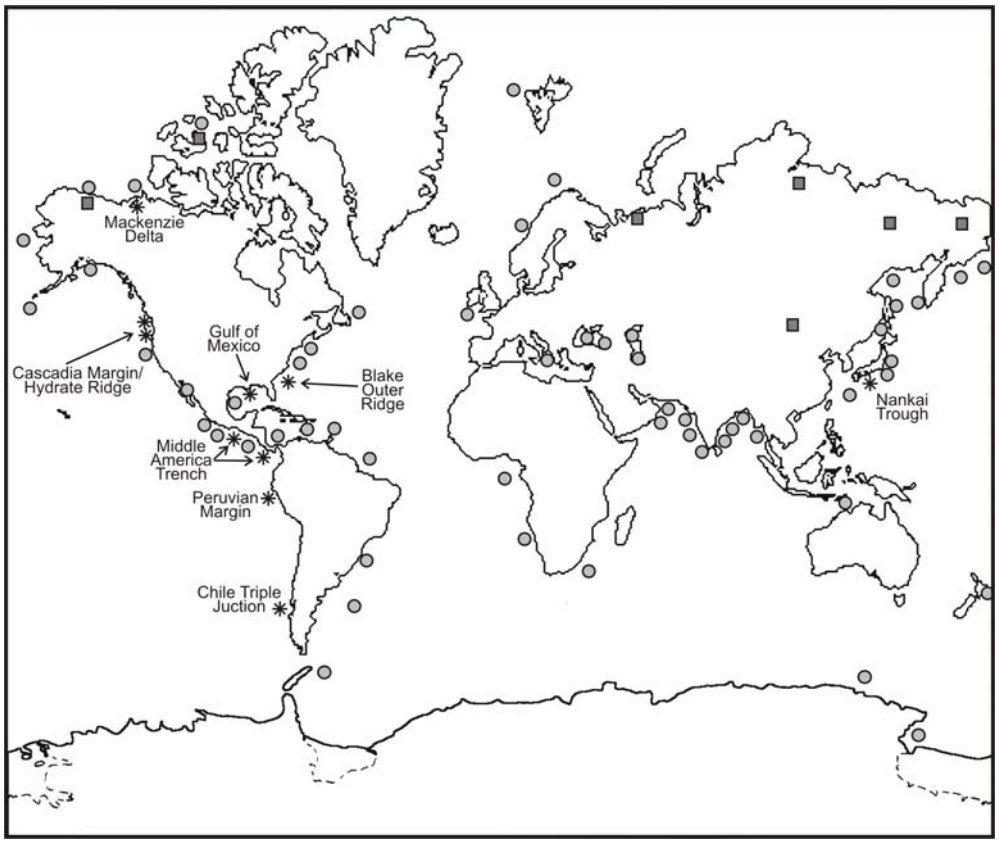

Figure C-1. Map of known and inferred hydrate occurrences, marine (circles) and permafrost (squares). Chemical and isotopic profile data locations, which are reviewed in this Appendix, are shown as asterisks and labeled (*). Adapted from Kvenvolden (*2000*).

C.2 Sample Collection and Analysis

One difficulty encountered in compiling and comparing data from different locations are the different collection and analytical methods. Gases are collected using the following methods: free gas (FG); headspace (HS); gas pockets; gas collection tube (GT); desorption; core cuttings; and pressure core

sampler (PCS), also known as a pressure core barrel (PCB). FG samples are taken from voids within the core liners, and provide ratios of relative abundance of the various gases. FG was the common sampling technique during the Deep Sea Drilling Program (DSDP). HS gas samples relate the amount of gas evolved to the volume of sediment from which it is derived by extracting a calibrated volume of sediment from the core which is sealed and heated. Gas concentrations analyzed by this method are limited by methane solubility at surface, and have little relationship with *in situ* methane concentrations (*Paull and Ussler 2001*). GT collect gas in inverted cylinders from core liners placed in specially prepared tubes as core is warmed in the laboratory. A more complete discussion of sampling methods is available (*Paull et al. 2000b, Paull and Ussler 2001*). It is worth noting that the different sampling methods produce significant differences in relative composition and concentrations (*Paull et al. 2000b*), and understanding of gas concentrations at *in situ* conditions is still rudimentary (*Paull and Ussler 2001*).

Every gas sampling method except PCS results in up to 99.8% of the gas loss during core recovery (*Paull et al. 2000b, Paull and Ussler 2001*); with the isotopically light $^{12}CH_4$ preferentially escaping from sediments (*Faber and Stahl 1983, Berner and Bertrand 1991*). Thus headspace gases are commonly depleted in CH_4 concentrations and enriched in ^{13}C relative to void and PCS gas *(Kvenvolden and Lorenson 2000, Wallace et al. 2000, Paull and Ussler 2001, Katz 2001*). Furthermore, both void and headspace gas are subject to core depressurization, and in all sampling methods the core is subject to temperature changes during retrieval. Thus, PCS is required for collecting and analyzing the true distributions and concentrations of hydrocarbon gases in oceanic sediments (*Dickens et al. 1997*). Sample collection is complicated by the difficulty of deploying a PCS (*Kvenvolden and Lorenson 2000*).

Carbon isotopic analytical techniques and mass spectrometers have improved over the course of the DSDP/ODP programs. Despite this, analytical precision of values reported here have remained between 0.2‰ and 0.15‰ in samples analyzed since 1985 (e.g. *Brooks et al. 1985, Matsumoto et al. 2000*).

C.3 Marine-Associated Hydrates

Due to different temperature regimes and sediment deposition, methane hydrates in marine environments are often grouped based on the type of margin on which they are found. Passive margins are characterized by fairly constant sediment deposition rates lower temperature and geothermal gradients, and a low advective methane flux (Figure C-2A). Accretionary margins consist of accumulated sediments and subvertically bedded materials, which are more heterogeneous than

sediments in passive margins due to horizontal tectonic movement (Figure C-2B). Temperatures and geothermal gradients are typically greater in an accretionary margin than a passive margin.

However, general similarities in diagenetic processes affecting methane and carbon isotopic compositions exist despite the different geologic conditions. Diagenetic processes affecting methane in deep-sea, continental margin sediments have been described (e.g. *Claypool and Kaplan 1974, Paull et al. 1994, Borowski et al. 1996, Borowski et al. 1997, Borowski et al. 2000b*). At most marine sites where methane is found, the interrelated diagenetic processes of microbial sulfate depletion, microbial methane production, and gas hydrate formation (*Paull et al. 1994, Borowski et al. 1996, Borowski et al. 2000a, Borowski 2004*) result in distinct zonation with depth. First, a sulfate reduction zone (SRZ), characterized by low methane concentration and decreasing sulfate concentrations, is found just beneath the sea-floor. Here, sulfate is consumed by sulfate-reducing microbes ($SO_4^{2-} + 2CH_2O \rightarrow H_2S^- + 2HCO_3^-$). At the base of the SRZ, the sulfate-methane interface (SMI), anaerobic methane oxidation (AMO) takes place ($CH_4 + SO_4^{2-} \rightarrow HCO_3^- + HS^- + H_2O$). Below the SMI, methane is abundant.

Based on molecular and isotopic compositions, the origin of methane in areas of hydrate accumulations may be either biogenic or thermogenic (*Milkov 2005a*). In marine sediments, bacterially generated methane is produced through CO_2 reduction ($CO_2 + 4H_2 \rightarrow CH_4 + H_2O$) (*Whiticar et al. 1986*). If methane concentrations and pressure and temperature conditions permit, there can be a zone of gas hydrate occurrence (GHOZ). Typically this occurs at some depth below the SMI. Because gas hydrate formation is dependent on methane concentrations, they may or may not be present throughout the entire gas hydrate stability zone (GHSZ). Whether or not the large concentrations of methane that are required to form methane hydrate are produced *in situ* or are transported upward or downward through advection/diffusion may depend on the site and is the subject of debate and may be site specific (e.g. *Paull et al. 1994*). Gas hydrates can occur in regions of high gas flux and low gas flux (Table C- and Table C-2). Free methane gas likely migrates through hydrate accumulation zones *(e.g. Shipboard Scientific Party 2002, Gorman et al. 2002, Torres et al. 2004, Netzeband et al. 2005, Liu and Flemings 2006).*

A bottom simulating reflector (BSR) is often (*e.g. Shipley et al. 1979*), but not always (*e.g. Pecher et al. 2001*) located near the base of the gas hydrate occurrence zone (GHOZ). The BSR is believed to be caused by the presence of free gas occupying between 1 and 4% of the pore space (*Bangs et al. 1993, Pecher et al. 2001, Hornbach et al. 2004*). Usually at or slightly below the BSR is the base of the gas hydrate stability zone (GHSZ). Only a few boreholes have penetrated the BSR,

and free gas beneath the BSR has only been directly measured at Blake Ridge (*Dickens et al. 1997*) and Hydrate Ridge (*Milkov et al. 2003*).

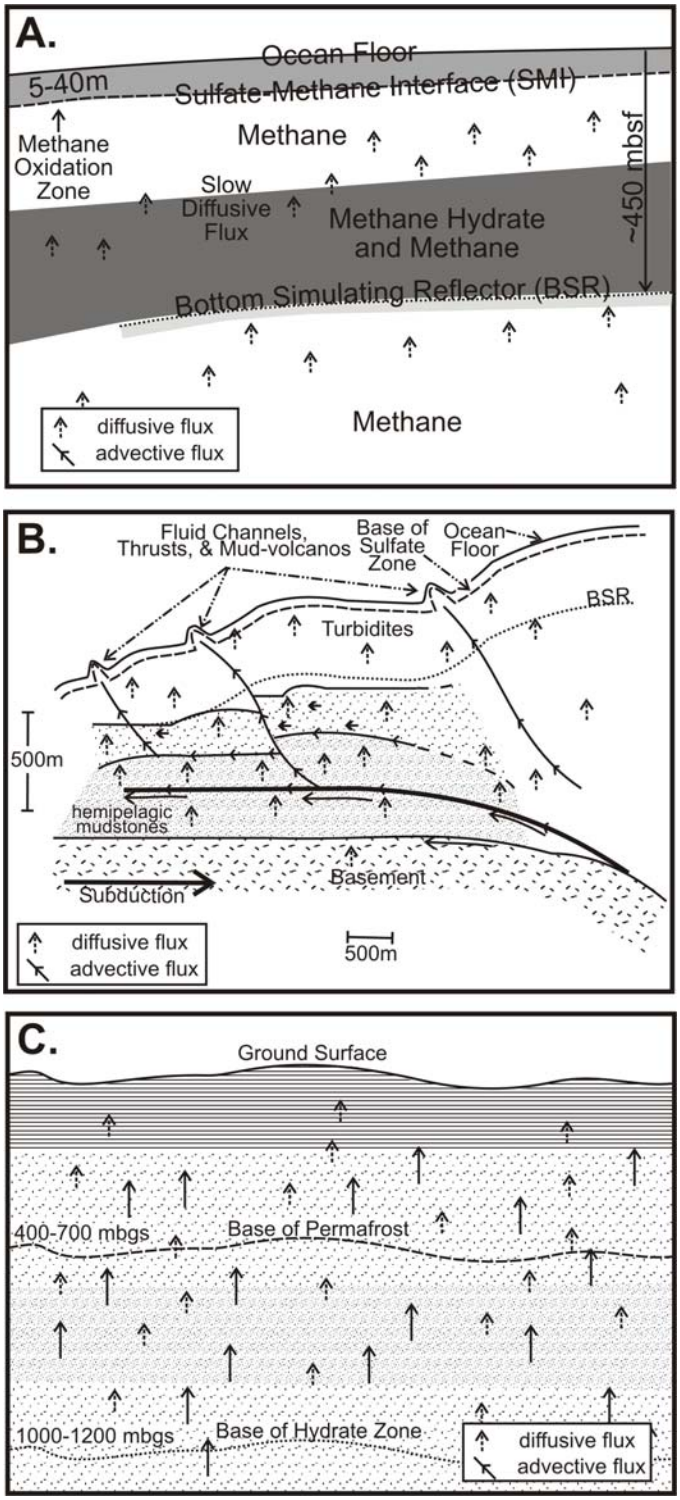

Figure C-2. Conceptualization of methane hydrate formation environments: (A) passive margins, Blake Ridge as an example (B) accretionary margins, (C) continental permafrost.

In marine environments, chemical and isotopic data from locations where methane hydrates occurrences have been found are available from both passive and accretionary margins. From passive margin study sites, data from deeper than 10 meters below sea floor (mbsf) is only available from the Blake Ridge study sites (e.g. *Claypool and Threlkeld 1983, Galimov et al. 1983, Brooks et al. 1983, Borowski et al. 1999, Borowski et al. 2000a,b, Paull et al. 2000a, Lorenson and Collett 2000*) and Gulf of Mexico (e.g. *Burke et al. 1986, Pflaum et al. 1986*). Deep chemical and isotopic data from methane hydrates occurrences are available from several active margin study sites, including the Cascadia Margin, Middle America Trench, Peruvian Outer Continental Margin, Chilean Triple Junction, and Nankai Trough. Two other passive margin study sites, Vøring Plateau, in the Norwegian Sea, and offshore New Jersey will be reviewed; however the presence or absence of methane hydrates at these locations was inconclusive in previously published literature. References for each of these study sites are provided in Table C- and Table C-2. As described previously, the locations of the SMI and BGHZ, and gas flux conditions are critical in understanding the occurrence of methane and methane hydrate. A summary of critical geologic information and identified gas hydrate occurrences from the individual passive margin sites may be found in Table C-, with site specific information from accretionary margin sites in Table C-2.

C.3.1 Marine Hydrate Isotopic Data

Previously, Claypool and Kaplan (*1974*), Borowski et al. (*1997*), and Borowski et al. (*1996*) have very clearly described a typical biogenic marine carbon-depth profile, where carbon cycling occurs as a result of anoxic methane oxidation and bacterial methane generation at the methane-sulfate interface. This impacts the carbon isotope compositions of both the methane and carbon dioxide pools (*Borowski et al. 1997*), resulting in extremely depleted $\delta^{13}C$ CH_4 and CO_2 values at the SMI (-85 to -103‰ and -30 to -51‰, respectively) compared with the isotopic values above or below the SMI. Steep isotopic gradients therefore exist near the SMI. This isotopic profile is observed in nearly every marine environment where biogenic methane formation occurs, regardless of the presence or absence of methane hydrates (e.g. *Borowski et al. 1997*).

However, at the four sites drilled at the northern and southern summits of Hydrate Ridge, there is no evidence in of carbon cycling even though the typical isotopic depletions of up to 40‰ are observed in CO_2 near the SMI (Figure C-4). Both summits are characterized by high upward advective gas and fluid flux (*Torres et al. 2002, Tryon et al. 2002*) and low sulfate concentrations (*Borowski 2005*) which are depleted within the first 5 to 15 cm of sediment, which is indicative of an extremely shallow SMI (*Boetius et al. 2000, Torres et al. 2002, Claypool et al. 2006*). Additionally, detectable

hydrogen sulfide to depths of 65 mbsf (*Westbrook et al. 1994, Borowski 2005*), and shallow gas hydrates, some containing hydrogen sulfide to depths of 20 mbsf (*Whiticar et al. 1995, Kastner et al. 1998, Milkov et al. 2005*).

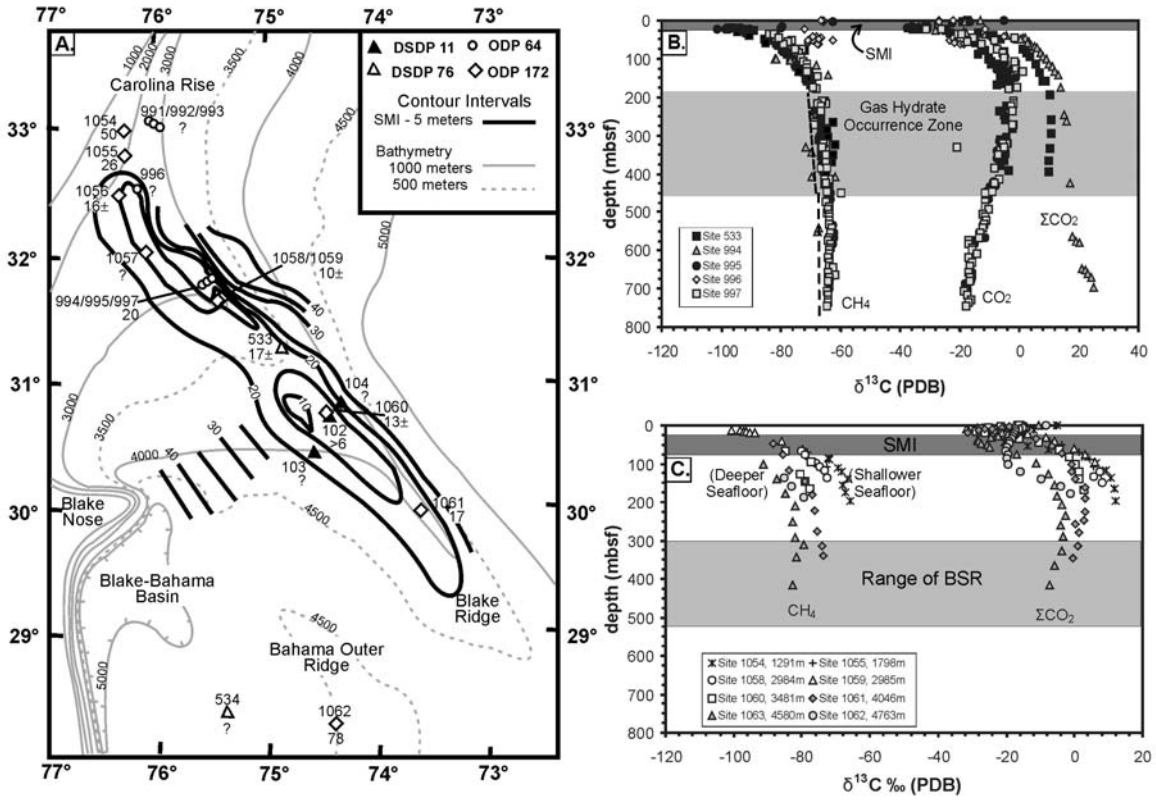

Figure C-3. Blake Ridge Data, DSDP/ODP Legs 11, 76, 164, and 172. (A) Site Locations with bathymetry and depth to sulfate-methane interface (from Borowski et al. 1999) (B) Legs 11, 76, and 164 (Galimov et al. 1983, Brooks et al. 1983, Claypool and Threlkeld 1983, Jenden and Gieskes 1983, Kvenvolden and Barnard 1983, Lorenson and Collett 2000, Paull et al. 2000a, Borowski et al. 2000a) (C) Leg 172 (Borowski et al. 2000b). Note the relationship between carbon isotope composition in methane and depth below sea level on Leg 172.

Currently, the occurrence of hydrogen sulfide in gas hydrates is unique to Hydrate Ridge (*Milkov et al. 2005*). It was suggested fluids originating from an intermediate depth mixed with in situ pore fluid within the active sulfate reduction zone allowed the formation of geologically young CH_4-H_2S hydrate (*Kastner et al. 1995b*).

The presence of H_2S in the gas hydrates could also indicate a recent increase in gas flux. An increasing methane gas flux could overwhelm sulfate reduction capacity, forcing the sulfate reduction zone to shallower depths. Methane hydrates could then form as the SRZ shallows, incorporating H_2S,

formed through sulfate reduction. Thus the methane hydrates and H_2S observed at the summits of Hydrate Ridge may be a record of deeper paleo-sulfate reduction zones. This idea would seem to be supported by the current model of gas formation and accumulation at the Southern Summit, suggesting free gas becomes stratigraphically trapped by hydrate until it is critically overpressured, decreasing the effective stress of sealing muds, allowing vertical leakage of the gas, which then precipitates as gas hydrates in shallow sediments (*Milkov et al. 2005*). Thus the vertical flux of gas varies through time, and the position of the SRZ could be expected to shift. Currently, gas flux at the southern summit is believed to be higher than at the northern summit, reflected in the much shallower H_2S at the southern summit (*Milkov et al. 2005*).

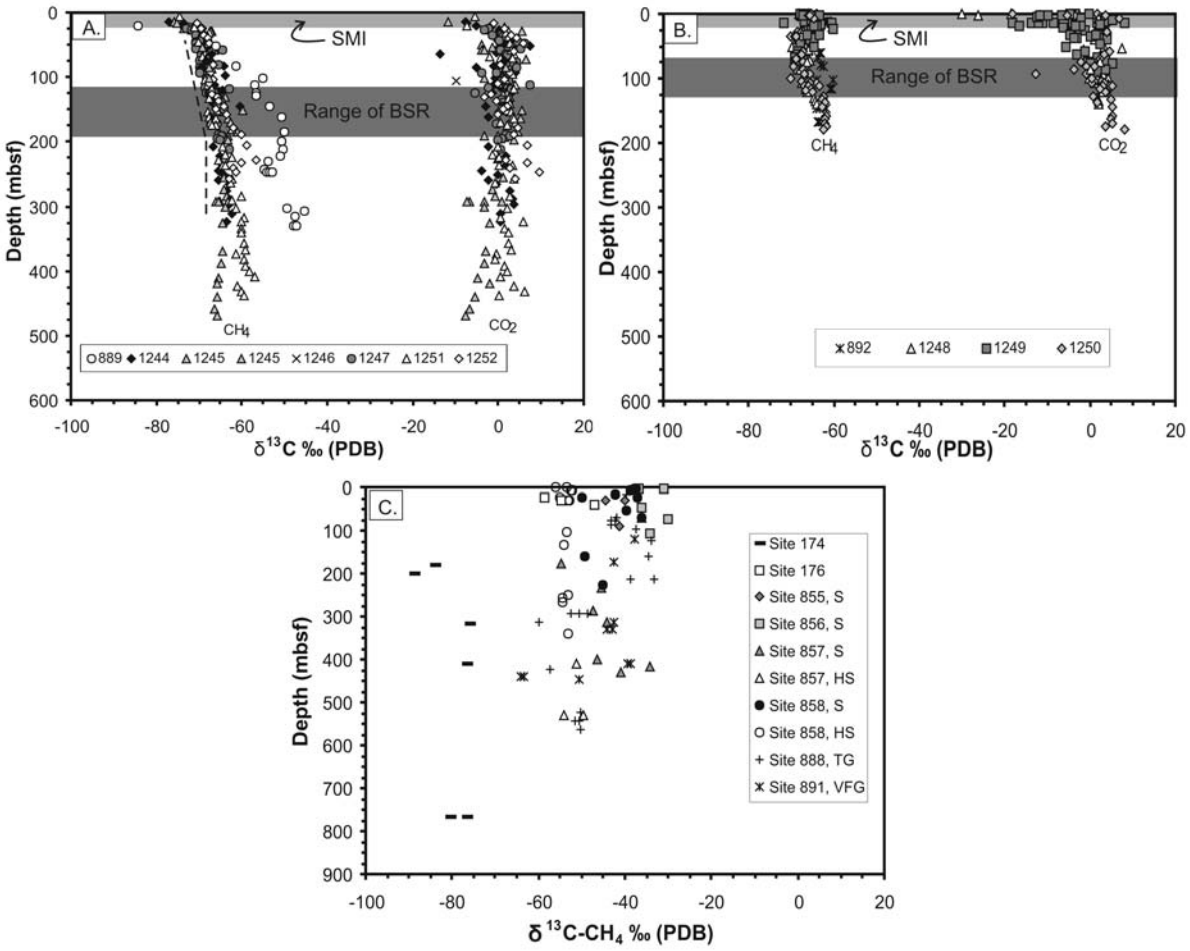

Figure C-4. Cascadia Margin (A) Sites with methane hydrates (B) sites with methane and hydrogen sulfide hydrates (C) sites without hydrates. Data from (Whiticar et al. 1994, Whiticar and Hovland 1995, Milkov et al. 2005, Claypool et al. 2006)

An example of an isotopic depth relationship that differs from the typical biogenic-marine profile is observed in data collected at Site 1250 at Hydrate Ridge, where the carbon isotopes of CO_2 behave as expected and show evidence of carbon cycling near the SMI, but the carbon isotopes of CH_4 do not. The CH_4 carbon isotopes range from around -65‰ near the seafloor, deplete to approximately -70‰ around 35 mbsf, enrich to -62‰ at around 125 mbsf, and then remain at that value until the bottom of the borehole (180 mbsf). This profile has a similar shape as those seen at other bacteriogenic marine sites, except carbon isotopic depletions are in the 5-8‰ range, and the minimum isotopic values do not occur near the current SMI. On the other hand, CO_2 isotopic trends shows depletions of up to 23‰ in shallow sediment just below the seafloor at the SMI from isotopic values of CO_2 sampled near the bottom of the borehole. The apparent de-coupling of CO_2 and CH_4 at this site has been attributed to <15% thermogenic gas migrating from depth mixing with microbial methane comprised of 20% microbial methane generated in surface sediments and 65% microbial methane venting from accretionary prism sediments (*Claypool et al. 2006*). Methane carbon isotope ratio depletions in bacteriogenic gas produced *in situ* are masked by the addition of migrating microbial and thermogenic gases.

While the carbon system at and above the sulfate-methane interface are well described, careful analyses of the area beneath the SMI reveals several assumptions may be incorrect and questions remain unexplained by the current model. The current hypothesis suggests the ^{13}C depletions at the SMI affect CH_4 and ΣCO_2 well below the SMI due to downward diffusion as ^{13}C-depleted ΣCO_2 is used as a substrate in bacterial methanogenesis (*Claypool and Kaplan 1974, Borowski et al. 1997, Paull et al. 2000a, Borowski et al. 2000a*).

Taking a closer look at all other marine sites with methane hydrates, which are typically found beneath the SMI, there is a slight $\delta^{13}C$-CH_4 enrichment with depth through the zone of hydrate occurrence (Figure C-3 - Figure C-7). With increasing depth beneath the SMI and starting within the zone of hydrate occurrence, the carbon isotope compositions of the CH_4 and ΣCO_2 pools commonly begin to diverge in areas of gas hydrate formation (e.g. *Borowski et al. 2000b*), as CH_4 becomes enriched with ^{13}C and .ΣCO_2 becomes enriched in ^{12}C. Thus, at sites with hydrates, the $\alpha^{13}C_{CH_4\text{-}\Sigma CO_2}$ begins to decrease beneath the SMI, indicating a slight decoupling of the CH_4-CO_2 systems.

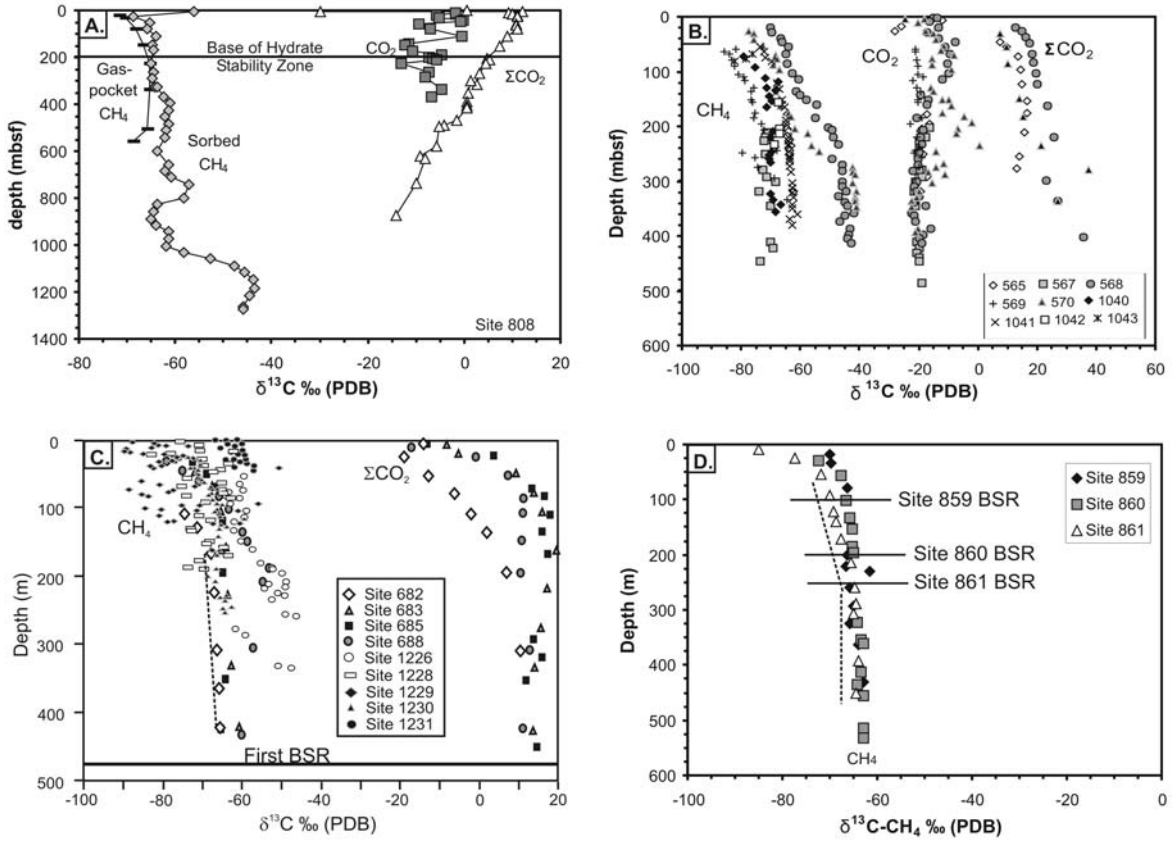

Figure C-5. Accretionary margin sites with gas hydrates. (A) Nankai Trough, ODP Leg 131, Site 808 (Berner and Faber 1993, Gamo et al. 1993). (B) Middle America Trench, Leg 84 (Claypool et al. 1985, Galimov and Shabaeva 1985a,b, Jeffrey et al. 1985), Leg 170 (Lückge et al. 2002). (C) Peruvian Outer Continental Margin (Whiticar and Suess 1990, Kvenvolden and Kastner 1990, Hinrichs et al. 2006). (D) Chilean Triple Junction (Waseda and Didyk 1995). Methane hydrates are absent at Middle America Trench Sites 567 and 1043.

The process or processes that cause the decoupling of the CH_4-CO_2 are not currently well understood. It is possible there is a similar process occurring at all sites, but currently there are multiple interpretations for the phenomenon, even for the same site. Possible explanations include mixing of upward migrating thermogenic gas with biogenic gas (e.g. *Claypool et al. 2006*), downward diffusion of isotopically light methane from the sulfate-methane interface (*Borowski et al. 1997*), and oxidation of methane in the absence of SO_4 (*Lorenson and Collett 2000, Milkov et al. 2005*). Two additional possible explanations which have not received much interest in the literature are: (1) slight fractionation of δ^{13}C-CH_4 due to gas hydrate formation, and (2) fractionation of mobile δ^{13}C-CH_4 by transport (diffusion or advection) through the zone of gas hydrate.

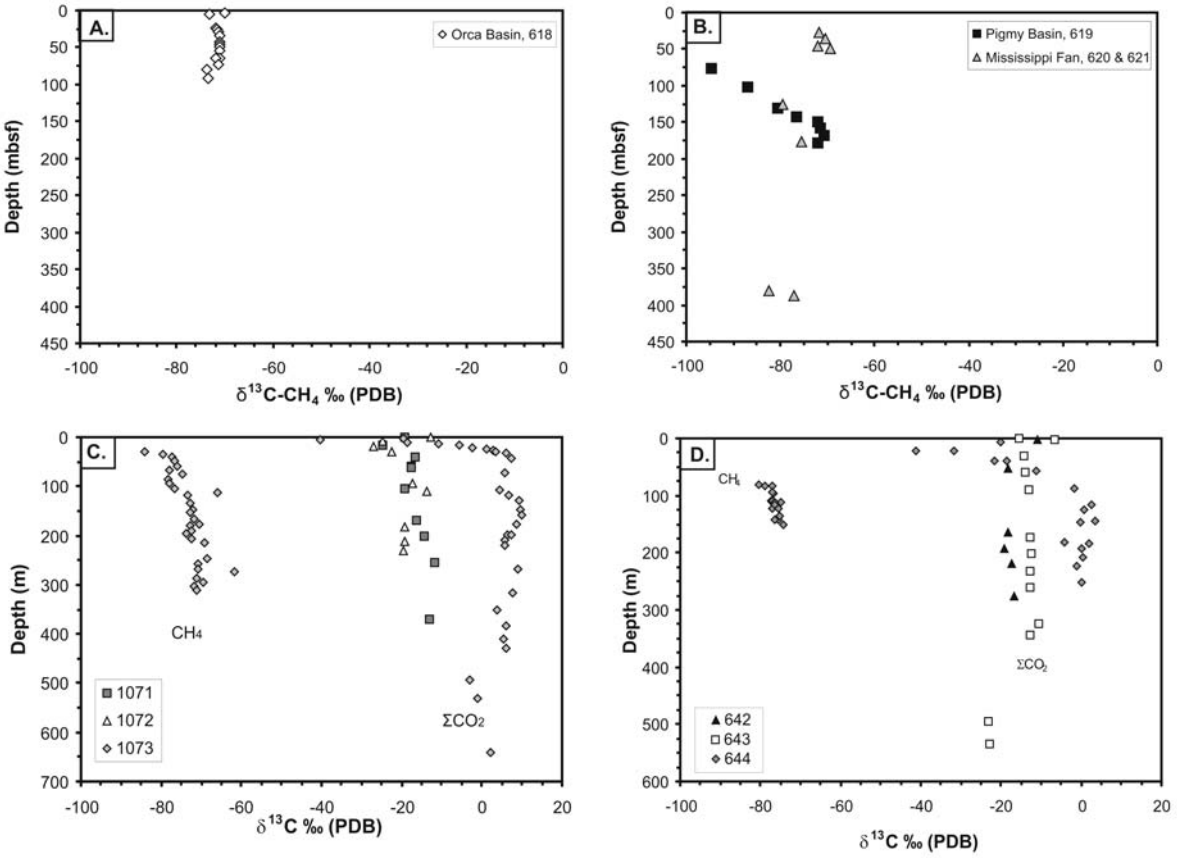

Figure C-6. Carbon isotope-depth profiles at other passive margin sites. Gulf of Mexico (Pflaum et al. 1986) sites (A) with gas hydrates and (B) without gas hydrates. Sites with probable, but unconfirmed gas hydrate (C) offshore New Jersey Leg 174A (Claypool et al. 2000) and (D) Vøring Plateau, Norway, Leg 104 (Vuletitch et al. 1989, Whiticar and Faber 1989a, Whiticar and Faber 1989b, Kvenvolden et al. 1989).

Fractionation of the isotopes in both water and gas due to gas hydrate formation was first proposed by Trofimuk et al. (*1974*). Since then, isotopic fractionation of hydrogen and oxygen has been clearly observed and reported due to hydrate structure formation from water (e.g. *Hesse and Harrison 1981, Hesse 2003*). However, isotopic fractionation of gas is not currently recognized, based on two lines of evidence (e.g. *Borowski et al. 1997*): (1) data collected from decomposing hydrates suggests carbon fractionation of methane does not occur in marine gas hydrates (e.g. *Brooks et al. 1983, Brooks et al. 1985*), and (2) the observation of similar isotopic trends in sediments where hydrates aren't stable, such as DSDP Site 147 in the Cariaco Basin (*Lyon 1973*) compared with sediments where hydrates have been observed and are stable, such as the Blake Ridge (*Borowski et al. 1997*) (Figure C-3).

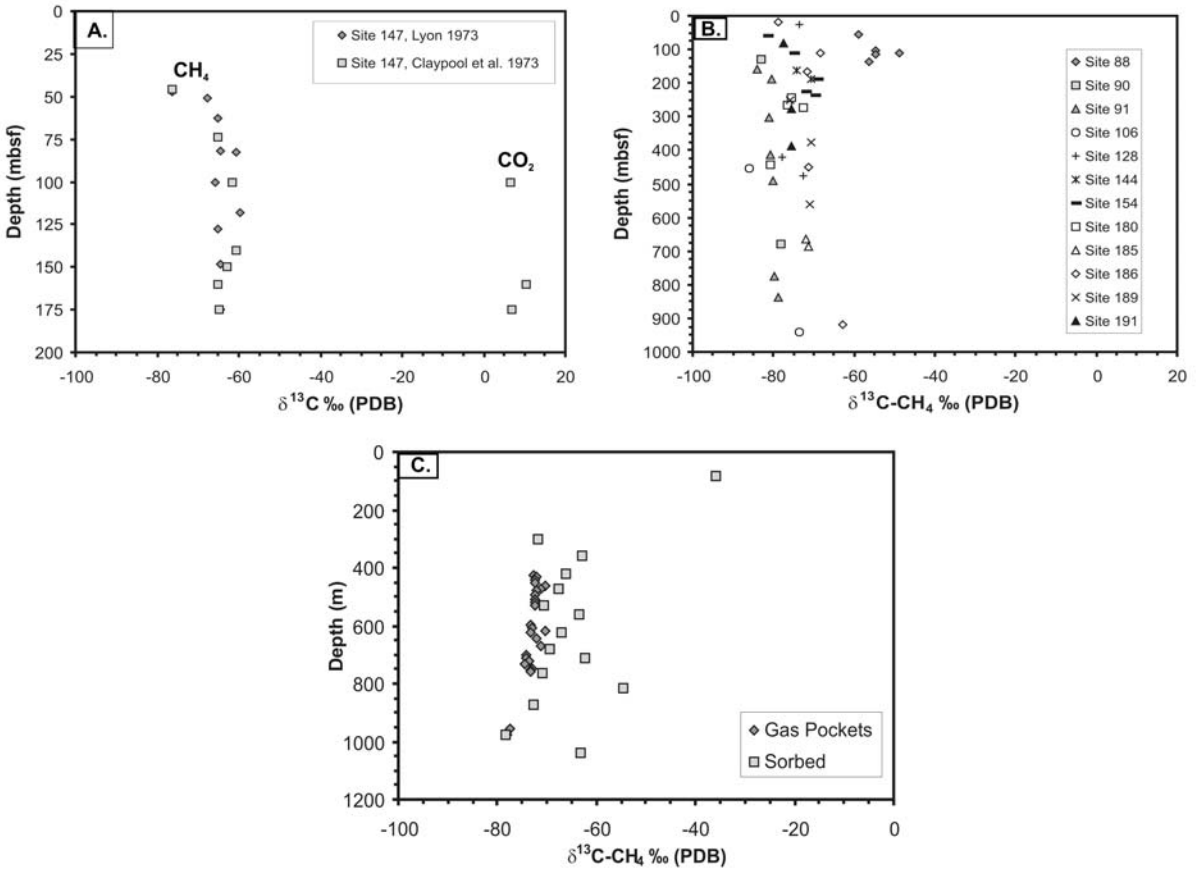

Figure C-7. Other marine gas profiles at sites without gas hydrates. (A) Cariaco Trench (Claypool et al. 1973, Lyon 1973), (B) various oceanic sites from early DSDP (Claypool et al. 1973), and (C) Philippines (Berner and Bertrand 1991).

The first argument, that significant carbon fractionation of methane has not been observed in marine gas hydrates, has been explored through melting of methane hydrate sampled by PCS. During gas hydrate melting experiments (*Brooks et al. 1983, Kvenvolden et al. 1984, Brooks et al. 1985*), a range of $\delta^{13}C\text{-}CH_4$ isotopic values (3‰-8‰) were observed (Figure C-8). The $\delta^{13}C\text{-}CH_4$ isotopic values vary asystematically, and it was uncertain whether the variance was real or an artifact of the procedure (*Kvenvolden et al. 1984*), thus the conclusion was made that carbon isotopic composition of the evolved C1 did not change significantly during the degassing period, and isotopic fractionation of the C1 gas was not observed during the PCB sampling (*Brooks et al. 1983*). Melted gas hydrate $\delta^{13}C\text{-}CH_4$ isotopic values are compared with gas measurements from nearby core collected by standard core collection techniques; including both void and headspace gas (*Milkov 2005a*). Further, "significantly different" $\delta^{13}C\text{-}CH_4$ in gas hydrates and adjacent voids are sometimes reported (e.g.

Milkov et al. 2005), but the gas hydrates may have crystallized in the past from a gas of a different composition than the gas currently migrating through surrounding sediments (*Milkov et al. 2005*).

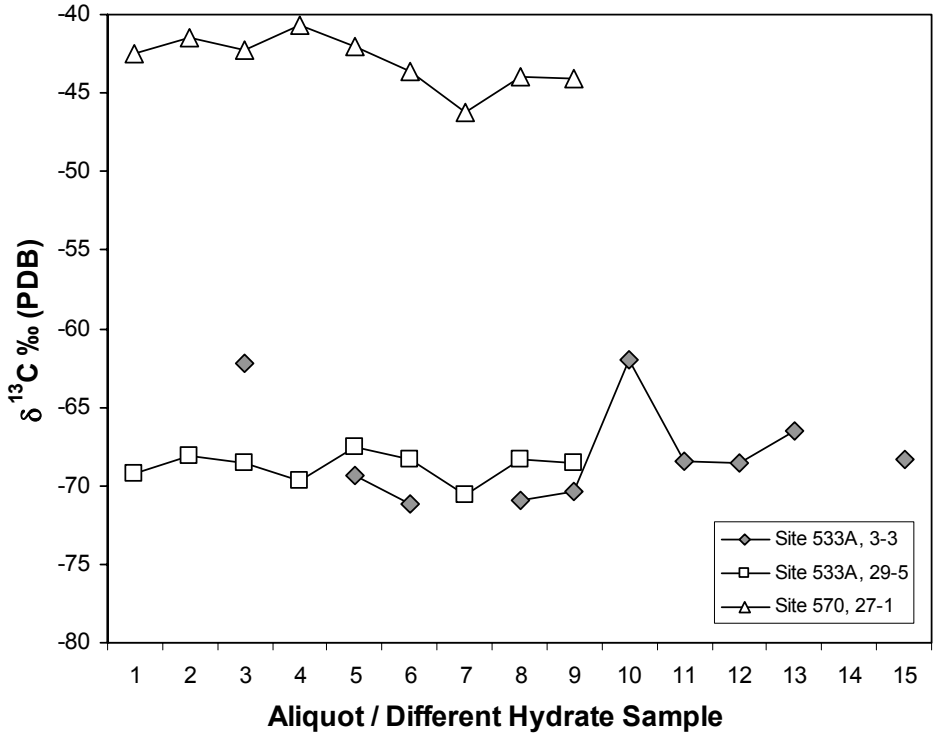

Figure C-8. Isotopic results of hydrate depressurization.

Situations where significantly different $\delta^{13}C\text{-}CH_4$ values are reported in adjacent gas hydrates and voids are treated as the exception, rather than the rule. However, with most sample collection techniques, up to 99.8% of the gas is lost during core recovery (*Paull et al. 2000b, Paull and Ussler 2001*). Furthermore, during core retrieval, the core is subject to temperature changes, and thus pressure changes in all sampling methods (including the PCS technique). Additionally, both void and headspace gases are subject to core depressurization, for all techniques except PCS. Because gas hydrates are stable under pressure and low temperature, at least partial gas release from the hydrates structure is often observed or assumed to have occurred in all sampling methods, including PCS (e.g. *Dickens and Kennedy 2000*). Therefore, there are currently no assurances the laboratory dissociated gas hydrates are actually being compared with free gas uncontaminated with gas released from hydrates during core retrieval. As gas hydrates can contain up to 164 times as much gas per cubic meter as free gas (*Sloan 1998*), even minor gas hydrate dissociation could significantly mask the

original free gas signature. Carbon isotope fractionation observed during degassing of methane from PCB has been attributed to kinetic fractionation associated with pressure loss (*Wallace et al. 2000*).

The second line of evidence against $\delta^{13}C\text{-}CH_4$ fractionation into methane-hydrate compares isotopic trends with depth in areas of gas hydrate formation versus areas where gas hydrates are not stable. This review has compiled all of the available carbon isotopic data which has been collected through areas of gas hydrate formation, as well as from other areas where gas hydrates do not occur (Figure C-3 - Figure C-7). At sites where gas hydrates are not present, neither an isotopic enrichment nor depletion is observed beneath the SMI zone. For instance, DSDP Site 147 in the Cariaco Trench, where methane hydrates are not stable (Figure C-7A), there is no enrichment or depletion of isotopic signatures. Other sites, drilled near gas hydrate occurrences but lacking in gas hydrates due to either P-T stability or gas quantity show no systematic enrichment or depletion with depth, such as Sites 888 and 891 at the Cascadia Margin or Sites 855, 856, 857, and 858 in the nearby Juan de Fuca plate (Figure C-4C).

One additional explanation for the observed enrichment with depth through the gas hydrate zone is diffusional fractionation. Early research suggested the potential for isotopic fractionation through diffusion (e.g. *Galimov 1967, May et al. 1968, Stahl et al. 1977*), but Fuex et al. (*1980*) argued strongly against any meaningful diffusive fractionation of $\delta^{13}C\text{-}CH_4$. Schoell (1983 a,b) therefore argued observed fractionations are actually due to mixing rather than diffusive fractionation; although he conceded the studies of Galimov (1967), May et al. (1968) and Stahl et al. (1977) may be "exceptional and not typical for most natural gases". More recent work (*Prinzhofer and Huc 1995, Pernaton et al. 1996, Prinzhofer and Pernaton 1997, Prinzhofer et al. 2000, Prinzhofer et al. 2001, Zhang and Krooss 2001*) revisited the idea of isotopic diffusive fractionation and concluded isotopic diffusion may occur. Isotopic fractionation coefficients of diffusive transport for methane and ethane were calculated by Schloemer and Krooss (*2004*). Isotopic fractionation associated with diffusion of carbon dioxide in aqueous solutions has also been measured (*O'Leary 1984*) and observed (e.g. *Cerling et al. 1991, Camarda et al. 2007*).

If transport related processes through the methane hydrate zone were causing fractionation of $\delta^{13}C\text{-}CH_4$, the carbon isotopes of ethane (C2) and propane (C3) could also be expected to fractionate. However, at the sites where $\delta^{13}C$-C2 and $\delta^{13}C$-C3 data were collected, $\delta^{13}C$ does not appear to fractionate in C2 and C3. This suggests neither diffusional nor advective transport is causing a fractionation of $\delta^{13}C\text{-}CH_4$ through the methane hydrate zone. Because Structure I hydrate consists primarily of methane with very little C2 and no C3, and a majority of naturally occurring hydrates recovered are Structure I (e.g. *Kvenvolden 1995*, *Sloan 1998, Milkov 2005a*), carbon isotope

fractionation due to methane hydrate formation could cause a fractionation of carbon isotopes in CH_4 but not in C2 or C3.

Several researchers have commented on exclusion of gas species, such as ethane and/or propane, from Structure I and II gas hydrates causing changes to gas composition in the geologic column, unrelated to gas formation (e.g. *Sloan 1998, Sassen et al. 2000, Sassen et al. 2001a, Sassen et al. 2001b, Milkov et al. 2004*). This fractionation is due to both mass and atomic size. It could also account for observations of ethane and propane collecting beneath hydrate formation zones (e.g. *Collett and Dallimore 1999*), which are often attributed to an increase in the proportion of thermogenic gas beneath and through the hydrate column (e.g. *Milkov et al. 2004*). Oxygen isotope fractionation between water incorporated in hydrate and liquid water occurs, resulting in $\delta^{18}O$ enrichment in the hydrate (e.g. *Hesse and Harrison 1981*). Amongst the noble gases Ar, Kr, and Xe, heavier noble gases are also preferentially incorporated into the hydrate structure, such that Xe incorporates more than Kr, which incorporates more than Ar (*Dickens and Kennedy 2000, Winckler et al. 2002*).

C.4 Permafrost-Associated Hydrates

Permafrost methane hydrates accumulations have been found in the North Slope of Alaska (*Collett et al. 1990*), in the Mackenzie Delta and Arctic islands of northern Canada (*Dallimore and Collett 1995, Dallimore et al. 1999, Majorowicz and Osadetz 1999, Majorowicz and Osadetz 2001, Dallimore and Collett 2005*), and in sedimentary sequences of the Siberian Platform (*Yakushev and Chuvilin 2000*). All known occurrences of permafrost hydrates are found in sedimentary and sedimentary basin sequences. The only published profiles of molecular and isotopic data with sufficient data resolution for this review are from the Mallik wellfield of the Mackenzie Delta. While isotopic data were reported by Dallimore and Collett (*1995*) in the nearby Taglu wellfield, the data coverage is not of sufficient resolution (five analyses in 413m) for this discussion.

In the Mackenzie Delta, two boreholes, Mallik 2L-38 and 5L-38, were drilled within 110m of each other as part of an international research program (*Lorenson et al. 1999, Uchida et al. 1999, Collett et al. 2005, Lorenson et al. 2005, Waseda and Uchida 2005*). In Mallik 2L-38, the base of ice-bonded permafrost was around 600 mbgs, with ice-bearing permafrost (corresponding to -1°C) observed to 640 mbgs (*Dallimore et al. 1999b*) and gas hydrates between 890 and 1106 mbgs (*Lorenson et al. 1999*). The base of ice bearing permafrost in the Mallik 5L-38 borehole is 605 mbgs (*Henninges et al. 2005*). Gas hydrate in this borehole occupies between 80 and 90% of the pore spaces between 891 and 1107 mbgs (*Lorenson et al. 2005*), but smaller amounts of gas hydrate (0-

40% porosity) was observed in geophysical logs to 800mbgs, where geophysical log reporting begins (*Collett et al. 2005, Collett and Lee 2005, Takayama et al. 2005*). Both boreholes were completed near the base of the gas hydrate zone.

The carbon isotopic compositions of methane in the permafrost boreholes do not show the same smooth variations with depth (Figure C-9) as the marine hydrates. This is attributed to the complex geology and the depositional setting, which results in differences in hydrocarbon trapping, fluid flow and gas transport. The carbon isotopic composition of methane is variable through the permafrost, then becomes more enriched with depth through the hydrate zone beneath the permafrost, and then slightly depleted in the area just beneath the gas hydrate stability zone. Most of the gas hydrate observed was Structure I (*Tulk et al. 1999*). Ice bonded permafrost acts as a partial seal inhibiting hydrocarbon gas migration, as evidenced by local concentration maximums of CO_2, C_2, C_3, nC_4, iC_5, and many of the C_6 and C_7 isomers, which have regional maximums around 600 mbgs (*Lorenson et al 1999, Collett and Dallimore 1999*). $C_1/(C_2+C_3)$ ratios also spikes at the base of the ice bearing permafrost (640 mbgs); increasing from 100 to 500, then decreases back to 100.

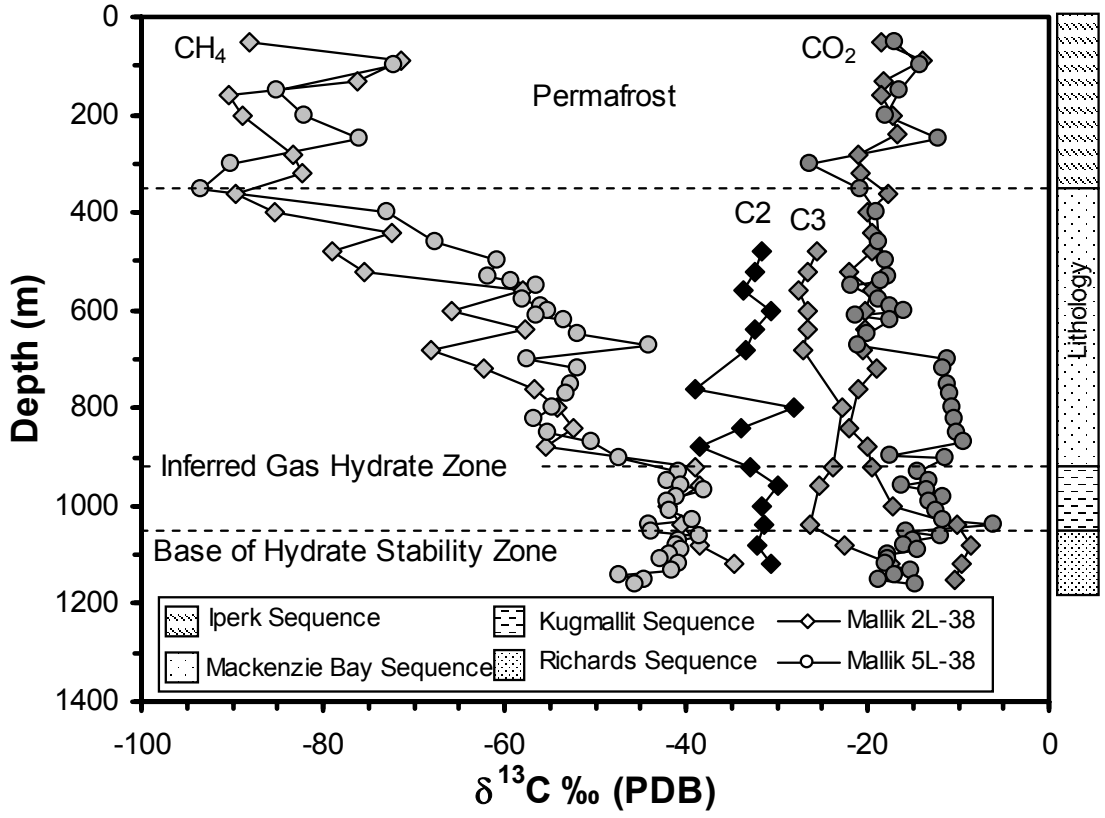

Figure C-9. Permafrost depth trends from the Mackenzie Delta, Mallik 2L-38 (Lorenson et al. 1999) and Mallik 5L-38 boreholes (Lorenson et al. 2005).

Permafrost methane hydrates are more complex than marine hydrate occurrences. The available $\delta^{13}C$ profiles are currently restricted to the Mackenzie Delta, Canada. In the Mallik 2L-38 and 5L-38 boreholes, there is a significant change in $\delta^{13}C$-CH_4 through the zone of hydrate occurrence (Figure C-9) from the zones above or below. The zone of hydrate stability is subject to change, because of temperature changes as a result of the glacial-interglacial cycle. These temperature changes are therefore more extreme in permafrost environments than subocean bottom environments (e.g.*Collett 1994*). Subsurface temperatures are currently within the zone of hydrate stability throughout the drilled column. Trapping mechanisms are a key factor in the formation of methane hydrates in permafrost environments (*Collett 1994*), and complex lithology within the hydrate occurrence zone in the Mallik boreholes further complicates interpretations.

C.5 Summary

Gas hydrates have been sampled in marine and subpermafrost environments. The most common naturally occurring hydrates are Structure I, consisting of primarily methane and water. The methane may be of either bacteriogenic or thermogenic origin. Because of temperature and pressure constraints, gas hydrates are extremely difficult to sample and study. In borehole studies, the pressure core barrel sampling method has been the only sampling method able to ensure degassing does not occur during sample recovery.

At marine hydrate locations, isotopic compositions of methane are affected by diagenetic processes. Typically, in the near sub-surface zone, isotopic fractionation due to methane oxidation occurs, enriching the methane carbon isotopic composition relative to deeper gas. However, carbon cycling with the CO_2 pool results in extreme ^{13}C depletion in methane near the base of the sulfate oxidizing zone (*Borowski et al. 1997*). Sometimes, but not always, a zone of just methane gas exists beneath the oxidizing zone. Methane carbon isotopes typically enrich substantially in ^{13}C through this zone. ^{13}C enrichment continues but with a fixed slope through the zone of gas hydrate occurrence. Beneath this zone, the ^{13}C profile typically stabilizes. However, very little data is available from beneath the gas hydrate zone.

The $\delta^{13}C$-CO_2-depth profile typically mimics the $\delta^{13}C$-CH_4 profile from the seafloor to the top of the gas hydrate zone, evidence of a constant fractionation factor between the carbon source pool (CO_2) and the product (CH_4). However the two carbon pools usually decouple at some depth, often near the gas hydrate occurrence zone. Most commonly this is attributed to mixing of bacteriogenic with thermogenic gas, downward diffusion of isotopically light methane from the sulfate-methane interface, methane oxidation in the absence of SO_4. Two hypotheses which have

received less support in the literature are slight fractionation of $\delta^{13}C\text{-}CH_4$ or fractionation of mobile $\delta^{13}C\text{-}CH_4$ by the transport process.

Several other processes related to gas hydrate formation were noted in the marine environment. Ethane and/or propane gas exclusion from Structure I or II gas hydrates is likely to create ambiguity when using gas compositions to determine gas origins. Certain noble gases are also preferentially incorporated into the hydrate structure. Although isotopic fractionation within gas molecules has not been observed, hydrogen and oxygen isotopes readily fractionate between liquid water and the hydrate structure.

Permafrost associated hydrates have been studied in arctic regions of North America and Asia. These hydrates are all associated with oil and gas producing sedimentary units. Two research boreholes drilled as part of the Mallik gas hydrate research program have the most extensive isotopic-depth datasets available from permafrost areas. The stratigraphy greatly complicates the carbon isotopic-depth profile. However, evidence indicates gases within the hydrate are of thermogenic origins, with bacteriogenic gases located in upper sections.

Table C-1. Site characteristics of the passive margin marine hydrate occurrences discussed in this paper.

	Site / Borehole	Ocean Depth (mbsl[1])	Gas Flux	SMI[3] (mbsf[4])	GHOZ[5] (mbsf)	BSR[6] (mbsf)
Blake Ridge						
Leg 11	102	3426				~600
	104	3811				~600
Leg 76	533	3194	Low	9.8-14.4		~600
Leg 164	994	2797	Low	20-22.5	180-460	None
	995	2778		20-22.5	180-460	440
	996	2166	High	4	0-60(EOH)	None
	997	2770	Low	23	180-460	464
Leg 172	1054	1291		50		~300
	1055	1798		26		~320
	1058	2984		12		~450
	1059	2985		13		~450
	1060	3481		13		~490
	1061	4046		17		~510
	1062	4763		75		
	1063	4580				
Gulf of Mexico						
Leg 96	618	2422	Low	3, 20, or		
	619	2274		80?		
	620	2612				
	621	2485				
New Jersey						
Leg 174	1071	88				
	1072	98				
	1073	639				
Vøring Plateau						
Leg 104	642	1292				
	643	2779				
	644	1226		6-22	Suggested?	

Table C-2. Site characteristics of the accretionary margin marine hydrate occurrences discussed in this paper.

	Site / Borehole	Ocean Depth (mbsl[1])	Gas Flux	SMI[3] (mbsf[4])	GHOZ[5] (mbsf/mbgs)	BSR[6] (mbsf)
Cascadia Margin						
Leg 146	888	2516				
	889	1316				224
	891	2663				
	892	674	Low	<20	0-68	68-74
Leg 204	1244	895	Low	8	137	128
	1245	871	Low	7	149	134, 158
	1246	850	Low	8	115	114-121
	1247	834	Low	11	156	128, 152
	1248	830	High		131	115, 145
	1249	777	High		136	115
	1250	796	High		133	114
	1251	1210		4		193
	1252	1040		5		170
Chilean Triple Junction						
Leg 141	859	2741				100
	860	2146				200
	861	1652				250
Juan de Fuca Plate						
Leg 139	855	2444		none	None	None
	856	2420		limited	None	None
	857	2420		~200	None	None
	858	2426		~200	None	None
Middle America Trench						
Leg 84	565	3099	Low		yes	not obsrv.
	567	5510			None	not obsrv.
	568	2020	Low		yes	
	569	2754			evidence	not obsrv.
	570	1708	Low		yes	not obsrv.
Leg 170	1040	4177			25-350 (?)	NO
	1041	3306	Low		120-280	no
	1042	3581			65-85	no
	1043	4312			None	no
Nankai Trough						
Leg 87	582	4879				
	583	4629				
Leg 131	808	4674		3-6	90-140,	none
Peruvian Outer Continental Margin						
Leg 112	679	450			No hydrates	None
	682	3788				477
	683	3071				None(529)
	685	5070	Low			612
	686	446			No hydrates	None
	688	3820	Low		120-430	473
Leg 201	1226	3297		No full	Gas-Poor	
	1228	252		depletion	(N-H?)	
	1229	105.5		38,90 S		
	1230*	5086		reappear	CH4 Gas	
	1231	4827		no full	poor	
				depletion	75-252	
				no full		
				depletion		

Appendix D.

Canadian and Fennoscandian Shield $\delta^{37}Cl$ and $\delta^{81}Br$ Data

Table D-1. Canadian and Fennoscandian Shield $\delta^{37}Cl$ and $\delta^{81}Br$ data from this study.

Borehole / Sample Loc	Depth m	$\delta^{81}Br$ ‰	$\delta^{37}Cl$ ‰	$^{87}Sr/^{86}Sr$	Ca mg/l	Na mg/l	Mg mg/l	Sr mg/l	Br mg/l	Cl mg/l	TDS g/l	$\delta^{18}O$ ‰	$\delta^{2}H$ ‰	$\delta^{13}C$-C1 ‰	$\delta^{2}H$-C1 ‰
Canada															
Elliot Lake-Dennison Mine															
DEN-3100 FZ	945	0.52	-0.15	0.73095	2700	3410	3.8	111	59	8830	15.2	-13.1	-88		
JV 906	945	0.79	-0.05	0.72852	2470	2324	4.9	60	53	8035	13.0	-14.1	-100	-36.1	-308
#30876 - EOH	945	0.85	-0.36	0.72492	4400	4700	5.9		52	14250	23.7	-11.5	-75	-37.4	-297
Elliot Lake-Panel Mine															
PAN 1249 Drift	381	0.78	0.98	0.75333	1970	1940	32	50	22	6050	10.1	-15.1	-108		
PAN 603 XCUT	381	1.17	0.24	0.75191	1080	1350	30	28	18	3850	6.4	-14.4	-102		
Eye-Dashwa Lakes Pluton – Atikokan															
ATK 5-4B	980	0.27	-0.35	0.70700	8980	816	1	220	137	18100	28.5	-9.5	-70		
ATK 1 - 9A	880	0.74	-0.29	0.70613	11900	1830	4		141	25400	40.1	-9.8	-72		
ATK 5-6B	1050	1.29	-0.5	0.70614	7460	779	1		119	12200	21.0	-9.1	-84		
Timmins - Kidd Creek Mine															
Kidd Creek		0.17	-0.45		27000	10200	3370		1200	80000	122	-13	-45	-39.8	-349
Lynn Lake – SGM Fox															
SGM 2000-1	610	0.26	-0.23	0.71091	1740	1040	16		5.7	4220	7.3	-18.3	-139		
SGM 2600-1	792	0.29	0.32	0.7115	2280	1000	351		37	5770	9.6	-16.2	-101		
Matagami-Matagami Mine															
R36	1800	0.33	-0.64		61300	14800	3400		1785	143581	227	-12.3	-42	-52.0	-356
R28-85		0.65	0.12	0.70866	563	300	41	14.6	16	1296	2.3	-14.4	-106	-54.5	-396
Matagami – Norita Mine															
Norita4W-0		insuf.	0.05											-47.7	-423
Norita 4W-85		0.83	0.1	0.70885	26300	11800	3800	813	1075	75331	120	-12.4	-69	-47.7	-423
Slave Province – Lupin Mine															
1130-64-Lu/GTK118	1130	0.41	-0.33		361	533	20	6.5	22	1590	2.6	-23.4	-181	-50.3	-330
890-188-Lu/GTK119	890	0.54	-0.19		407	526	56	9.3	27	1780	2.8	-22.8	-178	-55.0	-340
1130-192-Lu/GTK130	1130	0.69	-0.26		5860	8140	70		357	25200	39.9	-22.5	-172	-42.4	-329
1130-273 (30/11/04)	1130	0.84	-0.27		1460	1760	44	31.9	82	6700	10.2	-23.2	-179	-46.3	-340
Sudbury – Copper Cliff South Mine															
CCS Lev2050 Sta 844	325	0.68													
CCS-4000	1219	1.25	-0.03	0.70954	77300	13900	1420		1640	153000	258	-10.6	-47	-35.0	-325
CCS-500-842-1	152	insuf.		0.72476	217	70	104	1.7		38	1.9	-12.2	-80		

Borehole / Sample Loc	Depth m	$\delta^{81}Br$ ‰	$\delta^{37}Cl$ ‰	$^{87}Sr/^{86}Sr$	Ca mg/l	Na mg/l	Mg mg/l	Sr mg/l	Br mg/l	Cl mg/l	TDS g/l	$\delta^{18}O$ ‰	$\delta^{2}H$ ‰	$\delta^{13}C$-C1 ‰	$\delta^{2}H$-C1 ‰
CCS2050-1	625	insuf.	0.11	0.73924	590	440	45	5.7		985	3.5	-11.4	-82		
Sudbury –Fraser Mine															
Fr 33-170b	1006	0.23	-0.25	0.71166	4650	2400	2.2	88	88	13900	21.7	-12.7	-78		
Fr 33-192	1006	0.32	-0.22	0.71197	3825	2200	1.9	73	74	11000	17.7	-12.8	-78		
Sudbury – North Mine															
N3646b	1600	0.18	-0.26												
N3640b	1600	0.19	-0.13	0.71508	64000	21000	29		1370	153000	240	-10.3	-42	-26.6	-155
N3640a	1600	0.25	-0.54	0.71535	63800	18500	24		1200	166200	250	-10.9	-44	-26.5	-162
N3644b	1650	0.59	-0.19	0.71585	6200	22000	48	1700	1530	168000	256			-27.7	-203
Sudbury – Strathcona Mine															
ST31-178	1000	0.30	-0.6	0.71063	41300	8200	11		507	67700	119	-10.5	0	-29	-133
Thompson – Thompson Mine															
1002-2	305		-0.35	0.72347	820	908	145	15	34	3120	5.4	-17.4	-131		
T3-344b*** (or T3-27377-84)	610	0.01	-0.78		31800	20500	1310		570	74400	129	-15.3	-107	-54.5	-285
T3-2000'	610	0.11	-0.15	0.72289	4540	2740	160	80	111	12600	20.3	-17.9	-127		
2400-1	732	0.23	-0.12	0.72266	2650	1690	300	56	69	7830	14.5	-15.6	-122		
BL 4400	1341	0.31	-0.26		44300	28000	1960		10	119000	194	-12.9	-76	-52	-280
2200-1	671	0.37	-0.19	0.72197	4840	2930	233		115	13700	22.5	-15.0	-115		
Val d'Or – Sigma Mine															
#10680 - 95'	1737	0.69	0.04	0.71698	2600	313	0.1		69	4950	8.4	-13.4	-97	-46.3	-301
#12042-150	1737	0.90	0.03	0.7135	40310	7795	515	452	1107	82930	142	-13.8	-83	-46.3	-332
Yellowknife – Con Mine															
YK3464	1372	0.06	-0.61	0.71334	26400	18800	406		756	82700	130	-19.0	-126		
YK2043	1372	0.15	-0.54	0.71146	30000	18600	880		800	85000	135	-19.1	-11		
Con 4500-5	1372	0.16	-0.19		48530	19730	563	785	946	118420	189	-16.3	-93		
Con 4500-6b	1372	0.18	-0.13	0.71291	54400	35800	1340	1570	1150	135000	230	-15.0	-82		
Con 4500-6c	1372	0.20	-0.05	0.71221	57300	32600	920	1640	1520	142000	237	-14.4	-71		
Con 4500-1c	1372	0.23	-0.22	0.71266	49400	27900	712	1190	1180	132800	214	-15.7	-84		
4900-Negus	1494	0.39	-0.06	0.71382	43760	18000	304	690	885	105870	170	-17.5	-104		
Yellowknife – Giant Mine															
5	457		-0.02	0.71312	1400	1600	174	48	97	5250	8.9	-19.1	-152		
10	610		0.04	0.71048	757	784	95	13	21	1900	4.6	-19.0	-155		
2000-800N-16161	610	0.37	0.52	0.70757	22910	6850	489		393	48684	80	-17.4	-77	-51.3	-330
4	335	0.94	-0.15	0.71353	648	757	115		36	2360	4.2	-19.2	-163		
2000 #11011	610	1.02	-0.09	0.71194	7375	7065	785		244	25400	42	-20.0	-144	-51.3	-330
Finland															
Enonkoski															
Enon-366	995	1.77	0.62		1340	2516	747		82	8870	13.8	-13.9	-98	-67	-297
Hästholmen															
		0.26	0.00		730	1586	244		16.5	4161	*7.0*	-10.5	-76		
Juuka-Miihkali															
Ju91-341 (360)	341	1.4	0.37		1218	2433	39		34	5600	9.5	-12.8			
87/116/320 (311)	311	1.68	0.08		8900	6900	3.4		174	24540	41	-10.5	-19	-29	-281

Borehole / Sample Loc	Depth	$\delta^{81}Br$	$\delta^{37}Cl$	$^{87}Sr/^{86}Sr$	Ca	Na	Mg	Sr	Br	Cl	TDS	$\delta^{18}O$	$\delta^{2}H$	$\delta^{13}C$-C1	$\delta^{2}H$-C1
	m	‰	‰		mg/l	mg/l	mg/l	mg/l	mg/l	mg/l	g/l	‰	‰	‰	‰
Miihk-116-2475	750	1.70	0.80		8050	5190	1.2		177	20500	34	-10.4	-13	-29	-268
Miihk-116-3190	946	1.70	1.02		16700	38600	228		507	78700	134	-11.0	-7	-29	-281
Ju91–576 (610)	576	1.71	0.31		1234	2481	41		38	5630	9.3				
87/116/20 (19)	19	1.79	-0.45		7400	5600	3.8		154	19600	33	-10.6		-29	-284
87/116/520 (508)	508	1.81	0.15	0.71381	8900	6300	3.4		174	24460	40	-10.2	-21	-29	-279
Ju91-57 (60)	57	1.90	0.27		1257	2528	41		39	5600	9.5	-13.0			
Ju91-660 (621)	621	1.94	0.37		1191	2323	39		3	5580	9.2	-12.7			
JuMi91-138.2-C/L	138	insuf.	1.52												
Mantsala															
MHA2/9 855m	855	0.68	-0.36	0.71881	12700	6870	16.9		253	30300	*50*	-12.1	-84		
MHA2/91 905m	905	0.68	-0.54						253	30300	50				
MHA 1/92/850m	850	1.25	0.24		835	1010	1.5		16.1	2880	4.9	-11.2	-75		
Noormarkku															
PO-43	503	1.06	0.13	0.71871	9320	4870	104		155	26200	41	-11.3	-86	-44.1	-288
Palmottu															
R387	264	insuf.	0.78												
Pori															
301m	301	1.72	0.53		28100	8573	80		475	57100	92	-8.1	-54	-36.6	-372
420m	420	2.04	0.44		26200	6860	68		574	64000	93	-8.3	-46		
Ylivieska															
YL 313/92	550	0.89	0.01		6300	12400	4470		450	42300	66	-13.4	-30	-45.5	-340

* $\delta^{81}Br$ value from Shouakar-Stash et al. (*2005b*)
**Other chemical and isotopic data are previously published
***Indicates new $\delta^{37}Cl$ or $^{87}Sr/^{86}Sr$ analysis
****T3-27377-84?

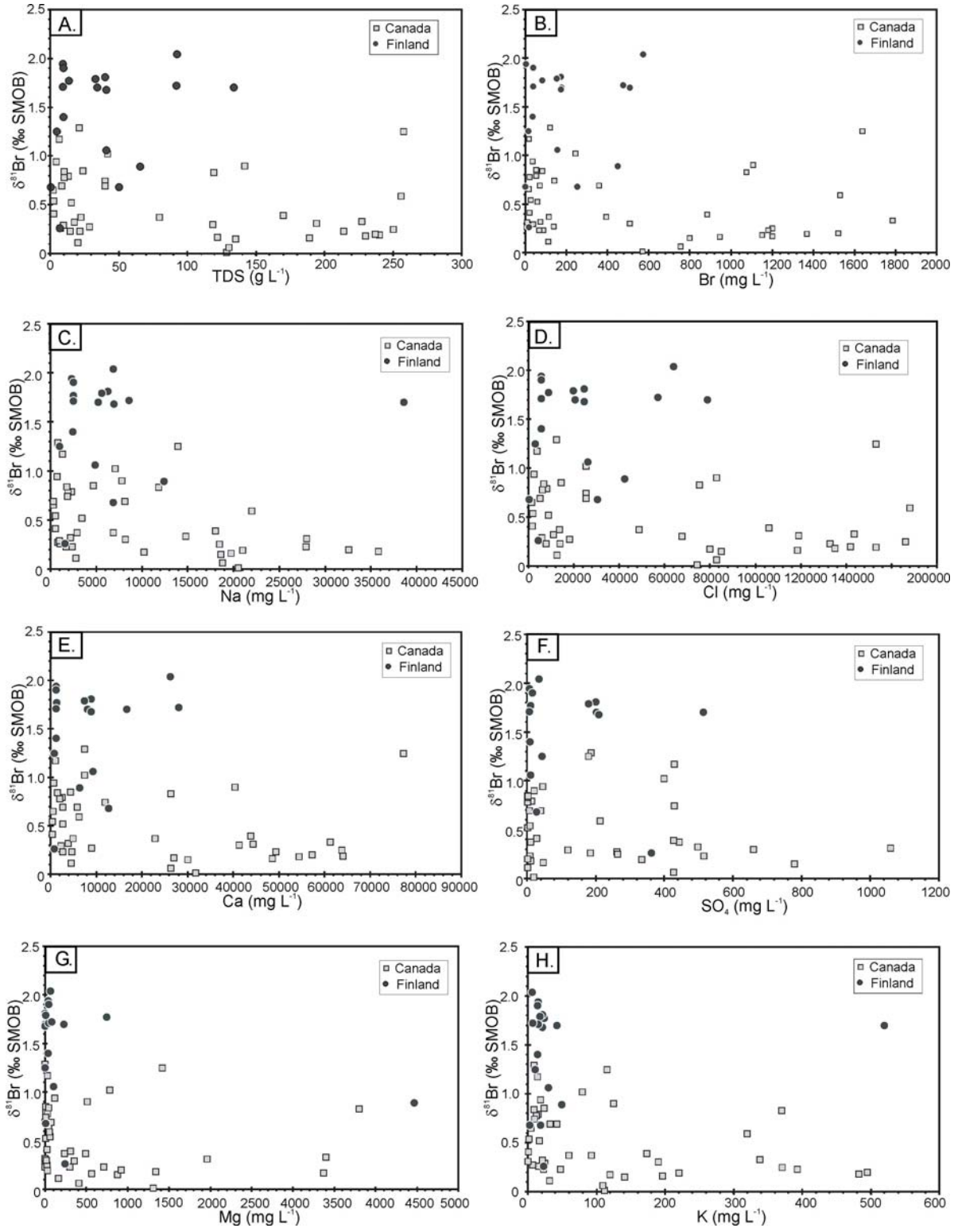

Figure D-1. δ^{81}Br vs. (A) TDS, (B) Br, (C) Na, (D) Cl, (E), Ca, (F), SO4, (G) Mg, and (H) K for Canadian and Fennoscandian Shield groundwaters.

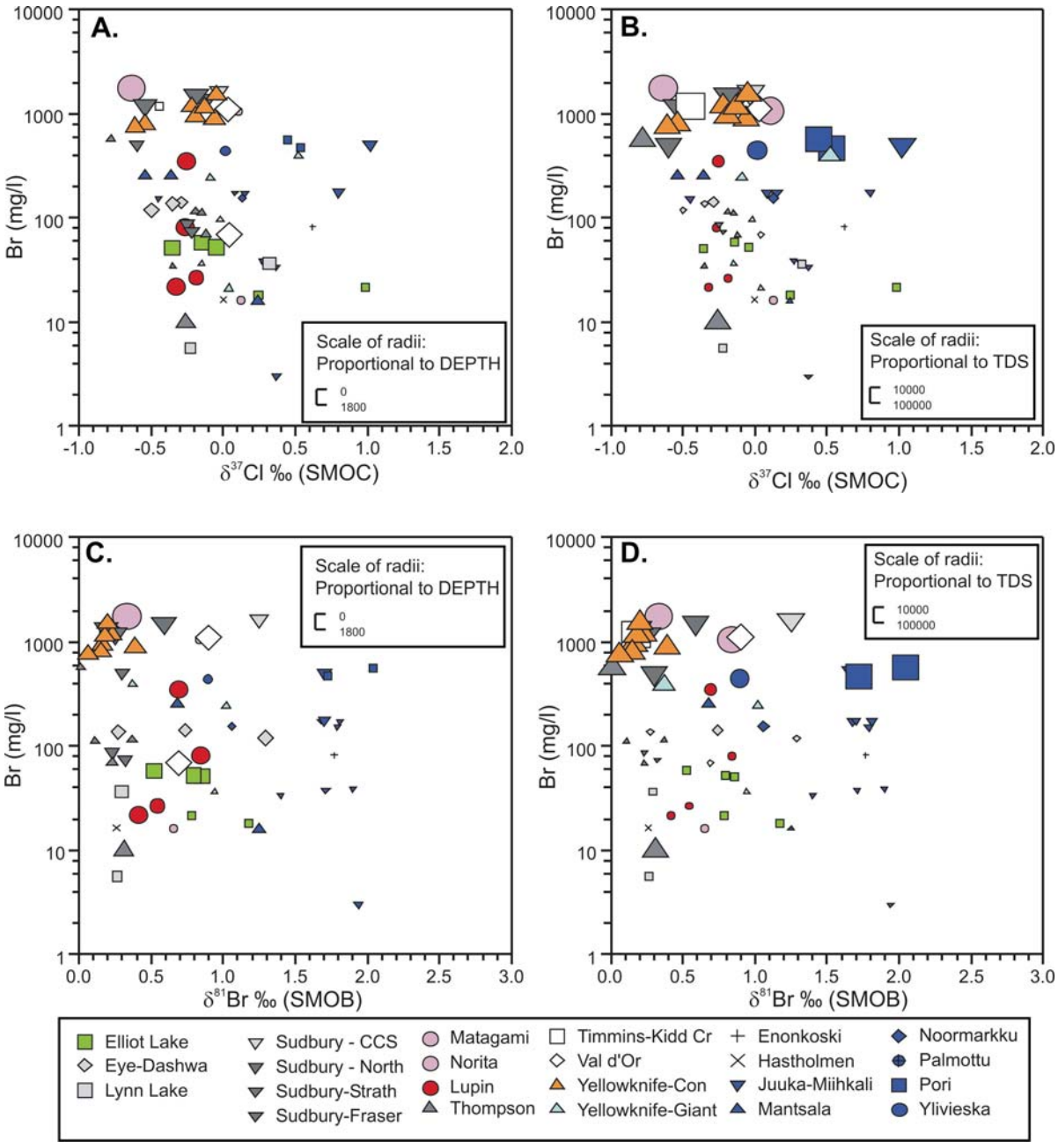

Figure D-2. Br vs. $\delta^{37}Cl$ (A, B) and vs. $\delta^{81}Br$ (C, D) for Canadian and Fennoscandian Shield groundwaters. Symbols are scaled relative to depth in A and C (larger symbols sampled deeper) and relative to TDS in B and D (larger symbols are brines).

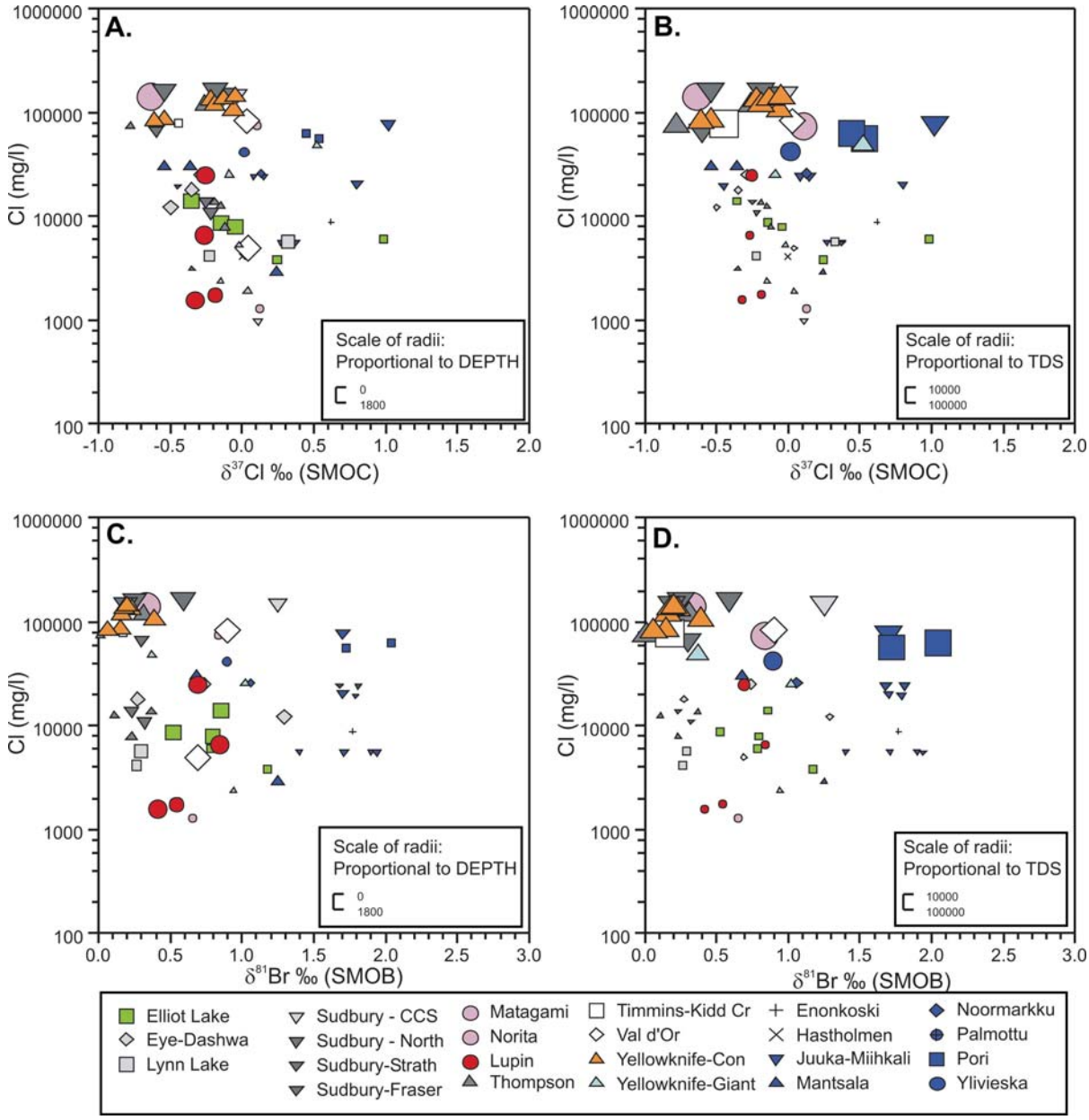

Figure D-3. Cl vs. δ^{37}Cl (A, B) and vs. δ^{81}Br (C, D) for Canadian and Fennoscandian Shield groundwaters. Symbols are scaled relative to depth in A and C (larger symbols sampled deeper) and relative to TDS in B and D (larger symbols are brines).

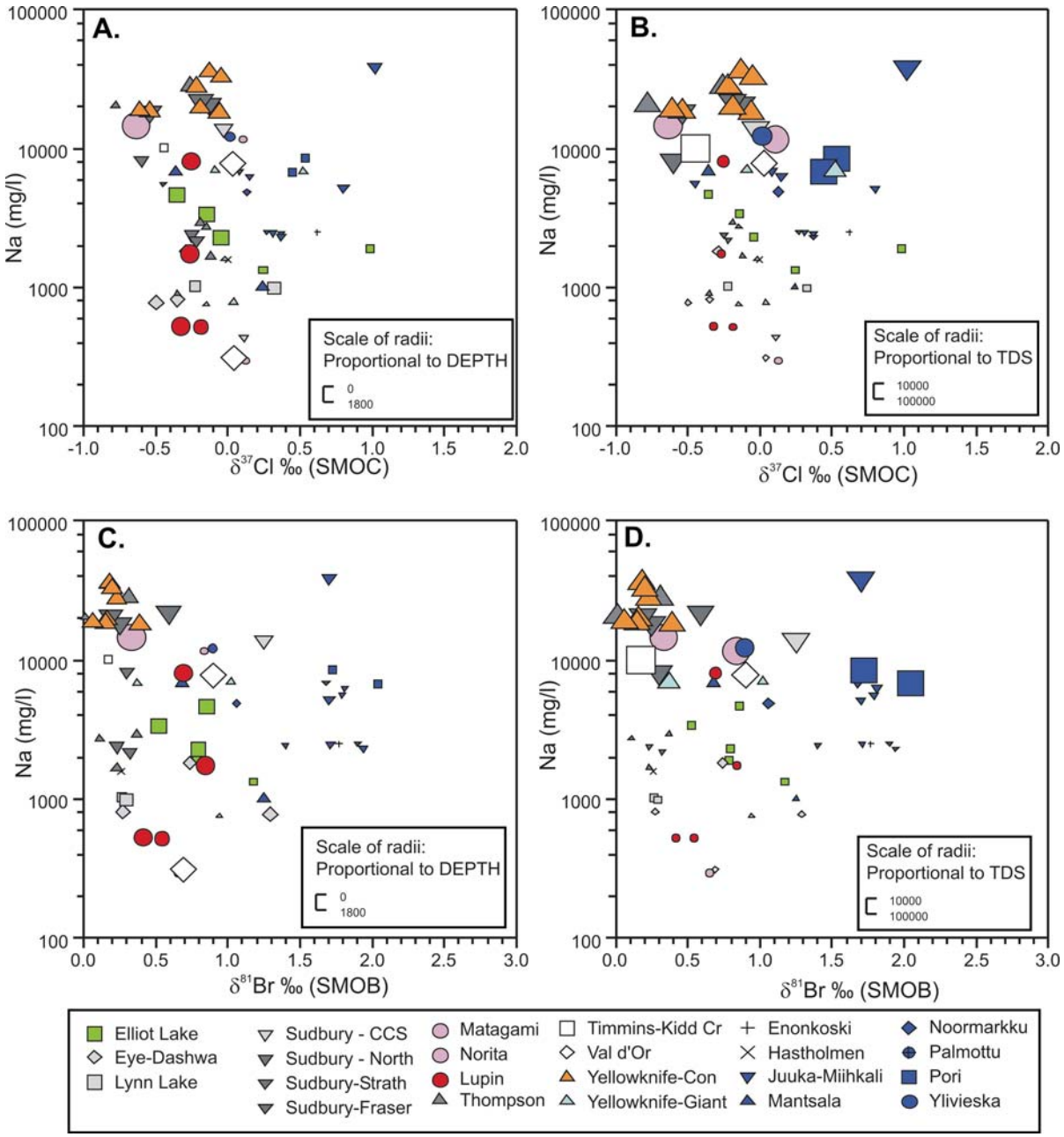

Figure D-4. Na vs. $\delta^{37}Cl$ (A, B) and vs. $\delta^{81}Br$ (C, D) for Canadian and Fennoscandian Shield groundwaters. Symbols are scaled relative to depth in A and C (larger symbols sampled deeper) and relative to TDS in B and D (larger symbols are brines).

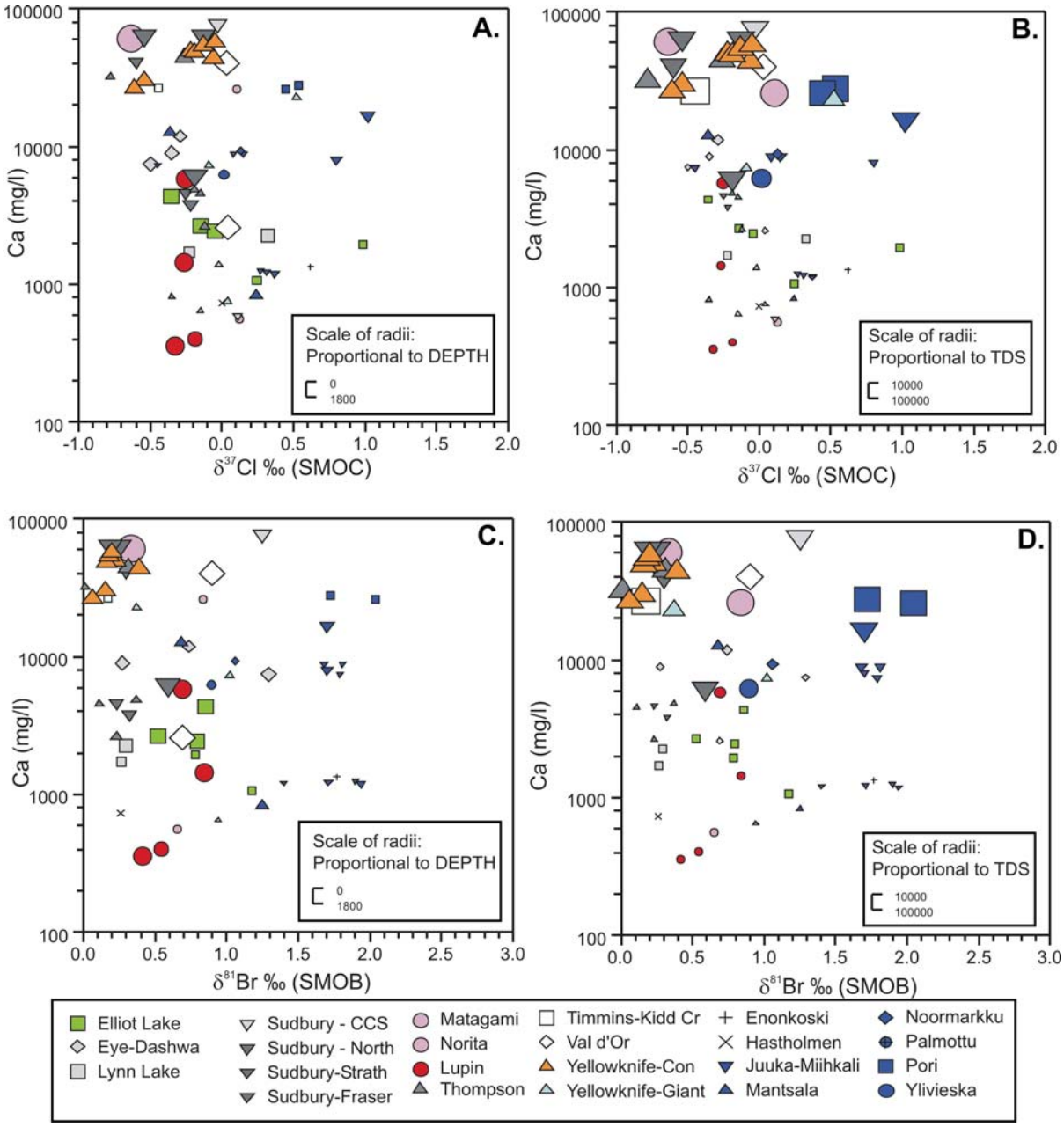

Figure D-5. Ca vs. $\delta^{37}Cl$ (A, B) and vs. $\delta^{81}Br$ (C, D) for Canadian and Fennoscandian Shield groundwaters. Symbols are scaled relative to depth in A and C (larger symbols sampled deeper) and relative to TDS in B and D (larger symbols are brines).

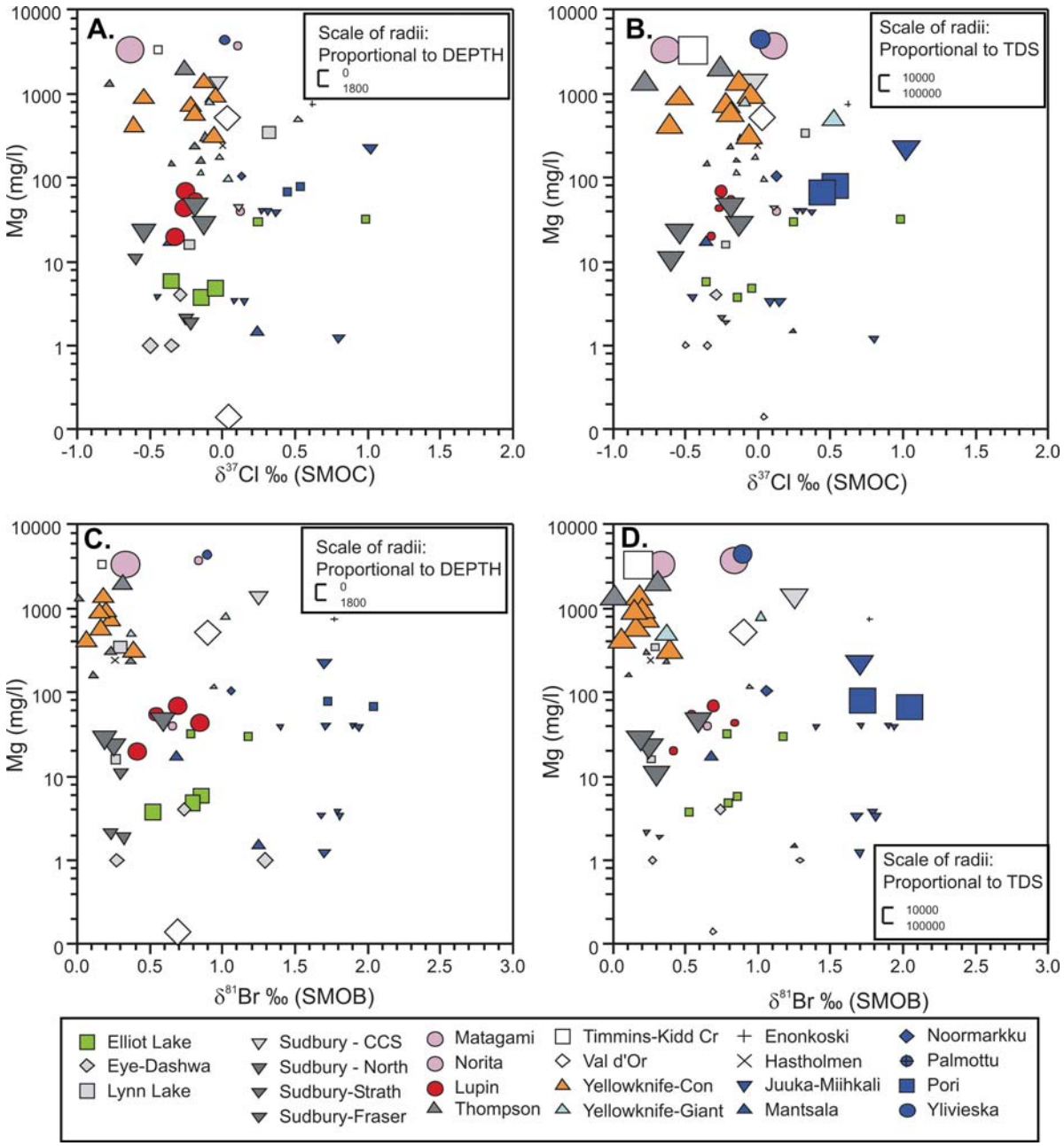

Figure D-6. Mg vs. $\delta^{37}Cl$ (A, B) and vs. $\delta^{81}Br$ (C, D) for Canadian and Fennoscandian Shield groundwaters. Symbols are scaled relative to depth in A and C (larger symbols sampled deeper) and relative to TDS in B and D (larger symbols are brines).

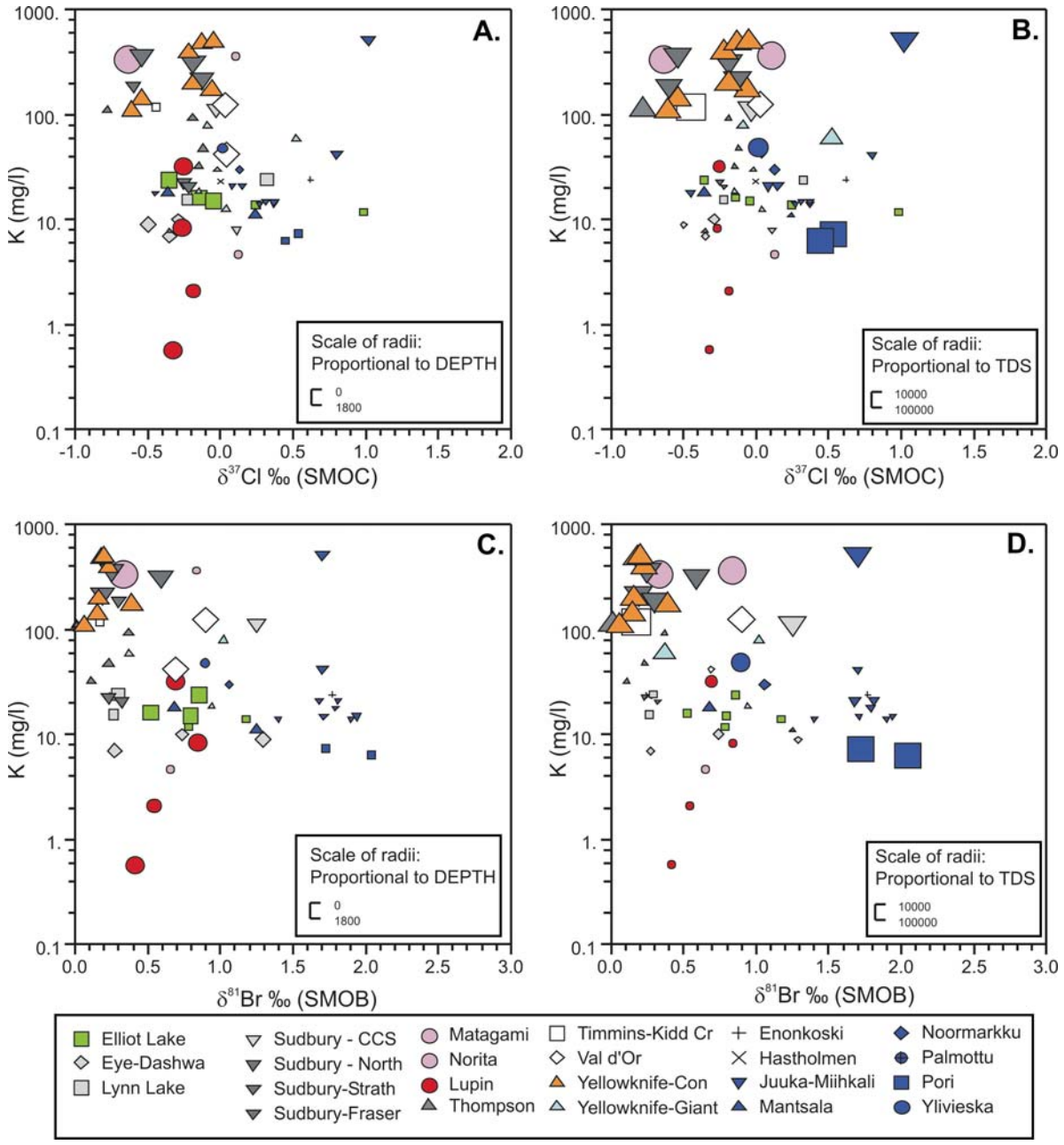

Figure D-7. K vs. $\delta^{37}Cl$ (A, B) and vs. $\delta^{81}Br$ (C, D) for Canadian and Fennoscandian Shield groundwaters. Symbols are scaled relative to depth in A and C (larger symbols sampled deeper) and relative to TDS in B and D (larger symbols are brines).

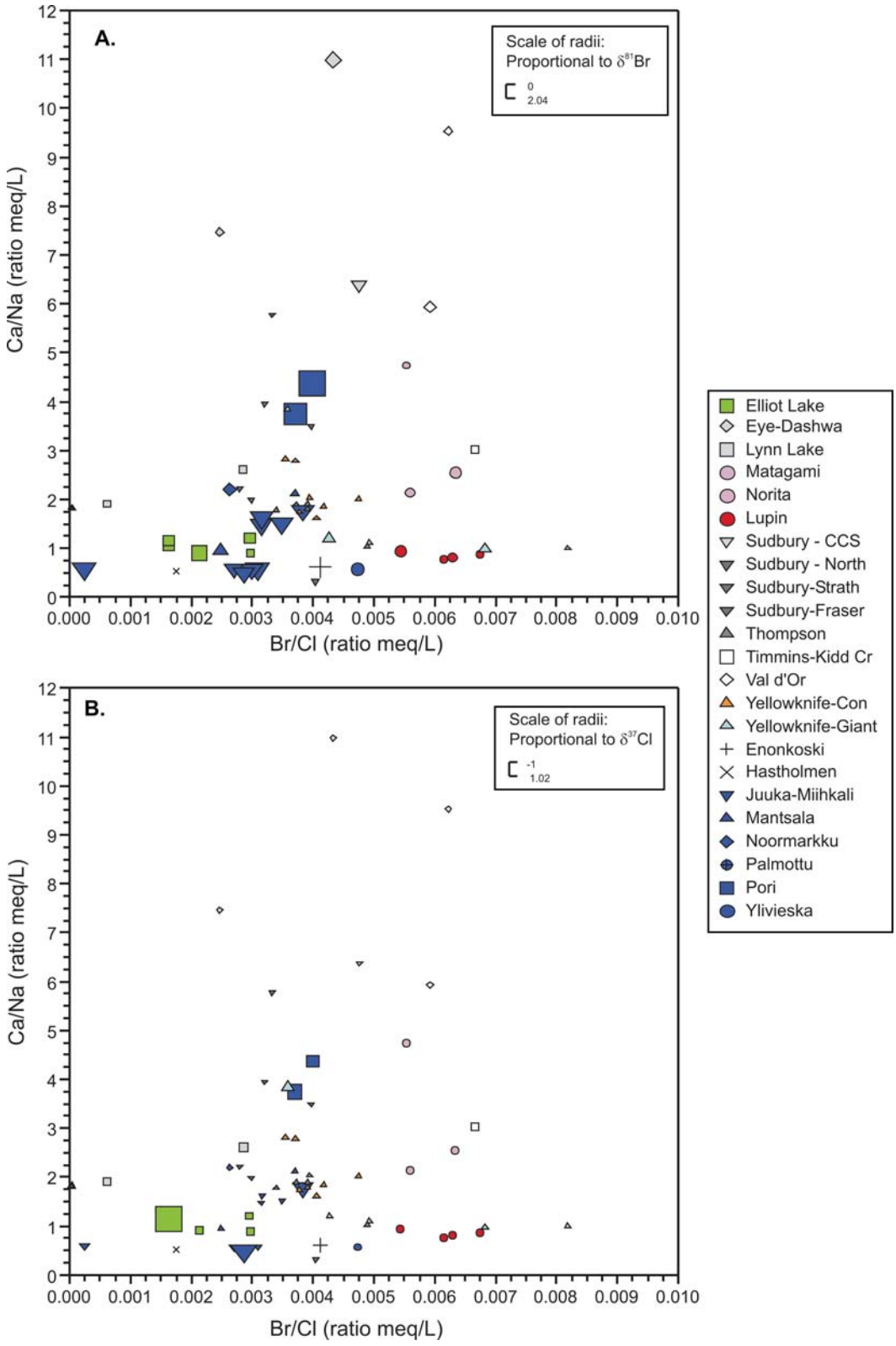

Figure D-8. Ca/Na vs. Br/Cl for Canadian and Fennoscandian Shield groundwaters. Symbol size is relative to δ^{81}Br (A) and δ^{37}Cl (B). Larger symbols represent more enriched samples.

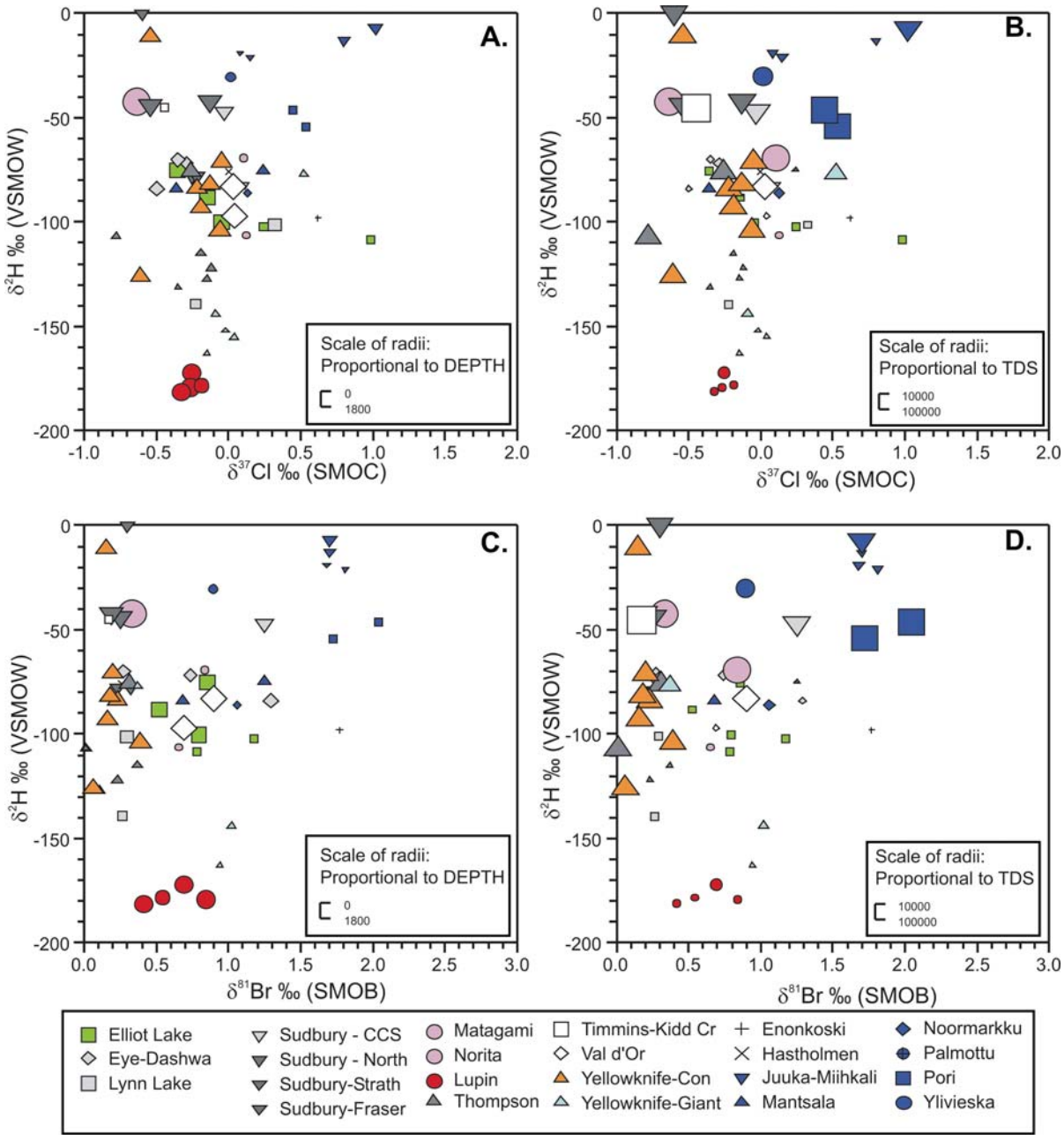

Figure D-9. δ^2H vs. $\delta^{37}Cl$ (A, B) and vs. $\delta^{81}Br$ (C, D) for Canadian and Fennoscandian Shield groundwaters. Symbols are scaled relative to depth in A and C (larger symbols sampled deeper) and relative to TDS in B and D (larger symbols are brines).

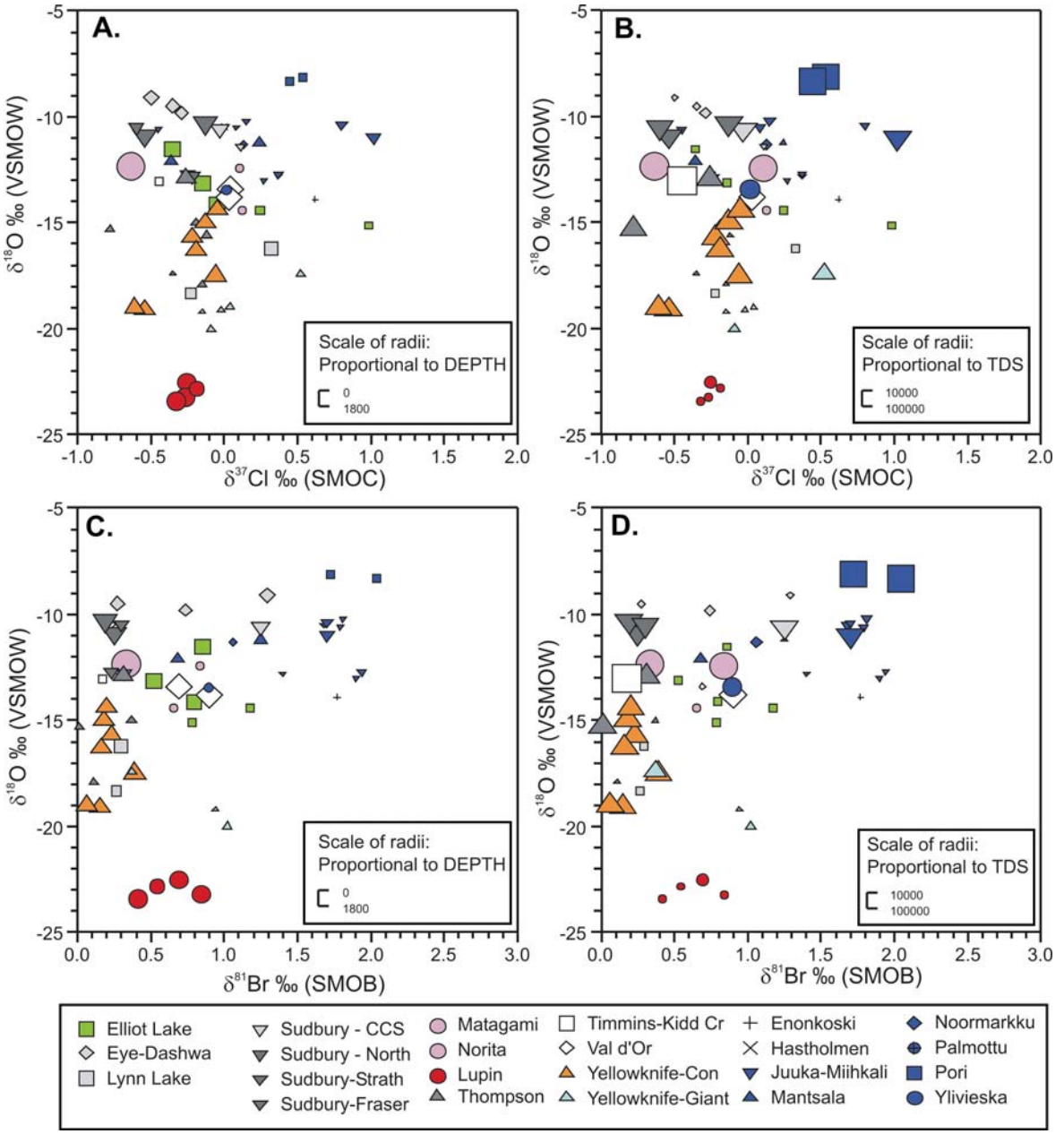

Figure D-10. $\delta^{18}O$ vs. $\delta^{37}Cl$ (A, B) and vs. $\delta^{81}Br$ (C, D) for Canadian and Fennoscandian Shield groundwaters. Symbols are scaled relative to depth in A and C (larger symbols sampled deeper) and relative to TDS in B and D (larger symbols are brines).

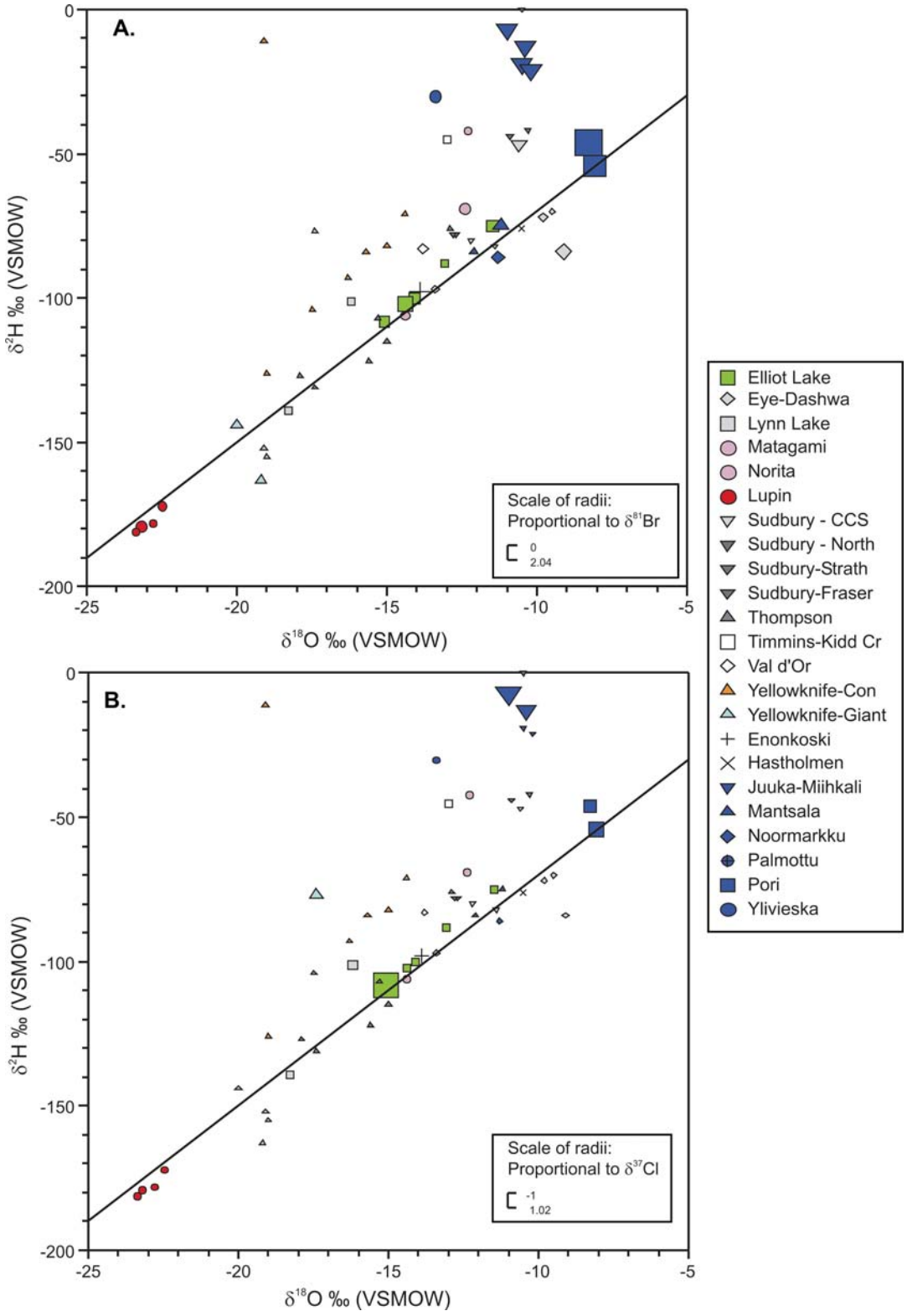

Figure D-11. $\delta^{18}O$ vs. $\delta^{2}H$ for Canadian and Fennoscandian Shield groundwaters. Symbol size is relative to $\delta^{81}Br$ (A) and $\delta^{37}Cl$ (B). Larger symbols represent more enriched samples.

References

ACIA. 2004. *Impacts of a Warming Arctic: Arctic Climate Impact Assessment*. Cambridge University Press, http://www.acia.uaf.edu.

Aiuppa, A., C. Federico, A. Franco, G. Giudice, S. Gurrieri, S. Inguaggiato, M. Liuzzo, A.J.S. McGonigle, M. Valenza. 2005. Emission of bromine and iodine from Mount Etna volcano. *Geochemistry, Geophysics, Geosystems* **6,** 10.1029/2005GC00965.

Alexeev S.V. and L.P. Alexeeva. 2002. Ground ice in the sedimentary rocks and kimberlites of Yakutia, Russia. *Permafrost Periglac. Process.* **13**, 53-59.

Alexeev S. V. and L.P. Alexeeva. 2003. Hydrogeochemistry of the permafrost zone in the central part of the Yakutian diamond-bearing province, Russia. *Hydrogeol. J.* **11**, 574-581.

Anderson, N.J., R. Harriman, D.B. Ryves, S.T. Patrick. 2001. Dominant factors controlling variability in the ionic composition of West Greenland lakes. *Arctic, Antarctic, and Alpine Research* **33,** 418-425.

Andrews, J.N. 1985. The isotopic composition of radiogenic helium and its use to study groundwater movement in confined aquifers. *Chem. Geol.* **49,** 339-351.

Appel, P.W.U. 1997. High bromine contents and low Cl/Br ratios in hydrothermally altered Archaean komatiitic rocks, west Greenland. *Precambrian Res.* **82**, 177-189.

Bada, J.L., C. Bigham, S.L. Miller. 1994. Impact melting of frozen oceans on the early Earth: implications for the origin of life. *PNAS* **91,** 1248-1250.

Bada, J.L. 2004. How life began on Earth: a status report. *Earth and Planetary Science Letters* **226,** 1-15.

Bakermans, C., D.J. McGown, T. Ruskeeniemi, L. Ahonen, J. Telling, C. Boettiger, R. Ho, B. Soffientino, S.A. DiFurio, S.M. Pfiffner, B. Sherwood-Lollar, S. Frape, R. Stotler, L.M. Pratt, R.E. Sloup, T.A. Vishnivetskaya, T.C. Onstott. Microbial sulfur cycling in subpermafrost saline fracture water at the Lupin Gold Mine, Nunavut, Canada. Submitted to *Environmental Microbiology* Feb. 2008.

Ballentine, C.J., R. Burgess, B. Marty. 2002. Tracing fluid origin, transport and interaction in the crust. *Reviews in Mineralogy & Geochemistry,* **47**, 481-538.

Balobaev, V.T. 1991. Geothermometry of permafrost of North Asia. Novosibirsk, Nauka, 192pp. (in Russian).

Bangs, N.L.B., D.S. Sawyer, X. Golovchenko. 1993. Free gas at the base of the gas hydrate zone in the vicinity of the Chile Triple Junction. *Geology* **21,** 905-908.

Banks, D.A., R. Green, R.A. Cliff, B.W.D. Yardley. 2000. Chlorine isotopes in fluid inclusions: determination of the origins of salinity in magmatic fluids. *Geochim. Cosmochim. Acta* **64,** 1785-1789.

Barker, J.F. and S.J. Pollack 1984. The geochemistry and origin of natural gases in Souther Ontario. *Bull. Can. Pet. Geol.* **32,** 313-326.

Battye, N.J. 2002. Noble gases in Canadian Shield groundwters from the Con Mine, Yellowknife, N.W.T. M.Sc. Thesis, University of Ottawa, Ottawa, Ontario, Canada.

Beerling, D.J., M.R. Lomas, M.R. D.R. Gröcke. 2002. On the nature of methane gas-hydrate dissociation during the Toarcian and Aptian oceanic anoxic events. *American Journal of Science* **302,** 28-49.

Bein, A. and A. Arad. 1992. Formation of saline groundwaters in the Baltic region through freezing of seawater during glacial periods. *J. of Hydrol.* **140**, 75-87.

Bentley, H.W, F.M. Phillips, S.N. Davis. 1986. Chlorine-36 in the terrestrial environment. In *Handbook of Environmental Isotope Geochemistry*, eds. P. Fritz and J. –C. Fontes, Elsevier, Amsterdam, **2,** 427-480.

Bernard, B.B., J.M. Brooks and W.M. Sackett. 1976. Natural gas seepage in the Gulf of Mexico. *Earth and Planetary Science Letters* **31,** 48-54.

Berner, U. and P. Bertrand. 1991. Light hydrocarbons in sediments of the Sulu Sea Basin (Site 768): genetic characterization by molecular and stable isotope composition. *In* Silver, E.A., Rangin, C., von Breymann, M.T., et al. (eds.), *Proceedings of Ocean Drilling Program, Scientific Results* **124,** 227-232.

Berner, U. and E. Faber. 1988. Maturity related mixing model for methane, ethane, and propane, based on carbon isotopes. *Org. Geochem*. **13,** 67-72.

Berner, U. and E. Faber. 1993. Light hydrocarbons in sediments of the Nankai accretionary prism (Leg 131, Site 808). In *Proceedings of the Ocean Drilling Program, Scientific Results* **131,** 185-195.

Berndt, M.E., D.E. Allen, W.E. Seyfried, Jr. 1996. Reduction of CO_2 during serpentinization of olivine at 300°C and 500 bar. *Geology* **24**, 351-354.

Berndt, M.E. and W.E. Seyfried, Jr. 1997. Calibration of Br/Cl fractionation during subcritical phase separation of seawater: possible halite at 9 to 10°N East Pacific Rise. *Geochim. Cosmochim. Acta* **61,** 2849-2854.

BGC Engineering Inc. 2005. Permafrost Monitoring Results, High Lake Project, NU. Draft Report prepared for Wolfden Resources Ltd., November 4, 2005.

Biddle, J.F., C.H. House, J.E. Brenchley. 2005. Microbial stratification in deeply buried marine sediment reflects changes in sulfate/methane profiles. *Geobiology* **3,** 287-295.

Blomqvist, R. 1999. *Hydrogeochemistry of Deep Groundwaters in the Central Part of the Fennoscandian Shield*. Report YST-101, -41. Geological Survey of Finland, Nuclear Waste Disposal Research.

Blomqvist, R., T. Ruskeeniemi, J. Kaija, L. Ahonen, M. Paananen, J. Smellie, B. Grundfelt, K. Pedersen, J. Bruno, L. Perez del Villar, E. Cera, K. Rasilainen, P. Pitkanen, J. Suksi, J. Casanova, D. Read, S.K. Frape. 2000. *The Palmottu Natural Analogue Project. Phase II: Transport of Radionuclides in a Natural Flow System at Palmottu.* Final Report, EUR 19611 EN, 174p. European Commission. Nuclear Science and Technology.

Blowes, D.W. and M.J. Logsdon. 1998. Diavik Geochemistry Baseline Report. Prepared for Diavik Diamond Mines Inc.

Blyth, A. 1993. The study of fracture filling calcite in the Fennoscandian and Canadian Shields as an indicator of past thermal and fluid history. M.Sc. Thesis, University of Waterloo, Waterloo, Ontario, Canada.

Blyth, A, S. Frape, R. Blomqvist, P. Nissinen. 2000. Assessing the past thermal and chemical history of fluids in crystalline rock by combining fluid inclusion and isotopic investigations of fracture calcite. *Appl. Geochem.* **15**, 1417-1437.

Blyth, A. 2004. Radioactive waste disposal in the crystalline rock of Scandinavia: case studies of the far-field environment. Ph.D. Dissertation, University of Waterloo, Waterloo, Ontario, Canada.

Blyth, A., Frape, S., Ruskeeniemi, T., and Blomqvist, R. 2004. Origins, closed system formation and preservation of calcites in glaciated crystalline bedrock: evidence from the Palmottu natural analogue site, Finland. *Appl. Geochem.* **19**, 675-686.

Bobrowski, N., G. Hönninger, B. Galle, U. Platt. 2003. Detection of bromine monoxide in a volcanic plume. *Nature* **423,** 273-276.

Boetius, A., K. Ravenschlag, C.J. Schubert, D. Rickert, F. Widdel, A. Gieseke, R. Amann, B.B. Jørgensen, U. Witte, and O. Pfannkuche. 2000. A marine microbial consortium apparently mediating anaerobic oxidation of methane. *Nature* **407,** 623-626.

Bonifacie, M., J.L. Charlou, N. Jendrzejewski, P. Agrinier, J.P. Donval. 2005. Chlorine isotopic compositions of high temperature hydrothermal vent fluids over ridge axis. *Chem. Geol.* **221,** 279-288.

Bonifacie, M., N. Jendrzejewski, P. Agrinier, M. Coleman, F. Pineau, M. Javoy. 2007a. Pyrohydrolysis-IRMS determination of silicate chlorine stable isotope compositions. Applications to oceanic crust and meteorite samples. *Chem Geol.* **242,** 187-201.

Bonifacie, M., C. Monnin, N. Jendrzejewski, P. Agrinier, M. Javoy. 2007b. Chlorine stable isotopic composition of basement fluids of the eastern flank of the Juan de Fuca Ridge (ODP Leg 168). *Earth and Planetary Science Letters* **260,** 10-22.

Borowski, W.S., C.K. Paull, and W. Ussler III. 1996. Marine pore-water sulfate profiles indicate in situ methane flux from underlying gas hydrate. *Geology* **24(7),** 655-658.

Borowski, W.S., C.K. Paull, W. Ussler III. 1997. Carbon cycling within the upper methanogenic zone of continental rise sediments: an example from the methane-rich sediments overlying the Blake Ridge gas hydrate deposits. *Marine Chemistry* **57,** 299-311.

Borowski, W.S., C.K. Paull, W. Ussler III. 1999. Global and local variations of interstitial sulfate gradients in deep-water, continental margin sediments: sensitivity to underlying methane and gas hydrates. *Marine Geology* **159,** 131-154.

Borowski, W.S., T.M. Hoehler, M.J. Alperin, N.M. Rodriguez, C.K. Paull. 2000a. Significance of anaerobic methane oxidation in methane-rich sediments overlying the Blake Ridge gas hydrates. *In*: C.K. Paull, R. Matsumoto, P.J. Wallace, and W.P. Dillon (eds.), *Proceedings of the Ocean Drilling Program, Scientific Results* **164,** 87-99.

Borowski, W.S., N. Cagatay, Y. Ternoi, C.K. Paull. 2000b. Data report: carbon isotopic composition of dissolved CO_2, CO_2 gas, and methane, Blake-Bahama Ridge and Northeast Bermuda Rise, ODP Leg 172. *In* Keigwin, L.D., Rio, D., Acton, G.D., and Arnold, E. (Eds.), *Proceedings of the Ocean Drilling Program, Scientific Results* **172,** 1-16 [Online]. Available from World Wide Web: http://www-odp.tamu.edu/publications/172_SR/VOLUME/CHAPTERS/SR172_03.PDF>

Borowski, W.S. 2004. A review of methane and gas hydrates in the dynamic stratified system of the Blake Ridge region, offshore southeastern North America. *Chem. Geol.* **205,** 311-346.

Borowski, W.S. 2005. Dissolved sulfide concentration and sulfur isotopic composition of sulfide and sulfate in pore waters, ODP Leg 204, Hydrate Ridge and vicinity, Cascadia margin, offshore Oregon. *In*: A.M. Trehu, G. Bohrmann, M.E. Torres, F.S. Colwell (Eds.) *Proc. ODP, Sci. Results* **204**, 1-13 [Online]. Available from World Wide Web: http://www-odp.tamu.edu/publications/204_SR/VOLUME/CHAPTERS/105.PDF. [Cited 2008-06-27].

Bottinga, Y. 1969. Calculated fractionation factors for carbon and hydrogen isotope exchange in the system calcite-carbon dioxide-graphite-methane-hydrogen-water vapor. *Geochim. Cosmochim. Acta* **33,** 49-64.

Bottomley, D.J., M. Gascoyne, D.C. Kamineni. 1990. The geochemistry, age, and origin of groundwater in a mafic pluton, East Bull Lake, Ontario, Canada. *Geochim. Cosmochim. Acta* **54,** 933-1008.

Bottomley, D.J., D.C. Gregoire, K.G. Raven. 1994. Saline groundwaters and brines in the Canadian Shield: geochemical and isotopic evidence for a residual evaporite brine component. *Geochim. Cosmochim. Acta* **58,** 1483-1498.

Bottomley, D.J., A. Katz, L.H. Chan, A. Starinsky, M. Douglas, I.D. Clark, K.G. Raven. 1999. The origin and evolution of Canadian Shield brines: evaporation or freezing of seawater? New lithium isotope and geochemical evidence from the Slave Craton. *Chem Geol.* **155**, 295-320.

Bottomley, D.J., R. Renaud, T. Kotzer, I.D. Clark. 2002. Iodine-129 constraints on residence times of deep marine brines in the Canadian Shield. *Geology* **30,** 587-590.

Bottomley, D.J., L.H. Chan, A. Katz, A. Starinsky, I.D. Clark. 2003. Lithium isotope geochemistry and origin of Canadian Shield brines. *Ground Water* **41,** 847-856

Bottomley, D.J. and I.D. Clark. 2004. Potassium and boron co-depletion in Canadian Shield brines: evidence for diagenetic interactions between marine brines and basin sediments. *Chem. Geol.* **203,** 225-236.

Bottomley, D.J., I.D. Clark, N. Battye, T. Kotzer. 2005. Geochemical and isotopic evidence for a genetic link between Canadian Shield brines, dolomitization in the Western Canada Sedimentary Basin, and Devonian calcium-chloridic seawater. *Can. J. Earth Sci.* **42,** 2059-2071.

Brady, H.T. and B. Batts. 1981. Large salt beds on the surface of the Ross Ice Shelf, near Black Island, Antarctica. *Journal of Glaciology* **27**, 11-18.

Brimblecombe, P., S.L. Clegg, T.D. Davies, D. Shooter, and M. Tranter. 1987. Observations of the preferential loss of major ions from melting snow and laboratory ice. *Wat. Res.* **21**, 1279-1286.

Brooks, J.M., L.A.Barnard, L.A., D.A. Wiesenburg, M.C. Kennicutt, K.A. Kvenvolden. 1983. Molecular and isotopic compositions of hydrocarbons at Site 533, Deep Sea Drilling Project Leg 76. *In*: Sheridan, R.E., Gradstein, F.M., et al. (Eds), *Initial Reports, DSDP* **76,** 377-389.

Brooks, J.M., H.B. Cox, W.R. Bryant, M.C. Kennicutt II, R.G. Mann, and T.J. McDonald. 1985. Association of gas hydrates and oil seepage in the Gulf of Mexico. *Advances in Organic Geochemistry* **10,** 221-234.

Bryant, J.G. 1995. 37/35 chlorine isotope relationship to other halides, inorganic geochemistry and geology in groundwaters of the Fennoscandian and Canadian Shields. MSc Project, Dept. of Earth Sciences, University of Waterloo.

Bucher, K. and I. Stober. 2000. Composition of groundwaters in the crystalline basement. In *Hydrogeology of Crystalline Rocks*, I. Stober and K. Bucher (eds), Kluwer Academic Publishers, Water Science and Technology Library **34,** 141-175.

Buffett B. and D. Archer. 2004. Global inventory of methane clathrate: sensitivity to changes in the deep ocean. *Earth and Planetary Science Letters* **227,** 185-199.

Bullis, H.R., Hureau, R.A., and Penner, B.D. 1994. Distribution of gold and sulfides at Lupin, Northwest Territories. *Econ. Geol.* **89**, 1217-1227.

Bureau, H., H. Keppler, N. Métrich. 2000. Volcanic degassing of bromine and iodine: experimental fluid/melt partitioning data and applications to stratospheric chemistry. *Earth Planet. Sci. Lett.* **183,** 51-60.

Burke, R.A., W.M. Sackett, J.M. Brooks. 1986. Hydrogen and carbon isotope compositions of methane from deep sea drilling project Site 618, Orca Basin. *In* Bouma, AH, Coleman, JM, Meyer, AW, et al. (eds.), *Initial Reports of Deep Sea Drilling Project, Leg* **96,** 777-780.

Burke, R.A., Jr. 1993. Possible influence of hydrogen concentration on microbial methane stabe hydrogen isotopic composition. *Chemosphere* **26,** 55-67.

Burn, C.R. 2002. Tundra lakes and permafrost, Richards Island, western Arctic coast, Canada. *Can. J. Earth Sci*. **39**, 1281-1298.

Burt, T.P. and P.J. Williams. 1976. Hydraulic conductivity in frozen soils. *Earth Surf. Processes* **1,** 349-360.

Burton, H.R. 1981. Chemistry, physics and evolution of Antarctic saline lakes: a review. *Hydrobiologia* **82**, 339-362.

Camarda, M., S. De Gregorio, R. Favara, S. Gurrieri. 2007. Evaluation of carbon isotope fractionation of soil CO_2 under an advective-diffusion regimen: a tool for computing the isotopic composition of unfractionated deep source. *Geochim. Cosmochim. Acta* **71,** 3016-3027.

Capo, R.C. and D.J. DePaolo. 1990. Seawater strontium isotopic variations from 2.5 million years ago to the present. *Science* **249,** 51-55.

Carlson, C.A., F.M. Phillips, D. Elmore, H.W. Bentley. 1990. Chlorine-36 tracing of salinity sources in the Dry Valleys of Victoria Land, Antarctica. *Geochimica et Cosmochimica Acta* **54**, 311-318.

Cary, J.W. and H.F. Mayland. 1972. Salt and water movement in unsaturated frozen soil. *Soil Sci. Soc. Am. Proc.* **6,** 549-555.

Cecil, L.D. 2000. Origin of Chlorine-36 in the eastern Snake River Plain aquifer, Idaho: Implications for describing ground water contamination near a nuclear facility. Ph.D. Dissertation, University of Waterloo, Waterloo, Ontario, Canada.

Cerling, T.E., D.K. Solomon, J. Quade, J.R. Bowman. 1991. On the isotopic composition of carbon in soil carbon dioxide. *Geochemica et Cosmochimica Acta*, **55,** 3403-3405.

Chand, S. and T.A. Minshull. 2003. Seismic constraints on the effects of gas hydrate on sediment physical properties and fluid flow: a review. *Geofluids* **3(4),** 275-289.

Channer, D.M.DeR., C.E.J. de Ronde, E.T.C. Spooner. 1997. The Cl^--Br^--I^- composition of ~3.23 Ga modified seawater: implications for the geological evolution of ocean halide chemistry. *Earth Planet. Sci. Lett.* **150,** 325-335.

Chiaradia, M., D. Banks, R. Cliff, R. Marschik, A. de Haller. 2006. Origin of fluids in iron oxide-copper-gold deposits: constraints from $\delta^{37}Cl$, $^{87}Sr/^{86}Sr_i$ and Cl/Br. *Miner. Deposita* **41,** 565-573.

Clark, I. and P. Fritz. 1997. *Environmental Isotopes in Hydrogeology*. Lewis Publishers: Boca Raton, 328p.

Clark, I.D., R. Matsumoto, S.R. Dallimore, B. Lowe, and J. Loop. 1999. Isotope constraints on the origin of pore waters and salinity in the permafrost and gas hydrate core intervals of the JAPEX/JNOC/GSC Mallik 2L-38 gas hydrate research well. In *Scientific Results from JAPEX/JNOC/GSC Mallik 2L-38 Gas Hydrate Research Well, Mackenzie Delta, Northwest Territories, Canada,* (ed.) S.R. Dallimore, T. Uchida, and T.S. Collett. *Geological Survey of Canada Bulletin* **544,** 177-188.

Clark, I.D., M. Douglas, K. Raven, and D. Bottomley. 2000. Recharge and preservation of Laurentide glacial melt water in the Canadian Shield. *Ground Water* **5,** 735-742.

Claypool, G.E., B.J. Presley, and I.R. Kaplan. 1973. Gas analyses in sediment samples from Legs 10, 11, 13, 14, 15, 18, and 19. *In*: J.S. Creager, D.W. Scholl, et al. (eds), *Initial Reports of the Deep Sea Drilling Project* **19,** 879-884.

Claypool, G.E. and I.R. Kaplan. 1974. The origin and distribution of methane in marine sediments. *In* I.R. Kaplan. (Ed.), Natural Gases in Marine Sediments. Plenum, New York, p. 99-139.

Claypool, G.E. and C.N. Threlkeld. 1983. Anoxic diagenesis and methane generation in sediments of the Blake Outer Ridge, Deep Sea Drilling Project Site 533, Leg 76. *In*: R.E. Sheridan, F.M. Gradstein, et al. (Eds), *Initial Reports, DSDP* **76,** 391-402.

Claypool, G.E., C.N. Threlkeld, P.N. Mankiewicz, M.A. Arthur, T.F. Anderson. 1985. Isotopic composition of interstitial fluids and origin of methane in slope sediment of the Middle America Trench, Deep Sea Drilling Project, Leg 84. *in* R. von Huene, J. Aubouin, et al. (eds), *Initial Reports, DSDP* **84,** 683-691.

Claypool, G.E., A.K. Vuletich, C. Rennison. 2000. Data report: Carbon isotopic composition of inorganic carbon and methane dissolved in pore waters at Sites 1071, 1072, and 1073. *In* N. Christie-Blick, J.A. Austin Jr., and M.J. Malone. (Eds.), *Proceedings of the Ocean Drilling Program, Scientific Results*, **174A,** 1-7 [Online]. Available from WWW: http://www-odp.tamu.edu/publications/174A_SR/Volume/CHAPTERS?SR174A01.PDF [Cited 2007-01-29]

Claypool, G.E., A.V. Milkov, Y.-J. Lee, M.E. Torres, W.S. Borowski, H. Tomaru. 2006. Microbial methane generation and gas transport in shallow sediments of an Accretionary Complex, Southern Hydrate Ridge (ODP Leg 204), Offshore Oregon, USA. *In*: A.M. Tréhu, G. Bohrmann, M.E. Torres, and F.S. Colwell, (Eds). *Proceedings of the Ocean Drilling Program, Scientific Results* **204,** 1-52 [Online]. Available from World Wide Web: <http://www-odp.tamu.edu/publications/204_SR/VOLUME/CHAPTERS/113.PDF>. [Cited 2007-02—08].

Clifford, S.M. 1993. A model for the hydrologic and climatic behavior of water on Mars. *J. Geophys. Res.* **98**, 10973-11016.

Coleman, D.D., J.B. Risatti, M. Schoell. 1981. Fractionation of carbon and hydrogen isotopes by methane-oxidizing bacteria. *Geochim. Cosmochim. Acta* **45,** 1033-1037.

Collett, T.S., K.A. Kvenvolden, L.B. Magoon. 1990. Characterization of hydrocarbon gas within the stratigraphic interval of gas-hydrate stability on the North Slope of Alaska, U.S.A. *Appl. Geochem.* **5,** 279-287.

Collett, T.S. 1992. Potential of gas hydrates outlines. *Oil and Gas Journal* **9025,** 84-87.

Collett, T.S. 1993. Natural gas hydrates of the Prudhoe Bay and Kuparuk River area, North Slope, Alaska. *AAPG Bull*. **77,** 793-812.

Collett, T.S. 1994. Permafrost associated gas hydrate accumulations. *Annals of the New York Academy of Sciences* **715,** 247-269.

Collett, T.S. and G.D. Ginsburg. 1998. Gas hydrates in the Messoyakha Gas Field of the West Siberian Basin – a re-examination of the geologic evidence. *Int. J. of Offshore and Polar Eng.* **8,** 22-29.

Collett, T.S. and S.R. Dallimore. 1999. Hydrocarbon gases associated with permafrost in the Mackenzie Delta, Northwest Territories, Canada. *Appl. Geochem.* **14,** 607-620.

Collett, T.S., K.A. Kvenvolden, L.B. Magoon. 1990. Characterization of hydrocarbon gas within the stratigraphic interval of gas-hydrate stability on the North Slope of Alaska, U.S.A. *Appl. Geochem.* **5,** 279-287.

Collett, T.S. and M.W. Lee. 2005. Electrical-resistivity well-log analysis of gas hydrate saturations in the JAPEX/JNOC/GSC et al. Mallik 5L-38 gas hydrate production research well. In *Scientifice Results from the Mallik 2002 Gas Hydrate Production Research Well Program, Mackenzie Delta, Northwest Territories, Canada*, S.R. Dallimore and T.S. Collett (eds.). *Geological Survey of Canada, Bulletin* **585**, 8p.

Collett, T.S., R.E. Lewis, S.R. Dallimore. 2005. JAPEX/JNOC/GSC et al. Mallik 5L-38 gas hydrate production research well downhole well-log and core montages. *In Scientifice Results from the Mallik 2002 Gas Hydrate Production Research Well Program, Mackenzie Delta, Northwest Territories, Canada*, (eds.) S.R. Dallimore and T.S. Collett. *Geological Survey of Canada, Bulletin* **585**, 23p.

Cooke, R.U. and I.J. Smalley. 1968. Salt weathering in deserts. *Nature* **220**, 1226-1227.

Craig, H. 1961. Isotopic variations in meteoric waters. *Science* **133,** 1833-1834.

Craig, H. and B. Hom. 1968. Relationships of deuterium, oxygen-18, and chlorinity in the formation of sea ice. *Trans. Am. Geophys. Union* **49,** 216-217.

Cragin, J.H., A.J. Gow, A. Kovacs. 1986. Chemical fractionation of brine in the McMurdo Ice Shelf, Antarctica. *Journal of Glaciology* **32**, 307-313.

Cranston, R.E. 1999. Pore-water geochemistry, JAPEX/JNOC/GSC Mallik 2L-38 gas hydrate research well. In *Scientific Results from JAPEX/JNOC/GSC Mallik 2L-38 Gas Hydrate Research Well, Mackenzie Delta, Northwest Territories, Canada,* (ed.) S.R. Dallimore, T. Uchida, and T.S. Collett. *Geological Survey of Canada Bulletin* **544,** 165-175.

Criss, R.E. 1999. Principles of stable isotope distribution. New York, Oxford University Press, 254pp.

Cumberland Resources Ltd. 2005. Meadowbank Gold Project, Baseline Physical Ecosystem Report. 68p.

Dallimore, S.R. and T.S. Collett. 1995. Intrapermafrost gas hydrates from a deep core hole in the Mackenzie Delta, Northwest Territories, Canada. *Geology* **23(6)**,527-530.

Dallimore, S.R., T. Uchida, T.S. Collett. (eds) 1999a. Scientific results from JAPEX/JNOC/GSC Mallik 2L-38 Gas Hydrate Research Well, Mackenzie Delta, Northwest Territories, Canada. *Geological Survey of Canada Bulletin* **544**.

Dallimore, S.R., T. Uchida, T.S. Collett. 1999b. Overview of science program, JAPEX/JNOC/GSC Mallik 2L-38 gas hydrate research well. *In* Scientific Results from the JAPEX/JNOC/GSC Mallik 2L-38 Gas Hydrate Research Well, Mackenzie Delta, Northwest Territories, Canada, (eds.) S.R. Dallimore, T. Uchida, and T.S. Collett. *Geological Survey of Canada Bulletin* **544**, p. 11-17.

Dallimore, S.R. and Collett, T.S. (eds) 2005. Scientific Results from the Mallik 2002 Gas Hydrate Production Research Well Program, Mackenzie Delta, Northwest Territories, Canada. *Geological Survey of Canada Bulletin* **585**.

Dansgaard, W. 1964. Stable isotopes in precipitation. *Tellus* **16,** 436-468.

Davidson, D.W., D.G. Leaist, R. Hesse. 1983. Oxygen-18 enrichment in the water of a clathrate hydrate. *Geochim. Cosmochim. Acta* **47**, 2293-2295.

de Graaf, W., P. Wellsbury, R.J. Parkes, T.E. Cappenberg. 1996. Comparison of acetate turnover in methanogenic and sulfate-reducing sediments by radiolabeling and stable isotope labeling and by use of specific inhibitors: evidence for isotopic exchange. *Appl. Environ. Microbiol.* **62,** 772-777.

Desaulniers, D.E., J.A. Cherry, P. Fritz. 1981. Origin, age, and movement of porewater in argillaceous Quaternary deposits at four sites in southwestern Ontario. *J. Hydrol.* **50,** 231-257.

Desaulniers, D.E., R.S. Kaufmann, J.A. Cherry, H.W. Bentley. 1986. ^{37}Cl-^{35}Cl variations in a diffusion-controlled groundwater system. *Geochim Comochim. Acta* **50**, 1757-1764.

Des Marais, D.J., J.H. Donchin, N.L. Nehring, A.H. Truesdell. 1981. Molecular carbon isotopic evidence for the origin of geothermal hydrocarbons. *Nature* **292,** 826-828.

Deyhle, A., A. Kopf, S. Frape, R. Hesse. 2003. Evidence for fluid flow in the Japan Trench foearc using isotope geochemistry (Cl, Sr, B); results from ODP Site 1150. *The Island Arc* **13,** 258-270.

Dicken, R.C., S.K. Frape, P. Fritz, R.E.J. Leech, R. Pearson. 1984. Groundwater chemistry to depths of 1000m in low permeability granitic rocks of the Canadian Shield. *International Groundwater Conference on Groundwater Resources Utilization and Contaminant Hydrogeology, Proceedings* **2,** 357-371.

Dickens, G.R., C.K. Paull, P. Wallace and the ODP Leg 164 Scientific Party. 1997. Direct measurement of in situ methane quantities in a large gas-hydrate reservoir. *Nature* **385,** 427-428.

Dickens, G.R. and B.M. Kennedy. 2000. Noble gas in methane hydrate from the Blake Ridge. *In*: Paull, C.K., Matsumoto, R., Wallace, P.J., and Dillon, W.P. (eds.), *Proceedings of the Ocean Drilling Program, Scientific Results* **164,** 165-170.

Dickens, G.R. 2001. Modeling the global carbon cycle with a gas hydrate capacitor: significance for the latest Paleocene Thermal Maximum. In: *Natural Gas Hydrate: Occurrence, Distribution, and Detection*, Geophysical Monograph 124, 19-38.

Dietz, R.S. 1964. Sudbury structure as an astrobleme. *J. Geol.* **72,** 412-434.

Doig, F. 1994. Bacterial methanogenesis in Canadian Shield groundwaters. M.Sc. Thesis, University of Toronto, Toronto, Ontario.

Douglas, M.C. 1997. Mixing and temporal variation in the groundwater flow system at the Con Mine, Yellowknife, N.W.T., Canada: An analogue for a radioactive waste repository. M.Sc. Thesis, University of Ottawa, Ottawa, Ontario.

Douglas, M., I.D. Clark, K. Raven, D. Bottomley. 2000. Groundwater mixing dynamics at a Canadian Shield mine. *J. Hydrol.* **235,** 88-103.

Douglas, M.S.V. and J.P. Smol. 1994. Limnology of high arctic ponds (Cape Herschel, Ellesmere Island, N.W.T.). *Arch. Hydrobiol.* **131,** 401-434.

Dutkiewicz, A., J. Ridley, R. Buick. 2003. Oil-bearing CO2-CH4-H2O fluid inclusions: oil survival since the Palaeoproterozoic after high temperature entrapment. *Chem. Geol.* **194**, 51-79.

Dyke, A.S., J.T. Andrews, P.U. Clark, J.H. England, G.H. Miller, J. Shaw, J.J. Veillette. 2002. The Laurentide and Innuitian ice sheets during the Last Glacial Maximum. *Quat. Sci. Rev.* **21,** 9-31.

Dyke, A.S. and V.K. Prest. 1987. Late Wisconsinan and Holocene history of the Laurentide Ice Sheet. *Géographie Physique et Quaternaire* **41,** 237-263.

Eastoe, C.J., J.A. Guilbert, R.S. Kaufmann. 1989. Preliminary evidence for fractionation of stable chlorine isotopes in ore-forming hydrothermal systems. *Geology* **17,** 285-288.

Eastoe, C.J. and J.M. Guilbert. 1992. Stable chlorine isotopes in hydrothermal processes. *Geochim. Cosmochim. Acta* **56,** 4247-4255.

Eastoe, C.J. and T.M. Peryt. 1999. Stable chlorine isotope evidence for non-marine chloride in Badenian evaporites, Carpathian mountain region. *Terra Nova* **11**, 118-123.

Eastoe, C.J., A. Long, L.S. Knauth, L.P. 1999. Stable chlorine isotopes in the Palo Duro Basin, Texas: evidence for preservation of Permaian evaporite brines. *Geochim. Cosmochim. Acta* **63,** 1375-1382.

Eastoe, C.J., A. Long, L.S. Land, J.R. Kyle. 2001. Stable chlorine isotopes in halite and brine from the Gulf Coast Basin: brine genesis and evolution. *Chem. Geol.* **176,** 343-360.

Eastoe, C.J., T.M. Peryt, O.Y. Petrychenko, S. Geisler-Cussey. 2007. Stable chlorine isotopes in Phanerozoic evaporites. *Appl. Geochem.* **22,** 575-588.

Edmunds, W.M. 1996. Bromine geochemistry of British groundwaters. *Mineralogical Magazine* **60,** 275-284.

Eggenkamp, H.G.M. 1994. The geochemistry of chlorine isotopes. Ph.D. Dissertation, Utrecht University, The Netherlands.

Eggenkamp, H.G.M., J.J. Middleburg, R. Kreulen. 1994. Preferential diffusion of ^{35}Cl relative to ^{37}Cl in sediments of Kau Bay, Halmahera, Indonesia. *Chem. Geol.* **116,** 317-325.

Eggenkamp, H.G.M. and R.D. Schuiling. 1995. $\delta^{37}Cl$ variations in selected minerals: a possible tool for exploration. *J. Geochem. Explorartion* **55,** 249-255.

Eggenkamp, H.G.M., R. Kreulen, A.F. Koster van Groos. 1995. Chlorine stable isotope fractionation in evaporites. *Geochim. Cosmochim. Acta* **59,** 5169-5175.

Eggenkamp, H.G.M., A. Pouya, M.L. Coleman. 1997. Can diffusion and shale compaction be causes of chlorine isotope fractionation in basinal brines? *Geofluids Conf. Ext. Abstr.* 322-325.

Eggenkamp, H.G.M. and M.L. Coleman. 2000. Rediscovery of classical methods and their application to the measurement of stable bromine isotopes in natural samples. *Chem. Geol.* **167,** 393-402.

Elliott, J.C., E. Dykes, P.E. Mackie. 1981. Structure of bromapatite and the radius of the bromide ion. *Acta Cryst.* **B37,** 435-438.

Enami, M., J.G. Liou, D.K. Bird. 1992. Cl-bearing amphibole in the Salton Sea geothermal system, California. *Can. Mineral.* **30**, 1077-1092.

Epstein, S. and T.K. Mayeda. 1953. Variation of the ^{18}O content of waters from natural sources. *Geochim. Cosmochim. Acta* **4,** 213-224.

Ericksen, G.E. 1981. Geology and origin of the Chilean nitrate deposits. USGS Prof. Paper 1188, 37p.

Ershov, E.D. and V.S. Yakushev. 1992. Experimental research on gas hydrate decomposition in frozen rocks. *Cold Regions Science and Technology* **20**, 147-156.

Espley, G.H. 1969. Experience with permafrost in gold mining. In: *Proceedings of the 3rd Canadian Conference on Permafrost, 14-15 Jan, 1969*, 59-64.

Ethier, A., I.D. Clark, S.R. Dallimore, R. Matsumoto, P. Middlestead. 2005. High-resolution isotope geochemistry of the gas hydrate-free gas transition in the JAPEX/JNOC/GSC et al. Mallik 5L-38 gas hydrate production research well. In *Scientific Results from the Mallik 2002 Gas Hydrate Production Research Well Program, Mackenzie Delta, Northwest Territories, Canada*, (ed.) S.R. Dallimore and T.S. Collett, *Geological Survey of Canada Bulletin* **585**, 11p.

Faber, E. and J.W. Stahl. 1983. Analytical procedure and results of an isotope geochemical surface survey in an area of the British North Seas. *In* Brooks, J (ed.), Petroleum Geochemistry and Exploration of Europe. *Geological Society Special Publication London* **11,** 51-63.

Fabryka-Martin J., S.N. Davis, D. Elmore. 1987. Applications of 129I and 36Cl to hydrology. *Nucl. Instrum. Meth. Phys. Res.* **B29**, 361-371.

Fabryka-Martin, J., D.O. Whittemore, S.N. Davis, L., P.W. Kubik, P. Sharma. 1991. Geochemistry of halogens in the Milk River aquifer, Alberta, Canada. *Appl. Geochem.* **6,** 447-464.

Feux, A.N. 1980. Experimental evidence against an appreciable isotopic fractionation of methane during migration. *In:* A.G. Douglas, J.R. Maxwell (Eds.), *Advances in Organic Geochemistry, 1979*, Pergamon, Oxford, pp. 725-732.

Fontes, J.-Ch., P. Fritz, D. Louvat, J.-L. Michelot. 1989. Aqueous sulfates from the Stripa groundwater system. *Geochim. Cosmochim. Acta* **53,** 1783-1789.

Ford, R.C. and N.A. Duke. 1993. Concentration of gold during retrograde metamorphism of Archean banded iron formations, Slave Province, Canada. *Can. J. Earth Sci.* **30**, 1566-1581.

Franklyn, M.T. 1987. Sr isotopic composition of saline waters and host rock in the Eye-Daswa Lakes Pluton, Atikokan, Ontario. M.Sc. Thesis, McMaster University, Hamilton, Ontario.

Franklyn, M.T., R.H. McNutt, D.C. Kaqmineni, M. Gascoyne, S.K. Frape. 1991. Groundwater 87Sr/86Sr values in the Eye-Dashwa Lakes Pluton, Canada: evidence of Plagioclase-water reactions. *Chem. Geol.* **86**, 111-122.

Frape, S.K. and P. Fritz. 1981. The Occurrence and Geochemistry of Groundwaters on the Canadian Shield. Report to AECL, project 002-08-18.

Frape, S.K. and P. Fritz. 1982. The chemistry and isotopic composition of saline groundwaters from the Sudbury Basin, Ontario. *Can. J. Earth Sci.* **19,** 645-661.

Frape, S.K., P. Fritz, R.H. McNutt. 1984. Water-rock interaction and chemistry of groundwater from the Canadian shield. *Geochim. Cosmochim. Acta* **48**, 1617-1627.

Frape, S.K. and P. Fritz. 1987. Geochemical trends for groundwater from the Canadian shield. In *Saline Water and Gases in Crystalline Rocks*, Paper 33 (eds. P. Fritz and S.K. Frape). Geological Association of Canada, Memorial University, Newfoundland, pp. 19-38.

Frape, S.K., A.R. Blyth, M.G. Jones, R. Blomqvist, E.L. Tullborg, R.H. McNutt, F. McDermott, M. Ivanovich. 1992. A comparison of calcite fracture mineralogy and geochemistry for the Canadian and Fennoscandian shields. *7th International Symposium on Water Rock Interaction* **1,** 787-791.

Frape, S.K., G. Bryant, R. Blomqvist, T. Ruskeeniemi. 1995. Evidence from stable chlorine isotopes for multiple sources of chloride in groundwaters from crystalline shield environments. In *Symposium on Isotopes in Water Resources Management*. United Nations Educational, Scientific and Cultural Organization, Vienna, Vol. 1, *IAEA-SM-336-24* pp. 19-30.

Frape, S.K., G. Bryant, P. Durance, J.C. Ropchan, J. Doupe, R. Blomqvist, P. Nissinen, J. Kaija. 1998. The source of stable chlorine isotopic signatures in groundwaters from crystalline shield rocks. *Proceedings of the 9th International Symposium on Water Rock Interaction* pp. 223-226.

Frape, S.K., A. Blyth, R. Blomqvist, R.H. McNutt, and M. Gascoyne. 2004. Deep Fluids in the Continents: II. Crystalline Rocks, pp 541-580. In *Surface and Ground Water, Weathering, and Soils* (ed. J.I. Drever), v. 5 *Treatise on Geochemistry* (eds. H.D. Holland and K.K. Turekian), Elsevier – Pergamon, Oxford.

Frape, S.K., R.L. Stotler, T. Ruskeeniemi, L. Ahonen, M. Paannanen, and M.Y. Hobbs, M.Y. 2004b. Hydrogeochemistry of groundwaters at and below the base of the Permafrost at Lupin: Report of Phase II. Ontario Power Generation Report No: 06819-REP-01300-10047-R00.

Frape, S.K., Shouakar-Stash, O., Pačes, T., Stotler, R. 2007. Geochemical and isotopic characteristics of the waters from crystalline and sedimentary structures of the Bohemian Massif. *Water Rock Interaction 12*, Kunming, China (eds: T.D. Bullen and Y Wang), **1**, 727-733.

Freeze, R.A. and J.A. Cherry. 1979. *Groundwater.* Prentice Hall, Englewood Cliffs, NJ. 604p.

Freifeld, B.M., T.C. Onstott, E. Chan, L.M. Pratt, A. Johnson, R. Stotler, B. Holden, S. Frape, S. Pfiffner, S. DiFurio, T. Ruskeeniemi, I. Neill. 2008. Deployment of a deep borehole observatory at the High Lake Project Site, Nunavut, Canada. *Permafrost – 9th International Conference*, **1,** 469-474.

French, H.M. 1996. *The Periglacial Environment*. Addison Wesley Longman, Essex, UK, 2nd Edition, 341p.

Friedman, I. and J.R. O'Neil. 1977. Data of Geochemistry, 6th edition. Chapter KK. Compilation of Stable Isotope Fractionation Factors of Geochemical Interest. *USGS Professional Paper* **440**.

Fritz, P. and S.K. Frape. 1982. Saline groundwaters in the Canadian shield – a first overview. *Chem. Geol.* **36**, 179-190.

Fritz, P., S.K. Frape, M. Miles. 1987. Methane in the crystalline rocks of the Canadian Shield. In *Saline Water and Gases in Crystalline Rocks*. Special Paper 33 (eds. P. Fritz and S.K. Frape). Geological Association of Canada, Memorial University, Newfoundland, pp. 211-223.

Fritz, P. S.K. Frape, R.J. Drimmie, E.C. Appleyard, K. Hattori. 1994. Sulfate in brines in the crystalline rocks of the Canadian Shield. *Geochim. Cosmochim. Acta* **58,** 57-65.

Fuex, N. 1980. Experimental evidence against an appreciable isotopic fractionation of methane during migration. *Organic Chemistry* **12,** 725-732.

Fuge, R. 1979. Water-soluble chlorine in granitic rocks. *Chem. Geol.* **25,** 169-174.

Fumi, F.G. and M.P. Tosi. 1964a. Ionic sizes and born repulsive parameters in the NaCl-type alkali halides – I: The Huggins-Mayer and Pauling forms. *J. Phys. Chem. Solids* **25**, 31-43.

Fyfe, W.S. 1987. The fluid inventory of the crust and its influences on crustal dynamics. In: P. Fritz and S.K. Frape (eds.), *Saline Water and Gases in Crystalline Rocks*, Geological Association of Canada, Special Paper 33, 1-3.

Galimov, E.M. 1967. ^{13}C enrichment of methane during passage through rocks. *Geochemistry International* **4,** 1180-1181.

Galimov, E.M., V.I. Vernadsky, and K.A. Kvenvolden. 1983. Concentrations and carbon isotopic compositions of CH_4 and CO_2 in gas from sediments of the Blake Outer Ridge, Deep Sea Drilling Project Leg 76. *In*: Sheridan, R.E., Gradstein, F.M., et al. (Eds.), *Initial Reports, DSDP* **76,** 403-407.

Galimov, E.M. and I.J. Shabaeva. 1985a. Carbon isotope composition of CH_4 and CO_2 in sediments of the Middle American Trench. *in* von Huene, R., Aubouin, J., et al. (Eds.), *Initial Reports, DSDP* **84,** 693-694.

Galimov, E.M. and I.Y. Shabayeva. 1985b. Carbon isotope compsition of CH_4 and CO_2 in sediments of the Guatemala Trench (DSDP Leg 84). *International Geology Review* **27,** 651-658.

Gamo, T., M. Kastner, U. Berner, J.M. Gieskes. 1993. Carbon isotope ratio of total inorganic carbon in pore waters associated with diagenesis of organic material at Site 808, Nankai Trough. In: *Proceedings of the Ocean Drilling Program, Scientific Results* **131,** 159-163.

Gartner Lee Limited. 2005. Field Report High Lake Project Hydrogeology 2005. Prepared for Wolfden Resources Inc. Ref. GLL 51-025.

Gartner Lee Limited. 2006a. Field Report High Lake Project Hydrogeology 2006. Prepared for Wolfden Resources Inc. Ref. GLL 61-014.

Gartner Lee Limited. 2006b. Appendix A: Hydrogeological Modelling of the Proposed High Lake Mine. Prepared for Wolfden Resources. Reference GLL 41-120.

Gascoyne, M. and H.P. Schwarcz. 1986. Radionuclide migration over recent geologic time in a granititc pluton. *Chem. Geol.* **59,** 75-86.

Gascoyne, M., Davison, C.C., Ross, J.D., Pearson, R. 1987. Saline groundwaters and brines in plutons in the Canadian shield. In *Saline Water and Gases in Crystalline Rocks*. Special Paper 33 (eds. P. Fritz and S.K. Frape). Geological Association of Canada, Memorial University, Newfoundland, pp. 53-68.

Gascoyne, M., J.D. Ross, A. Purdy, S.K. Frape, R.J. Drimmie, P. Fritz, R.N. Betcher. 1989. Evidence for penetration of sedimentary basin brines into an Archean granite of the Canadian Shield. *Proc. 6th Symp. Water-Rock Interaction Malvern, Aug. 1989,* 243-245.

Gascoyne, M. and D.A. Thomas. 1997. Impact of blasting on groundwater composition in a fracture in Canada's Underground Research Laboratory. *J. of Geophys. Res.* **102(B1),** 573-584.

Gascoyne, M. 2000. A review of published literature on the effects of permafrost on the Hydrogeochemistry of bedrock. POSIVA Report 2000-9, 53p.

Gerasimov, I.P. and K.K. Markov. 1941. The glacial period in the territory of the U.S.S.R. In: *Review: The History of Glaciation in Northern Eurasia*, C.C. Nikiforoff (ed.), *Geographical Review* **31**, 343-345.

Gerlach, T.M. 2004. Volcanic sources of tropospheric ozone-depleting trace gases. *Geochemistry, Geophysics, Geosystems* **5,** 10.1029/2004GC000747.

Geusebroek, P.A. and N.A. Duke. 2004. An update on the geology of the Lupin Gold Mine, Nunavut, Canada. *Explor. Mining Geol*. **13,** 1-13.

Gibson, J.J. 1996. Non-steady isotopic methods for estimating lake evaporation: development and validation in arctic Canada. Ph.D. Dissertation, University of Waterloo, Waterloo, Ontario, Canada.

Gibson, J.J., T.W.D. Edwards, T.D. Prowse. 1999. Pan-derived isotopic composition of atmospheric water vapour and its variability in northern Canada. *J. of Hydrol.* **217**, 55-74.

Gibson, J.J. 2002. Short-term evaporation and water budget comparisons in shallow Arctic lakes using non-steady isotope mass balance. *J of Hydrol.* **264**, 242-261.

Gibson, J.J. and T.W.D. Edwards. 2002. Regional water balance trends and evaporation-transpiration partitioning from a stable isotope survey of lakes in northern Canada. *Global Biogeochemical Cycles* **16,** doi: 10.1029/2001GB001839.

Gibson, J.J., S.J. Birks, T.W.D. Edwards. 2008. Global prediction of δA and δ^2H-$\delta^{18}O$ evaporation slopes for lakes and soil water accounting for seasonality. *Global Biogeochemical Cycles* **22,** doi: 10.1029/2007GB002997.

Ginsburg, G.B. and Y.V. Neizvestnov. 1973. Hydrodynamic and hydrochemical processes in the area of the cooling of the earth's crust. In *Proceedings of the 2nd International Conference on Permafrost, Yakutsk, USSR, July 13-28, 1973 – USSR Contribution*, p. 377-381.

Gitterman, K.E. 1937. Thermal analysis of sea water. CRREL TL 287. USA Cold Regions Research and Engineering Laboratory, Hanover, NH.

Godon, A., N. Jendrzejewski, M. Castrec-Rouelle, A. Dia, F. Pineau, J. Boulègue, and M. Javoy. 2004a. Origin and evolution of fluids from mud volcanoes in the Barbados accretionary complex. *Geochim. Cosmochim. Acta* **68**, 2153-2165.

Godon, A., N. Jendrzejewski, H.G.M. Eggenkamp, D.A. Banks, M. Ader, M.L. Coleman, F. Pineau. 2004b. A cross-calibration of chlorine isotopic measurements and suitability of seawater as the international reference material. *Chem. Geol.* **207,** 1-12.

Golder Associates Ltd. 2004. Report on Predictions of Brackish Water Upwelling in Open Pits Meadowbank Project Nunavut. Submitted to Cumberland Resources Ltd. Ref #: 03-1413-078.

Goodarzi, F., O.R. Eckstrand, L. Snowdon, B. Williamson, L.D. Stasiuk. 1992. Thermal metamorphism of bitumen in Archean rocks by ultramafic volcanic flows. *Int. J. Coal Geol.* **20,** 165-178.

Gooseff, M.N., D.M. McKnight, W.B. Lyons, and A.E. Blum. 2002. Weathering reactions and hyporheic exchange controls on stream water chemistry in a glacial meltwater stream in the McMurdo Dry Valleys. *Water Resources Research* **38**, 1279, doi:10.1029/2001WR000834.

Gorman, A.R., W.S. Holbrook, M. Hornbach, K.L. Hackwith, D. Lizarralde, and I.A. Pecher. 2002. Migration of methane gas through the hydrate stability zone in a low-flux hydrate province. Geology, v. 30: 327-330.

Grasby, S., K. Osadetz, R. Betcher, F. Render. 2000. Reversal of the regional-scale flow system of the Williston basin in response to Pleistocene glaciation. *Geol.* **28,** 635-638.

Gray, D.M. and Granger, R.J. 1986. {In situ} measurements of moisture and salt movement in freezing soils. *Canadian Journal of Earth Sciences* **23**, 696-704.

Greene, S. 2005. Noble gases of the Canadian Shield from the Lupin and Con mines, Canada, as indicators of deep groundwater flow dynamics and residence time. M.Sc. Thesis, University of Ottawa, Ottawa, Ontario.

Groen, J. J. Welstra, A.G.C.A. Meesters. 2000. Salinization processes in paleowaters in coastal sediments of Suriname: evidence from δ^{37}Cl analysis and diffusion modeling. *J. Hydrology* **234,** 1-20.

Guha, J. and R. Kanwar. 1987. Vug brines-fluid inclusions: a key to understanding of secondary gold enrichment processes and the evolution of deep brines in the Canadian Shield. In *Saline Water and Gases in Crystalline Rocks*. Special Paper 33 (eds. P. Fritz and S.K. Frape). Geological Association of Canada, Memorial University, Newfoundland, pp. 95-101.

Haeckel, M., E. Suess, K. Wallmann, and D. Rickert. 2004. Rising methane gas bubbles form massive hydrate layers at the seafloor. *Geochim. Cosmochim. Acta*, **68**, 4335-4345

Häkli, T.A. 1971. Silicate nickel and its application to the exploration of nickel ores. *Bull. Geol. Soc. Finland* **43,** 247-263.

Halonen, S. 1990. Ylivieskan, Ranuan ja Keminmaan kerrosintrusioden mineralogiasta. Geologian tutkimuskeskus, Ydinjätteidensijoitus – tutkimukset, Työraportti 2-90, 15p.

Hamilton, P.B., K. Gajewski, D.E. Atkinson, D.R.S. Lean. 2001. Physical and chemical limnology of 204 lakes from the Canadian Arctic Archipelago. *Hydrobiologia* **457,** 133-148.

Hanley, J.J. and J.E. Mungall. 2003. Chlorine enrichment and hydrous alteration of the Sudbury Breccia hosting footwall Cu-Ni-PGE mineralization at the Fraser Mine, Sudbury, Ontario, Canada. *The Canadian Mineralogist* **41,** 857-881.

Hanley, J.J., J.E. Mungall, T. Pettke, E.T.C. Spooner, C.J. Bray. 2005. Ore metal redistribution by hydrocarbon-brine and hydrocarbon-halide melt phases, North Range footwall of the Sudbury Igneous Complex, Ontario, Canada. *Mineralium Deposita* **40,** 237-256.

Hanley, J., D. Ames, J. Barnes, Z. Sharp, and T. Pettke. 2006. Stable isotope evidence for multiple sources of Cl in ore fluids at the Sudbury Igneous Complex, Ontario, Canada. *The Gangue*, issue **90**, p. 1, 6-10.

Hansen, J., M. Sato, R. Ruedy, K. Lo, D.W. Lea, M. Medina-Elizade. 2006. Global temperature change. *PNAS* **103,** 14288-14293.

Hanshaw, B.B. and B. Hallet. 1978. Oxygen isotope composition of subglacially precipitated calcite: possible paleoclimatic implications. *Science* **200**, 1267-1270.

Hardie, L.A. 1996. Secular variation in seawater chemistry: an explanation for the coupled secular variation in the mineralogies of marine limestones and potash evaporites over the past 600 m.y. *Geology* **24,** 279-283.

Härme, M. 1978. Kallioperäkartean seliykset, lehdet 2043 ja 2044. Geological Map of Finland 1: 100,000, 51p.

Hedenquist, J.W. and J.B. Lowenstern. 1994. The role of magmas in the formation of hydrothermal ore deposits. *Nature* **370** 519-527.

Hein, J.R., W.R. Normark, B.R. McIntyre, T.D. Lorenson, C.L. Powell III. 2006. Methanogenic calcite, ^{13}C-depleted bivalve shells, and gas hydrate from a mud volcano offshore Southern California. *Geology* **34,** 109-112.

Henninges, J., J. Schrötter, K. Erbas, and E. Huenges. 2005. Temperature field of the Mallik gas hydrate occurrence – implication on phase changes and thermal properties. In *Scientific Results from the Mallik 2002 Gas Hydrate Production Research Well Program, Mackenzie Delta, Northwest Territories, Canada*, S.R. Dallimore and T.S. Collett (eds), Geological Survey of Canada, Bulletin 585, 14p.

Hermann, A.G., D. Knake, J. Schneider, H. Peters. 1973. Geochemistry of modern seawater and brines from salt pans: main components and bromine distribution. *Contr. Mineral. Petrol.* **40,** 1-24.

Hermann, A.G. 1980. Bromide distribution between halite and NaCl-saturated seawater. *Chem. Geol.* **28,** 171-177.

Herut, B., A. Starinsky, A. Katz, A. Bein, A. 1990. The role of seawater freezing in the formation of subsurface brines. *Geochimica et Cosmochimica Acta* **54,** 13-12.

Hesse R. and W.E. Harrison. 1981. Gas hydrates (clathrates) causing pore-water freshening and oxygen-isotope fractionation in deep-water sedimentary sections of terrigenous continental margins. *Earth Planet. Sci. Lett.* **55** 453-462.

Hesse, R., J. Lebel, and J.M. Gieskes. 1985. Interstitial water chemistry of gas-hydrate bearing sections on the Middle America Trench Slope, Deep Sea Drilling Project Leg 84. *In*: R. von Huene, J. Aubouin, et al. (Eds.), *Initial Reports DSDP* **84**. pp. 727-737.

Hesse, R., S.K. Frape, P.K. Egeberg, and R. Matsumoto. 2000. Stable isotope studies (Cl, O, and H) of intersititial waters from Site 997, Blake Ridge gas hydrate field, west Atlantic. In: C.K. Paull, R. Matsumoto, P.J. Wallace, and W.P. Dillon (Eds.) *Proceedings of the Ocean Drilling Program, Scientific Results* **164,** 129-137

Hesse, R. 2003. Pore water anomalies of submarine gas-hydrate zones as tool to assess hydrate abundance and distribution in the subsurface: What have we learned in the past decade? *Earth-Science Reviews* **61** 149-179.

Hesse, R., P.K. Egeberg, and S.K. Frape. 2006. Chlorine stable isotope ratios as tracer for pore-water advection rates ina submarine gas-hydrate fiel: implication for hydrate concentration. *Geofluids* **6,** 1-7.

Hester, K.C., R.M. Dunk, S.N. White, P.G. Brewer, E.T. Peltzer, and E.D. Sloan. 2007. Gas hydrate measurements at Hydrate Ridge using Raman spectroscopy. *Geochim. Cosmochim. Acta* **71,** 2947-2959.

Hinrichs, K.-U., J.M. Hayes, W. Bach, A.J. Spivack, L.R. Hmelo, N.G. Holm, C.G. Johnson, S.P. Sylva. 2006. Biological formation of ethane and propane in the deep marine subsurface. *Proc. National Acad. Sci.* **103**, 14684-14689.

Holbrook, W.S., H. Hoskins, W.T. Wood, R.A. Stephen, D. Lizarralde and Leg 164 Science Party. 1996. Methane hydrate and free gas on the Blake Ridge from vertical seismic profiling. *Science* **273,** 1840-1843.

Holbrook, W.S., D. Lizarralde, I.A. Pecher, A.R. Gorman, K.L. Hackwith, M. Hornbach, D. Saffer. 2002. Escape of methane gas through sediment waves in a large methane hydrate province. *Geology* **30(5),** 467-470.

Holland, M.M. and C.M. Bitz. 2003. Polar amplification of climate change in coupled models. *Clim. Dynam.* **21,** 221-232.

Holland, H.D., J. Horita, W.E. Seyfried. 1996. On the secular variations in the composition of Phanerozoic marine potash evaporites. *Geology* **24**, 993-996.

Hornbach, M.J., D.M. Saffer, W.S. Holbrook. 2004. Critically pressured free-gas reservoirs below gas-hydrate provinces. *Nature* **427,** 142-144.

Hyndman, R.D., J.P. Foucher, M. Yamano, A. Fisher and Scientific Team of Ocean Drilling Program Leg 131. 1992. Deep sea bottom-simulating-reflectors: calibration of the base of the hydrate stability field as used for heat flow estimates. *Earth and Planetary Science Letters* **109,** 289-301.

Ito, E. and A.T. Anderson Jr. 1983. Submarine metamorphism of gabbros from the Mid-Cayman Rise: petrographic and mineralogic constraints on hydrothermal processes at slow-spreading ridges. *Contrib. Mineral. Petrol.* **82,** 371-388.

Ito, E., D.M. Harris, A.T. Anderson Jr. 1983. Alteration of oceanic crust and geologic cycling of chlorine and water. *Geochim. Cosmochim. Acta* **47,** 1613-1624.

James, A.T. 1983. Correlation of natural gas by use of carbon isotopic distribution between hydrocarbon components. *AAPG Bull.* **67,** 1176-1191.

Jeffrey, A.W.A., R.C. Pflaum, T.J. McDonald, J.M. Brooks, K.A. Kvenvolden. 1985. Isotopic analysis of core gases at Sites 565-570, Deep Sea Drilling Project Leg 84. *in* von Huene, R., Aubouin, J., et al. (eds.), *Initial Reports, DSDP* **84,** 693-694.

Jenden, P.D. and J.M. Gieskes. 1983. Chemical and isotopic composition of interstitial water from Deep Sea Drilling Project Sites 533 and 534. *In*: Sheridan, R.E., Gradstein, F.M., et al. (Eds). *Initial Reports, DSDP* **76,** 453-461.

Jenden, P.D. 1985. Analysis of gases in the Earth's crust. *Gas Research Institute Report,* **GRI-85/0106**, 222p.

Jenden, P.D. and Kaplan, I.R. 1986. Comparison of microbial gases from the Middle America Trench and Scripps Submarine Canyon: implications for the origin of natural gas. *Appl. Geochem.* **1,** 631-646.

Johnson, L.H., R. Burgess, G. Turner, H.J. Milledge, J.W. Harris. 2000. Noble gas and halogen geochemistry of mantle fljuids: comparison of African and Canadian diamonds. *Geochim. Cosmochim. Acta* **64,** 717-732.

Jones, M.G. 1987. A study of the late-stage secondary fracture mineralization at sites across the Precambrian Canadian Shield. MSc. Thesis, Dept. of Earth Sciences, University of Waterloo, Waterloo, Ontario, Canada.

Jordan, A. 2003. Volcanic formation of halogenated organic compounds. In: *The Handbook of Environmental Chemistry*, **3(Part P)**, 121-139.

Jorgenson, M.T., Y.L. Shur, E.R. Pullman. 2006. Abrupt increase in permafrost degradation in Arctic Alaska. *Geophys. Res. Lett.* **33,** 10.1029/2005GL024960.

Kamineni, D.C. 1986. A petrochemical study of calcic amphiboles from the East Bull Lake anorthosite-gabbro layered complex, District of Algoma, Ontario. *Contrib. Mineral. Petrol.* **93,** 471-481.

Kamineni, D.C. 1987. Halogen-bearing minerals in plutonic rocks: a possible source of chlorine in saline groundwater in the Canadian Shield. In *Saline Water and Gases in Crystalline Rocks*. Special Paper 33 (eds. P. Fritz and S.K. Frape). Geological Association of Canada, Memorial University, Newfoundland, pp. 69-79.

Kastner, M., J.C. Sample, M.J. Whiticar, M. Hovland, B.A. Cragg, and J.R. Parkes. 1995b. Geochemical evidence for fluid flow and diagenesis at the Cascadia convergent margin. *In*: Carson, B., Westbrook, G.K., Musgrave, R.J., and Suess, E. (Eds.). *Proceedings of the Ocean Drilling Program, Scientific Results* **146,** 375-384.

Kastner, M., K.A. Kvenvolden, and T.D. Lorenson. 1998. Chemistry, isotopic composition, and origin of a methane-hydrogen sulfide hydrate at the Cascadia subdubtion zone.*Earth and Planetary Science Letters* **156,** 173-183.

Katz, B.J. 2001. Geochemical investigation of Sites 1108 and 1109, Leg 180. *In*: Huchon, P., Taylor, B., Klaus, A. (eds.), *Proceedings Ocean Drilling Program, Scientific Results* **180** [Online]. Available from World Wide Web: http://www-odp.tamu.edu/publications/180_SR/151/151.htm. [Cited 2007-06-11].

Kaufmann, R.S. 1984. Chlorine in ground water: stable isotope distribution. Ph.D. Diss. University of Arizona, Tuscon. 150p.

Kaufmann, R., A. Long, H. Bentley, and S. Davis. 1984. Natural chlorine isotope variations. *Nature* **309,** 338-340.

Kaufmann, R., S.K. Frape, P. Fritz, H. Bentley. 1987. Chlorine stable isotope composition of Canadian Shield brines.In *Saline Water and Gases in Crystalline Rocks*. Special Paper 33 (eds. P. Fritz and S.K. Frape). Geological Association of Canada, Memorial University, Newfoundland, pp. 89-93.

Kaufmann, R.S. 1989. Equilibrium exchange models for chlorine stable isotope fractionation in high temperature environments. In *Proc. 6th Int. Symp. Water-Rock Interaction* edited by D.L. Miles, 365-368.

Kaufmann, R.S., S.K. Frape, R. McNutt, C. Eastoe. 1993. Chlorine stable isotope distribution of Michigan Basin formation waters. *Appl. Geochem.* **8**, 403-407.

Kay, B.D. and P.H. Groenevelt. 1983. The redistribution of solutes in freezing soil: exclusion of solutes. In *Proc. 4th Int. Conf. on Permafrost, Jul 17-22, Fairbanks, Alaska.* Washington, D.C.: National Academy Press, p. 584-588.

Keatley, B.E., M.S.V. Douglas, J.P. Smol. 2007. Physical and chemical limnologyical characteristics of lakes and ponds across environmental gradients on Melville Island, Nunavut/N.W.T., High Arctic Canada. *Fundamental and Applied Limnology, Archiv für Hydrobiologie* **168,** 355-376.

Kelly, W.C., R.O. Rye, A. Livnat. 1986. Saline minewaters of the Keweenaw Peninsula, northern Michigan: their nature, origin, and relation to similar deep waters in Precambrian crystalline rocks of the Canadian Shield. *Am. J. Sci.* **286,** 281-308.

Kendall, C. and R. Aravena. 2000. Nitrate isotopes in groundwater systems. In P.G. Cook and A.L. Herczeg (Eds)*, Environmental Tracers in Subsurface Hydrology*, Kluwer Academic Publishers, p. 261-297.

Kennett, J.P., K.G. Cannariato, I.L. Hendy, R.J. Behl. 2000. Carbon isotopic evidence for methane hydrate instability during Quaternary Interstadials. *Science* **288,** 128-133.

Killawee, J.A., I.J. Fairchild, J.-L. Tison, L. Janssens, and R. Lorrain. 1998. Segregation of solutes and gases in experimental freezing of dilute solutions: implications for natural glacial systems. *Geochimica et Cosmochimica Acta* **62**, 3637-3655.

King, J.E., W.J. Davis, C. Relf, R.W. Avery. 1988. Deformation and plutonism in the Western Contwoyto Lake map area, central Slave province, District of Mackenzie, N.W.T. *Geol. Surv. of Canada, Paper* **88-1C,** 161-176.

King, J.E., W.J. Davis, T. Van Nostrand, C. Relf. 1989. Geology of the western Contwoyto Lake map area, District of Mackenzie, N.W.T. *Canada Geological Survey Paper* **89-1C**.

Kipfer, R., W. Aeschbach-Hertig, F. Peeters, M. Stute. 2002. Noble gases in lakes and ground waters. *Reviews in Mineralogy & Geochemistry,* **47**, 615-700.

Kirschvink, J.L. and T.D. Raub. 2003. A methane fuse for the Cambrian explosion: carbon cycles and true polar wander. *C.R. Geoscience* **335,** 65-78.

Kiyosu, Y. and S. Imaizumi. 1996. Carbon and hydrogen isotope fractionation during oxidation of methane by metal oxides at temperatures from 400°C to 530°C. *Chem. Geol.* **133,** 279-287.

Kleinberg, R.L., C. Flaum, D.D. Griffin, P.G. Brewer, G.E. Malby, E.T. Peltzer, J.P. Yesinowski. 2003. Deep sea NMR: Methane hydrate growth habit in porous media and its relationship to hydraulic permeability, deposit accumulation, and submarine slope stability. *J. Geophys. Res.* **108**, No. B10, 2508, doi: 10,1029/2003JB002389

Konrad, J.-M. and A.W. McCammon. 1990. Solute partitioning in freezing soils. *Can. Geotech. J.* **67**, 726-736.

Kopf, A., G. Mora, A. Deyhle, S. Frape, R. Hesse. 2003. Fluid geochemistry in the Japan Trench forearc (ODP Leg 186): a synthesis. In: K. Suyehiro, I.S. Sacks et al. *Proceedings of the Ocean Drilling Program, Scientific Results (CD-ROM)* **186,** 23pp. [Accessible at http://www-odp.tamu.edu/publications/186_SR/117/117.htm January 2008].

Kozłowski, A. and Ł. Karwowski. 1974. Chlorine/bromine ratio in fluid inclusions. *Econ. Geol.* **69,** 268-271.

Kroopnick, P. and H. Craig. 1972. Atmospheric oxygen – isotopic composition and solubility fractionation. *Science* **175,** 54-55.

Krouse, H.R. and B. Mayer. 2000. Sulphur and oxygen isotopes in sulphate. In *Environmental Tracers in Subsurface Hydrology*, eds. P. Cook and A.L. Herczeg, Kluwer Academic Publishers, p. 195 -231.

Kukkonen, I.T. and J. Šafanda. 2001. Numerical modeling of permafrost in bedrock in northern Fennoscandia during the Holocene. *Global and Planetary Change* **29,** 259-273.

Kullerud, K. 1996. Chlorine-rich amphiboles: interplay between amphibole composition and an evolving fluid. *Eur. J. Mineral.* **8**, 355-370.

Kumke, T., M. Ksenofontova, L. Pestryakova, L. Nazarova, H.-W. Hubberten. 2007. Limnological characteristic of lakes in the lowlands of Central Yakutia, Russia. *J. Limnol.* **66,** 40-53.

Kusky, T.M. 1989. Accretion of the Archean Slave Province. *Geol.* **17,** 63-67.

Kvenvolden, K.A. and L.A. Barnard, L.A. 1983. Gas hydrates of the Blake Outer Ridge, Site 533, Deep Sea Drilling Project, Leg 76. *In*: R.E. Sheridan, F.M. Gradstein, et al. (Eds). *Initial Reports DSDP* **76,** 353-365.

Kvenvolden, K.A., G.E. Claypool, C.N. Threlkeld, and E.D. Sloan. 1984. Geochemistry of a naturally occurring massive marine gas hydrate. *Organic Geochemistry* **6,** 703-713.

Kvenvolden, K.A. and T.J. McDonald. 1985. Gas hydrates of the Middle America Trench – Deep Sea Drilling Project Leg 84. *In:* R.von Huene, J. Aubouin, et al. (eds.), *Initial Reports DSDP* **84,** 667-682.

Kvenvolden, K.A. 1988. Methane hydrate – a major reservoir of carbon in the shallow geosphere? *Chem. Geol.* **71,** 41-51.

Kvenvolden, K.A., M. Golan-Bac, T.J. McDonald, R.C. Pflaum and J.M. Brooks. 1989. Hydrocarbon gases in sediment of the Vøring Plateau, Norwegian Sea. *In*: O. Eldholm, J. Thiede, E. Taylor, et al. (Eds). *Proceedings of the Ocean Drilling Program, Scientific Results* **104,** 319-326.

Kvenolden K.A. and M. Kastner, M. 1990. Gas hydrates of the Peruvian outer continental margin. In: E. Suess, R. Von Huene, et al. (eds.) *Peru Continental Margin Proc. Ocean Drill Program Sci Results* **112** 517-526.

Kvenvolden, K.A. 1993. Gas hydrates-geological perspective and global change. *Reviews of Geophysics* **31,** 173-187.

Kvenvolden, K.A. 1995. A review of the geochemistry of methane in natural gas hydrate. *Organic Geochemistry* **23,** 997-1008.

Kvenvolden, K.A. 1998. Methane-hydrate-A major reservoir of carbon in the shallow geosphere? *Chemical Geology* **71,** 41-51.

Kvenvolden, K.A. 2000. Natural gas hydrate: introduction and history of discovery. *In* Natural Gas Hydrate in Oceanic and Permafrost Environments; M.D. Max (ed.), Kluwer Academic Publishers, p. 9-16.

Kvenvolden, K.A. and T.D. Lorenson. 2000. Methane and other hydrocarbon gases in sediment from the southeastern North American continental margin. *In* C.K. Paull, R. Matsumoto, P.J. Wall and W.P. Dillon (Eds.), *Proceedings of the Ocean Drilling Program, Scientific Results* **164,** 29-36.

Kvenvolden, K.A. and T.D. Lorenson. 2001. The global occurrence of natural gas hydrate. *In*: C.K. Paull, and W.P. Dillon (eds.), Natural Gas Hydrates: Occurrence, Distribution, and Dynamics. *AGU Monograph Series* **124,** 3-18

Lahermo, P.W. and P.H. Lampen. 1987. Brackish and saline groundwaters in Finland. In *Saline Water and Gases in Crystalline Rocks*, Special Paper 33 (eds. P. Fritz and S.K. Frape). Geological Association of Canada, Memorial University, Newfoundland, pp. 103-109.

Lahermo, P.W., S. Halonen, L. Ahonen, K. Pirttisalo, J. Mitrega. 1989. Deep groundwater conditions at Miihkali, Eastern Finland. In: D.G. Miles (ed.) *Water-Rock Interaction, 6th International Symposium, Malvern, Aug. 3-8, 1989*, p. 405-408.

Lancet, H.S. and E. Anders. 1970. Carbon isotope fractionation in the Fischer-Tropsch synthesis of methane. *Science* **170,** 980-982

Lary, D.J. and R. Toumi. 1997. Halogen-catalyzed methane oxidation. *J. Geophys. Res.* **102,** 23,421-23,428.

Lee, C. Y.J. Kim, H. Tanimoto, N. Bobrowski, U. Platt, T. Mori, K. Yamamoto, C.S. Hong. 2005. High ClO and ozone depletion observed in the plume of Sakurajima volcano, Japan. *Geophys. Res. Letters* **32,** 10.1029/2005GL023785.

Lemieux, J.-M. 2006. Impact of the Wisconsinian Glaciation on Canadian Continental Groundwater Flow. Ph.D. thesis, Department of Earth Sciences, University of Waterloo, Waterloo, Ontario, Canada.

Lemieux, J.-M., E.A. Sudicky, W.R. Peltier, L. Tarasov. 2008. Dynamics of groundwater recharge and seepage over the Canadian landscape during the Wisonsinian glaciation. *J. of Geophys. Res.* **113,** F01011, doi:10.1029/2007JF000838.

Lemieux, J.-M., E.A. Sudicky, W.R. Peltier, L. Tarasov. 2008b. Simulating the impact of glaciations on continental groundwater flow systems: 1. relevant processes and model formulation. *J. Geophys. Res.* **113,** F03017, doi: 10.1029/2007JF000928

Lemieux, J.-M., E.A. Sudicky, W.R. Peltier, L. Tarasov. 2008c. Simulating the impact of glaciations on continental groundwater flow systems: 2. model application to the Wisconsinian glaciation over the Canadian landscape. *J. Geophys. Res.* **113,** F03018, doi: 10.1029/2007JF000929.

Levy, M. S.L. Miller, K. Brinton, J.L. Bada. 2000. Prebiotic synthesis of adenine and amino acids under Europa-like conditions. *Icarus* **145**, 609-613.

Lewis, G.J. and T.G. Thompson. 1950. The effect of freezing on the sulphate/chlorinity ratio of sea water. *Journal of Marine Research* **9**, 211-217.

Liebscher, A., V. Lüders, W. Heinrich, G. Schettler. 2006a. Br/Cl signature of hydrothermal fluids: liquid-vapour fractionation of bromine revisited. *Geofluids* **6**, 113-121.

Liebscher, A., J. Barnes, Z. Sharp. 2006b. Chlorine isotope vapor-liquid fractionation during experimental fluid-phase separation at 400°C/23 MPa to 450°C/42 MPa. *Chem. Geol.* **234,** 340-345

Lim, D.S.S., M.S.V. Douglas, J.P. Smol., D.R.S. Lean. 2001. Physical and chemical limnological characteristics of 38 lakes and ponds on Bathhurst Island, Nunavut, Canadian High Arctic. *Internat. Rev. Hydrobiol.* **86,** 1-22.

Lim, D.S.S. and M.S.V. Douglas. 2003. Limnological characteristics of 22 lakes and ponds in the Haughton Crater Region of Devon Island, Nunavut, Canadian High Arctic. *Arctic, Antarctic, and Apline Research* **35,** 509-519.

Lim, D.S.S., M.S.V. Douglas, J.P. Smol. 2005. Limnology of 46 lakes and ponds on Banks Island, N.W.T., Canadian Arctic Archipelago. *Hydrobiologia* **545,** 11-32.

Liu, X. and P.B. Flemings. 2006. Passing gas through the hydrate stability zone at southern Hydrate Ridge, offshore Oregon. *Earth and Planetary Science Letters* **241,** 211-226.

Longstaffe, F.J. 2000. An Introduction to stable oxygen and hydrogen isotopes and their use as fluid tracers in sedimentary systems. *Fluids and Basin Evolution*, Kurt Kyser (ed), Mineralogical Association of Canada Short Course Series, **28,** 115-162.

Lorenson, T.D., M.J. Whiticar, A. Waseda, S.R. Dallimore, T.S. Collett. 1999. Gas Composition and isotopic geochemistry of cuttings, core, and gas hydrate from the JAPEX/JNOC/GSC Mallik 2L-38 gas hydrate research well; *in* Scientific Results from JAPEX/JNOC/GSC Mallik 2L-38 Gas Hydrate Research Well, Mackenzie Delta, Northwest Territories, Canada, (ed.) S.R. Dallimore, T. Uchida, and T.S. Collett; *Geological Survey of Canada, Bulletin* **544**, 143-163.

Lorenson, T.D. and T.S. Collett. 2000. Gas content and composition of gas hydrate from sediments of the southeastern North American continental margin. *In*: C.K. Paull, R. Matsumoto, P.J. Wallace, and W.P. Dillon (eds.), *Proceedings of the Ocean Drilling Program, Scientific Results* **164,** 37-46.

Lorenson, T.D., M.J. Whiticar, T.S. Collett, S.R. Dallimore, and J.A. Dougherty. 2005. Complete gas composition and isotopic geochemistry from the JAPEX/JNOC/GSC et al. Mallik 5L-38 gas hydrate production research well: cuttings, core, gas hydrate, and production well testing results. *in* Dallimore, S.R. and Collett, T.S. (eds), Scientific Results from the Mallik 2002 Gas Hydrate Production Research Well Program, Mackenzie Delta, Northwest Territories, Canada. *Geological Survey of Canada, Bulletin* **585**, 19p.

Lückge, A., M. Kastner, R. Littke, B. Cramer. 2002. Hydrocarbon gas in the Costa Rica subduction zone: primary composition and post-genetic alteration. *Organic Geochemistry* **33,** 933-943.

Lüders, V., D.A. Banks, P. Halbach. 2002. Extreme Cl/Br and δ^{37}Cl isotope fractionation in fluids of modern submarine hydrothermal systems. *Mineralium Deposita* **37,** 765-771.

Lundström, U. and Å. Olin. 1986. Bromide concentration in Swedish precipitation, surface and ground waters. *Wat. Res.* **20**, 751-756.

Lyon, G.L. 1973. Interstitial water studies, Leg 15 – chemical and isotopic composition of gases from Cariaco Trench sediments. *In*:B.C. Heezen, I.D. MacGregor, et al. (eds.), *Initial Reports of the Deep Sea Drilling Project* **20,** 773-774.

Lyons, W.B. and K.A. Welch. 1997. Lithium in waters of a polar desert. *Geochim. Cosmochim. Acta* **61**, 4309-4319.

Lyons, W.B., K.A. Welch, P. Sharma. 1998. Chlorine-36 in the waters of the McMurdo Dry Valley lakes, southern Victoria Land, Antarctica: Revisited. *Geochim. Cosmochim. Acta* **62,** 185-191.

Lyons, W.B., S.K. Frape, K.A. Welch. 1999. History of McMurdo Dry Valley lakes, Antarctica, from stable chlorine isotope data. *Geology* **27,** 527-530.

Lyons, W.B., K.A. Welch, G. Snyder, J. Olesik, E.Y. Graham, G.M. Marion, R.J. Poreda. 2005. Halogen geochemistry of the McMurdo dry valley lakes, Antarctic: Clues to the origin of solutes and lake evolution. *Geochim. Cosmochim. Acta* **69,** 305-323.

MacDonald, I.M. 1986. Water-rock interaction in felsic rocks of the Canadian Shield. MSc. Thesis, Dept. of Earth Sciences, University of Waterloo, Waterloo, Ontario, Canada.

MacDonald, G.J. 1990. Role of methane clathrates in past and future climates. *Climatic Change* **16,** 247-281.

MacGeehan, P.J. 1978. The geochemistry of altered volcanic rocks at Matagami, Quebec: a geothermal model for massive sulphide genesis. *Can. J. Earth Sci.* **15,** 551-570.

MacGeehan, P.J. and W.H. MacLean. 1980. An Archean sub-seafloor geothermal system, 'calc-alkali' trends, and massive sulphide genesis. *Nature* **286,** 767-771.

MacGeehan, P.J., W.H. Maclean, A.J. Bonenfant. 1981. Exploration significance of the emplacement and genesis of massive sulphides in the Main Zone at the Norita Mine, Matagami, Quebec. *CIM Bull.* **74(828)**, 59-75

Mackay, J.R. and L.M. Lavkulich. 1974. Ionic and oxygen isotopic fractionation in permafrost growth. *Geol. Surv. Can.,* Paper 74-1, Part B. 255-256.

Mackay, J.R. 1992. Lake stability in an ice-rich permafrost environment: examples from the western Arctic coast. *In* Aquatic ecosystems in semi-arid regions: implications for resource management (eds. R.D. Robarts and M.L. Bothwell). National Hydrology Research Institute, Environment Canada, Saskatoon. Symposium Series **7**, 1-26.

Maekawa T. and N. Imai. 2000. Hydrogen and oxygen isotope fractionation in water during gas hydrate formation. *Annals New York Academy of Sciences* **912** 452-459.

Magenheim, A.J. 1995. Oceanic borehole fluid chemistry and analysis of chlorine stable isotopes in silicate rocks. Ph.D. dissertation, University of California, San Diego, 184p.

Magenheim, A.J., A.J. Spivack, P.J. Michael, J.M. Gieskes. 1995. Chlorine stable isotope composition of the oceanic crust: implications for Earth's distribution of chlorine. *Earth and Planetary Science Letters* **131,** 427-432.

Majorowicz, J.A. and K. Osadetz. 1999. Basic geological and geophysical indications of gas hydrate distribution and volume in Canada. *Geological Survey of Canada, Open File Report* **3780**, 21p, + 16figures.

Majorowicz, J.A. and K.A. Osadetz. 2001. Gas hydrate distribution and volume in Canada. *AAPG Bull.* **85(7),** 1211-1230.

Makogon, Y.F., F.A. Trebin, A.A. Trofimuk, V.P. Tsarev, and N.V. Cherskiy. 1971. Detection of a pool of natural gas in a solid (hydrated gas) state. *Doklady Akademii Nauk SSSR* **196,** 203-206.

Makogon, Y.F. 1981. Hydrates of Natural Gas. Pennwell, Tulsa, Oklahoma, 237p.

Mallard, W.G., F. Westley, J.T. Herron, R.F. Hampson, D.H. Frizzel. 1993. *NIST Chemical Kinetics Database: Version 5.0*. National Institute of Standards and Technology, Gaithersburg, MD.

Marion, G.M. and S.A. Grant. 1994. FREZCHEM: a chemical-thermodynamic model for aqueous solutions at subzero temperatures. CRREL Spec. Rep. 94-18. USA Cold Regions Research and Engineering Laboratory, Hanover, NH.

Marion, G.M. 1995. Freeze-Thaw Processes and Soil Chemistry. US Army Corps of Engineers, Cold Regions Research and Engineering Laboratory, Special Report 95-12.

Marion, G.M. 1997. A theoretical evaluation of mineral stability in Don Juan Pond, Wright Valley, Victoria Land. *Antarctic Science* **9**, 92-99.

Marion, G.M. and R.E. Farren. 1999. Mineral solubilities in the Na-K-Mg-Ca-Cl-SO4-H2O system: a re-evaluation of the sulphate chemistry in the Spencer-Møller-Weare model. *Geochim. Cosmochim. Acta* **63,** 1305-1318.

Marion, G.M., R.E. Farren, A.J. Komrowski. 1999. Alternative pathways for seawater freezing. *Cold Regions Science and Technology* **29**, 259-266.

Markl, G., M. Musashi, K. Bucher. 1997. Chlorine stable isotope composition of granulites from Lofoten, Norway: Implications for the Cl isotopic composition and for the source of Cl enrichment in the lower crust. *Earth and Planetary Science Letters* **150,** 95-102.

Markl, G. and K. Bucher. 1998. Composition of fluids in the lower crust inferred from metamorphic salt in lower crustal rocks. *Nature* **391**, 781-783.

Martin, J.B. 1999. Nonconservative behavior of Br^-/Cl^- ratios during alteration of volcaniclastic sediments. *Geochim. Cosmochim. Acta* **63,** 383-391.

Martini, A.M., Walter, L.M., Budai, J.M., Ku, T.C.W., Kaiser, C.J., and Schoell, M. 1998. Genetic and temporal relations between formation waters and biogenic methane, Upper Devonian Antrim Shale, Michigan Basin, USA. Geochimica et Cosmochimica Acta, v. 62(10): 1699-1720.

Martini, A.M., L.M. Walter, T.C.W. Ku, J.M. Budai, J.C. McIntosh, M. Schoell. 2003. Microbial production and modification of gases in sedimentary basins: a geochemical case study from a Devonian shale gas play, Michigan Basin. *AAPG Bull.* **87,** 1355-1375.

Maas, R., M.T. McCulloch, I.H. Campbell, P.R. Coad. 1986. Sm-Nd and Rb-Sr dating of an Archean massive sulfide deposit: Kidd Creek, Ontario. *Geology* **14,** 585-588.

Matsumoto, R. and W.S. Borowski. 2000. Gas hydrate estimates from newly determined oxygen isotope fractionation ($\alpha_{GH\text{-}IW}$) and $\delta^{18}O$ anomalies of the interstitial waters: Leg 164, Blake Ridge. In: C.K. Paull, R. Matsumoto, P.J. Wallace, and W.P. Dillon (eds) *Proc. Ocean Drill. Program Sci. Results* **164,** 59-66.

Matsumoto, R., T. Uchida, A. Waseda, T. Uchida, S. Takeya, T. Hirano, K. Yamada, Y. Maeda, T. Okui. 2000. Occurrence, structure, and composition of natural gas hydrate recovered from the Blake Ridge, Northwest Atlantic. *In*: Paull, C.K., Matsumoto, R., Wallace, P.J., and Dillon, W.P. (eds.), *Proceedings of the Ocean Drilling Program, Scientific Results* **164**, 13-28.

Matsumoto, R., H. Tomaru, Y.F. Chen, H. Lu, I.D. Clark. 2005. Geochemistry of the interstitial waters of the JAPEX/JNOC/GSC et al. Mallik 5L-38 gas hydrate production research well. In *Scientific Results from the Mallik 2002 Gas Hydrate Production Research Well Program, Mackenzie Delta, Northwest Territories, Canada*, (ed.) S.R. Dallimore and T.S. Collett, *Geological Survey of Canada Bulletin* **585**, 14p.

May, F., W. Freund, E.P. Müller, K.P. Dostal. 1968. Modellversuche über isotopenfraktionierung von erdgaskomponenten während der migration. *Zeitschrift fur Angewandte Geologie*, **14**, 376-380.

Mazor, E. 1972. Paleotemperatures and other hydrological parameters deduced from noble gases dissolved in groundwaters; Jordan Rift Valley, Israel. *Geochem. Cosmochim. Acta* **36,** 1321-1336.

McCaffrey, M.A., B. Lazar, H.D. Holland. 1987. The evaporation path of seawater and the coprecipitation of Br- and K+ with halite. *J. Sed. Petrology* **57**, 928-937.

McCollom, T.M. and J.S. Seewald. 2001. A reassessment of the potential for reduction of dissolved CO_2 to hydrocarbons during serpentinization of olivine. *Geochim. Cosmochim. Acta* **65,** 3769-3778.

McCollom, T.M. and J.S. Seewald. 2003. Experimental study of the hydrothermal reactivity of organic acids and acid anions: II. Acetic acid, acetate, and valeric acid. *Geochim. Cosmochim. Acta* **67,** 3645-3664.

McNutt, R.H., S.K. Frape, P. Fritz. 1984. Strontium isotopic composition of some brines from the Precambrian Shield of Canada. *Isotope Geoscience* **2,** 205-215.

McNutt, R.H. 1987. Sr-87/Sr-86 as indicators for rock-water interactions: applications to brines found in Precambrian age rocks from Canada. In *Saline Water and Gases in Crystalline Rocks*. Special Paper 33 (eds. P. Fritz and S.K. Frape). Geological Association of Canada, Memorial University, Newfoundland, pp. 81-93.

McNutt, R.H., M. Gascoyne, D.C. Kamineni. 1987. $^{87}Sr/^{86}Sr$ values in groundwaters of the East Bull Lake Pluton, Superior Province, Ontario, Canada. *Appl. Geochem.* **2,** 93-101.

McNutt, R.H., S.K. Frape, P. Fritz, M.G. Jones, I.M. MacDonald. 1990. The $^{87}Sr/^{86}Sr$ values of Canadian Shield brines and fracture minerals with applications to groundwater mixing, fracture history, and geochronology. *Geochim. Cosmochim. Acta* **54**, 202-215.

Melezhik, V.A., A.E. Fallick, M.M. Filippov, O. Larsen. 1999. Karelian shungite – an indication of 2.0-Ga-old metamorphosed oil-shale and generation of petroleum: geology, lithology, and geochemistry. *Earth-Sci. Reviews* **47,** 1-40

Michael, P.J. and J.G. Schilling. 1989. Chlorine in Mid-Ocean Ridge magmas: evidence for assimilation of seawater-influenced components. *Geochim. Cosmochim. Acta* **53**, 3131-3143.

Michelot, J.-L., H. Bentley, I. Brissaud, D. Elmore, J.-Ch. Fontes. 1983. Progress in environmental isotope studies (^{36}Cl, ^{34}S, ^{18}O) at the Stripa site. *Proc. Symp. Isotope Hydrology, IAEA Vienna,* 207-209.

Michelot J.-L. and J.-Ch. Fontes. 1987. Two case studies on the origin of aqueous sulphate. In *Studies on Sulphur Isotope Variations in Nature: Proc. Adv. Group Meet., IAEA, Vienna June 1985*, 65-76.

Michelot, J.-L., H. Bentley, I. Brissaud, D. Elmore, J.-Ch. Fontes. 1983. Progress in environmental isotope studies (^{36}Cl, ^{34}S, ^{18}O) at the Stripa site. *Proc. Symp. Isotope Hydrology, IAEA, Vienna,* 207-209.

Michelutti, N., M.S.V. Douglas, D.C.G. Muir, X. Wang, J.P. Smol. 2002. Limnological characteristics of 38 lakes and ponds on Axel Heiberg Island, High Arctic Canada. *Internat. Rev. Hydrobiol.* **87,** 385-399.

Milkov, A.V., G.E. Claypool, Y.-J. Lee, W. Xu, G.R. Dickens, W.S. Borowski. 2003. In situ methane concentrations at Hydrate Ridge, offshore Oregon; new constraints on the global gas hydrate inventory. *Geology* **31,** 833-836.

Milkov, A.V. 2004. Global estimates of hydrate-bound gas in marine sediments: how much is really out there? *Earth-Sci. Rev.* **66,** 183-197.

Milkov, A.V., G.E. Claypool, Y.-J. Lee, M.E. Torres, W.S. Borowski, H. Tomaru, R. Sassen, P.E. Long, and ODP Leg 204 Scientific Party. 2004. Ethane enrichement and propane depletion in subsurface gases indicate gas hydrate occurrence in marine sediments at southern Hydrate Ridge, offshore Oregon. *Org. Geochem.* **35,** 1067-1080.

Milkov, A.V. 2005a. Molecular and stable isotope compositions of natural gas hydrates: a revised global dataset and basic interpretations in the context of geological settings. *Org. Geochem.* **36,** 681-702.

Milkov, A.V. 2005b. In situ methane concentrations at Hydrate Ridge, offshore Oregon: new constraints on the global gas hydrate inventory. *Geology* **31,** 833-836.

Milkov, A.V., G.E. Claypool, Y.-J. Lee, R. Sassen. 2005. Gas hydrate systems at Hydrate Ridge offshore Oregon inferred from molecular and isotopic properties of hydrate-bound and void gases. *Geochim. Cosmochim. Acta* **69**, 1007-1026.

Mingram, B. and K. Bäuer. 2001. Ammonium concentration and nitrogen isotope composition in metasedimentary rocks from different tectonometamorphic units of the European Variscan Belt. *Geochim. Cosmochim. Acta* **65,** 273-287.

Mironenko, M.V., S.A. Grant, G.M. Marion, R.E. Farren. 1997. FREZCHEM2: a chemical-thermodynamic model for aqueous solutions at subzero temperatures. CRREL Rep. 97-5. USA Cold Regions Research and Engineering Laboratory, Hanover, NH.

Mislowack, B.J., T.C. Onstott, D. Sigman, M. Borscik, B. Sherwood-Lollar, G. Lacrampe-Couloume, M Fogel. 2008. The role of geologic nitrogen in deep subsurface terrestrial ecosystems. Submitted to *Chem. Geol.*

Miyakawa, S., H.J. Cleaves, S.L. Miller. 2002a. The cold origin of life: A. implications based on the hydrolytic stabilities of hydrogen cyanide and formamide. *Origin of Life and Evolution of the Biosphere* **32,** 195-208.

Miyakawa, S., H.J. Cleaves, S.L. Miller. 2002b. The cold origin of life: B. implications based on pyrimidines and purines produced from frozen ammonium cyanide solutions. *Origins of Life and Evolution of the Biosphere* **32,** 209-218.

Montgomery, J. 1994. An isotopic study of CH_4 and associated N_2 and H_2 gases in Canadian Shield mining environments. M.Sc. Thesis, University of Toronto, Toronto, Ontario.

Morrison, J. 1991. Compositional constraints on the incorporation of Cl into amphiboles. *Am. Mineral.* **76,** 1920-1930.

Morrison, J., T. Brockwell, T. Merren, F. Fourel, and A.M. Phillips. 2001. On-line high-precision stable hydrogen isotopic analyses on nanoliter water samples. *Analytical Chem.* **73,** 3570-3575.

Moser, H. (Ed.) 1977. Jahresbericht 1977. Internal report of the Institute fur radiohydrometrie GSF Munich **169,** 70-71.

Mossman, D.J., B. Nagy, D.W. Davis. 1993. Hydrothermal alteration of organic matter in uranium ores, Elliot Lake, Canada: Implications for selected organic-rich deposits. *Geochim. Cosmochim. Acta* **57,** 3251-3259.

Mungall, J.E. and J.M. Brenan. 2003. Experimental evidence for the chalcophile behavior of the halogens. *The Canadian Mineralogist* **41,** 207-200.

Mungall, J.E., D.E. Ames, and J.J. Hanley. 2004. Geochemical evidence from the Sudbury structure for crustal redistribution by large bolide impacts. *Nature* **429**, 546-548.

Musashi, M., T. Oi, H.G.M. Eggenkamp, Y. Yato, M. Matsuo. 2007. Anion-exchange chromatographic study of the chlorine isotope effect accompanying hydration. *J. Chromatography A* **1140**, 121-125.

National Research Council of Canada. 1988. Glossary of Permafrost and Related Ground-Ice Terms. Associate Committee on Geotechnical Research, Permafrost Subcommittee. *Technical Memorandum No.* **142**, Ottwaw, Canada; 156p.

National Research Council of the National Academies. 2008. *Assessment of the NASA Astrobiology Institute*. 68p.

Natural Resources Canada. 1995. Canada – Permafrost. The National Atlas of Canada, 5th Edition, MCR 4177.

Negrel, P. J. Casanova, R. Blomqvist, J. Kaija, S. Frape. 2003. Strontium isotopic characterization of the Palmottu hydrosystem (Finland); water-rock interaction and geochemistry of groundwaters. *Geofluids* **3,** 161-175.

Negrel, P, J. Casanova, R. Blomqvist. 2005. $^{87}Sr/^{86}Sr$ of brines from the Fennoscandian Shield; a synthesis of groundwater isotopic data from the Baltic Sea region. *Can. J. Earth Sci.* **42,** 273-285.

Nelson K.H. and T.G. Thompson. 1954. Depostion of salts from sea water by frigid concentration. *Journal of Marine Research* **13**, 166-182.

Nezat, C.A., W.B. Lyons, and K.A. Welch. 2001. Chemical weathering in streams of a polar desert (Taylor Valley, Antarctica). *Geological Society of America Bulletin* **113**, 1401-1408.

Netzeband, G.L., C.P. Hübscher, D. Gajewski, J.W.G. Grobys, and J. Bialas. 2005. Seismic velocities from the Yaquina forearc basin off Peru: evidence for free gas within the gas hydrate stability zone. *International Journal of Earth Science (Geol Rundsch)* **94,** 420-432.

Nijland, T.G., J.B. Jansen, and C. Maijer. 1993. Halogen geochemistry of fluid during amphibolite-granulite metamorphism as indicated by apatite and hydrous silicates in basic rocks from the Bamble Sector, South Norway. *Lithos* **30,** 167-189.

Nisbet, E.G. 1990. The end of the ice age. *Canadian Journal of Earth Sciences* **27,** 148-157.

Nisbet, E.G. 1992. Sources of atmospheric CH_4 in early postglacial time. *Journal of Geophysical Research* **97(D12),** 12859-12867.

Nisbet, E.G. 2002. Have sudden large releases of methane from geological reservoirs occurred since the Last Glacial Maximum, and could such releases occur again? *Phil. Trans. R. Soc. Lond. A* **360,** 581-607.

Nordstrom, D.K. 1986. Hydrogeochemical interpretation of the groundwater at the Hästholmen site, Finland. Voimayhtiöiden Ydinjätetoimikunta (Nuclear Waste Commission of Finnish Power Companies) Report YJT-86-32.

Nordstrom, D.K. and T. Olsson. 1987. Fluid inclusions as a source of dissolved salts in deep granitic groundwaters. In *Saline Water and Gases in Crystalline Rocks*. Special Paper 33 (eds. P. Fritz and S.K. Frape). Geological Association of Canada, Memorial University, Newfoundland, pp. 111-119.

Nordstrom, D.K., S. Lindblom, R.J. Donahoe, C.C. Barton. 1989a. Fluid inclusions in the Stripa granite and their possible influence on the groundwater chemistry. *Geochim. Cosmochim. Acta* **53,** 1741-1755.

Nordstrom, D.K., T. Olsson, L. Carsson, P. Fritz. 1989b. Introduction to the hydrogeochemical investigations within the international Stripa project. *Geochim. Cosmochim. Acta* **53,** 171-1726.

Nurmi, P.A. and I.T. Kukonen. 1986. A new technique for sampling water and gas from deep drill holes. *Canadian J. Earth Sci.* **23**, 1450-1454.

Nurmi, P.A., I.T. Kukkonen, P. Lahermo. 1988. Geochemistry and origin of saline groundwaters in the Fennoscandian Shield. *Appl. Geochem.***3,** 185-203.

NWMO. 2005. Choosing a Way Forward. The Future Management of Canada's Used Nuclear Fuel. Final Study Report. Nuclear Waste Management Organization, Toronto, Ontario, Canada.

Oberti, R., L. Ungaretti, E. Cannillo, F.C. Hawthorne. 1993. The mechanism of Cl incorporation in amphibole. *Am. Mineral.* **78,** 746-752.

O'Leary, M.H. 1984. Measurement of the isotope fractionation associated with diffusion of carbon dioxide in aqueous solution. *J. Phys. Chem.* **88**: 823-825.

O'Neil, J.R. 1968. Hydrogen and oxygen isotope fractionation between ice and water. *J. Phys. Chem.* **72,** 3683-3684.

Orberger, B., G. Friedrich, E. Woermann. 1990. The distribution of halogens and carbon in PGE-bearing ultramafics of the Acoje ophiolite block, Zambales, Philippines. *J. of Geochem. Explor.* **37,** 147-169.

Oremland, R.S., M.J. Whiticar, F.E. Strohmaier, R.P. Kiene. 1988. Bacterial ethane formation from reduced, ethylated sulfur compounds in anoxic sediments. *Geochim. Cosmochim. Acta* **52,** 1895-1904.

Overpeck, J., K. Hughen, D. Hardy, R. Bradley, R. Case, M. Douglas, B. Finney, K. Gajewski, G. Jacoby, A. Jennings, S. Lamoureus, A. Lasca, G. MacDonald, J. Moore, M. Retelle, S. Smith, A. Wolfe, G. Zielinski. 1997. Arctic environmental change of the last four centuries. *Science* **278,** 1251-1256.

Paktunç, A.D. 1984. Metamorphism of the ultramafic rocks of the Thompson Mine, Thompson Nickel Belt, Northern Manitoba. *Canadian Mineralogist* **22,** 77-91.

Palmén, J. and P. Hellä. 2003. Summary of the water sampling and analysis results at the Olkiluoto Site, Eurajoki. POSIVA Working Report 2003-19, 82p.

Pan, Y. and P. Dong. 2003. Bromine in scapolite-group minerals and sodalite: XRF microprobe analysis, exchange experiments, and application to skarn deposits. *The Canadian Mineralogist* **41,** 529-540.

Paull, C.K., W. Ussler III, W. S.Borowski. 1994. Sources of biogenic methane to form marine gas hydrates. *New York Academy of Sciences Annals* **715,** 392-409.

Paull, C.K., R. Matsumoto, P.J. Wallace, et al. 1996. Proceedings of Ocean Drilling Program, Initial Reports, v. 164.

Paull, C.K., T.D. Lorenson, W.S. Borowski, W. Ussler III, K. Olsen, N.M. Rodriguez. 2000a. Isotopic composition of CH4, CO2 species, and sedimentary organic matter within smaples from the Blake Ridge: gas source implications. *In*: Paull, C.K., Matsumoto, R., Wallace, P.J., and Dillon, W.P. (eds.), Proceedings of the Ocean Drilling Program, Scientific Results v. 164: 67-78.

Paull, C.K., T.D. Lorenson, G. Dickens, W.S. Borowski, W. Ussler III., and K. Kvenvolden. 2000b. Comparisons of *in situ* and core gas measurements in ODP Leg 164 bore holes. Annals of the New York Academy of Sciences, v. 912: 23-31.

Paull, C.K. and Ussler IIII, W. 2001. History and significance of gas sampling during the DSDP and ODP. *In*: Paull, C.K. and Dillon W.P. (eds.), Natural Gas Hydrates: Occurrence, Distribution, and Dynamics. *AGU Monograph Series* **124,** 53-66.

Pearson, F.J., Jr. 1987. Models of mineral controls on the composition of saline groundwaters of the Canadian Shield. In *Saline Water and Gases in Crystalline Rocks*, Special Paper 33 (eds. P. Fritz and S.K. Frape). Geological Association of Canada, Memorial University, Newfoundland, pp. 39-51.

Pecher, I.A., N. Kukowski, C. Huebscher, J. Greinert, J. Bialas, and the GEOPECO Working Group. 2001. The link between bottom-simulating reflections and methane flux into the gas hydrate stability zone – new evidence from Lima Basin, Peru Margin. *Earth Planet. Sci. Lett.* **185,** 353-354.

Perfect, E., P.H. Groenevelt, and B.D. Kay. 1991. Transport phenomena in frozen porous media. In *Transport Processes in Porous Media*. Dordrecht: Kluwer Academic Publishers, p. 243-270.

Pernaton, E., A. Prinzhofer, F. Schneider. 1996. Reconsideration of methane isotope signature as a criterion for the genesis of natural gas: Influence of migration on isotopic signatures. *Revue de l'Institut Français du Pétrole* **51(5)**, 635-651.

Person, M.A., D. Cohen, A. Marksamer. 2006. Pleistocene recharge mechanisms on the Atlantic continental shelf. *Geological Society of America Annual Meeting* **38,** 334.

Person, M., J. McIntosh, V. Bense, V.H. Remenda. 2007. Pleistocene hydrology of North America: the role of ice sheets in reorganizing groundwater flow systems. *Rev. of Geophys.* **45**, RG3007, 10.1029/2006RG000206.

Petersilie, I.A. and H. Sörensen. 1970. Hydrocarbon gases and bituminous substances in rocks from the Ilímaussaq alkaline intrusion, south Greenland. *Cont. to the Mineral. Of Ilímaussaq,* No. 18, 59-76.

Pfiffner, S.M., Onstott, T.C., Ruskeeniemi, T., Talikka, M., Bakermans, C., McGown, D., Chan, E., Johnson, A., Phelps, T.J., Difurio, S.A., Pratt, L.M., Stotler, R., Telling, J., Sherwood-Lollar, B., Neill, I., Zerbin, B. Challenges for coring deep permafrost on Earth and Mars. *Astrobiology* **8,** 623-638.

Pflaum, R.C., J.M. Brooks, H.B. Cox, M.C. Kennicutt, II, and D.-D. Sheu. 1986. Molecular and isotopic analysis of core gases and gas hydrates, Deep Sea Drilling Project Leg 96. I*n* A.H. Bouma, J.M. Coleman, A.W. Meyer, et al., (eds.), *Initial Reports of Deep Sea Drilling Project, Leg 96*: 781-784.

Philippot, P., P. Agrinier, M. Scambelluri. 1998. Chlorine cycling during subduction of altered oceanic crust. *Earth and Planetary Science Letters* **161**, 33-44.

Philippot, P., V. Busigny, M. Scambelluri ,P. Cartigny. 2007. Oxygen and nitrogen isotopes as tracers of fluid activities in serpentinites and metasediments during subduction. *Mineralogy and Petrology* **91,** 11-24.

Phillips, F.M. and H.W. Bentley. 1987. Isotopic fractionation during ion filtration: 1. Theory. *Geochim. Cosmochim. Acta.***51,** 683-695.

Phillips, F.M. 2000. Chlorine-36. In *Environmental Tracers in Subsurface Hydrology*, eds. P. Cook and A.L. Herczeg, Kluwer Academic Publishers, p. 299 -348.

Piché, M., J. Guha, R. Daigneault. 1993. Stratigraphic and structural aspects of the volcanic rocks of the Matagami Mining Camp, Quebec: implications for the Norita ore deposit. *Econ. Geol.* **88,** 1542-1558.

Pinnekar, Y.V. 1973. Interaction of cryolithosphere and subsurface water in deep horizons of artesian basins. In *Proceedings of the 2nd International Conference on Permafrost, Yakutsk, USSR, July 13-28, 1973 – USSR Contribution*, p.433-435.

Pitkanen, P., A. Luukkonen, P. Ruotsalainen, H. Leino-Forsman, U. Vuorinen. 1999. Geochemical modeling of groundwater evolution and residence time at the Olkiluoto site. POSIVA Report 98-10, 184p.

Posiva. 2000. Disposal of spent fuel in Olkiluoto bedrock – programme for research, development and technical design for the pre-construction phase. POSIVA 2000-14.

Price, P.B. 2007. Microbial life in glacial ice and implications for a cold origin of life. *FEMS Microbiology Ecology* **59,** 217-231.

Prinzhofer, A.A. and A.Y. Huc. 1995. Genetic and post-genetic molecular and isotopic fractionations in natural gases. *Chem. Geol.* **126,** 281-290.

Prinzhofer, A. and E. Pernaton. 1997. Isotopically light methane in natural gas: bacterial imprint or diffusive fractionation? *Chem. Geol.* **142** 193-200.

Prinzhofer, A., M.R. Mello, and T. Takaki. 2000. Geochemical characterization of natural gas: a physical multivariable approach and its applications in maturity and migration estimates. *AAPG Bull.* **84(8),** 1152-1172.

Prinzhofer, A., M.R. Mello, and T. Takaki. 2001. Geochemical characterization of natural gas: a physical multivariable approach and its applications in maturity and migration estimates: Reply. *AAPG Bull.* **85(12),** 2114-2117.

Priscu, J.C. and B.C. Christner. 2004. Earth's icy biosphere. *Microbial Diversity and Bioprospecting* (Bull AT, ed), pp. 130-145. ASM Press, Washington, D.C.

Purdy, A. 1989. Aqueous sulfate in the Lac du Bonnet Batholith groundwater system. M.Sc. thesis, Univ. Waterloo.

Qiu, G., W. Sheng, C. Huang, K. Zheng. 1988. Direction of ion migration during cooling and freezing processes. In *Proc., 5th Int. Conf. on Permafrost, 2-5 August, Trondheim, Norway.* Trondheim, Norway: Tapir Publishers, v. **1**, 442-447.

Raab, M. and B. Spiro. 1991. Sulfur isotopic variations during seawater evaporation with fractional crystallization. *Chem. Geol. (Iso. Geosci. Sec.)* **86,** 323-333.

Ransom B., A.J. Spivack, M. Kastner. 1995. Stable Cl isotopes in subduction-zone pore waters: implications for fluid-rock reactions and the cycling of chlorine. *Geology* **23**, 715-718.

Redding, C., M. Schoell, J.C. Monin, B. Durand. 1980. Hydrogen and carbon isotopic composition of coals and kerogens. In: A.G. Douglas and J.R. Maxwell (eds). *Advances in Organic Geochemistry 1979*. Pergamon, Oxford, pp. 711-723.

Rehtijärvi, P. 1984. Enrichment of bromine and chlorine in Proterozoic serpentinites from the Outokumpu Cu-Co ore district, Finland. *Econ. Geol.* **79,** 549-552.

Retallack G.J. and E.S. Krull E.S. 2006. Carbon isotope evidence for terminal-Permian methane outbursts and their role in extinctions of animals, plants, coral reefs, and peat swamps. *Geological Society of America Special Paper* **399,** 249-268.

Richardson, C. 1976. Phase relationships in sea ice as a function of temperature. *J. Glaciol.* **17**, 507-519.

Richet, P., Y. Bottinga, M. Javoy. 1977. A review of hydrogen, carbon, nitrogen, oxygen, sulphur, and chlorine stable isotope fractionation among gaseous molecules. *Ann. Rev. Earth Plant. Sci.* **5,** 65-110.

Ringer, W.E. 1906a. Über die Veränderungen in der Zusammensetzung des Meereswassersalzes beim Ausfrieren. *Verh. Rijksst. Onderz. Zeeviss*. **3**, 1-55.

Ringer, W.E. 1906b. De veranderingen in samenstelling van zeewater bij het bevriezen. *Chem. Weekbl.* **3**, 223-249.

Ritenhouse, G. 1967. Bromine in oilfield waters and its use in determining the possibilities of origin of these waters. *AAPG Bull.* **51,** 2430-2440.

Robert, F. and A.C. Brown. 1986a. Archean gold-bearing quartz veins at the Sigma Mine, Abitibi Greenstone Belt, Quebec: Part I. geologic relations and formation of the vein system. *Econ Geol.* **81,** 578-592.

Robert, F. and A.C. Brown. 1986b. Archean gold-bearing quartz veins at the Sigma Mine, Abitibi Greenstone Belt, Quebec: Part II. Vein paragenesis and hydrothermal alteration. *Econ. Geol.* **81,** 593-616.

Roberts, R.G. 1975. The geological setting of the Mattagami Lake Mine, Quebec: a volanogenic massive sulphide deposit. *Econ. Geol.* **70,** 115-129.

Roedder, E. 1984. Fluid Inclusions. *Reviews in Mineralogy,* v. 12. Mineral. Soc. America.

Romanov, V.P. and G.P. Levchenko. 1989. Migration of salts in freezing soils. *Soviet Engineering Geology* **2**, 44-51.

Romanov, V.P. and G.P. Levchenko. 1989. Migration of salts in freezing soils. *Soviet Engineering Geology* **2**, 44-51.

Rosenfeld, W.D. and S.R. Silverman. 1959. Carbon isotope fractionation in bacterial production of methane. *Science* **130,** 1658-1659.

Rossi, A.P. 1999. Investigation of permafrost groundwater discharge at Screech Lake, NWT: a preliminary conceptual model for natural, flowing cryo-artesian conditions through a coupled talik in the continuous permafrost zone. MSc Thesis, Dept. of Earth Sciences, University of Waterloo, Waterloo, Ontario, Canada.

Rühland, K. and J.P. Smol. 1998. Limnological characteristics of 70 lakes spanning arctic treeline from Coronation Gulf to Great Slave Lake in the Central Northwest Territories, Canada. *Internat. Rev. Hydrobiol.* **83,** 183-203.

Ruskeeniemi, T., R. Blomqvist, A. Lindberg, L. Ahonen, S.K. Frape. 1996. *Hydrogeochemistry of Deep Groundwaters of Mafic and Ultramafic Rocks in Finland*. POSIVA-96-21, Posiva Oy, 123p.

Ruskeeniemi, T., M. Paananen, L. Ahonen, J. Kaija, A. Kuivamäki, S. Frape, L. Moren, P. Degnan. 2002. Permafrost at Lupin : Report of Phase 1. Geological Survey of Finland, YST-112. 59 p. + 3 app.

Ruskeeniemi, T., L. Ahonen, M. Paananen, S. Frape, R. Stotler, M. Hobbs, J. Kaija, P. Degnan, R. Blomqvist, M. Jensen, K. Lehto, L. Moren, I. Puigdomenech, M. Snellman. 2004. Permafrost at Lupin: Report of Phase II. Geological Survey of Finland, Nuclear Waste Disposal Research. Report YST-119, 89 p.

Rye, D.M. and R.O. Rye. 1974. Homestake Gold Mine, South Dakota: 1, Stable Isotope Studies. *Econ. Geol.* **69**, 293-317.

Sackett, W.M., S. Nakaparskin, S. Dalrymple. 1970. Carbon isotope effects in methane production by thermal cracking. In *Advances in Organic Geochemistry* (eds G.D. Hobson and G.C. Speers). pp 37-53. Pergamon Press.

Salvi, S. and A.E. Williams-Jones. 1997. Fischer-Tropsch synthesis of hydrocarbons during sub-solidus alteration of the Strange Lake peralkaline granite, Quebec/Labrador, Canada. *Geochim. Cosmochim. Acta.* **61,** 83-99.

Sassen, R., S.T. Sweet, D.A. DeFreitas, A.V. Milkov. 2000. Exclusion of 2-methylbutane (isopentane) during crystallization of structure II gas hydrate in sea-floor sediment, Gulf of Mexico. *Org. Geochem.* **31,** 1257-1262.

Sassen, R., S.L. Losh, L. Cathles III, H.H. Roberts, J.K. Whelan, A.V. Milkov, S.T. Sweet, D.A. DeFreitas. 2001a. Massive vein-filling gas hydrate: relation to ongoing gas migration from the deep subsurface in the Gulf of Mexico. *Marine and Petroleum Geology* **18,** 551-560.

Sassen, R., S.T. Sweet, A.V. Milkov, D.A. DeFreitas, M.C. Kennicutt II. 2001b. Thermogenic vent gas and gas hydrate in the Gulf of Mexico slope: Is gas hydrate decomposition significant? *Geology* **29(2),** 107-110.

Schauble, H.P., G.R. Rossman, H.P. Taylor Jr. 2003. Theoretical estimates of equilibrium chlorine-isotope fractionations. *Geochim. Cosmochim. Acta* **67,** 3267-3281.

Schilling, J.-G., C.K. Unni, and M.L. Bender. 1978. Origin of chlorine and bromine in the oceans. *Nature* **273,** 631-636.

Schilling, J.-G., M.B. Bergeron, R. Evans, and J.V. Smith. 1980. Halogens in the mantle beneath the North Atlantic. *Philosophical Transactions of the Royal Society of London. Series A, Mathematical and Physical Sciences* **297,** 147-178**.**

Schoell, M. 1980. The hydrogen and carbon isotopic composition of methane from natural gases of various origins. *Geochim. Cosmochim. Atca* **44,** 649-661.

Schoell, M. 1983a. Genetic characterization of natural gases. *AAPG Bull.* **67**, 2225-2238.

Schoell, M. 1983b. Isotope techniques for tracing migration of gases in sedimentary basins. *Journal of Geological Society of London*, **140,** 415-422.

Schoell, M. 1984. Recent advances in petroleum isotope geochemistry. *Org. Geochem.* **6,** 645-663.

Schloemer, S. and B.M. Krooss. 2004. Molecular transport of methane, ethane, and nitrogen and the influence of diffusion on the chemical and isotopic composition of natural gas accumulations. *Geofluids* **4,** 81-108.

Schwarcz, H.P., M. Gascoyne, and D.C. Ford. 1982. Uranium-series disequilibrium studies of granite rocks. *Chem. Geol.* **36,** 87-102.

Serreze M.C. and J.A. Francis. 2006. The arctic amplification debate. *Climatic Change* **76,** 241-264.

Sessions, A.L., S.P. Sylva, R.E. Summons, J.M. Hayes. 2004. Isotopic exchange of carbon-bound hydrogen over geologic timescales. *Geochim. Cosmochim. Acta* **68,** 1545-1559.

Shakur, M.A. 1982. $\delta^{34}S$ and $\delta^{18}O$ variations in terrestrial sulfates. Ph.D. Thesis, Univ. Calgary.

Shannon, R.D. 1976. Revised effective ionic radii and systematic studies of interatomic distances in halides and chalcogenides. *Acta Crystallogr.* **A32**, 751-767.

Sharp, Z.D. and J.D. Barnes. 2004. Water-soluble chlorides in massive seafloor serpentinites: a source of chloride in subduction zones. *Earth and Planetary Science Letters* **226,** 243-254.

Sharp, Z.D., J.D. Barnes, A.J. Brearley, M. Chaussidon, T.P. Fischer, and V.S. Kamenetsky. 2007. Chlorine isotope homogeneity of the mantle, crust and carbonaceous chondrites. *Nature* **446**, 1062-1065.

Shauble, E.A., G.R. Rossman, and H.P. Taylor, Jr. 2003. Theoretical estimates of equilibrium chlorine-isotope fractionations. *Geochim. Cosmochim. Acta* **67,** 3267-3281.

Sherwood-Lollar, B., P. Fritz, S.K. Frape, S.A. Macko, S.M. Weise, and J.A. Welhan. 1988. Methane occurrences in the Canadian Shield. *Chem. Geol.* **71,** 223-236.

Sherwood-Lollar, B. 1990. Origins and implications of methane in the crystalline environment – the Canadian and Fennoscandian Shields.. Ph.D. Dissertation, University of Waterloo, Waterloo, Ontario.

Sherwood Lollar, B., S.K. Frape, P. Fritz, S.A. Macko, J.A. Welhan, R. Blomqvist, P.W. Lahermo. 1993a. Evidence for bacterially generated hydrocarbon gas in Canadian Shield and Fennoscandian Shield rocks. *Geochim. Cosmochim. Acta* **57,** 5073-5086.

Sherwood Lollar, B., S.K. Frape, S.M. Weise, P. Fritz, S.A. Macko, J.A. Welhan. 1993b. Abiogenic methanogenesis in crystalline rocks. *Geochim. Cosmochim. Acta* **57,** 5087-5097.

Sherwood Lollar, B., S.M. Weise, S.K. Frape, J.F. Barker. 1994. Isotopic constraints on the migration of hydrocarbon and helium gases of southwestern Ontario. *Bull. Can. Petrol. Geol*., **42,** 283-295.

Sherwood Lollar, B., T.B. Westgate, J.A. Ward, G.F. Slater, G.L. Lacrampe-Couloume. 2002. Abiogenic formation of alkanes in the Earth's crust as a minor source for global hydrocarbon reservoirs. *Nature* **416,** 522-524.

Sherwood Lollar, B., G. Lacrampe-Couloume, G.F. Slater, J. Ward, D.P. Moser, T.M. Gihring, L.H. Lin, T.C. Onstott. 2006. Unraveling abiogenic and biogenic sources of methane in the Earth's deep subsurface. *Chem. Geol.* **226,** 328-339.

Shiegl, W.E. and J.C. Vogel. 1970. Deuterium content of organic matter. *Earth Planet. Sci. Lett.* **7,** 307-313.

Shipboard Scientific Party. 2002. Proceedings of the Ocean Drilling Program, initial reports, v. 204.

Shouakar-Stash, O., Drimmie, R.J., Morrison, J., Frape, S.K., Heemskerk, A.R., Mark, W.A. 2000. On-line D/H analysis for water, natural gas, and organic solvents by manganese reduction. *Anal. Chem.* **72,** 2664-2666.

Shouakar-Stash, O., R.J. Drimmie, S.K. Frape. 2005a. Determination of inorganic chlorine stable isotopes by continuous flow isotope ratio mass spectrometry. *Rapid Commun. in Mass Spectrom.* **19**, 121-127.

Shouakar-Stash, O., S.K. Frape, R.J. Drimmie. 2005b. Determination of bromine stable isotopes using continuous-flow isotope ratio mass spectrometry. *Anal. Chem.* **77**, 4027-4033.

Shouakar-Stash, O., Alexeev, S.V., Frape, S.K., Alexeeva, L.P., and Drimmie, R.J. 2007. Geochemistry and stable isotopic signatures, including chlorine and bromine isotopes, of the deep groundwaters of the Siberian Platform, Russia. *Applied Geochemistry* **22**, 589-605.

Shouakar-Stash, O. 2008. Evaluation of Stable Chlorine and Bromine Isotopes in Sedimentary Formation Fluids. PhD dissertation, Department of Earth and Environmental Sciences, University of Waterloo, Waterloo, ON, Canada.

Sie, P.M.J. 1999. Evaluation of groundwaters at Stripa and south central Sweden using stable chlorine isotopes. M.Sc. Thesis, University of Waterloo, Waterloo, Ontario, Canada.

Sie, P.M.J. and S.K. Frape. 2002. Evaluation of the groundwaters from the Stripa mine using stable chlorine isotopes. *Chem. Geol.* **182,** 565-582.

Siemann, M.G. and M. Schramm. 2000. Thermodynamic modeling of the Br partition between aqueous solutions and halite. *Geochim. Cosmochim. Acta* **64**, 1681-1693.

Siemann, M.G. and M. Schramm. 2002. Henry's and non-Henry's law behavior of B in simple marine systems. *Geochim. Cosmochim. Acta* **66** 1387-1399.

Siemann, M.G. 2003. Extensive and rapid changes in seawater chemistry during the Phanerozoic: evidence from Br contents in basal halite. *Terra Nova* **15,** 243-248.

Siegel, D.I. and R.J. Mandle. 1984. Isotopic evidence for glacial melt water to the Cambrian-Ordovician Aquifer, north-central United States. *Quat. Res.* **22,** 328-335.

SKB. 1992. SKB 91, Final disposal of spent nuclear fuel, importance of the bedrock for safety. Swedish Nuclear Fuel and Waste Management Co (SKB), Stockholm, Technical Report 92-20, 197p.

SKB. 2004. Interim main report of the safety assessment SR-Can. Swedish Nuclear Fuel and Waste Management Co (SKB), Stockhom, TR-04-11, 378p.

Sloan, E.D. 1998. Clathrate Hydrates of Natural Gases. Marcel Dekker Inc

Smalley, P.C., R. Blomqvist, A. Raheim. 1988. Sr isotopic evidence for discrete saline components in stratified ground waters from crystalline bedrock, Outokumpu, Finland. *Geology* **16,** 354-357.

Smellie, J.A.T., Waber, H.N., and Frape, S.K. 2003. Matrix fluid chemistry experiment, Final Report, June 1998-March 2003. SKB Technical Report TR-03-18, 162p.

Smith, M.W. and D.W. Riseborough. 1983. Permafrost sensitivity to climatic change. *Int. Conf. on Permafrost, Proceedings,* **4,** 1178-1183.

Smith, S.L., Burgess, M.M., and Heginbottom, J.A. 2001. Permafrost in Canada, a challenge to northern development. In *A Synthesis of Geological Hazards in Canada*, (ed.) G.R. Brooks. Geological Survey of Canada, Bulletin 548.

Solomon, D.K. and E.A. Sudicky. 1991. Tritium and helium-3 isotope ratios for direct estimation of spatial variations in groundwater recharge. *Water Resour. Res.* **27,** 2309-2319.

Souchez, R.A. and J. Jouzel. 1984. On the isotopic composition in delta D and delta (super 18) O of water and ice during freezing. *Journal of Glaciology* **30,** 369-372.

Spencer, R.J., N. Møller, and J.H. Weare. 1990. The prediction of mineral solubilities in mineral waters: a chemical equilibrium model for the Na-K-Ca-Mg-Cl-SO_4-H_2O system at temperatures below 25°C. *Geochim. Cosmochim. Acta* **54**, 575-590.

Spivack, A.J., M. Kastner, B. Ransom. 2002. Elemental and isotopic chloride geochemistry and fluid flow in the Nankai Trough. *Geophysical Research Letters* **29** 10.1029/2001GL014122.

SRK Consulting. 2005. Groundwater Assessment, Doris North Project, Hope Bay Nunavut, Canada. Prepared for Miramar Hope Bay Limited. Project No. 1CM014.006.

Stahl, W.J., G. Wollanke, H. Boigk. 1977. Carbon and nitrogen isotope data of Upper Carboniferous and Rotliegend natural gases from North Germany and their relationship to the maturity of the organic source material. *In*: Campos, R. and Gonji, J. (eds), *Advnaces in Organic Geochemistry 1975*, 539-559.

Stahl, W. 1979. Carbon isotopes in petroleum geochemistry. In: F. Jager and J.C. Unziker (Eds.), *Lectures in Isotope Geology*. Springer, New York, pp. 274-283.

Starinsky, A. and A. Katz. 2003. The formation of natural cryogenic brines. *Geochim. Cosmochim. Acta* **67(8),** 1475-1484.

Stark, S.C., B.V. O'Grady, H.R. Burton, P.D. Carpenter. 2003. Frigidly concentrated seawater and the evolution of Antarctic Saline Lakes. *Aust. J. Chem.* **56**, 181-186.

Stella. G.F. S. Stein, T.H. Dixon, M. Craymer, T.S. James, S. Mazzotti, R.K. Dokka. 2007. Observation of glacial isostatic adjustment in "stable" North America with GPS. *Geophys. Res. Lett.* **34,** L02306, doi: 10.1029/2006GL027081.

Stewart, M.K. 1974. Hydrogen and oxygen isotope fractionation during crystallization of mirabilite and ice. *Geochim. Cosmochim. Acta* **38,** 167-172.

Stewart, M.A. and A.J. Spivack. 2004. The stable-chlorine isotope compositions of natural and anthropogenic materials. In: C.M. Johnson, B.L. Beard, and F. Albarède (eds), *Geochemistry of Non-Traditional Isotopes*, Reviews in Mineralogy and Geochemistry **55,** 231-254.

Stober, I. and K. Bucher. 2000. Hydraulic properties of continental crust. *In*: Stober, I., K. Bucher, (eds), Hydrogeology of Crystalline Rocks, Kluwer Academic Publishers, *Water and Science Technology Library* **34,** 53-78.

Stotler, R.L., S.K. Frape, T. Ruskeeniemi, L. Ahonen, M. Paannanen, M.Y. Hobbs, M. Zhang. 2007. Hydrogeochemistry of groundwaters at and below the base of the permafrost at Lupin: Report of Phase III. Ontario Power Generation Nuclear Waste Management Division, Report No: 06819-REP-01200-xxxxx-R00.

Stotler, R.L., B. Holden, S.K. Frape, T. Ruskeeniemi, M. Talikka, B.M. Freifeld. 2008. High Lake permafrost comparison site: Permafrost Phase IV. Nuclear Waste Management Organization, Report No.: NWMO TR-2007-xx.

Stuiver M. and H.A. Polach. 1977. Discussion: reporting of C-14 data. *Radiocarbon* **19**, 355-363.

Sugiura, T., Y. Mizutani, S. Oana. 1963. Fluorine, chlorine, bromine, and iodine in volcanic gases. *The Journal of Earth Sciences, Nagoya University* **11,** 272-278.

Suzuoki, T. and T. Kimura. 1973. D/H and 18O/16O fractionation in ice-water system. Mass Spectrometry **21,** 229-233.

Symonds, R.B., W.I. Rose, T.M. Gerlach, P.H. Briggs, R.S. Harmon. 1990. Evaluation of gases, condensates, and SO2 emissions from Augustine volcano, Alaska: the degassing of a Cl-rich volcanic system. *Bull. Volcanol.* **52,** 355-374.

Szatmari, P. 1989. Petroleum formation by Fischer-Tropsch synthesis in plate tectonics. *AAPG Bull.* **73,** 989-998.

Takayama, T., M. Nishi, T. Uchida, K. Akihisa, F. Sawamura, K. Ochiai. 2005. Gas hydrate saturation analysis using density and nuclear magnetic resonance logs from the JAPEX/JNOC/GSC et al. Mallik 5L-38 gas hydrate production research well. *In* Scientifice Results from the Mallik 2002 Gas Hydrate Production Research Well Program, Mackenzie Delta, Northwest Territories, Canada, (eds.) S.R. Dallimore and T.S. Collett. *Geological Survey of Canada, Bulletin* **585**, 8p.

Taran, Y.A., G.A. Kliger, V.S. Sevastianov. 2007. Carbon isotope effects in the open-system Fischer-Tropsch synthesis. *Geochim. Cosmochim. Acta* **71,** 4474-4487.

Tarasov, L. and W.R. Peltier. 2004. A geophysically constrained large ensemble analysis of the deglacial history of the North American ice-sheet complex. *Quat. Sci. Rev.* **23,** 359-388.

Tarasov, L. and W.R. Peltier. 2005. Arctic freshwater forcing of the Younger Dryas cold reversal. *Nature* **435**, 662-665.

Tarasov, L. and W.R. Peltier. 2007. The co-evolution of continental ice cover and permafrost extent over the last glacial-interglacial cycle in North America. *J. Geophys. Res. Earth Surface*, **112**, F02S08, doi:10.1029/2006JF000661.

Taylor, A.E. 1999. Modelling the thermal regime of permafrost and gas hydrate deposits to determine the impact of climate warming, Mallik field area. In: *Scientific Results from JAPEX/JNOC/GSC Mallik 2L-38 Gas Hydrate Research Well, Mackenzie Delta, Northwest Territories, Canada,* S.R. Dallimore, T. Uchida, and T.S. Collett (eds.). Geological Survey of Canada Bulletin 544, p. 391-401.

Taylor, C.B. 1977. Tritium enrichment of environmental waters by electrolysis: development of cathodes exhibiting high isotopic separation and precise measurement of tritium enrichment factors. *Proceedings of the International Conference of Low-Radioactivity Measurements and Applications,* Slovenski Pedagogicke Nakladatelstvo, Bratislava, p. 131-140.

Taylor, H.P. 1977b. Water/rock interactions and the origin of H_2O in granitic batholith. *J. Geol. Soc. (Lond.)* **133,** 509-558.

Therriault, A.M., A.D. Fowler, R.A.F. Grieve. 2002. The Sudbury Igneous Complex: a differentiated impact melt-sheet. *Econ. Geol.* **97**, 1521-1540.

Therrien, R., R.G. McLaren, E.A. Sudicky, S.M. Panday. 2007. Hydrosphere: A three-dimensional numerical model describing fully-integrated subsurface and surface flow and solute transport. Groundwater Simulations Group, Waterloo, ON, Canada.

Thompson, T.G. and K.H. Nelson. 1954. Desalting of sea water by freezing. *Refrigerating Engineer* **32**, 44-48.

Thompson, T.G. and K.H. Nelson. 1956. Concentration of brines and deposition of salts from sea water under frigid conditions. *American Journal of Science* **254**, 227-238.

Tolstikhin, N.I. and V.M. Maksimov. 1955. Yakutskiy artesianskiy basseyn (Yakutsk artesian basin). *Zapiski LGI* (*Notes of Leningrad Mining Istitute* imeni G.V Plekhanov) **31**.

Tolstikhin, N.I. and O.N. Tolstikhin. 1974. Groundwater and Surface Water in the Permafrost Region. In: *Gneral Permafrost Studies*, P.I. Melnikov and O.N. Tolstikhin (eds.), USSR Academy of Sciences, Novosibirsk, English translation published by Environment Canada, Inland Waters Directorate, Ottawa, Technical Bulletin No. 97, 25p. (translation published 1976).

Tomaru, H., R. Matsumoto, Y.F. Chen, H. Lu, I.D. Clark. 2005. Evolution of a gas hydrate system as recorded by oxygen and hydrogen isotopes of the interstitial waters of the JAPEX/JNOC/GSC et a. Mallik 5L-38 gas hydrate production research well. In *Scientific Results from the Mallik 2002 Gas Hydrate Production Research Well Program, Mackenzie Delta, Northwest Territories, Canada*, (ed.) S.R. Dallimore and T.S. Collett, *Geological Survey of Canada Bulletin* **585**, 12p.

Tomaru, H., M.E. Torres, R. Matsumoto, W.S. Borowski. 2006. Effect of massive gas hydrate formation on the water isotopic fractionation of the gas hydrate system at Hydrate Ridge, Cascadia Margin, offshore Oregon. *Geochem. Geophys. Geosys.* **7,** 10.1029/2005GC001207.

Toran, L. and Harris, R.F. 1989. Interpretation of sulphur and oxygen isotopes in biological and abiological sulphide oxidation. *Geochim. Cosmochim. Acta*, **53**, 2341-2348.

Torres, M.E., K. Wallmann, A.M. Tréhu, G. Bohrmann, W.S. Borowski, H. Tomaru. 2004. Gas hydrate growth, methane transport, and chloride enrichment at the southern summit of Hydrate Ridge, Cascadia margin, off Oregon. *Earth Planet Sci Let.* **226,** 225-241.

Tosi, M.P and F.G. Fumi. 1964. Ionic sizes and born repulsive parameters in the NaCl-type alkali halides – II: The generalized Huggins-Mayer form. *J. Phys. Chem. Solids* **25**, 45-52.

Tréhu, A.M., P.E. Long, M.E. Torres, G. Bohrmann, F.R. Rack, T.S. Collett, D.S. Goldberg, A.V. Milkov, M. Riedel, P. Schultheiss, N.L. Bangs, S.R. Barr, W.S. Borowski, G.E. Claypool, M.E. Delwiche, G.R. Dickens, E. Gracia, G. Guerin, M. Holland, J.E. Johnson, Y.-J. Lee, C.-S. Liu, X. Su, B. Teichert, H. Tomaru, M. Vanneste, M. Watanabe, J.L. Weinberger. 2004. Three-dimensional distribution of gas hydrate beneath southern Hydrate Ridge: constraints from ODP Leg 204. *Earth and Planetary Science Letters* **222,** 845-862.

Trofimuk, A.A., N.V. Cherskiy, V.P. Tsarev. 1974. Mechanism of fractionation of isotopes of water and gas in crustal zones of hydrate formation. *Doklady Akademii Nauk SSSR* **215** 1226-1229.

Tryon, M.D., K.M. Brown, M.E. Torres. 2002. Fluid and chemical flux in and out of sediments hosting methane hydrate deposits on Hydrate Ridge, OR, II: Hydrogeological processes. *Earth and Planetary Science Letters* **201,** 541-557.

Tulk, C.A., C.I. Ratcliffe, J.A. Ripmeester. 1999. Chemical and physical analysis of natural gas hydrate from the JAPEX/JNOC/GSC Mallik 2L-38 gas hydrate research well. *in* Scientific Results from JAPEX/JNOC/GSC Mallik 2L-38 Gas Hydrate Research Well, Mackenzie Delta, Northwest Territories, Canada, (ed.) S.R. Dallimore, T. Uchida, and T.S. Collett; *Geological Survey of Canada, Bulletin* **544**, p. 251-262.

TVO. 1992. Final disposal of spent fuel in the Finnish bedrock, technical plans and safety assessment [in Finnish with English abstract]. Nuclear Waste Commission of Finnish Power Companies, Helsinki, YJT-92-31, 136p.

Tyutyunov, T. 1964. *An Introduction to the Theory of the Formation of Frozen Rocks*. Translated by J.O.H. Muhlhaus, edited by N. Rast. Pergamon Press, NY.

Uchida, T., R. Matsumoto, A. Waseda, T. Okui, K. Yamada, T. Uchida, S. Okada, O. Takano. 1999. Summary of physicochemical properties of natural gas hydrate and associated gas-hydrate-bearing sediments, JAPEX/JNOC/GSC Mallik 2L-38 gas hydrate research well, by the Japanese research consortium. *in* Scientific Results from JAPEX/JNOC/GSC Mallik 2L-38 Gas Hydrate Research Well, Mackenzie Delta, Northwest Territories, Canada, (ed.) S.R. Dallimore, T. Uchida, and T.S. Collett; *Geological Survey of Canada, Bulletin* **544**, p. 205-228.

Unni, C.K. and J.-G. Schilling. 1978. Cl and Br degassing by volcanism along the Reykjanes Ridge and Iceland. *Nature* **272,** 19-23.

Ussler III, W., and C.K. Paull. 1995. Effects of ion exclusion and isotopic fractionation on pore water geochemistry during gas hydrate formation and decomposition. *Geo-Mar. Lett.* **15** 37-44.

Ussler, W. III, and C.K. Paull. 2001. Ion exclusion associated with marine gas hydrate deposits. In: *Natural Gas Hydrates: Occurrence, Distribution, and Detection,* Geophysical Monograph **124**, 41-65.

Vakimäe, R., M Böse, F.A. Michel, and B.J. Moormann. 1995. Changes in permafrost conditions. *Quaternary International* **28**, 113-118.

Valyashko, M.G. 1956. Geochemistry of bromine in the processes of salt deposition and the use of the bromine content as a genetic and prospecting criterion. *Geochemistry* **6**, 570-589.

Van Everdingen, R.O. 1976. Geocryological terminology. *Canadian Journal of Earth Sciences* **13**, 862-867.

Van Everdingen, R.O. 1990. Ground-water hydrology. In Northern Hydrology: Canadian Perspectives, T.D. Prowse & C.S.L Ommanney (eds), National Hydrological Research Institute NHRI Science Report No. 1, Environment Canada, Saskatoon, Canada, 77-101.

Vanko, D.A. 1986. High-chlorine amphiboles from oceanic rocks: product of highly-saline hydrothermal fluids? *Am. Mineral.* **71**, 51-59.

Vidstrand, P. 2003. Surface and subsurface conditions in permafrost areas – a literature review. SKB Technical Report TR-03-06.

Vieno, T. and A.T.K. Ikonen. 2005. Plan for Safety Case of Spent Fuel Repository at Olkiluoto. Posiva Report 2005-1, Posiva, 69p.

Villemant, B. and G. Boudon. 1999. H_2O and halogen (F, Cl, Br) behaviour during shallow magma degassin processes. *Earth Plant. Sci. Lett.* **168,** 271-286.

Volpe, C.M. 1998. Stable chlorine isotope variations in the atmosphere. PhD Disseration, University of California San Diego.

Voytov G.I. 1991. Chemical and carbon-isotope fluctuations in free gases (gas jets) in the Khibiny. *Geokhimiya* **6,** 769-780.

Vuletich, A.K., C.N. Threlkeld, G.E. Claypool. 1989. Isotopic composition of gases and interstitial fluids in sediment of the Vøring Plateau, ODP Leg 104, Site 644. *In*: Eldholm, O., Thiede, J., Taylor, E., et al. (eds), *Proceedings of the Ocean Drilling Program, Scientific Results* **104,** 281-283.

Waber, H.N. and S.K. Frape. 2002. Djupförvarsteknik Matrix Fluid Chemistry Experiment, Synthesis Report: Drillcore pore water leaching studies and borehole water. *SKB Technical Document* TD-03-02, 67p.

Waldron, S., J.M. Lansdown, E.M. Scott, A.E. Fallick, A.J. Hall. 1999. The global influence of the hydrogen isotope composition of water on that of bacteriogenic methane from shallow freshwater environments. *Geochim. Cosmochim. Acta* **63,** 2237-2245.

Wallace, P.J., G.R. Dickens, C.K. Paull, W. Ussler III. 2000. Effects of retrieval and degassing on the carbon isotope composition of methane in gas hydrate- and free gas- bearing sediments from the Blake Ridge. *In*: C.K. Paull, R. Matsumoto, P.J. Wallace, W.P. Dillon, (eds.), *Proceedings of Ocean Drilling Program, Scientific Results* **164,** 101-112.

Wang, B. 1990. Permafrost and groundwater conditions, Huola River Basin, Northeast China. *Permafrost and Periglacial Processes* **1**, 45-52.

Waseda, A., and B.M. Didyk. 1995. Isotope compositions of gases in sediments from the Chile Continental Margin. In: Lewis, S.D., Behrmann, J.H., Musgrave, R.J., and Cande, S.C. (eds). *Proceedings of the Ocean Drilling Program, Scientific Results* **141,** 307-312.

Waseda, A. and T. Uchida. 2005. Organic geochemistry of gas, gas hydrate, and organic matter from the JAPEX/JNOC/GSC et al. Mallik 5L-48 gas hydrate production research well. In: S.R. Dallimore and T.S. Collett (ed.), Scientific Results from the Mallik 2002 Gas Hydrate Production Research Well Program, Mackenzie Delta, Northwest Territories, Canada. *Geological Survey of Canada Bulletin* **585**, 11p.

Washburn, A.L. 1979. Geocryology: A survey of periglacial processes and environments. Second Edition. Edward Arnold (Publisher) Ltd. ISBN 0-7131-6119-1.

Webster, J.D. 2004. The exsolution of magmatic hydrosaline chloride liquids. *Chem. Geol.* **210,** 33-48.

Weitemeyer, K.A. and B.A. Buffett. 2006. Accumulation and release of methane from clathrates below the Laurentide and Cordilleran ice sheets. *Global and Planetary Change* **53,** 176-187.

Westbrook, G.K., B. Carson, R.J. Musgrave, et al. 1994. *Proceedings of the Ocean Drilling Program, Initial Reports* **146** (part 1).

Westgate, T.D. 1998. Compositional and carbon isotopic characteristics of abiogenically derived hydrocarbons at the Kidd Creek Mine, Timmins, Ontario. M.Sc. Thesis, University of Toronto, Toronto, Ontario.

Whiticar, M.J., E. Faber, M. Schoell. 1986. Biogenic methane formation in marine and freshwater environments: CO_2 reduction vs. acetate fermentation – isotope evidence. *Geochim. Cosmochim. Acta* **50**, 693-709.

Whiticar, M.J., and E. Faber. 1989a. Carbon, hydrogen, and oxygen isotope distribution in the interstitial fluids of ODP Leg 104, Holes 642B, 642D, 643A, and 644A, Vøring Plateau, Norwegian Sea. In: Eldholm, O., Thiede, J., Taylor, E., et al. (eds.) *Proceedings of the Ocean Drilling Program, Scientific Results* **104,** 285-290.

Whiticar, M.J. and E. Faber. 1989b. Molecular and stable isotope composition of headspace and total hydrocarbon gases at ODP Leg 104, Sites 642, 643, and 644, Vøring Plateau, Norwegian Sea. In: Eldholm, O., Thiede, J., Taylor, E., et al. (eds.) *Proceedings of the Ocean Drilling Program, Scientific Results* **104,** 327-334.

Whiticar, M.J. and E. Suess. 1990. Characterization of sorbed volatile hydrocarbons from the Peru Margin, Leg 112, Sites 679, 680/681, 682, 684, and 686/687. *In:* E. Suess, R. von Huene, et al. (Eds.) *Proc. ODP, Sci. Res.* **112,** 527-538.

Whiticar, M.J. 1994. Correlation of natural gases with their sources. In: L.B. Magoon and W.G. Dow (eds.), *The Petroleum System-From Source to Trap*, AAPG Memoir **60,** 261-283.

Whiticar, M.J., E. Faber, J.K. Whelan, and B.R.T. Simoneit. 1994. Thermogenic and bacterial hydrocarbon gases (free and sorbed) in Middle Valley, Juan de Fuca Ridge, Leg 139. In: Mottl, M.J., Davis, E.E., Fisher, A.T., and Slack, J.F. (Eds). *Proceedings of the Ocean Drilling Program, Scientific Results* **139**, 467-477.

Whiticar, M.J. and M. Hovland. 1995. Data Report: Molecular and stable isotope analyses of sorbed and free hydrocarbon gases of Leg 146, Cascadia and Oregon Margins. In: *Proceedings of the Ocean Drilling Program Scientific Results* **146 (pt. 1),** 439-449.

Whiticar, M.J., M. Hovland, M. Kastner, and J.C. Sample. 1995. Organic geochemistry of gases, fluids, and hydrates at the Cascadia Accretionary Margin. *In*: B. Carson, G.K. Westbrook, R.J. Musgrave, and E. Suess (Eds.). *Proceedings of the Ocean Drilling Program, Scientific Results* **146,** 385-397.

Whiticar, M.J. 1996. Stable isotope geochemistry of coals, humic kerogens, and related natural gases. *Int. J. Coal Geol*. **32,** 191-215.

Whiticar, M.J. 1999. Carbon and hydrogen isotope systematics of bacterial formation and oxidation of methane. *Chem. Geol.* **161,** 291-314.

Willemse, N.W., O. van Dam, P.-J. van Helvoort, R. Dankers, M. Brommer, J. Schokker, T.E. Valstar, H. de Wolf. 2004. Physical and chemical limnology of a subsaline athalassic lake in West Greenland. *Hydrogiologia* **524,** 167-192.

Williams, J.R. and R.O. van Everdingen. 1973. Groundwater investigations in permafrost regions of North America: a review. In *Proceedings of the 2nd International Conference on Permafrost, Yakutsk, USSR, July 13-28, 1973 – North American Contribution*, p. 435-446.

Winckler, G., Aeschbach-Hertig, W., Holocher, J., Kipfer, R., Levin, I., Poss, C., Rehder G., Suess, E, and Schlosser P. 2002. Noble gases and radiocarbon in natural gas hydrates. *Geophys. Res. Lett.* **29(10),** 1423, 10.1029/2001GL014013.

Woulé Ebongué, V., N. Jendrzejewski, F. Walgenwitz, F. Pineau, M. Javoy. 2005. Chlorine isotope residual salt analysis: A new tool to investigate formation waters from core analyses. *AAPG Bull.* **89,** 1005-1018.

Wright, J.F., A.E. Taylor, S.R. Dallimore, F.M. Nixon. 1999. Estimating in situ gas hydrate saturation from core temperature observations, JAPEX/JNOC/GSC Mallik 2L-38 gas hydrate research well. In: *Scientific Results from JAPEX/JNOC/GSC Mallik 2L-38 Gas Hydrate Research Well, Mackenzie Delta, Northwest Territories, Canada* (ed.) S.R. Dallimore, T. Uchide, and T.S. Collett. *Geol. Surv. Canada Bull.* **544,** 101-108.

Yakushev, V.S. and E.M. Chuvilin. 2000. Natural gas and gas hydrate accumulations within permafrost in Russia. *Cold Regions Sci. Tech.* **31,** 189-197.

Yanagisawa, F. and H. Sakai. 1983. Thermal decomposition of barium sulfate vanadium pentaoxide silica glass mixtures for preparation of sulfur-dioxide in sulfur isotope ratio measurements. *Anal. Chem.* **55,** 985-987.

Yapp, C.J. and S. Epstein. 1977. Climatic implications of D/H ratios of meteoric water over North America (9500-22,000 B.P.) as inferred from ancient wood celluslose C-H hydrogen. *Earth Planet. Sci. Lett.* **34,** 333-350.

Yershov, E.D. 1998. General Geocryology. Cambridge University Press, 580.

Youngman, M.J. 1989. Dissolved gases and radioelements in groundwaters. PhD Thesis, The British Library, West Yorkshire. 422p.

Yoshida, M., I. Makino, N. Yonehara, I. Iwasaki. 1965. The fractionation of halogen compounds through the process of the volatilization and the sublimation from volcanic rocks on heating. *Bull. Chem. Soc. Japan* **38,** 1436-1443.

Yoshida, M., K. Takahashi, N. Yonehara, T. Ozawa, I. Iwasaki. 1971. The fluorine, chlorine, bromine, and iodine contents of volcanic rocks in Japan. *Bull. Chem. Soc. Japan* **44,** 1844-1850.

Zhang, M. and S.K. Frape. 2002. Permafrost: evolution of shield groundwater compositions during freezing. Ontario Power Generation Report No: 06819-REP-01200-10098-R00.

Zhang, M., M.Y. Hobbs, S.K. Frape, D.K. Nordstrom, J.W. Ball, R.B. McCleskey. 2004. Stable chlorine isotopic composition of geothermal waters from Yellowstone National Park. *Proc. Int. Symp. Water-Rock Int.* **v.11**, 233-236.

Zhang, M., S.K. Frape, A.J. Love, A.L. Herczeg, B.E. Lehmann, U. Beyerle, R. Purtschert. 2007. Chlorine stable isotope studies of old groundwater, southwester Great Artesian Basin, Australia. *Appl. Geochem.* **22,** 557-574.

Zhang, T. and B.M. Kroos. 2001. Experimental investigation on the carbon isotope fractionation of methane during gas migration by diffusion through sedimentary rocks at elevated temperature and pressure. *Geochim. Cosmochim. Acta*, **65,** 2723-2742.

Zhu, C. and D.A. Sverjensky. 1992. F-Cl-OH partitioning between biotite and apatite. *Geochim. Cosmochim. Acta* **56,** 3435-3467.

Ziegler, K. and F.J. Longstaff. 2000. Multiple episodes of clay alteration at the Precambrian/Paleozoic unconformity, Appalachian Basin: isotopic evidence for long-distance and local fluid migrations. *Clays and Clay Minerals* **48,** 474-493.